FLORIDA HURRICANE LOSS MITIGATION PROGRAM

2021 ANNUAL REPORT

January 1, 2022

Prepared by

Florida Division of Emergency Management

Ron DeSantis
Governor

Kevin Guthrie
Director

TABLE OF CONTENTS

EXECUTIVE SUMMARY

Pursuant to Subsection 215.559 (6), Florida Statutes (F.S.), this document provides a full report and accounting of activities and evaluation of such activities conducted by the Hurricane Loss Mitigation Program (HLMP). The time period covered by this report is July 1, 2020 through June 30, 2021, or State Fiscal Year (FY) 2021. Based on Section 215.559 (1), F.S., the Hurricane Loss Mitigation Program is established in the Division of Emergency Management (Division). The Division receives an annual appropriation of $10 million from the investment income of the Florida Hurricane Catastrophe Fund, authorized under the Florida General Appropriation Act and Section 215.555 (7) (c), F.S. The Public Shelter Retrofit Program, Tallahassee Community College's (TCC) Mobile Home Tie-Down Program, Florida International University's (FIU) Hurricane Research Program and Mitigation Program account for a combined $6.5 million, or sixty-five (65%) percent of the FY 2021 $10 million appropriation. The remaining thirty-five (35%) percent is used to distribute a community mitigation grant that includes both flood and wind retrofits of Florida residences and public outreach and education about retrofits to citizens and local government officials and their staff.

The Shelter Retrofit Program and TCC's Mobile Home Tie-Down Program have separate reporting requirements under Section 252.385, F.S., and Section 215.559(2)(a), F.S., respectively. Included in this report is a project analysis of the Public Shelter Retrofit Program, expenditure report for the Tallahassee Mobile Home Tie-Down Program, summary of FIU's Hurricane Research Program progress, and programmatic analysis of the Hurricane Loss Mitigation Program.

BACKGROUND

In the aftermath of Hurricane Andrew, the Florida Legislature created a series of programs to stabilize the economy and insurance industry. These programs consist of the following:

- Citizens Property Insurance Corporation (formed from a merger of the Florida Windstorm Underwriting Association and the Florida Residential Property and Casualty Joint Underwriting Association), the state insurance plan for residents unable to obtain a conventional homeowners insurance policy;

- The Florida Hurricane Catastrophe Fund, Section 215.555 F.S., a re-insurance fund established to limit insurance exposure after a storm;

- The Bill Williams Residential Safety and Preparedness Act, which in 1999 created the Hurricane Loss Mitigation Program, Section 215.559 F. S., with an annual appropriation of $10 million.

Pursuant to Section 215.559 (1) F. S., the Hurricane Loss Mitigation Program is established within the Division of Emergency Management. The Division receives an annual appropriation of $10 million from the investment income of the Florida Hurricane Catastrophe Fund authorized under the Florida General Appropriation Act and Section 215.555 (7) (c) F. S. The purpose of the $10 million annual appropriation is to provide funding to local governments, state agencies, public and private educational institutions, and nonprofit organizations to support programs that improve hurricane preparedness, reduce potential losses in the event of a hurricane, and to provide research and education on how to reduce hurricane losses.

The funds are also to be used for programs that will assist the public in determining the suitability of upgrades to structures and in the financing of such upgrades, or to protect local infrastructure from potential damage from a hurricane.

Specific Program Areas and Funding Levels

Shelter Retrofits - Pursuant to Section 215.559(2)(a), F. S., $3 million of the annual $10 million appropriation for the Hurricane Loss Mitigation Program is directed to retrofit existing public facilities to enable them to be used as public shelters. An annual report of the state's shelter retrofit program, entitled the Shelter Retrofit Report, is prepared annually and separately submitted to the Governor and the Legislature pursuant to Section 252.385, F.S. The remaining $7 million of the appropriation is allocated according to different subsections in Section 215.559, F. S., as described below.

Tallahassee Community College (TCC) – Pursuant to Section 215.559(2)(a), F. S., TCC is given an annual allocation of $2.8 million or 40 percent of the remaining $7 million. These funds are administered by TCC and are to be used to mitigate future losses for mobile homes and to provide tie-downs for mobile homes in communities throughout the State of Florida. Please see Appendix A for TCC's FY 2021 Progress Report and Appendix B for TCC's FY 2020 Final Report (extended due to COVID).

Florida International University (FIU) – Pursuant to Section 215.559(3), F. S., FIU is allocated $700,000, or 10 percent, of the remaining $7 million. The funds are administered by FIU and dedicated to hurricane research at the Type I Center of the State University System to support hurricane loss reduction devices and techniques. Please see Appendix C for FIU's FY 2021 Final Report and Appendix D for FIU's FY 2020 Final Report (extended due to COVID).

Hurricane Loss Mitigation Program (HLMP) – The remaining $3.5 million provides grant funding to governmental entities, nonprofit organizations, and qualified for-profit organizations as a means to improve the resiliency of residential, community, and government structures within their communities. The HLMP advertises funding through a Request for Proposal which utilizes a benefit-cost analysis for each of the submitted projects in order to ensure that the recommended mitigation retrofits remain cost-effective.

Hurricane Loss Mitigation Program

PROGRAM ACTIVITIES

HLMP Funding Distribution -

In June 2020, the Division issued a Request for Proposal for projects funded during the FY 2021 for the annual amount of $3.5 million as appropriated by Section 215.559, F.S. A review panel appointed by the Division selected eligible applicants based on priority, need, benefit, and alignment with local mitigation strategy projects. Based on this evaluation process, the Division contracted with 14 grant recipients to conduct wind mitigation retrofits to homes. These grant recipients are: Centro Campesino, Pompano Beach, Carrabelle, Miami Dade Community Action & Human Services Department, St. Lucie Habitat for Humanity, Banyan Health, City of Bradenton, City of Lauderdale Lakes, City of Deerfield Beach, Calhoun County, North Lauderdale, Memorial Health, Gulf County, and Franklin County. The project agreements were funded with an initial period of performance closeout date of June 30, 2021.

Due to statewide concerns surrounding the COVID-19 pandemic, extensions were granted as needed for December 31, 2021. The extensions were granted due to the halting of many projects and the supply chain bottlenecks of construction equipment and materials.

HLMP Outreach –

Pursuant to Section 215.559, F. S., the Hurricane Loss Mitigation Program was set to expire on June 30, 2021. Outreach efforts were limited due to the statute expiration and mainly focused on the FloridaDisaster.org website for public outreach. This site provides citizens and potential recipients all the information and forms needed to apply to the HLMP program. It also includes an additional hurricane retrofit guide to help citizens make informed decisions on how to prepare their homes from potentially hazardous weather.

Program Management -

HLMP is working toward adopting processes that have proven success in the Mitigation Bureau's federal grant programs. HLMP project and grant management training programs are continuously evolving to include the best practices experienced by the state-funded grant program and federal grant management programs. Additionally, custom scope templates have been designed for the various newly permissible mitigation project types that are being managed by HLMP. These new scopes are Florida specific, project specific, and provide clear instruction on the compliance requirements set forth by the State of Florida, the Division of Emergency Management, and the Bureau of Mitigation.

PROGRAM ANALYSIS

FY 2021 Recipients

Figure 1.1 shows all HLMP awards for FY 2021. All fourteen projects were residential wind mitigation type projects. Figure 1 also shows the award amount and the amount spent to date. Due to COVID-19, many of these projects were extended to December 31, 2021. Due to these extensions, the current amount spent is much lower than in previous years. All currently active projects are proceeding on schedule and are projected to close with most, if not all funds spent.

Recipient	Award Amount	Spent to Date	Project Type
DEM-HL00035 Centro Campesino	$ 194,000.00	$ 190,700.00	Residential Wind Mitigation
DEM-HL00036 City of Pompano Beach	$ 194,000.00	$ 145,108.57	Residential Wind Mitigation
DEM-HL00037 City of Carrabelle	$ 194,000.00	$ 14,689.60	Residential Wind Mitigation
DEM-HL00038 Miami-Dade CAHSD	$ 194,000.00	$ -	Residential Wind Mitigation
DEM-HL00039 St.Lucie Habitat for Humanity	$ 194,000.00	$ 55,383.50	Residential Wind Mitigation
DEM-HL00041 City of Bradenton	$ 194,000.00	$ 51,640.83	Residential Wind Mitigation
DEM-HL00042 City of Lauderdale Lakes	$ 194,000.00	$ 1,938.00	Residential Wind Mitigation
DEM-HL00043 City of Deerfield Beach	$ 194,000.00	$ 8,190.97	Residential Wind Mitigation
DEM-HL00044 Calhoun County	$ 194,000.00	$ -	Residential Wind Mitigation
DEM-HL00045 City of North Lauderdale	$ 194,000.00	$ 6,775.35	Residential Wind Mitigation
DEM-HL00046 Memorial Healthcare	$ 194,000.00	$ -	Residential Wind Mitigation
DEM-HL00047 Gulf County	$ 194,000.00	$ 8,198.25	Residential Wind Mitigation
DEM-HL00048 Franklin County	$ 194,000.00	$ -	Residential Wind Mitigation
Total	**$ 2,522,000.00**	**$ 482,625.07**	

Figure 1.1

Benefit Cost Analysis

Figure 1.2 shows the benefit cost analysis benefits and return on investment that were generated for the FY 2021 project. As displayed, there was a 36% overall return on investment for the FY 2021 projects, which is a strong return on investment.

Recipient	BCA Generated Benefits	Cost	Return on Investment
Residential			
DEM-HL00035 Centro Campesino	$ 252,517.00	$ 181,000.00	39%
DEM-HL00036 City of Pompano Beach	$ 214,452.00	$ 175,130.00	22%
DEM-HL00037 City of Carrabelle	$ 210,216.00	$ 205,348.00	2%
DEM-HL00038 Miami-Dade CAHSD	$ 410,532.00	$ 159,776.00	156%
DEM-HL00039 St.Lucie Habitat for Humanity	$ 304,112.00	$ 187,253.00	62%
DEM-HL00041 City of Bradenton	$ 202,778.00	$ 175,906.00	15%
DEM-HL00042 City of Lauderdale Lakes	$ 205,094.00	$ 146,275.00	40%
DEM-HL00043 City of Deerfield Beach	$ 228,122.00	$ 144,185.00	58%
DEM-HL00044 Calhoun County	$ 158,435.00	$ 90,637.00	74%
DEM-HL00045 City of North Lauderdale	$ 202,536.00	$ 191,482.00	5%
DEM-HL00046 Memorial Healthcare			
DEM-HL00047 Gulf County	$ 241,849.00	$ 221,155.00	9%
DEM-HL00048 Franklin County	$ 423,683.00	$ 373,423.00	13%
TOTAL	**$ 3,054,326.00**	**$ 2,251,570.00**	**36%**

Figure 1.2

FY 2022 New Projects

Figure 1.3 shows all the approved HLMP projects for FY 2022, which has a balanced set of residential wind mitigation projects and non-residential wind mitigation projects.

Newly Awarded Recipient	Award Amount	Project Type
DEM-HL00040 Banyan Health	$ 194,000.00	Non-Residential Wind Mitigation
DEM-HL00049 DeSoto County	$ 194,000.00	Non-Residential Wind Mitigation
DEM-HL00050 City of Chattahoochee	$ 194,000.00	Residential Wind Mitigation
DEM-HL00051 Escambia County	$ 194,000.00	Residential Wind Mitigation
DEM-HL00052 City of Bristol	$ 194,000.00	Residential Wind Mitigation
DEM-HL00053 Crisis Housing Solutions	$ 194,000.00	Residential Wind Mitigation
DEM-HL00054 Emerald Coast Regional Council	$ 194,000.00	Residential Wind Mitigation
DEM-HL00055 City of Flagler Beach	$ 194,000.00	Non-Residential Wind Mitigation
DEM-HL00056 West Palm Beach Housing Authority	$ 194,000.00	Non-Residential Wind Mitigation
DEM-HL00057 City of Edgewater	$ 194,000.00	Non-Residential Wind Mitigation
DEM-HL00058 City of Panama City	$ 194,000.00	Non-Residential Wind Mitigation

Figure 1.3

FY 2020 Closed Projects

Figure 1.4 shows all the completed projects from FY 2020, which had over 3.5 million spent retrofitting residential and public properties.

Closed Project	Award Amount	Amount Spent	Project Type
DEM-HL00008 Vizcaya Museum	$ 194,000.00	$ 193,999.38	Flood Mitigation
DEM-HL00010 City of North Lauderdale	$ 194,000.00	$ 186,505.29	Residential Wind Mitigation
DEM-HL00011 City of Bradenton	$ 194,000.00	$ 161,731.16	Residential Wind Mitigation
DEM-HL00013 Eckerd College INC	$ 194,000.00	$ 194,000.00	Wind Mitigation
DEM-HL00014 City of Deerfield Beach	$ 194,000.00	$ 185,449.32	Residential Wind Mitigation
DEM-HL00015 Rebuild Northwest Florida	$ 194,000.00	$ 194,000.00	Residential Wind Mitigation
DEM-HL00016 St. Lucie County	$ 194,000.00	$ 193,116.79	Residential Wind Mitigation
DEM-HL00018 Centro Campesino	$ 194,000.00	$ 193,825.00	Residential Wind Mitigation
DEM-HL00019 Adopt a Hurricane Family	$ 194,000.00	$ 193,850.00	Residential Wind Mitigation
DEM-HL00020 Flagler County	$ 194,000.00	$ 194,000.00	Residential Wind Mitigation
DEM-HL00021 Laser Wind Retrofit	$ 194,000.00	$ 182,906.17	Residential Wind Mitigation
DEM-HL00022 Town of Southwest Ranches	$ 194,000.00	$ 194,000.00	Storm Water Drainage Project
DEM-HL00023 City of Sunrise	$ 194,000.00	$ 194,000.00	Public Wind Mitigation
DEM-HL00024 City of Lauderdale Lakes	$ 194,000.00	$ 123,076.52	Residential Wind Mitigation
DEM-HL00026 Miami-Dade CAHSD	$ 194,000.00	$ 192,367.17	Residential Wind Mitigation
DEM-HL00027 City of Pompano Beach	$ 194,000.00	$ 194,000.00	Residential Wind Mitigation
DEM-HL00028 City of Carrabelle	$ 194,000.00	$ 194,000.00	Residential Wind Mitigation
DEM-HL00029 Coral Springs Improvement	$ 194,000.00	$ 194,000.00	Wind Mitigation
DEM-HL00030 Franklin County	$ 194,000.00	$ 59,783.42	Residential Wind Mitigation
DEM-HL00032 Emerald Coast Regional Council	$ 194,000.00	$ 162,078.57	Residential Wind Mitigation
TOTAL	**$ 3,880,000.00**	**$ 3,580,688.79**	

Figure 1.4

PROGRAM GOALS AND RECOMMENDATIONS

The Division of Emergency Management is committed to developing programs to educate the public on ways to reduce the impact of a disaster. It is essential that the Division continue to work with Florida homeowners, local governments, non-profit organizations and state agencies to reduce the risk of hurricane losses. Research must continue to develop stronger wind mitigation measures to protect the residents of Florida and increase structural survivability for residences. Additionally, through a comprehensive outreach approach, more communities will have an opportunity to participate in the grant program.

The Division has the following goals for the Hurricane Loss Mitigation Program:

- Continue refining grant management activities in the Salesforce platform for better reporting and process improvement,

- Where possible, leverage HLMP funds with other funds from federal, state, local government or private sources, and

- Partner with Recovery Regional Coordinators (RRC) to enhance HLMP outreach efforts.

Observations and Recommendations:

Observation - Grant recipients and contractors are continually under a confined time constraint for awarding and expending the appropriated funds within one fiscal year. Project solicitation, awarding, contracting, sub-contracting, actual mitigation retrofits and project closeout must be completed by the end of each fiscal year. This condensed time frame does not allow the Division or its participants sufficient time to take full advantage of the funding provided.

Recommendation – Extend the funding and budget authority for the annual appropriation for up to two years. This would allow the Division's contracts to start upon full execution and have a period of performance that would expire at the end of the second fiscal year.

Shelter Retrofit Program

PROGRAM ACTIVITIES

Shelter Retrofit Funding

In 2017, the Hurricane Loss Mitigation Program began managing the Shelter Survey and Retrofit Program's grants and contracting responsibilities. HLMP applied current grant management processes to both existing and new projects being managed by the Shelter Retrofit Program. With the resources available to the Mitigation Bureau's Finance Unit, tracking shelter payments, contracting, and reporting have become streamlined processes within HLMP's daily operations.

The Hurricane Loss Mitigation Program has worked with the Mitigation Bureau's Technical Unit to design and streamline processes for the project management of the Shelter Retrofit Program. Modernized Scopes of Work have been finalized with the collaboration of the Shelter Retrofit Program, Technical Unit, and Hurricane Loss Mitigation Program. New review processes and detailed requirements within the Scope of Work will strengthen regulation and monitoring while providing the recipient with a clearer understanding of their goals and objectives.

Executed Projects

Figure 2.1 displays the four shelter retrofit agreements that were executed in FY 2021, totaling $1,110,900.00.

Recipient	Award Amount
DEM-SR00031 Pinellas County	$ 27,500.00
DEM-SR00032 Alachua County	$ 166,000.00
DEM-SR00033 Bay County	$ 557,200.00
DEM-SR00035 School Board of Clay County	$ 360,200.00
TOTAL	**$ 1,110,900.00**

Figure 2.1

Closed Projects

Figure 2.2 below summarizes the nine projects were closed in FY 2021, totaling in $1,277,771.00.

Recipient	Amount Spent
HLMPSR17-020B Clay County	$ 101,440.00
HLMPSR18-001 City of South Bay	$ 332,501.00
DEM-SR00004 Orange County (WITHDRAWN)	$ -
DEM-SR00006 Orange County	$ 15,000.00
DEM-SR00007 South Florida State College	$ 40,000.00
DEM-SR00009 University of Florida	$ 399,035.00
DEM-SR00012 Lee County (WITHDRAWN)	$ -
DEM-SR00024 Jefferson County School Board	$ 370,440.00
DEM-SR00031 Pinellas County	$ 19,355.00
TOTAL	**$1,277,771.00**

Figure 2.2

Active Projects

Figure 2.3 shows all nineteen projects that were active at the end year of FY 2021. Fifteen of these projects were executed in previous fiscal years and four were executed during FY 2021. The projects that take place can be divided into three major categories; Engineering Study, Genset, and Retrofit. An Engineering Study determines the viability of a building for retrofitting. A Genset project installs the necessary electrical components to connect a generator to a building. Retrofit projects focus on hardening the envelope of a building.

Recipient	Projects	Project Type	# of Locations
HLMPSR17-020A Clay County	Orange Park High School	Engineering Study	5
	Asbury Lake Jr High School	Gen Set	
	Oakleaf High School	Retrofit	
	Fleming Island High School	Retrofit	
	Keystone Heights High School	Retrofit	
DEM-SR00001 Seminole County	Winter Springs High School	Retrofit	4
	Teague Middle School	Gen Set	
	Teague Middle School	Retrofit	
	Lawton Chiles Middle School	Gen Set	
	Lawton Chiles Middle School	Retrofit	
	Lyman High School	Gen Set	
	Lyman High School	Retrofit	
DEM-SR00005 Orange County	South Econ Rec Gym	Retrofit	5
	West Orange Rec Gym	Retrofit	
	Silver Star Rec Gym	Retrofit	
	Meadow Woods Rec Gym	Retrofit	
	Goldenrod Rec Gym	Retrofit	
DEM-SR00010 Walton County	Freeport High School	Gen Set	1
DEM-SR00013 Bay District Schools (Deer Point)	Deerpoint Elementary	Retrofit	1
DEM-SR00014 Bay District Schools (Bozeman)	Bozeman Learning Center	Retrofit	1
DEM-SR00018 School Board of Sarasota	Taylor Ranch Elementary	Retrofit	3
	Gulf Gate Elementary	Retrofit	
	North Port High School	Retrofit	

Figure 2.3

(Figure 2.3 cont.)

DEM-SR00020 School Board of Lake County	East Ridge High School	Retrofit	17
	Carver Middle School	Retrofit	
	Eustis Middle School	Retrofit	
	Mt. Dora High School	Retrofit	
	Leesburg High School	Retrofit	
	Tavares High School	Retrofit	
	Umatilla High School	Engineering Study	
	Umatilla High School	Retrofit	
	Eustis Middle School	Retrofit	
	Astatula Elementary School	Retrofit	
	Astatula Elementary School	Gen Set	
	Villages Elementary School	Gen Set	
	Villages Elementary School	Retrofit	
	Lost Lake Elementary School	Retrofit	
	Lost Lake Elementary School	Gen Set	
	Leesburg Elementary School	Gen Set	
	Umatilla Elementary School	Gen Set	
	Spring Creek Elementary Schools	Gen Set	
	Round Lake Elementary School	Gen Set	
	East Ridge Middle School	Gen Set	
	Tavares Middle School	Retrofit	
DEM-SR00021 School District of DeSoto County	West Elementary School	Retrofit	3
	Nocatee Elementary School	Retrofit	
	DeSoto High School	Retrofit	
DEM-SR00022 School Board of Brevard County	Oak Park Elementary School	Gen Set	1
DEM-SR00025 Walton County	Walton High School	Gen Set	1
DEM-SR00027 Marion County	Belleview High School	Retrofit	6
	Belleview Middle School	Retrofit	
	Legacy Elementary School	Retrofit	
	Saddlewood Elementary School	Retrofit	
	South Ocala Elementary School	Retrofit	
	West Port High School	Retrofit	
DEM-SR00028 Indian River State College	IRSC Okeechobee Conference Center	Gen Set	1
DEM-SR00029 Sumter County School Board	Wildwood Elementary School	Gen Set	1
DEM-SR00030 School Board of Polk County	Ben Hill Griffin JR Elementary School	Retrofit	5
	Frostproof Middle Senior School	Retrofit	
	Ft Meade/SR High	Retrofit	
	Ridge Community High School	Gen Set	
	Berkley Charter Elementary School	Retrofit	
DEM-SR00031 Pinellas County	Palm Harbor Activity Center	Engineering Study	1
DEM-SR00032 Alachua County	Freedom Center	Retrofit	1
	Freedom Center	Gen Set	
DEM-SR00033 Bay County	Bay County Public Library	Retrofit	1
	Bay County Public Library	Gen Set	
DEM-SR00035 School Board of Clay County	Rideout Elementary	Retrofit	1

Engineering Study	3
Retrofit	45
Gen Set	20
Total	**68**

PROGRAM GOALS AND RECOMMENDATIONS

Shelter Retrofit Program

Under the guidance of the Hurricane Loss Mitigation Program, the Shelter Retrofit Program has grown in scope and efficiency. By collaborating with the Infrastructure Unit, we continue to eradicate shelter deficits throughout the state. From better reporting to improved funding accountability, the program looks forward to providing greater resiliency and preparedness for future disasters and events throughout the state.

The Division has the following goals to accomplish in the next Fiscal Year:

- Meet the Legislature goal to eliminate the deficit of safe public hurricane evacuation shelter space in any region of the state,
- Continue refining grant management activities in the Salesforce platform for better reporting and process improvement,
- Maintain a strong relationship between the Infrastructure staff and Mitigation staff, and
- Tour final inspections with the Technical Unit to better understand the methodology used when performing inspections.

2020-2021 ANNUAL REPORT
TALLAHASSEE COMMUNITY COLLEGE
MOBILE HOME TIE DOWN PROGRAM

The Mobile Home Tie-Down Program continued to be a successful program during the 2020-2021 fiscal year, however reduced homeowner participation due to COVID-19 continued.

Program Highlights:

- New RFP 2020-04 was advertised and approved with vendors Storm Ready Services (M&B Enterprises) and Timberline Construction Group for statewide services.
- Changes to the new RFP:
  - The RFP requested a price point for non-removable skirting as recommended by the advisory council. After review, the advisory council decided non-removable skirting would not be included in the service contracts for FY20/21.
  - The RFP incorporated a limitation of 10% price variance between approved vendors. A number of parks on the waiting list do not or no longer have established, functioning HOAs requiring more direct individualized services. A single RFP was issued allowing for vendors to provide services to either individuals or parks under one contract.
  - The RFP allowed for vendors to select a region rather than statewide service.
- The use of Quality Assurance Inspectors was continued, both for the Individual component and for the Parks served by new vendor Timberline, as TCC was still under travel restrictions.
- The Florida Department of Highway Safety and Motor Vehicles (D.H.S.M.V.), Division of Motor Vehicles, Manufactured Housing Section completed a random inspection of a minimum of 10% of the homes for the Parks component. This inspection verifies the items were actually installed by the vendor and installed according to the manufacturer's specifications.
- The online application site was suspended due to non-renewal of F.S. 215.559 and the extensive waiting list. No new applications have been accepted since 6/1/2020.

Impact of COVID-19:

COVID restrictions continued to impact the services provided this program year. The state emergency declaration for COVID delayed contract negotiations and execution until the 2nd quarter of the program year. Priority was given to utilize the remaining FY1920 NCE funds; completion numbers were included in the FY1920 final report. In addition, most parks do not have the capability to host large HOA meetings with the recommended social distancing guidelines, although some allowed for multiple HOA meetings outside and/or with small

groups. Homeowners who were outside the state were restricted from traveling back to Florida and limited participation in the program.

Final Numbers:

Thirty-one (31) park site visits were completed throughout the year. The following deliverables were completed during this process:

- Interviews with management and/or homeowner association representatives.
- Visual inspections of all homes within the community.
- Intake training for the homeowners' association representatives.

During the 2020-2021 program year fourteen (14) initial resident meetings were conducted by the Program Contractors. In several parks, meetings had to be repeated to maximize resident participation and reduce participant count for social distancing. These meetings were conducted with homeowner's association board members, volunteers and, on many occasions, most residents of a particular community. Many parks did not allow for HOA meetings to be held due to COVID concerns and program information had to be disseminated "door-to-door" within the community, which also affected participation.

TCC completed six hundred eighty-six (686) homes this past year as compared to two thousand forty-one (2,141) homes the previous year. The program was successfully completed in nine (9) mobile home communities, (with three partially completed to be finalized in 2021-22) across nine (9) different Florida counties. One million fourteen thousand one hundred twenty ($1,014,120) was utilized of the FY2021 DEM-HL00033 grant, or 36% grant utilization.

Community/Park Name	**Address**	**City**	**County**	**# Homes Served**
River Haven *split b/t FY1920 and FY2021	10100 Burnt Store Rd	Punta Gorda	Charlotte	14*
Crystal Lake RV Resort	14960 Collier Blvd	Naples	Collier	47
Harbor Oaks MHP	3990 Picciola Rd	Fruitland Park	Lake	55
Heartland Estates MHP	1701 W Commerce Ave	HAINES CITY	Polk	82
Homes of Ponce de Leon	1901 US HWY 17-92	Indialantic	Brevard	10
Indian Rocks Estates	12701 126th Ave N	Largo	Pinellas	29
Lake Arrowhead Part 1	2860 North Tamiami Trail	N. Ft. Myers	Lee	165
Laurel Estates Part 1	2760 Deerfield Dr	N. Ft. Myers	Lee	33
Paddock Park	8880 SW 27th Ave	Ocala	Marion	17
Sherwood Forest Part 1	5300 West Irlo Bronson Hwy	Kissimmee	Osceola	60
Jamaica Bay	15235 S Tamiami Trl	Ft. Myers	Lee	181
Individual Homes	Details provided in program reports			25

Moving Forward:

- TCC requested and received an executed no cost extension to utilize the remaining FY2021 funds.
- Currently the database has a listing of 115 outstanding parks and 39 individual applications remaining. With that in mind TCC is not accepting new applications until the waiting list is a more manageable size and a determination is made for continuing the grant program.
- The two vendors selected through RFP 2020-04 were offered renewals for FY21/22; Timberline Construction Group declined due to low participation rates, of which we agree may continue in FY22 as COVID variants continue to spread.
- Storm Ready Services has the capacity to provide full services for this program moving forward. TCC has reserved the right to issue an RFP or localized service contract agreements to meet DEM obligations.
- Restricted access and concern over community health will likely continue to impact the program.

Please refer any questions relating to this report or the Program in general to:

Amy Bradbury
Director of Financial Services
Tallahassee Community College
444 Appleyard Drive
Tallahassee, FL 32304
850.201.8519
amy.bradbury@tcc.fl.edu

2019-2020 ANNUAL REPORT – NCE ADDENDUM
TALLAHASSEE COMMUNITY COLLEGE
MOBILE HOME TIE DOWN PROGRAM

The Mobile Home Tie-Down Program continued to be a successful program during the 2019-2020 fiscal year.

Program Highlights:

- Multiple vendor contracts were renewed as allowed and stated in the 2017 RFP and renewed 2020 RFP. Over the normal and extended program period we had three vendor agreements.
- The Individual Component of the program was renewed, but expanded to $183,540 due to increased individual interest, and the ability to complete additional individual homes during COVID park delays.
- The use of Quality Assurance Inspectors was continued, but only for the Individual Component.
- The Florida Department of Highway Safety and Motor Vehicles (D.H.S.M.V), Division of Motor Vehicles, Manufactured Housing Section completed a random inspection of a minimum of 10% of the homes for the Parks Component. This inspection verifies the items were actually installed by the vendor and installed according to the manufacturer's specifications.
- TCC adapted outreach material and forms in Spanish.
- An office assistant continued to address the majority of homeowner phone calls, and answered general homeowner questions in a timely manner.
- Correspondence for application acceptance and vendor award notification moved to a mostly electronic format, and a Hurricane Season information flyer was sent at the start of the program year.
- The online application site was updated to include additional data points: county, park manager and park HOA contact details.
- 337 new applications were accepted, including 70 park applications and 261 individual applications.
- On June 1, 2020 the online application was closed due to the extensive waiting list of parks and homes due to be served.
- Public Record Requests from a Florida resident requesting information on parks served and parks on the waiting list were shared with communities and brought additional attention to the program.
- As noted above, a new RFP was required and incorporated the following:
    - The RFP requested a price point for non-removable skirting as recommended by the advisory council. Service to non-removable skirting was reviewed and based

on the information received in the RFP responses the advisory board did not recommend expanding services.
    - The RFP incorporated a limitation of 10% price variance between approved vendors.
    - A number of parks on the waiting list do not or no longer have established, functioning HOAs requiring more direct individualized services. These parks are now classified as individuals. One RFP was issued rather than two, allowing for a single contract to provide services to individuals or parks.
    - The RFP allowed for vendors to select a region rather than statewide service. Additionally, as in years past, the RFP information was distributed to all licensed mobile home installers. These steps were done to encourage smaller, local vendors to participate in the program. This did not provide the results expected as three state-wide vendors submitted proposals.
- The NCE of the FY1920 grant funds was requested, approved, and fully utilized in 2021.

Impact of COVID-19:

COVID restrictions impacted in the 4th quarter of the program year allowing for little recovery to address the impact. DEM granted extension through FY2021. COVID risks and parks closure to public access almost halted mitigation. DHSMV Inspections on mitigation conducted were also delayed in March/April 2020 due to state COVID travel restrictions, but were fortunately completed allowing for the vendors to invoice TCC for services in June. Most parks canceled HOA meetings, although some allowed for multiple HOA meetings with small groups. Homeowners who were outside the state were not traveling back to participate in the program. COVID continued to impact participation in the program and progress of mitigation efforts through FY21. Occasionally work paused due to area outbreaks, and homeowners were reluctant to increase exposure risk as expected.

Final Numbers:

One hundred thirty-(130) site visits were completed. These visits include community evaluations utilizing the comprehensive assessment tool and the following deliverables were completed during this process:

- Interviews with management and/or homeowner association representatives. Visual inspections of all homes within the community.
- Intake training for the homeowners' association representatives.

During the 2019-2020 program year and extension period thirty-two (32) initial resident meetings were conducted by the Program Contractors. In several parks, meetings had to be

repeated to maximize resident participation and reduce headcount for social distancing. These meetings were conducted with homeowner's association board members, volunteers and, on many occasions, most residents of a particular community. Several parks would not allow community meetings at all and resulted in program information to be disseminated "door-to-door."

TCC completed two thousand one hundred forty-one (2,141) homes this year (with the NCE) as compared to two thousand and seventy-four (2,074) homes the prior FY19 program year. The program was successfully completed in twenty-nine (29) mobile home communities across fifteen (15) different Florida counties. In all two million two hundred seventeen thousand seven hundred ten dollars ($2,217,710) dollars were expensed on the grant spending 79.20% of the allocated funds during the initial grant year, primarily due to the cessation of mitigation activities due to the COVID travel, inspection and community access restrictions. The program was able fully to expend 100% of the remaining funds during the no cost extension period.

Community/Park Name	Address	City	County	# Homes Served
Westwinds Village MHP	5316 53rd Ave E	Bradenton	Manatee	163
Magnolia Manor	4190 71st St. N	St. Petersburg	Pinellas	107
Lakeshore Villas	115401 Lakeshore Villas St	Tampa	Hillsborough	88
Strawberry Ridge	3419 FL-60	Valrico	Hillsborough	75
Briarwood	5644 Regency Blvd	Port Orange	Volusia	61
Briny Breezes	5000 N Ocean Blvd	Boynton Beach	Palm Beach	224
Fairhaven Pt 1	5757 66th Street N	St. Petersburg	Pinellas	21
Fairhaven Pt 2	5757 66th Street N	St. Petersburg	Pinellas	62
Harborview MHP	24325 Harborview Rd	Punta Gorda	Charlotte	47
Lamplighter MHC Pt 2	3202 Nova Rd. S	Port Orange	Volusia	89
Maplewood Village MHP	201 Cape Ave.	Cocoa	Brevard	61
Maranatha Village	11 Maranatha Blvd	Sebring	Highlands	48
Park Hill	10101 Burnt Store Rd	Punta Gorda	Charlotte	33
Riviera Golf Estates / Riviera Village	425 Charlemagne Blvd	Naples	Collier	282
Suncoast	6010 Ridge Rd	Port Richey	Pasco	67
Tropical Breeze Estates Pt 1	4820 Mockingbird Dr	Boynton Beach	Palm Beach	96
Palm Beach MHP Pt 1	300 Cypress Dr	Lake Worth	Palm Beach	79
Bonfire Mobile Village	10140 County Rd. 44	Leesburg	Lake	100
Carriage Court East	3475 S Goldenrod Rd	Orlando	Orange	18
Cedar Cove MHC	7020 Captain Kidd Ave	Sarasota	Sarasota	7
Colony Point	3909 Briaridge Circle, W.	Sebring	Highlands	18

Groveland MHP	4651 West Eau Gallie Blvd	West Melbourne	Brevard	5
Haselton Village	14 Coral St	Eustis	Lake	15
Hollandale	2600 Pineapple Ave	Melbourne	Brevard	13
Lake Deer MHP	3301 Avenue G NW	Auburndale	Polk	38
Lake Rich Village MHP	7777 46th Ave. N.	St. Petersburg	Pinellas	50
Palm Beach MHP Pt 2	300 Cypress Dr	Lake Worth	Palm Beach	1
Pinelake Gardens	6854 SE Morningside Dr	Stuart	Martin	36
Sunny Pines RV and MHP	1200 U.S. Highway 27 S	Sebring	Highlands	37
Tropical Breeze Estates Part 2	4820 Mockingbird Dr	Boynton Beach	Palm Beach	11
Woodland Lakes	1901 US HWY 17/92	Lake Alfred	Polk	83
River Haven (*split with DEM-HL00033)	10100 Burnt Store Rd	River Haven	Charlotte	14*
Individual Homes	Details provided in program reports			99

Moving Forward

- Currently the database has a listing of 115 outstanding parks and 39 individual applications. The estimated wait time is 5-7 years. With that in mind TCC is continuing to not accept new applications until the waiting list is a more manageable size.

Please refer any questions relating to this report or the Program in general to:

Amy Bradbury
Director, Director of Financial Services
Tallahassee Community College
444 Appleyard Drive
Tallahassee, FL 32304
850.201.8519
amy.bradbury@tcc.fl.edu

A Resource for the State of Florida

HURRICANE LOSS REDUCTION FOR HOUSING IN FLORIDA

FINAL REPORT
For the Period October 16, 2020 to June 30, 2021

A Research Project Funded by:
The State of Florida Division of Emergency Management
Through Contract #DEM-HL00034-B0076

Prepared by
The International Hurricane Research Center (IHRC)
Florida International University (FIU)

July 30, 2021

Final Report

Table of Contents

Section 1
Executive Summary

Six major efforts were identified by the International Hurricane Research Center (IHRC) for the Hurricane Loss Mitigation Program (HLMP) Fiscal Year 2020-21. Funding was dedicated to areas of structural mitigation analysis, integrated flood modeling analysis, social science and education and outreach. In keeping with the comprehensive agenda of the research topics for this project, the IHRC organized a multidisciplinary team of researchers, students and support staff to complete the stated objectives. The following is a summary of research findings:

Research Area 1: Quantification of Wind Driven Rain (WDR) Intrusion Through Shuttered Sliding Glass Door Systems (PI: Dr. Arindam Gan Chowdhury)

The objective of the proposed research was to experimentally and analytically assess wind-induced water intrusion through typical sliding glass door systems installed in residential mid-rise buildings. Another aim of this project is to investigate the wind-driven-rain (WDR) impact with and without the presence of common shuttering systems, namely aluminum storm panels and accordion-style shutters. This project investigated water intrusion through a full-scale sliding glass door system installed on a large-scale building model. To accomplish the goals, wind-driven-rain (WDR) tests were conducted for multiple wind directions, test durations and wind speeds to study their effects on water intrusion through the sliding glass door system. Water intrusion effects were studied with respect to wind speed, test duration, and wind direction for configurations with and without shuttering systems. Pressure equalization across shuttered sliding glass doors was also investigated. The following list summarizes the research findings:

- The highest differential pressure on the sliding glass door occurred at the 0° wind direction and it decreased in magnitude as the model was rotated toward 45°.
- Shutters provided a sheltering effect and resulted in a lower and more uniform pressure differential on the sliding glass door when compared to the non-shuttered test cases.
- Significant water intrusion was observed for all test configurations during the 130 mph wind speed tests.
- Substantial differences in the water intrusion volumes were observed between the aluminum storm panel configuration and the accordion shutter system configuration.
- There was a general trend that the volume of water intrusion increased as the test duration increased. This trend was most significant for the aluminum storm panels at 100 mph.
- Results at lower wind speed suggest that oblique wind directions may be vulnerable to high levels of water intrusion.

This study demonstrated that significant levels of water intrusion can occur during conditions well below design-level. This project also demonstrated that variability could exist among various shuttering systems with regards to their potential sheltering effect for reducing water intrusion. More research is needed to investigate the impact of different shutter installation methods, types, and geometries to discover optimal installation techniques for potentially reducing water intrusion effects. Future research should more thoroughly investigate water intrusion at oblique angles under higher wind speed conditions to confirm this observation.

The new knowledge regarding will help quantify usefulness of shutters to reduce the risk of WDR intrusion. The Florida Public Hurricane Loss Model (FPHLM) can use the test-based data to estimate WDR loss reduction benefit provided by shutters using a risk modeling platform. The data also provide means for minimizing water intrusion. Thus, the research is important for Florida and Floridians in terms of understanding WDR intrusion and what types of shutters may help to reduce water intrusion. The research activities helped in training students with expertise in hurricane damage mitigation. The team plans to disseminate project results through journal publication and report. Also, video recording of the testing is planned to be made publicly available by FIU IHRC/EEI to demonstrate the water intrusion, helping researchers, stakeholders, and citizens to observe water penetration through the sliding glass door.

Research Area 2: Aerodynamic Loading of Residential Buildings Subjected to Experimental Downbursts and Hurricanes (PI: Dr. Amal Elawady)

Downbursts are non-stationary, transient, localized high wind events that constitute considerable damage to buildings and other structures. The importance to develop a physical large-scale downburst outflow simulator is essential to enable investigating for aerodynamics of buildings and other infrastructure systems. Recently, the research team at the Wall of Wind (WOW) Experimental Facility (EF) has been able to develop a large-scale downburst simulator that is able to produce downburst outflows of relatively large size that can allow testing of low-, mid- and high-rise buildings. A series of simulated downburst outflow tests have been conducted on a spatial-temporal grid pattern consisting of various horizontal locations at various heights in an open terrain to characterize the outflow and validate it to real downburst events.

In this study, a two part process is explained. First the validation of a novel large-scale downburst simulator at the Wall of Wind. The flow characterization is evaluated based on three main criteria which includes the formation of a rolling vortex through smoke visualization, the spike or peak zone found in the time history of each downburst test run, and finally the validation of a ‘nose shaped’ vertical profile that is compared to previous recorded real downbursts. The use of a large-scale downburst simulator open up new venues of testing for the transient aerodynamics of low-, mid- and high-rise buildings. Three buildings were tested, a low-rise building, a mid-rise building and a high-rise building in a length scale of 1:100 in open terrain. The goal was to evaluate the aerodynamics of downbursts and compare these to the conventional ABL loading considerations and determine the differences represented in a normalized pressure coefficients. Comparing the contours and pressure coefficient magnitudes amongst ABL versus downbursts, it was revealed that the overall the aerodynamic trend is basically similar; however, the pressure coefficients vary. This was particularly pronounced for the case of the high rise building. More investigations are needed to assess the possible scaling effects that may affect the resulting pressures. Also, since downburst impact on high rise buildings seems significantly different compared to ABL-induced aerodynamics, it is suggested that the dynamic response of a tall building subjected to downbursts is studied to assess the downburst-induced vibrations and dynamic response factors.

Research Area 3: Codification Wind-induced Loads on Irregular Shaped Buildings Phase II (PI: Dr. Ioannis Zisis)

Extreme wind events have been responsible for significant human and economic losses. The low-rise residential structures, which compose most of the built environment, have sustained considerable damages due to wind-induced loads. Current wind provisions presented (e.g. ASCE 7-16) provide design guidelines for low-rise structures, however, these guidelines are based on wind tunnel data performed in the late 70s with rectangular models results. Advancements in technology have led to the design of more complicated structures with uncommon shapes (identified as irregular shaped/plans). Several research investigations have studied the effect of plan irregularities on the overall pressure distributions; however, the majority have been aimed for mid-to high-rise structures, overlooking the most commonly used low-rise residential structures.

In previous DEM investigations, several irregular shapes were identified by observing a considerable number of satellite images of South Florida residential areas. It was concluded that the shapes varied significantly, however, C, L, T shapes were observed to be recurrent. During this investigation, a new shape with an S plan was identified. From these shapes, four irregular and one rectangular-shaped model of scales 1 to 100 were built. The rectangular model was built to be used as a benchmark for comparison with other available databases like NIST. Note that the models' ratios were different from the previous investigation and resembled square footage typically found on the field.

The models were tested in the new Atmospheric Boundary Layer Wind Tunnel (ABLWT) located in the Laboratory for Wind Engineering Research (LWERT) at Florida International University (FIU). This wind tunnel (of test section 6 by 8 feet in height, width, and 60 feet in overall length) was calibrated/configured to produce an open terrain with a z0=0.01m where the models were tested at ~180mph full-scale wind speed from 0 to 345 degrees wind directions at 15 degrees increments. Pressure measurements were obtained from the 350+ pressure taps that the models were instrumented with, and pressure coefficients were obtained for generating contour plots and area-averaged envelope curves.

The research concluded that irregular-shaped structures may develop considerably more critical zones of suction in walls and roof sections due to the increased number of corners, making these building shapes more susceptible to wind-induced damages. A comprehensive database of wind pressures has been produced for the considered building geometries. The preliminary codification exercise shows that current wind provisions may also underestimate the wind loads on Irregular-shaped buildings. This work will be continued as more data from additional geometries become available that will add the necessary level of confidence.

Research Area 4: Development of integrated storm tide and freshwater flooding model Phase 4 (PI: Dr. Keqi Zhang and Dr. Yuepeng Li)

In the previous phases, IHRC developed the prototype SSFOF (Storm Surge and Freshwater Overland Flooding) model which can simulate the compound effect of tide, storm surge and rainfall runoff during hurricane impact. The SSFOF model has been proven to be stable, robust, and efficient, and is one of the most advanced full-physics Nonlinear Shallow Water Equation (NSWE) based depth-averaged storm surge models. Previous reports have focused on applying the SSFOF model to large domain simulations covering particularly South Florida and North

Florida regions. While a large computational domain at region scale is necessary for storm surge simulations, local geometrical and bathymetric characteristics may be compromised in those simulations, due to the limitations of current computational capacity.

In this phase, the study was focused on a relatively local area around the Panama City FL, whose boundary is delineated according to the HU-8 watershed boundary dataset. This study investigates the hurricane induced compound storm surge and rainfall runoff flooding impact on the Panama City area. The simulations include not only a historical hurricane event Michael (2018) with measured NEXRAD (The Next Generation Weather Radar) rainfall data, but also synthetic hurricanes in combination with synthetic rainfall amount and duration, since Hurricane Michael (2018) is surge dominated.

The deliverables for the 2020-21 research period included:

- The riverine flooding module was built in the current SSFOF model, and a fine grid covering Panama City was generated.
- A more reliable and updated digital elevation data set, The Continuously Updated Digital Elevation Model (CUDEM) - 1/9 Arc-Second Resolution (3 meters), was collected and employed into the current model, to replace 5 meters Lidar Digital Elevation Model (DEM) data covering the North Florida region from U.S. Geological Survey (USGS) or Florida Geographic Data Library (FGDL).
- The population in the originally proposed study region Panhandle and Apalachicola bay is generated, and the adjacent rivers and stream were resolved.
- With the newly generated grid, recent historical hurricanes Michael (2018) was simulated. Since Ivan (2004) didn't have significant impact to Panama City, three synthetic hurricanes simulation are performed with different moving speed and landfall locations.
- Current model has the ability to simulate the storm surge induced by wind, astronomical tide, rainfall runoff, and riverine flooding simultaneously. The compound flooding of storm surge, tide, and rainfall runoff at the Panama City area are investigated, using historical Hurricane Michael (2018) and synthetic hurricane events.

In detail, a nesting technique was developed into the model to provide the boundary conditions at the shoreline, which are the water level and the flow velocity interpolated from the pre-computed storm surge results in large domains. The rainfall data is applied during the local domain computation, and the riverine flooding due to rainfall are directly resolved through applying a refined grid along the rivers instead of using upstream river discharge boundary conditions. The Continuously Updated Digital Elevation Model (CUDEM) - 1/9 Arc-Second Resolution (3 meters) Bathymetric-Topographic Tiles that is being developed by NOAA's National Centers for Environmental Information (NCEI) were been employed for the bathymetry and topography.

The finest grid resolution of the local computational domain is at the order of 50 m, particularly around the Panama City, coastal areas, and major rivers. An enhanced data map of the Manning

coefficients representing the effects of different land covers on the flooding has been generated using the same approach as previously reported. Also for the rainfall runoff module, the same Curve Number (CN) based approach is employed and a data map of the CNs has been produced. The rainfall data associated with Hurricane Michael (2018) is downloaded from the NEXRAD database and interpolated onto the local computational grid through Python scripts.

In general, it is found that heavy rainfall (20 inches in 1 day) during extreme rainfall dominated scenarios would cause significant flooding both in the Panama City and around the Deer Point Lake areas to the north of the city. It is also confirmed that a larger rainfall rate would lead to higher maximum inundation depth. If Michael (2018) made landfall at the west side of the city, much severer storm surge could occur around the city. If a hurricane forwarding speed was also reduced by half, the peak water level caused by storm surge could increase by approximately 30% at the Deer Point Lake areas. Simulations have also been carried out by replacing the original rainfall amount of Michael (2018) with a much severer rainfall (20 inches in 1 day). The results show that such rainfall could increase the peak water level by nearly 35%, depending on the location and the time period of rainfall. On the other hand, when shifting the track of Michael (2018) to the west side of the Panama City, the same extreme rainfall amount would prolong the flooding time period by days but would not increase the peak water levels significantly. In both cases, it is concluded that estimating the compound rainfall and storm surge flooding through simple superposition would cause significant errors.

Research Area 5: Improving Individual Preparedness for Hurricanes: Lessons to be Learned From Longitudinal Survey Data Collected from Florida (PI: Jeff Czajkowski)

This study is part of a multi-year research effort on hurricane preparedness by coastal residents in Florida which aims to give insights into determinants of hurricane preparedness behavior. In order to design policies to improve disaster preparedness researchers need to have a better understanding of individual decision making during a threat of a disaster as well as in its aftermath, and in particular obtain insights into why some people are well prepared and others not, which may be related to behavioral characteristics, like risk perceptions. However, most studies of individual natural disaster risk perceptions and their relation to risk reduction activities rely on cross-sectional data that is collected at one point in time after the disaster has occurred, while risk perceptions and preparedness activities evolve over time. Therefore, researchers collected data on risk perceptions and preparations in real-time during the 2020 hurricane season and under the direct threat of impacts from flooding and wind from Hurricane Eta to gain insights into how households prepare, take risk reduction measures, evacuate and/or have insurance, and study the factors that explain these decisions. Moreover, researchers conducted a follow up survey of the same households six months after the storm and coinciding with the beginning of the 2021 hurricane season to examine how preparedness activities, risk perceptions, and other factors that drive disaster preparedness have changed over time. While the real-time survey provides an important and relatively unique understanding of preparation activities during the heightened threat of the hurricane, the follow-up survey provides a longitudinal view of preparation activities that is critical to understanding factors which drive these activities, given that risk perceptions and preparedness activities evolve over time especially in the wake of

events – including record breaking near-miss storms and pandemics. Based on these insights the team draw lessons for improving individual preparedness for future hurricanes.

Specifically, the team address results obtained from a survey conducted on November 10th and 11th of 2020, shortly before hurricane Eta made landfall near Cedar Key in Florida, and a survey conducted between May 26th and June 7th 2021, at the start of the 2021 hurricane season. Researchers are interested in the drivers of insurance uptake and whether risk reduction effort is a substitute or a complement to insurance uptake, i.e. whether there is moral hazard or advantageous selection concerning flood insurance in Florida. Moreover, the team examines how individual intentions to evacuate for a storm threat are influenced by concerns about becoming infected by COVID-19. Finally, since in the U.S., there is no one "base policy" for property insurance that can cover all disaster perils, homeowners need to acquire a significant amount of information and knowledge to understand their homeowner's insurance policies and make informed decisions about their coverage options including separate polices, deductibles, and coverage limits. Consequently, we also demonstrate the complexity of property insurance in the U.S. and understand the difference in the determinants of insurance coverage purchase by various policyholder types through statistical analyses of the identified policyholder type data.

In particular, using the real-time survey conducted just ahead of what was Hurricane Eta's impact the team are able to address a particular research gap on the relationship between flood insurance coverage and the implementation of emergency preparedness measures. As these measures are applied shortly before or during immediate hurricane threats, preferences for taking emergency measures may differ compared to a low-threat situation. The team finds advantageous selection for both emergency and ex ante flood risk reduction measures for both surveys, meaning that individuals with flood insurance coverage are more likely to engage in these risk reduction activities, which is in contrast to results found in an earlier study using survey data obtained during a low-risk situation in New York city. Furthermore, researchers find that advantageous selection is largely driven by high levels of perceived worry about flood damage as well as perceived social norms for uptake of insurance and risk reduction measures. By focusing on survey respondents that are particularly cautious or uncautious we find that the former are more likely to worry about flooding, have experience with flooding, and perceive a social norm for preparedness, whereas uncautious individuals are less likely to have experience with flooding and perceive a lower social norm for preparedness. These results suggest that uptake of both insurance and risk reduction measures can be improved by raising awareness of flood risk and social norms. Flood awareness can be improved by communicating flood probabilities and consequences through advertisement campaigns, while social norms may be enhanced by giving households information on disaster preparedness by others and signaling that this is the proper thing to do.

The U.S. 2020 hurricane season was extraordinary because of a record number of named storms coinciding with the COVID-19 pandemic. This study draws lessons on how individual hurricane preparedness is influenced by the additional risk stemming from a pandemic, which turns out to be a combination of perceptions of flood and pandemic risks that have opposite effects on preparedness behavior. Our statistical analyses investigating the factors influencing evacuation intentions during Hurricane Eta in November 2020 show that older individuals are less likely to evacuate under a voluntary order, because they are more concerned about the consequences of

becoming infected by COVID-19. The results of the survey in June 2021 at the start of the 2021 hurricane season point towards similar impacts of COVID-19 risk perceptions on evacuation intentions. Although the effect of COVID-19 on evacuation intention has become slightly smaller, it is still an issue for the 2021 hurricane season despite lower COVID-19 infections and hospitalization compared with 2020 due to the ongoing vaccination campaign.

The team discusses the implications of the findings on evacuation intentions for risk communication and emergency management policies. Examples during the COVID-19 pandemic are: including COVID-19 mitigation measures in hurricane preparedness kits, such as hand sanitizer and mouth masks, abiding by social distancing rules during an evacuation, and planning ahead to identify safe evacuation locations. Moreover, government agencies can send more tailored communication messages to older people to alleviate their concerns over COVID-19 or improve their flood risk perceptions. Emergency management policies should create safe evacuation shelters where COVID-19 risks are well controlled and communicate their COVID-19 measures to the public to increase people's confidence in shelters' safety.

In terms of the analysis of the various policyholder type decisions, the team finds that the determinants of insurance coverage purchase of different policyholder types are different. This is because policyholders' demand for different types of insurance policies can be a different function of their locations, demography, house characteristics, risk perceptions, etc. For example, we find that the mandated purchase of an NFIP flood policy is not driven by the value of building and contents, the demographic characteristics, and the individuals' financial difficulty due to COVID-19, whereas these factors can impact the voluntary purchase of flood insurance. Having a basement positively affects the voluntary purchase of private flood insurance products and negatively impacts the voluntary purchase of an NFIP policy because the NFIP policy does not cover the contents in the basement. The purchase of windstorm coverage is driven by different factors than flood insurance. Being a homeowner significantly increases the probability of having windstorm coverage. The objective windstorm risk has a strong and positive relation with windstorm coverage, and the effect is stronger for the wind-only policy type. Compared to the standard market buyers, the residual market buyers of wind coverage are more significantly and positively affected by the experience of having trouble getting or renewing the wind insurance due to an increase in disaster activities.

The statistical analyses of different types of policyholders' hurricane insurance purchase determinants can help public policy officials to better understand the incentives of different policyholder types to purchase insurance and come up with policies that better target specific types of homeowners. Although our data and analysis are limited to Florida, the results could be relevant and informative to all coastal states that aim to increase the uptake rate of insurance coverage.

Research Area 6 Education and Outreach Programs to Convey the Benefits of Various Hurricane Loss Mitigation Devises and Techniques (PI: Erik Salna)

The IHRC developed and coordinated education and outreach activities to build on the foundation of previous work under this grant and showcased the hurricane-loss mitigation objectives of the HLMP.

For the 2020-21 performance period, the below mentioned educational partnerships, community events, and outreach programs were developed:

Wall of Wind Mitigation Challenge (WOW! Challenge): Friday, March 26th, 2021
(Due to COVID-19, Miami-Dade County Public Schools requested the competition be done virtually.)
The International Hurricane Research Center (IHRC), located on the campus of Florida International University (FIU), has developed the Wall of Wind Mitigation Challenge (WOW! Challenge), a judged competition for South Florida high school students. As the next generation of engineers to address natural hazards and extreme weather, this STEM education event features a competition between high school teams to develop innovative wind mitigation concepts and real-life human safety and property protection solutions. The mitigation concepts are tested live at the FIU NHERI Wall of Wind (WOW) Experimental Facility (EF), located on FIU's Engineering Campus.

- The objective for the 2021 Wall of Wind Mitigation Challenge was for students to design a wind mitigation solution to reduce the impact of wind scour on a building's flat roof.
- Each student team was supplied with a model flat roof and their wind mitigation solution had to prevent gravel on the roof from being blow away by hurricane-force winds.
- The student teams prepared three components for the competition: a physical test, an oral presentation, and a written technical paper.
- The competition included teams from five South Florida high schools.
- *First Place* was awarded to G. Holmes Braddock Senior High School.
- *Second Place* was awarded to Miami Coral Park Senior High School.
- *Third Place* was awarded to MAST Academy.
- A complete scoring summary can be found on the following link: https://www.ihrc.fiu.edu/wp-content/uploads/2021/07/2021_WOW_CHALLENGE_RESULTS_SUMMARY.pdf

Media exposure resulted in great positive visibility in the community for the IHRC, FIU and FDEM's message of mitigation:

- FIU News: https://news.fiu.edu/2021/virtual-wall-of-wind-challenge-inspires-high-school-students-to-tackle-real-world-problems?utm_source=Newsletter&utm_medium=Email&utm_campaign=FIU%20Newsletter

Eye of the Storm (Science, Mitigation & Preparedness) In-Person Event: May 15th, 2021
The Museum of Discovery & Science (MODS), located in Fort Lauderdale, FL, assisted the IHRC in planning, coordinating and facilitating this free admission public education event that showcased special hands-on, interactive activities and demonstrations teaching hurricane science, mitigation and preparedness.

- For this year's onsite, in-person Eye of the Storm, the Museum of Discovery and Science (MODS) in Fort Lauderdale had COVID-19 protocols in place for all staff, partners, vendors, participants, volunteers, and public: Healthy Scientists Make Healthy Choices Protocol | MODS.
- A record 3,750 visitors attended Eye of the Storm, showcasing special interactive activities and demonstrations teaching hurricane science, mitigation and preparedness.

- A Participant Post Survey showed 62.16% of respondents increased their knowledge about wind engineering and mitigating hurricane damage and 67.57% will be taking steps to mitigate hurricane damage.

  Media exposure resulted in great positive visibility in the community for the IHRC, FIU and FDEM's message of mitigation.
- FIU News Website "University helps community prepare for hurricane season," June 7, 2021.

  NOAA Hurricane Awareness Tour: Cancelled due to COVID-19.

  Get Ready, America! The National Hurricane Survival Initiative: Cancelled due to lack of sponsorships.

A Resource for the State of Florida

SECTION 2
QUANTIFICATION OF WIND DRIVEN RAIN (WDR) INTRUSION THROUGH SHUTTERED SLIDING GLASS DOOR SYSTEMS

FINAL REPORT
(Period: 2020-2021)

A Research Project Funded by:
The State of Florida Department of Emergency Management

Prepared by
Dr. Arindam Gan Chowdhury
Mr. James Erwin

Graduate Students
Krishna Sai Vutukuru
Johnathan Estephan

Executive Summary

The objective of the proposed research is to experimentally and analytically assess wind-induced water intrusion through typical sliding glass door systems installed in residential mid-rise buildings. Another aim of this project is to investigate the wind-driven-rain (WDR) impact with and without the presence of common shuttering systems, namely aluminum storm panels and accordion-style shutters. This project investigated water intrusion through a full-scale sliding glass door system installed on a large-scale building model. To accomplish the goals, wind-driven-rain (WDR) tests were conducted for multiple wind directions, test durations and wind speeds to study their effects on water intrusion through the sliding glass door system. Water intrusion effects were studied with respect to wind speed, test duration, and wind direction for configurations with and without shuttering systems. Pressure equalization across shuttered sliding glass doors was also investigated. The following list summarizes the research findings:

- The highest differential pressure on the sliding glass door occurred at the 0° wind direction and it decreased in magnitude as the model was rotated toward 45°.
- Shutters provided a sheltering effect and resulted in a lower and more uniform pressure differential on the sliding glass door when compared to the non-shuttered test cases.
- Significant water intrusion was observed for all test configurations during the 130 mph wind speed tests.
- Substantial differences in the water intrusion volumes were observed between the aluminum storm panel configuration and the accordion shutter system configuration.
- There was a general trend that the volume of water intrusion increased as the test duration increased. This trend was most significant for the aluminum storm panels at 100 mph.
- Results at lower wind speed suggest that oblique wind directions may be vulnerable to high levels of water intrusion.

This study demonstrated that significant levels of water intrusion can occur during conditions well below design-level. This project also demonstrated that variability could exist among various shuttering systems with regards to their potential sheltering effect for reducing water intrusion. More research is needed to investigate the impact of different shutter installation methods, types, and geometries to discover optimal installation techniques for potentially reducing water intrusion effects. Future research should more thoroughly investigate water intrusion at oblique angles under higher wind speed conditions to confirm this observation.

The new knowledge regarding will help quantify usefulness of shutters to reduce the risk of WDR intrusion. The Florida Public Hurricane Loss Model (FPHLM) can use the test-based data to estimate WDR loss reduction benefit provided by shutters using a risk modeling platform. The data also provide means for minimizing water intrusion. Thus, the research is important for Florida and Floridians in terms of understanding WDR intrusion and what types of shutters may help to reduce water intrusion. The research activities helped in training students with expertise in hurricane damage mitigation. The team plans to disseminate project results through journal publication and report. Also, video recording of the testing is planned to be made publicly available by FIU IHRC/EEI to demonstrate the water intrusion, helping researchers, stakeholders, and citizens to observe water penetration through the sliding glass door.

Introduction

The use of shuttering systems on windows, doors and sliding glass doors is a common practice in hurricane-prone regions, such as Florida. Internal pressurization due to a broken window/door is not desirable during extreme wind events because this may lead to catastrophic damage to the building. Florida Building Code (FBC) recommends the use of shutters primarily to protect the building façade from flying debris. Shutter components are typically product-rated to resist the impact during hurricanes based on standardized testing methodologies. However, it is unclear whether various shutter systems can provide additional resistance to water intrusion into the buildings. To address this question, a previous study was performed at the FIU Wall of Wind Experimental Facility that investigated water intrusion through shutters, impact resistant and unprotected windows against hurricane force wind speeds on a large-scale building model with a 1:4 scale raindrop size distribution (RSD). The results showed that there was a significant decrease in the water intrusion for the shuttered and impact resistant windows compared to unprotected windows. Hence, it was concluded that in addition to providing resistance against flying debris, shutters may also provide resistance to water intrusion into the building. To expand on these results to other building components, the current project studies the effect of shutters on a full-scale sliding glass door. For this purpose, a building with full-scale sliding glass door model was tested against simultaneous wind and rain starting with wind speeds ranging from tropical storm to a major hurricane range. Further, a full-scale RSD (based on Tokay et al., 2008 Gamma model) is better simulated at WOW during the current testing.

The objective of the proposed research is to experimentally and analytically assess wind-induced water intrusion through typical sliding glass door systems installed in residential mid-rise buildings. Another aim of this project is to investigate the WDR impact with and without the presence of common shuttering systems, namely aluminum storm panels and accordion-style shutters. The results may help develop an understanding of the difference(s) between shutter types for rain intrusion vulnerability. To accomplish these goals, water tests were conducted for multiple wind directions, test durations and wind speeds to study their effects on water intrusion. Pressure equalization across shuttered sliding glass doors was also investigated.

Background

Tropical storms and hurricanes are typically associated with heavy rainfall. However, more attention is needed to improve the wind-driven rain resistance of the built environment. This is evident from recent post hurricane damage surveys conducted after hurricanes Irma, Michael, Florence, Harvey, Dorian, and Laura (Pinelli et al. 2018, Kijewski-Correa et al. 2021), which showed that water intrusion into the building is a prime factor for damage to interior contents – even for buildings that were otherwise structurally sound. Even with ongoing improvements to building codes and standards, such as Florida Building Code Testing and Standards (TAS) 201, 202 and 203, the water intrusion through the building façade remains a problem. Interaction of building materials with the environment is an important factor in the long-term durability of

buildings. The WDR effects on building façades is well-recognized in literature (e.g. Choi 1999, Straube and Burnett 2000, Blocken and Carmeliet 2004, Salzano et al. 2010, and Kubilay et. al 2014), and is especially important because potential mold and mildew growth may result in deterioration, serviceability disruptions and interior content damage.

Aerodynamically, when the wind flows into a rectangular building, at about two-thirds of the building height, flow separation happens and some air reaches up the face and top of the roof, some air flows sideways and around the corner, and the remaining air travels downward and form a vortex (as described by Wise et al., 1965). This airflow pattern can be used as wind-driven rain deposition guide. The rain deposition on a building is mainly dependent on oncoming wind velocity and rain drop size distribution (RSD). The amount of rain deposited on the wall of a building is almost half of the amount of rain measured in free air (Robinson and Baker 1975). Also, typically due to the deflection of air and rain, the deposit of rain is higher on the top and sides of a building in comparison to the remaining surfaces. Baheru et al., (2014a) and Vutukuru et al. (2020) identified that water intrusion into a building can be attributed to three categories: pathways, sources and driving forces, as shown in Figure 1.

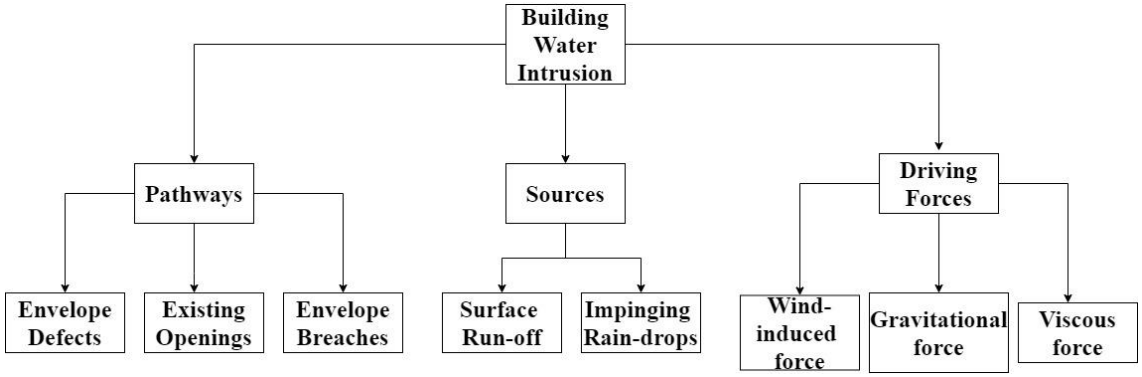

Figure 1: Attribute Classification for Rain Intrusion into the building (Vutukuru et al. 2020)

Specific to hurricane-prone regions in the U.S., damage assessment studies published by the Federal Emergency Management Agency (FEMA) following the active 2004 and 2005 Atlantic hurricane seasons identified several instances where significant losses to building interiors and contents directly resulted from water intrusion through various openings and breaches of the building envelope (FEMA 2005a, 2005b). Following Hurricane Irma in 2017, damage observations in Florida demonstrated that soffit failures were a primary source of WDR-related water intrusion into attic spaces, which led to interior damage; these observations prompted FEMA to publish a Recovery Advisory (RA) recommending more stringent soffit design and installation details (FEMA 2018). Existing risk assessment models include FEMA-HAZUS (discussed in Subramanian et al., 2014) and the Florida Public Hurricane Loss Model (FPHLM) (discussed in Baheru et al. 2014). However, the interior damage is treated as a function of the total volume of water entering a building, which is calculated based on semi-empirical models with assumed WDR parameters and engineering judgement (Baheru et al., 2014a). Due to a lack of quantitative data, there is a possibility of high-level uncertainty in the estimated water volume

in these semi-empirical methods. The current research project is aimed at reducing this level of uncertainty by providing a preliminary database of water intrusion volumes through a full-scale sliding glass door assemblies exposed to simulated hurricane wind and WDR conditions.

To date, several researchers have contributed to the development of important WDR parameters and prediction models. These models can be briefly classified into three categories. i) Experimental/Field measurements, ii) Numerical/CFD and iii) Empirical. Some very rare experimental simulations/field measurements include Straube and Burnett (2000), where a semi-empirical model was developed from data accumulated from more than 1,000 rain events (each of 15-min duration) on a test house at University of Waterloo. Blocken and Carmeliet (2005) described a novel setup for full-scale WDR measurements conducted on a model building instrumented at the Laboratory of Building Physics, Katholieke Universiteit Leuven, located in Flanders, Belgium. These results became a preliminary database of WDR deposition values for buildings. Kubilay et al. (2014) presented full-scale WDR measurements collected on the façades of two different cubic structures situated within a 3×3 array of 2 m cubes. This experimental setup was located in Dübendorf, Switzerland. Many researchers tried to mimic the behavior of water intrusion by modeling wind flow and raindrops using CFD. Choi (1993, 1994, 1999), proposed a method to determine the WDR deposition on building facades through CFD modeling of the wind flow pattern and raindrop trajectories around a building. Straube and Burnett (1998) studied the WDR-induced wetting, water penetration, and drying patterns for common brick veneer wall cladding systems and compared their results against existing test procedures developed by the American Society for Testing and Materials (ASTM) and the American Architectural Manufacturers Association (AAMA). Hangan (1999) developed a CFD model to predict raindrop trajectories and wetting patterns for two building shapes, and he compared the modeling results against experimental datasets obtained from boundary layer wind tunnel (BLWT) testing. Blocken and Carmeliet (2004) compiled a comprehensive summary of WDR literature, examining available information across various disciplines; their paper discussed experimental measurements, semi-empirical modeling methods which combined theoretical calculations with field measurements, and numerical simulations for WDR measurements and predictions with an emphasis on building science applications. Later these CFD models paved the way for the development of semi-empirical models. Abuku et al. (2009), Blocken and Carmeliet (2010), Blocken et al. (2010), and Blocken et al. (2011) compared the development and application of three different WDR models: a semi-empirical model developed by the International Standards Organization (ISO, 2009), the semi-empirical model developed by Straube and Burnett (1998, 2000), and the numerical CFD model first developed by Choi (1993, 1994) and then enhanced by Blocken and Carmeliet (2002, 2007). These papers demonstrated the ability of CFD modeling to produce reliable WDR deposition results but acknowledged the cost and complexity of the CFD modeling as two major limitations to its widespread practicality; the authors recognized the importance of the semi-empirical methods, despite their limitations, and argued that CFD modeling may enhance the overall accuracy and adoption of the semi-empirical models. Foroushani et al. (2014) conducted CFD modeling to investigate the effect of roof overhangs on WDR deposition. The study found that the overhang's ability to protect the building façade was dependent on its size and on the oncoming wind parameters. Further, the

presence of an overhang was able to protect the upper half of the building by reducing WDR deposition by as much as 80%, although the lower half of the building façade was generally unaffected by the presence of the overhang. Measured results were compared against predictions derived from two semi-empirical models, one of which underestimated the WDR and the other overestimated the average WDR.

Due to the specific geographical locations of most experimental datasets, the available WDR depositions were not measured under extreme wind and rain conditions associated with hurricanes. However, recent efforts have been made to characterize WDR parameters, such as raindrop size distribution (RSD) and rain rate, specifically during hurricanes, to better understand these extreme weather conditions. Tokay et al. (2008) reported fundamental rain parameters acquired by disdrometer field measurements during seven tropical cyclones during the 2004-2006 Atlantic hurricane seasons. These findings indicated relatively high concentrations of small and medium-sized raindrops during tropical cyclones, producing high values for the raindrop number concentration, the liquid water content, and the rain rate. Friedrich et al. (2013) reported RSD measurements gathered during Hurricane Ike in 2008 and also during convective thunderstorm events in the Great Plains region of the United States during 2010; this research discussed inherent limitations in disdrometer measurements during high wind events and recommended the use of articulating instruments during high wind measurements to reduce certain measurement errors. Numerical modeling of WDR effects under extreme wind conditions has also been attempted. Research by van de Lindt and Dao (2009), Dao and van de Lindt (2010) and Dao and van de Lindt (2012) combined CFD and finite element (FE) modeling to develop fragility curves for rainwater intrusion through a wood frame roof system applicable to residential construction. These results led to the development of a loss model for both structural and nonstructural damage in wood frame construction due to hurricanes, where the nonstructural losses were primarily attributed to rainwater intrusion (van de Lindt and Dao 2012).

Although full-scale measurements are necessary for validation of semi-empirical and numerical modeling of WDR effects, one major limitation to full-scale field measurements is the temporal dependence on natural wind and rain events to occur before useful data may be acquired. One method for overcoming this limitation is the development of large/full-scale testing facilities capable of simulating accurate and repeatable wind and WDR conditions. At the University of Florida (UF), Salzano et al. (2010) conducted an extensive study of water penetration at the window-wall interface using common installation methods for residential wood framing and concrete masonry walls. In this study, the window systems were tested in an air chamber under static air pressure conditions and cyclic air pressure conditions, as well as under dynamic WDR conditions generated by the UF Hurricane Simulator; the pressure and time of leakage were reported by Salzano et al. (2010), but water intrusion volumes were not measured. Van Straaten et al. (2010) explored the possibility of testing window assemblies under more accurate wind loading patterns when compared to a conventional test protocol, ASTM E331 (American Society for Testing and Materials 2000). To accomplish this, researchers installed a pressure load actuator (PLA) system over a full-scale window assembly. Pressure time histories obtained from

BLWT testing were reproduced by the PLA system to simulate realistic time-varying wind loads on the window. At Florida International University (FIU), Bitsuamlak et al. (2009) assessed water intrusion through secondary water barriers on a roof system under simulated hurricane conditions with the six-fan Wall of Wind (WOW) facility. Chowdhury et al. (2011) conducted similar experiments with the 6-fan WOW system to investigate water intrusion volumes through commonly installed roof vent devices. Baheru et al. 2014a and Baheru et al., 2014b reported their efforts to simulate hurricane-level wind and WDR conditions with the 12-fan WOW facility at FIU. Under these simulated conditions, Baheru et al., 2014c conducted a detailed study of water deposition on the façade of a 1:4 scale residential building model to improve the risk assessment methodology in the FPHLM.

Per *Florida Building Code* (FBC), sliding glass door systems installed in the High Velocity Hurricane Zone (HVHZ) may fall under the requirements of Testing and Application Standard (TAS) 201, 202, and 203. TAS 201 details windborne debris impact testing requirements, TAS 202 describes requirements for uniform static air pressure testing and water intrusion resistance, and TAS 203 designates the requirements for cyclic pressure loadings. Nonimpact-rated sliding glass doors are required to satisfy TAS 202 requirements only. One outcome of these testing standards is the experimental validation of door design pressure (DP), defined as the uniform static positive or negative air pressure that a door system is designed to withstand under service load conditions.

Considering the above testing standards, water intrusion in HVHZ is only addressed in the TAS 202 standard. The TAS 202 test procedure requires an application of 75% DP in the positive and negative directions for 30 s each, and then this process is repeated at 150% DP for the same 30 s durations. After the door assembly passes the uniform static pressure testing, water is then applied to the door at a minimum rate of 5 gallons per hour (gph) per square foot, which correlates to a rain rate of approximately 8.02 in/hr on the test specimen. The TAS protocol requires the rain simulation to occur with a minimum static air pressure of 15% DP applied across the sliding glass door for a duration of at least 15 min. It is hypothesized that this procedure does not adequately determine a sliding glass door assembly's ability to resist water intrusion for two reasons: First, the water intrusion requirements are conducted at only 15% DP, a much lower DP than what the sliding glass door may experience during hurricane-level WDR events under service conditions. Second, while the application of static air pressure is sufficient to determine the strength of the sliding glass door assembly, it does not replicate the dynamic time-dependent pummeling effect of the wind and rain on the sliding glass door assembly that would occur during an actual hurricane. Since the wind-induced inertial force is a primary driving force of water intrusion, the necessary dynamic interaction that may force water to flow through a potential envelope defect is lacking in the standard test protocols. This study tries to fill this knowledge gap by realistic dynamic wind testing, and it also aims to investigate the effect of test duration on the total amount of rain intrusion into the building.

Methodology

The current research study exposed a full-scale sliding glass door – installed on a large-scale test model – to wind and wind-driven rain conditions generated by the 12-fan WOW Experimental Facility (EF) at Florida International University (FIU). The large-scale building model considered during this study had been previously tested as part of a past research project. The test model was stored outdoors at the WOW facility between research projects, thus exposing the sliding glass door specimen to ambient South Florida weather conditions for a period of approximately two years before the current project. The test model itself was constructed from internal steel framing members attached to two reinforced concrete wall sections; the other two wall sections were sheathed with plywood panels, and the roof was also sheathed with plywood (Figure 2). The overall dimensions of the test model measured 2.4 × 3.2 × 3.4 m (8.0 × 10.4 × 11 ft, $B \times D \times H$). These dimensions were designed to keep the model engulfed within the WOW flow field. It is noted that, due to blockage limitations in the WOW flow field, the sliding glass door comprises a major portion of the windward wall of the building model, so the current study may be considered conservative in nature. The sliding glass door was secure to one of the test model's reinforced concrete walls with concrete anchors. During the original research project, the sliding glass door had been professionally installed and sealed on the test model in a manner consistent with typical field installations.

Figure 2: Large-scale building model with full-scale sliding glass door

The sliding glass door components were custom-built during the previous research project to replicate a sliding glass door unit that was no longer in production at the time of the research; the

estimated design pressure (DP) for the sliding glass door is 77.8 psf, controlled by the ¼" tempered glass chosen for construction of the specimen. Any penetrations through the sliding glass door framing from the previous research project's instrumentation were filled with Dow Corning 790 sealant and further covered with tape before the current research project commenced.

The test protocol for the current study was established to investigate the effects of wind speed, wind direction, experiment duration, and the potential sheltering effect of two common shuttering systems – aluminum storm panels and accordion shutters – on the volume of water intrusion accumulated inside the building model. The protocol considered three wind directions, 0°, 22.5°, and 45°, as defined in Figure 3.

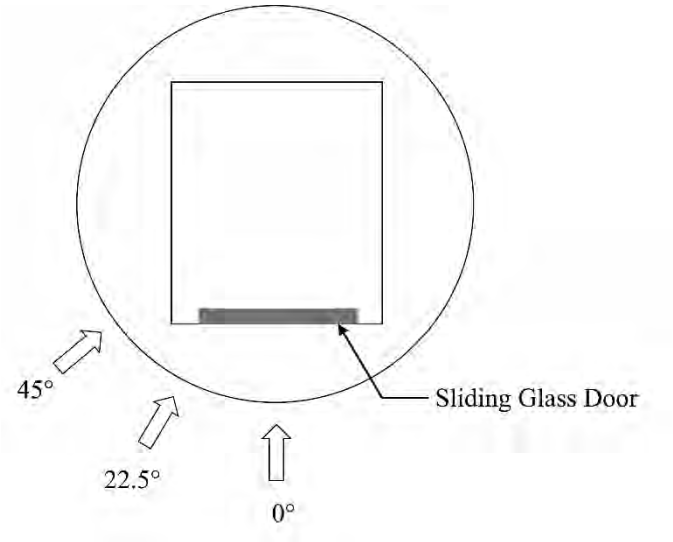

Figure 3: Wind directions (Plan View)

Raindrop Size Distribution

Before the building model was exposed to WOW-generated wind and wind-driven rain conditions, a series of free stream experiments was conducted to increase the size of the raindrop diameters injected into the WOW flow field. Past work by Baheru et al. (2014b) developed a 1:4 scale raindrop size distribution (RSD) at the WOW facility. For this project, work began to better simulate a full-scale 1:1 RSD in the WOW flow field. The 1:1 RSD experiments consisted of various trials with different water nozzle configurations to find an arrangement that would yield a satisfactory full-scale simulation. A precipitation imaging probe (PIP), manufactured by Droplet Measurement Technologies, was installed in the WOW field to measure the raindrop size distribution. To conduct these experiments, the PIP was generously loaned to FIU by colleagues at the University of Florida. The PIP was installed at the center of the WOW turntable (Figure 4), and it recorded droplet size data at WOW-generated wind speeds of 65, 100, and 130 mph.

Figure 4: PIP sensor installed on WOW turntable

The rain rate during the RSD tests was determined by measuring the total flow rate of water injected into the WOW wind field during the experiments. The flow rate was converted into an equivalent rain rate by dividing the volume of water per unit time by the area of the WOW wind field.

Pressure Distribution Study

A pressure study was conducted to quantify the net pressure distribution across the sliding glass door, as well as the changes to the net pressure distribution caused by the presence of the shutters. The pressure distribution on the sliding glass door was determined by installing 12 external pressure taps and four internal pressure taps on the sliding door panel. Because it would have been difficult to install pressure taps through the tempered glass on the sliding glass door, a mock door was constructed from plywood sheathing and nominal 2x4 lumber bracing. Pressure taps were drilled into the mock door, and the mock door was installed into the sliding glass door framing (Figure 5a). Dow Corning 790 sealant was applied around the mock door edges and allowed to cure to create an airtight installation. The pressure taps were connected to a Scanivalve ZOC33 pressure scanner (Figure 5b) and a DSM4000 data acquisition system. Pressure data was sampled at a rate of 520 Hz during this pressure study. Once the baseline pressure distribution had been measured on the sliding glass door alone, a shutter system was installed over the door, and the series of pressure measurements were repeated. During the shuttered pressure testing, the shutters themselves were instrumented with an additional 24 pressure taps (12 external pressure taps and 12 internal pressure taps, Figure 5c), bringing the total number of taps to 40 for the shuttered test cases (16 taps on the mock sliding glass door plus 24 taps on the shutters). Due to time and budget constraints, the pressure measurements were conducted with the aluminum storm panel shutters only (Figure 5d). It was assumed that the sheltering effect of the accordion shutter system would yield results comparable to the aluminum storm panels. A summary of the pressure distribution tests is shown in Table 1.

(a) Pressure model with instrumented mock door panel.

(b) Interior view of instrumented mock door showing Scanivalve pressure instrumentation

(c) Close-up view of interior and exterior pressure taps on aluminum storm panel

(d) Pressure model with instrumented mock door and instrumented storm panel shutters.

Figure 5: Pressure study building model

Table 1: Summary of Pressure Distribution Test Cases

Target Wind Speed (mph)	Wind Direction (deg)	Sampling Time (min)	Sampling Frequency (Hz)
Sliding Glass Door Only, No Shutter			
65	0	1	520
65	22.5	1	520
65	45	1	520
Sliding Glass Door with Aluminum Storm Panel			
65	0	1	520
65	22.5	1	520
65	45	1	520

Water Intrusion Study

Following the pressure study, a series of tests was conducted to quantify the total volume of water entering the building through the sliding glass door system, with and without the presence of shutters. To investigate the effect of wind speed, the sliding glass door was subjected to three different target wind speeds at the 0° wind direction: 65, 100, and 130 mph. The effect of test duration was investigated by testing each wind speed and wind direction for different test durations, ranging from 3-min to 15-min. Water intrusion effects were also investigated at the oblique wind directions of 22.5° and 45° for one wind speed only (65 mph).

The volume of water intrusion through the sliding glass door was captured by four plastic storage bins, acting as water catch basins. The storage bins were placed inside the building model along the bottom sill of the sliding glass door; several pieces of aluminum foil were taped to the inside edge of the sill and shaped to direct the water to flow into the catch basins (Figure 6). Any residual water that remained on the sliding glass door sill or the aluminum foil was collected by hand using PIG water absorbent mats. A GoPro camera was installed inside the building model during several test cases to record video of the water intrusion (Figure 7), helping the researchers identify source(s) of water penetration through the sliding glass door. Following each test case, the volume of water intrusion was determined by weighing the water collected in all four catch basins, plus the water absorbed by the absorbent pads, using an Ohaus R31P3 electronic balance and the weight-by-difference technique. The water weight for each catch basin and absorbent pad were summed together and reported as the total amount of water intrusion for a given test case. Between tests, the sliding glass door and catch basins were wiped down by hand with paper towels to help ensure that no residual water would be collected during the following test case. A summary of the water intrusion test cases is shown in Table 2; note that the series of test cases shown in Table 2 was applied to each of the three test configurations: no shutters, aluminum storm panels, and accordion shutters.

Figure 6: Interior view of water catch basins

Figure 7: GoPro camera inside building model during the water intrusion experiments.

Table 2: Summary of Water Intrusion Test Cases (Applies to No Shutter, Aluminum Storm Panel, and Accordion Shutter test configurations)

Target Wind Speed (mph)	Wind Direction (deg)	Test Duration (min)
65	0	3
65	0	6
65	0	9
65	0	12
65	0	15
100	0	3
100	0	6
100	0	9
130	0	3
130	0	6
130	0	9
65	22.5	3
65	22.5	9
65	22.5	15
65	45	3
65	45	9
65	45	15

Calculations

Pressure Distribution Study:
One goal of this project was to better understand the relationship between differential pressure and water intrusion through a sliding glass door. The pressure distribution was studied in terms of the pressure differential across the door, that is, the difference in pressure between the external and internal surfaces of the door panel. The recorded pressure time histories were converted into equivalent 3-sec gust differential pressure coefficients, $C_{P,3-sec}$, calculated according to the following equation:

$$C_{P,3-sec} = \frac{\Delta P}{0.5\rho V_{3-sec}^2} \quad (1)$$

In Equation 1, ΔP is the calculated maximum pressure differential between the external and internal surfaces of the door at a given pressure tap location, ρ is the density of air, and V_{3-sec} is the peak 3-sec gust wind speed at the building model's roof height. Free stream wind speed measurements were conducted with Turbulent Flow Instrumentation cobra probes to record wind speed time histories to determine V_{3-sec}.

Water Intrusion Study:
Baheru et al. (2014a) expressed water intrusion at a given location on the building façade in terms of two nondimensional parameters: the rain admittance factor (RAF) to quantify water intrusion due to direct impinging raindrops, and the surface runoff coefficient (SRC) to quantify water intrusion due to surface runoff rainwater. RAF and SRC are calculated by Equations 2 and 3, respectively:

$$RAF = \frac{RR_{b,\mathrm{DI}}}{RR_v} \quad (2)$$

$$SRC = \frac{RR_{b,\mathrm{SR}}}{RR_v} \quad (3)$$

The term $RR_{b,\mathrm{DI}}$ represents the rain rate at a given point on the building facade due to direct impinging raindrops, and the term $RR_{b,\mathrm{SR}}$ represents the rain rate at a given point on the building facade due to the surface runoff rainwater. In both equations, the term RR_v is the free stream wind driven rain rate measured at a given reference height. Values of $RR_{b,\mathrm{DI}}$ and $RR_{b,\mathrm{SR}}$ are calculated by Equations 4 and 5, respectively:

$$RR_{b,DI} = \frac{V_{o,\mathrm{DI}}}{A_o t} \quad (4)$$

$$RR_{b,SR} = \frac{V_{o,\mathrm{SR}}}{A_{\mathrm{SR}} t} \quad (5)$$

where, $V_{o,\mathrm{DI}}$ is the volume of water that enters an opening due to direct impinging raindrops, A_o is the area of the opening, $V_{o,\mathrm{SR}}$ is the volume of water that enters an opening due to surface runoff rainwater, and A_{SR} is the area of the building façade over which surface runoff rainwater may reach a given opening. For both equations, t is the duration of the WDR event. In general, the total volume of WDR intrusion through a given opening on a building envelope, V_{tot}, may be calculated as the sum of the water intrusion volume due to direct impinging raindrops, V_{DI}, and the water intrusion volume due to surface runoff rainwater, V_{SR}, as shown in Equation 6, below:

$$V_{tot} = V_{DI} + V_{SR} \tag{6}$$

Rather than distinguishing the volume of water intrusion attributed to direct impinging raindrops versus the volume water attributed to surface runoff, the current study focused on finding the total volume of water intrusion, V_{tot}, accumulated from both mechanisms impacting the sliding glass door simultaneously. Consequently, RAF and SRC values are not reported here. Instead, the observed water intrusion is reported as the total rain rate into the building through the window as a function of the total volume of water intrusion, symbolized here as $RR_{b,tot}$. Values of $RR_{b,tot}$ were calculated according to Equation 7, below.

$$RR_{b,tot} = \frac{V_{tot}}{A_e t} \tag{7}$$

In Equation 7, the total volume, V_{tot}, has the same meaning as defined in Equation 5, and t represents the duration of the WDR event. The term A_e was adopted here to represent the effective area of the sliding glass door and wall section for both direct impinging raindrops and surface runoff. The effective area was calculated as area of the sliding glass door itself (direct impinging raindrop region) plus the area of the wall directly above the sliding glass door (surface runoff region). Compared to the non-shuttered test case, a larger effective area was applied to the aluminum storm panel and accordion shutter test cases because the shutter systems extended wider than and below the sliding glass door dimensions opening.

Results

Raindrop Size Distribution

RSD measurements acquired from the PIP sensor during free stream experiments indicated that the best results came from an arrangement of 11 Teejet 8008E nozzles mounted to the center spire and one custom 3d printed nozzle mounted on each of the two outer spires of the WOW flow management section. A diagram of the nozzle layout is shown in Figure 8. This nozzle arrangement resulted in a water flow rate of approximately 26 gal/min into the wind flow – an equivalent simulated rain rate of approximately 9.3 in/hr across the WOW wind field. Figure 9 shows a normalized comparison of the WOW simulated 1:1 RSD against the target Gamma model reported by Tokay et al. (2013), which was based on field observations. The results show

reasonable agreement between the WOW simulation and the field measurements for rain drop diameters in the mid-range. It is acknowledged that additional work is needed to further improve the WOW 1:1 RSD simulation for drops having diameters larger than 2.25 mm and smaller than 1.5 mm. However, the excess number of larger diameter raindrops in the WOW flow field is consistent with the conservative nature of this current research study.

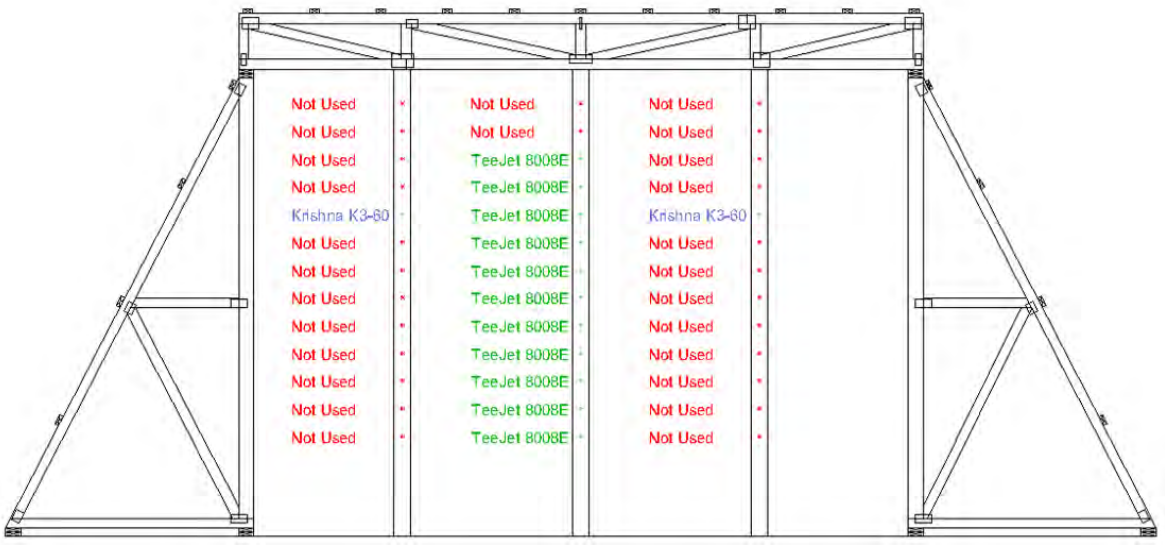

Figure 8: Water nozzle arrangement

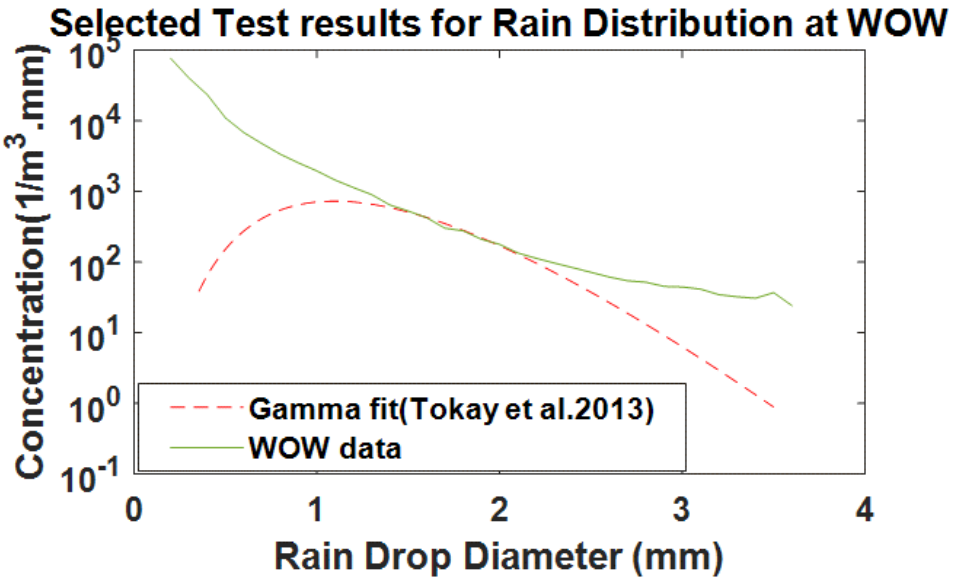

Figure 9: RSD simulation results

Pressure Distribution Study

The peak 3-sec gust pressure coefficients determined from the pressure time histories on the instrumented door panel have been plotted as contours. The coordinate system for the contour plots assumes an origin located at the bottom corner of the instrument mock door panel, as shown in Figure 10.

Figure 10: Coordinate system for pressure contour plots

Figure 11, Figure 12, and Figure 13 show the differential pressure distributions acting on the instrumented half of the sliding glass door for the respective 0°, 22.5°, and 45° test cases without shutters and with shutters. For the "No Shutter" test cases, Figure 11 indicates that the greatest overall pressure differential across the door panel occurred at the 0° wind direction, and that the overall highest measured pressure differential, $C_{P,3-sec} \approx 0.95$ is located at the top of the door panel near the center of the sliding glass door assembly. It is interesting to note that the observed pressure distribution on the sliding glass door became nearly uniform across the entire door when the shutters were installed (Figure 11b). Further, the shutters provided a sheltering effect on the sliding glass door at 0°, reducing the peak differential pressure coefficient from 0.95 to 0.63, a reduction of approximately 34%. Compared to the 0° wind direction, the net pressure distribution on the non-shuttered sliding glass door decreased in magnitude at the 22.5° wind direction, with the highest $C_{P,3-sec} = 0.42$. The sheltering effect of the shutters is again apparent at the 22.5° wind direction, with the highest $C_{P,3-sec}$ reducing to 0.35, a reduction of 16.7%. Once again, the differential pressure distribution became more uniform on the instrumented sliding glass door panel when the shutters were installed at the 22.5° wind direction. For the 45° wind direction, the measured differential pressures acting on the instrumented door were found to be zero for the non-shuttered test configuration. The presence of the shutters slightly increased the net pressure differential on the door to $C_{P,3-sec}$ values ranging from 0.05 to 0.07, but these values remain significantly lower than the 0° and 22.5° wind directions, indicating that the 45° wind direction is likely not a critical condition for water intrusion on the building model considered in this study.

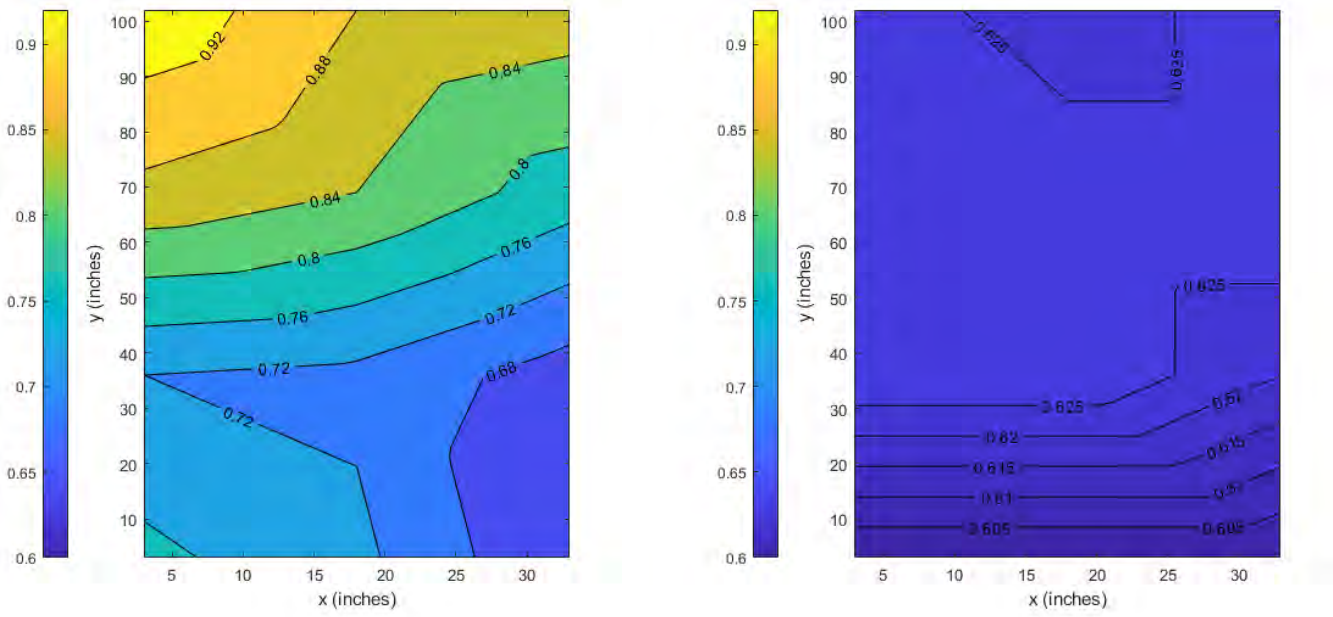

(a) No Shutter (b) With Aluminum Storm Panel

Figure 11: Peak differential 3-sec gust ($C_{P,3-sec}$) contours on sliding glass door for 0° wind direction

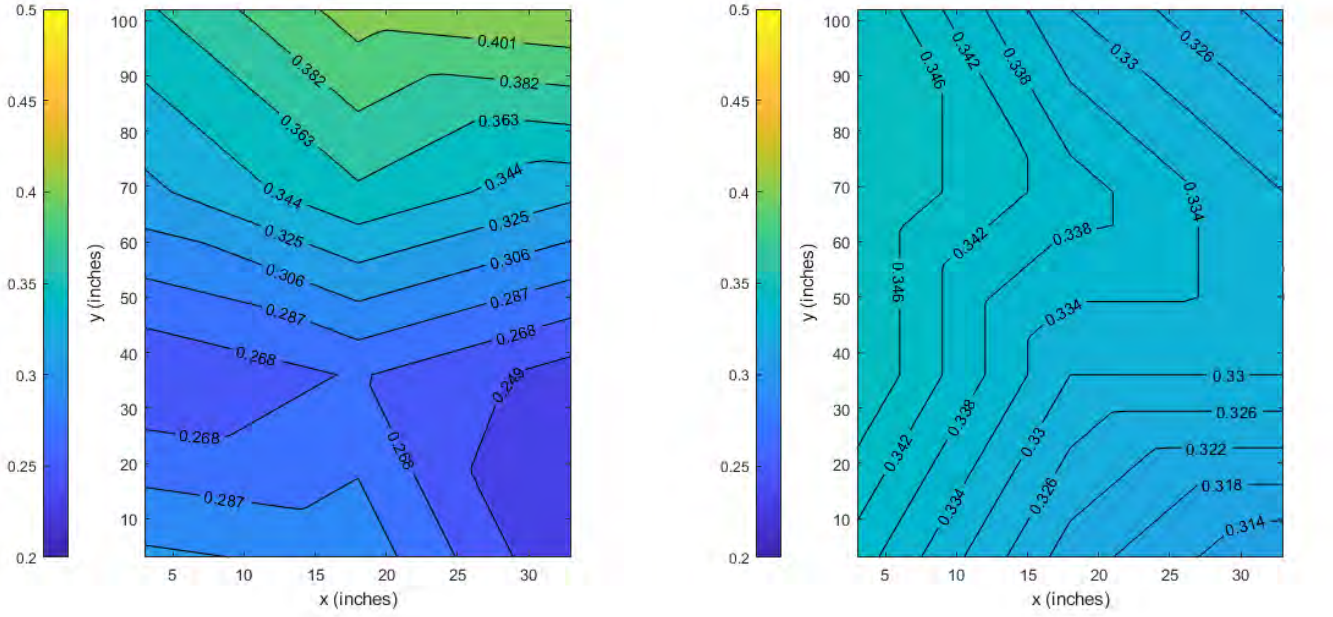

(a) No Shutter (b) With Aluminum Storm Panel

Figure 12: Peak differential 3-sec gust ($C_{P,3-sec}$) contours on sliding glass door for 22.5° wind direction

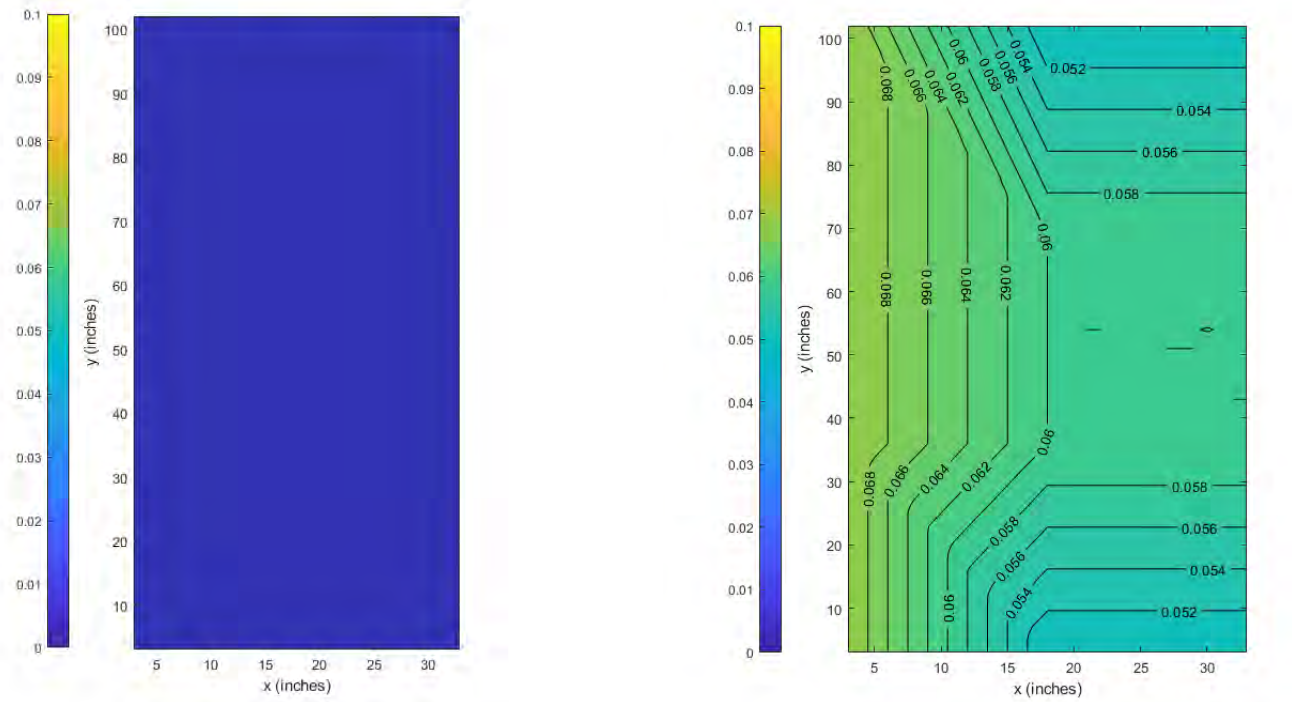

(a) No Shutter (b) With Aluminum Storm Panel

Figure 13: Peak differential 3-sec gust ($C_{P,3-sec}$) contours on sliding glass door for 45° wind direction

Water Intrusion Study

1. Effect of wind speed

To understand the effect of wind speed on water intrusion, Figure 14a-c shows plots of $RR_{b,tot}$ versus the target WOW wind speed. These figures were plotted for a constant wind direction of 0°, the wind direction that showed the highest overall pressure differential on the sliding glass door, and for experimental durations of 3-, 6-, and 9- min. The plots reveal a generally rising trend that indicates higher volumes of water intrusion occurred through the sliding glass door as the wind speed increased. For all test configurations, minimal amounts of water intrusion occurred at the 65 mph wind speed, but significant amounts of water intrusion were observed at 100 and 130 mph. Figure 14b and Figure 14c show that the water intrusion volumes were comparable between the non-shuttered configuration and the aluminum storm panel configuration at 100 mph and 130 mph, whereas the accordion shutter system demonstrated lesser amounts of water intrusion for all wind speeds in comparison to the other two configurations. Nevertheless, significant amounts of water intrusion were observed for all three test configurations at 130 mph.

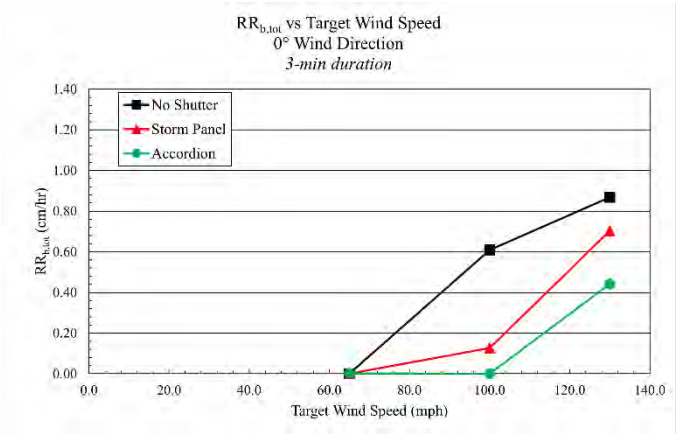

(a) 3-min test duration

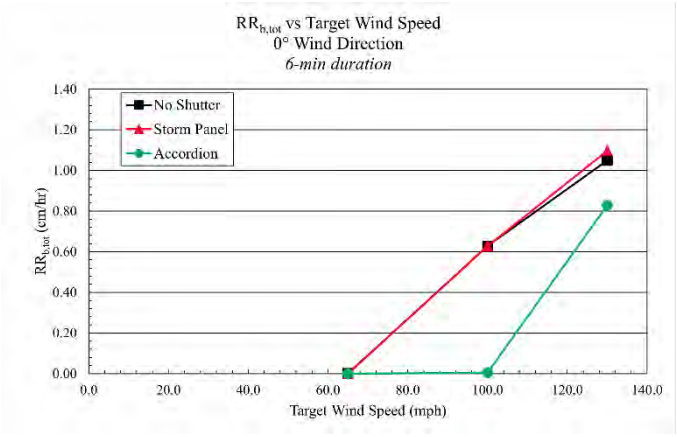

(b) 6-min test duration

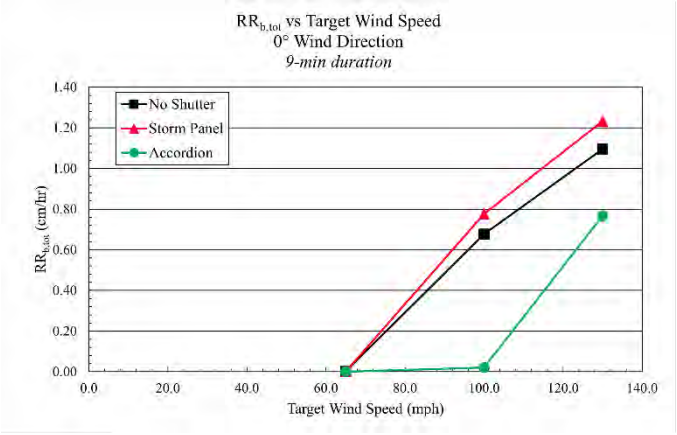

(c) 9-min test duration

Figure 14: Water Intrusion Volume ($RR_{b,tot}$) vs. Target Wind Speed

2. Effect of test duration

Figure 15 shows plots of $RR_{b,tot}$ versus test duration for the three target wind speeds, with a constant wind direction of 0°. The results in Figure 15, indicate that the total volume of water intrusion was negligible at 65 mph for all three test configurations, making it difficult to draw reliable conclusions about duration effects from the 65 mph data alone. For the 100 mph tests, the accordion shutter had a slight increase in water intrusion volume as the test duration increased from the 3-min to the 6-min and 9-min test cases, but the rate remained near 0 cm/hr for all accordion shutter tests at 100 mph. The aluminum storm panel data shows an increase in water intrusion volume during the 100 mph tests, ranging from 0.13 cm/hr at 3-min to 0.78 cm/hr at 9-min. The non-shuttered tests also revealed an increase in water intrusion volume as the test duration increased during the 100 mph tests; this trend was shallower and more linear in nature than the aluminum storm panel, and ranged from 0.61 cm/hr at 3-min to 0.68 cm/hr at 9-min. For the 130 mph test cases, the volume of water intrusion for the non-shuttered test configuration and the aluminum storm panel configuration both increased as the test duration increased, but the

change between the 3-min and 6-min tests was greater than the change between the 6-min and 9-min tests. For the accordion shutter system, the highest observed water intrusion rate at 130 mph occurred during the 6-min test duration (0.83 cm/hr), and slightly decreased to 0.77 cm/hr during the 9-min test duration, indicating that the trend for the accordion shutter differed from the other two test configurations. Overall, the amount of water intrusion was significantly higher as the wind speed increased for all test configurations considered.

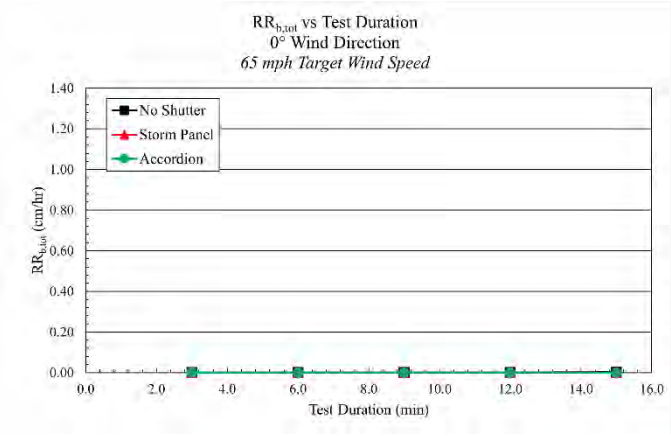

(a) 65 mph wind speed

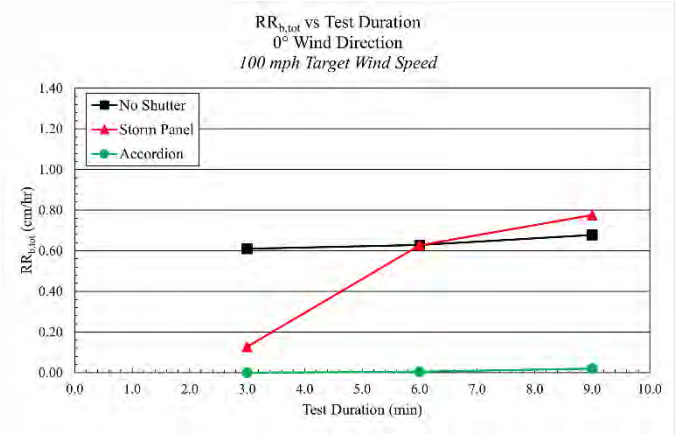

(b) 100 mph wind speed

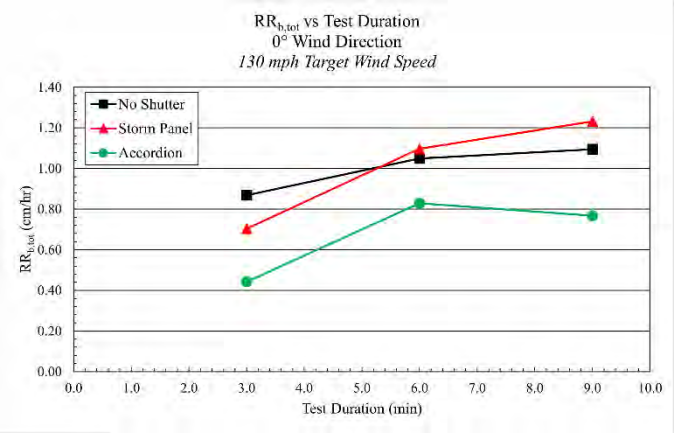

(c) 130 mph wind speed

Figure 15: Water Intrusion Volume ($RR_{b,tot}$) vs. Test Duration

3. Effect of wind direction

Wind direction effects were only investigated at 65 mph. The results for the non-shuttered test case are plotted in Figure 16 for a constant wind speed of 65 mph and test durations of 3-min, 9-min, and 15--min. The storm panel and accordion shutter test cases are not included in Figure 16 because no water intrusion was observed for either of the shuttered test cases at 0°, 22.5°, and 45° wind directions at a target wind speed of 65 mph. The trend in Figure 16 indicates that an

oblique wind direction may be critical for the unmitigated sliding glass door system because higher water intrusion rates were observed at 22.5° compared to both 0° and 45° wind directions. This trend remained consistent for all test durations. However, it should be noted that the overall rates of water intrusion reported in Figure 16 are relatively small (peak values range from 0.0063 to 0.0085 cm/hr) compared to the results from higher wind speeds tested at the 0° wind direction where peak values are orders of magnitude larger (peak values range from 0.8 to 1.2 cm/hr). Thus, it is recommended that future work should be done to consider additional tests of an unmitigated sliding glass door system subjected to oblique wind directions and higher wind speeds to verify the trend shown in Figure 16.

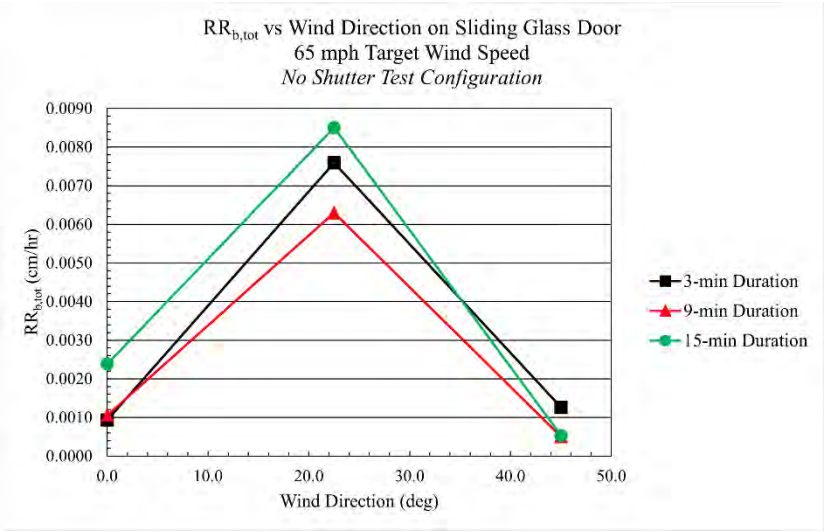

Figure 16: Water Intrusion Volume ($RR_{b,tot}$) vs. Wind Direction (65 mph, No Shutter)

4. Sources of water intrusion

Analysis of GoPro video footage revealed several locations on the sliding glass door system that were the predominant sources of leakage and pathways for water intrusion into the building model. Figure 17 - Figure 19 show screenshots of the GoPro videos for the no shutter test configuration, taken from the 130 mph 6-min duration tests at the 0° wind direction.

During the non-shuttered test cases, water intrusion predominantly occurred at several locations along the bottom of the sliding glass door, particularly at the corner regions where the glass met the aluminum extrusions, and at the seams between the door sill and the vertical framing members (Figure 17a); unique to the non-shuttered configuration only, an additional water intrusion pathway was observed at the upper joint of the central aluminum framing members between the two door panels (Figure 17b).

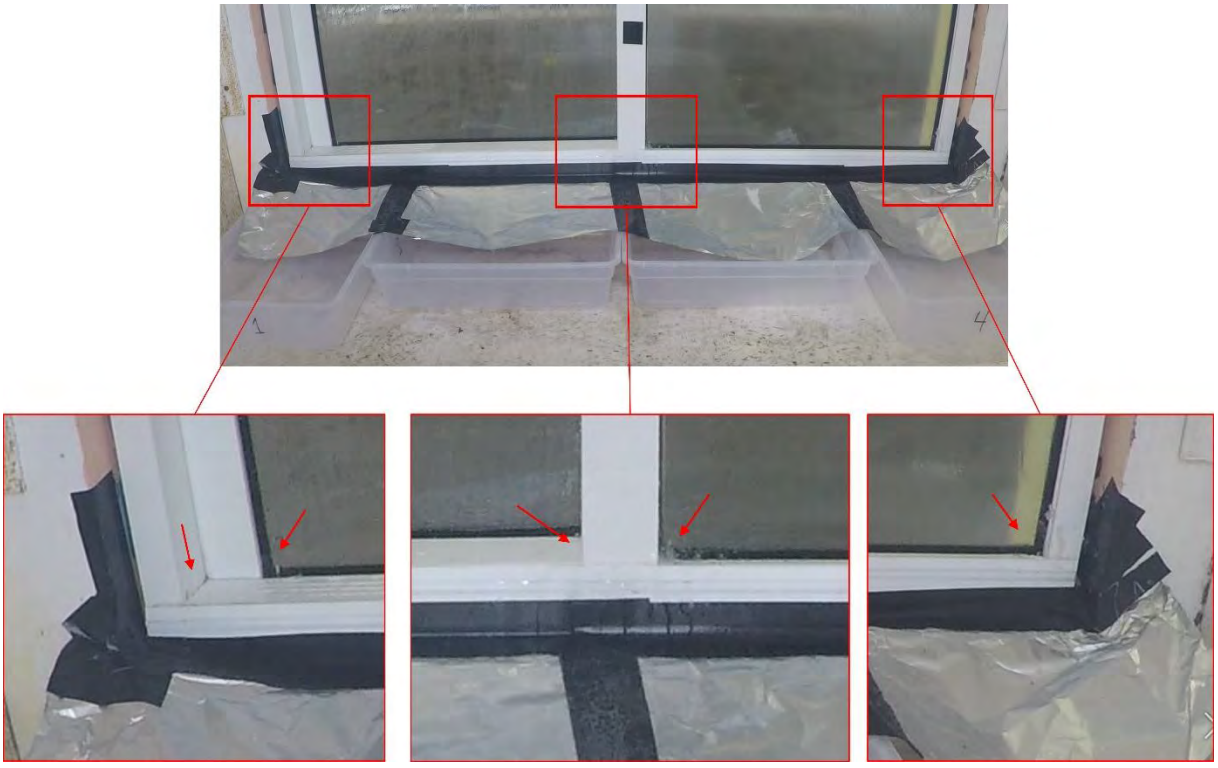

(a) Bottom of sliding glass door

(b) Top of sliding glass door

Figure 17: Water intrusion locations during the No Shutter configuration

Video from the aluminum storm panel and accordion shutter configurations revealed water intrusion along the bottom of the sliding glass door, in the same regions where the non-shuttered test case was vulnerable. However, the shuttered test cases did not indicate any water intrusion from the upper part of the sliding glass door. This may be attributed to the sheltering effect of the shutters and the reduction of the highest net pressure differential on the sliding glass door caused by the presence of the shutters. Screenshots from the 130 mph 6-min duration tests at the 0° wind direction are shown in Figure 18 and Figure 19 for the aluminum storm panel and accordion shutter test cases, respectively.

Figure 18: Water intrusion locations during the Aluminum Storm Panel configuration

Figure 19: Water intrusion locations during the Accordion Shutter configuration

Conclusions

This project investigated water intrusion through a full-scale sliding glass door system installed on a large-scale building model. Water intrusion effects were studied with respect to wind speed, test duration, and wind direction for configurations with and without shuttering systems. The following list summarizes the research findings:

- The highest differential pressures on the sliding glass door occurred at the 0° wind direction.
- The pressure differential on the sliding glass door decreased in magnitude as the model was rotated away from 0° toward 45°.
- The presence of the shutters resulted in a lower and more uniform pressure differential on the sliding glass door when compared to the non-shuttered test cases at 0° and 22.5°, evidence that the shutters provide a sheltering effect at these wind directions.

- For the test cases considered in this study, wind speeds had the greatest influence on the volume of water intrusion observed.
- Significant water intrusion was observed for all three test configurations during the 130 mph wind speed tests.
- Substantial differences in the water intrusion volumes were observed between the aluminum storm panel configuration and the accordion shutter system configuration at 100 mph and 130 mph wind speeds. More research is recommended to further validate this result and investigate possible reasons for these differences.
- At the 100 mph and 130 mph, there was a general trend that the volume of water intrusion increased as the test duration increased. This trend was most significant for the aluminum storm panels at 100 mph.
- Results from the 65 mph tests suggest that oblique wind directions may be vulnerable to high levels of water intrusion. Future research should more thoroughly investigate water intrusion at oblique angles under higher wind speed conditions to confirm this observation.

This study demonstrated that significant levels of water intrusion can occur during conditions well below design-level (the 130 mph tests correlate to approximately 45% DP for the sliding glass door). This project also demonstrated that variability could exist among various shuttering systems with regards to their potential sheltering effect for reducing water intrusion. More research is needed to investigate the impact of different shutter installation methods, types, and geometries to discover optimal installation techniques for potentially reducing water intrusion effects.

References

Abuku, M., Blocken, B., and Roels, S. (2009). "Moisture response of building facades to wind-driven rain: Field measurements compared with numerical simulations." *J. Wind Eng. Ind. Aerodyn.* 97, 197-207.

American Society for Testing and Materials (2000). "Standard test method for water penetration of exterior windows, skylights, doors, and curtain walls by uniform static air pressure difference." *ASTM E331-00.* West Conshohocken, PA.

Baheru, T., Chowdhury, A. G., and Pinelli, J. P. (2014a). "Estimation of wind-driven rain intrusion through building envelope defects and breaches during tropical cyclones." *Natural Hazards Review*, 16(2), 04014023.

Baheru, T., Chowdhury, A. G., Bitsuamlak, G., Masters, F. J., and Tokay, A., (2014b). "Simulation of wind-driven rain associated with tropical storms and hurricanes using the 12-fan Wall of Wind." *Build. Environ.*, 76, 18-29.

Baheru, T., Chowdhury, A. G., Pinelli, J. P., and Bitsuamlak, G., (2014c). "Distribution of wind-driven rain deposition on low-rise buildings: Direct impinging raindrops versus surface runoff." *J. Wind Eng. Ind. Aerodyn.* 133, 27-38.

Bitsuamlak, G. T., Chowdhury, A. G., and Sambare, D. (2009). "Application of a full-scale testing facility for assessing wind-driven-rain intrusion." *Build. Environ.*, 44(12), 2430–2441.

Blocken, B., and Carmeliet, J. (2002). "Spatial and temporal distribution of driving rain on a low-rise building." *Wind Struct.*, 5(5), 441-462.

Blocken, B., and Carmeliet, J. (2004). "A review of wind-driven rain research in building science." *J. Wind Eng, Ind. Aerodyn.*, 92, 1079-1130.

Blocken, B., and Carmeliet, J. (2005). "High-resolution wind-driven rain measurements on a low-rise building—experimental data for model development and model validation" *J. Wind Eng, Ind. Aerodyn.*, 93, 905-928.

Blocken, B, and Carmeliet, J. (2007). "On the errors associated with the use of hourly data in wind-driven rain calculations on building facades." *Atmos. Environ.*, 41(11), 2335–2343.

Blocken, B., and Carmeliet, J. (2010). "Overview of three state-of-the-art wind-driven rain assessment models and comparison based on model theory." *Build. Environ.*, 45, 691-703.

Blocken, B., Dezsö, G., van Beeck, J. and Carmeliet, J. (2010). "Comparison of calculation models for wind-driven rain deposition on building facades." *Atmos. Environ.*, 44, 1714-1725.

Blocken, B., Abuku, M., Nore, K., Briggen, P. M., Schellen, H. L., Thue, J. V., Roels, S., and Carmeliet, J. (2011). "Intercomparison of wind-driven rain deposition models based on two case studies with full-scale measurements." *J. Wind Eng, Ind. Aerodyn.*, 99, 448-459.

Choi, E. C. C. (1993). "Simulation of wind-driven rain around a building." *J. Wind Eng. Ind. Aerodyn.*, 46–47, 721–729.

Choi, E. C. C. (1994). "Determination of wind-driven rain intensity on building faces." *J. Wind Eng. Ind. Aerodyn.*, 51(1), 55–69.

Choi, E. C. C. (1999). "Wind-driven rain on building faces and the driving-rain index." *J. Wind Eng. Ind. Aerodyn.*, 79, 105-122.

Chowdhury, A. G., Bitsuamlak, G. T., Fu, T.-C., and Kawade, P. (2011). "A study on roof vents subjected to simulated hurricane effects." *Nat. Hazards Rev.*, 12(4), 158–165.

Dao, T. N., and van de Lindt, J. W. (2010). "Methodology for Wind-Driven Rainwater Intrusion Fragilities for Light-Frame Wood Roof Systems." *J. Struct. Eng.*, 136(6), 700-706.

Dao, T. N., and van de Lindt, J. W. (2012). "Loss Analysis for Wood Frame Buildings during Hurricanes. I: Structure and Hazard Modeling." *J. Perform. Constr. Fac.*, 26(6), 729-738.

FEMA. (2005a). "Mitigation assessment team report—Hurricane Charley in Florida; observations, recommendations, and technical guidance." *FEMA 488*, Washington, DC.

FEMA. (2005b). "Summary report on building performance, 2004 hurricane season." *FEMA 490*, Washington, DC.

FEMA. (2018) "Soffit Installation in Florida." *Hurricane Irma in Florida: Recovery Advisory 2*, Washington, DC.

Foroushani, S. S. M., Ge, H., and Naylor, D. (2014). "Effects of roof overhangs on wind-driven rain wetting of a low-rise cubic building: A numerical study." *J. Wind Eng. Ind. Aerodyn.*, 125, 38-51.

Friedrich, K., Higgins, S., Masters, F. J., and Lopez, C. R. (2013) "Articulating and Stationary PARSIVEL Disdrometer Measurements in Conditions with Strong Winds and Heavy Rainfall." *J. Atmos. Oceanic Tech.*, 30, 2063-2080.

Hangan, H. (1999). "Wind-driven rain studies. A C-FD-E approach." *J. Wind Eng. Ind. Aerodyn.*, 81, 323-331.

International Code Council, Inc. (2017). “Testing Application Standard (TAS) 201-94 Impact Test Procedures.” *2017 Florida Building Code—Test Protocols for High Velocity Hurricane Zone*, 978-1-60983-688-7.

International Code Council, Inc. (2017). “Testing Application Standard (TAS) 202-94 Criteria for Testing Impact and Nonimpact Resistant Building Envelope Components Using Uniform Static Air Pressure” *2017 Florida Building Code—Test Protocols for High Velocity Hurricane Zone*, 978-1-60983-688-7.

International Code Council, Inc. (2017). “Testing Application Standard (TAS) 203-94 Criteria for Testing Products Subject to Cyclic Wind Pressure Loading” *2017 Florida Building Code—Test Protocols for High Velocity Hurricane Zone*, 978-1-60983-688-7.

ISO, (2009). “Hygrothermal performance of buildings—calculation and presentation of climatic data part 3: Calculation of a driving rain index for vertical surfaces from hourly wind and rain data.” *ISO 2009; 15927-3*, Geneva, Switzerland.

Kijewski-Correa, T. L., Roueche, D. B., Mosalam, K. M., Prevatt, D. O., & Robertson, I. N. (2021). “StEER: A Community-Centered Approach to Assessing the Performance of the Built Environment after Natural Hazard Events.” *Frontiers in Built Environment*, *7*, 79.

Kubilay, A., Derome, D., Blocken, B., and Carmeliet, J. (2014). “High-resolution field measurements of wind-driven rain on an array of low-rise cubic buildings.” *Build. Environ.*, 78, 1-13.

Pinelli,J.P., Roueche, D., Kijewski-Correa,T., Plaz, F., Prevatt,D., Zisis, I., *et al.* (2018). “Overview of damage observed in regional construction during the passage of hurricane irma over the state of Florida” Proceedings of ASCE Forensic Engineering Conference 18, Reston, VA.

Robinson,G., and Baker, M.C. (1975). “Wind driven rain and buildings.” Technical Paper (National Research Council of Canada. Division of Building Research), 1975-07.

Salzano, C. T., Masters, F. J., and Katsaros, J. D. (2010). “Water penetration resistance of residential window installation options for hurricane-prone areas.” *Build. Environ.*, 45, 1373-1388.

Straube, J. F. and Burnett, E. F. P., (1998) "Driving Rain and Masonry Veneer," *Water Leakage Through Building Facades, ASTM STP 1314*, (R. J. Kudder and J. L. Erdly, Eds.), American Society for Testing and Materials.

Straube, J.F. and Burnett, E. F. P., (2000) "Simplified Prediction of Driving Rain Deposition." *Proc. of International Building Physics Conference*, Eindhoven, 375-382.

Subramanian, D., Salazar, J., Duenas-Osorio, L., & Stein, R. (2013). "Building and validating geographically refined hurricane wind risk models for residential structures." *Nat. Hazards Rev.*, 15(3), 04014002.

Tokay, A., Bashor, P. G., Habib, E., and Kasparis, T., (2008). "Raindrop Size Distribution Measurements in Tropical Cyclones." *Mon. Weather Rev.,* 136(5), 1669–1685.

van de Lindt, J. W., and Dao, T. N. (2009). "Performance-Based Wind Engineering for Wood-Frame Buildings." *J. Struct. Eng.*, 2009, 135(2): 169-177.

van de Lindt, J. W., and Dao, T. N. (2012). "Loss Analysis for Wood Frame Buildings during Hurricanes. II: Loss Estimation." *J. Perform. Constr. Fac.*, 26(6), 739-747.

Van Straaten, R. A., Kopp, G. A., and Straube, J. F. (2010). "Testing water penetration resistance of window systems exposed to "realistic" dynamic air pressures." In *Proceedings of International Conference of Building Envelope Systems and Technology (ICBEST),* Vancouver.

Vutukuru,K.S., Moravej, M., Elawady,A., and Chowdhury, A.G. (2020). "Holistic testing to determine quantitative wind driven rain intrusion for shuttered and impact resistant window." *J. Wind Eng. Ind. Aerodyn.*,206,104359.

Wise, A.F.E, Sexton,D.E., and Lillywhite,M.S.T. (1965). "Study of airflow around buildings." Technical paper, Building Research Station, England.

A Resource for the State of Florida

SECTION 3
AERODYNAMIC LOADING OF RESIDENTIAL BUILDINGS SUBJECTED TO EXPERIMENTAL DOWNBURSTS AND HURRICANES

A Research Project Funded by:
The State of Florida Department of Emergency Management

Prepared by
Dr. Amal Elawady
Dr. Dejiang Chen
Alvaro Mejia, PhD Candidate, FIU

International Hurricane Research Center
Florida International University

July 30, 2021

Executive Summary:

Downbursts are non-stationary, transient, localized high wind events that constitute considerable damage to buildings and other structures. The importance to develop a physical large-scale downburst outflow simulator is essential to enable investigating for aerodynamics of buildings and other infrastructure systems. Recently, the research team at the Wall of Wind (WOW) Experimental Facility (EF) has been able to develop a large-scale downburst simulator that is able to produce downburst outflows of relatively large size that can allow testing of low-, mid- and high-rise buildings. A series of simulated downburst outflow tests have been conducted on a spatial-temporal grid pattern consisting of various horizontal locations at various heights in an open terrain to characterize the outflow and validate it to real downburst events. For this reason, the two major goals of this report are to first assess the capabilities of the simulated downburst outflow and second is to assess the mean and peak pressure coefficients C_p on three low, mid and high-rise buildings obtained from downburst loading and compare these values to those obtained by Atmospheric Boundary Layer (ABL) simulation at the WOW. This study will explore the pressure distributions found in the transient nature of thunderstorm downburst hazards.

KEYWORDS: Downburst; Buildings; Non-stationarity; Outflow; Wall of Wind

1. Introduction

Downbursts are a non-stationary, transient, localized and intense weather phenomena formed at the mature stage of cell thunderstorm. Downburst winds are defined as a descending mass of cold air that strike the ground surface then transfers horizontally creating intensive divergent outflow in radial directions. Such impingement causes a sudden intense high winds near the ground, diverging radially in all directions with wind speeds ranging from 30 m/s up to 75 m/s. These high wind speeds are found to occur at heights between 5 m to 100 m which is the typical height range of civil infrastructure and buildings. These winds constitute a significant and unusual damage equivalent to catastrophic tornadoes (F2) that possibly cause total failure especially of low rise buildings and other structures. Wind loading on buildings and infrastructure attributed to hurricane and Atmospheric Boundary Layer (ABL) winds and downburst winds can be significantly different. These differences can be summarized as follows: (1) Downbursts are highly non-stationary events that are localized in space and in time. This makes collecting field measurements a challenging task as it is difficult to predict where and

when a downburst event will happen. This highlights the pressing need for realistic experimental simulations to test structural responses to such extreme wind events. (2) The spatial localization of the event may result in different loading scenarios compared to those expected from synoptic ABL winds. In addition, the geometrical configurations of the building with respect to the geometric characteristics of the outflow or main rolling vortex (e.g. height of the maximum wind speed and wind direction) need to be taken into consideration as a potential influential factor. (3) The time history of a downburst event is characterized by a localized peak zone winds that starts with a ramp-up, a plateau and ends with a ramp-down. Therefore, it is recommended by many researchers that the downburst time history should be decomposed into a running-mean and turbulence which highlights the temporal non-stationarity of the event. (4) Downburst mean vertical profile is characterized by a nose-shape where the maximum wind speed is occurring near the ground as opposed to the ABL wind profile where the windspeed increases as the height increases. This means that the peak zone wind speed resulting from a downburst event occurs within the range of typical structures heights. Therefore, the quantification of downburst wind loading and the corresponding structural response is expected to vary from those resulting from ABL events which urges further research and development. The significant differences between the ABL and downburst flow in addition to the lack of design guidelines that addresses the wind actions on buildings during a downburst event have motivated the WOW research team to investigate the feasibility to achieve downburst simulation at the WOW facility so that the dynamic and kinetic characteristics of downburst flows are properly produced in a large significant length scale.

2. Experimental methodology

The focus of the proposed research is to investigate the downburst outflow characterization and aerodynamic assessment of three building test configurations representing low-rise, mid-rise, and high-rise buildings. The wind loading distribution and corresponding values of the wind pressure coefficients (Cps) on the surfaces of these buildings configurations were subjected to ABL and downburst loadings. The analysis of both results will examine the differences and ultimately, help in determining if a modification can be proposed to the current design codes that are solely based on stationary ABL and without considering the aspect of high, short lived wind speeds near the ground that are characteristic to downbursts.

Task #1: Experimental investigations of downbursts and ABL wind loading on buildings.

Task #2: Comparative studies to assess aerodynamic loading of downbursts and ABL data tested previously by the WOW Facility. Three (3) testing configurations representing low-rise, mid-rise and high-rise building models were tested at the WOW facility. The building models will have the same geometry while three different heights and open terrain conditions are considered. The three models will represent: (A) a low-rise building; (B) a mid-rise building; and (C) a high-rise building. All three will be modeled using a length scales of 1:100. In this task, wind loads obtained for different wind directions will be evaluated to determine the mean and peak (i.e. minimum and maximum) values of the pressure coefficients (Cp) across all surfaces of the building and these will be assessed and evaluated for both the downburst and ABL cases, respectively.

3. Experimental facility

3.1 Wall of Wind

The NHERI Wall of Wind (WOW) is a large-scale, open jet, wind testing facility capable of simulating hurricane winds up to category 5 on a Saffir-Simpson scale reaching maximum horizontal wind speeds of 72 m/s (Chowdhury et al., 2017). The WOW consists of a 12-propeller fan matrix configuration arranged in 2 rows by 6 columns blowing large volumes of wind into a contraction section where it increases the wind velocity and subsequently shapes it into a rectangular flow inside a box with a cross-sectional area of 6.1 m wide by 4.3 m high. The longitudinal fetch of the flow management box is 9.75 m. The WOW is equipped with flow conditioning devices such as triangular spires and dynamic floor roughness elements that generate straight line ABL flows for different terrain configurations of choice. WOW is capable of generating large turbulent complex wind fields able to test full and large-scale structural models and their related components in order to examine the inherent weakness and susceptibility in their performance and connections. The open test section that is present outside the vicinity of the flow management box outlet receives the discharged flow and passes through a 4.9 m diameter turntable center where the test models are to be fixed at the base and with its center located at 6 m from the flow management box outlet. The test section allows a wide area for positioning various downstream locations at which single point velocity measurements can take place at various heights and various horizontal distances of interest.

(a) (b)

Figure 1 FIU NHERI Wall of Wind Experimental Facility showing (a) Rear end consisting of 12 fans positioned in an arch shaped, 2 rows by 12 columns and (b) front end consisting of the flow management box shooting the ABL wind flow jet

3.2 Downburst simulator at the WOW

A large-scale downburst simulator addition has recently been constructed at the WOW and is placed directly in front of the existing WOW flow management box outlet. The downburst simulator aim is to be able to produce large-scale downburst outflows travelling across the testing section of the WOW and be able to reproduce non-stationary, transient aerodynamics loads to various types of structures. The novelty of dealing with transient loading at a large-scale makes a great addition to the WOW so that it explores a new venue of different hazard mitigation studies. The lower region of the downburst simulator consists of two louver-slats, covering a lower opening of 1.52 m high by 5.94 m high. The slats are positioned vertically when closed and will open to a specified angle. The opening mechanism of the slat consists of a two counterweight systems (one at each side of the downburst simulator) connected to the slats with stainless steel rope, a system of pulleys and winches and these counterweights are heavier than the slats. These counterweights are suspended while the louver slats are held by power supplied electro-magnets. These electro-magnets are programmed by an electronic Arduino system that is programmed to shut the power supply to the electro-magnets holding the slats closed. As soon as the electro-magnets are no longer fed by the power supply, then these turn off and hence releasing the slats free. The counterweights will fall down and pull the ropes so that both louver slats open. The estimated rate of angular opening for the two louver slats to open is about 1.17 radians/sec. The upper slat dimensions are 5.89 m wide by 0.74 m long by 0.0127 m thick and the lower slat 5.89 m wide by 0.75 m long by 0.0127 m. The upper slat dimensions are

slightly less than the lower slats and their corresponding weight is about 133 kg each. The upper region of the downburst simulator consisted of a blockage completely covered by aluminum 8020 framing and plywood sheathing so that the wind coming from the flow management box is directed to the bottom region. It is important to note that downbursts manifest large wind velocities near the ground as opposed to ABL winds that is the opposite. A gravity gate (GG) placed behind the blockage and louver slats suspended by a system of electromagnets attached to a horizontal suspended beam was used to end the flow, i.e., to create the decay of the wind speeds. The GG was attached at each side along linear bearings. The approximate weight of the GG is 182 kilograms. The electromagnets were also part of the time automated Arduino system in which the suspended electromagnet's power supply was also shut down some specified and programmed time after the louver slats opened and the gravity gate slide down a height of 1.52 m into the ground and be stopped by shock absorbers. The estimated time for the gravity gate to fall down and completely shut the flow is of 0.8 sec.

4. Test Model Description

In order to evaluate the downburst aerodynamic loading on structures, it was decided to test three buildings to represent a low-rise, a mid-rise and a high-rise category to assess the downburst loading effects and how they compare with conventional ABL loading. The selected length scale to represent an open terrain is 1:100. The three buildings that are to be scaled are: low-rise building (A) with full scale dimensions 9.1 m long by 14 m wide by 4 m high; Mid-rise building (B) with full-scale dimensions 46 m long by 69 m wide by 20 m high; and finally high-rise building (C) with full-scale dimensions 91 m long by 137 m wide by 40 m high. The following Figure 2 show the buildings scaled down dimensions to represent a length scale of 1:100. The building has a gable roof with a small slope of 1.27 deg.

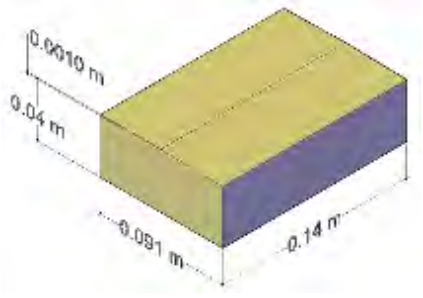

(A)

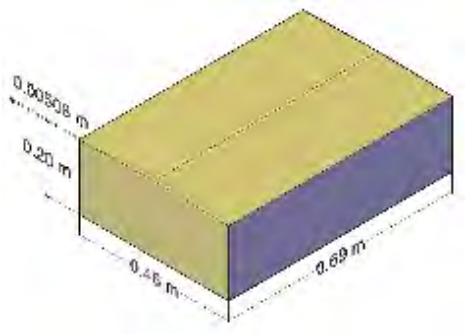

(B)

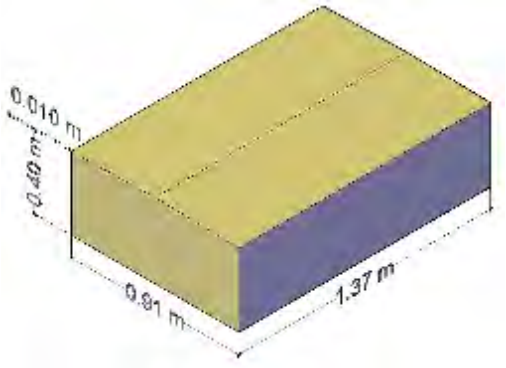

(C)

Figure 2 Three scale model buildings tested at a length scale 1:100 representing (a) a 4 m high low-rise building A (b) a 20 m high low-rise building B and (c) a 40 m high high-rise building C

5. Instrumentation and Testing Protocol

The downburst experiments started with the commissioning of the downburst simulator, followed by the flow characterization and ending with the aerodynamics of low, mid and high-rise buildings subjected under downburst loading. Phase 1 included a smoke generator that allowed the preliminary visualization of the main rolling vortex exiting the louver slats at a specified angle and travelling across the testing section of the WOW as seen in Figure 3. This was the first and quick check to determine whether the downburst simulator was creating the expected formation of a main rolling vortex to allow a much in depth flow characterization. Phase 2, 3 and 4 included downburst experiments solely based on the outflow characterization with the use of 3.175 mm O.D. by 304.8 mm long stainless steel pitot tubes connected to a 64 channel Scanivalve system with a sampling frequency of 512 Hz and a set of six (6) TFI series 100 Cobra probes with a sampling frequency of 2500 Hz. Both data acquisition systems were

used to measure the velocity flow field for each of the downburst simulation test runs. The idea of using the pitot tubes simultaneously with the Cobra probes is that the pitot tubes are smaller, larger in number and easier to maneuver and position at closely spaced point measurements.. The Cobra probe brings the ability to measure wind velocities in three directions in addition that measures wind velocities at a much higher sampling resolution compared to the pitot tubes, thus providing a high resolution turbulence analysis. Both data acquisition systems complement each other for a good quality analysis of the downburst outflow. These pitot tubes and Cobra probes were positioned side by side in a vertical rake that was free to move around the testing section at strategic locations within the testing section in front of the downburst simulator.

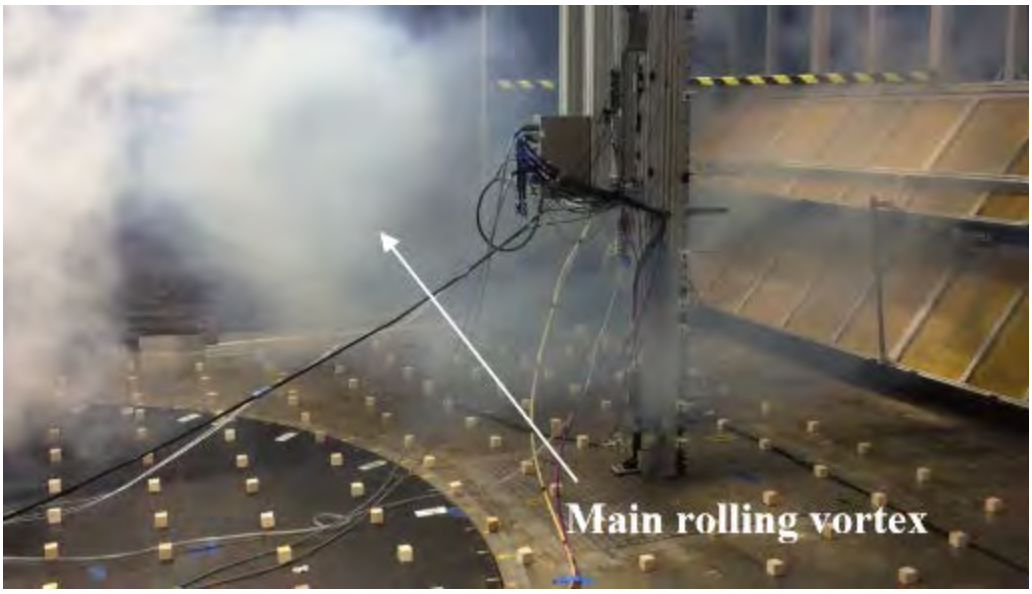

Figure 3 Formation of the downburst characteristic main rolling vortex during phase 1 commissioning with the downburst simulator two louver slats to be opened at a 45 deg with a wind fan throttle ratio of 45 deg.

Phase 2 used a moving dense vertical rake (Rake C) consisting of 64 pitot tubes and 6 cobra probes at strategic heights up to 2794 mm high to measure the downburst outflows at different locations downstream across the testing area. Figure 4 shows the strategic locations used during the commissioning phase 2 in determining the downburst outflow characterization, time histories and vertical velocity profiles and Figure 5 shows the dense rake used in the commissioning Phase 2.

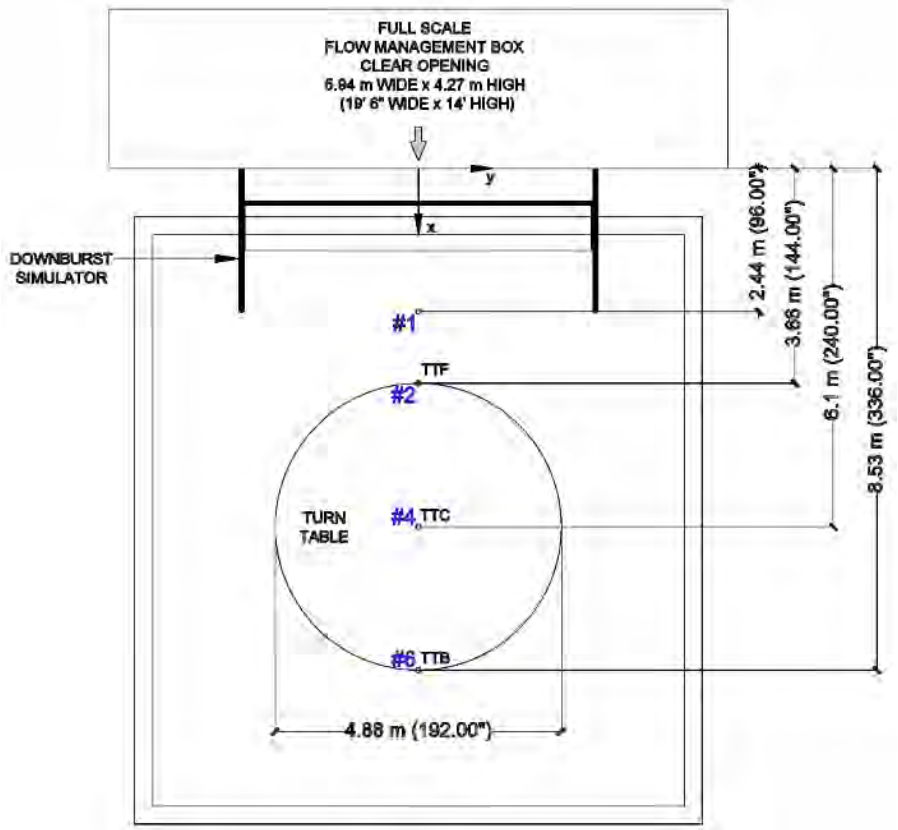

Figure 4 Plan view of WOW testing area showing the strategic locations of the flow commissioning on smooth terrain using Dense Rake C. TTF, TTC and TTB indicate the turntable front, center and back.

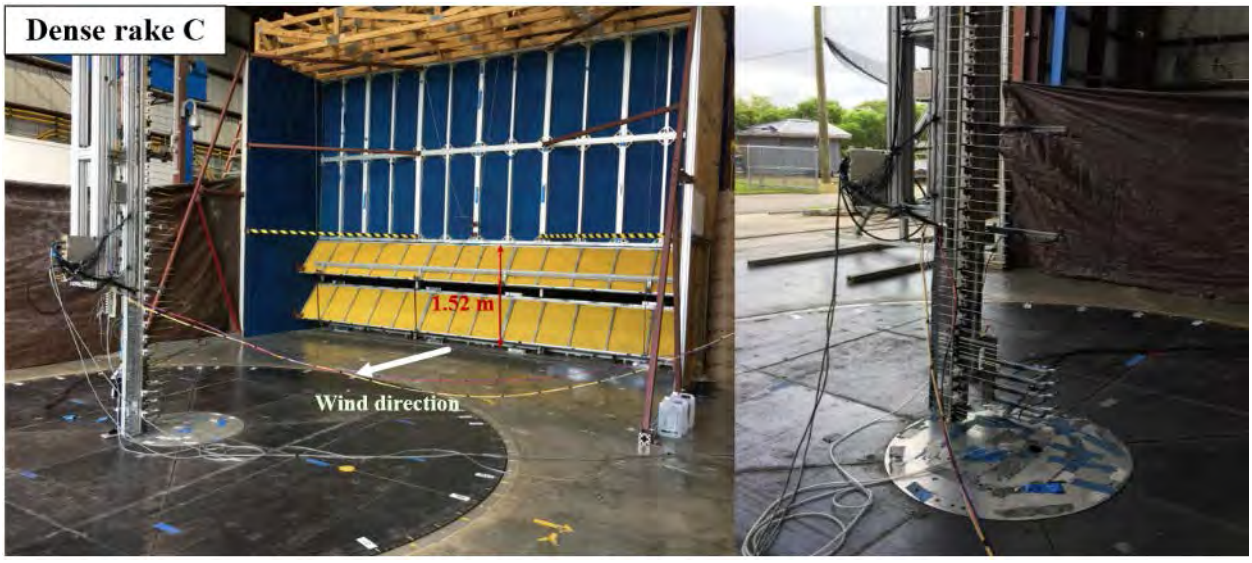

(a) (b)

Figure 5 Flow calibration using dense rake C (a) Downburst simulator with slats open to allow downburst outflow exit from the flow management box and travel across the testing section (b) Rake C positioned at the turn table center (TTC).

A pass-fail criteria check list was established for every downburst test run to determine the adequacy of the preliminary downburst outflow results. Phase 1 and phase 2 were described as the commissioning part of the downburst tests at WOW. The results were immediately analyzed on the spot, right after each downburst test run was completed to verify if any mistakes, wind leakage or bad data had occurred and observed. The pass-fail criteria were mainly based on three downburst important characteristics which include: First, the formation of a main rolling vortex travelling across the testing section area in a clockwise manner. The second was to verify if a significant spike or peak zone of a triangular shape was present in the horizontal velocity time histories of every test run and third was to verify if a 'nose' shape profile was observed in the vertical velocity profile of the horizontal velocities. When all three pass-fail criteria passed successfully, then the downburst test run was deemed a pass. Initially a sequence of trial tests considering a variation of the initial conditions were done. These initial conditions considered different wind fan throttles, louver slat angles (with respect the vertical plane positioned at 35 deg, 45 deg and 60 deg), different opening and closing of the louver slats (considering 3 sec, 5 sec, 15 sec and 30 sec) in a smooth terrain were tested and compared to identify which test provided a most realistic downburst outflow. As soon as the commissioning part of the test successfully passed, phase 3 and 4 were started, this time considering an open terrain representative using 38.1 mm x 38.1 mm x 38.1 mm cubic wooden blocks, hot glued to the ground and spaced in a squared grid pattern to determine their corresponding outflow measurements. The outflow speeds were measured, this time with two rakes (rake A and rake B) at which each rake consisted of 32 pitot tubes and 3 cobra probes. The positions of the pitot tubes and cobra probes can be seen in Figure A-5, A-6 and A-7 found in the Appendix. Rake A and Rake B had the exact height positions for the pitot tubes and cobra probes. The heights of the pitot tubes for each rake reached up to 2540 mm high. Rake A was a moving rake while rake B was kept fixed in the same place. The idea of the simultaneous measurements of two rakes for each test run was done for the purpose of determining the correlation in space and time within the same outflow. See Figure 6 for the strategic locations of moving rake A and fixed rake B and Figure 7 for overall view of both rakes.

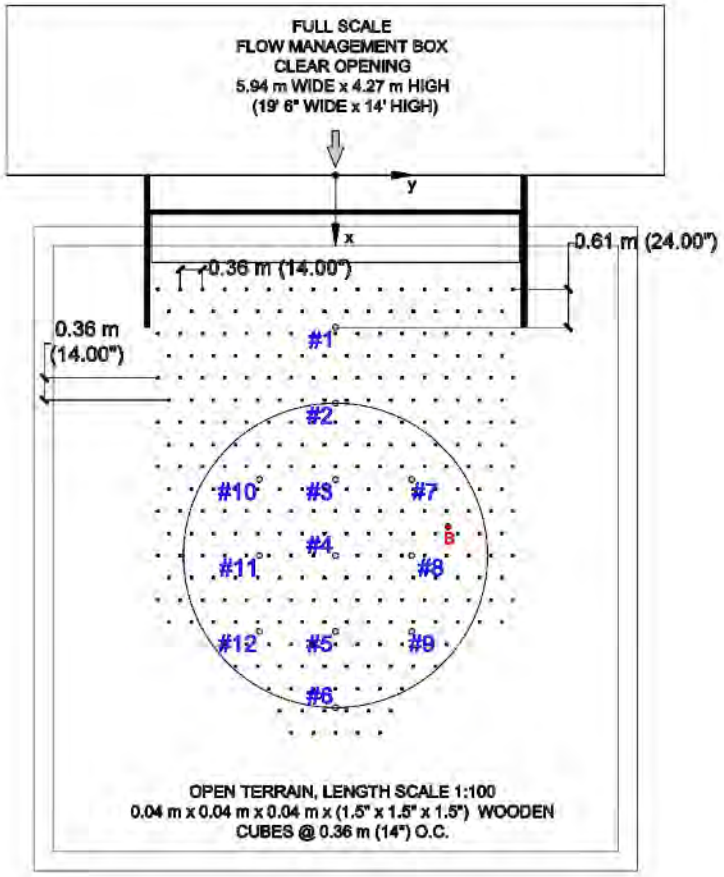

Figure 6 Plan view of WOW testing area showing the strategic locations for flow characterization measurements on 1:100 open terrain using a moving rake A and a fixed rake B

(a) (b)

Figure 7 Flow calibration using dense rake A and B (a) Overview of Rake A at location 1 and at the back fixed rake B (c) Overview towards the downburst simulator showing Rake A at location 9 and rake B at the fixed location

Phase 3 assessed the effect of the wooden cube roughness elements on the downburst outflow while phase 4 assessed the effect of increasing the wind velocities; two fan throttle ratios, 10% throttle and 15% throttle were considered.

As soon as a WOW downburst database of several test runs was established for all the different cases and most of the outflow results were agreed upon as a pass criterion, then phase 5 was initiated by considering the aerodynamic of downbursts on three different buildings: A, a mid-rise building B and a high-rise building C. Each of these three buildings were subjected to the downburst outflows generated by the WOW downburst simulator at three different wind directions (0, 45, and 90°) to determine the effect of non-stationary, transient downburst loading on each of the building surfaces (windward, leeward, side walls and roof). The corresponding normalized contour lines of the minimum, maximum and mean pressure coefficient values (C_p) were obtained to evaluate the downburst loading upon different building sizes. In addition, to evaluating downburst aerodynamic loading to low-, mid- and high-rise buildings, the results were also compared to those results obtained for the same buildings subjected to ABL wind loads of stationary nature. In the case of downbursts, the corresponding pressure coefficients will be based on a min, max and mean value given the non-stationary, short lived, transient nature of the downburst event within a peak zone versus the pressure coefficients of stationary ABL winds that have been tested and corrected with Partial Turbulence Simulation (PTS) as recommended by (Mooneghi et al., 2016; Moravej, 2018) which is a process in which larger scale models have a deficiency in the lower turbulence content due to the limitations in size of wind tunnels and require a post-processing correction to adjust the aerodynamics after testing so that the normalized pressure coefficients C_p approximate those found in a full-scale.

In phase 5, the three scale models representing a low-rise A, a mid-rise B and a high-rise building C were instrumented with a total of 204 pressure taps and connected to tubing of appropriate lengths so that these were also connected to four Scanivalve ZOC33 pressure scanners so that the scale model buildings subjected to downburst wind loads acquire the high-resolution time histories at each pressure tap. Based on the connector side and tap side tubing length, appropriate transfer function tubing length corrections were applied on the raw results to make sure the data represents a realistic value. The experimental pressure measurements were recorded for wind directions ranging from 0° to 90° at 45° intervals for each of the scale models

subjected to downburst outflows. For each downburst test run, the pressure data was recorded at a sampling rate of 520 Hz/channel on each tap for a 30 sec duration. The louver slat angles of the downburst simulator were set to open at 45 deg with respect the vertical plane, the fans were started for a total time of 30 seconds before opening the louver slats to allow pressure stabilization of the flow, then the louver slats were suddenly opened using an automated timing Arduino system. Then the louver slats remained open for a total of 10 seconds. The measured time histories were used to investigate the pressure coefficient distributions on the windward, leeward, two side walls and roof of each of the scale-models. The next Figure 8 shows the test set-up of all three buildings with respect the downburst simulator.

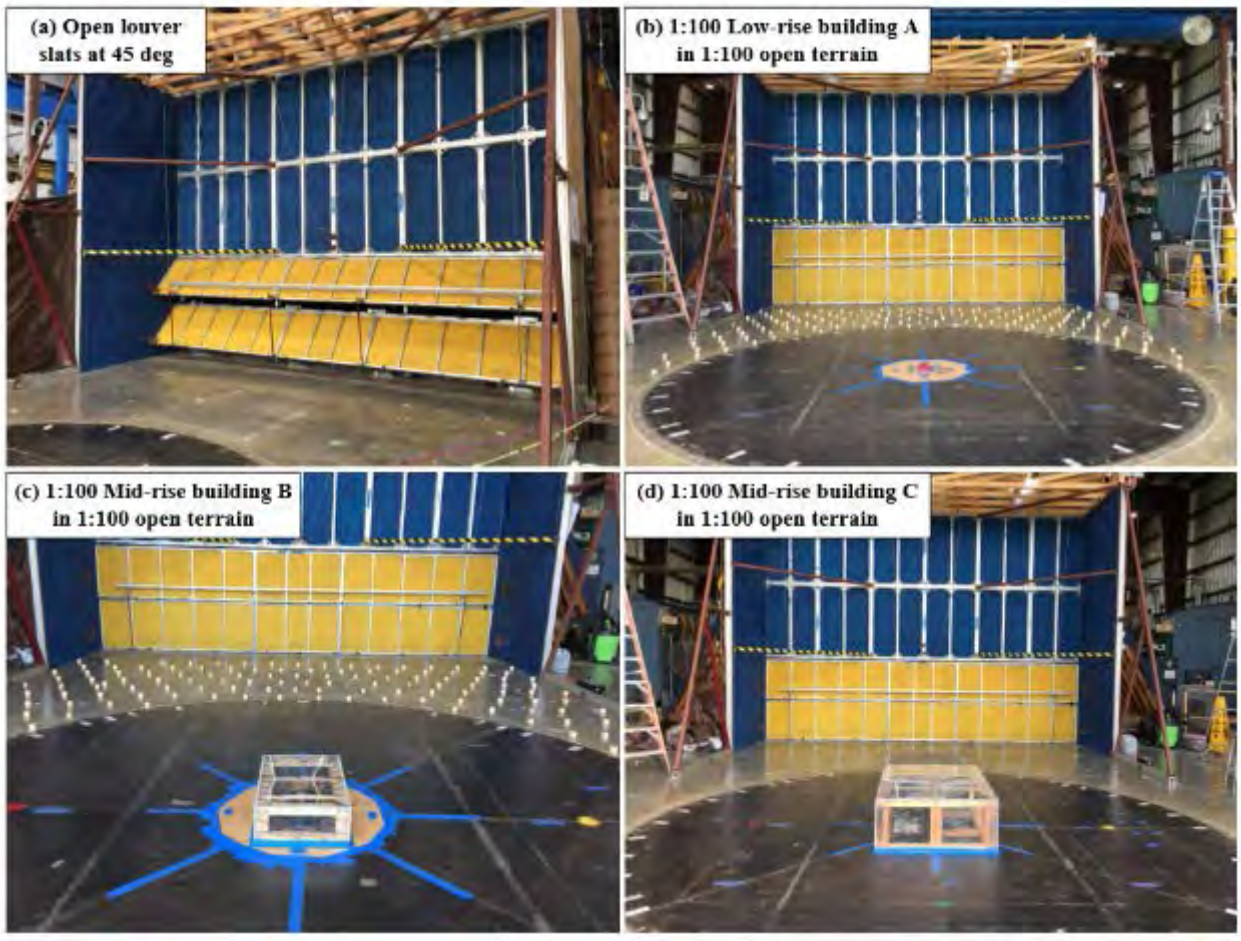

Figure 8 Downburst aerodynamic testing on three test configurations in a length scale 1:100 representing a low-rise building, a mid-rise and a high-rise building (a) Downburst simulator at WOW with the two louver slats opened (b) a 4 m high low-rise building A (c) a 20 m high mid-rise building B and (d) a 40 m high high-rise building C

6. Results and Discussion

The results described herein explore the flow characterization of the downburst outflows generated in the WOW testing area, the application of these downburst outflows to low-, mid- and high-rise buildings to determine the mean and peak pressure coefficient distribution on each building face and a comparison of these distributions to conventional ABL wind loading.

6.1 Flow characterization

For each downburst test, obtained data was analyzed by obtaining the normalized vertical profile of horizontal velocities at the Turntable Center (TTC) (i.e. location of interest as this is where the future scale models are to be placed). The 'nose' shape of these velocities are compared with previous real downburst events and former literature experiments to determine the validity of the current tests, as seen in Figure 9. The definitions of the test cases are provided in Appendix A. The horizontal wind velocities normalized with respect to the local maximum horizontal wind velocity $U_{\max}$.It can be seen that the quality of the tests can be measured by the existence of a shaded area that represents the boundaries of a series of real downbursts in Colorado from a campaign called JAWS and delineated by (Hjelmfelt, 1988).

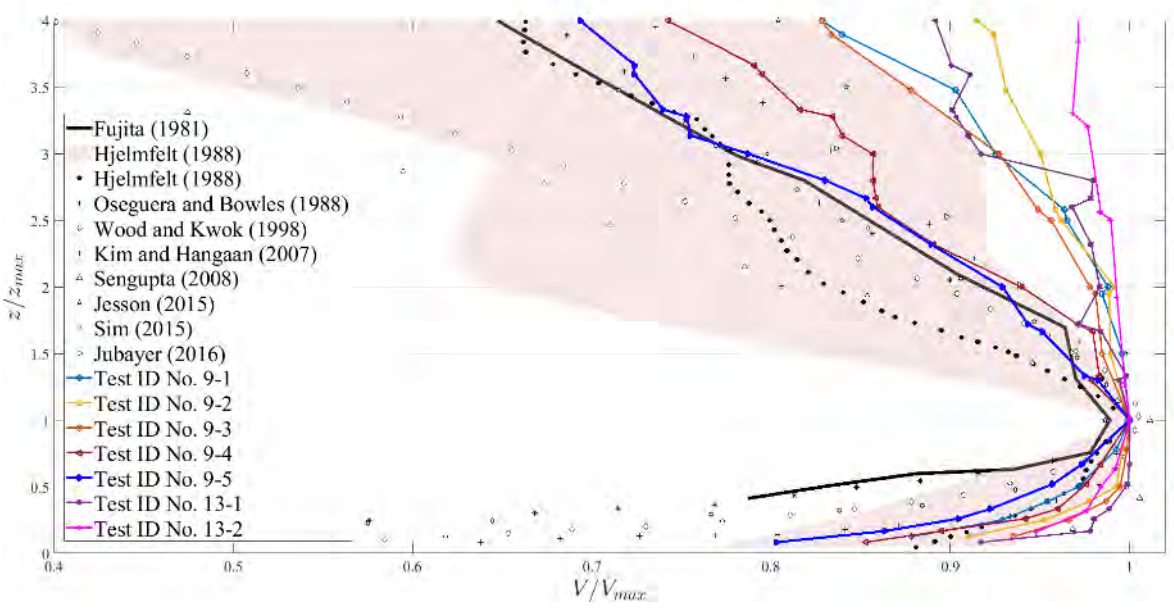

Figure 9 Vertical profile of horizontal wind velocities at the TTC for phase 2 flow characterization with slat angles at 45 deg and 60 deg at the turn table center (TTC)

The velocities in this validation Figure 9 show those tests that were conducted at the turntable center (TTC) in phase 2 and these velocities were extracted using a moving mean time window

T_{ave} based on the classical decomposition methods suggested by (Holmes et al., 2008; Solari et al., 2015). The method states that the total instantaneous wind velocity of a downburst at any height z at any time t and any downstream horizontal distance x is defined as the vector summation of a central moving average wind velocity and a fluctuating wind velocity as follows:

$$U(x,y,z,t) = \bar{U}(x,y,z,t) + u'(x,y,z,t) \quad (1)$$

where $U(x,y,z,t)$ is the total instantaneous wind velocity at height z and time t; $\bar{U}(x,y,z,t)$ is the slowly-varying, non-turbulent, moving mean wind velocity which is a deterministic function obtained from averaging the data using a convenient average time window T_{ave}; $u'(x,y,z,t)$ is the residual turbulent fluctuating wind velocity. The extraction of the slowly varying mean $\bar{U}(x,y,z,t)$ represent the moving mean horizontal velocities based on a time moving window visually selected to be a best fit for the time histories derived. From the tests herein, a value of $T_{ave}$of 0.5 sec was selected and applied to all the time histories for each pitot tube and cobra probe height. An example of this moving mean decomposition method can be seen in Figure 10 where the velocity is measured at the local peak height $z_{\max}$=152.4 mm.

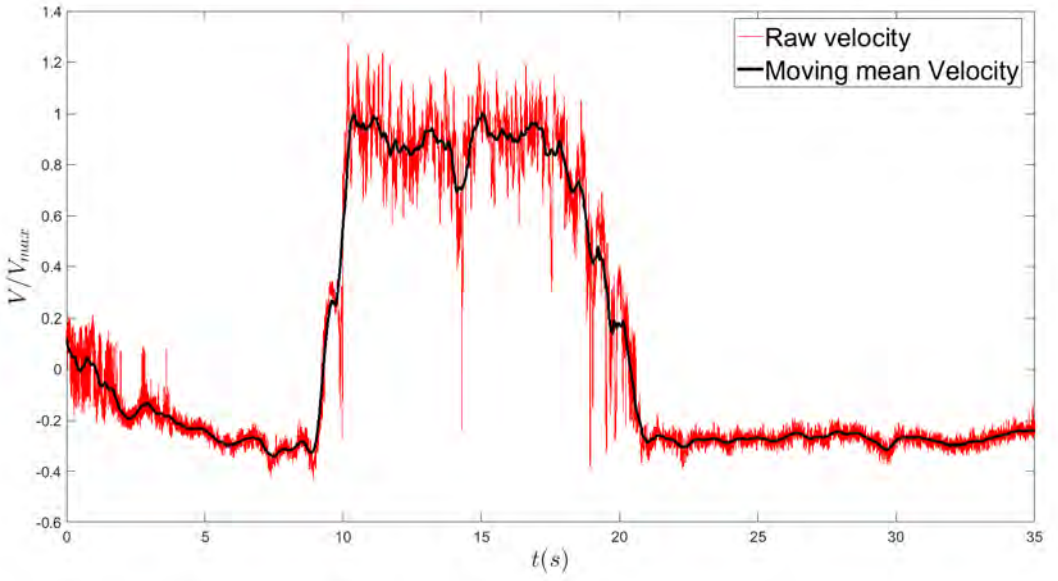

Figure 10 Time history for test ID ***No. 9-5****, at turntable center at height zmax=152.4 mm*

The moving mean velocity within the time history should follow smoothly the original velocity signal in a manner that passes through the middle of the signal and does not deviate away

excessively as seen in Figure 10. The results showed that using higher fan throttle ratios, the downburst outflows were enhanced. The louver slat angles opened at 30 deg also did not provide good results. The vertical velocity profiles at 30 deg louver slat angle did not provide an adequate 'nose' on the vertical profile of horizontal wind velocities but a series of large wind velocity variations between each successive probe height. These seemed to look like high perturbations in the flow and not properly displaying a characteristic ramp-up. The louver slats when opened at 60 deg did provide a realistic downburst time history with a well-defined ramp-up, the peak zone with a plateau, or short-lived stationarity region between the ramps, and a ramp-down. However, it was observed that in the vertical profile of horizontal velocities, two peak velocities were observed at different heights forming a "double" nose. When plotting the 60 deg louver slat angle, in the validation of normalized velocity profiles, the wind velocities tend to go over the acceptable "shaded area" that represents the inner and outer limits of the JAWS downburst events occurring in Colorado by (Hjelmfelt, 1988). The results obtained from the 45 deg louver slat provided the best results amongst any other angle as both the time histories and vertical velocity profiles did pass satisfactorily.

6.2 Turbulence characterization

The characterization and understanding of downburst outflow dynamics and vortex development requires a comprehensive analysis of statistical quantities such as the turbulence intensity, integral length scale, power spectral density (PSD), probability density function (PDF), autocorrelation coefficient and gust factors. However, a great difficulty exists in obtaining these statistical quantities due to the non-stationary and transient properties of downbursts. The analysis herein evaluates these statistical quantities to define their corresponding turbulence characterization. The instantaneous turbulence intensity of non-stationary winds, as in the case of downbursts, can be defined in the following equation as proposed by (Wang & Kareem, 2004; McCullough et al., 2014) as follows:

$$I_{u',T} = E\left[\frac{\sigma_{u',T}}{\overline{U}_T(t)}\right]_T \tag{2}$$

Where $E[\cdot]$ is the expected value within a short time interval T; $\sigma_{u',T}$ is the standard deviation of the residual fluctuating wind velocity u' within a time interval T known herein as the peak zone and $\overline{U}_T(t)$ is a time varying mean wind velocity which is considered herein to be equal to the

mean of the moving mean velocity within the peak zone. Figure 11 shows the corresponding variation of turbulence intensity profile for a conventional ABL stationary wind where the definition of turbulence intensity is taken as the standard deviation of the fluctuation wind velocity divided by the mean velocity. Figure 12 shows the turbulence intensity for the downburst flow generated at the WOW. For both cases, ABL and downburst, it can be seen that the turbulence intensity is a 'mirror image' of the velocity profile. In the case of downbursts, the natural phenomena involves an increase of the velocity with height up to the nose tip or peak height $z_{\max}$. Above the peak height the velocity decreases reaching zero where the center of the rolling vortex is found. This decrease allows a large increase of turbulence intensity.

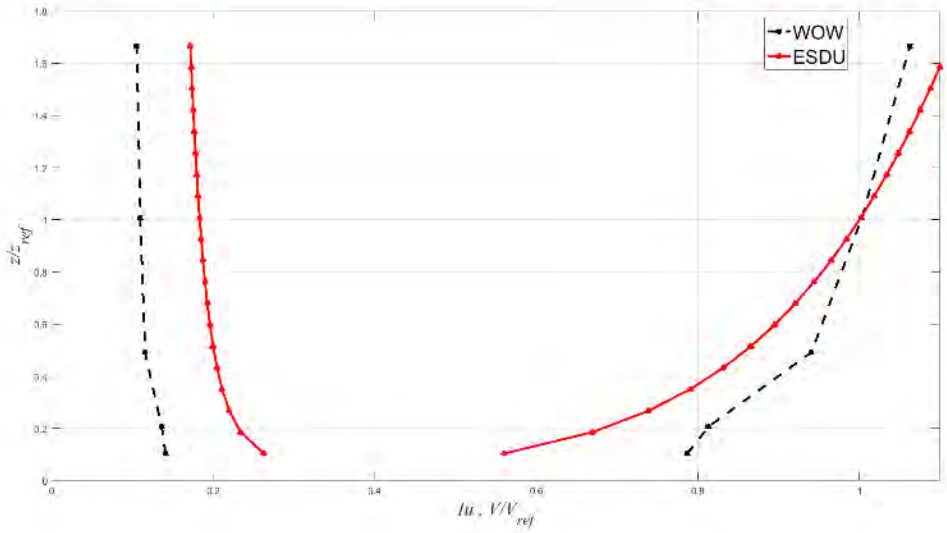

Figure 11 Vertical profile of turbulence intensity and horizontal wind velocities for ABL flow test at the TTC

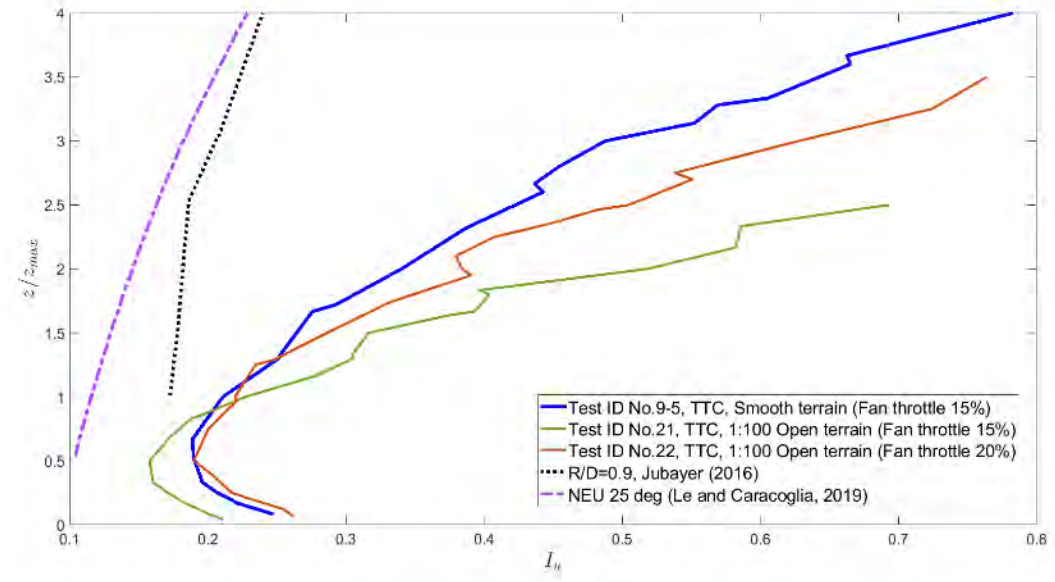

Figure 12 Turbulence intensity profile for downburst test ID No. 9-5 at the TTC using pitot tubes

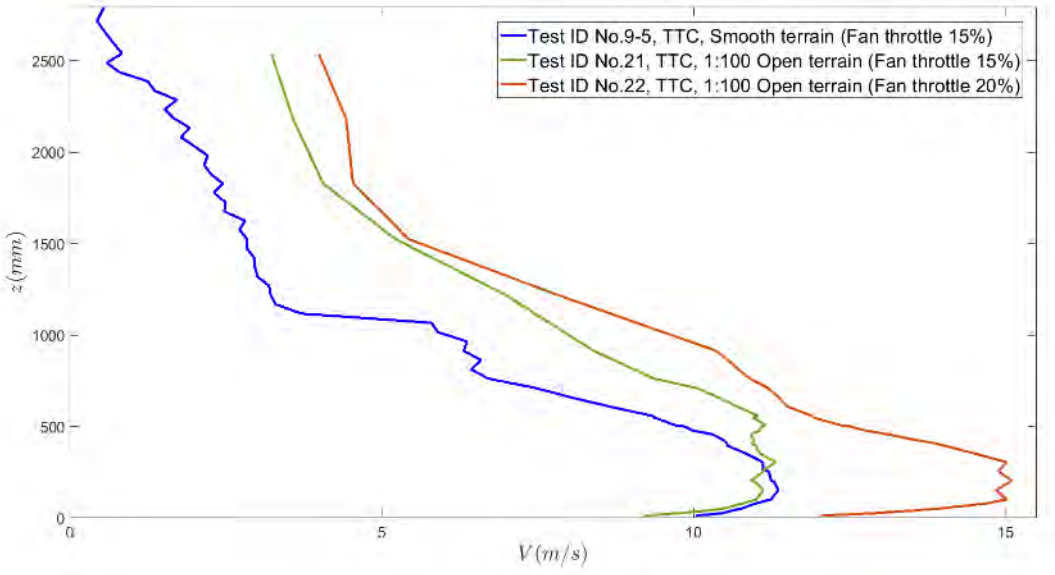

Figure 13 Vertical profile of horizontal wind velocities for test ID No. 9-5 using pitot tubes at the TTC

The turbulence integral length scales represent the average size of an eddy within the turbulent flow. The values of these can be obtained by either autocorrelation method or spectral fit (Van Fossen et al., 1995). For the case of downbursts, a Solari's PSD model exists that is suitable for transient events where a nondimensionalized PSD can be applied to a reduced turbulence

fluctuation within the peak zone and this model has proven to provide very good and reliable results (Solari et al., 2015).

Figure 14 shows the dimensionalized PSD of the residual fluctuations $u'$and moving mean velocity $\overline{U}$ within the peak zone in order to determine a comparison between the pitot tube and the cobra probe measurements at an identical height of 50.8 mm at the turn table center. It can be seen that the downburst fluctuation has an adequate Von Karman model fit (Von Karman, 1948) for both probe cases and no deficiency is seen in neither of the low frequency end, thus allowing a disregard of the use of Partial Turbulence Simulation (PTS) method for the aerodynamic building analysis subjected to downbursts.

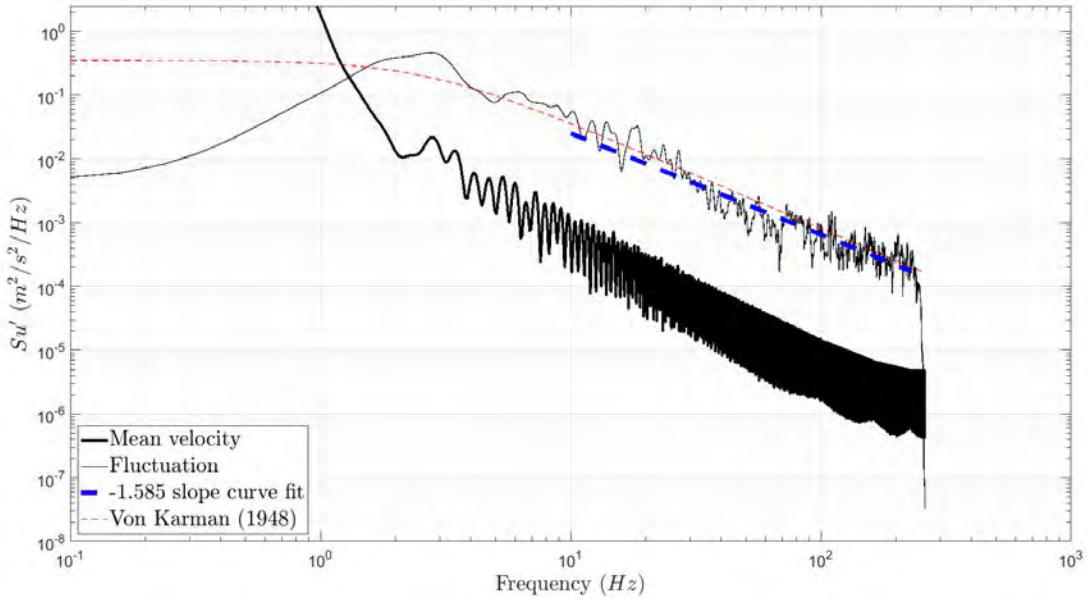

(a)

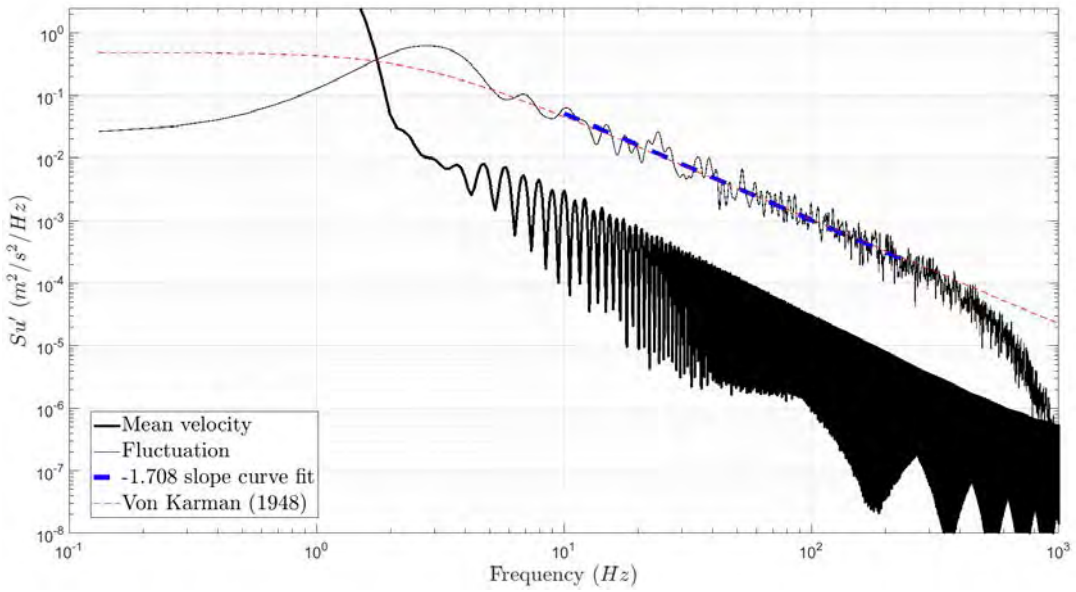

(b)

Figure 14 Comparison of Dimensionalized Power Spectral Density for test ID No. 9-5 at height of 50.8 mm between (a) Pitot tube and (b) Cobra probes at the turntable center TTC

For the case of non-dimensionalized PSD considering a non-dimensional, reduced turbulence fluctuation within the peak zone described by Solari (Solari et al., 2015), the Von Karman PSD model did very well as Solari's model as seen in Figure 15.

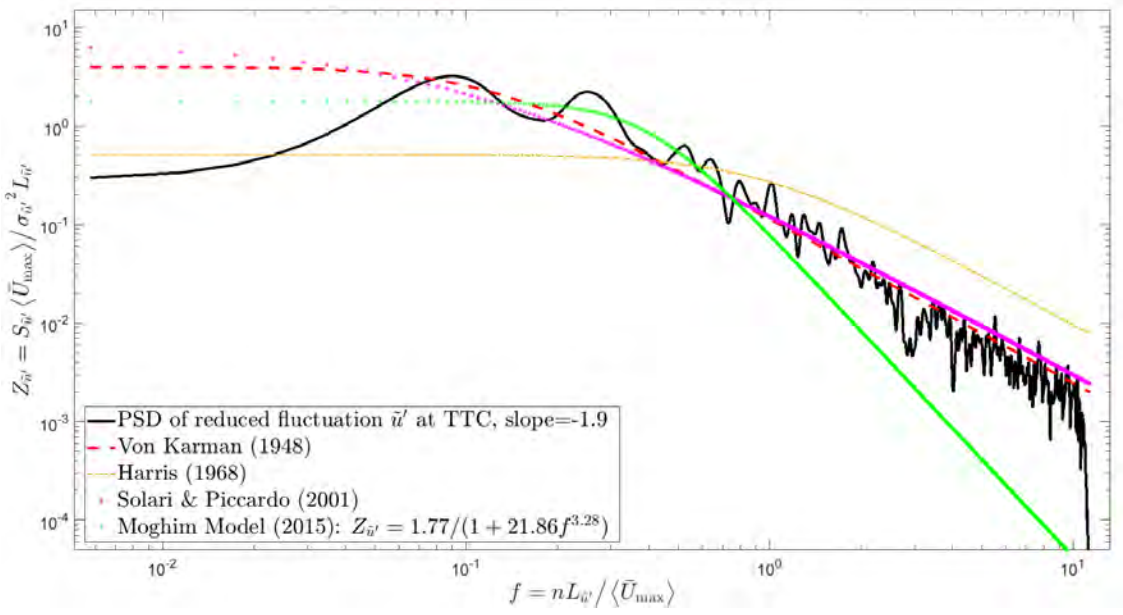

(a)

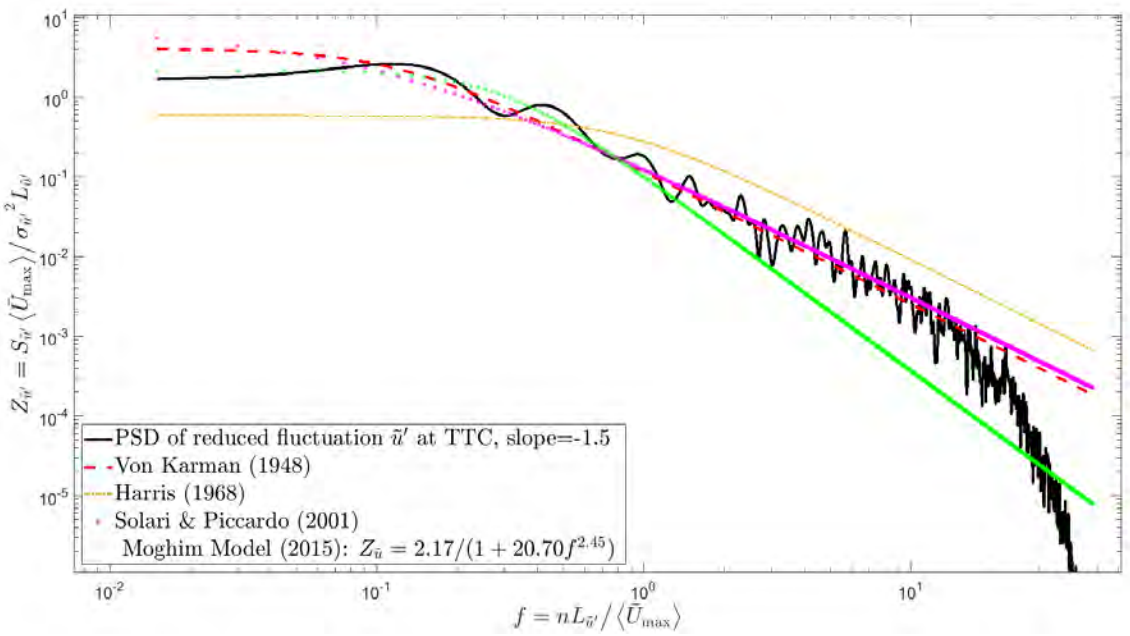

(b)

Figure 15 Non-dimensionalized Power Spectral Density for test ID No. 9-5 at height of 50.8 mm between (a) Pitot tube and (b) Cobra probes at the turntable center TTC

By non-dimensionalizing the turbulence fluctuations, the reduced turbulence can be analyzed similarly as ABL conventional statistical methods by allowing this new turbulence be well within the stationarity Gaussianity. Figure 16 shows the value of the statistical moments and deviation. For a Gaussian distribution, the mean should be zero with a unit standard deviation. The values of negentropy, kurtosis and skewness are indicators of how deviated from Gaussianity the experimental values obtained in the WOW were.

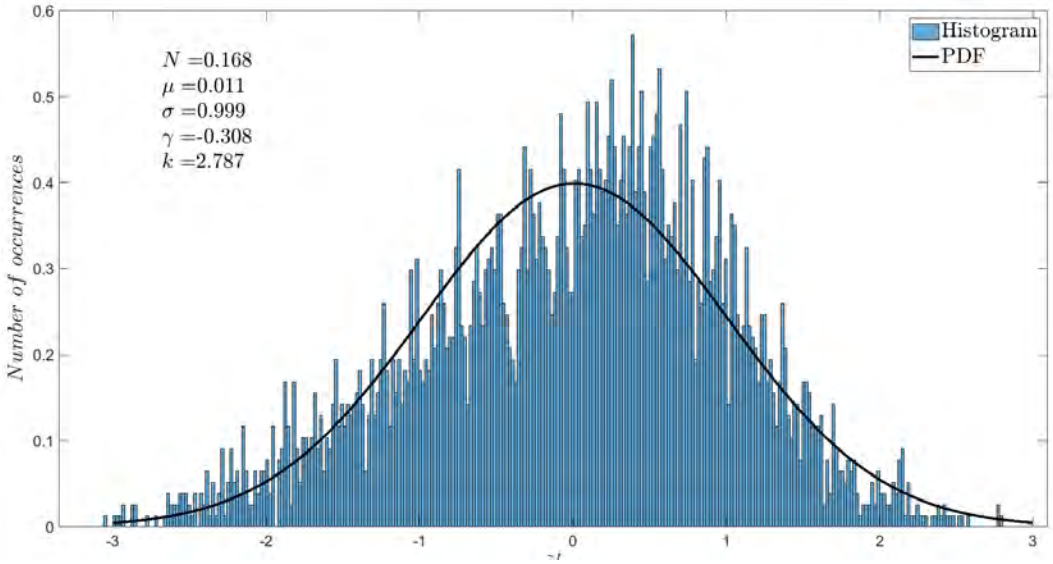

(a)

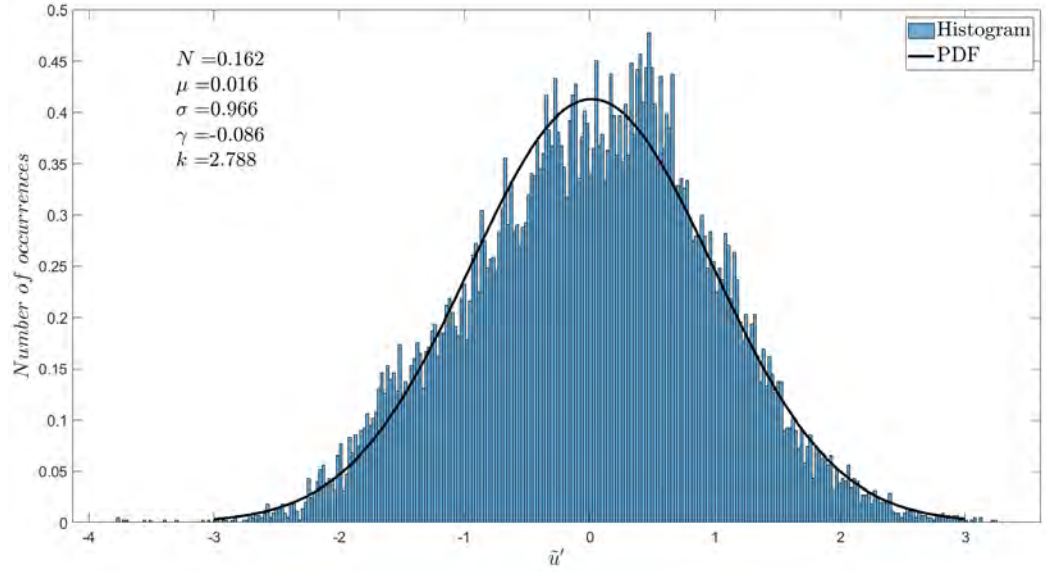

(b)

Figure 16 Histogram of Gaussianity measure for the Non-dimensionalized Power Spectral Density for test ID No. ***9-5*** *at height of 50.8 mm between (a) Pitot tube and (b) Cobra probes at the turntable center TTC*

From the turbulence analysis based on autocorrelation and PSD methods, the following Table 1 shows the calculated values of turbulence integral length scale L_u^x for pitot tubes and cobra probes. It can be seen that the Von Karman and Solari integral length values are close

Table 1. Reference velocities and corresponding integral length scales derived from autocorrelation and PSD from downburst data

		Reference velocities at roof eave height (m/s)		Integral length scales L_u^x at each roof height based on downburst outflow (m)					
Building designation	Roof heights (mm)	40% fan throttle ABL	15% fan throttle Downburst	Von Karman Dimensional spectral fit		Von Karman Nondimensional spectral fit		Solari Nondimensional spectral fit	
				Pitot tube	Cobra probe	Pitot tube	Cobra probe	Pitot tube	Cobra probe
A	39.62	13.62	10.61	0.34	0.45	0.43	0.51	0.35	0.42
B	198.12	17.6	11.29	0.26	0.54	0.34	0.54	0.28	0.44
C	396.24	21.74	10.54	0.25	0.51	0.35	0.49	0.30	0.41

6.2 Building aerodynamic analysis

The evaluation of C_p and a comparison regarding this value takes into consideration a variety of challenges and assumptions as the natural dynamics of both flows is entirely different. In the case of ABL versus downbursts, the idea is to determine which method is most appropriate to determine C_p considering the transient nature of downbursts. In the case of ABL wind loading, the differential pressure acting normal on the building surface is normalized with respect a reference velocity as follows:

$$C_p = \frac{p - p_{atmospheric}}{\frac{1}{2}\rho_{air}\bar{U}_{ref}^2} \quad (3)$$

where the numerator is the differential pressure of p with respect the reference atmospheric static pressure; U_{ref} is the reference velocity that is measured at the roof eave height of the corresponding building model when the building is not present at ABL flow. A single mean value can be applied to the entire time history of the ABL test for both the pressure p and the velocity U_{ref} as the test duration for the ABL tests analyzed herein was only 1 minute. On the other hand, when the event is a downburst, typically these events cannot use the same time averaging window T_{ave} of a stationary event because downbursts occur over durations shorter

than those associated with the stationary events (Lombardo, 2009). The C_p equation 3 used in ABL flows can no longer be applicable to downbursts. Several authors like (Lombardo, 2009; Iida et al., 2015; Jesson et al., 2015; Lombardo et al., 2018; Asano et al., 2019) have attempted to develop a representative equation for Cp that best describes the non-stationarity existent in the pressure and velocity field in downbursts taking into consideration the duration of the peak zone T. (Lombardo, 2009) has attempted to define the C_p equation with different time averages T_{ave}. (Asano et al., 2019) used a mean pressure value of the pressure field and considered a maximum instantaneous wind velocity as for reference velocity $U_{\max,T}$. For the study herein, the following equation used here is based on a T_{ave} of 0.5 sec applied for both, the moving pressure field and velocity field that are dependent on time as follows:

$$C_p(t) = \frac{E\left[p(t) - p_{atmospheric}\right]_T}{\frac{1}{2}\rho_{air}\,\bar{U}^2_{\max,ref,T}} \qquad (4)$$

where E() is the expected value of the differential pressure within the peak zone, expected value being either a minimum, mean or maximum value divided by the square of the reference velocity at the corresponding roof height when the building is not present in a downburst flow. The differential pressure is dependent on time and a good approach is to consider the peak zone duration T. The $\overline{U}_{\max.ref}$ is the maximum instantaneous value (or envelope) of the moving mean velocity within the peak zone. This value is obtained in an arbitrary way as there is no true solution. Following these equations, Figures 17-19show the comparisons made for the $C_{p,mean}$ amongst ABL and downbursts test cases. The fan throttle ration for the ABL cases were of 40% whereas the ones for downburst cases corresponded to 15%. The Reynolds number may not agree but basing the comparison of the normalized C_p values on quasi-steady theory, then a comparison can be drawn. Figure 19 shows that, for the 0 deg, all surfaces are exhibiting positive pressures, while for the 90, 180, and 270 deg, the pressure distribution exhibit negative values for all sides. This is unexpected and we suspect something might went wrong with the test instrumentations. So, further investigation is ongoing.

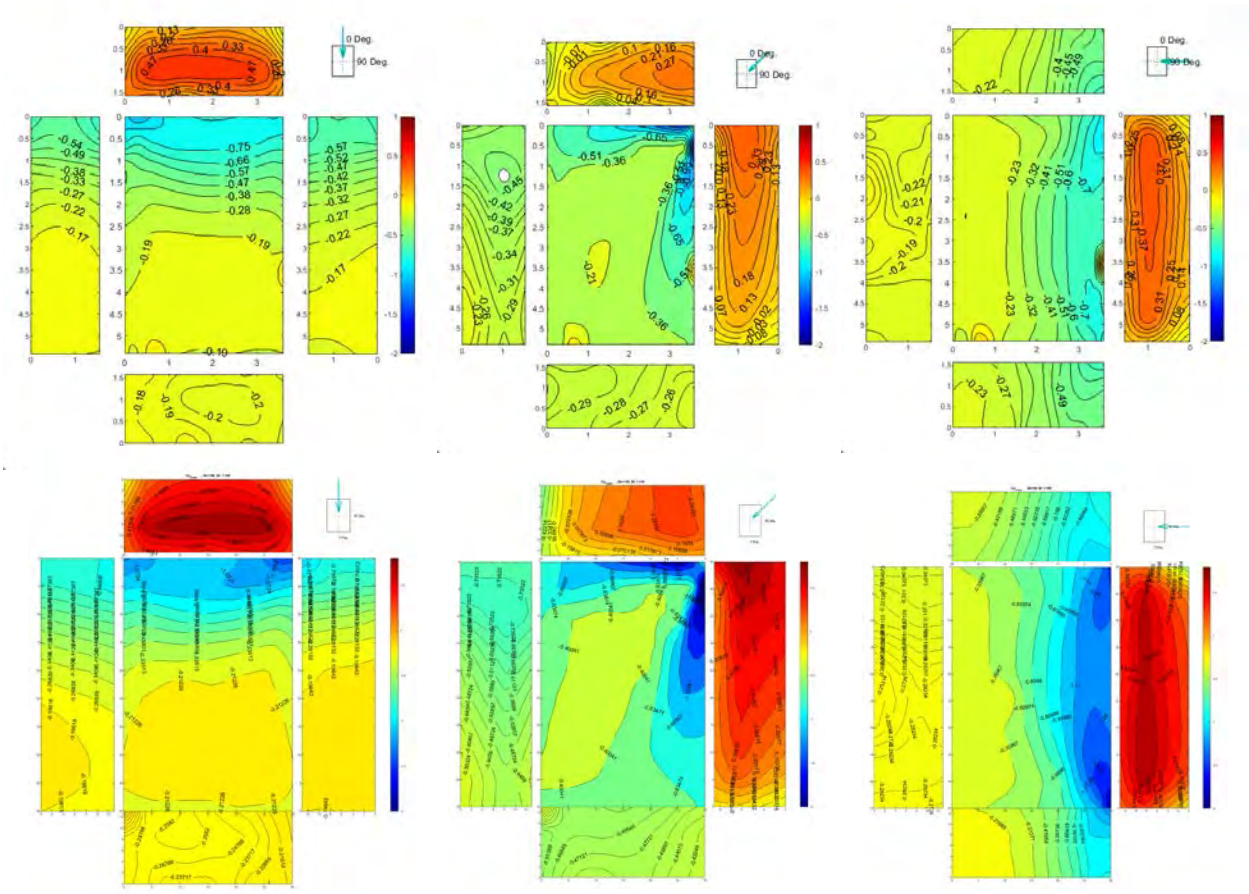

Figure 17 Determination of mean Cp,mean for Downburst (upper row) versus ABL (lower row) loading for the low-rise building A

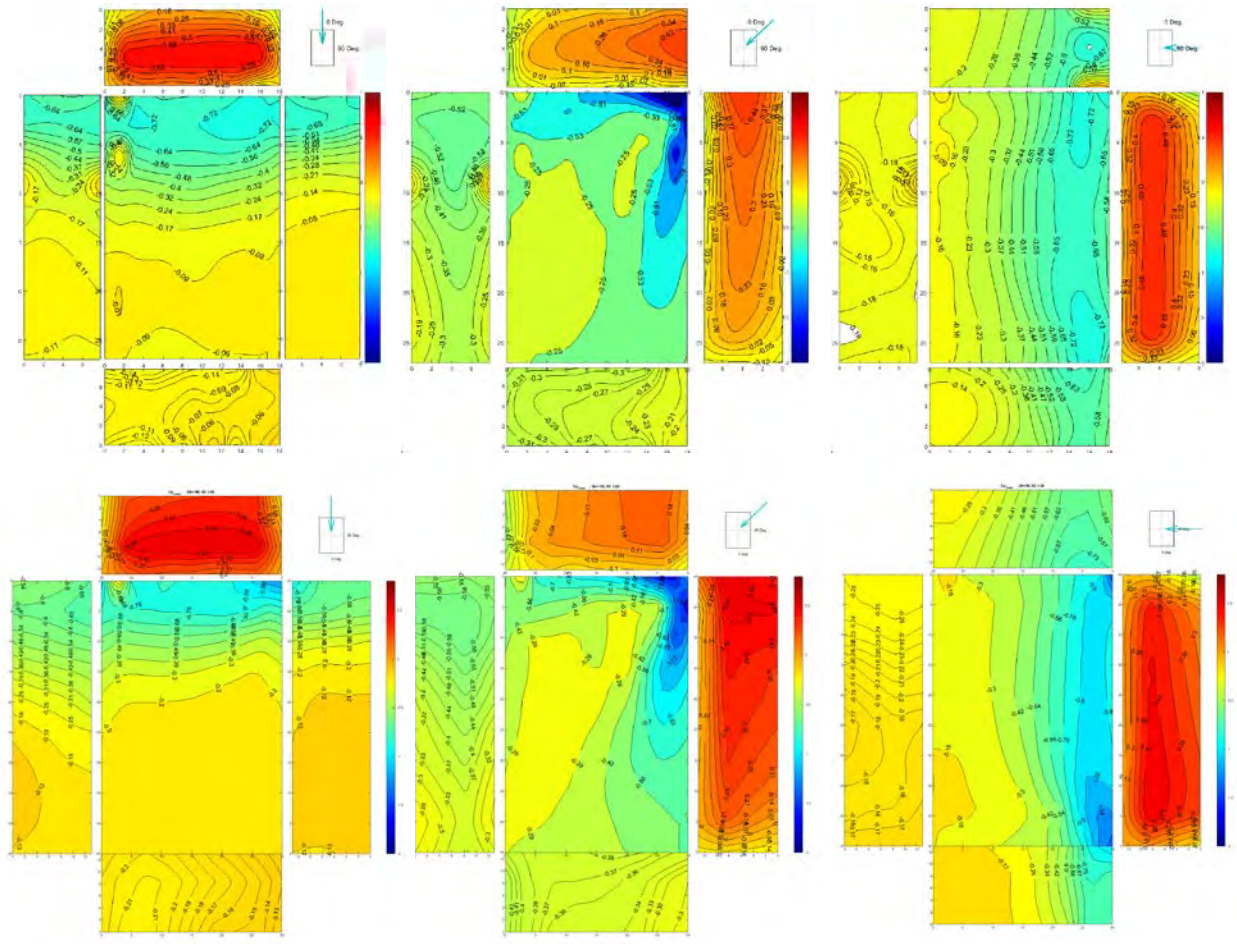

Figure 18 Determination of mean Cp,mean for Downburst (upper row) versus ABL (lower row) loading for the mid-rise building B

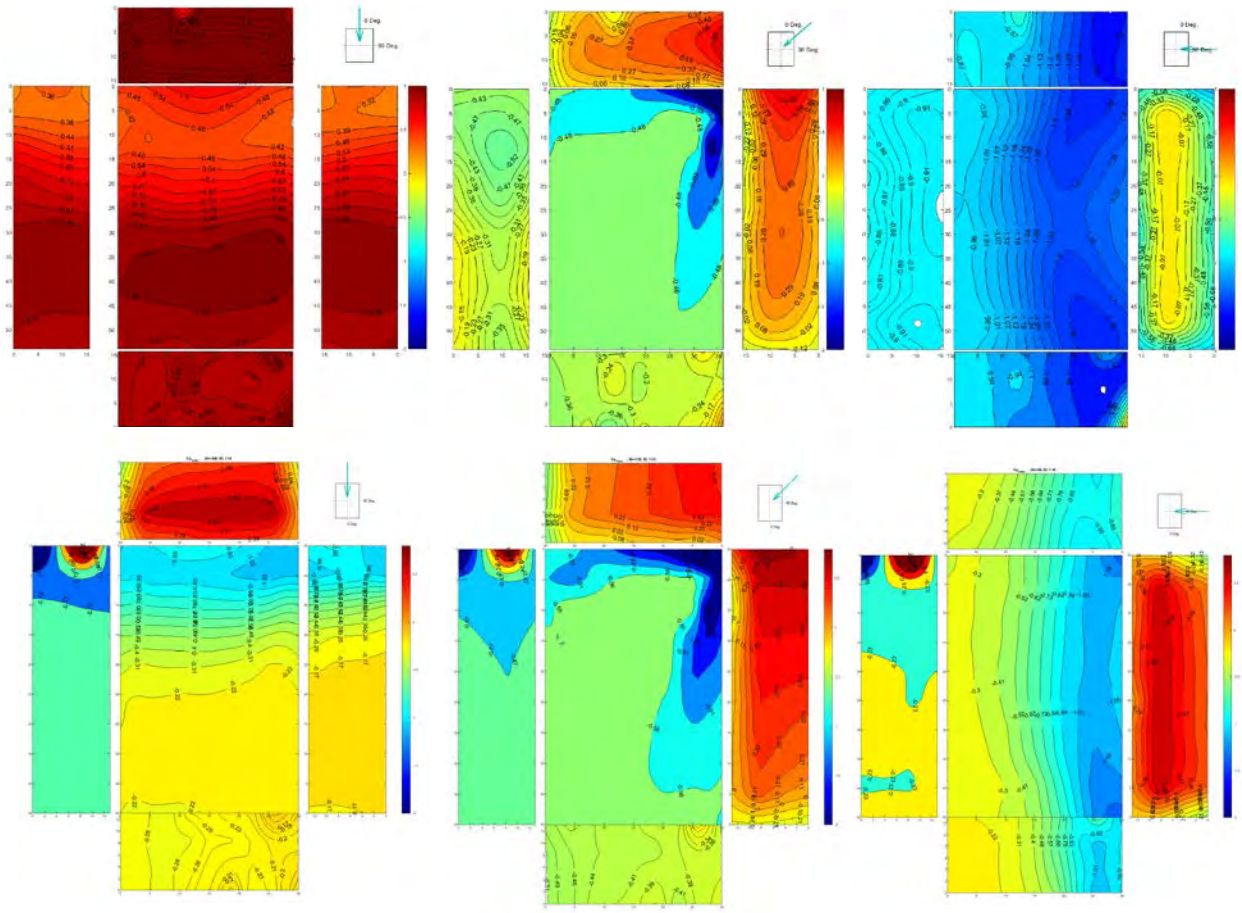

Figure 19 Determination of mean Cp,mean for Downburst (upper row) versus ABL (lower row) loading for the high-rise building C

From the pressure coefficients contours, Table 2 was derived based on mean of the C_p's observed for the building surfaces. In the table, the building sides were named based on a 0 deg wind as following: the windward "Side 1", side walls "Side 2 and 3", leeward "Side 4" roof "Side 5".

Table 2. Cp value comparison between ABL versus downburst on each building face subjected to three wind directions for low-rise building A

Low-rise building A	ABL	Downburst
Azimuth/building side	Mean Cp	Mean Cp
0 deg		
Side 1	0.51	0.32
Side 2	-0.33	-0.30
Side 3	-0.24	-0.19
Side 4	-0.42	-0.25

Side 5	-0.45	-0.30
45 deg		
Side 1	0.03	0.09
Side 2	0.32	0.15
Side 3	-0.48	-0.28
Side 4	-0.58	-0.34
Side 5	-0.70	-0.33
90 deg		
Side 1	-0.65	-0.33
Side 2	0.47	0.24
Side 3	-0.51	-0.37
Side 4	-0.30	-0.21
Side 5	-0.73	-0.33

Table 3. Cp value comparison between ABL versus downburst on each building face subjected to three wind directions for mid-rise building B

Mid-rise building B	ABL	Downburst
Azimuth/building side	Mean Cp	Mean Cp
0 deg		
Side 1	0.31	0.37
Side 2	-0.24	-0.20
Side 3	-0.18	-0.09
Side 4	-0.34	-0.25
Side 5	-0.33	-0.25
45 deg		
Side 1	-0.017	0.13
Side 2	0.22	0.16
Side 3	-0.36	-0.26
Side 4	-0.44	-0.38
Side 5	-0.53	-0.38
90 deg		
Side 1	-0.49	-0.37
Side 2	0.26	0.31
Side 3	-0.35	-0.35
Side 4	-0.20	-0.17

Side 5	-0.54	-0.39

Table 4. Cp value comparison between ABL versus downburst on each building face subjected to three wind directions for high-rise building C

High-rise building C	ABL	Downburst
Azimuth/building side	Mean Cp	Mean Cp
0 deg		
Side 1	0.40	1.48
Side 2	-0.36	0.77
Side 3	-0.24	0.88
Side 4	-0.31	0.77
Side 5	-0.44	0.77
45 deg		
Side 1	0.098	0.27
Side 2	0.26	0.24
Side 3	-0.42	-0.28
Side 4	-0.50	-0.34
Side 5	-0.72	-0.38
90 deg		
Side 1	-0.62	-1.17
Side 2	0.34	-0.33
Side 3	-0.52	-1.15
Side 4	-0.12	-0.90
Side 5	-0.68	-1.17

And based on the contour plots and table 2 through 4, the following were observed:

- An overall similar trend in the pressure distribution was found amongst ABL and downbursts. However, the magnitude of the pressure coefficients vary. This difference might have resulted from the superposition between the corner vortex formation and the suction derived from the main rolling vortex passing over the building in the case of downburst winds.

- There are strong suction (negative) pressure coefficients found on the roof and exacerbating when the wind direction impact the building at 45 deg. These high suction pressures are an indication of strong vorticity due to the conical vortices forming at the roof edges. The roof suction pressure coefficient are always higher in the ABL case over downbursts.
- Comparing downburst to ABL, no significant difference in mean pressure coefficients was found for both Model A and B (low-rise and mid-rise buildings). This may support the hypothesis that ABL-induced pressure coefficients could be sufficient for downburst cases.
- Comparing downburst to ABL, the maximum and minimum mean pressure coefficients on the high-rise building model C was significantly higher for the downburst case.

The results indicate that in some cases downburst flow causes higher positive and negative pressures than these measured under ABL winds. More investigations are ongoing at the WOW facility to assess these preliminary observations and to extend this study to assess the maximum and minimum local and area-averaged pressures.

7. Conclusions

In this study, a two part process is explained. First the validation of a novel large-scale downburst simulator at the Wall of Wind. The flow characterization is evaluated based on three main criteria which includes the formation of a rolling vortex through smoke visualization, the spike or peak zone found in the time history of each downburst test run, and finally the validation of a 'nose shaped' vertical profile that is compared to previous recorded real downbursts. The use of a large-scale downburst simulator open up new venues of testing for the transient aerodynamics of low-, mid- and high-rise buildings. Three buildings were tested, a low-rise building, a mid-rise building and a high-rise building in a length scale of 1:100 in open terrain. The goal was to evaluate the aerodynamics of downbursts and compare these to the conventional ABL loading considerations and determine the differences represented in a normalized pressure coefficients. Comparing the contours and pressure coefficient magnitudes amongst ABL versus downbursts, it was revealed that the overall the aerodynamic trend is basically similar; however, the pressure coefficients vary. This was particularly pronounced for the case of the high rise building. More investigations are needed to assess the possible scaling effects that may affect the

resulting pressures. Also, since downburst impact on high rise buildings seems significantly different compared to ABL-induced aerodynamics, it is suggested that the dynamic response of a tall building subjected to downbursts is studied to assess the downburst-induced vibrations and dynamic response factors.

Acknowledgements

The authors of the downburst project wish to thank the NHERI Wall of Wind staff to make this advancement a further possibility for research and development.

References

Asano, K., Iida, Y., & Uematsu, Y. (2019). Laboratory study of wind loads on a low-rise building in a downburst using a moving pulsed jet simulator and their comparison with other types of simulators. *Journal of Wind Engineering and Industrial Aerodynamics*, *184*, 313–320.

Chowdhury, A., Zisis, I., Irwin, P., Bitsuamlak, G., Pinelli, J.-P., Hajra, B., & Moravej, M. (2017). Large-scale experimentation using the 12-fan wall of wind to assess and mitigate hurricane wind and rain impacts on buildings and infrastructure systems. *Journal of Structural Engineering*, *143*(7), 4017053.

Fujita, T. T. (1981). Tornadoes and downbursts in the context of generalized planetary scales. *Journal of the Atmospheric Sciences*, *38*(8), 1511–1534.

Hjelmfelt, M. R. (1988). Structure and life cycle of microburst outflows observed in Colorado. *Journal of Applied Meteorology*, *27*(8), 900–927.

Holmes, J. D., Hangan, H. M., Schroeder, J. L., Letchford, C. W., & Orwig, K. D. (2008). A forensic study of the Lubbock-Reese downdraft of 2002. *Wind and Structures, An International Journal*. https://doi.org/10.12989/was.2008.11.2.137

Iida, Y., Uematsu, Y., & Gavanski, E. (2015). A study of downburst-induced wind loading on buildings. *Journal of Wind Engineering*, *40*(2), 40–49.

Jesson, M., Sterling, M., Letchford, C., & Haines, M. (2015). Aerodynamic forces on generic buildings subject to transient, downburst-type winds. *Journal of Wind Engineering and Industrial Aerodynamics*, *137*, 58–68.

Lombardo, F. T. (2009). *Analysis and interpretation of thunderstorm wind flow and its effects on a bluff body*. Texas Tech University.

Lombardo, F. T., Mason, M. S., & de Alba, A. Z. (2018). Investigation of a downburst loading event on a full-scale low-rise building. *Journal of Wind Engineering and Industrial Aerodynamics*, *182*, 272–285.

Makita, H. (1991). Realization of a large-scale turbulence field in a small wind tunnel. *Fluid Dynamics Research*, *8*(1–4), 53.

McCullough, M., Kwon, D. K., Kareem, A., & Wang, L. (2014). Efficacy of averaging interval for nonstationary winds. *Journal of Engineering Mechanics*, *140*(1), 1–19.

Mooneghi, M. A., Irwin, P., & Chowdhury, A. G. (2016). Partial turbulence simulation method for predicting peak wind loads on small structures and building appurtenances. *Journal of Wind Engineering and Industrial Aerodynamics*, *157*, 47–62.

Moravej, M. (2018). *Investigating scale effects on analytical methods of predicting peak wind loads on buildings*.

Romanic, D., Chowdhury, J., Chowdhury, J., & Hangan, H. (2019). *Investigation of abrupt changes in thunderstorm velocity record*. *September 2012*, 13–16.

Solari, G., Burlando, M., De Gaetano, P., & Repetto, M. P. (2015). Characteristics of thunderstorms relevant to the wind loading of structures. *Wind and Structures*, *20*(6), 763–791.

Van Fossen, G. J., Simoneau, R. J., & Ching, C. Y. (1995). *Influence of turbulence parameters, Reynolds number, and body shape on stagnation-region heat transfer*.

Von Karman, T. (1948). Progress in the statistical theory of turbulence. *Proceedings of the National Academy of Sciences of the United States of America*, *34*(11), 530.

Wang, L., & Kareem, A. (2004). Modeling of non-stationary winds in gust-fronts. *9th ASCE Specialty Conference on Probabilistic Mechanics and Structural Reliability*, 1–6.

Appendix A Downburst simulator and flow characterization

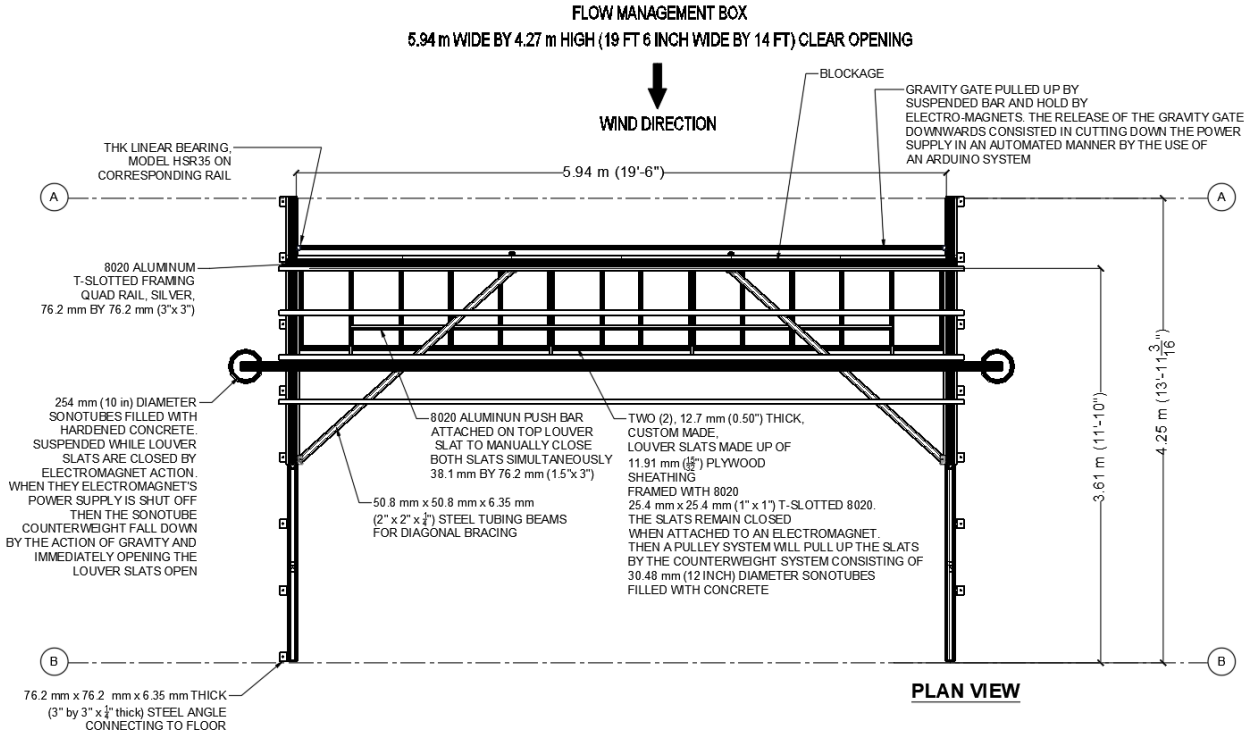

Figure A-1 Downburst simulator placed in front of the flow management box at the Wall of Wind (WOW) plan view

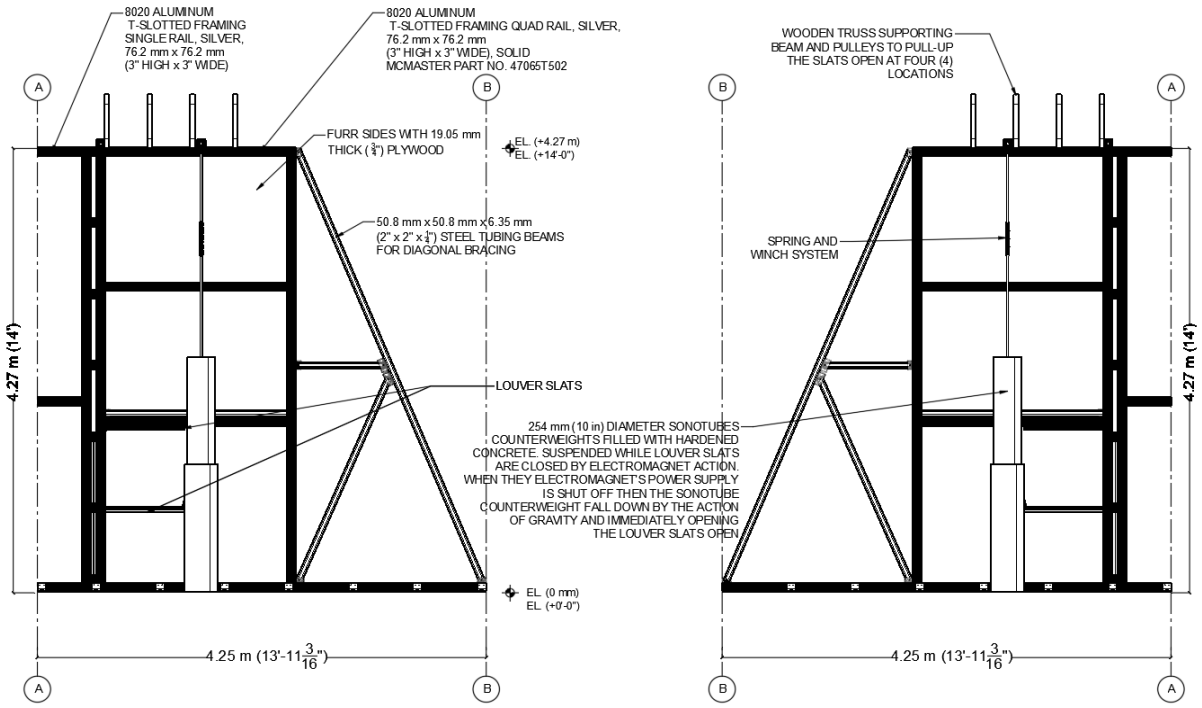

Figure A-2 Downburst simulator placed in front of the flow management box at the Wall of Wind (WOW) side elevation view

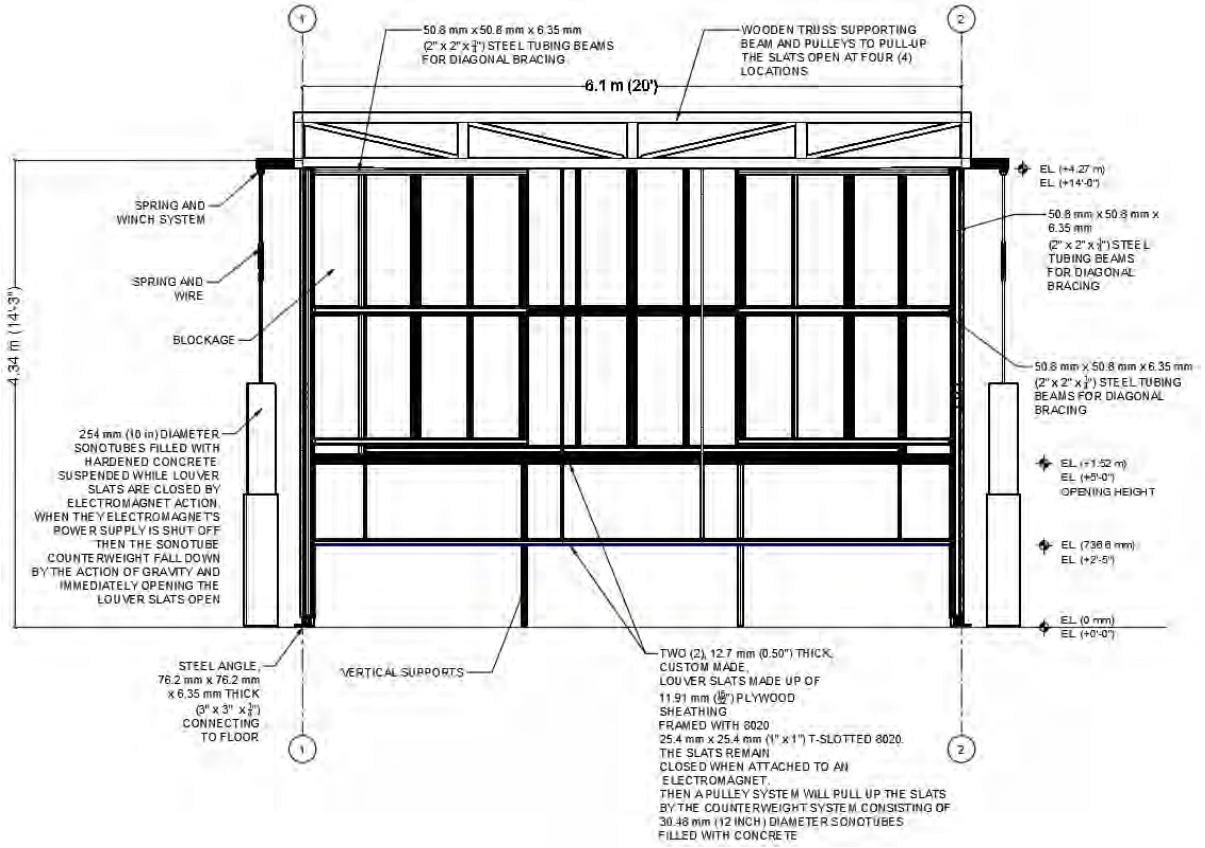

Figure A-3 Downburst simulator placed in front of the flow management box at the Wall of Wind (WOW) front elevation view

Figure A-4 Downburst simulator picture placed in front of the flow management box at the Wall of Wind (WOW) with two louver slats closed

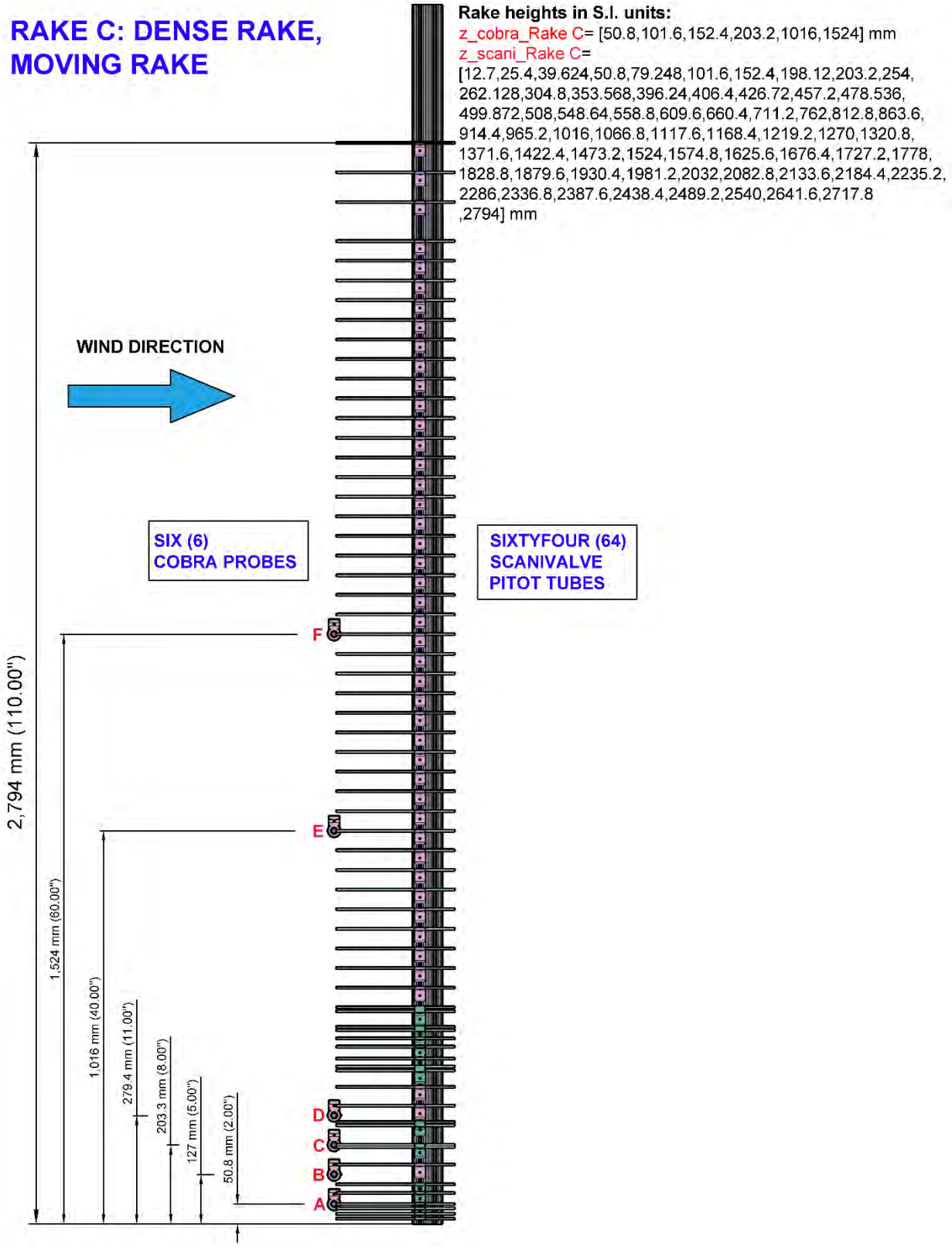

Figure A-5 Dense rake C consisting of sixty-four pitot tubes and six cobra probes

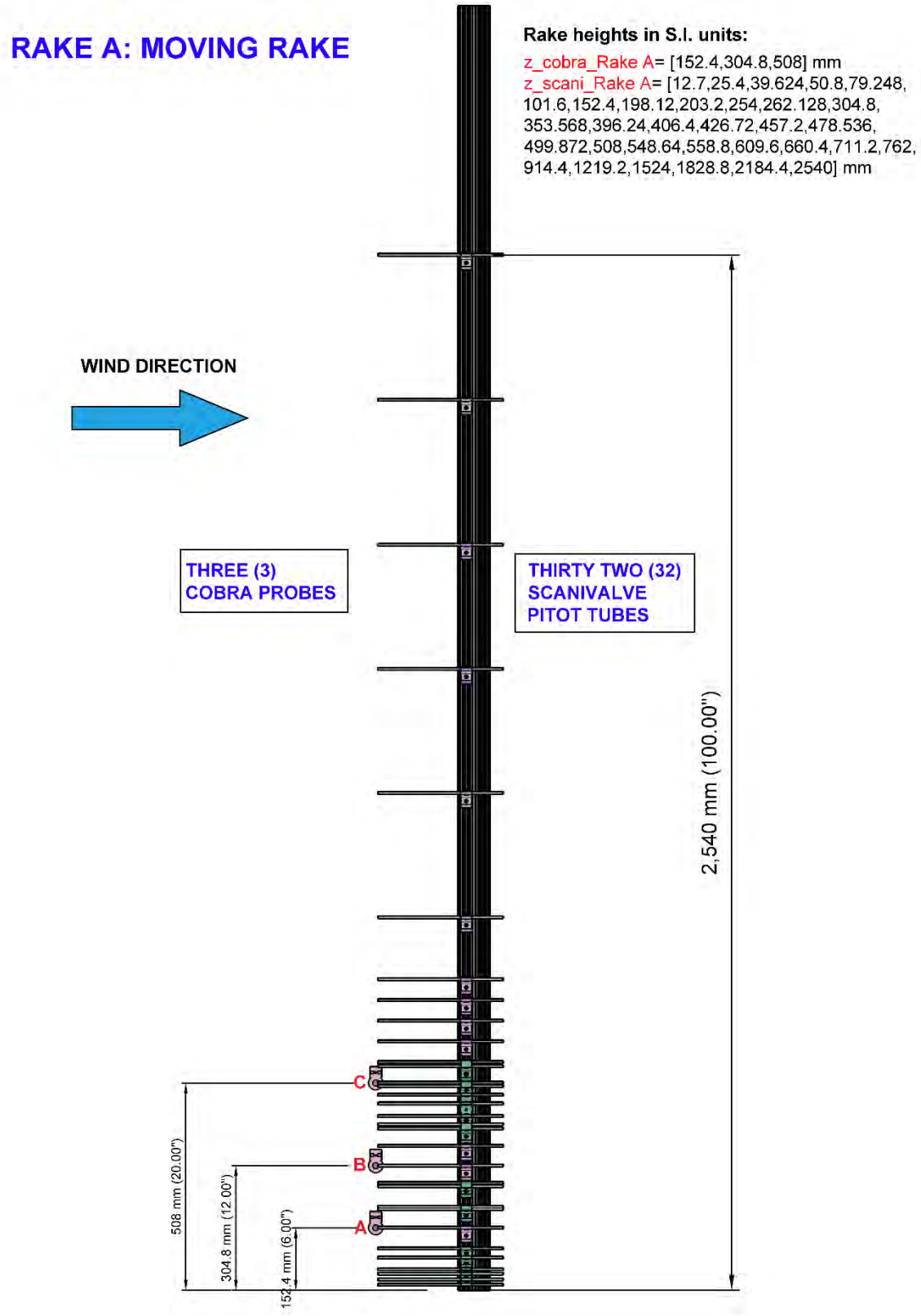

Figure A-6 Moving Rake A consisting of thirty two pitot tubes and six cobra probes

.

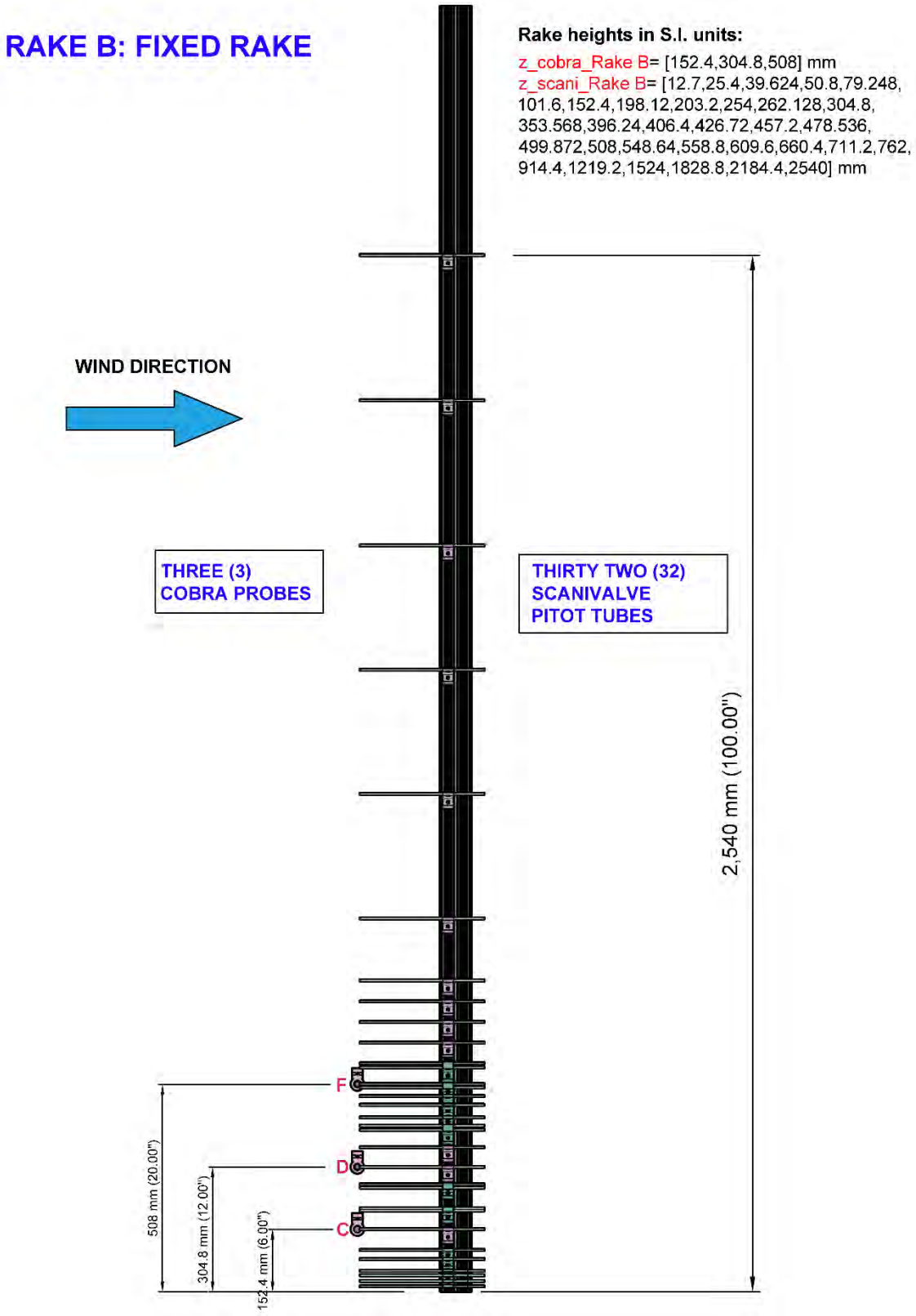

Figure A-7 Fixed rake B consisting of thirty two pitot tubes and six cobra probes

Table A-8. Downburst tests pass-fail criteria during Downburst commissioning Phase 2, 3 and 4

Test ID		Controlling Parameters				Test output			Test criteria	
Test ID No	Loca-tion ID No	Slat angle (deg)	Initial Fan throttle ratio (%)	Opening duration (sec)	Closing method	U_{max} (m/s)	z_{max} (m)	Peak zone duration (sec)	Pass	Fail
9-1	4	45	15	15	Gravity Gate	11.7	0.10	16.70	✓	
9-2	4	45	15	Continuous	None	10.5	0.10	17.77	✓	
9-3	4	45	15	15	Close slats manually	11.9	0.10	16.41	✓	
9-4	4	45	15	15	Close slats manually	11	0.10	17.00	✓	
9-5	4	45	15	10	Close slats manually	11.2	0.15	11.10	✓	
13-1	4	60	15	10	Close slats manually	10.3	0.20	13.30	✓	
13-2	4	60	15	10	Close slats manually	10.3	0.10	12.11	✓	
21 Rake A	4	45	15	10	Close slats manually	11	0.15	12.18	✓	
21 Rake B	B	45	15	10	Close slats manually	1.8	0.61	12.86		X
22 Rake A	4	45	20	10	Close slats manually	15	0.20	11.73	✓	
22 Rake B	B	45	20	10	Close slats manually	14.7	0.20	11.78	✓	

*Foot Note: The values presented in this table herein are based on a moving time average window of Tave=1 sec as it was initially done during commissioning and flow characterization check. The Tave was later changed to 0.5 sec for further analysis on turbulence and aerodynamic of the buildings.

Appendix B Downburst aerodynamics on low-rise TTU buildings

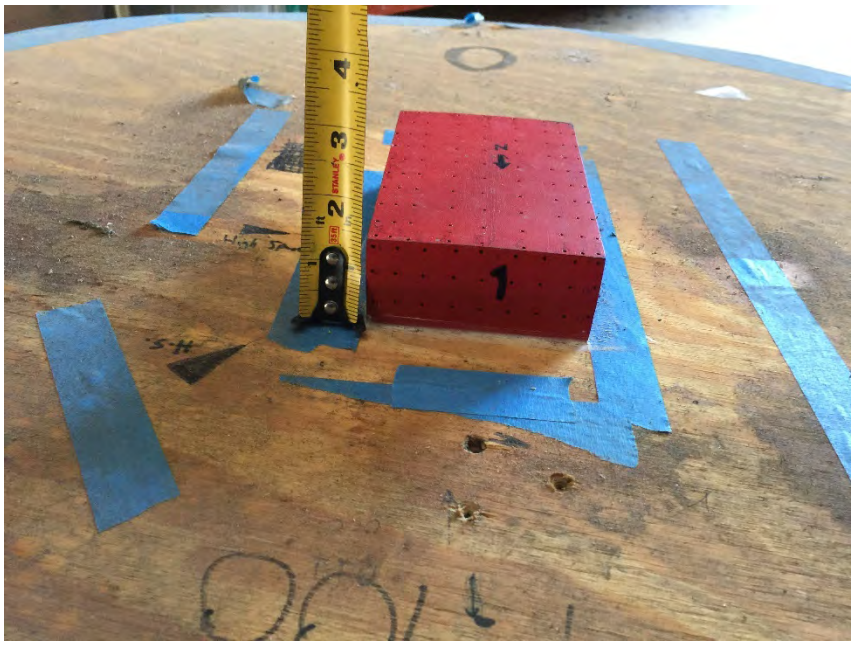

Figure B1-1 Low-rise building A, scaled in 1:100

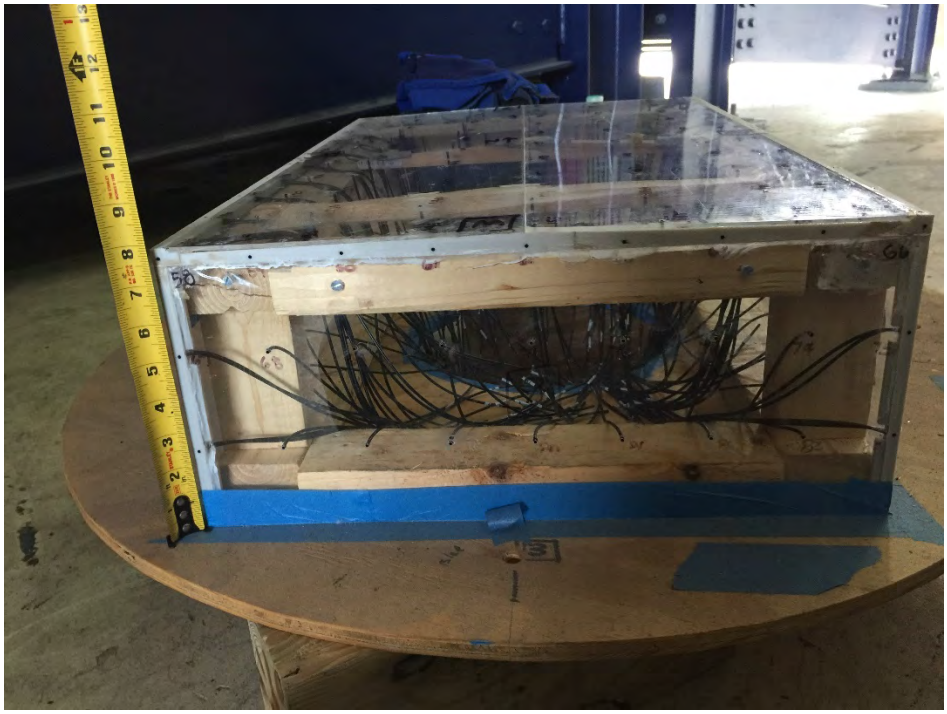

Figure B1-3 Mid-rise building B, scaled in 1:100

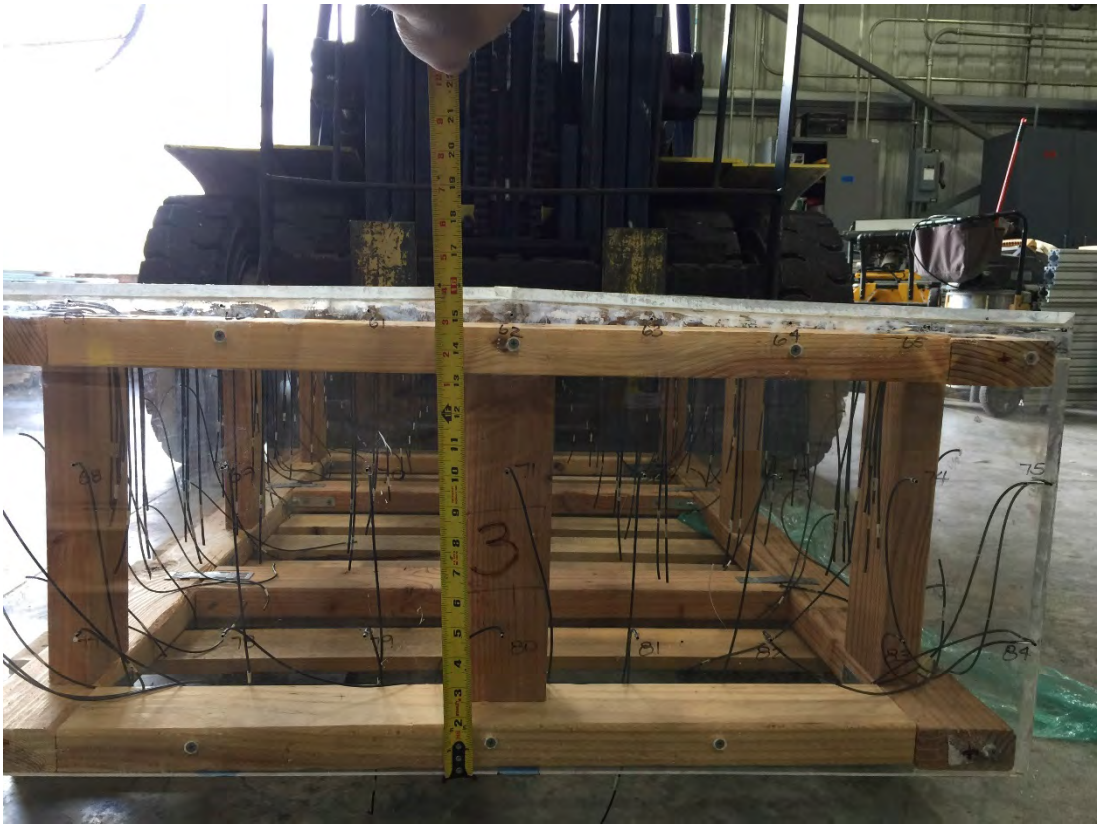

Figure B1-4 High-rise building C, scaled in 1:100

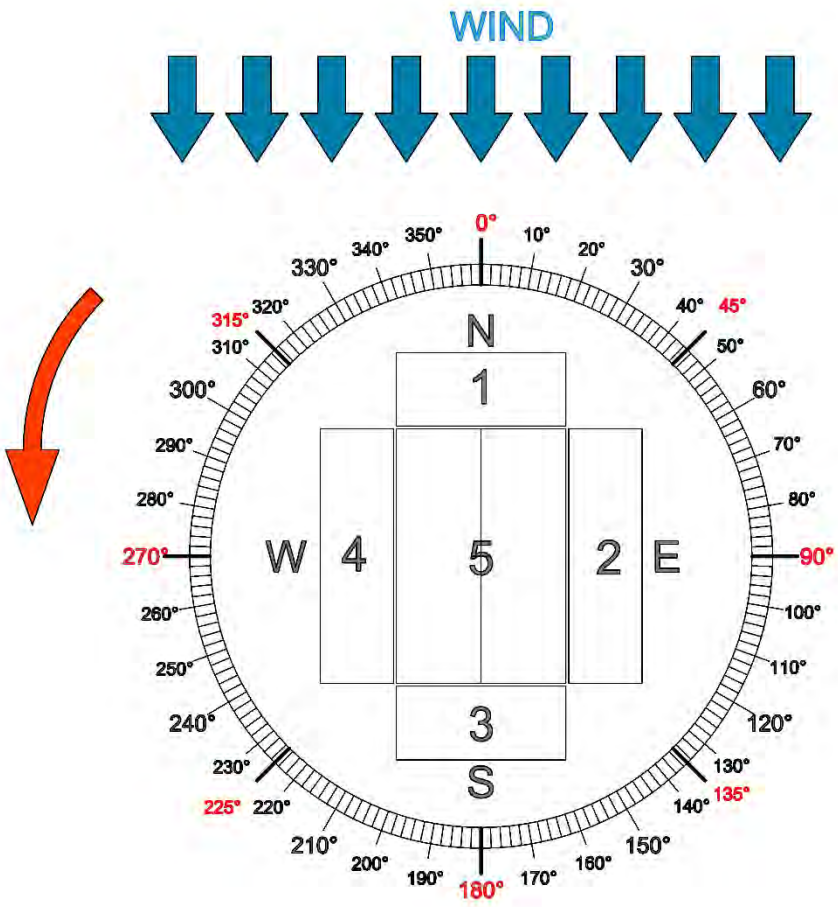

Figure B1-5 International wind convention for aerodynamic testing used herein for the TTU buildings. The building is rotated counterclockwise at which the zero degree is facing north. The angles represent the azimuth angles.

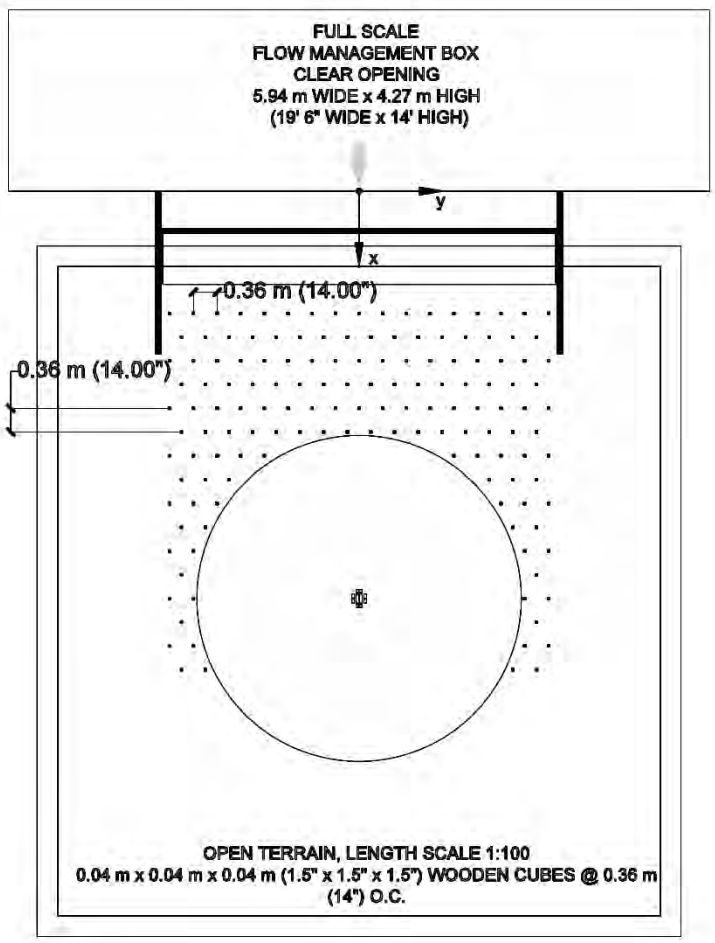

Figure B1-6 Low-rise building A placed in an open terrain scale of 1:100

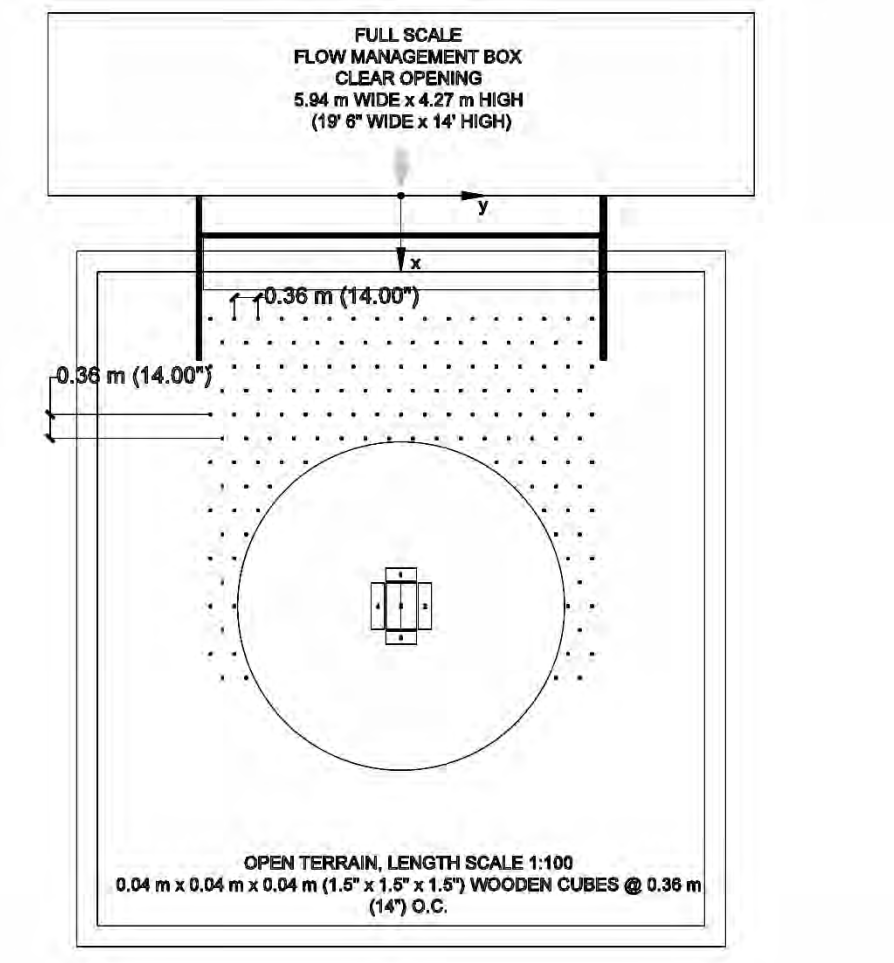

Figure B1-4 Low-rise building B placed in an open terrain scale of 1:100

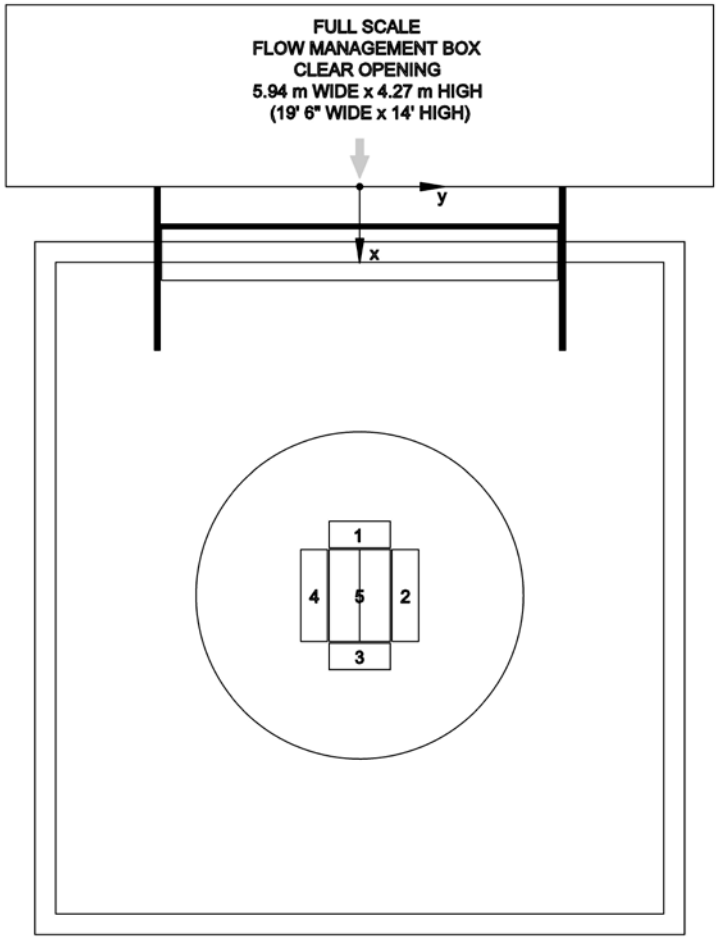

Figure B1-4 Mid-rise building C placed in an open terrain scale of 1:100

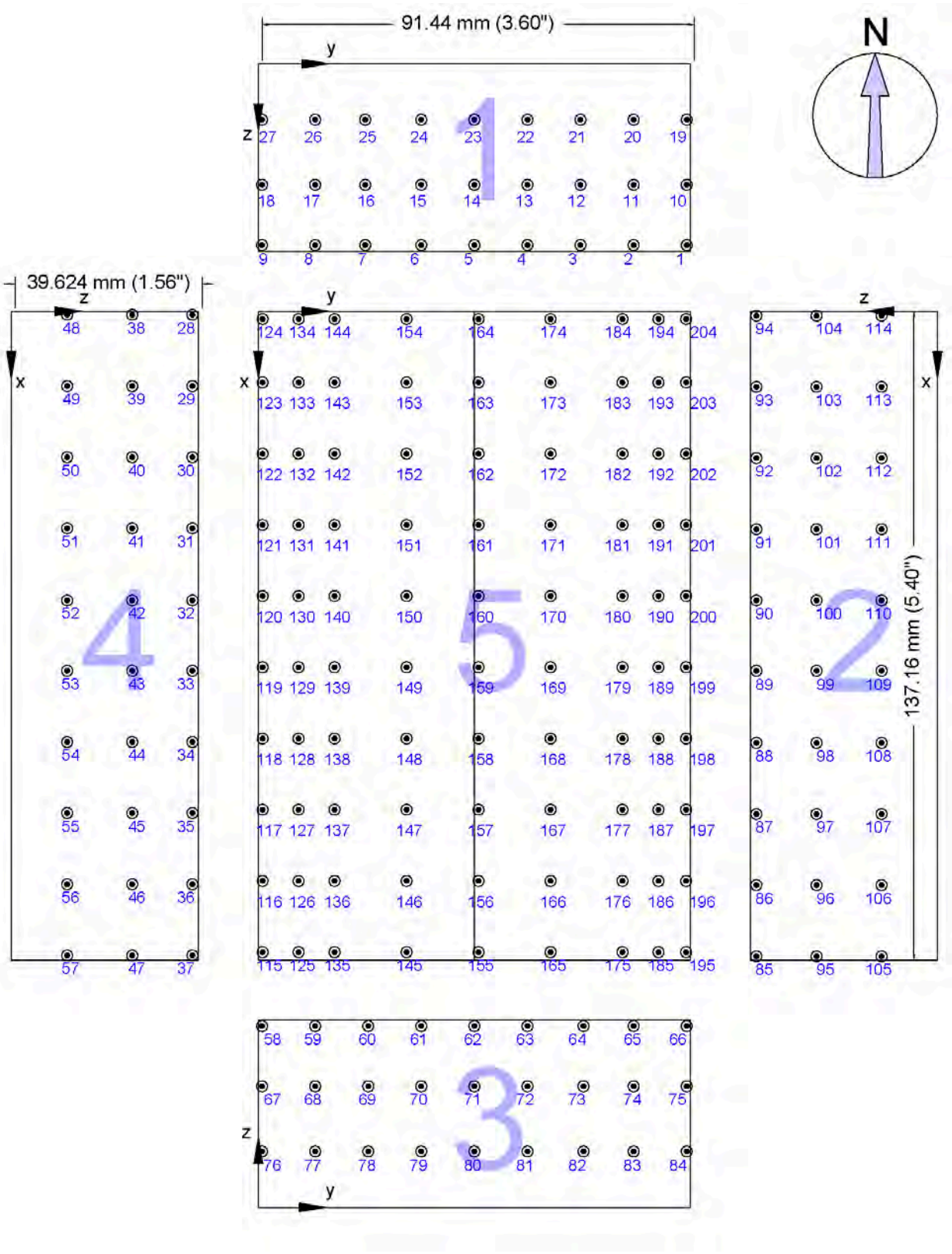

Figure B1-5 Geometrical and tap configuration for low-rise building A in a length scale of 1:100

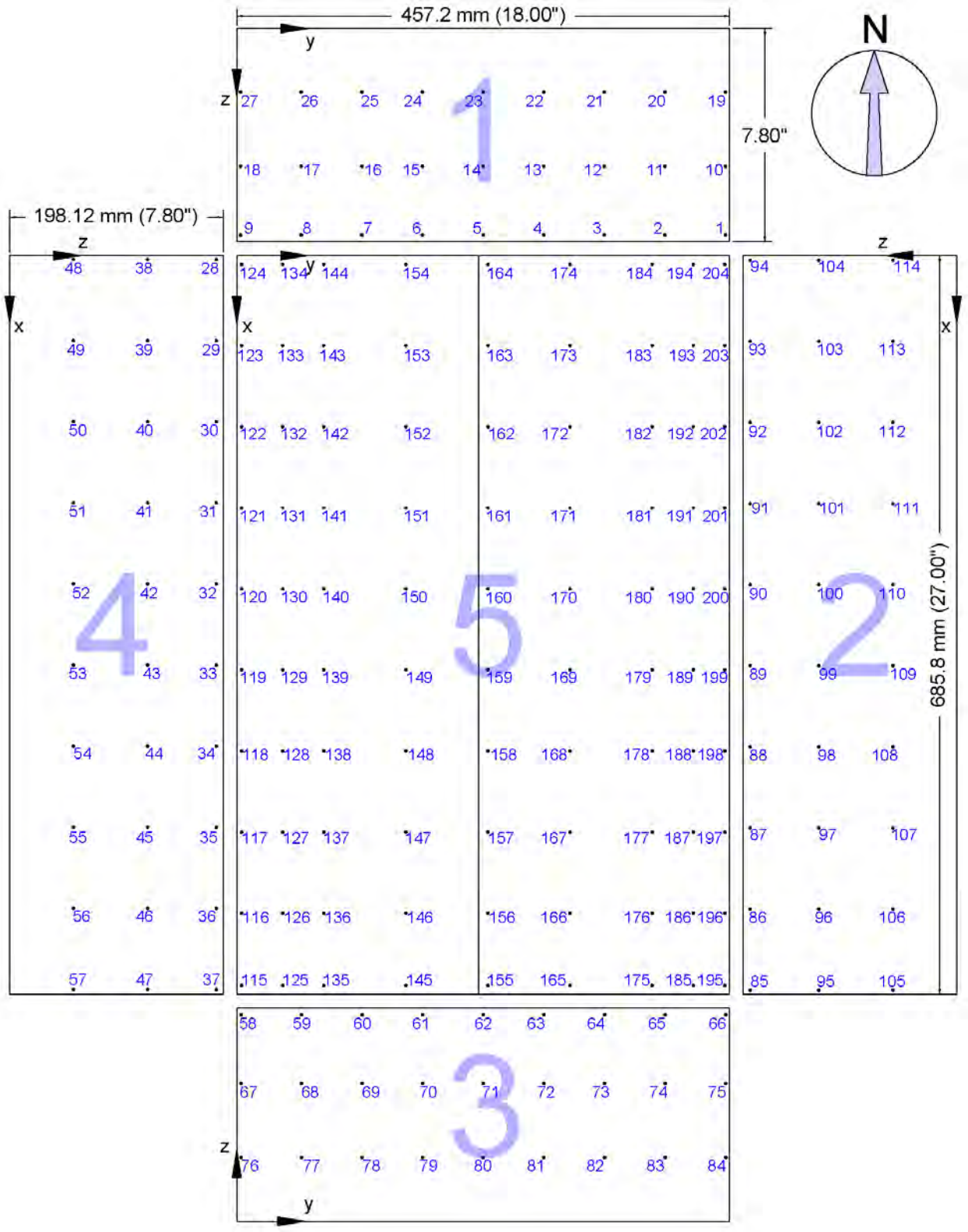

Figure B1-6 Geometrical and tap configuration for mid-rise building B in a length scale of 1:100

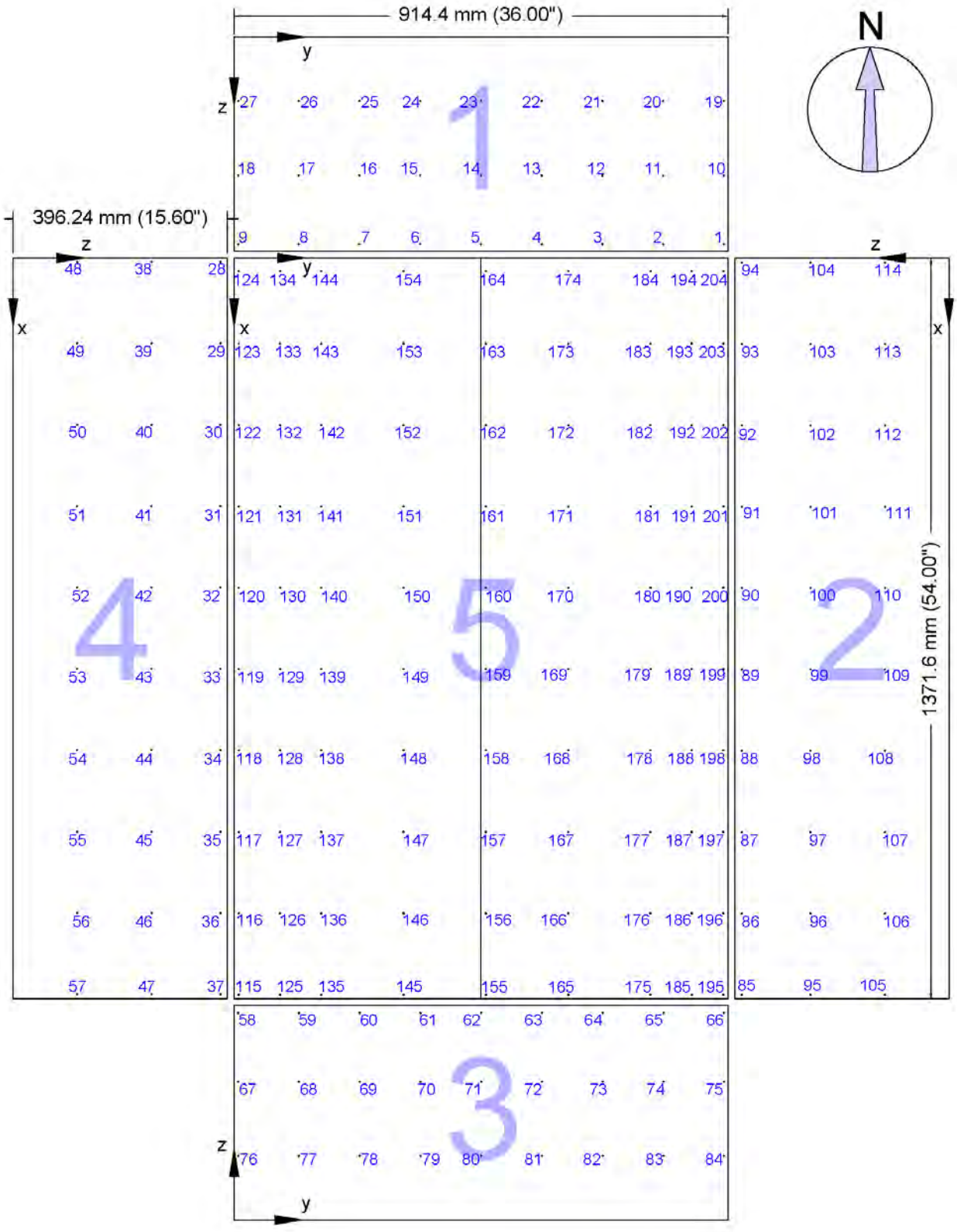

Figure B1-7 Geometrical and tap configuration for high-rise building C in a length scale of 1:100

SECTION 4
Codification Wind-induced Loads on Irregular Shaped Buildings Phase II

A Report Submitted to:
The State of Florida Division of Emergency Management

Prepared by:
Principal Investigator:
Ioannis Zisis, PhD (izisis@fiu.edu)
Manuel A. Matus (mmatu016@fiu.edu)

Department of Civil and Environmental Engineering
Florida International University
In Partnership with
The International Hurricane Research Center (IHRC)
Florida International University

July 30, 2021

Table of Contents

List of Figures

Executive Summary

Extreme wind events have been responsible for significant human and economic losses. The low-rise residential structures, which compose most of the built environment, have sustained considerable damages due to wind-induced loads. Current wind provisions presented (e.g. ASCE 7-16) provide design guidelines for low-rise structures, however, these guidelines are based on wind tunnel data performed in the late 70s with rectangular models results. Advancements in technology have led to the design of more complicated structures with uncommon shapes (identified as irregular shaped/plans). Several research investigations have studied the effect of plan irregularities on the overall pressure distributions; however, the majority have been aimed for mid-to high-rise structures, overlooking the most commonly used low-rise residential structures.

In previous DEM investigations, several irregular shapes were identified by observing a considerable number of satellite images of South Florida residential areas. It was concluded that the shapes varied significantly, however, C, L, T shapes were observed to be recurrent. During this investigation, a new shape with an S plan was identified. From these shapes, four irregular and one rectangular-shaped model of scales 1 to 100 were built. The rectangular model was built to be used as a benchmark for comparison with other available databases like NIST. Note that the models' ratios were different from the previous investigation and resembled square footage typically found on the field.

The models were tested in the new Atmospheric Boundary Layer Wind Tunnel (ABLWT) located in the Laboratory for Wind Engineering Research (LWERT) at Florida International University (FIU). This wind tunnel (of test section 6 by 8 feet in height, width, and 60 feet in overall length) was calibrated/configured to produce an open terrain with a z_0=0.01m where the models were tested at ~180mph full-scale wind speed from 0 to 345 degrees wind directions at 15 degrees increments. Pressure measurements were obtained from the 350+ pressure taps that the models were instrumented with, and pressure coefficients were obtained for generating contour plots and area-averaged envelope curves.

The research concluded that irregular-shaped structures may develop considerably more critical zones of suction in walls and roof sections due to the increased number of corners, making these building shapes more susceptible to wind-induced damages. A comprehensive database of wind pressures has been produced for the considered building geometries. The preliminary codification exercise shows that current wind provisions may also underestimate the wind loads on Irregular-shaped buildings. This work will be continued as more data from additional geometries become available that will add the necessary level of confidence.

1. Introduction

The US has been impacted by several natural disaster events which have caused substantial economic and human losses. Since 1980, 291 weather and climate disasters have occurred, and the overall cost of these events reaches 1.905 trillion dollars (NOAA, 2021). Of the entirety of the built environment, most of the residential structures fall under the category of low-rise structures and can be found in vast residential areas around US cities. Advancements in building, architectural, and construction techniques have resulted in structures having much more complicated shapes than rectangular and squared shapes. There have been several investigations on the effect of wind-induced loads on irregular shaped structures, however, the majority have focused on mid-to high-rise buildings overlooking the low-rise residential side (Shao et al., 2019, Uematsu et al., 1999, Stathopoulos et al., 1993, Mashalkar et al., 2015, Gomez et al., 2005, Lee et al., 2016, Souvik et al., 2014, Yi et al., 2016, Yi et al., 2017, Yi et al., 2020, Zhao et al., 2017).

The current wind load provisions (e.g. ASCE 7-16) are based on studies performed on regular-shaped buildings from 30+ years ago (Akins et al., 1977, Davenport et al., 1977 and Stathopoulos 1979). There are more recent databases (National Institute of Standards and Technology (NIST) and Tokyo Polytechnic University (TPU)) with better technological advancements to record and analyze data that engineers could utilize for the safe design of structures; however, these are also based on investigations performed on regular shaped structures (Ho et al., 2005 and Tamura et al., 2005).

Based on the above mentioned, it can be concluded that there is a need to further investigate the effect of wind on irregular-shaped low-rise structures to better understand their performance, better design them and thus significantly reduce the damages produced by extreme wind events. The current work completes the research carried out in the two previous projects funded in the 2019 and 2020 Florida DEM funding cycles. That work has identified three dominant irregular shapes via satellite imagery (i.e. T, L, and C). Further reconnaissance of aerial images allowed for the identification of S shapes, which also appears to be common, as can be seen in Figure 1 a) and b).

For this study, five different models of the 1:100 scale (with different length to width ratios than previous years) were constructed. The shapes were T, C, L, S, and a Rectangular (R) model (to be used as a baseline). These models were tested in the new atmospheric boundary layer wind tunnel (ABLWT) in the Laboratory for Wind Engineering Research (LWER) located at Florida International University (FIU).

a)

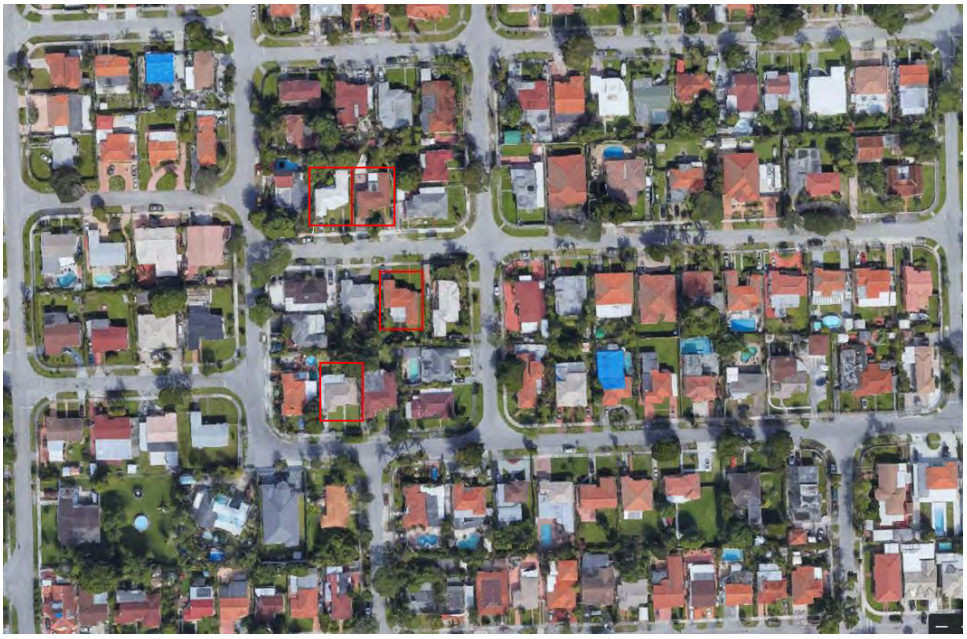

b)

Figure 1: Aerial photo from the Miami area (photo was taken using Google Maps)

2. Facility and Experimental Procedure

2.1. Wind Tunnel

The tests were carried out in the newly constructed Atmospheric Boundary Layer Wind Tunnel (ABLWT) in the Laboratory for Wind Engineering Research (LWER), located at Florida International University (FIU), Figure 2. The wind tunnel has a test section of 8 feet wide by 6 feet high and 60 feet overall length (Matus et al., 2021). This wind tunnel is made up of different sections like a) Fans, b) Wide-

angle Diffuser, c) Settling Chamber, d) Contraction, e) Fetch and f) Turntable section (Figure 3 to Figure 7). The turntable, placed downwind of the wind tunnel, allows for housing the models and testing them in different wind directions, see Figure 8. The spires and roughness elements can be manually adjusted to achieve the desired exposure (open, suburban, or urban), see Figure 9 and Figure 10. The configuration chosen for the spires and roughness elements were adjusted to reproduce an open terrain profile with z_0=0.01m and the scale of the models was set to 1:100.

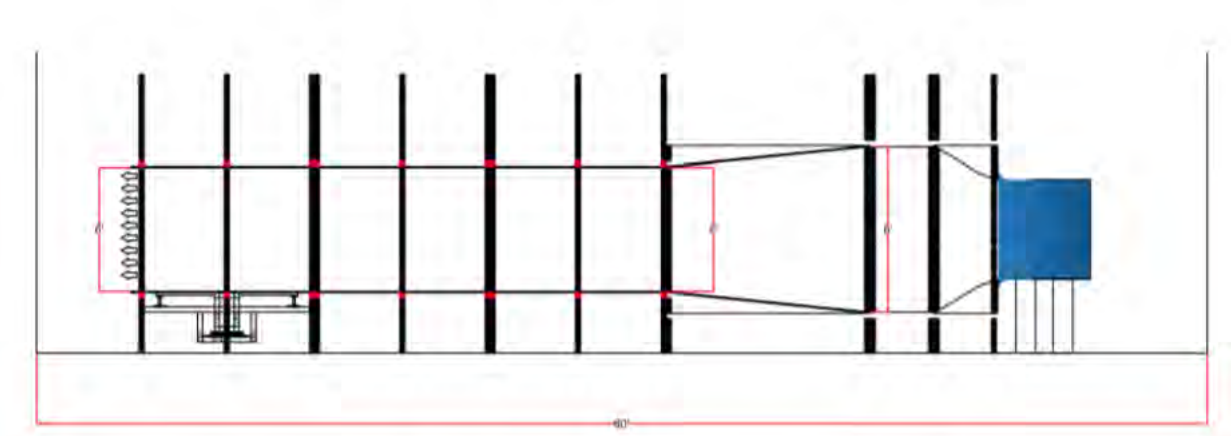

Figure 2: ABL flow generation mechanism schematic for the ABLWT

Figure 3. Fans section

Figure 4. Wide-angle diffuser section

Figure 5. Settling chamber section

Figure 6. Contraction section

Figure 7. Fetch and turntable sections

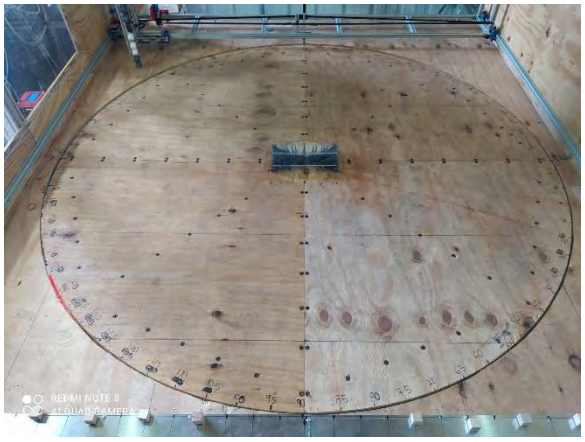

Figure 8: Turntable

Figure 9: Spires

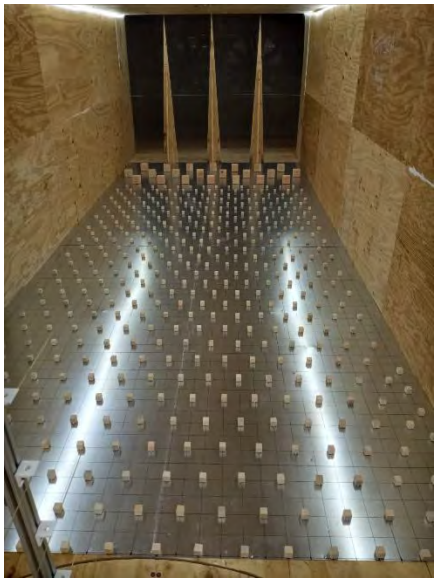

Figure 10: Roughness elements

2.2. Flow Simulation

The wind field was calibrated to represent an open terrain with roughness exposure of z_0=0.01m. To measure the wind characteristics of the ABLWT, twelve Cobra Probes were installed at the center of the turntable at heights 1.5, 3, 4.5, 8, 10, 12, 14, 16, 20, 22, 24, and 26 inches from the ground. The reference height used for generating the profiles was 26 inches and the mean roof height of the models was approximately 1.5 inches. From the Cobra Probes, it was observed that the wind field mean wind speed had a good agreement with the Engineering Science Data Unit (ESDU) 1:100 scale profile, and the same was observed for the turbulence intensity (I_u) profile, as shown in Figure 11 (ESDU, 2001). The Power Spectrum Density (PSD) profile provides valuable information on the capacity of the wind tunnel to reproduce all the eddies sizes naturally produced in the wind, and this can be seen in Figure 12, where power along the frequency domain is matching with the expected full-scale values.

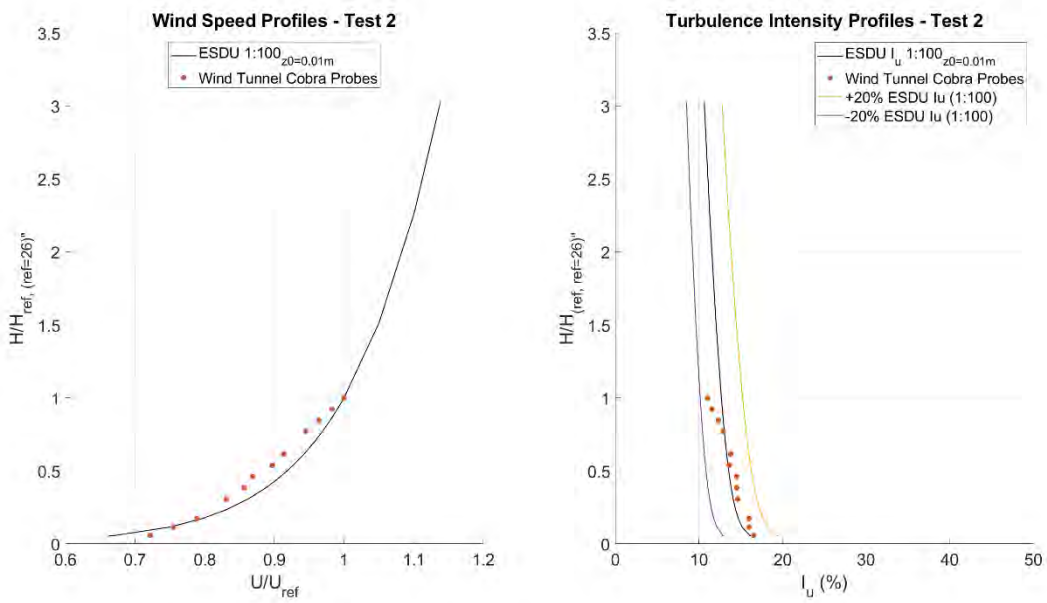

Figure 11. Wind and turbulence intensity (U and Iu) profiles

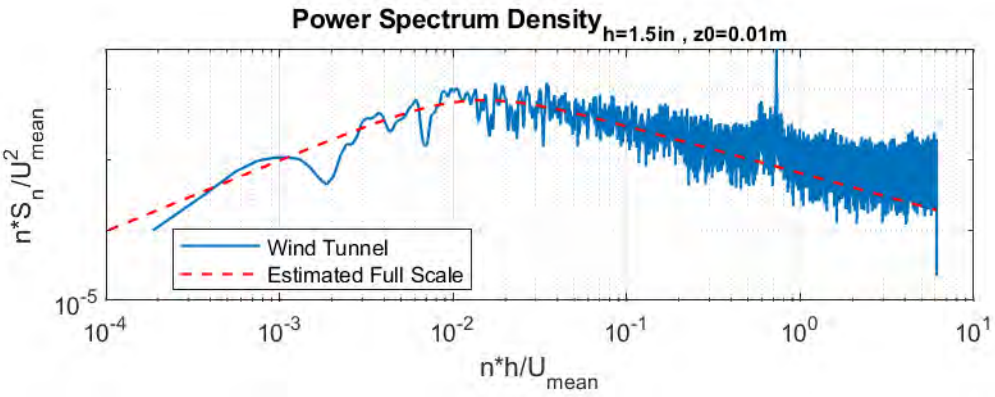

Figure 12. Power spectrum density profile

2.3. Models Description

For this investigation, five different models were identified, designed, and built. The models were designed to be as realistic as possible and to match those found in real communities. The footprints were made to represent a residential home of approximately 1000 – 1600 square feet, except from the rectangular model which was a replica of the NIST database model and was used as a baseline (Ho et al.,

2005). The irregular-shaped models were 3D printed with Fused Deposition Modeling (FDM) equipment while the rectangular model was built out of 3/8” thick plexiglass parts cut with a CNC machine.

The layout of each model (front, topside, and elevation views) are shown in Figure 13 to Figure 17. Please note dimensions are in full scale. Models T, L, C, S, and R were instrumented with 331, 333, 363, 367, and 330 pressure taps.

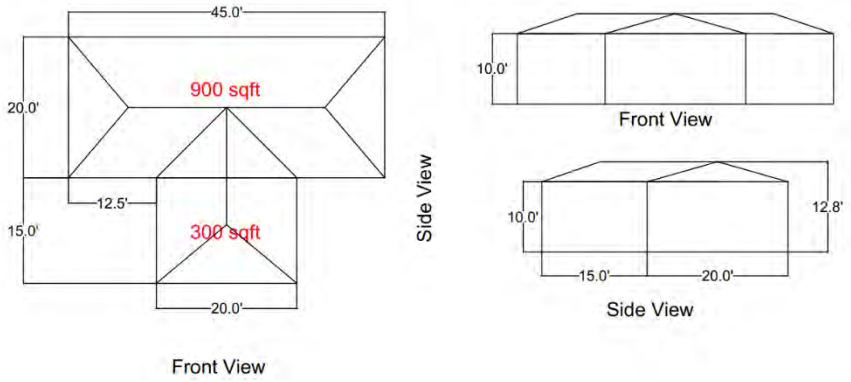

Figure 13. Model T (layouts)

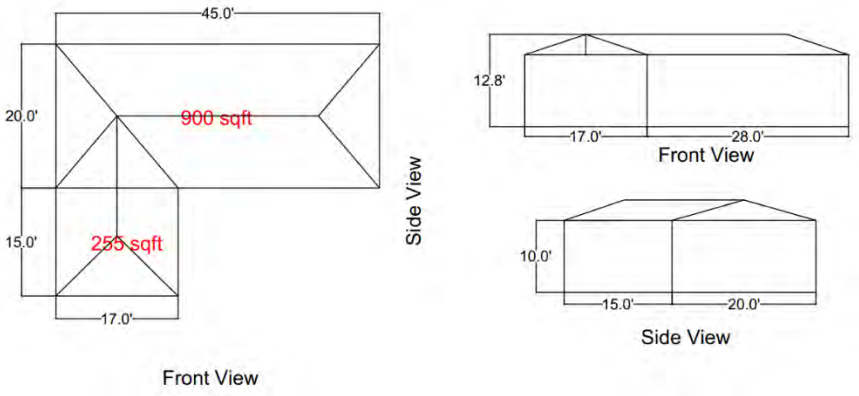

Figure 14. Model L (layouts)

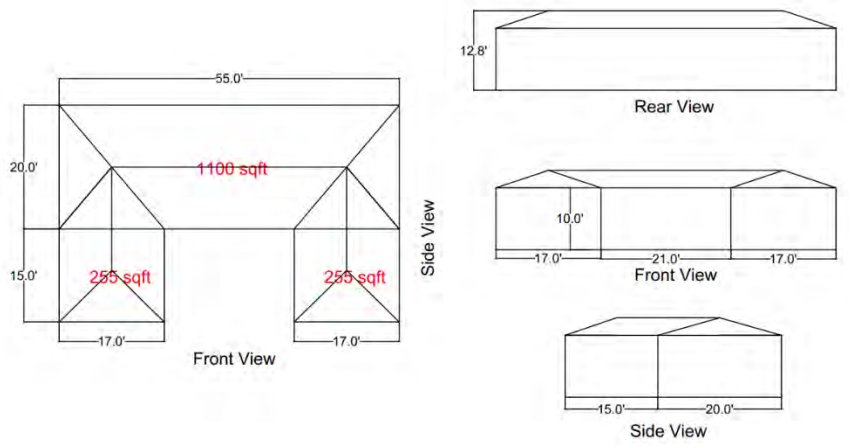

Figure 15. Model C (layouts)

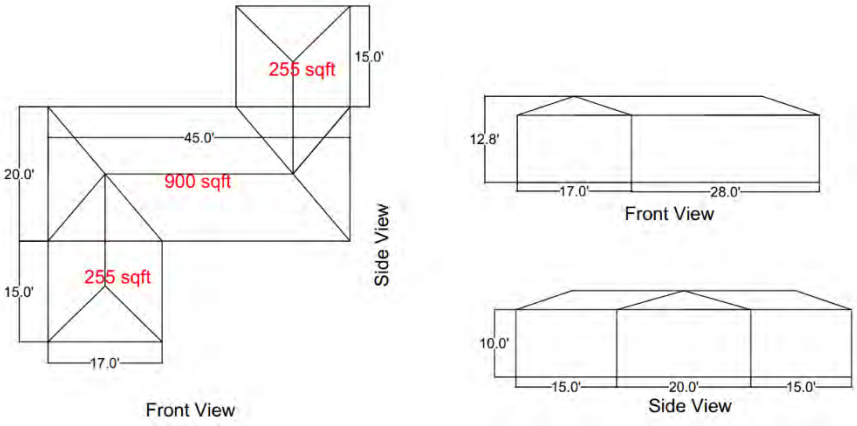

Figure 16. Model S (layouts)

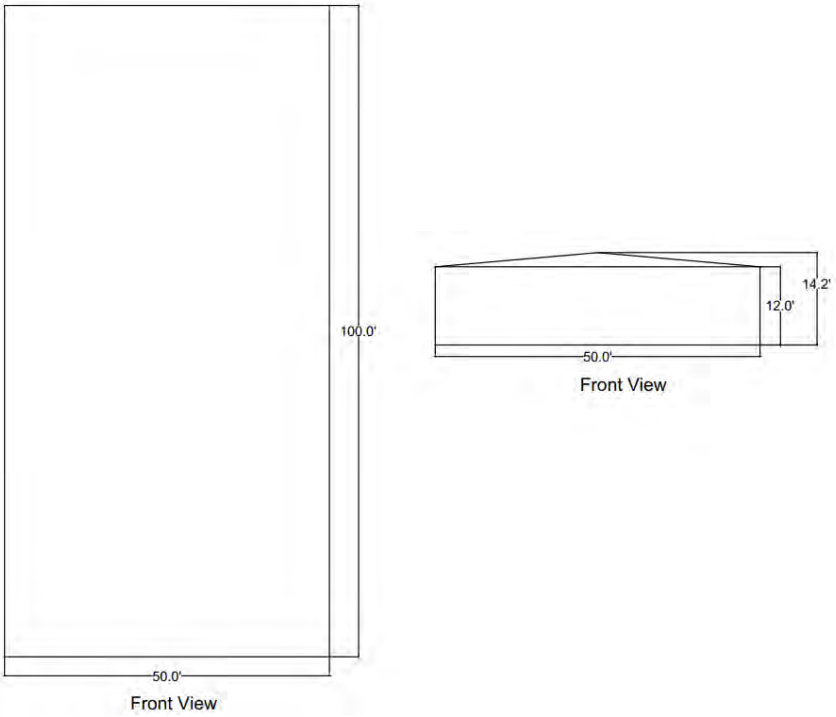

Figure 17. Model R (layouts)

2.4. Test Protocol

All five models were tested at the ABLWT at 50% throttle, which provides a mean wind speed in a free stream of approximately 20 mph. The models were tested for a 1-minute duration from 0 to 345 degrees at every 15 degrees wind direction increment (as shown in Figure 18). The Scanivalve system, used to record the pressures of each pressure tap, was set to collect the data at 520 Hz sampling frequency. The raw data was applied a transfer function to account for the distortion produced by the tubing length (Irwin et al., 1979).

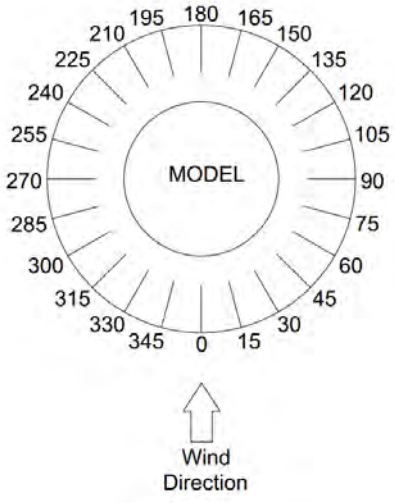

Figure 18. Wind directions

2.5. Pressure Coefficients

The results presented in this report are in the form of mean and peak pressure coefficients. The pressure coefficient, C_P, is a dimensionless number that describes the relative pressures acting on the surfaces of the models. Such a dimensionless result allows the transfer of experimental results to full scale as well as comparisons to wind standards and other available databases.

The formula for the pressure coefficient is as follow:

$$C_p = \frac{p - p_0}{\frac{1}{2}\rho V^2} \quad (1)$$

Where, $p - p_0$ is the pressure (obtained from the Scanivalve) readings and is the pressure difference between the static pressure and the pressure read by the pressure taps. The dynamic pressure is $\frac{1}{2}\rho V^2$, where ρ is air-density and V is wind-speed. For simplicity, the units were manipulated to end

up with a simpler equation that would require inputting the pressure difference in $^{lb}/_{ft^2}$ and the wind speed in miles per hour (mph). The formula for this is then:

$$C_p = \frac{p - p_0}{0.002556\, V^2} \tag{2}$$

The wind speed used as V is wind speed obtained from wind speed measurements obtained from the cobra probe installed at mean roof height (that is 1.5" height).

For the mean pressure coefficient, the mean wind speed was used, for what the formula would then become:

$$C_{p,mean} = \frac{p - p_0}{0.002556 V_{mean}^2} \tag{3}$$

The 3-sec peak pressure coefficients were obtained using the Best Linear Unbiased Estimate (BLUE) extreme value analysis. This method estimates extreme values for negative and positive pressures applied to n epochs. Extremes were estimated for probabilities of non-exceedance P1, which was set to 76%, while n was set to 100 (Cook et al., 1985). A MATLAB code has been developed by NIST and it is available for public use.

3. Results

3.1. NIST vs ABLWT

To validate the experimental procedures in the newly developed wind tunnel, the rectangular model results obtained from the ABLWT were compared/validated against a NIST database rectangular model. The rectangular model built at the ABLWT was an exact copy of a NIST database model (of 1:100 scale), but the pressure tap layout was varied. It must be noted that the model taken from the NIST database was identified as Test 3 in the report (Ho et al., 2005).

For comparison, a line of pressure taps was selected; i.e. the line of pressure taps bisected the model in half from the windward wall, roof, and leeward roof (red line in Figure 19). For the validation, the mean and peak (maximum and minimum) Cp_s were plotted. The x-axis represents the location (in full-scale dimensions) of each pressure tap along the total length of the bisecting line, where the origin is located at the base of the windward wall. Results obtained show good agreement for both mean and peak pressure coefficients between the NIST and ABLWT models (Figure 20 to Figure 22). At 90 degrees, there is a small variation between the models' peak pressure coefficients, and this may be due to the location of the pressure taps along the red bisecting line from the ridge of the model as well as surface roughness length differences (Stathopoulos, 1982; Tieleman, 1992).

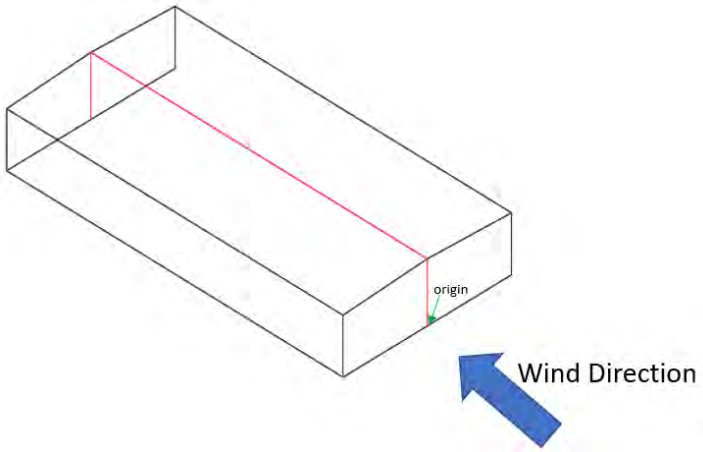

Figure 19. NST vs ABLWT pressure taps line of comparison

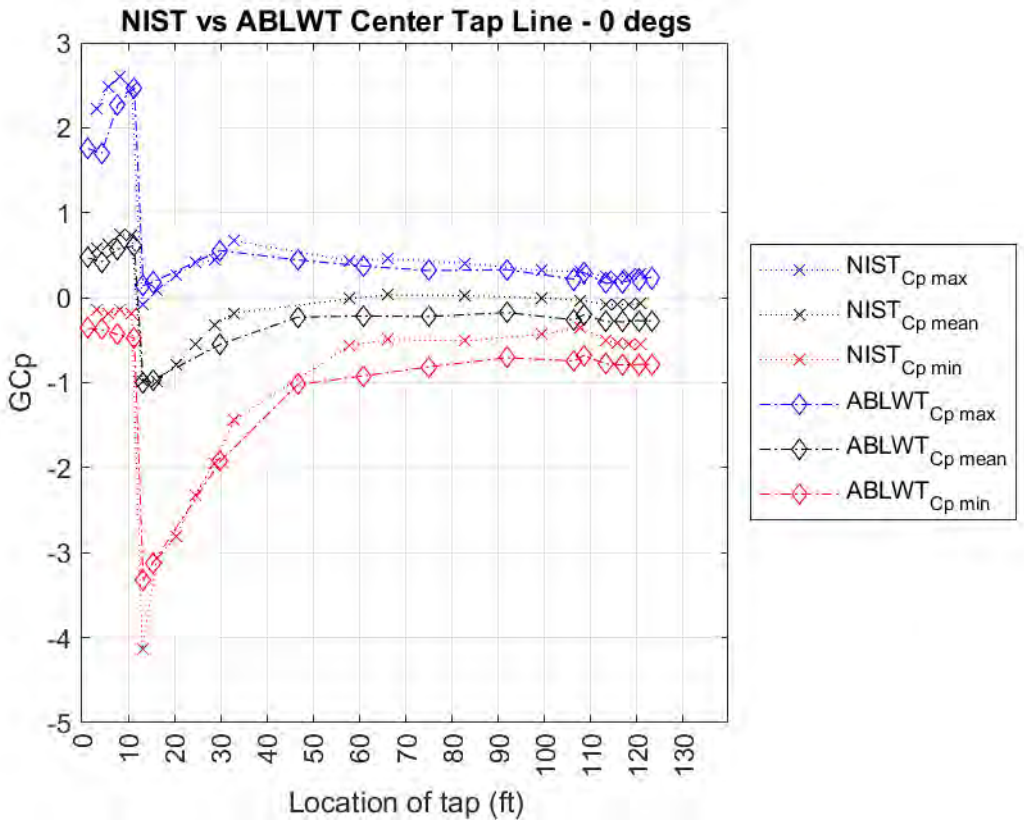

Figure 20. Comparison at 0 degrees

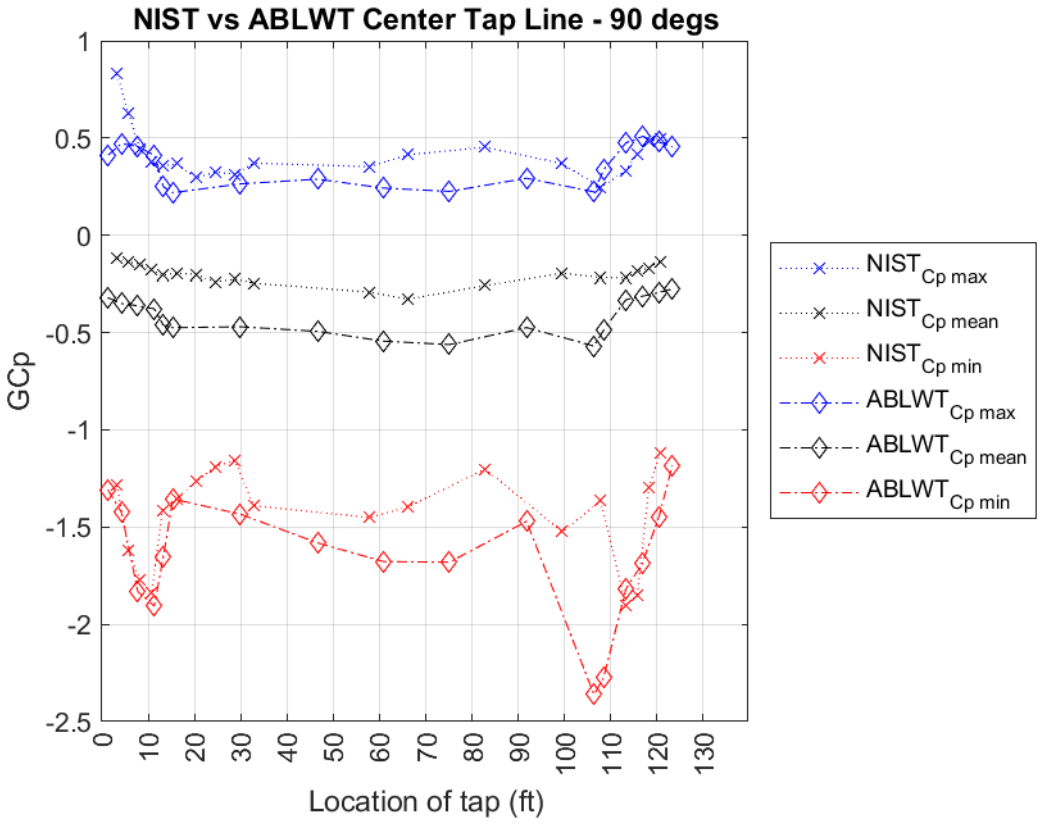

Figure 21. Comparison at 90 degrees

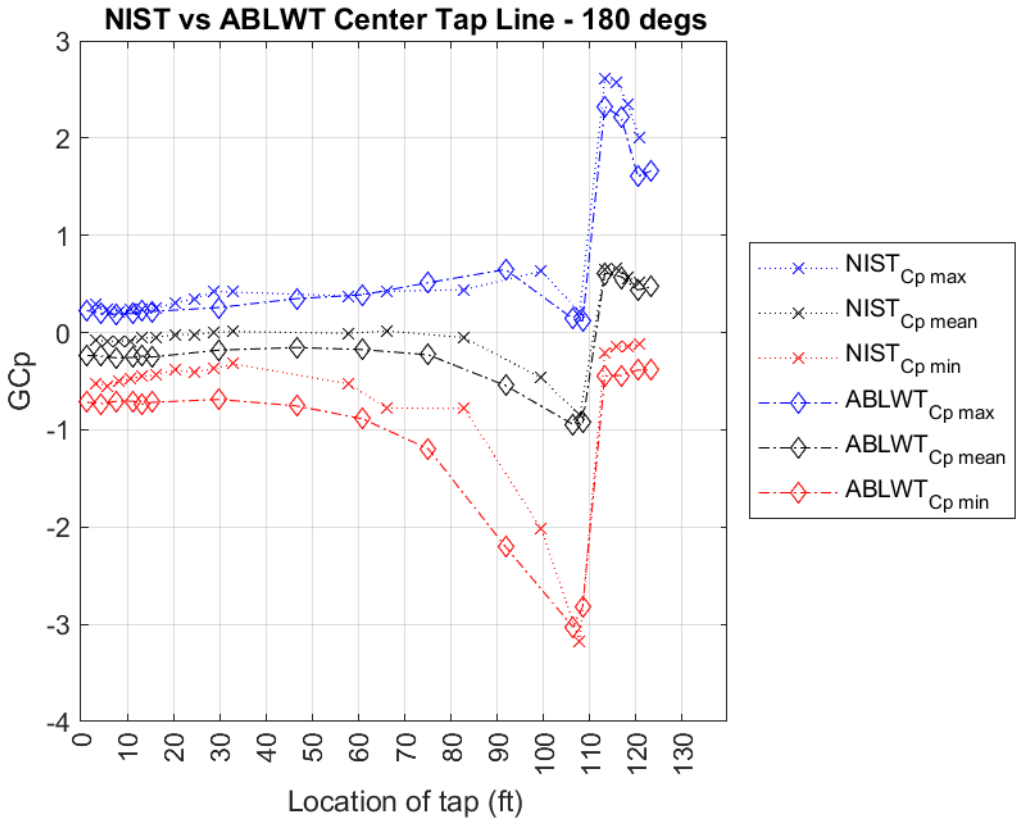

Figure 22. Comparison at 180 degrees

3.2. Mean Pressure Coefficients

The mean pressure coefficients at 0-degree wind direction, for models T, L, C, and S, are presented in Figure 23 to Figure 26. Contour plots for the rest of the wind directions can be found in the Appendix A section.

3.2.1. Model T

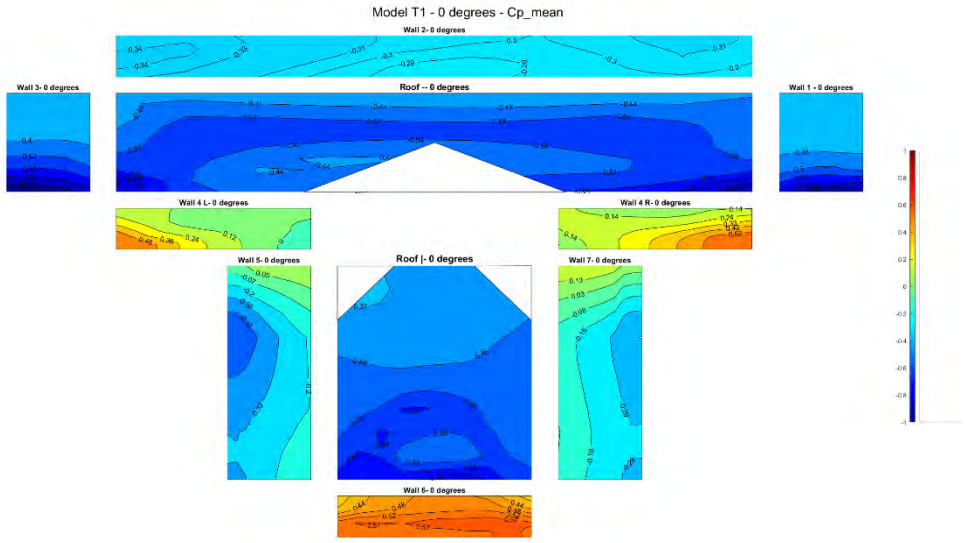

Figure 23. Cp mean at 0 degrees for model T

3.2.2. Model L

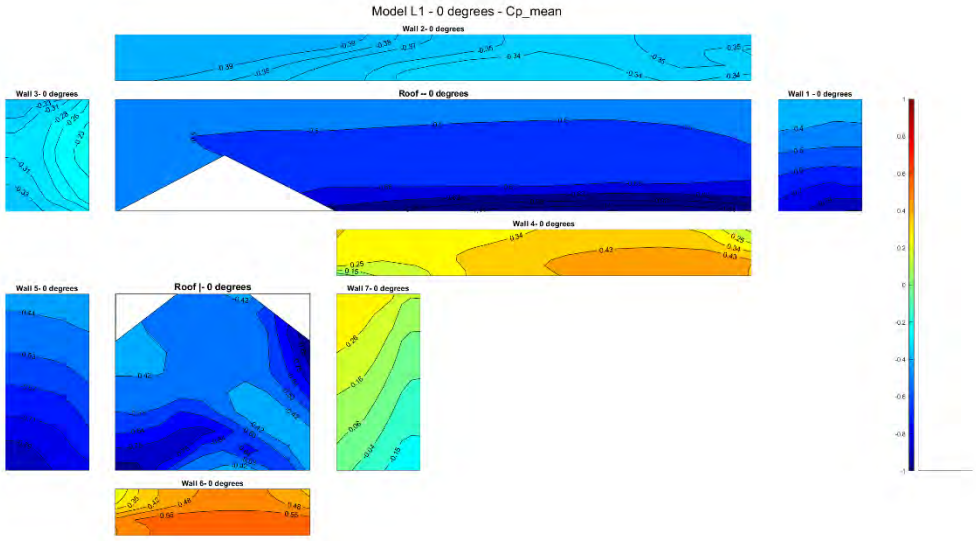

Figure 24. Cp mean at 0 degrees for model L

3.2.3. Model C

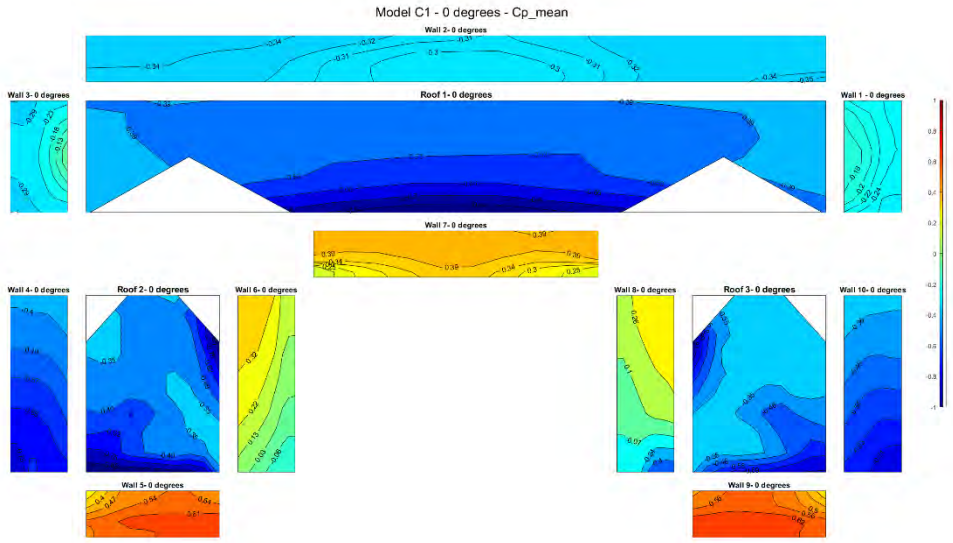

Figure 25. Cp mean at 0 degrees for model C

3.2.4. Model S

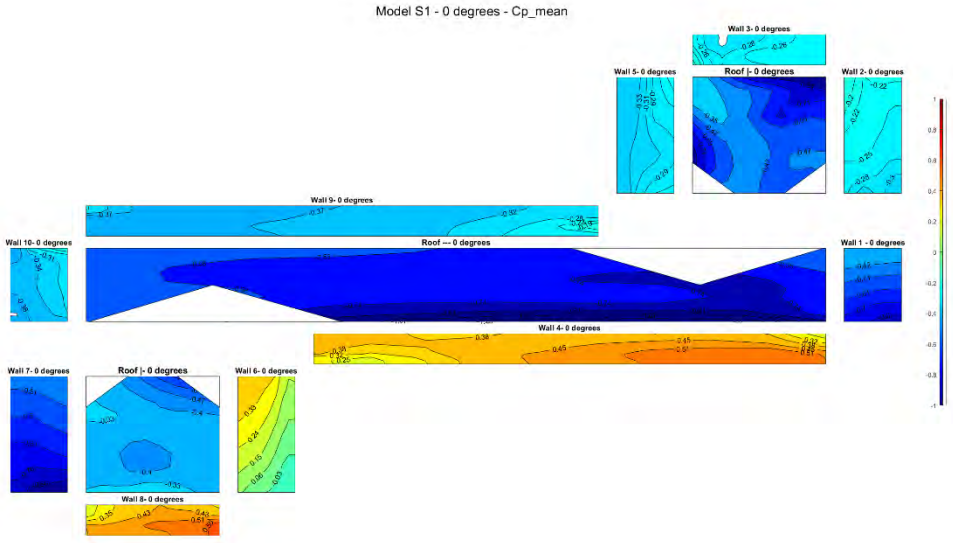

Figure 26. Cp mean at 0 degrees for model S

3.3. Critical Peak Pressure Coefficients

The 3-sec critical peak pressure coefficients, $C_{P\text{-}3sec,\ max}$ and $C_{P\text{-}3sec,\ min}$, were calculated using the Best Linear Unbiased Estimator (BLUE) method analysis (Lieblein, 1974). These values were obtained for each pressure tap of all models at all wind angles of attack. The highest value for each pressure tap, among all the wind angles of attack, was identified and a contour plot was generated for both, maximum and minimum C_P (see Figure 27 to Figure 34). It must be noted that the peak pressure coefficients were obtained from the pressure coefficients calculated using the 3-seconds averaged wind velocity. The minimum peak Cp contour plots at each wind direction are presented in Appendix B.

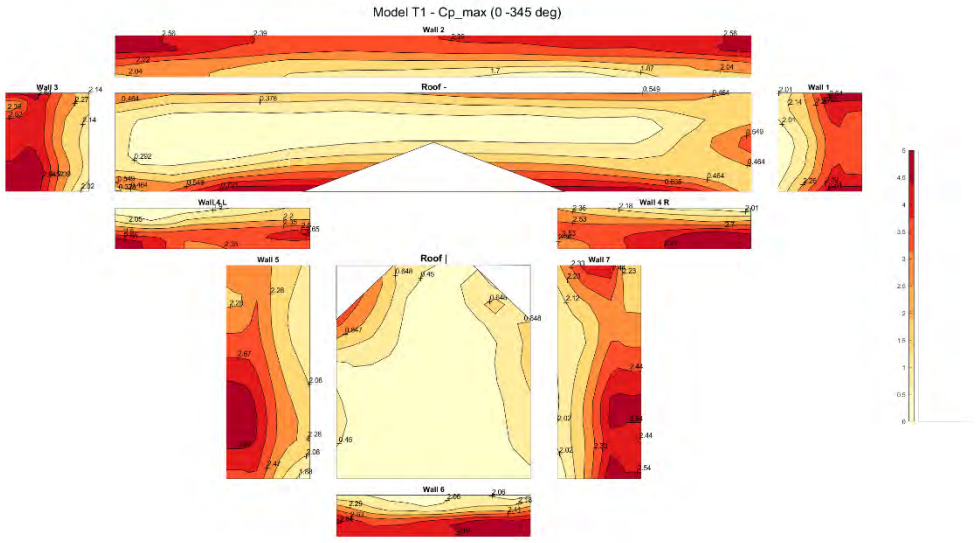

Figure 27. Maximum peak Cp for model T

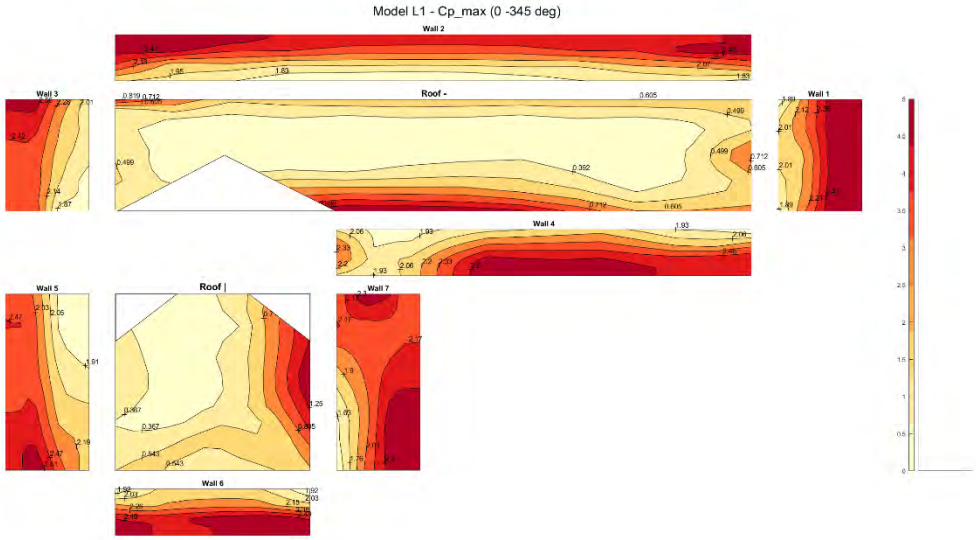

Figure 28. Maximum peak Cp for model L

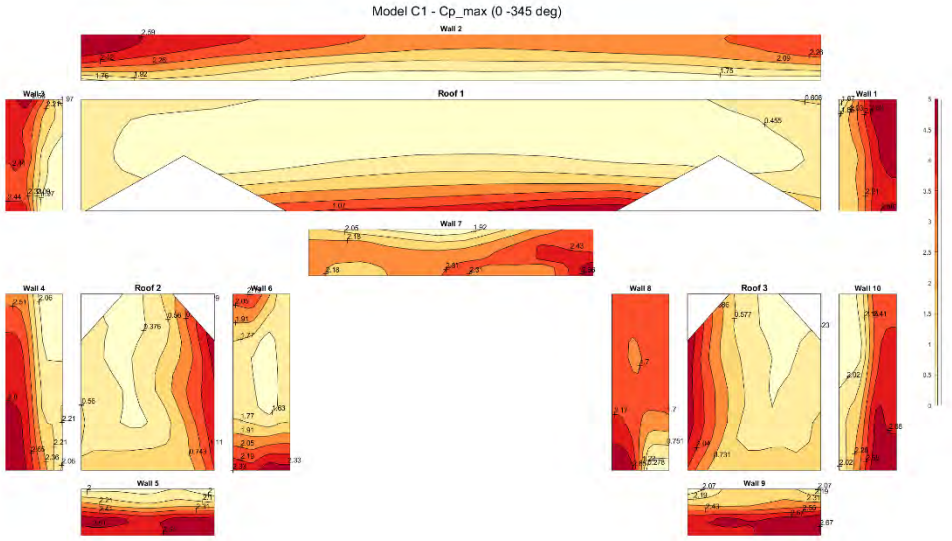

Figure 29. Maximum peak Cp for model C

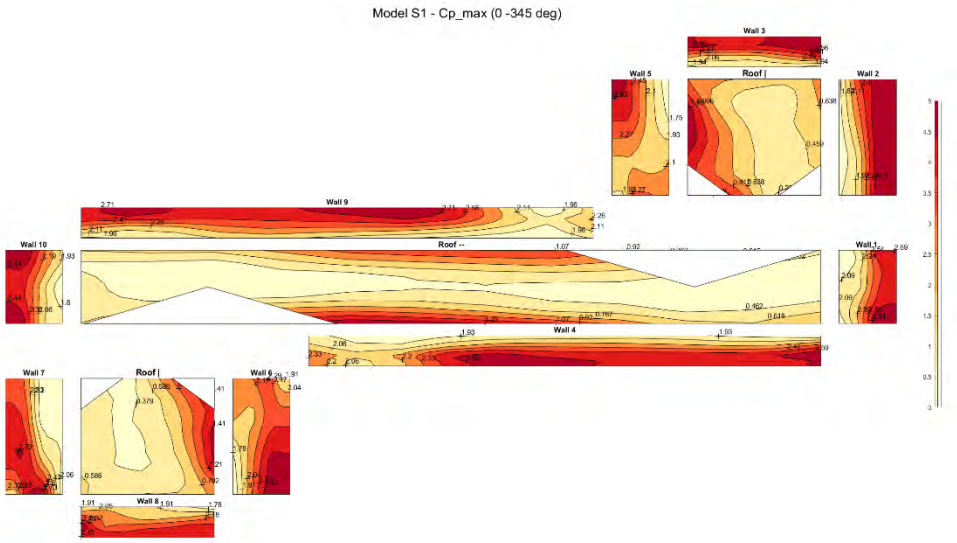

Figure 30. Maximum peak Cp for model S

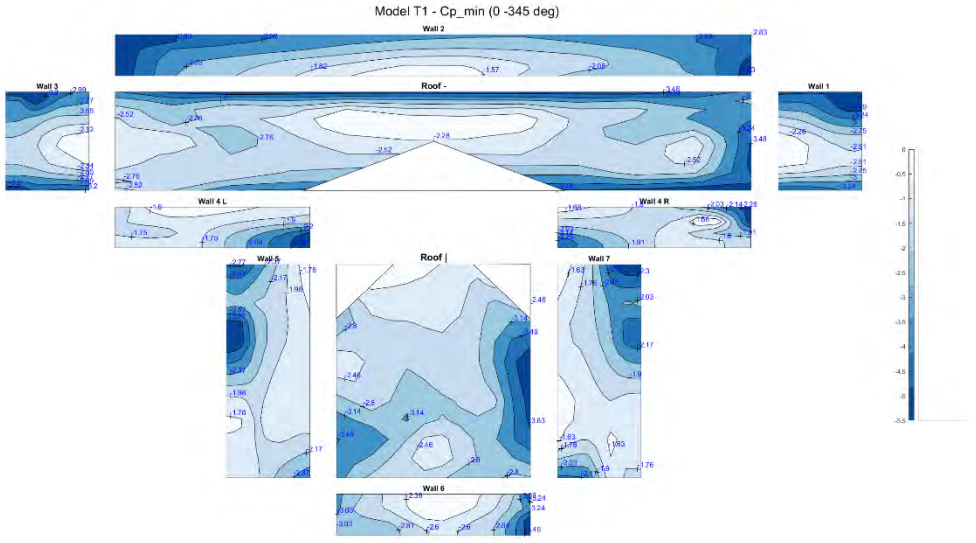

Figure 31. Minimum peak Cp for model T

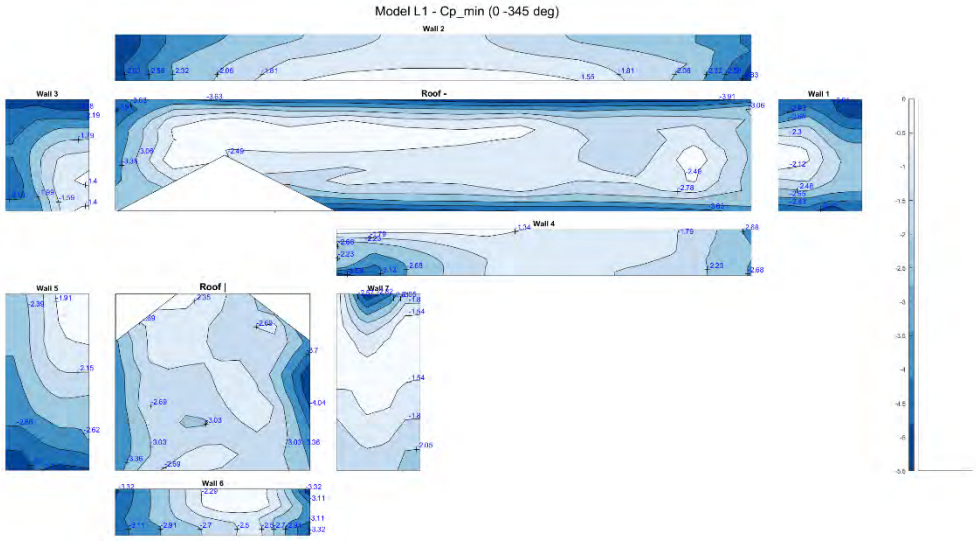

Figure 32. Minimum peak Cp for model L

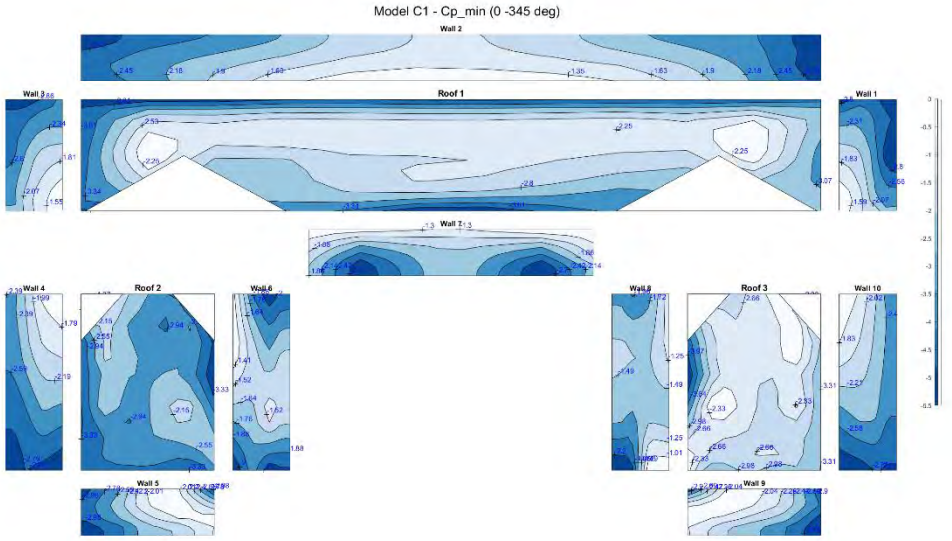

Figure 33. Minimum peak Cp for model C

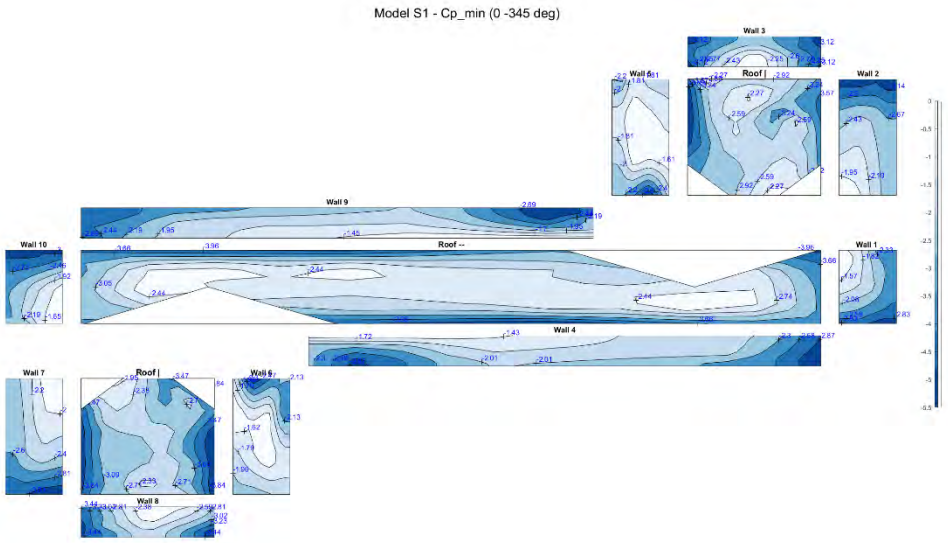

Figure 34. Minimum peak Cp for model S

3.4. Area Averaging

The generation of area-averaged graphs was obtained by using the critical peak pressure coefficients by finding different combinations of pressure-tap tributary areas. The combinations were obtained using areas as small as a single pressure tap to multiple pressure taps. The first step was to create matrices that would include all the possible combinations of all the pressure taps for the sections being compared. The summation of the product of the pressure-tap pressure coefficients and the tributary area, of the selected combination, was obtained to be divided by the total tributary area. The equation below was used:

$$Area\ Averaged\ C_p = \frac{\sum_1^i C_{pi} * A_i}{\sum_1^i A_i} \qquad (4)$$

With the above equation, the area-averaging scatter plot was generated. It must be noted that all areas are reported as full-scale. Also, to be able to compare the research findings to the current wind provisions, the pressure coefficients in this section were obtained using the 3-second wind speed.

3.5. Codification Process

To codify the area averaging graphs shown in the previous section, the graphs were modified to have a logarithmic measure of surface area (x-axis) and thus have the same format provided in ASCE 7. In the current wind provisions, the envelope graphs are provided for different zones of the walls and roof (Figure 35 and Figure 36), while in these experimental results all zones are included in one single line/graph, which is one graph for wall and one graph for the roof surfaces (see Figure 37 and Figure 38). After the properties of the graphs were matched, the graphs were divided into three different parts: for walls, the envelope

curves range from 1 to 10 ft^2, from 10 to 500 $ft^{2,}$ and from 500 to 1000 ft^2 (for positive and negative pressure coefficients) and for the roof they range from 1 to 2 ft^2, from 2 to 100 ft^2, from 100 to 1000 ft^2 (for the positive pressure coefficients), from 1 to 10 ft^2, from 10 to 100 ft^2 and from 100 to 1000 ft^2 (for the negative pressures). It should be noted that the enveloping of the experimental data is more effective when a very high number of building models has been tested. In this section, the envelope curves were generated following a similar approach to the one presented in Stathopoulos (1979). Please note that the below-presented envelope curves should not be considered conclusive and should be treated as preliminary cases for comparison purposes only.

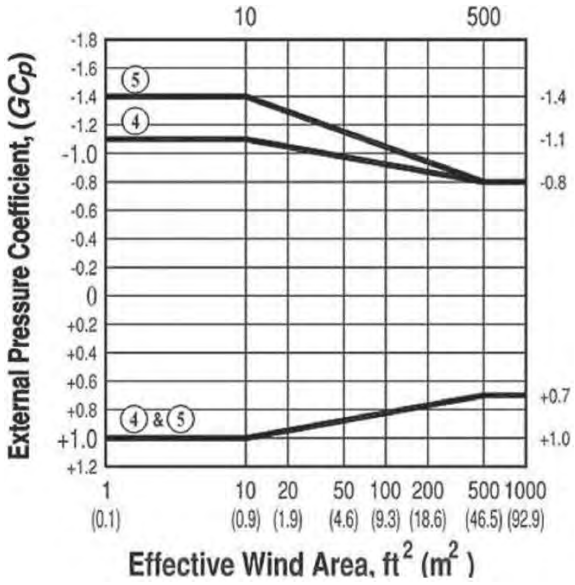

Figure 35: External Pressure Coefficient (GCp) - Walls (ASCE 7-16)

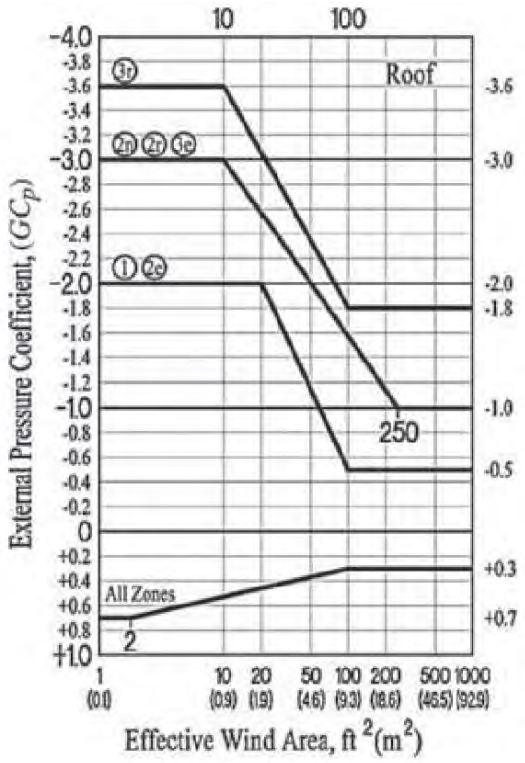

Figure 36: External pressure coefficients (GCp) - Roof (ASCE 7-16)

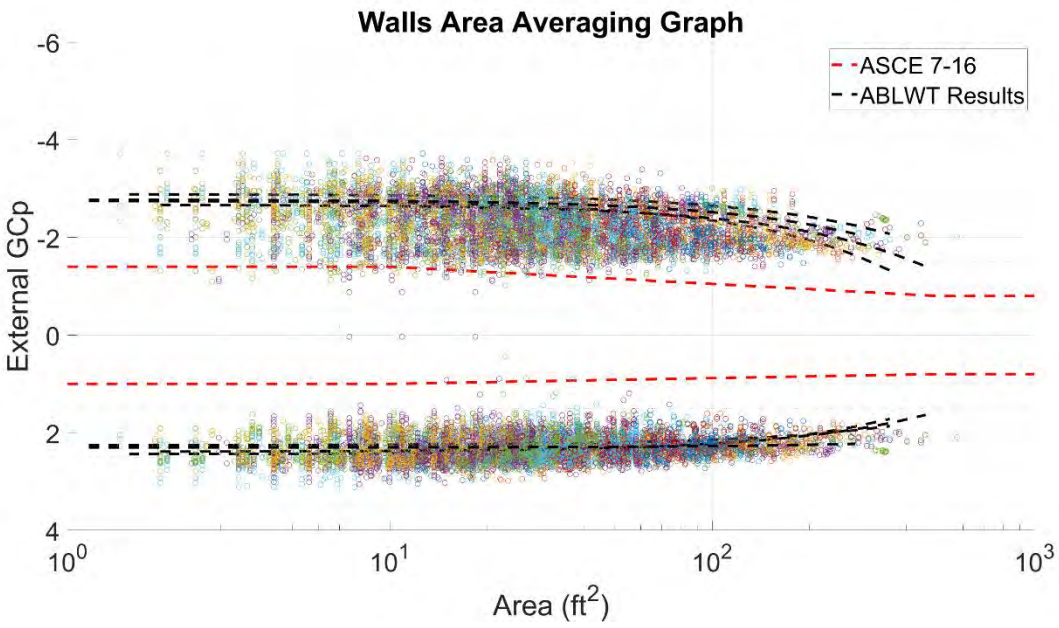

Figure 37: Codification graph for walls

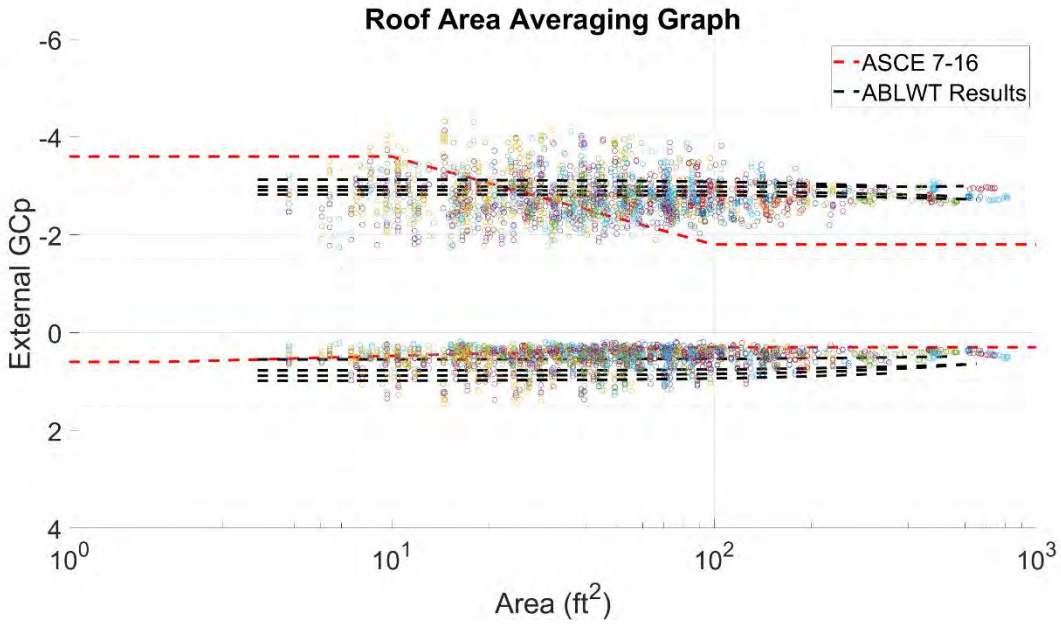

Figure 38: Codification graph for roofs

4. Conclusions

Extreme wind events have caused substantial damages to civil engineered structures, especially on the residential side. Investigations have been performed to better understand the effect of wind-induced forces on structures and provide better design criteria. The current wind load provisions provide design guidelines; however, these are based on wind tunnel investigations that used regular-shaped structures that are no longer representative of the average single-family home. Most of the research that is relevant to this topic considered mostly mid-and high-rise buildings leaving a lot of unanswered questions on the wind-induced performance of irregular-shaped low-rise buildings.

This investigation performed wind tunnel testing on four low-rise irregular-shaped structures. The shapes were T, L, C, and S and were identified via satellite imagery of South Florida residential areas. A rectangular model was built to be used as a baseline against previous databases (e.g. NIST) and results provided a good agreement between the tested models and the NIST database model. Mean and peak pressure coefficients contour plots were generated for all models, resulting in the very first wind load database for irregular-shaped buildings. Moreover, a lot of critical information on high suction zones can be extracted from these results which might assist in reducing the wind-induced damage on low-rise buildings of more complex shapes.

One of the most important outcomes of this newly established pressure database is the potential to use the data for codification purposes. Design guidelines provide envelope curves that can be used for the design of different building components and cladding (C&C). Thus, the findings from the current work were used to develop ASCE 7 type envelope curves. These preliminary comparisons revealed that the current wind provisions may underestimate the pressures on irregular-shaped structures but more geometries and shapes are needed to increase the confidence in this codification process

Acknowledgments

Special thanks to the Florida Division of Emergency Management (FDEM) for funding this research project and to the laboratory for Wind Engineering Research (LWER) team for the guidance and support during the pre-testing, testing, and post-testing activities required for the execution of this research project.

References

Akins, R. E., Peterka, J. A., and Cermak, J.E. 1977. “Mean force and moment coefficients for buildings in turbulent boundary layers.” Journal of Wind Engineering and Industrial Aerodynamics. 2 (3): 195–209. https://doi.org/10.1016/0167-6105 (77)90022-8.

American Society of Civil Engineers (ASCE). 2016. ASCE Standard, Minimum Design Loads for Buildings and Other Structures, ASCE.

Cook, N.J. 1985. "The designer's guide to wind loading of building structures." British Research Establishment 1985 Table C3, vol. Part 1, pp. 321-323.

Davenport, A. G., Surry, D. and Stathopoulos, T. 1977. “Wind loads on low-rise buildings: Final report of phases I and II, parts 1 and 2”. BLWT Rep. No. SS8-1977. London, ON, Canada: University of Western Ontario.

ESDU 85020. 2001. Characteristics of atmospheric turbulence near the ground Part II: single point data for strong winds (neutral atmosphere).

Gomes, M.G., Rodrigues, A.M., and Mendes, P. 2005. "Experimental and numerical study of wind pressures on irregular-plan shapes." Journal of Wind Engineering and Industrial Aerodynamics, Volume 93, Issue 10, October 2005, Pages 741-756. https://doi.org/10.1016/j.jweia.2005.08.008.

Ho, T. C. E., D. Surry, D. Morrish, and Kopp, G.A. 2005. “The UWO contribution to the NIST aerodynamic database for wind loads on low buildings. Part 1: Archiving format and basic aerodynamic data.” Journal of Wind Engineering and Industrial Aerodynamics. 93 (1): 1–30. https://doi.org/10.1016/j.jweia .2004.07.006

Irwin, P., Cooper, K.R., and Girard, R. 1979. "Correction of distortion effects caused by tubing systems in measurements of fluctuating pressures." Journal of Wind Engineering and Industrial Aerodynamics, Volume 5, Issues 1–2, October 1979, Pages 93-107. https://doi.org/10.1016/0167-6105(79)90026-6.

Lee, Y.T., Boo, S.L., Lim, H.C., Misutani, K. 2016. “Pressure distribution on rectangular buildings with changes in aspect ratio and wind direction.” Wind and Structures. Vol. 23, No. 5 (2016) 465-483. http://dx.doi.org/10.12989/was.2016.23.5.465.

Lieblein, J. 1974. “Efficient methods of extreme-value methodology.” Technical Analysis Division, Institute for Applied Technology, National Bureau of Standards. Final Report NBSIR 74-602.

Mashalkar B.S., Patil, G.R., and Jadhav, A.S. 2015. "Effect of plan shapes on the response of buildings subjected to wind vibrations." IOSR Journal of Mechanical and Civil Engineering (IOSR-JMCE), e-ISSN : 2278-1684, p-ISSN : 2320–334X, p. 80-89.

Matus, M., Mostafa, K., Sarma, H., Schwartz, B., Zisis, I. 2021. “Design and development of a new boundary layer wind tunnel at Florida International University.” 6th American Association for Wind Engineering Workshop. Clemson, SC.

NOAA National Centers for Environmental Information (NCEI) U.S. Billion-Dollar Weather and Climate Disasters. 2021. https://www.ncdc.noaa.gov/billions/, DOI: 10.25921/stkw-7w73.

Shao, S., Tian T., Yang Q.S., Stathopoulos, T. 2019. “Wind-induced cladding and structural loads on low-rise buildings with 4:12-sloped hip roofs.” Journal of Wind Engineering and Industrial Aerodynamics, Volume 193, October 2019, 103948. https://doi.org/10.1016/j.jweia.2019.103948.

Souvik, C., Sujit, K.D., and Ashok, K.A. 2012. "Wind load on irregular plan shaped tall building - a case study." Wind and Structures, Volume 19, Number 1, July 2014, pages 59-73. http://dx.doi.org/10.12989/was.2014.19.1.059.

Stathopoulos, T. 1979. “Turbulent Wind Action on Low Rise Buildings.” Ph.D. Thesis, The University of Western Ontario, London, Ontario, Canada.

Stathopoulos, T. 1982. “Wind loads on low-rise buildings: a review of the state of the art.” Centre for building studies, Concordia University, Montreal, Quebec, Canada.

Stathopoulos, T., Zhou, Y. 1993. "Computation of wind pressures on L-shaped buildings." Journal of Engineering Mechanics, Vol. 119, Issue 8 (August 1993). https://doi.org/10.1061/(ASCE)0733-399(1993)119:8(1526).

Tamura, Y., Kareem, A., Solari, G., Kwok, K., Holmes, J.D., and Melbourne, W.H. 2005. “Aspects of the dynamic wind-induced response of structures and codification”. Wind Structures. 8 (4): 251–268. https://doi .org/10.12989/was.2005.8.4.251.

Tieleman, H.W. 1992. “Problems associated with flow modeling procedures for low-rise structure.” Journal of Wind Engineering and Industrial Aerodynamics, Volume 42, Issues 1–3, October 1992, Pages 923-934. https://doi.org/10.1016/0167-6105(92)90099-V.

Uematsu, Y. and Isyumov, N. 1999. "Wind Pressures Acting on Low-rise Buildings." Journal of Wind Engineering and Industrial Aerodynamics, Volume 82, Issues 1–3, August 1999, Pages 1-25. https://doi.org/10.1016/S0167-6105(99)00036-7.

Yi L., Duan, R.B., Li, Q.S., Li, Y.G., Li. C. 2020. “Research on the characteristics of wind pressures on L-shaped tall buildings.” Advances in Structural Engineering. http://dx.doi.org/10.1177/1369433220906934.

Yi L., Li, Q.S. 2016. “Wind-induced response-based optimal design of irregular-shaped tall buildings.” Journal of Wind Engineering and Industrial Aerodynamics. 155 (2016) 1978-207. http://dx.doi.org/10.1016/j.jweia.2016.06.001.

Yi L., Li, Q.S., Chen, F. 2017. “Wind tunnel study of wind-induced torques on L-shaped tall buildings.” Journal of Wind Engineering and Industrial Aerodynamics. 167 (2017) 41-50. http://dx.doi.org/10.1016/j.jweia.2017.04.013.

Zhao, D.X., He, B.J. 2017. “Effects of architectural shapes on surface wind pressure distribution: Case studies of oval-shaped tall buildings”. Journal of Building Engineering. 2017. 12 (2017) 219-228. http://dx.doi.org/10.1016/j.jobe.2017.06.009.

Appendix A: Average Pressure Coefficients

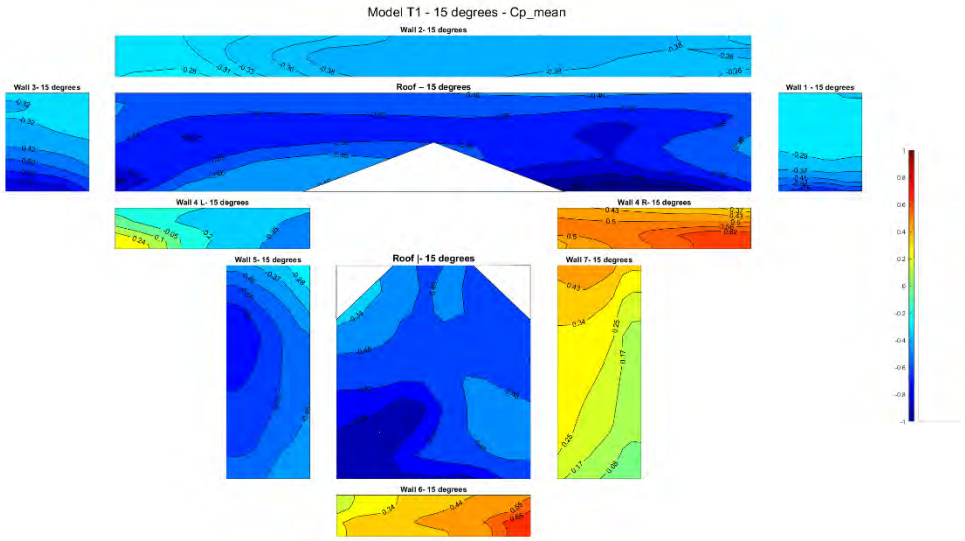

A 1. Mean Cp at 15 degrees for model T

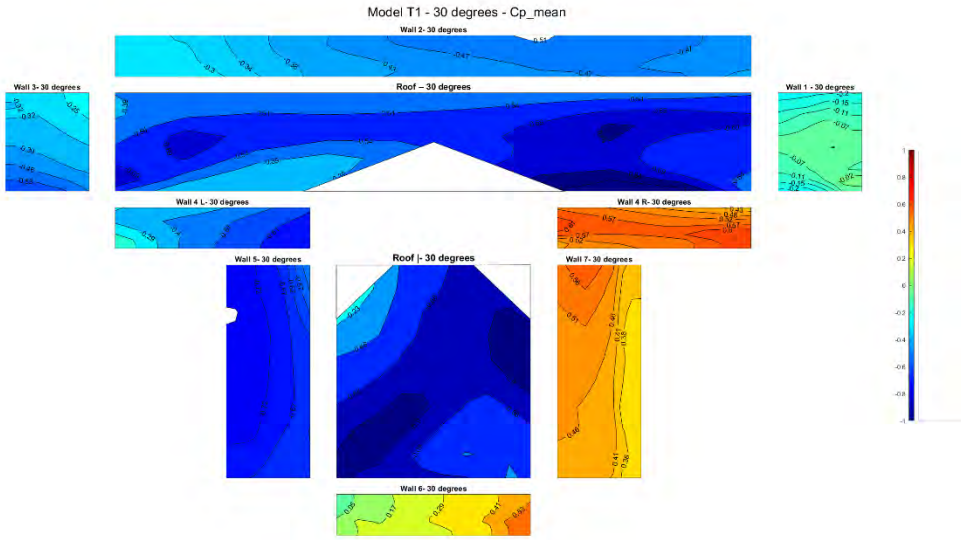

A 2. Mean Cp at 30 degrees for model T

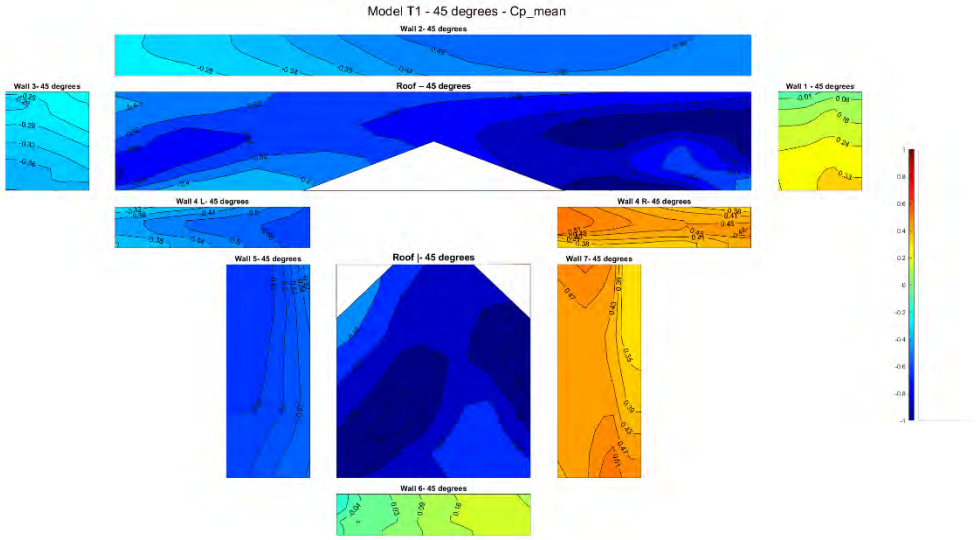

A 3. Mean Cp at 45 degrees for model T

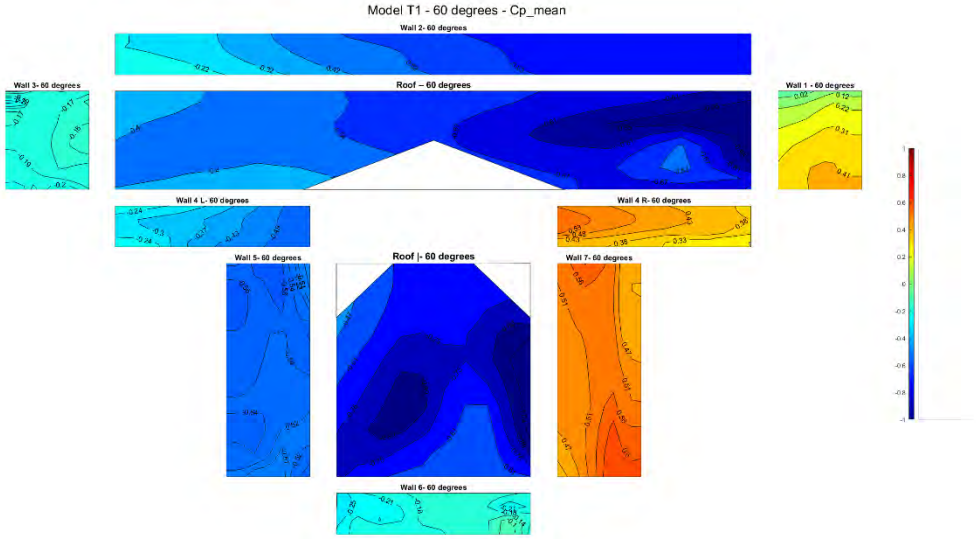

A 4. Mean Cp at 60 degrees for model T

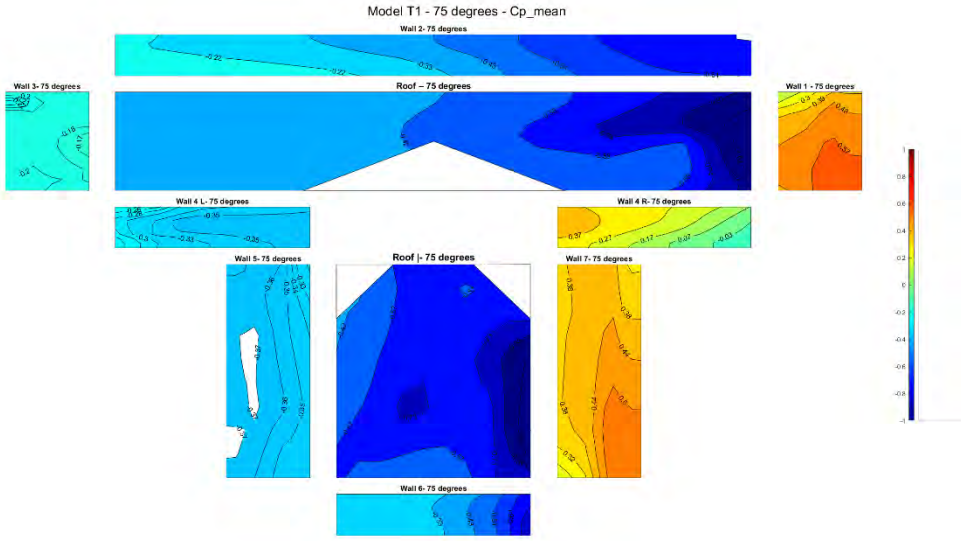

A 5. Mean Cp at 75 degrees for model T

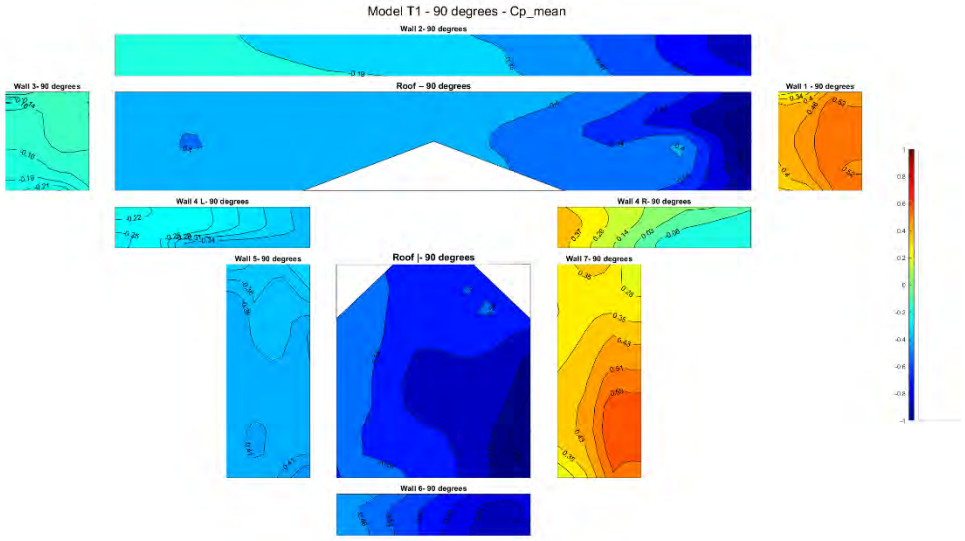

A 6. Mean Cp at 90 degrees for model T

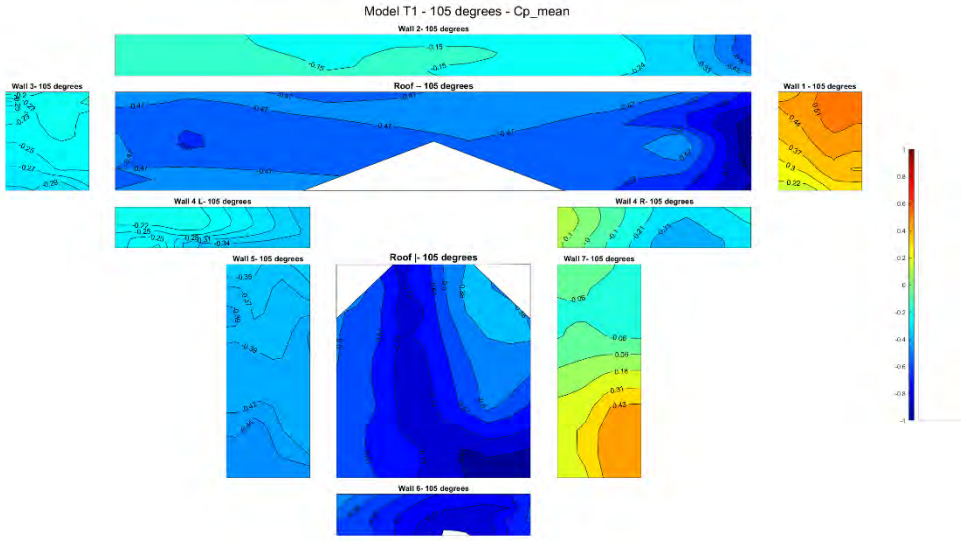

A 7. Mean Cp at 105 degrees for model T

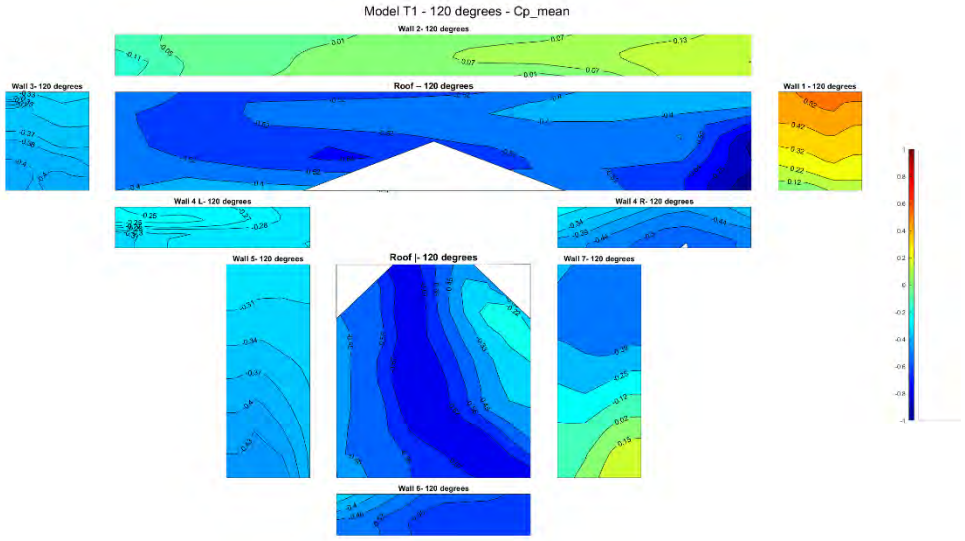

A 8. Mean Cp at 120 degrees for model T

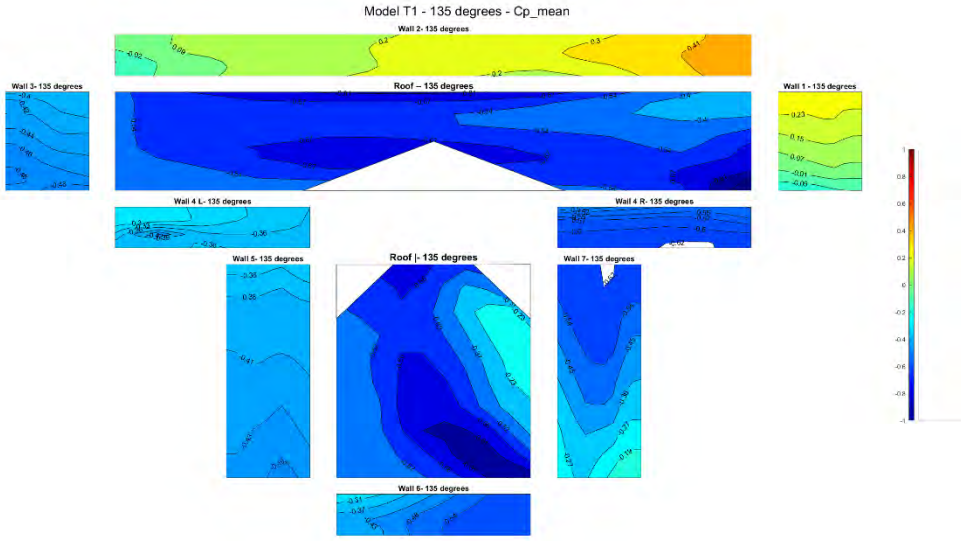

A 9. Mean Cp at 135 degrees for model T

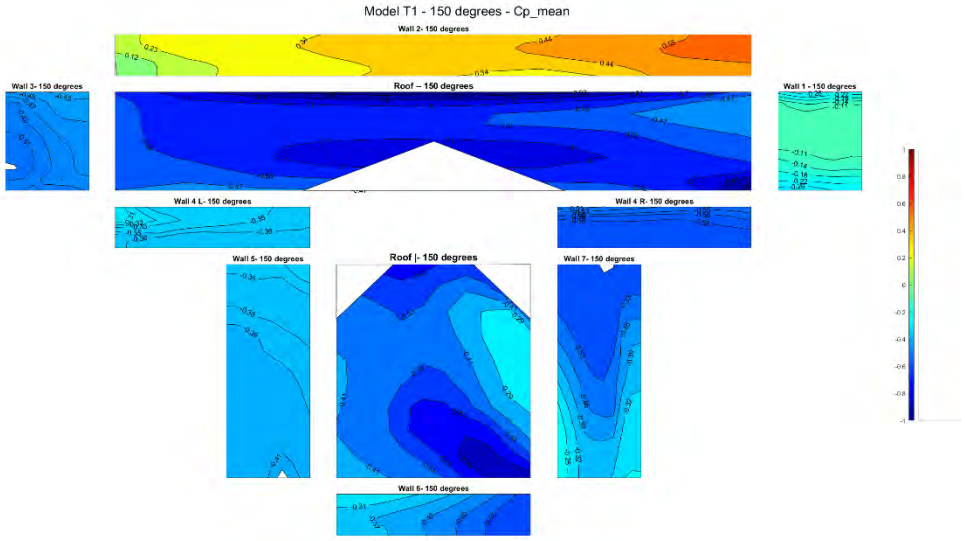

A 10. Mean Cp at 150 degrees for model T

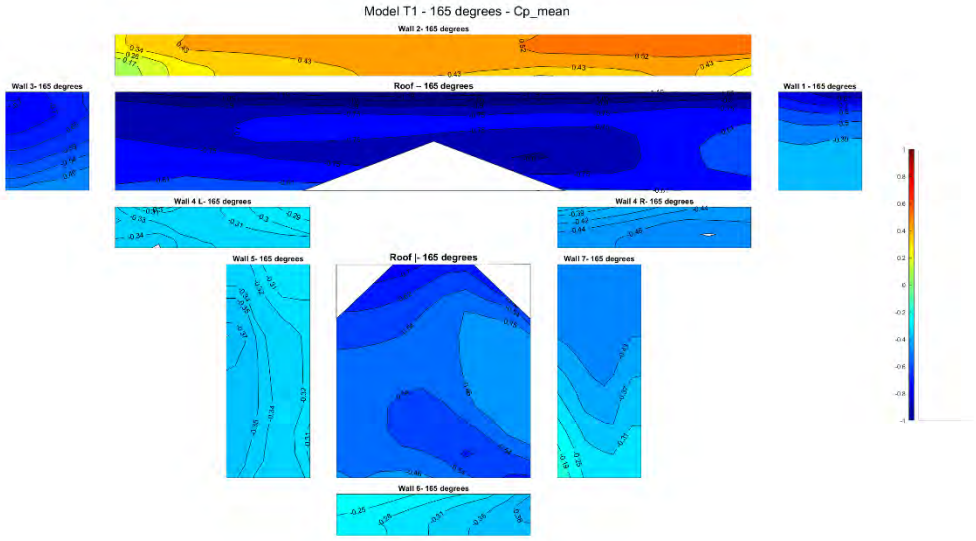

A 11. Mean Cp at 165 degrees for model T

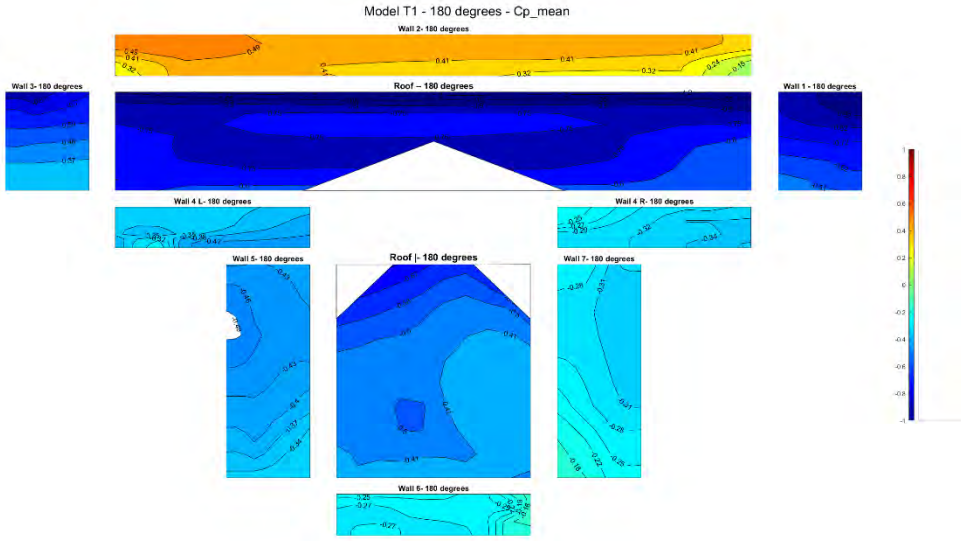

A 12. Mean Cp at 180 degrees for model T

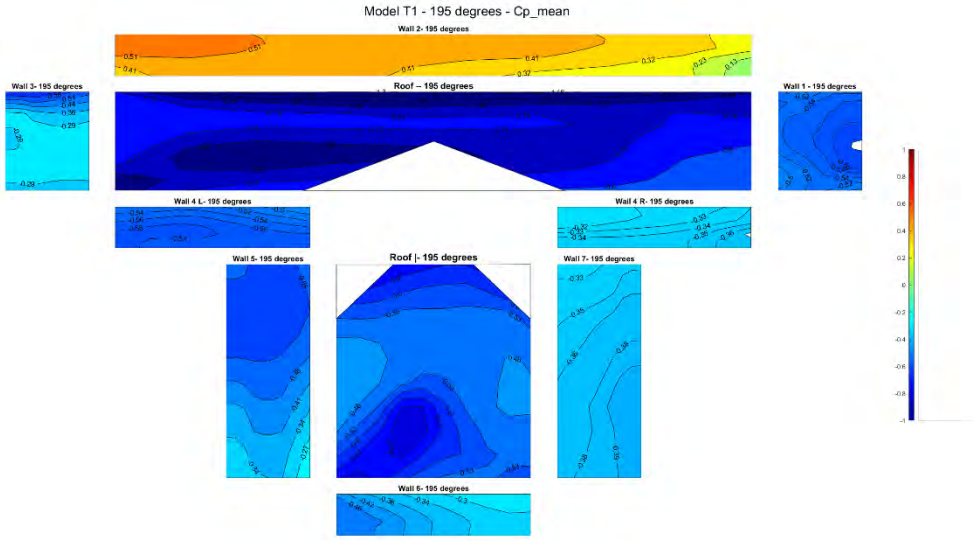

A 13. Mean Cp at 195 degrees for model T

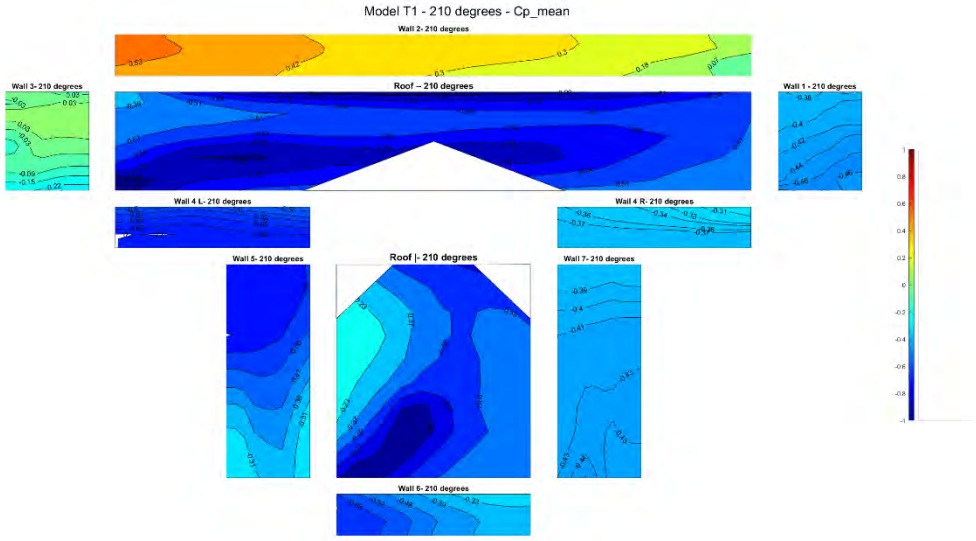

A 14. Mean Cp at 210 degrees for model T

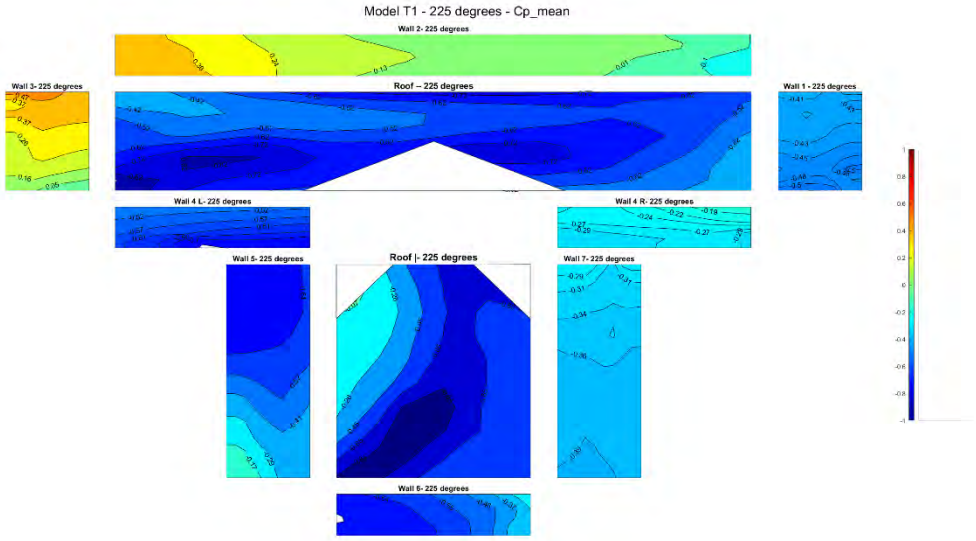

A 15. Mean Cp at 225 degrees for model T

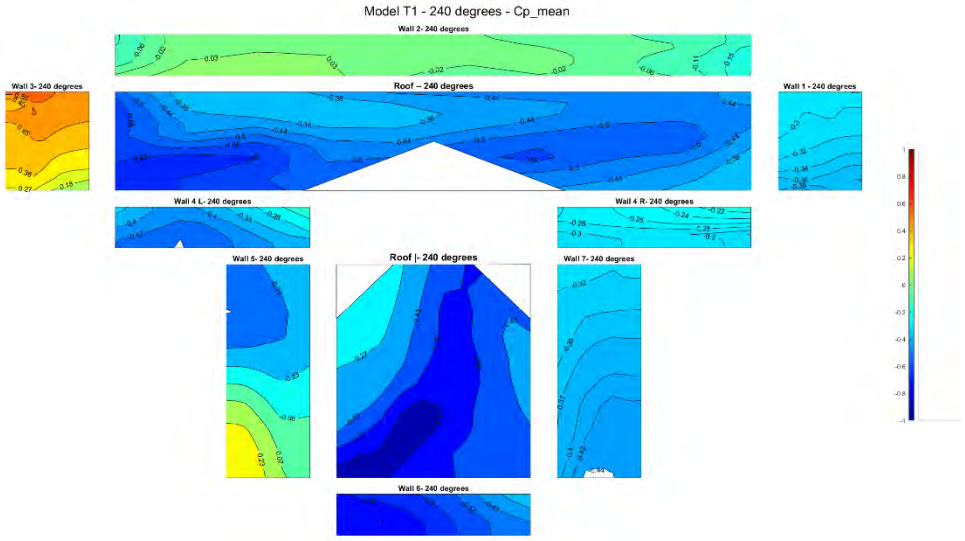

A 16. Mean Cp at 240 degrees for model T

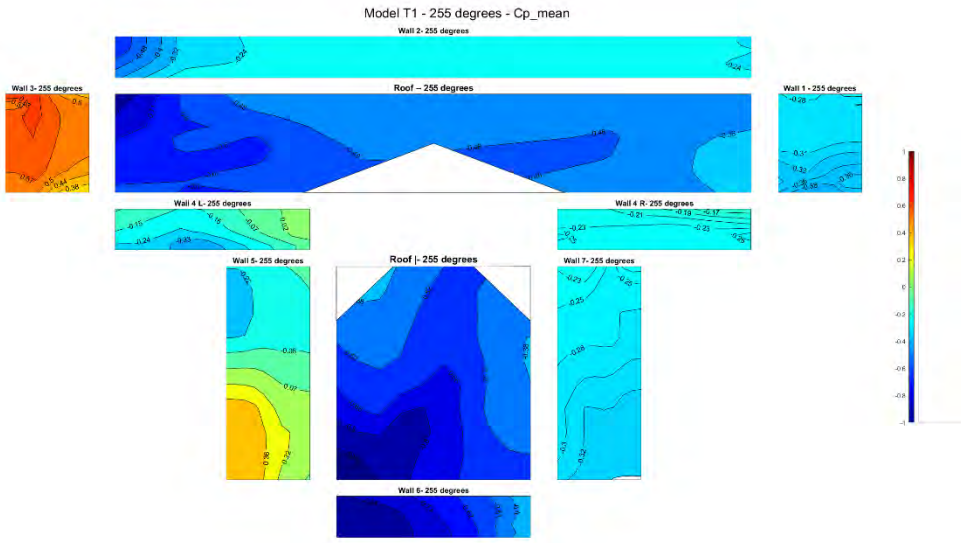

A 17. Mean Cp at 255 degrees for model T

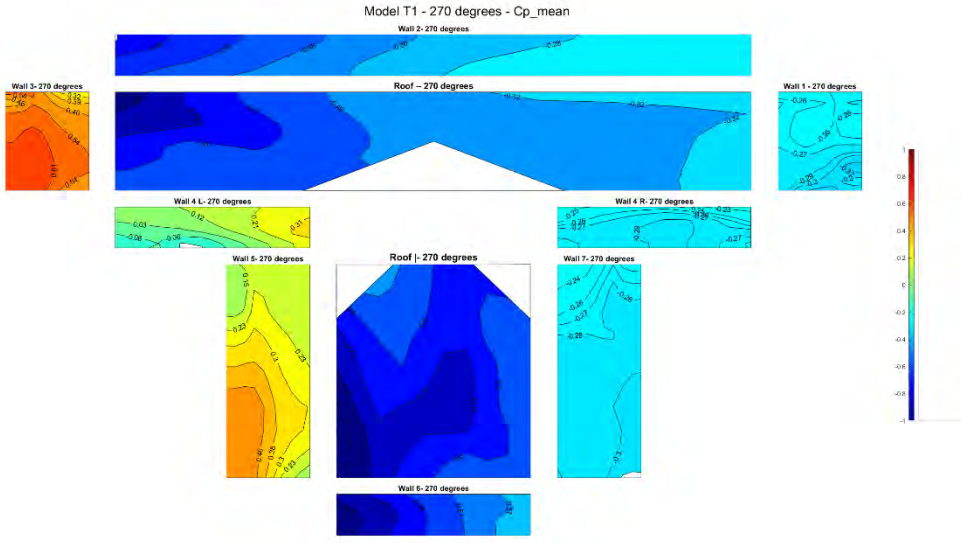

A 18. Mean Cp at 270 degrees for model T

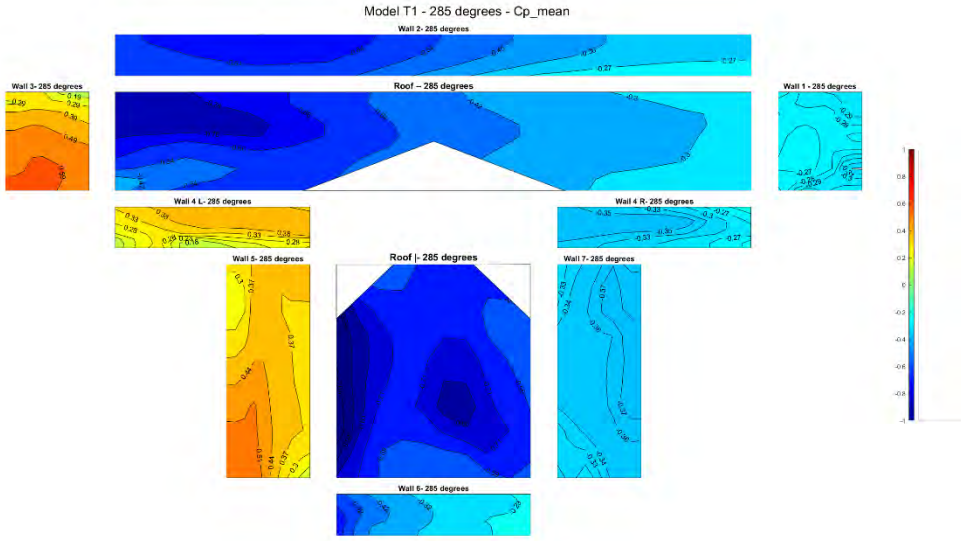

A 19. Mean Cp at 285 degrees for model T

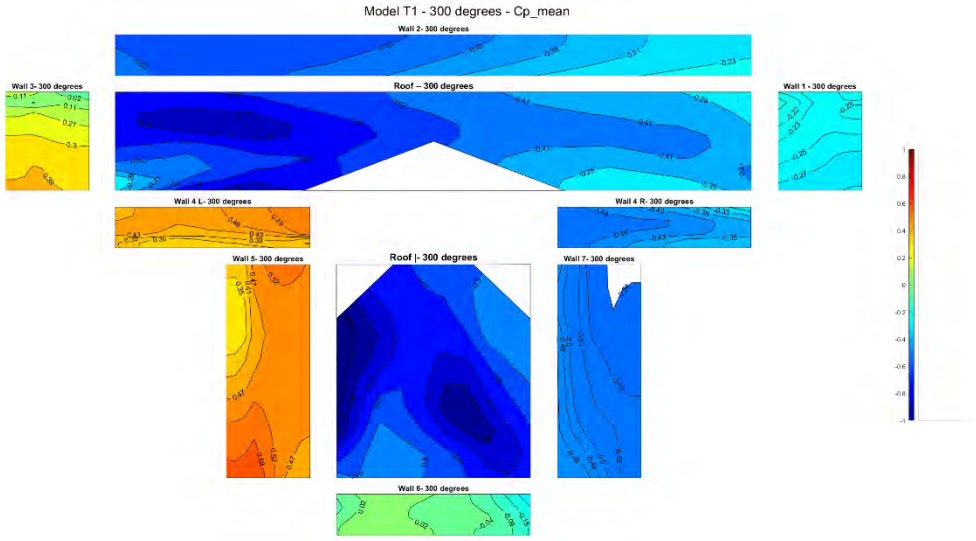

A 20. Mean Cp at 300 degrees for model T

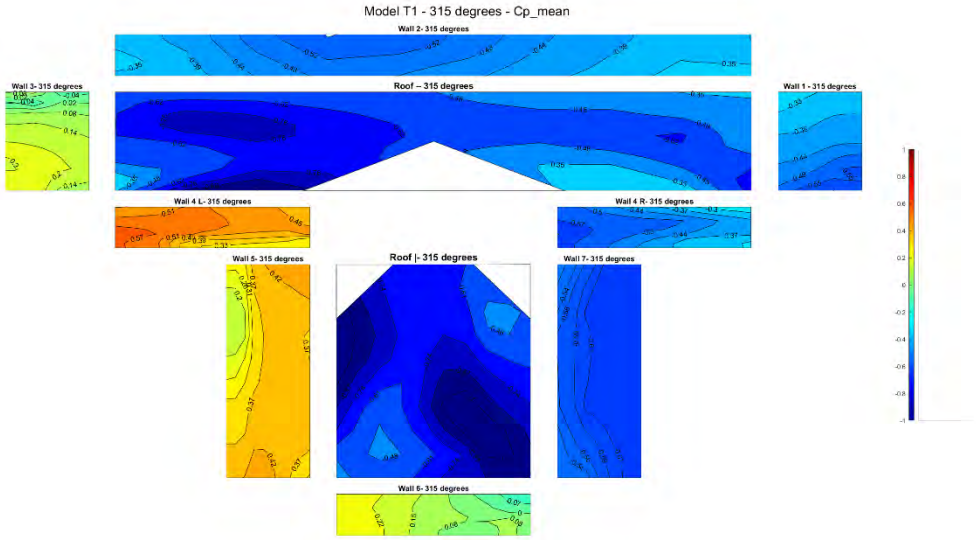

A 21. Mean Cp at 315 degrees for model T

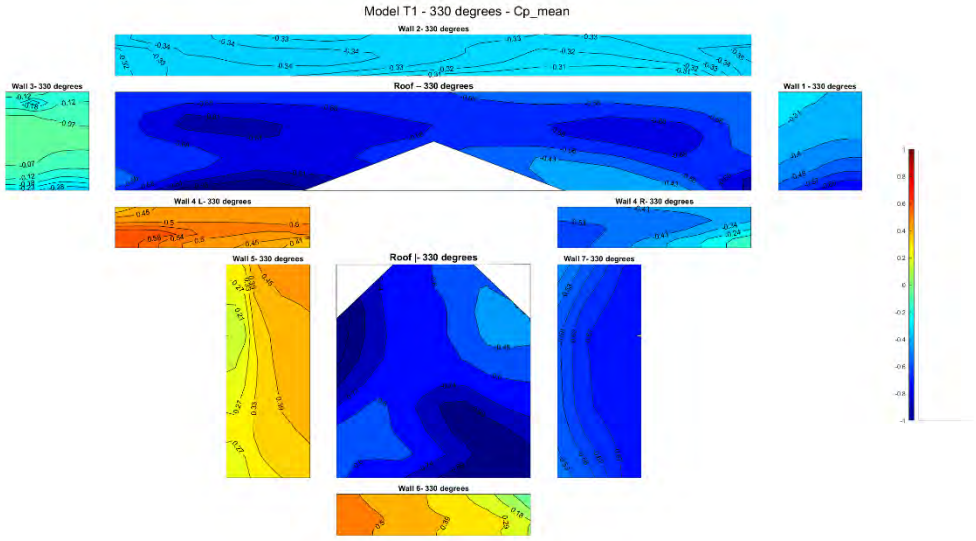

A 22. Mean Cp at 330 degrees for model T

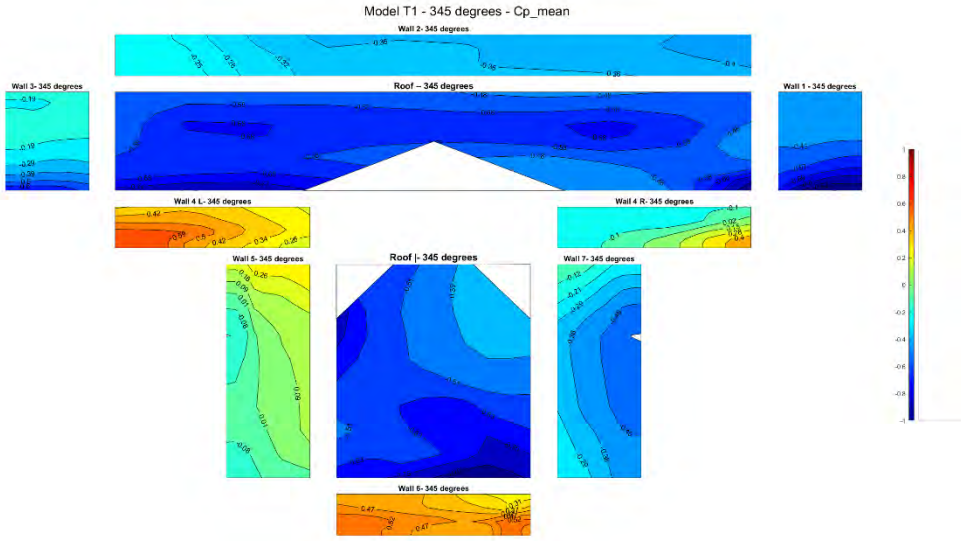

A 23. Mean Cp at 345 degrees for model T

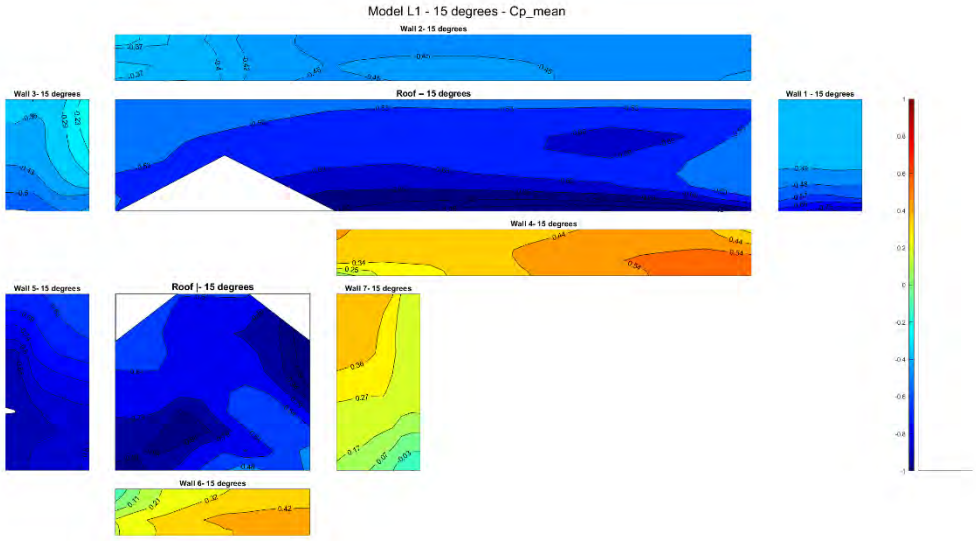

A 24. Mean Cp at 15 degrees for model L

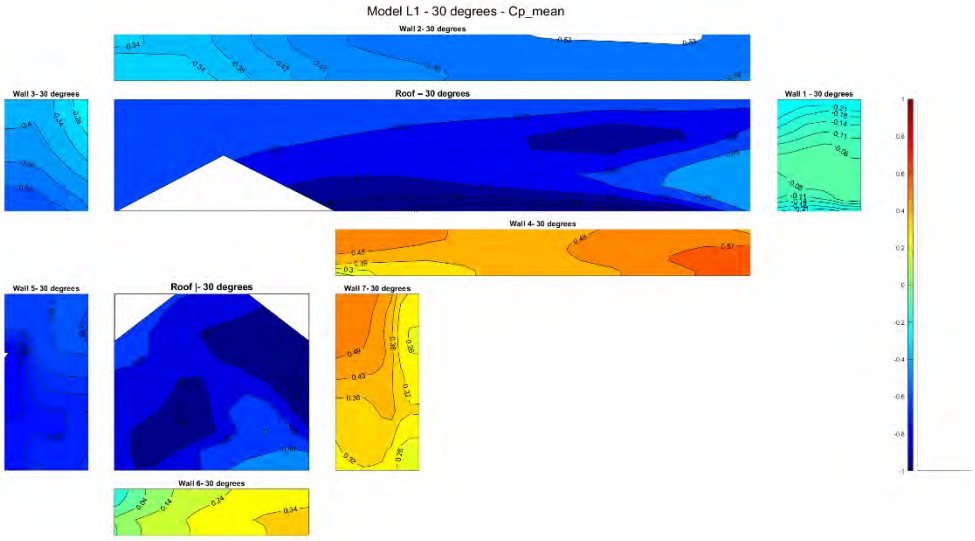

A 25. Mean Cp at 30 degrees for model L

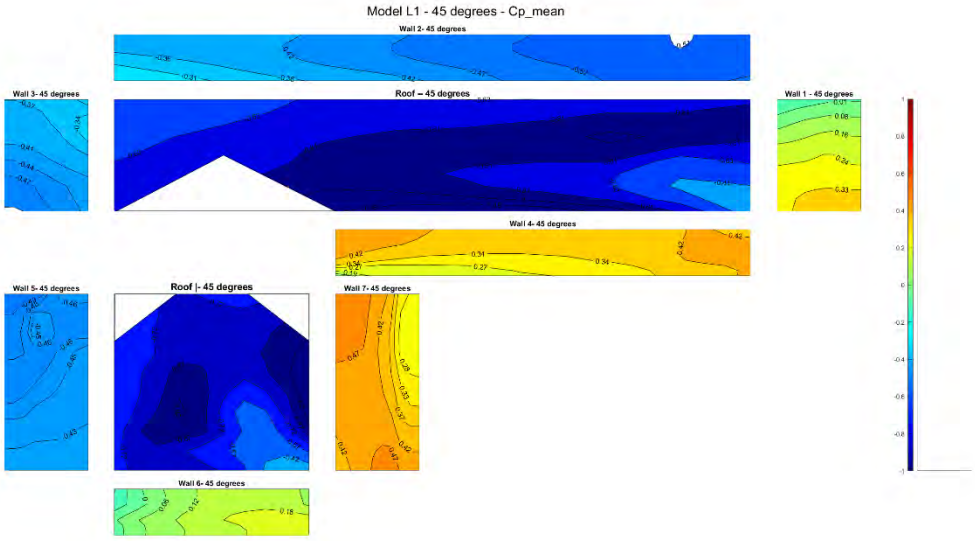

A 26. Mean Cp at 45 degrees for model L

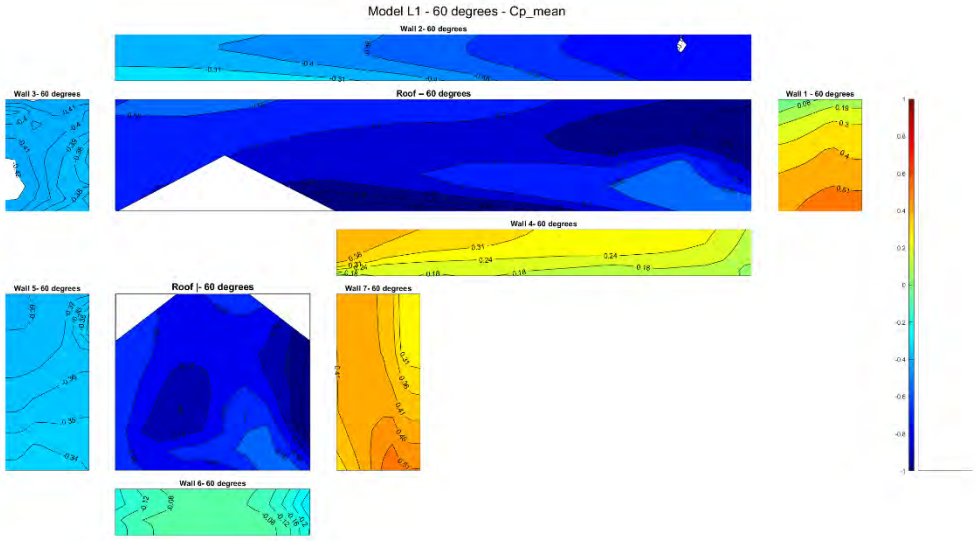

A 27. Mean Cp at 60 degrees for model L

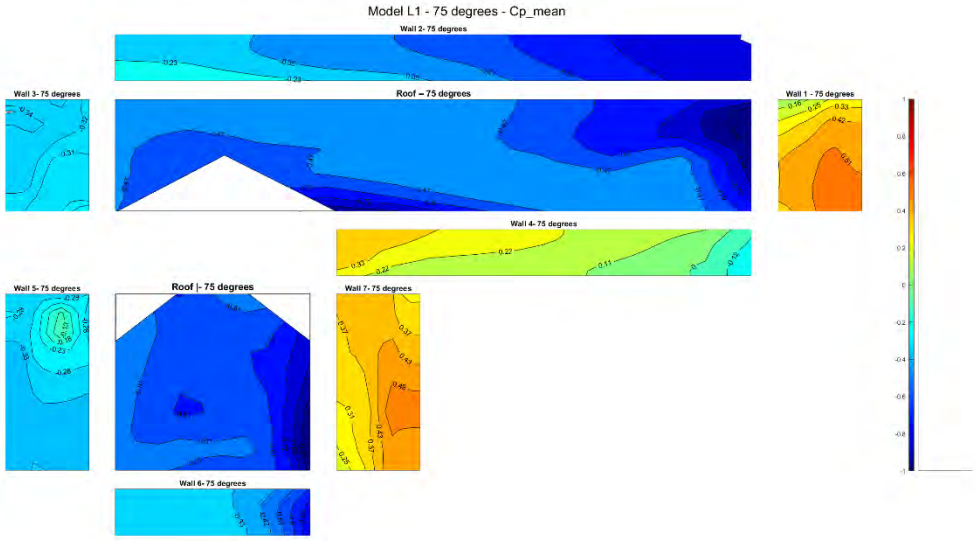

A 28. Mean Cp at 75 degrees for model L

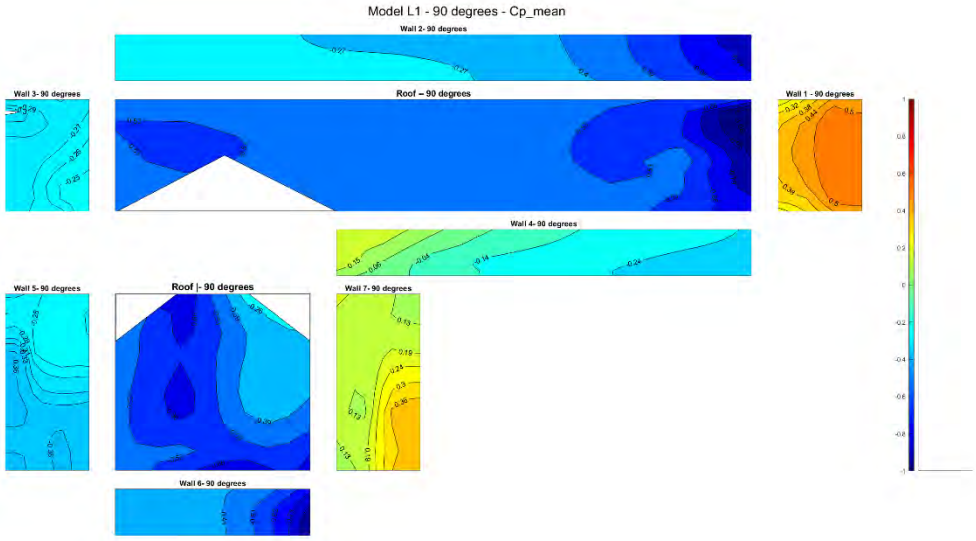

A 29. Mean Cp at 90 degrees for model L

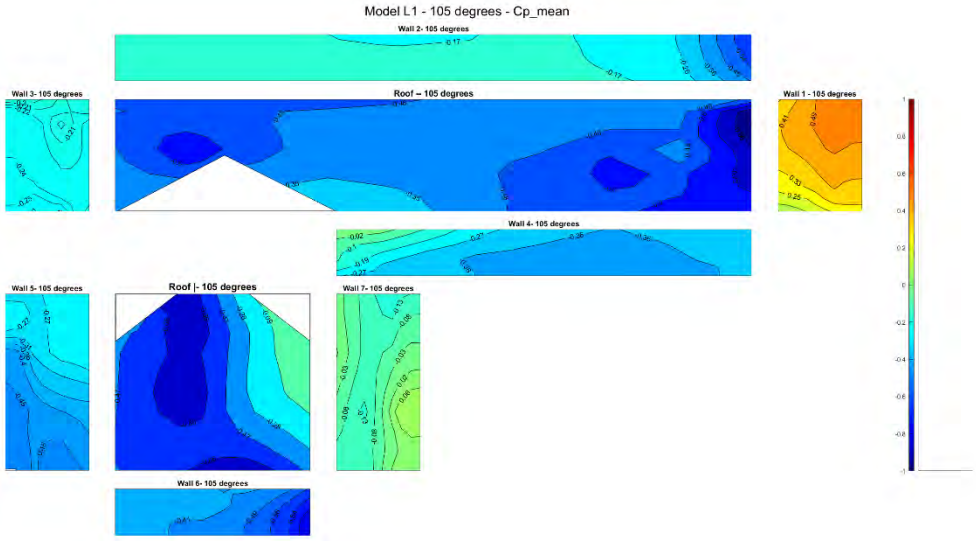

A 30. Mean Cp at 105 degrees for model L

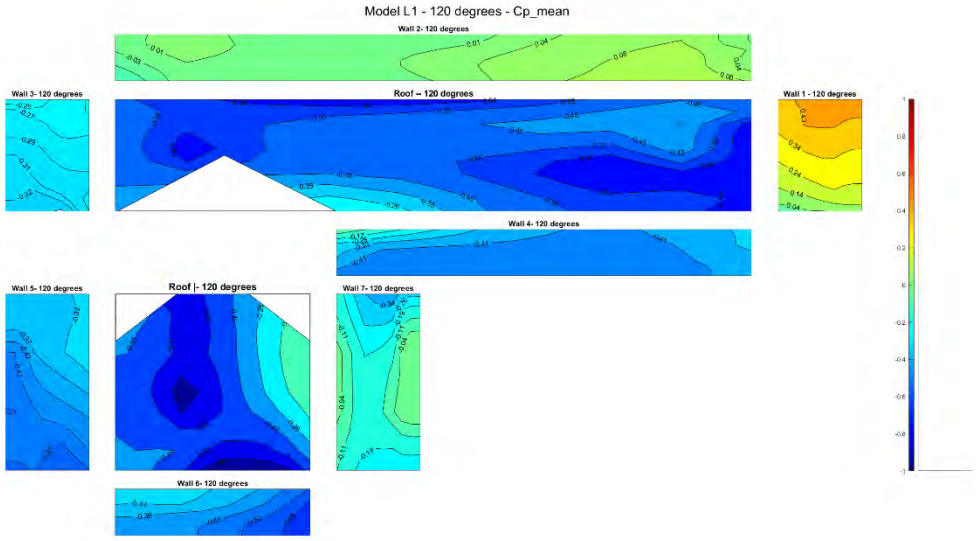

A 31. Mean Cp at 120 degrees for model L

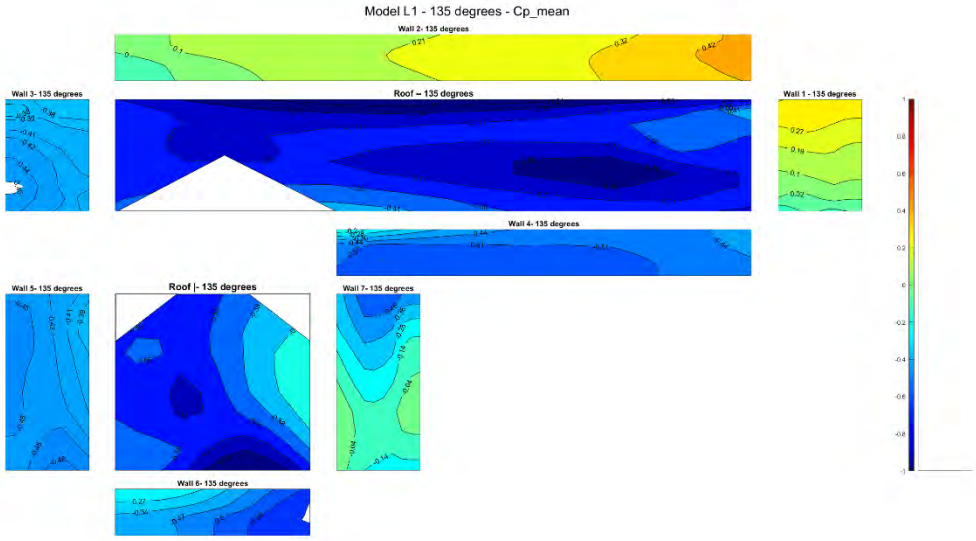

A 32. Mean Cp at 135 degrees for model L

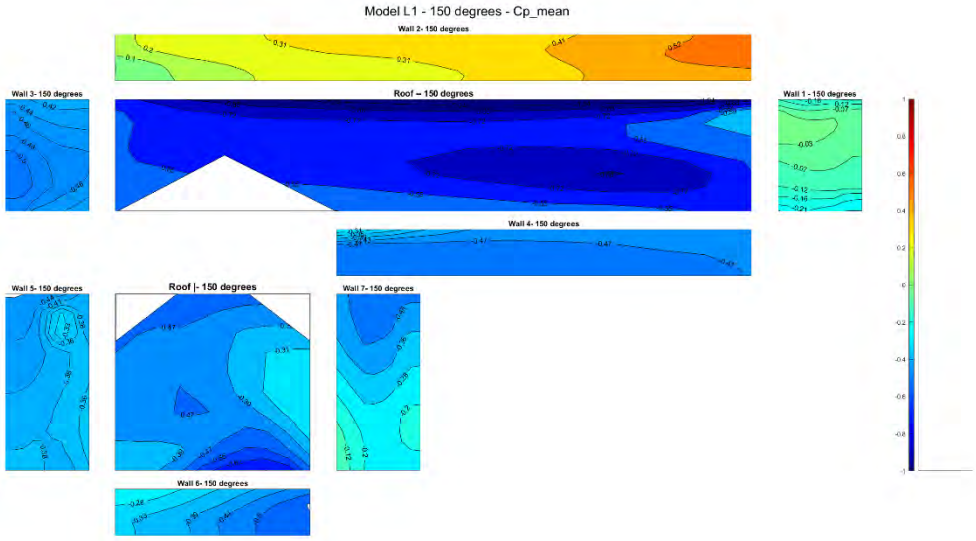

A 33. Mean Cp at 150 degrees for model L

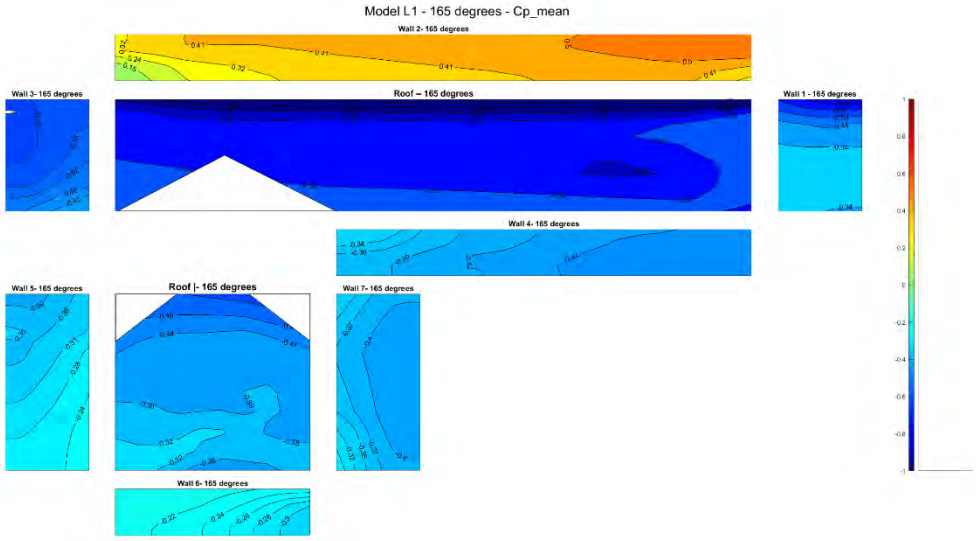

A 34. Mean Cp at 165 degrees for model L

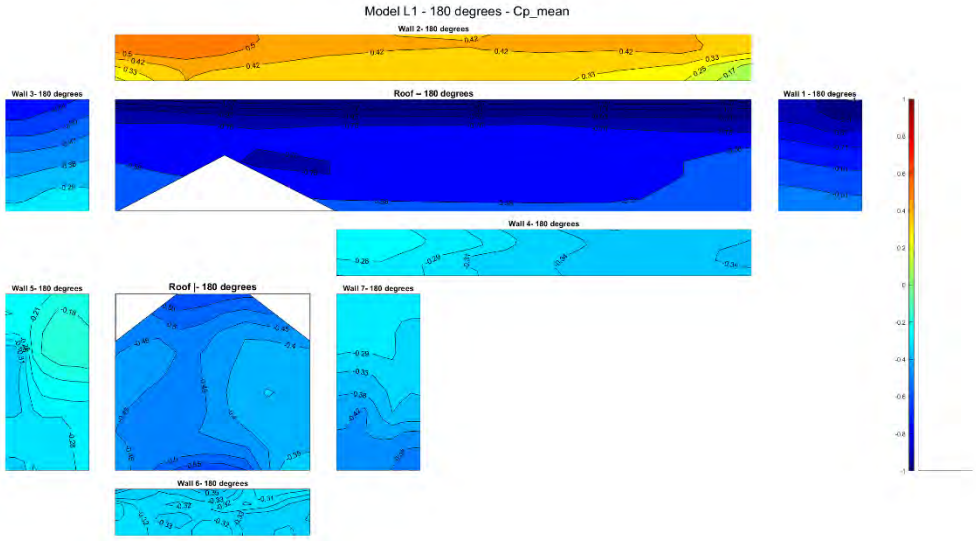

A 35. Mean Cp at 180 degrees for model L

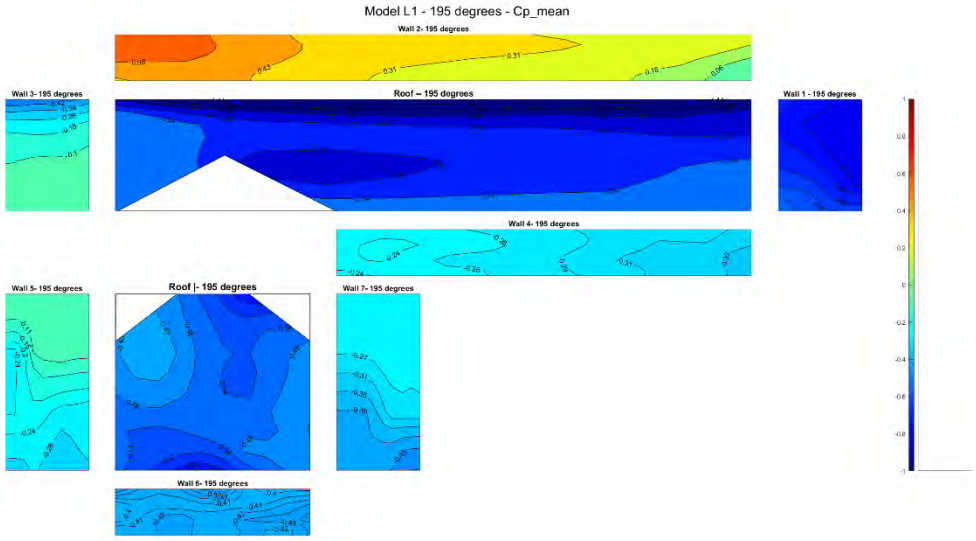

A 36. Mean Cp at 195 degrees for model L

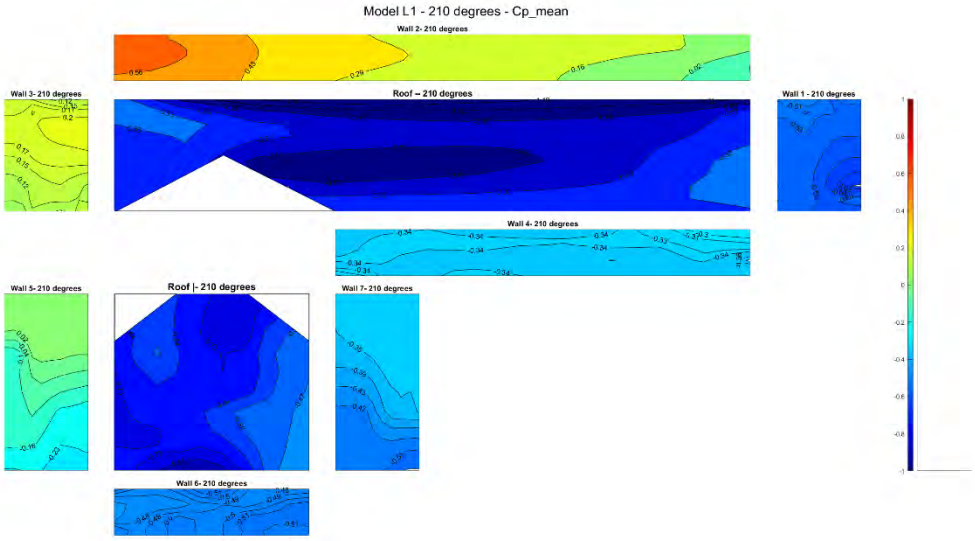

A 37. Mean Cp at 210 degrees for model L

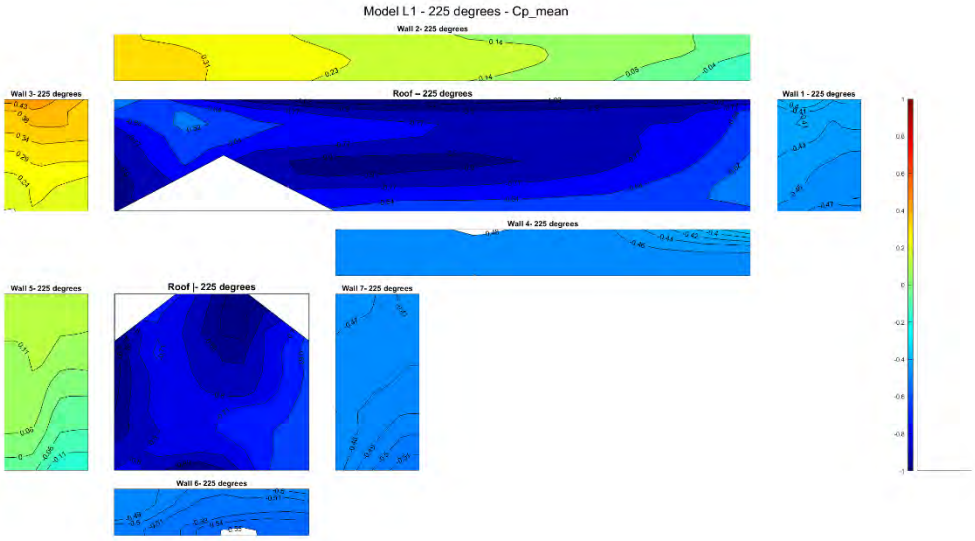

A 38. Mean Cp at 225 degrees for model L

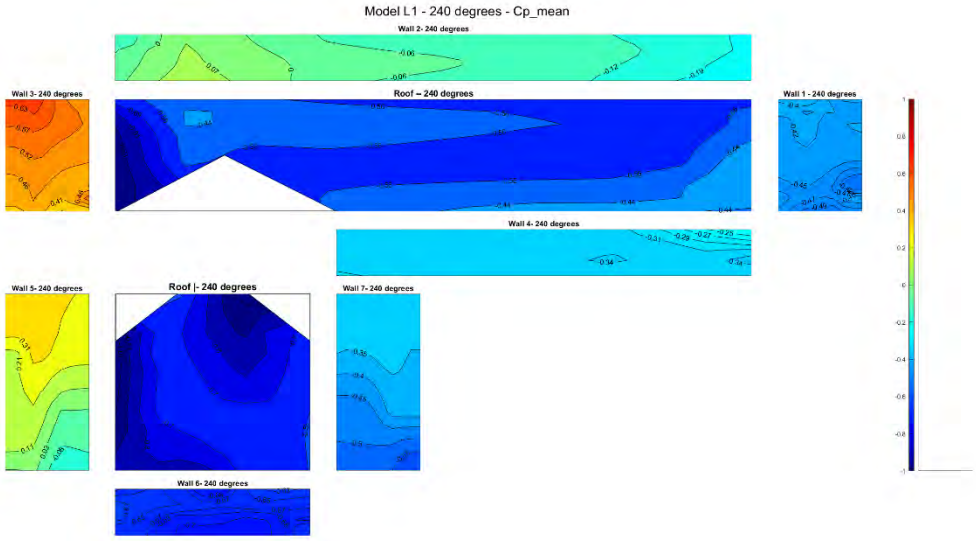

A 39. Mean Cp at 240 degrees for model L

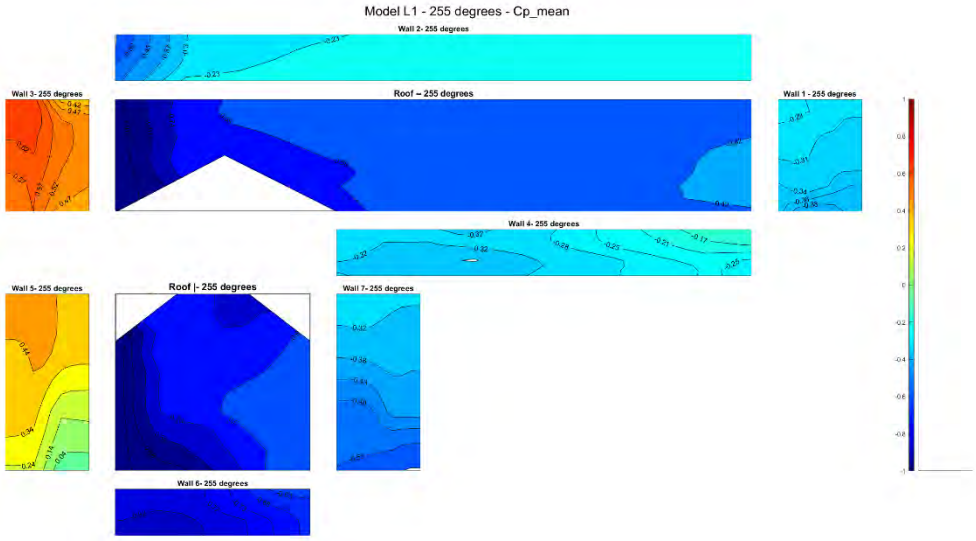

A 40. Mean Cp at 255 degrees for model L

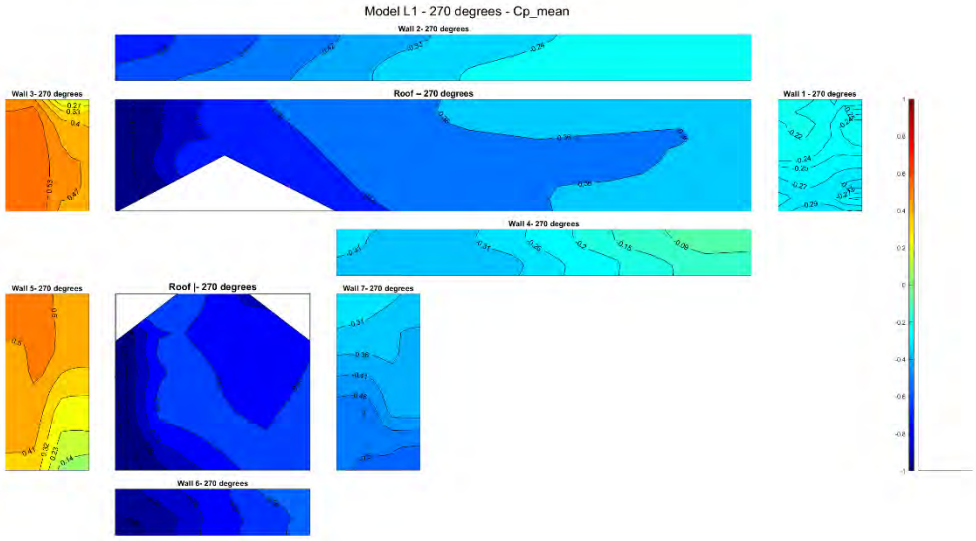

A 41. Mean Cp at 270 degrees for model L

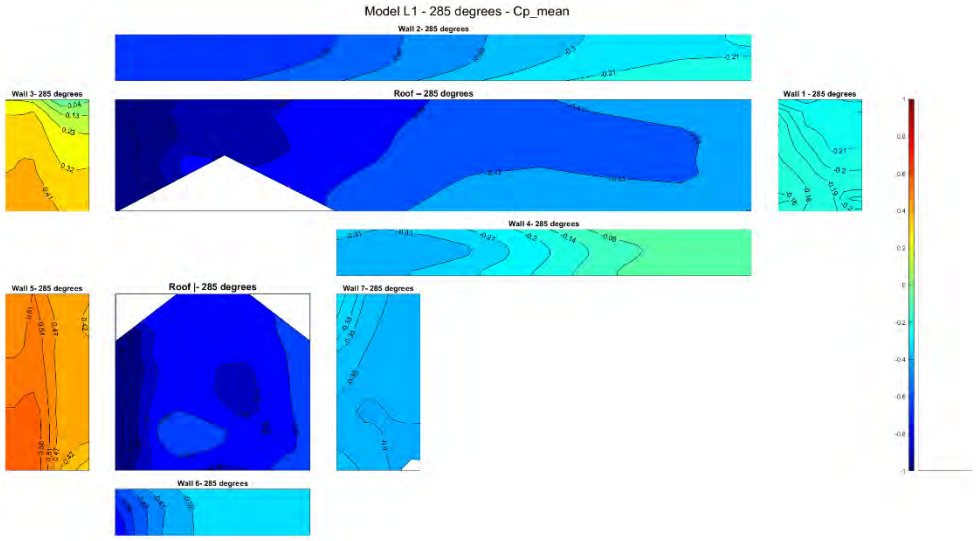

A 42. Mean Cp at 285 degrees for model L

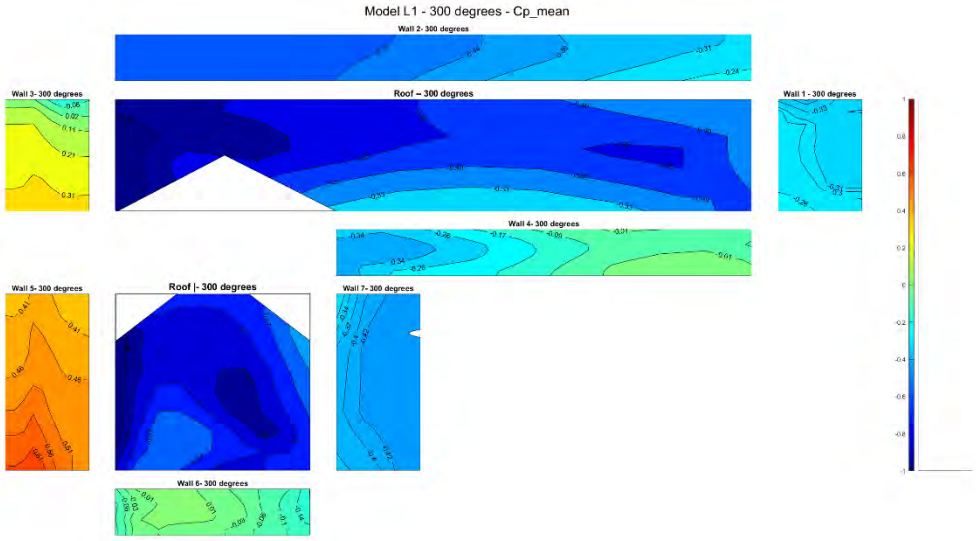

A 43. Mean Cp at 300 degrees for model L

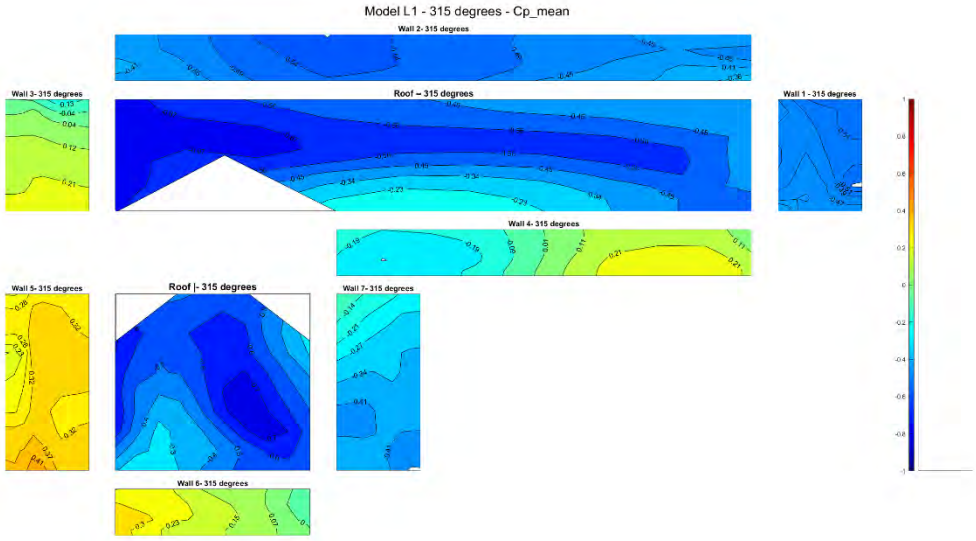

A 44. Mean Cp at 315 degrees for model L

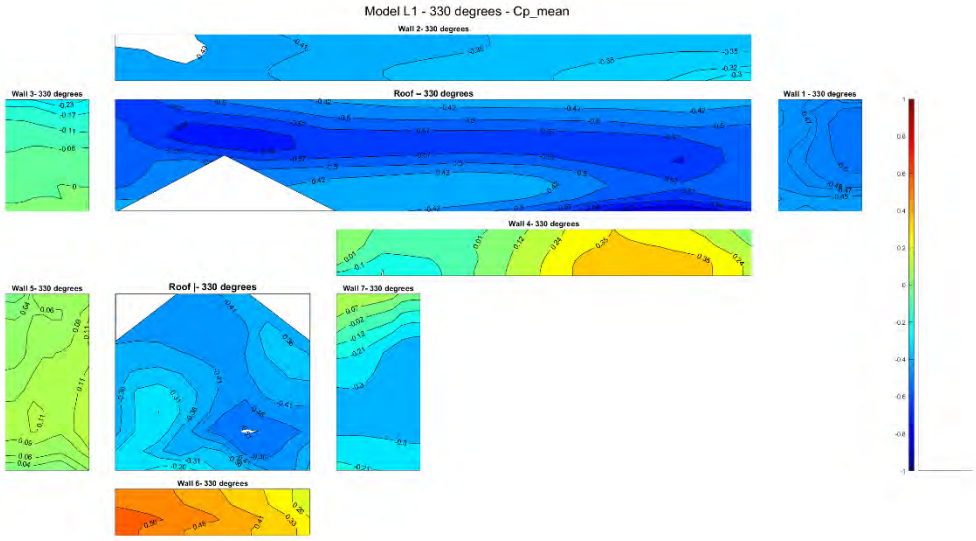

A 45. Mean Cp at 330 degrees for model L

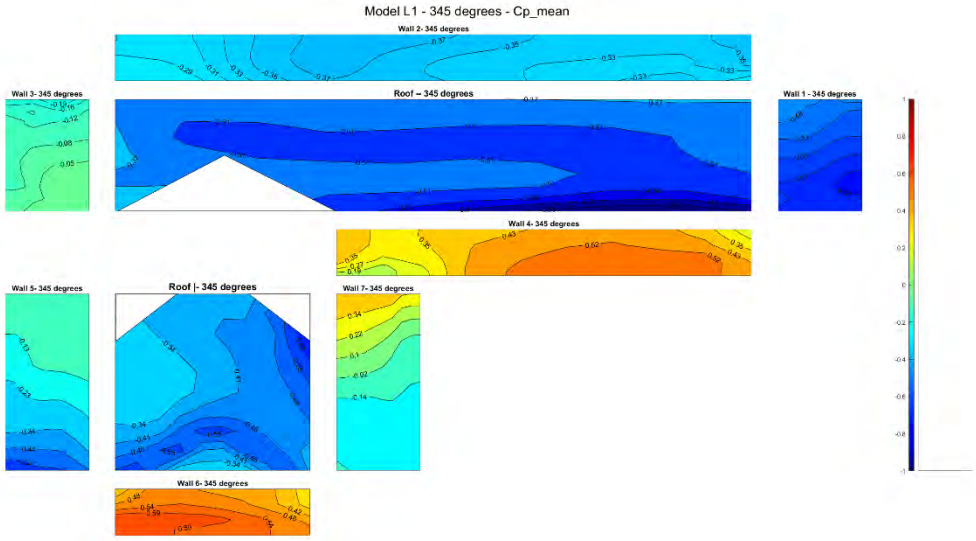

A 46. Mean Cp at 345 degrees for model L

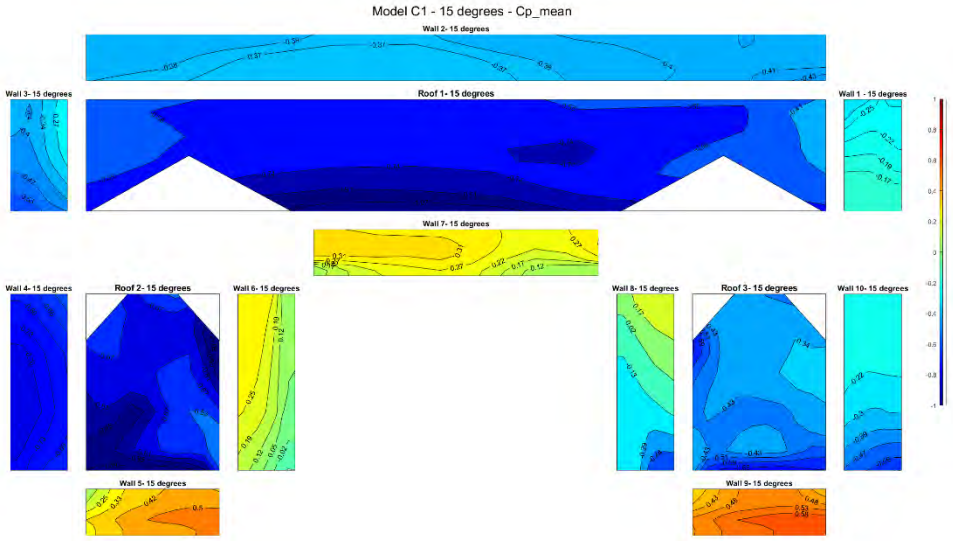

A 47. Mean Cp at 15 degrees for model C

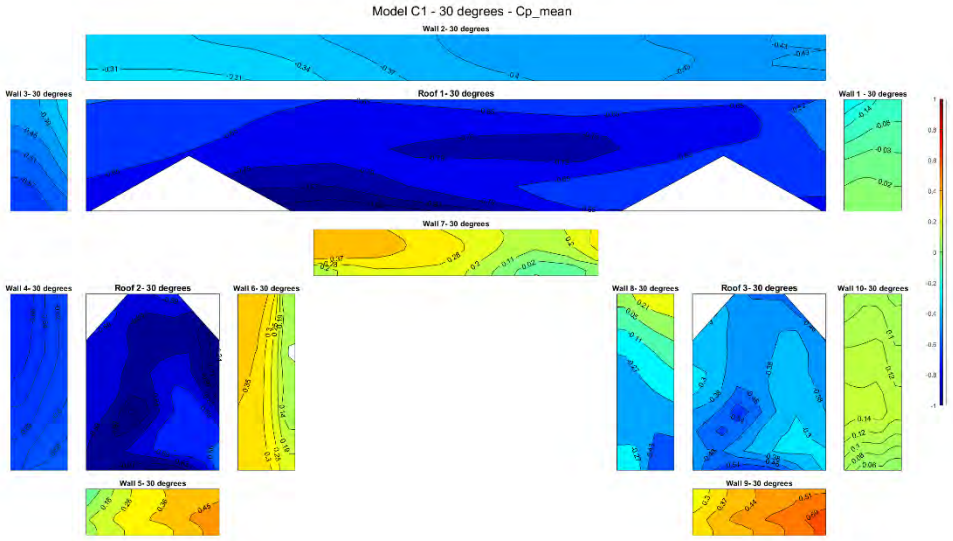

A 48. Mean Cp at 30 degrees for model C

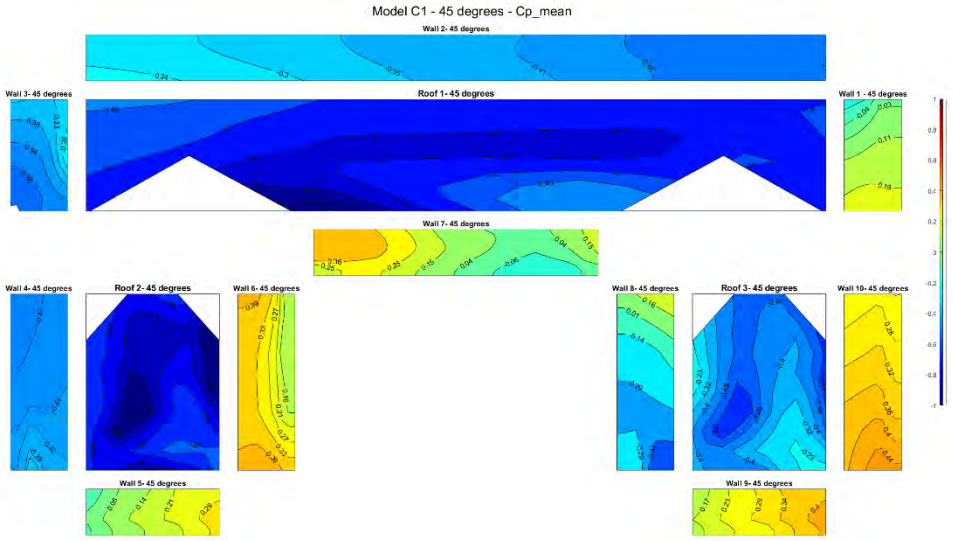

A 49. Mean Cp at 45 degrees for model C

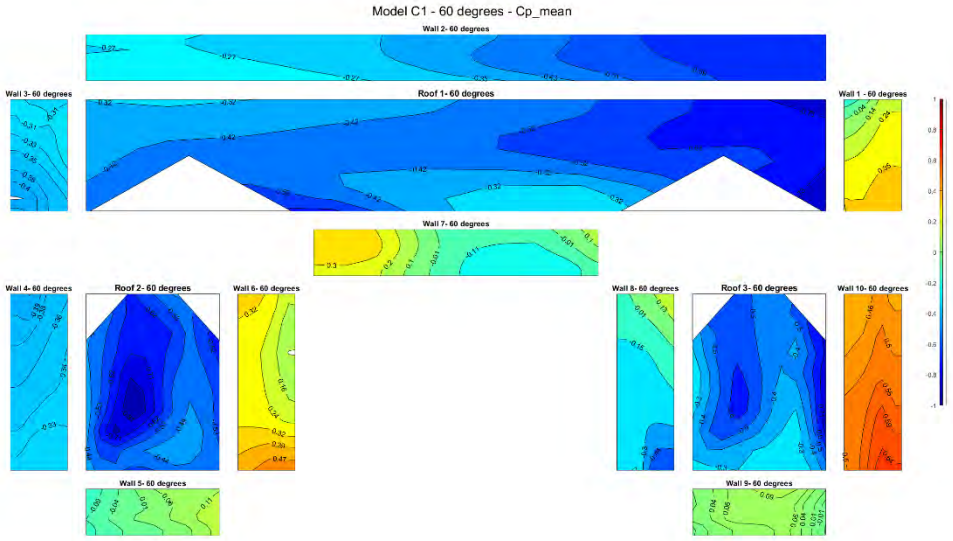

A 50. Mean Cp at 60 degrees for model C

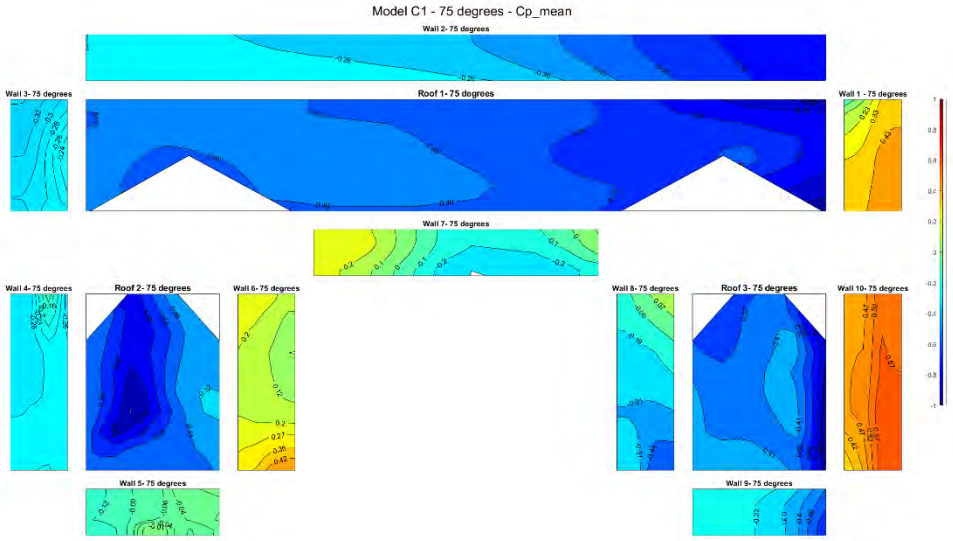

A 51. Mean Cp at 75 degrees for model C

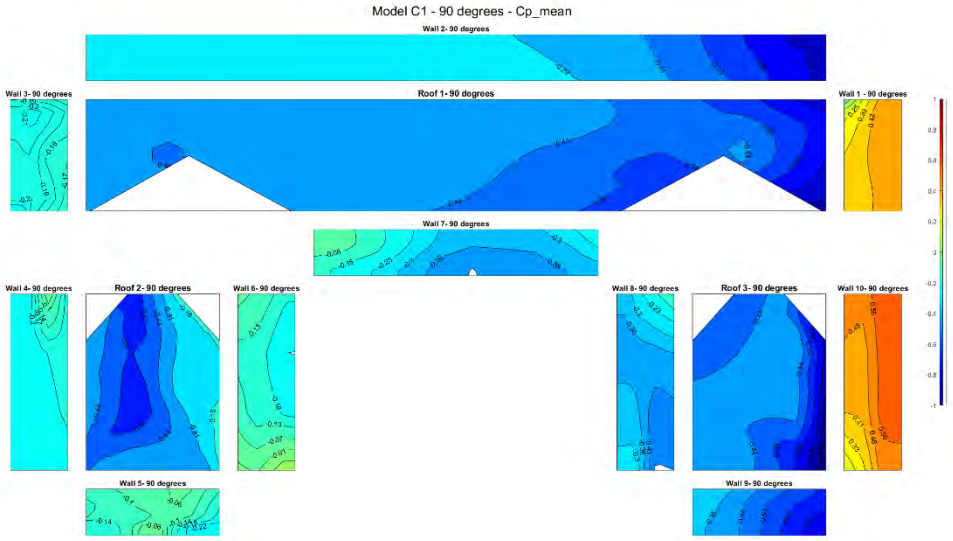

A 52. Mean Cp at 90 degrees for model C

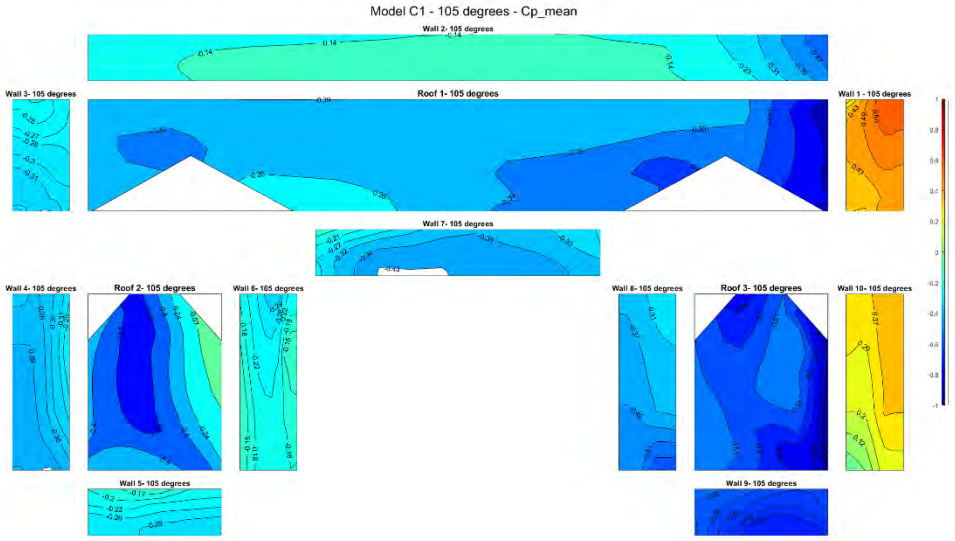

A 53. Mean Cp at 105 degrees for model C

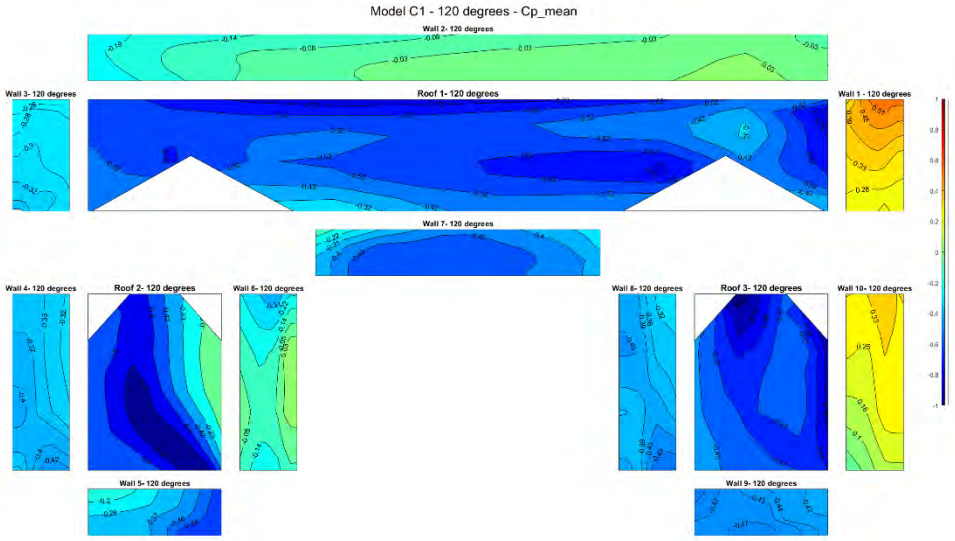

A 54. Mean Cp at 120 degrees for model C

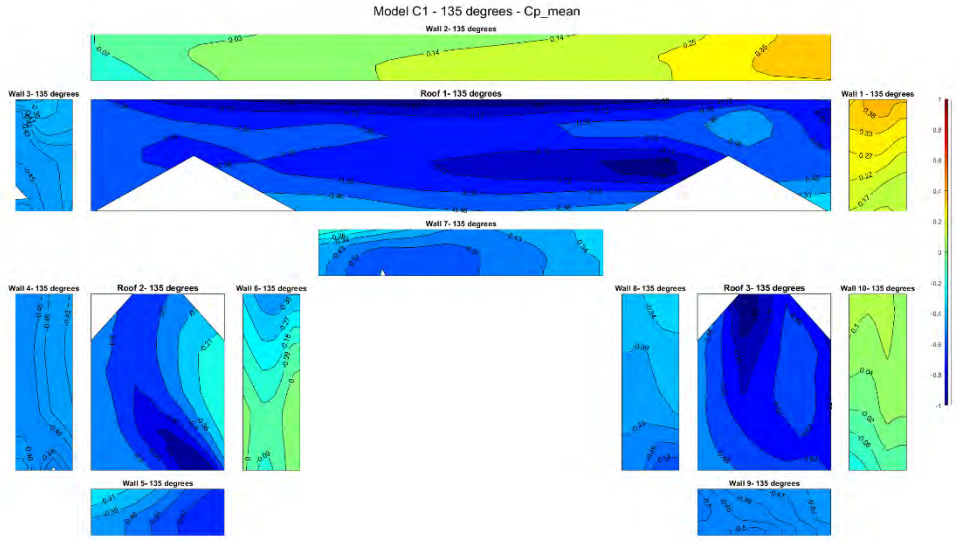

A 55. Mean Cp at 135 degrees for model C

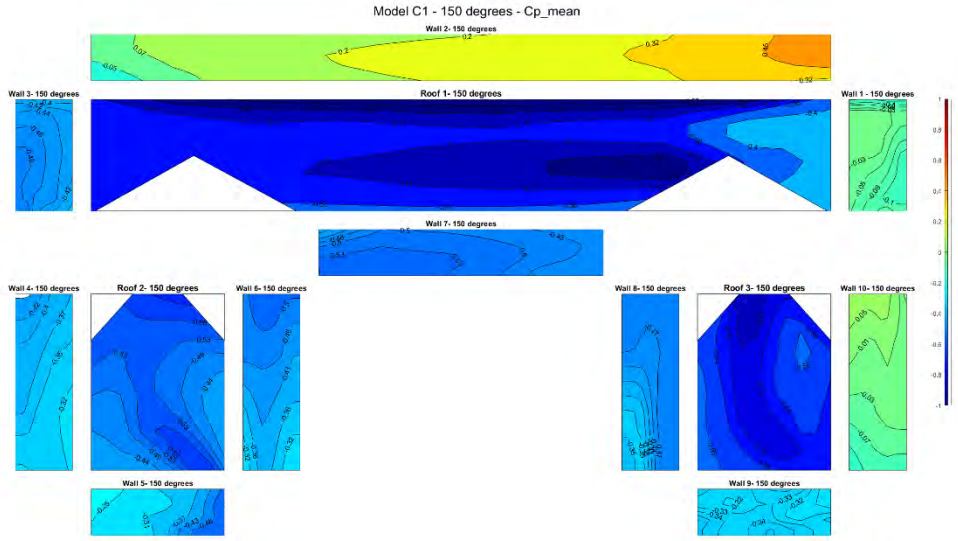

A 56. Mean Cp at 150 degrees for model C

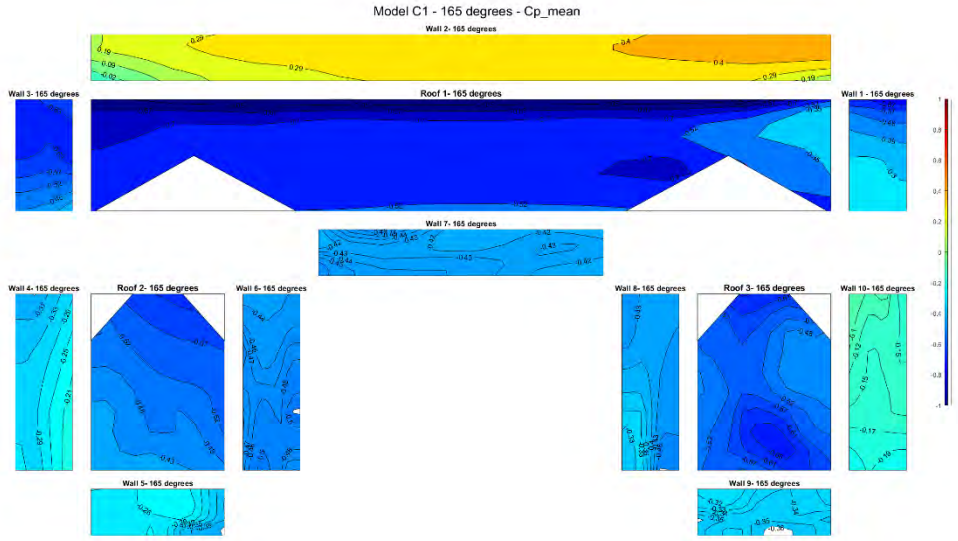

A 57. Mean Cp at 165 degrees for model C

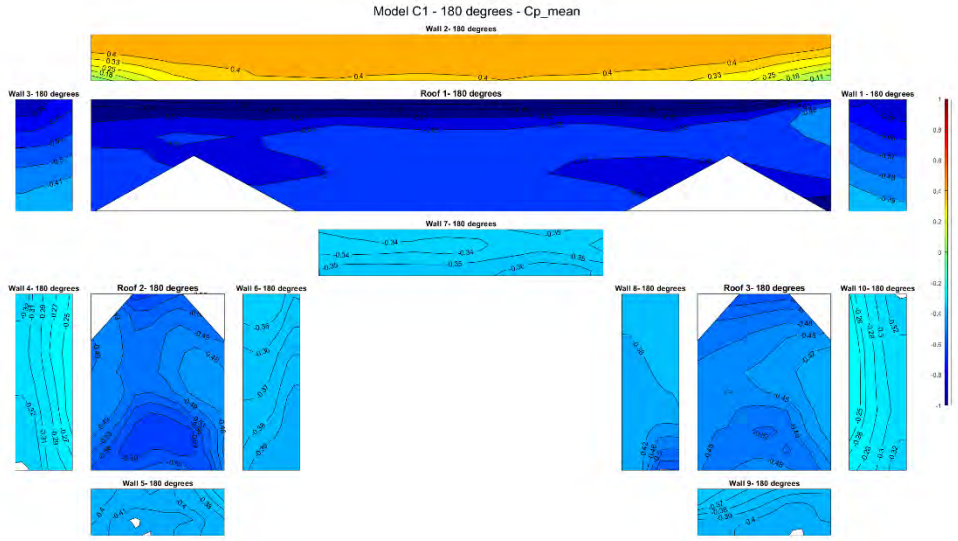

A 58. Mean Cp at 180 degrees for model C

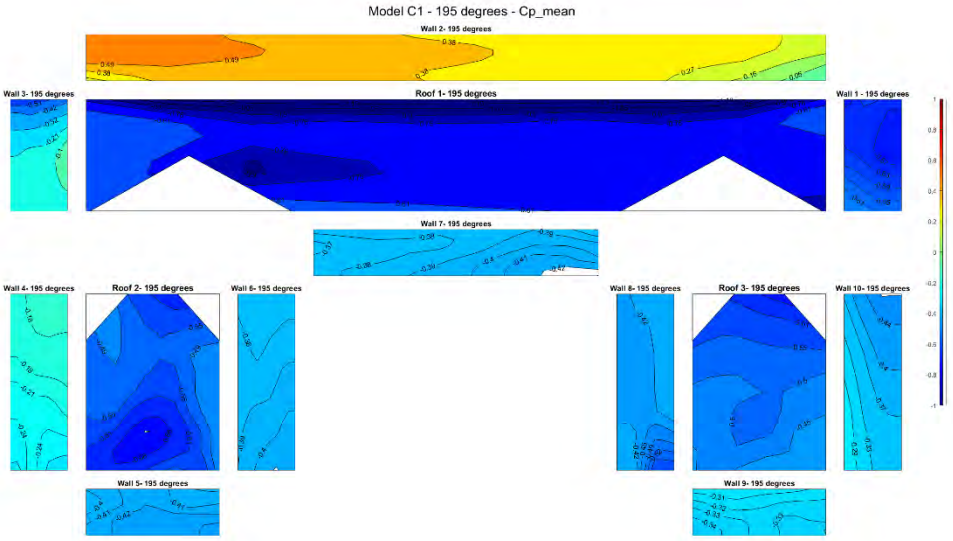

A 59. Mean Cp at 195 degrees for model C

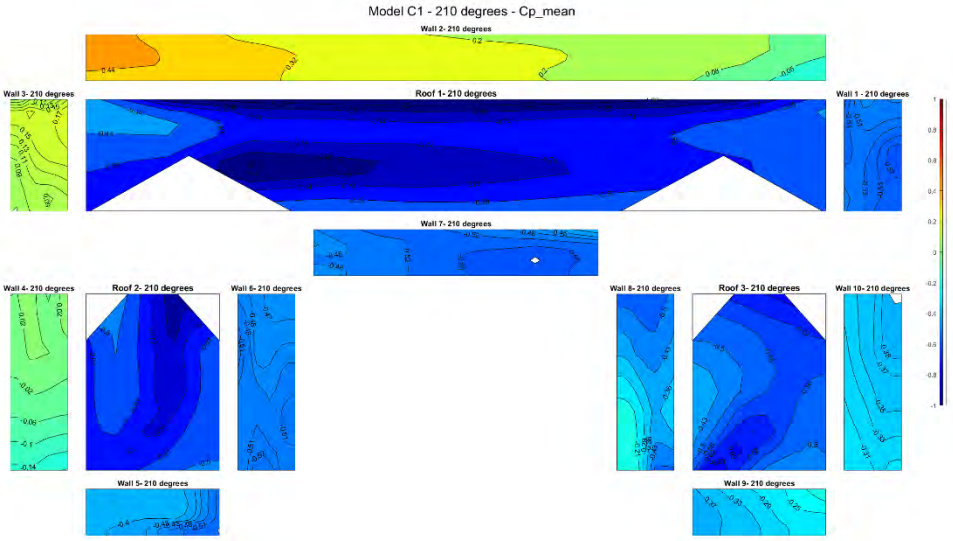

A 60. Mean Cp at 210 degrees for model C

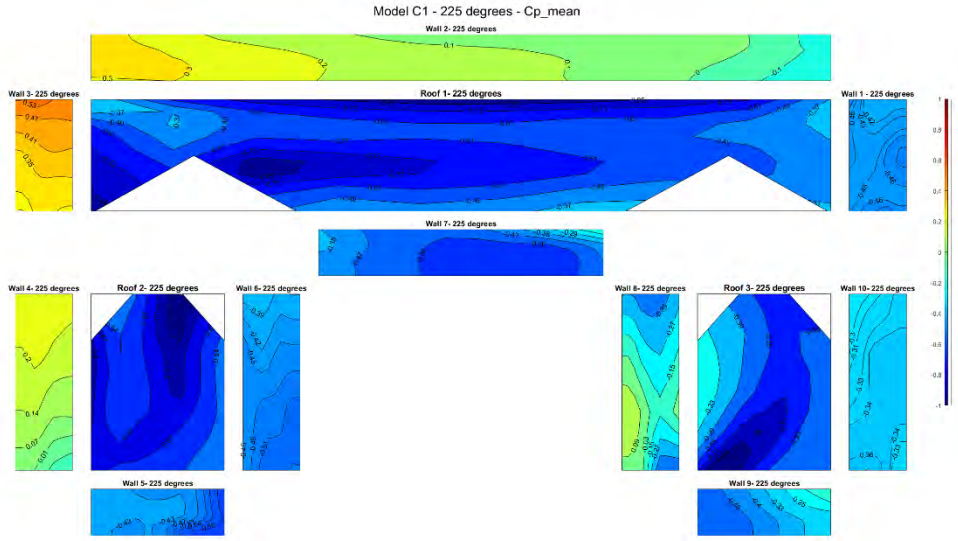

A 61. Mean Cp at 225 degrees for model C

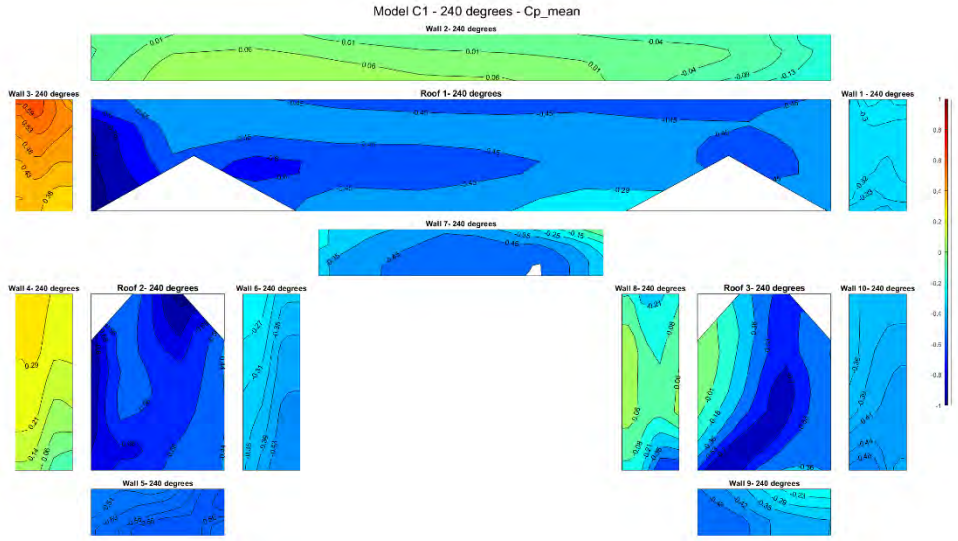

A 62. Mean Cp at 240 degrees for model C

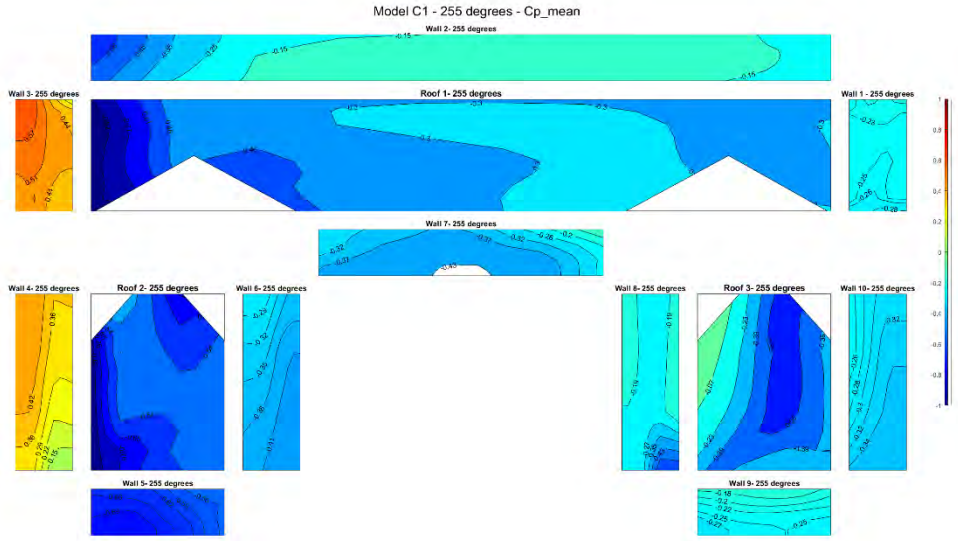

A 63. Mean Cp at 255 degrees for model C

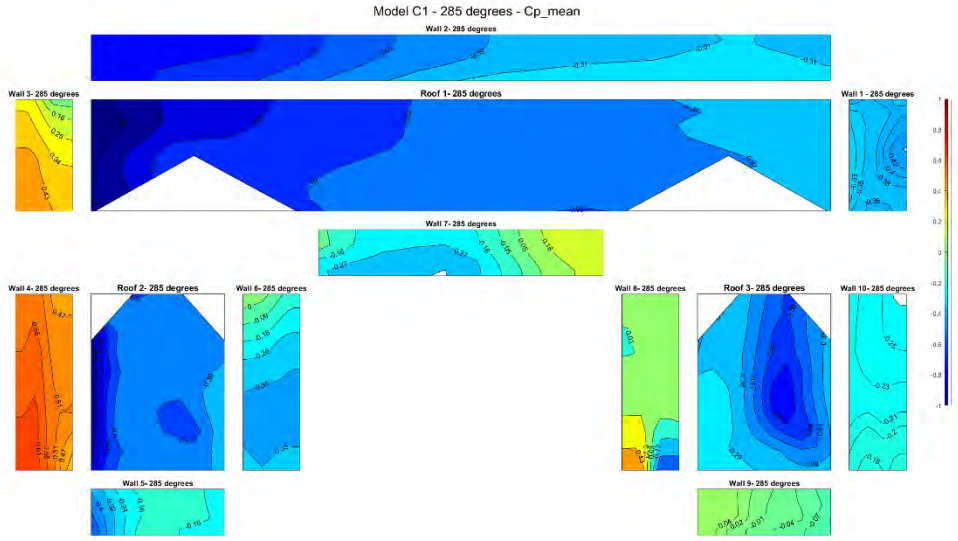

A 64. Mean Cp at 285 degrees for model C

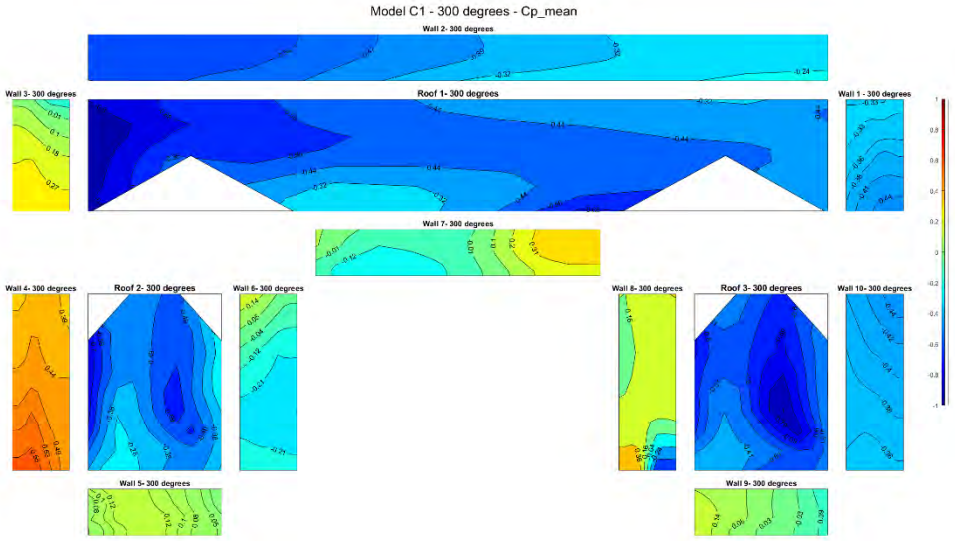

A 65. Mean Cp at 300 degrees for model C

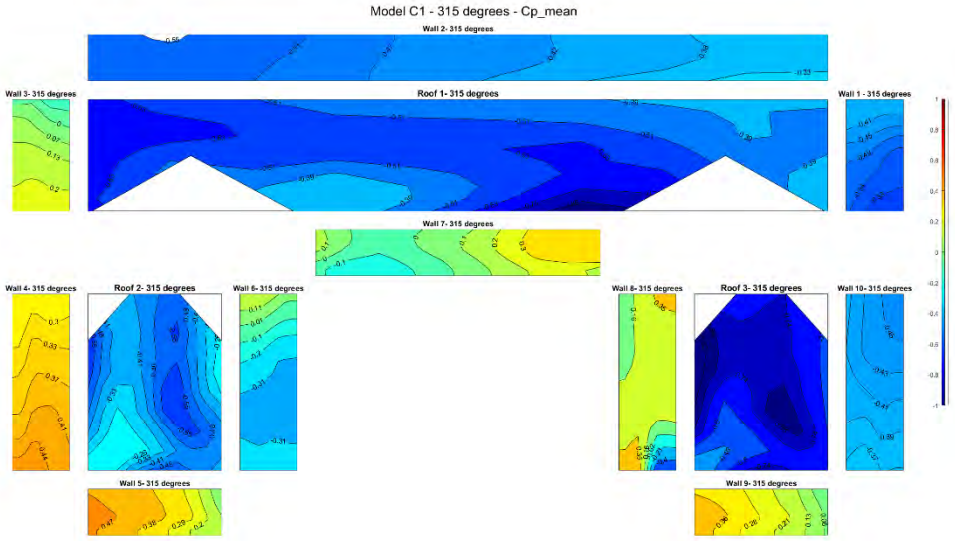

A 66. Mean Cp at 315 degrees for model C

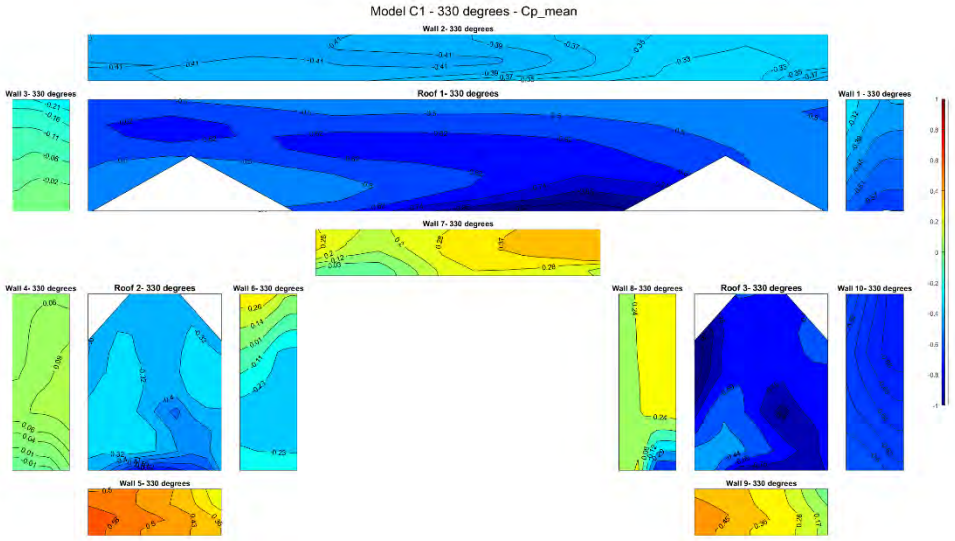

A 67. Mean Cp at 330 degrees for model C

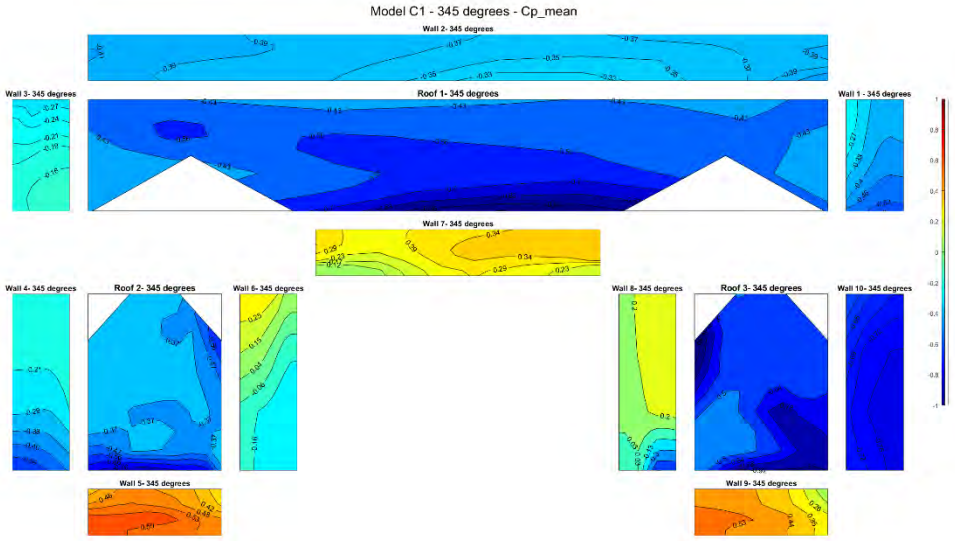

A 68. Mean Cp at 345 degrees for model C

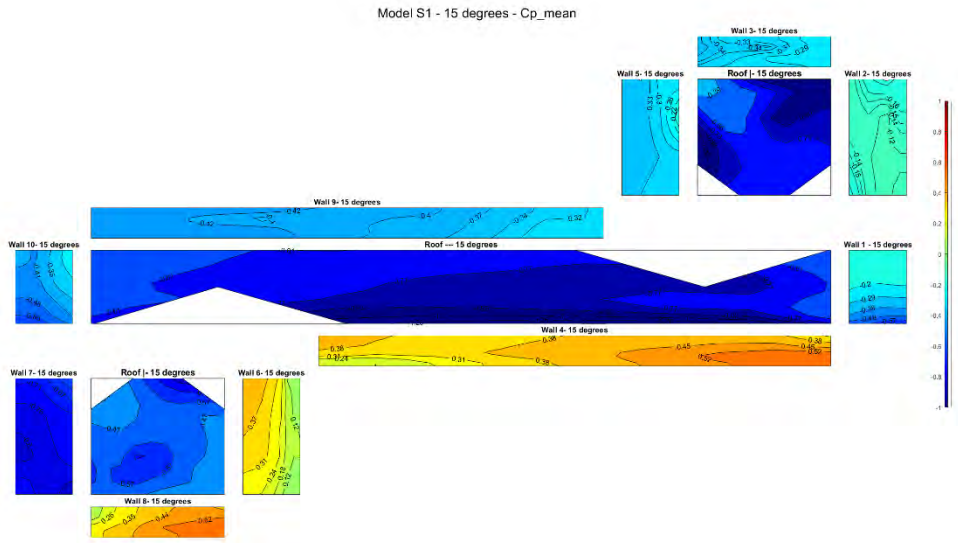

A 69. Mean Cp at 15 degrees for model S

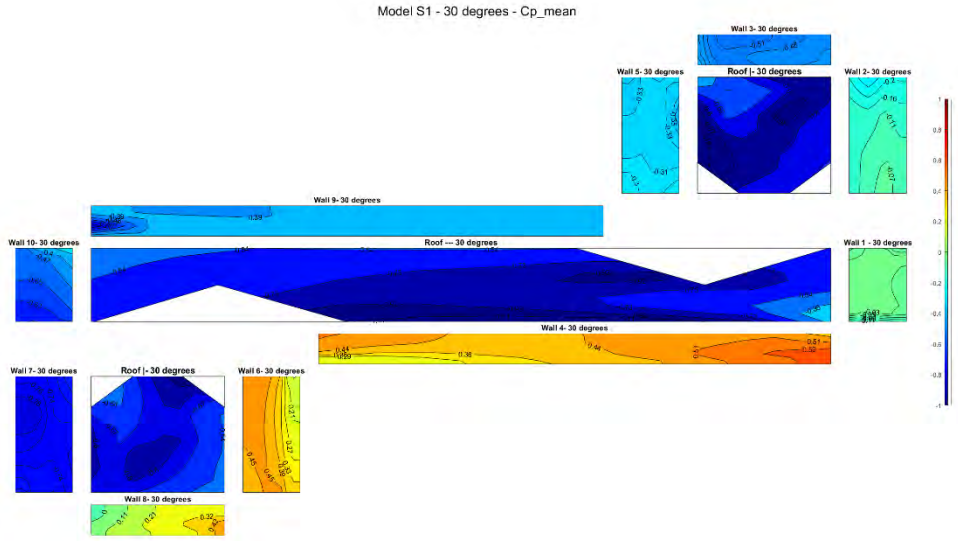

A 70. Mean Cp at 30 degrees for model S

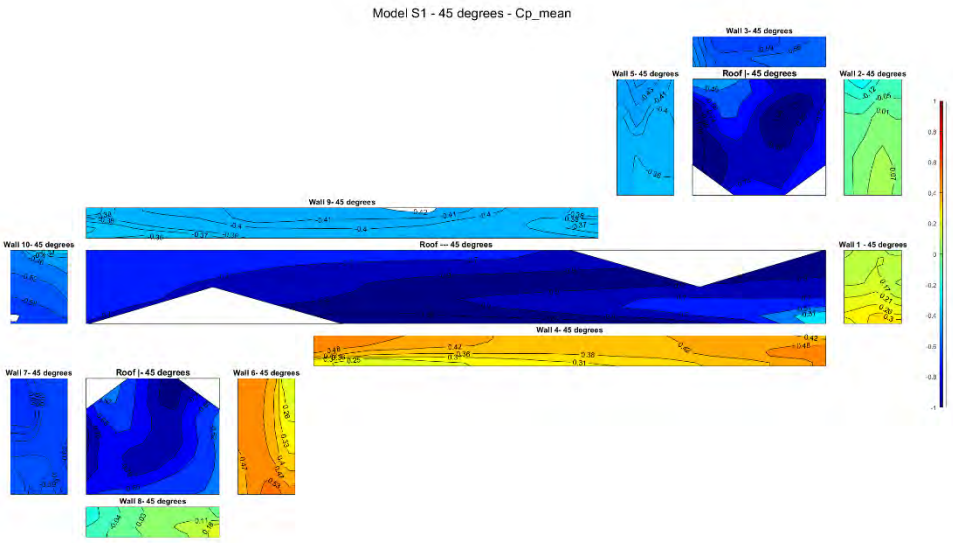

A 71. Mean Cp at 45 degrees for model S

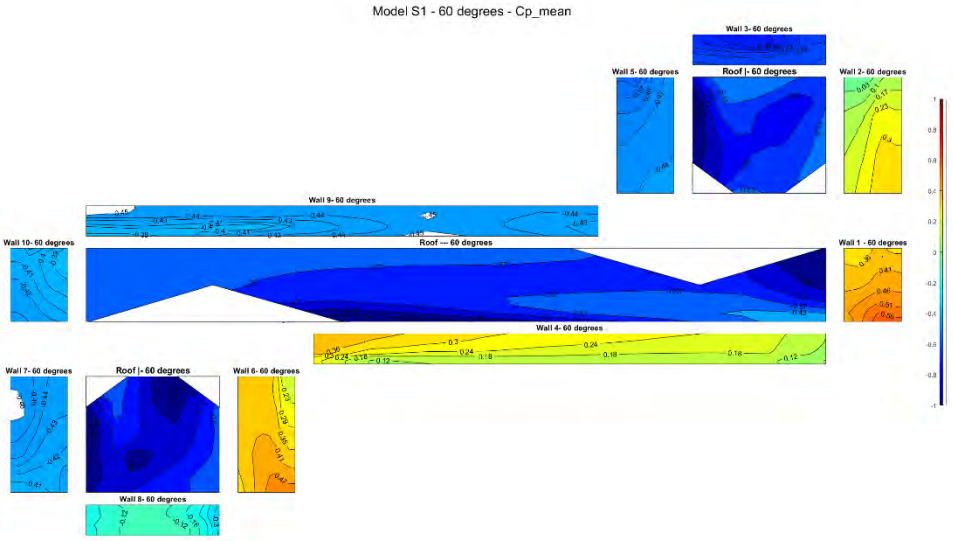

A 72. Mean Cp at 60 degrees for model S

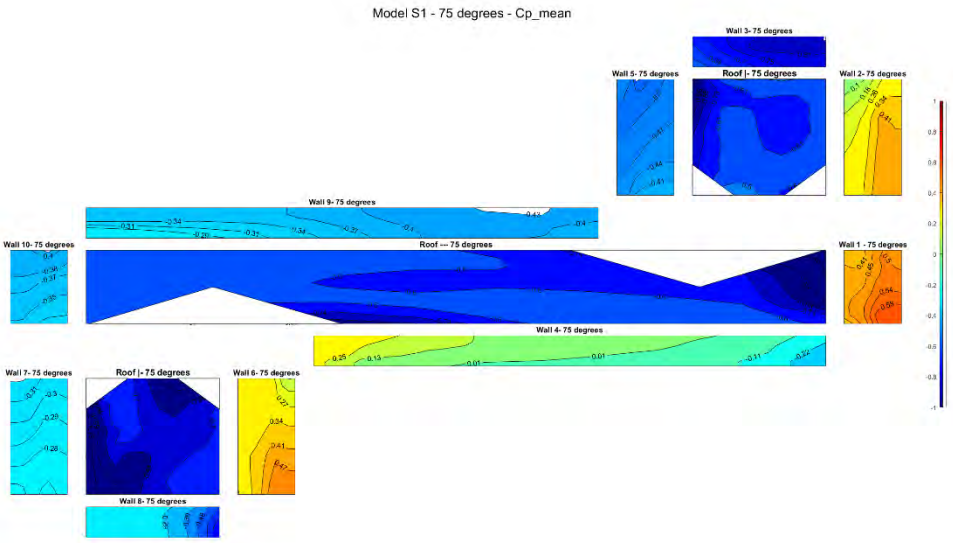

A 73. Mean Cp at 75 degrees for model S

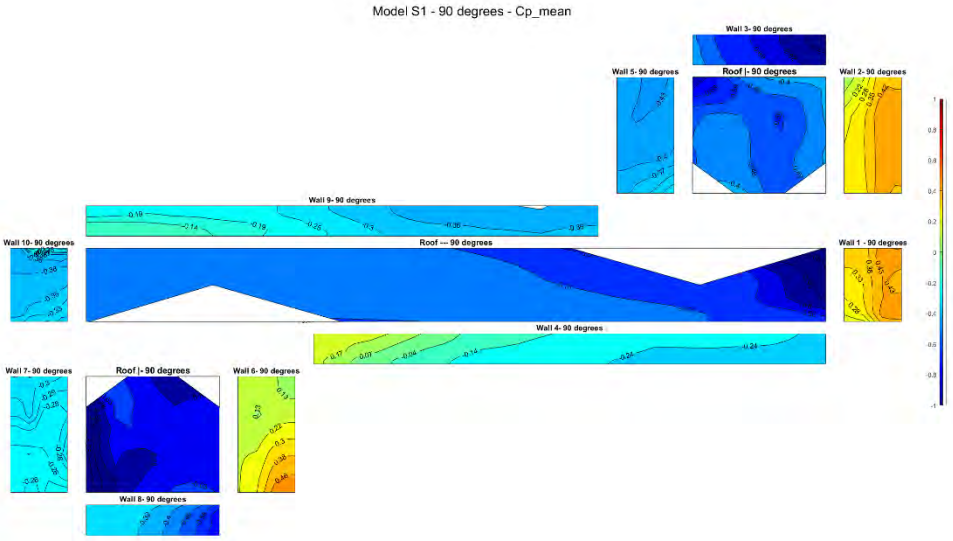

A 74. Mean Cp at 90 degrees for model S

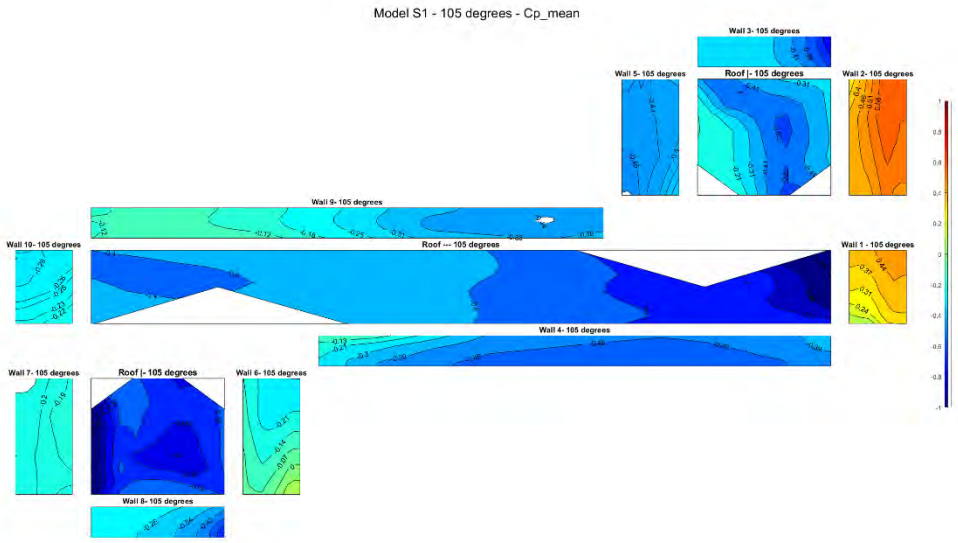

A 75. Mean Cp at 105 degrees for model S

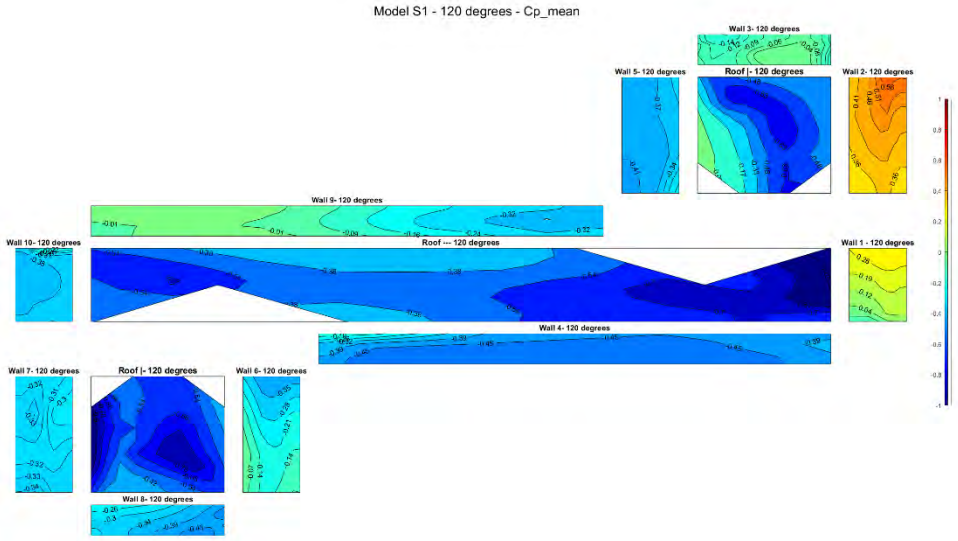

A 76. Mean Cp at 120 degrees for model S

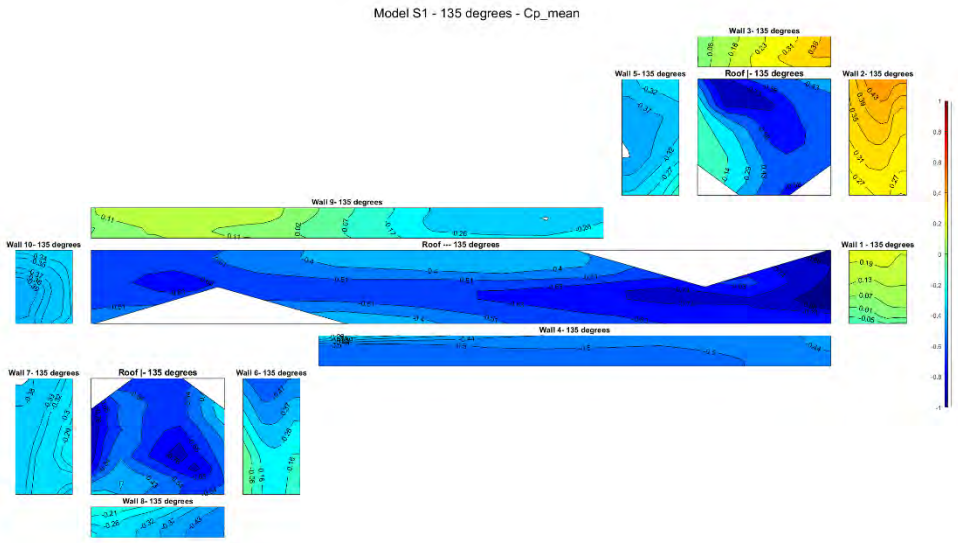

A 77. Mean Cp at 135 degrees for model S

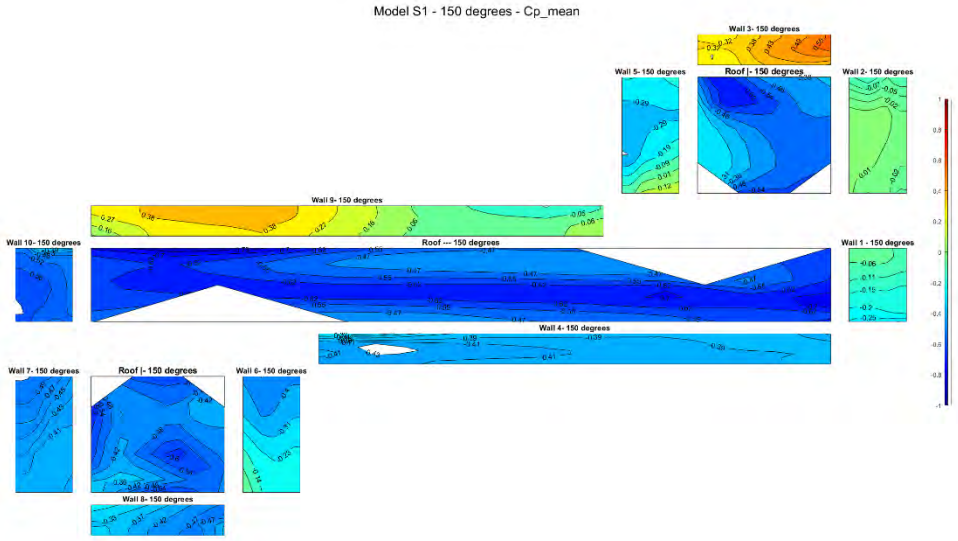

A 78. Mean Cp at 150 degrees for model S

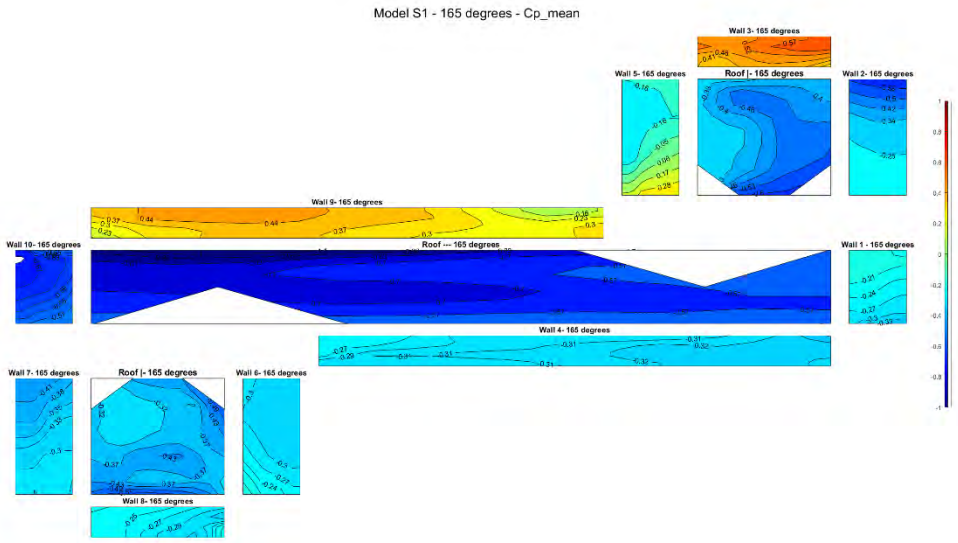

A 79. Mean Cp at 165 degrees for model S

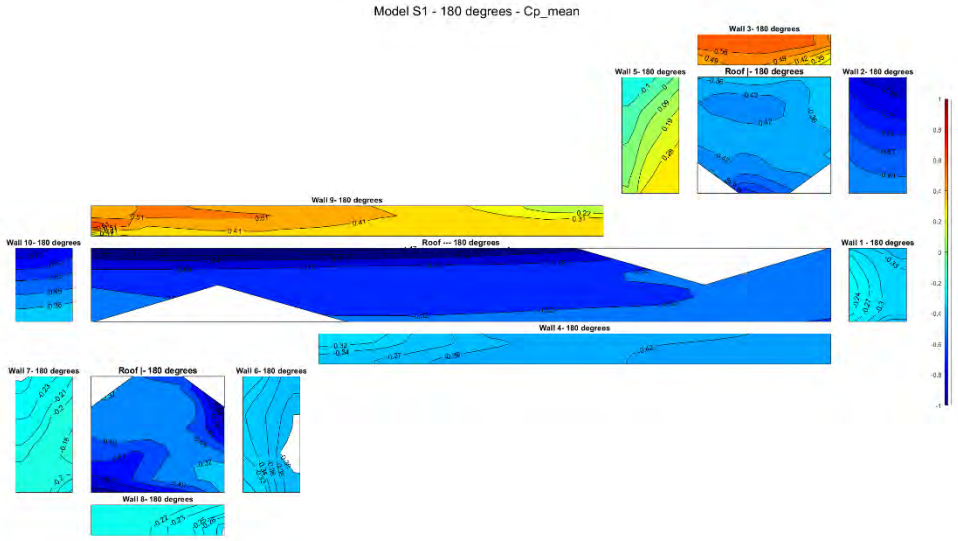

A 80. Mean Cp at 180 degrees for model S

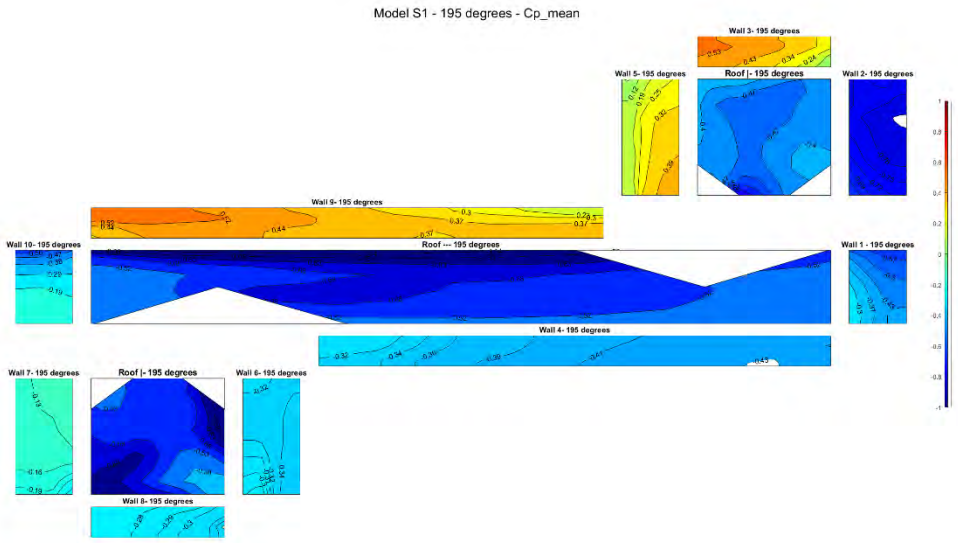

A 81. Mean Cp at 195 degrees for model S

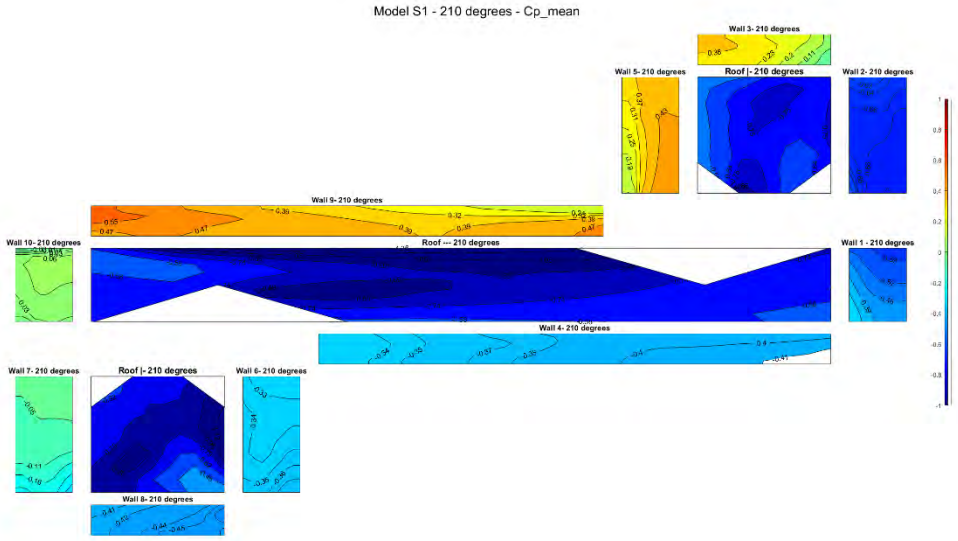

A 82. Mean Cp at 210 degrees for model S

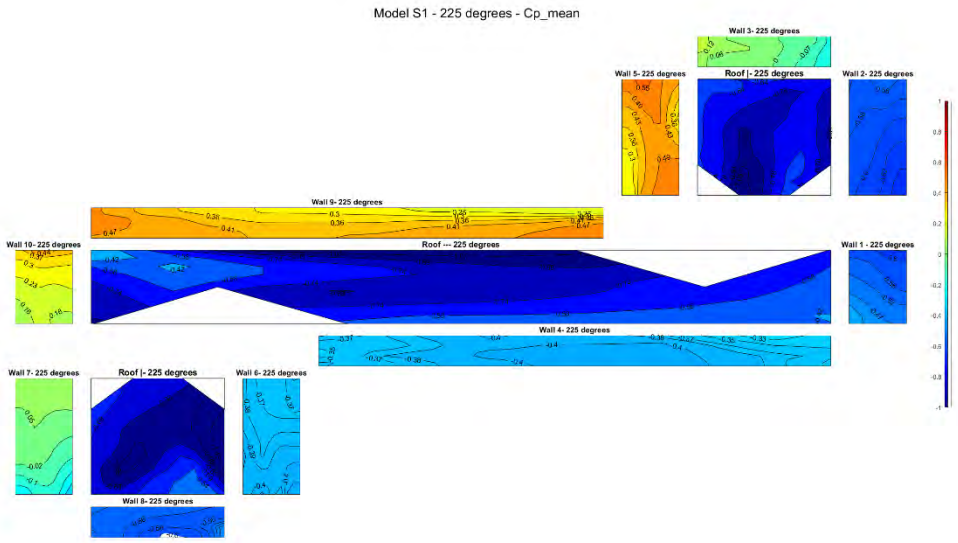

A 83. Mean Cp at 225 degrees for model S

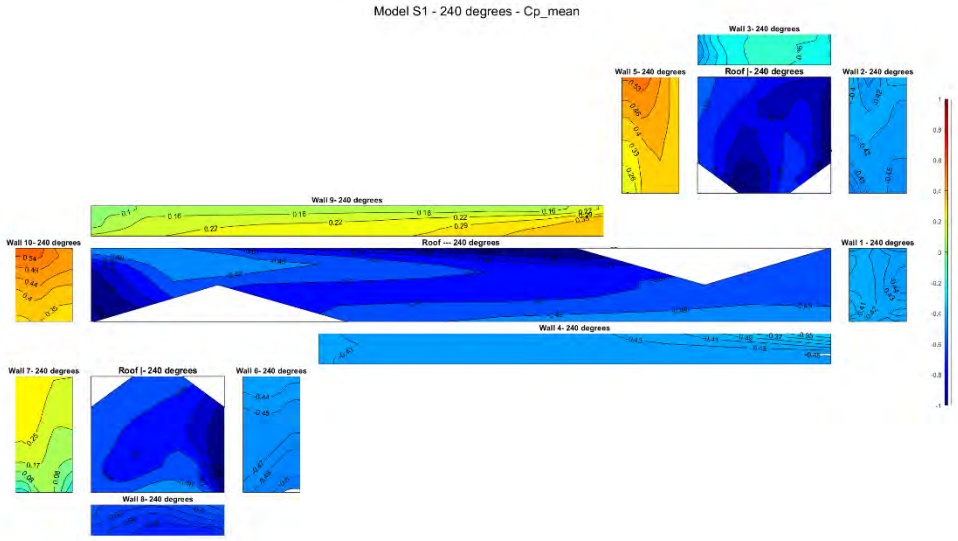

A 84. Mean Cp at 240 degrees for model S

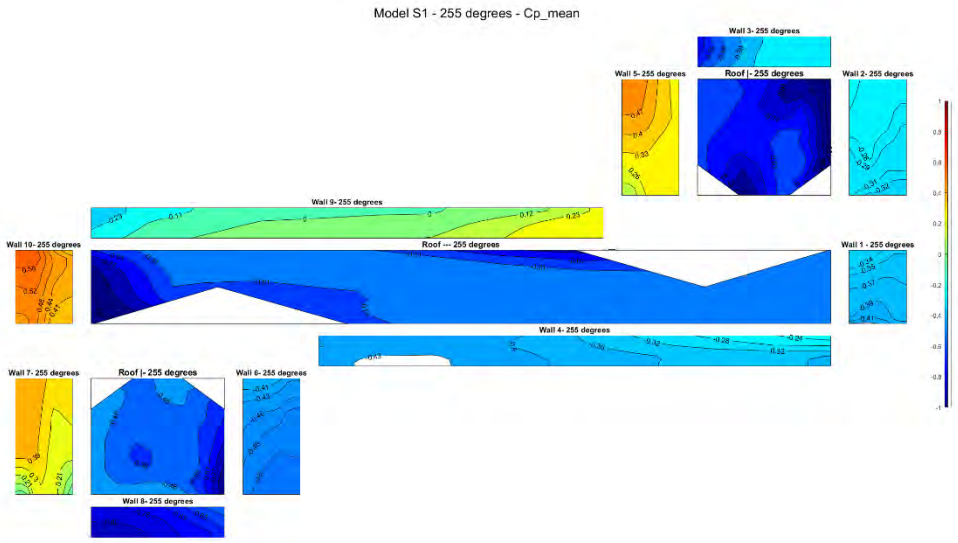

A 85. Mean Cp at 255 degrees for model S

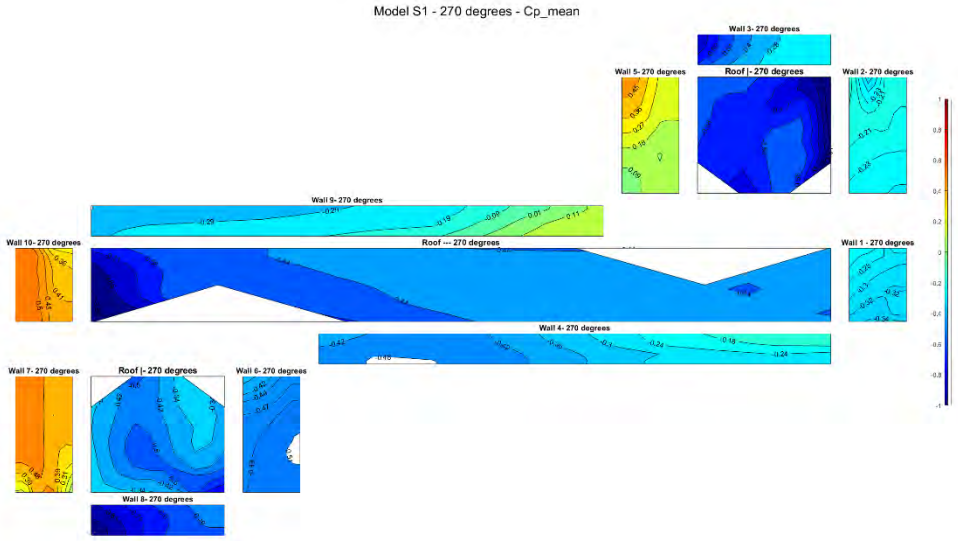

A 86. Mean Cp at 270 degrees for model S

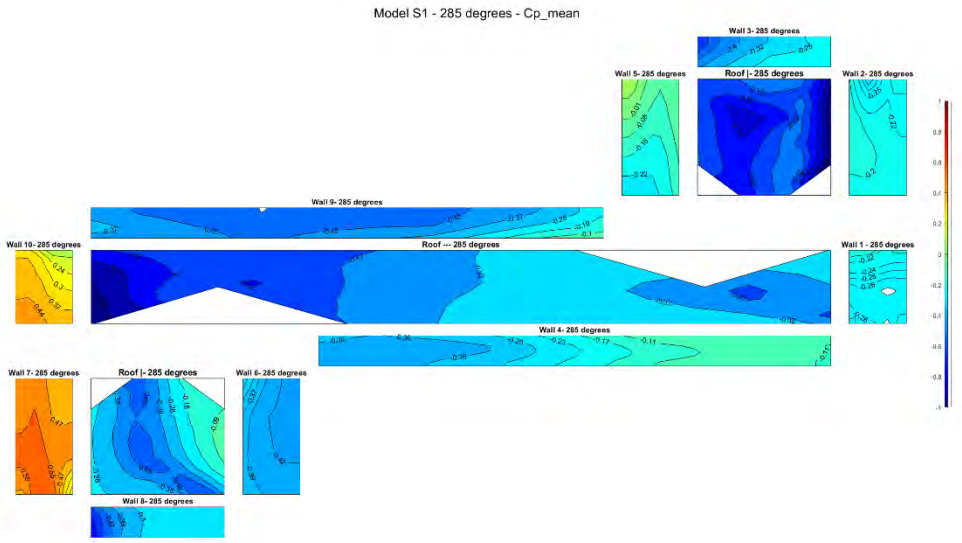

A 87. Mean Cp at 285 degrees for model S

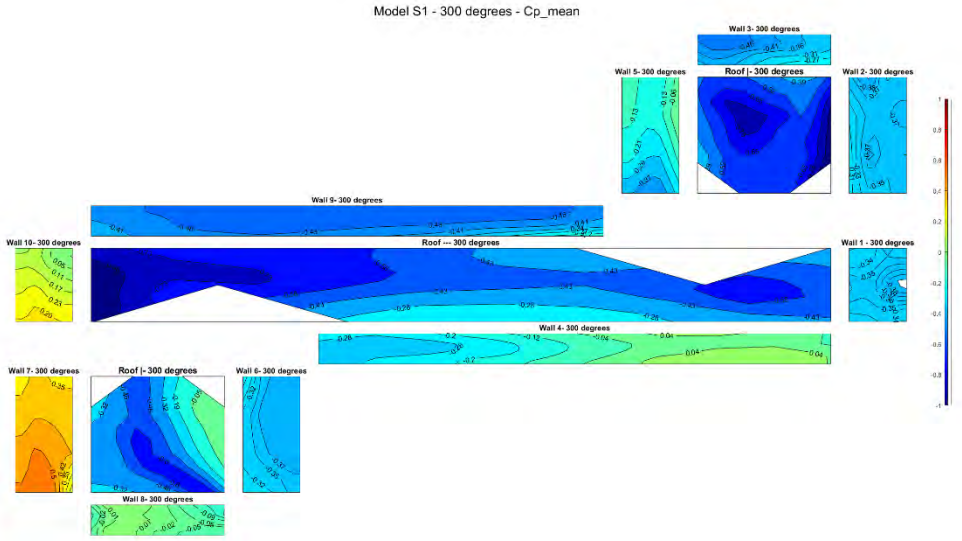

A 88. Mean Cp at 300 degrees for model S

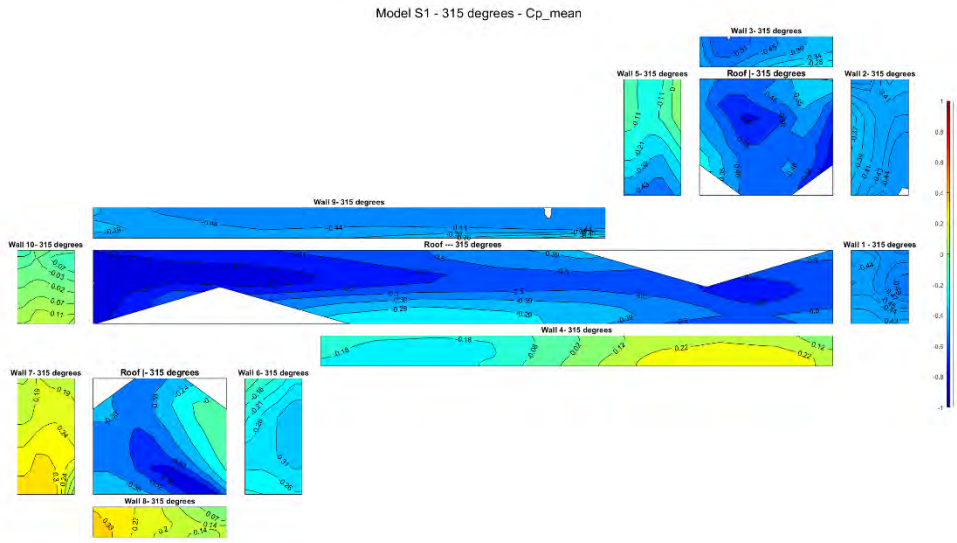

A 89. Mean Cp at 315 degrees for model S

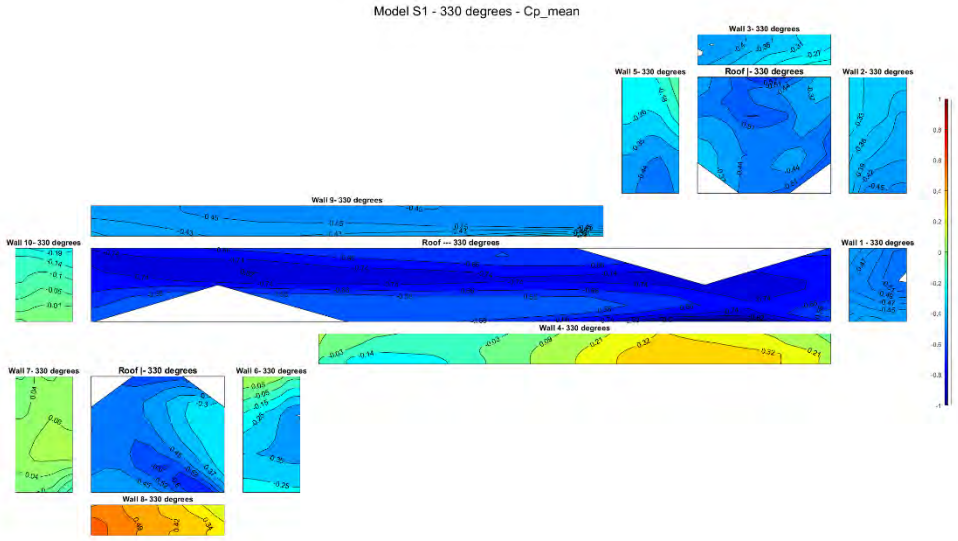

A 90. Mean Cp at 330 degrees for model S

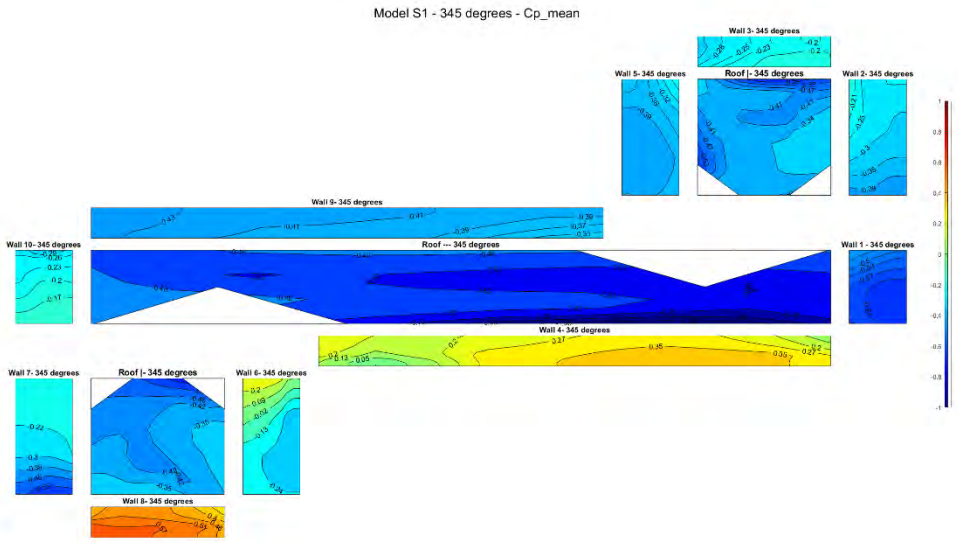

A 91. Mean Cp at 345 degrees for model S

Appendix B: Minimum Peak Pressure Coefficients

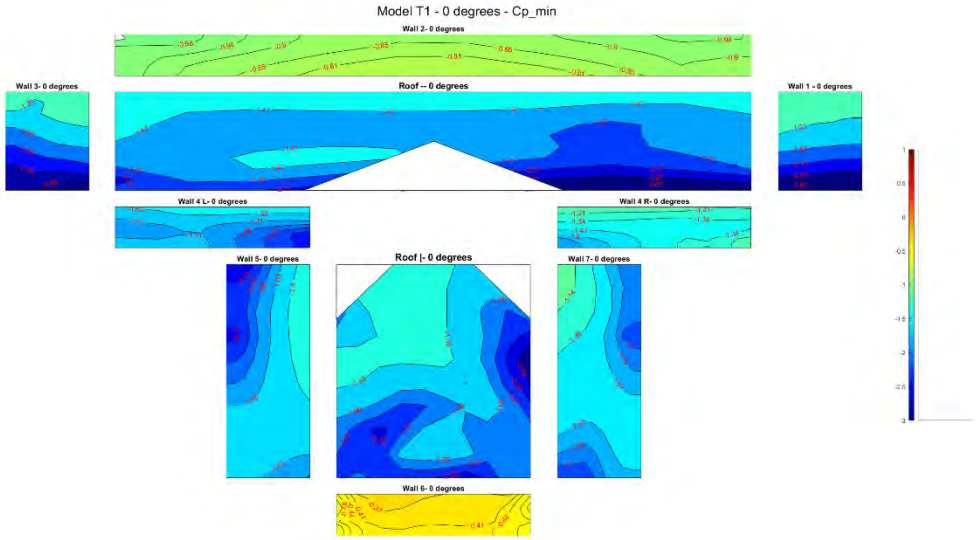

B 1. Minimum peak Cp at 0 degrees for model T

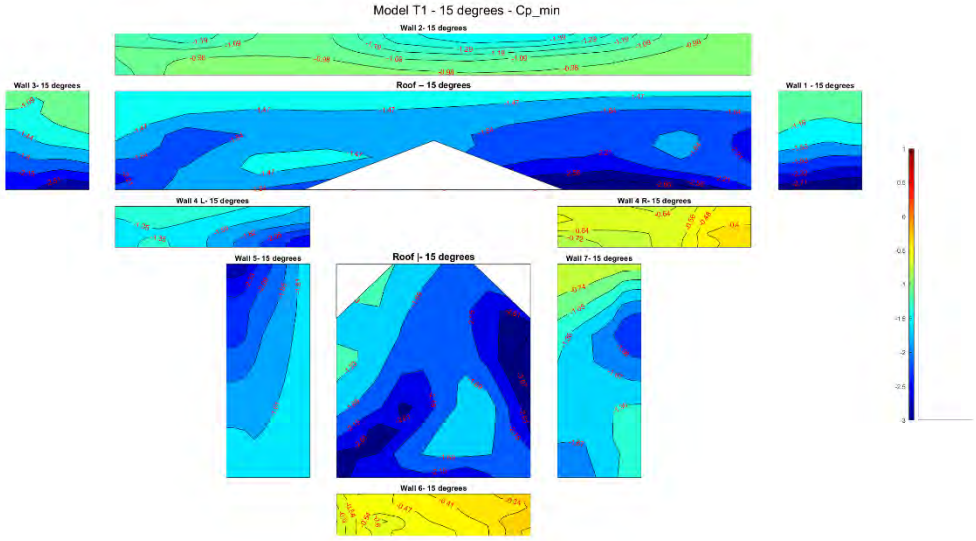

B 2. Minimum peak Cp at 15 degrees for model T

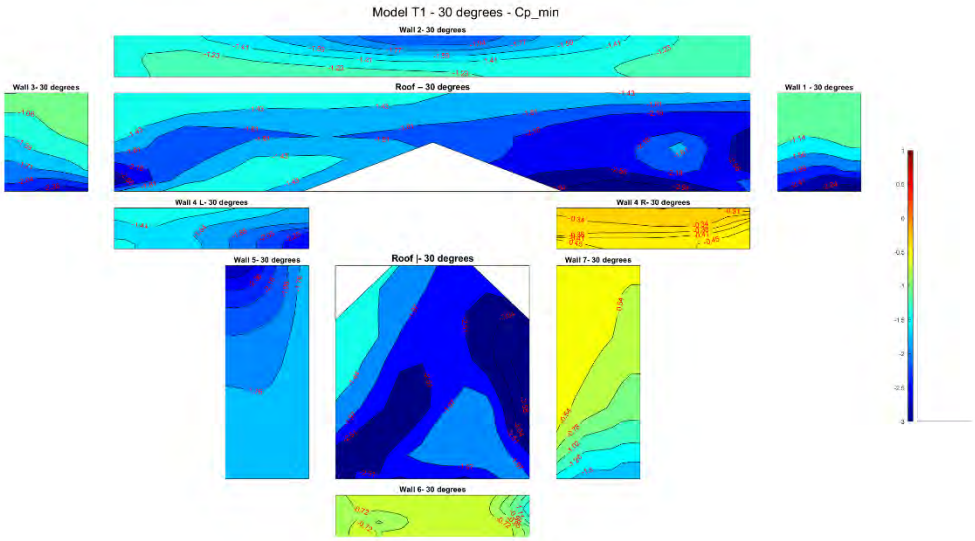

B 3. Minimum peak Cp at 30 degrees for model T

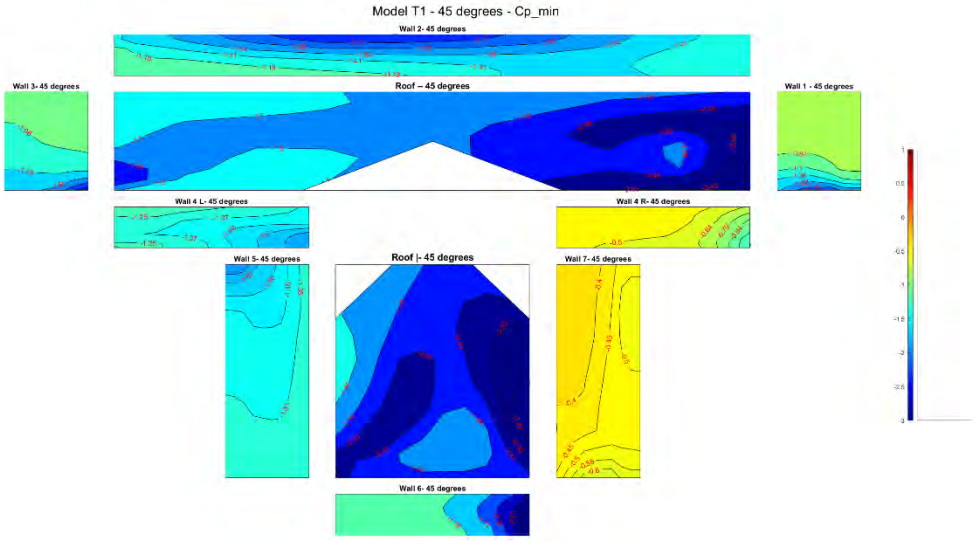

B 4. Minimum peak Cp at 45 degrees for model T

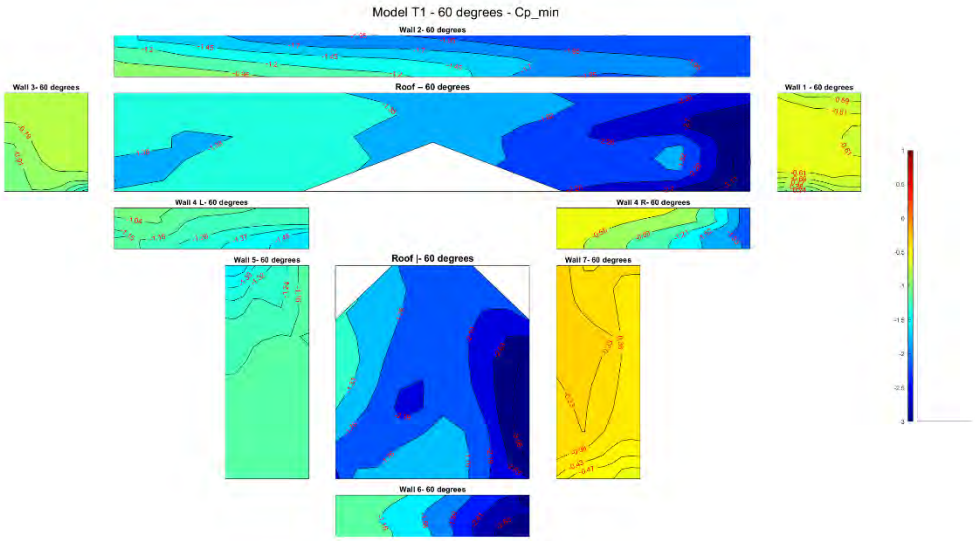

B 5. Minimum peak Cp at 60 degrees for model T

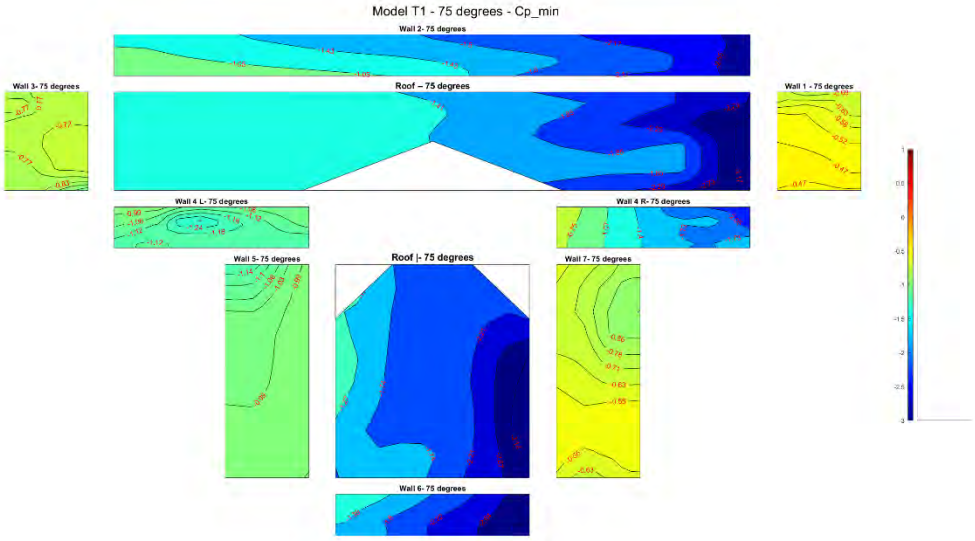

B 6. Minimum peak Cp at 75 degrees for model T

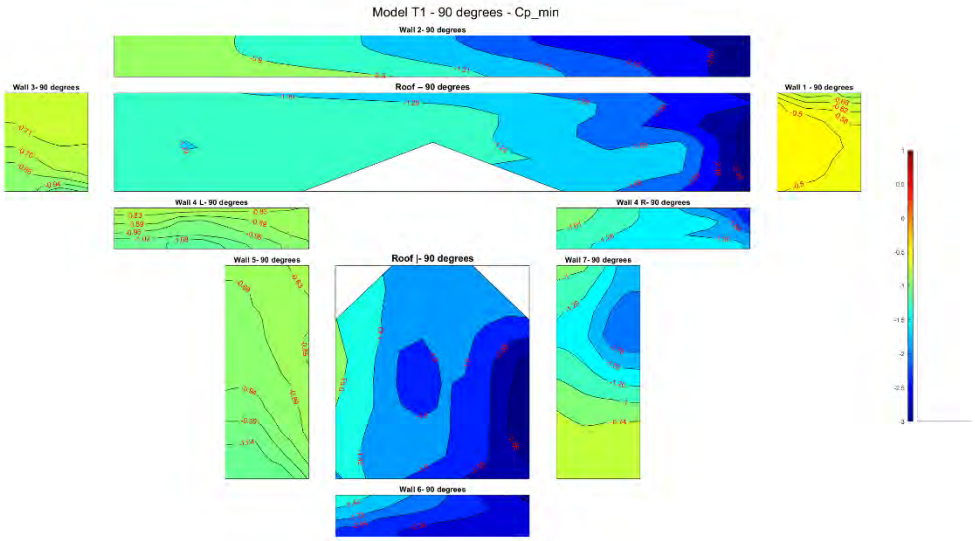

B 7. Minimum peak Cp at 90 degrees for model T

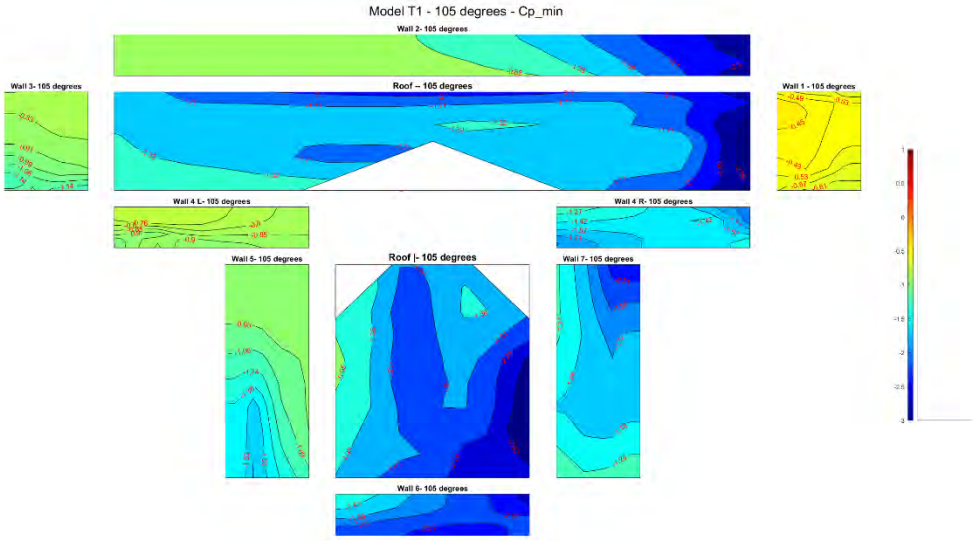

B 8. Minimum peak Cp at 105 degrees for model T

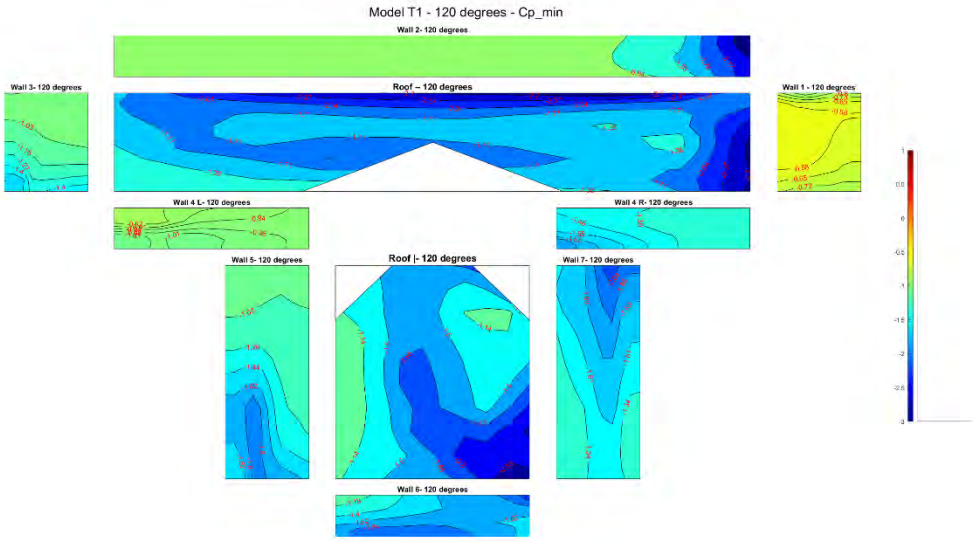

B 9. Minimum peak Cp at 120 degrees for model T

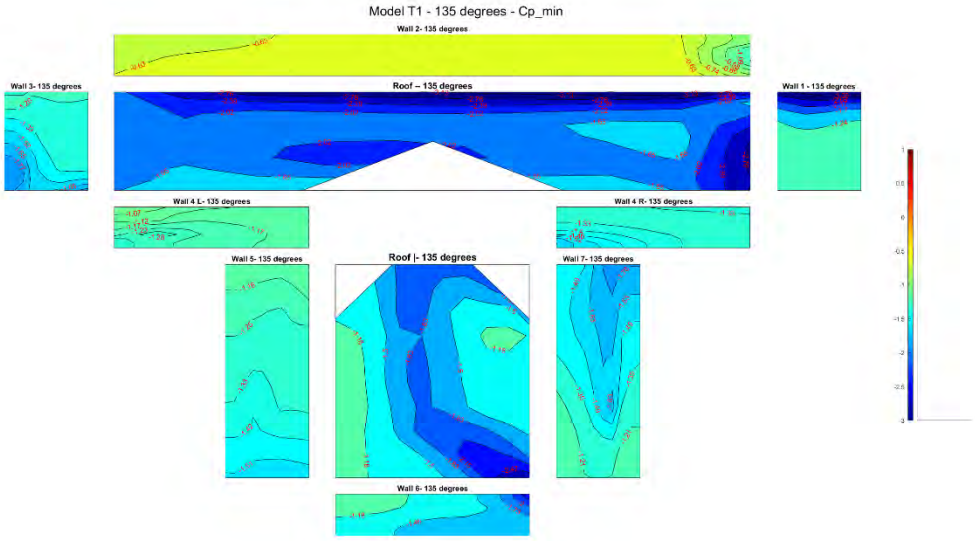

B 10. Minimum peak Cp at 135 degrees for model T

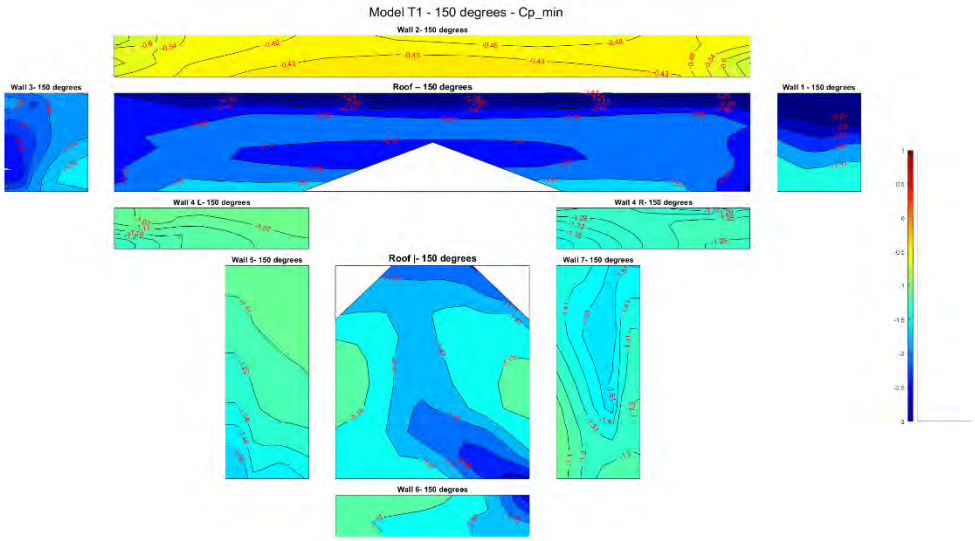

B 11. Minimum peak Cp at 150 degrees for model T

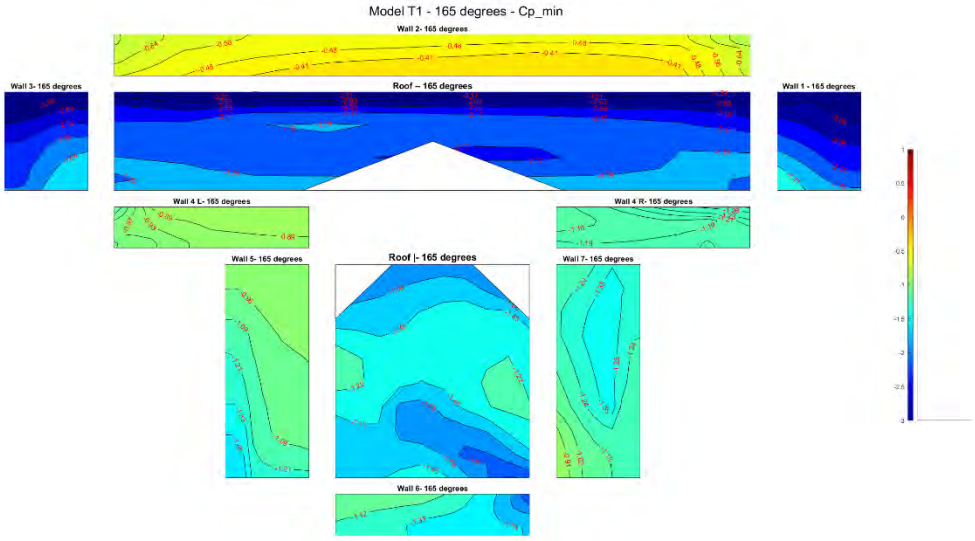

B 12. Minimum peak Cp at 165 degrees for model T

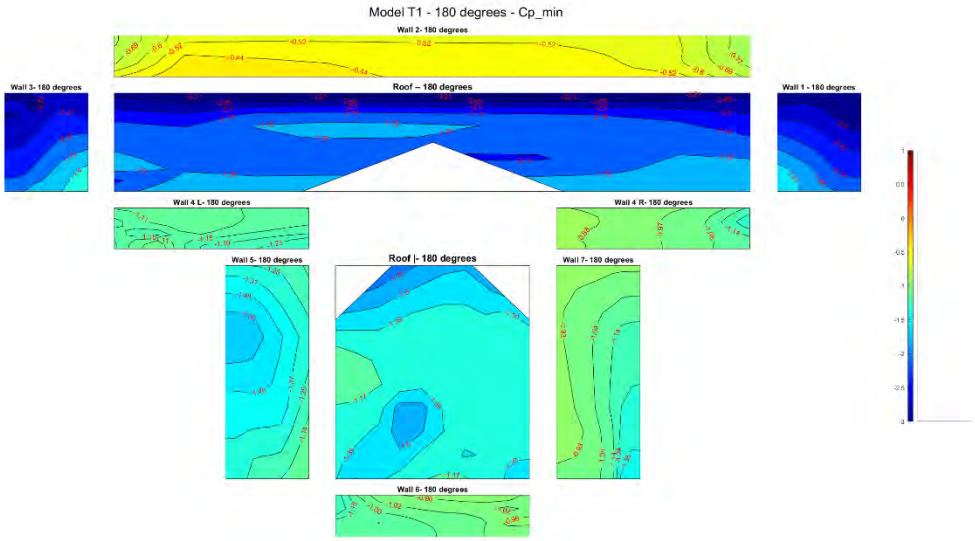

B 13. Minimum peak Cp at 180 degrees for model T

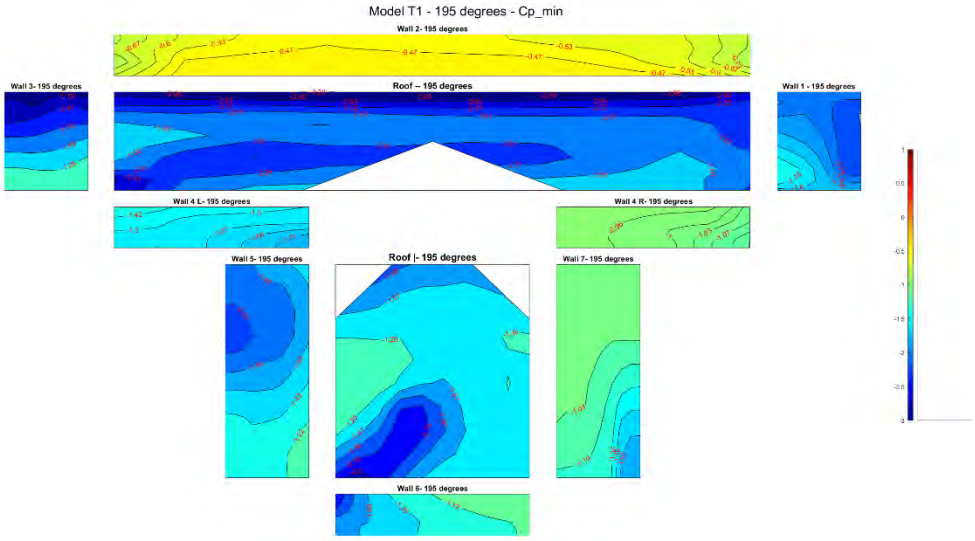

B 14. Minimum peak Cp at 195 degrees for model T

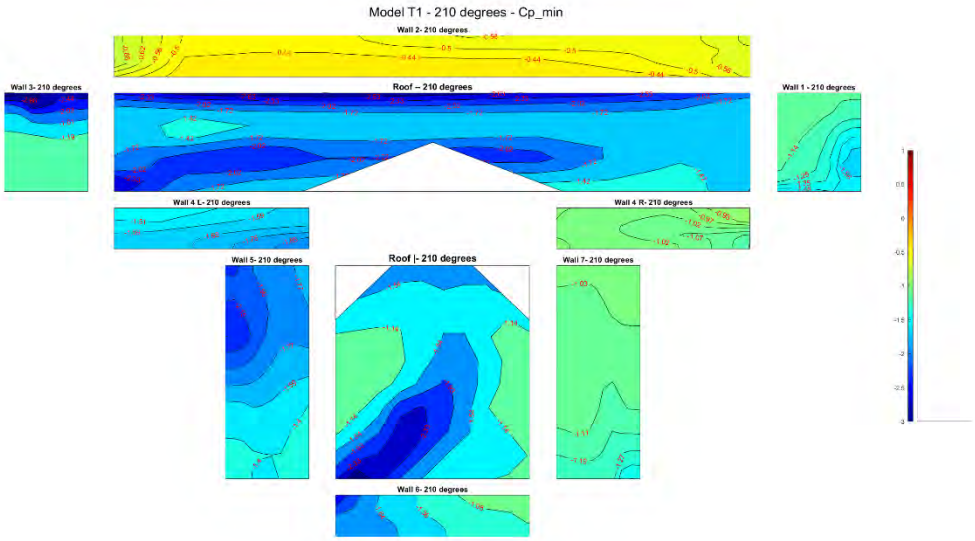

B 15. Minimum peak Cp at 210. degrees for model T

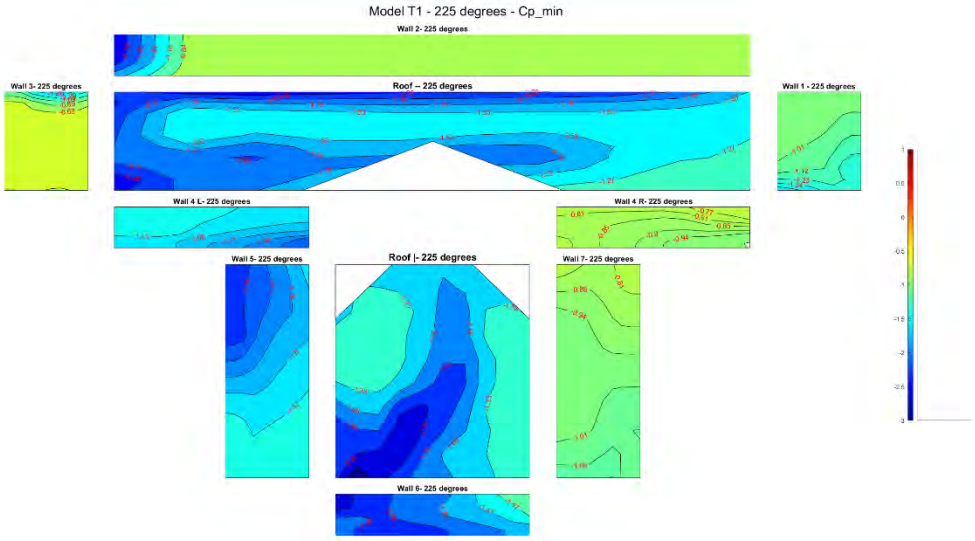

B 16. Minimum peak Cp at 225 degrees for model T

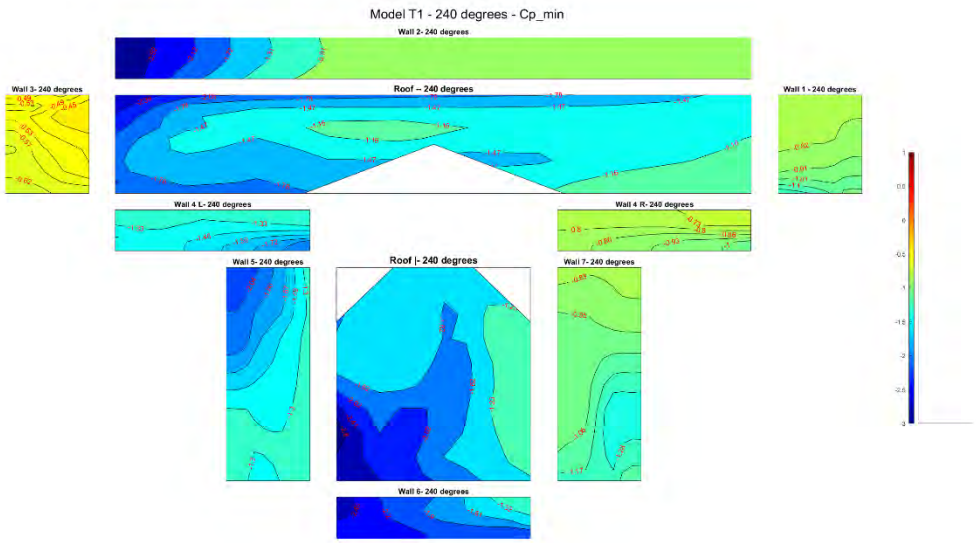

B 17. Minimum peak Cp at 240 degrees for model T

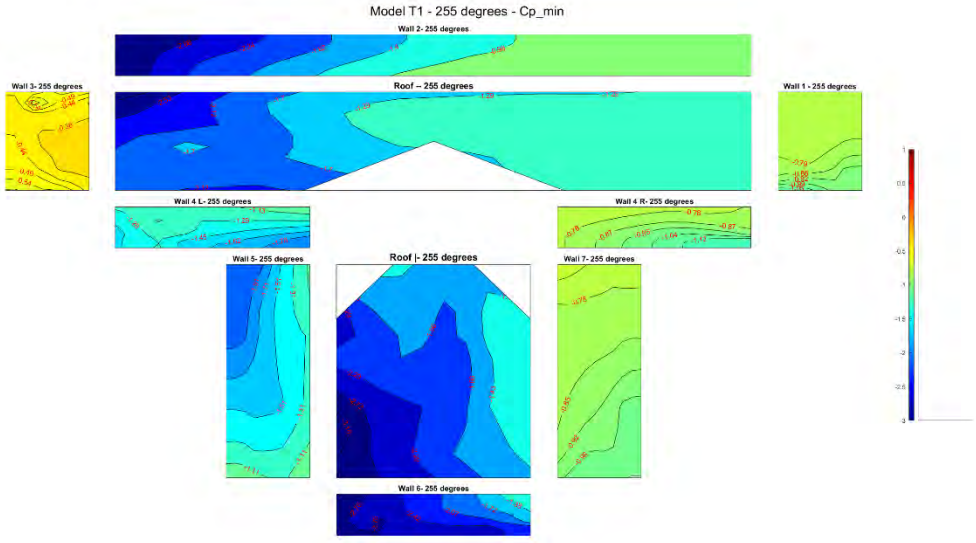

B 18. Minimum peak Cp at 255 degrees for model T

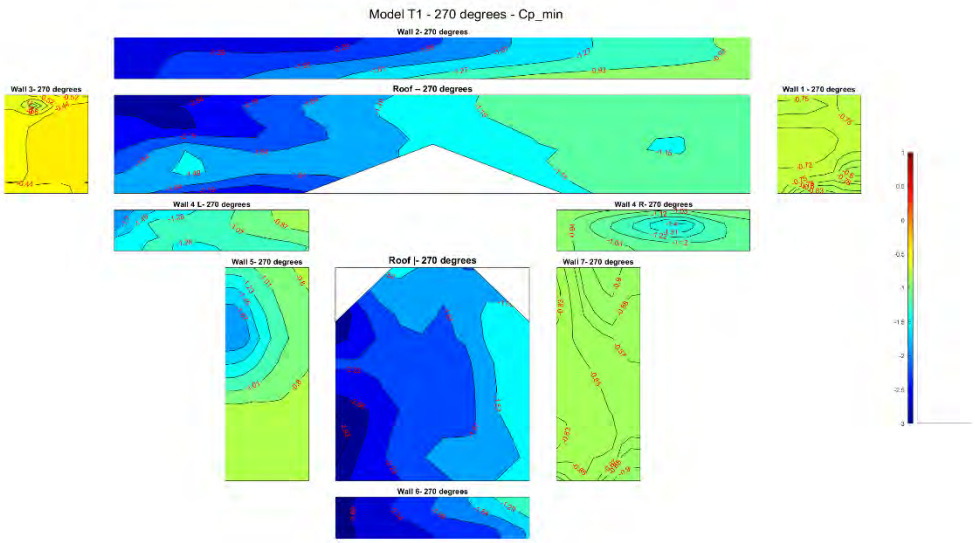

B 19. Minimum peak Cp at 270 degrees for model T

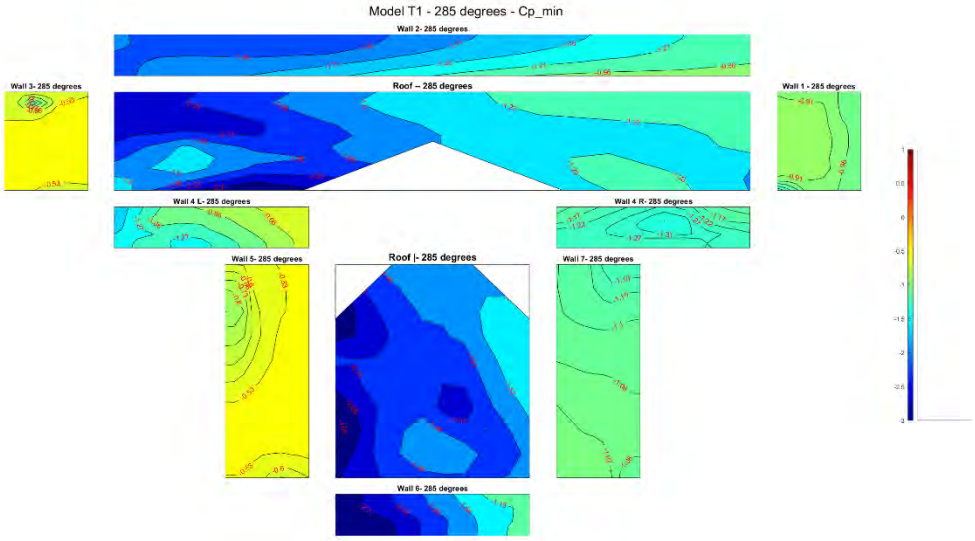

B 20. Minimum peak Cp at 285 degrees for model T

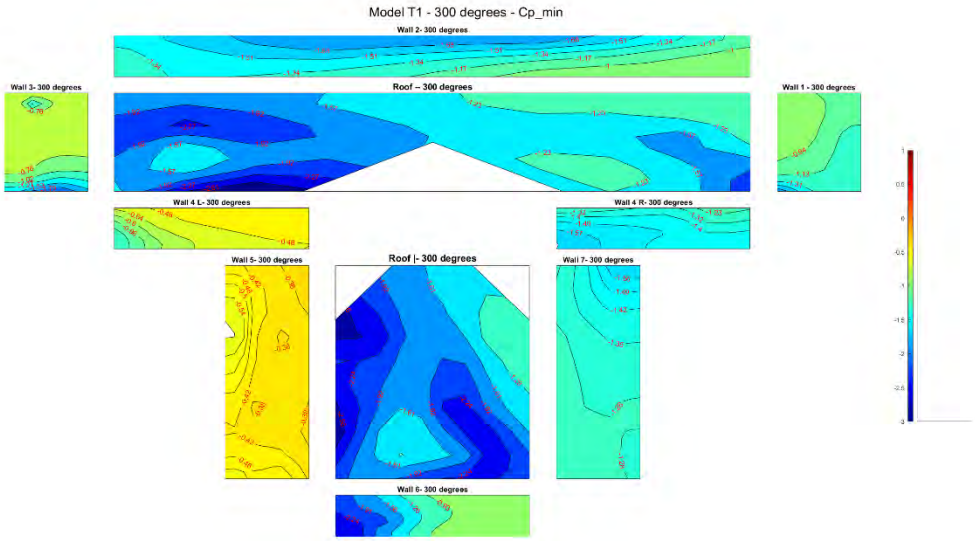

B 21. Minimum peak Cp at 300 degrees for model T

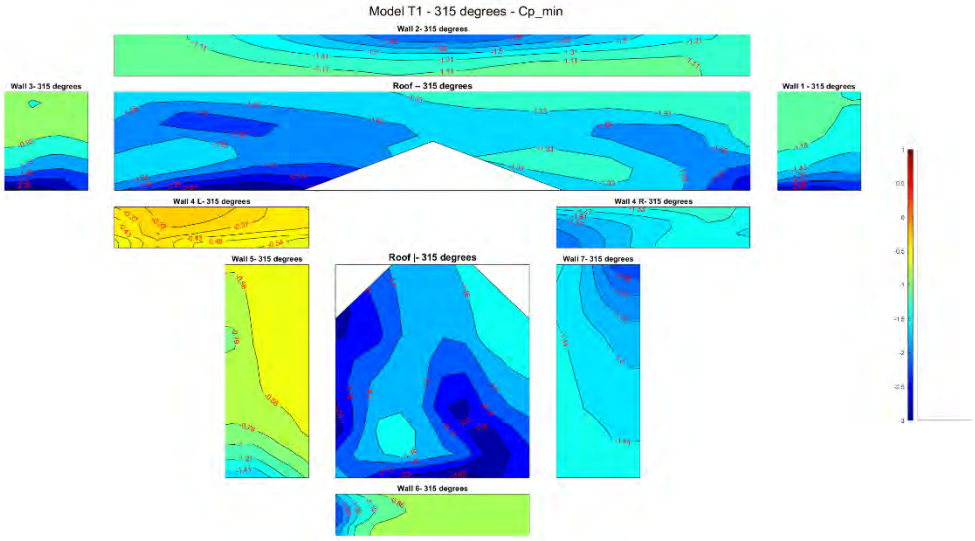

B 22. Minimum peak Cp at 315 degrees for model T

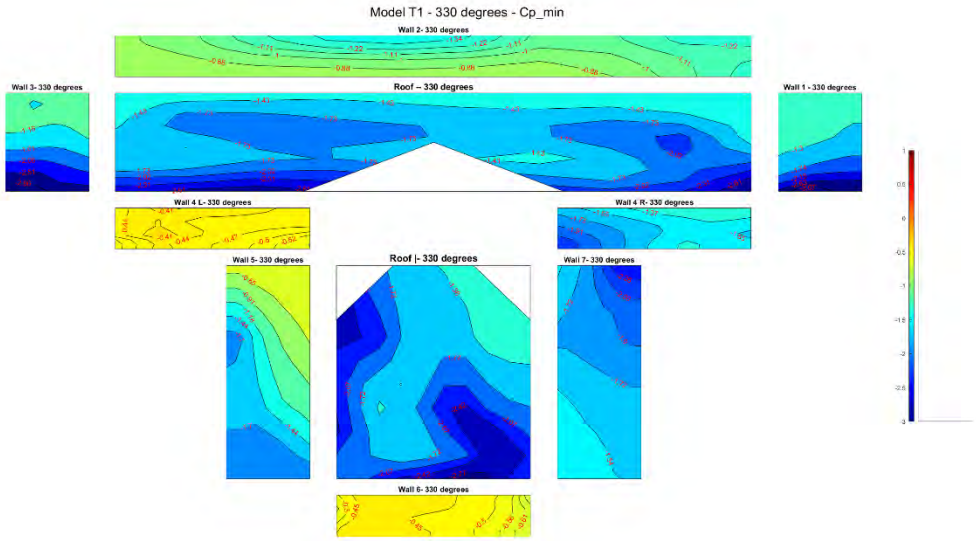

B 23. Minimum peak Cp at 330 degrees for model T

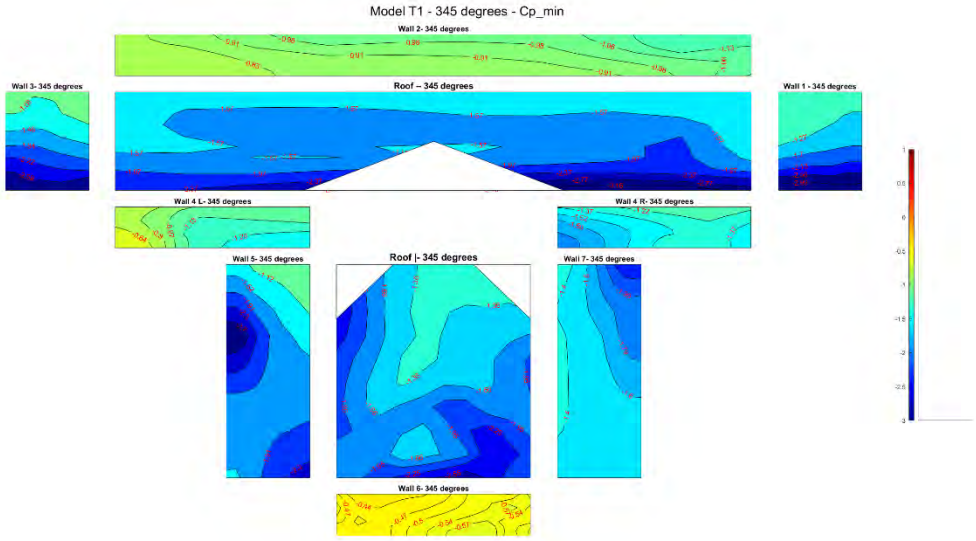

B 24. Minimum peak Cp at 345 degrees for model T

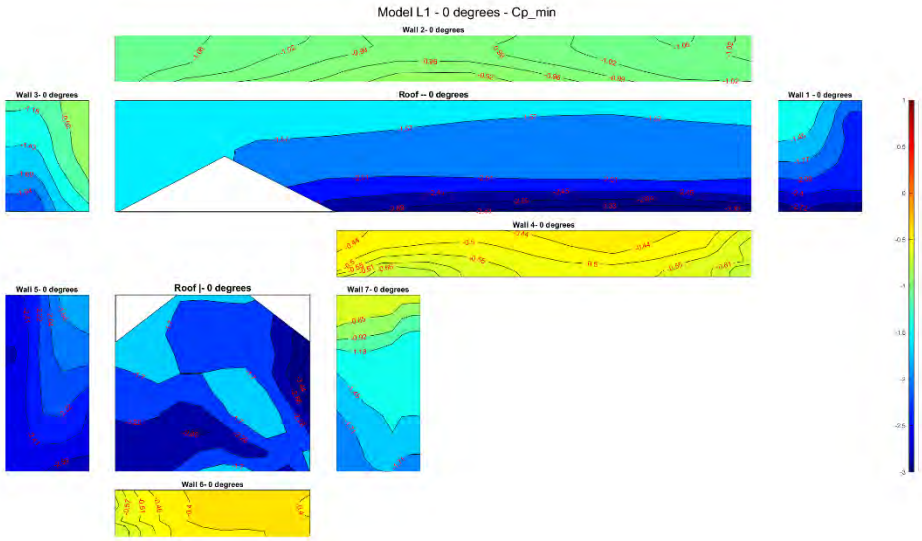

B 25. Minimum peak Cp at 0 degrees for model L

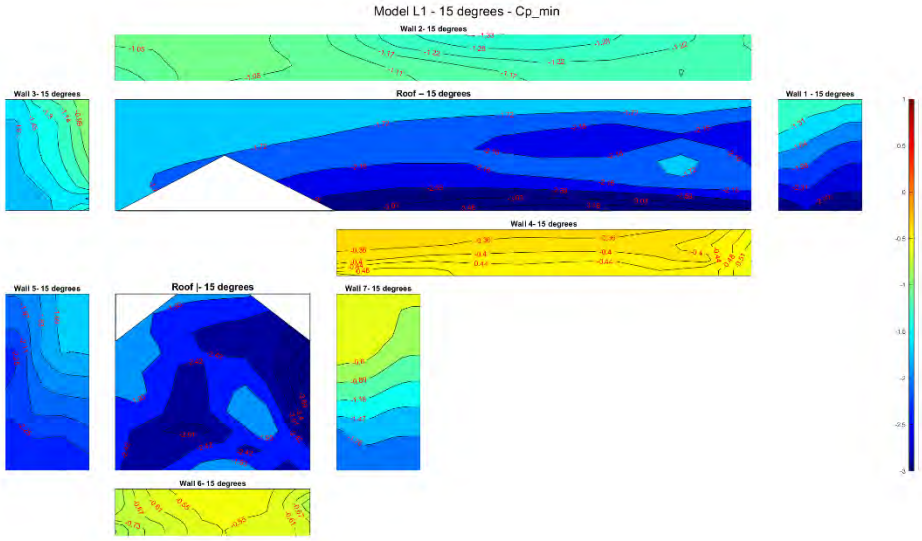

B 26. Minimum peak Cp at 15 degrees for model L

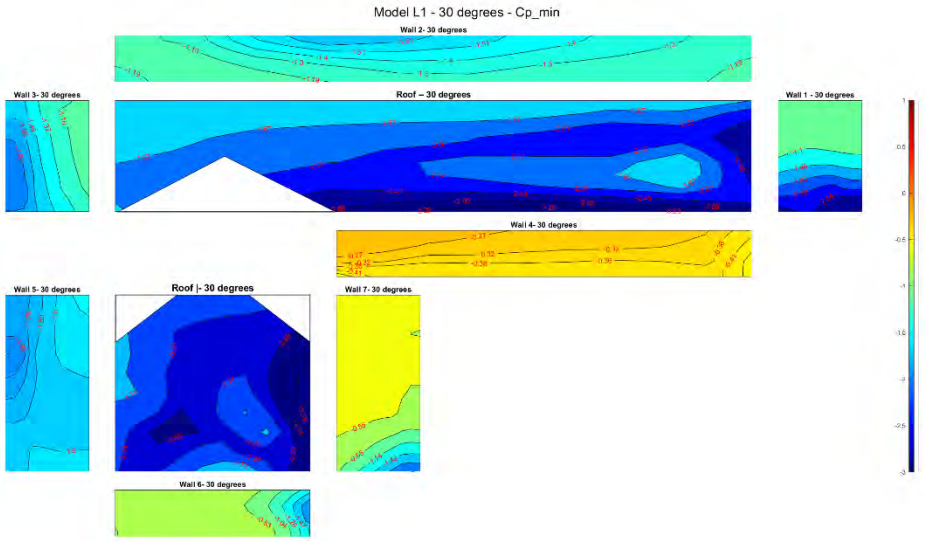

B 27. Minimum peak Cp at 30 degrees for model L

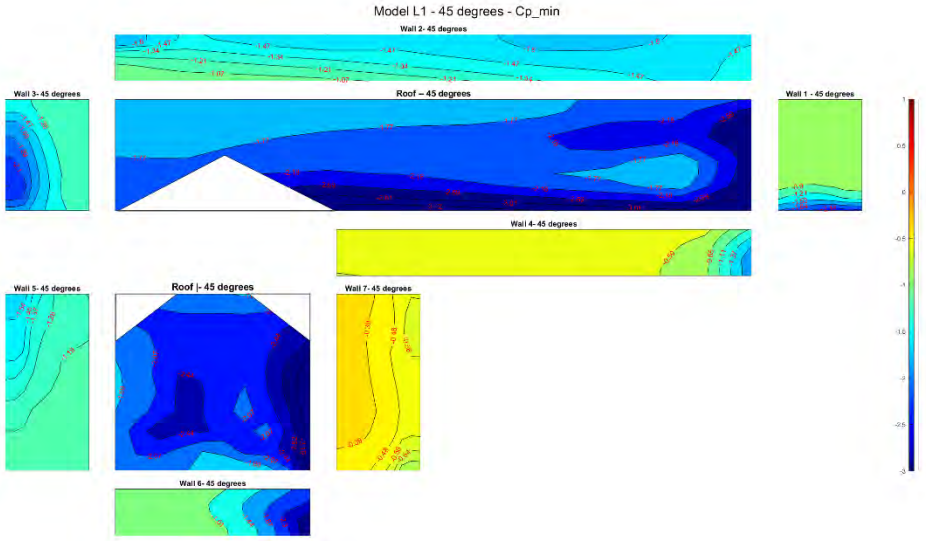

B 28. Minimum peak Cp at 45 degrees for model L

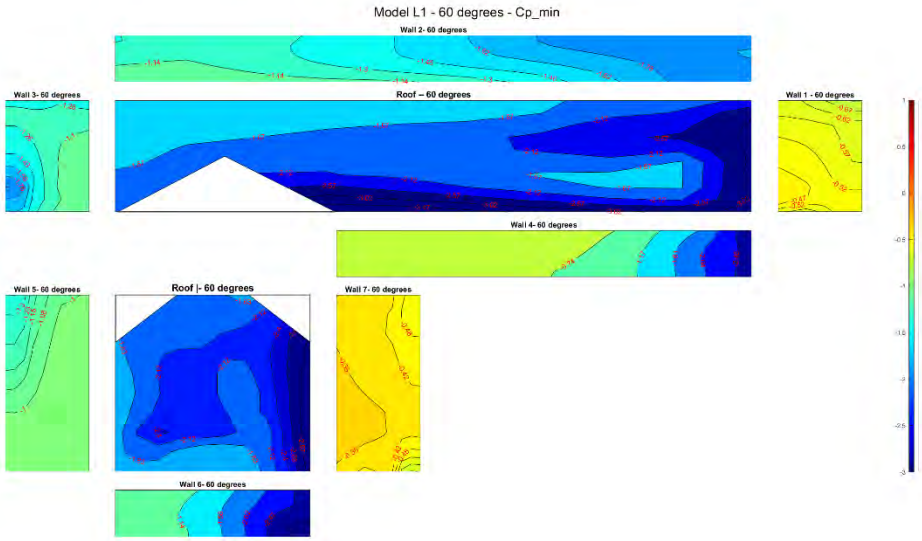

B 29. Minimum peak Cp at 60 degrees for model L

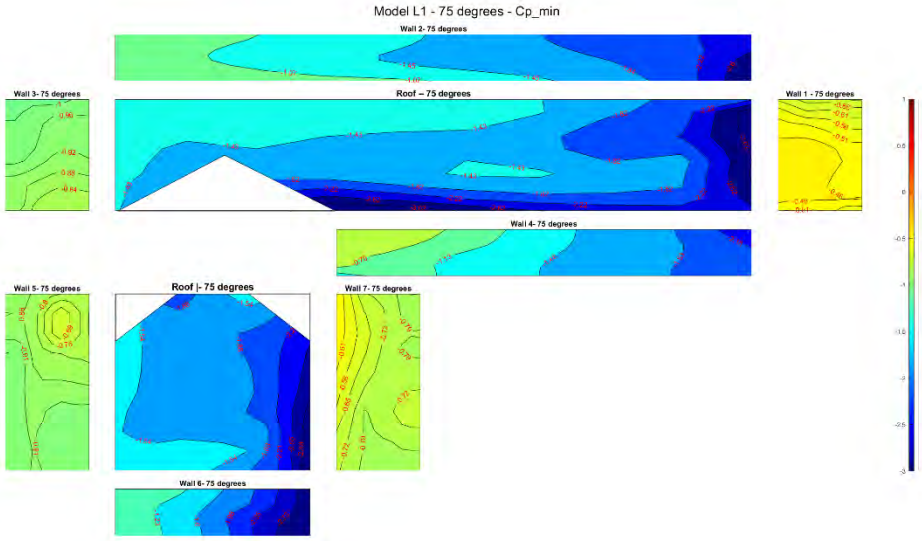

B 30. Minimum peak Cp at 75 degrees for model L

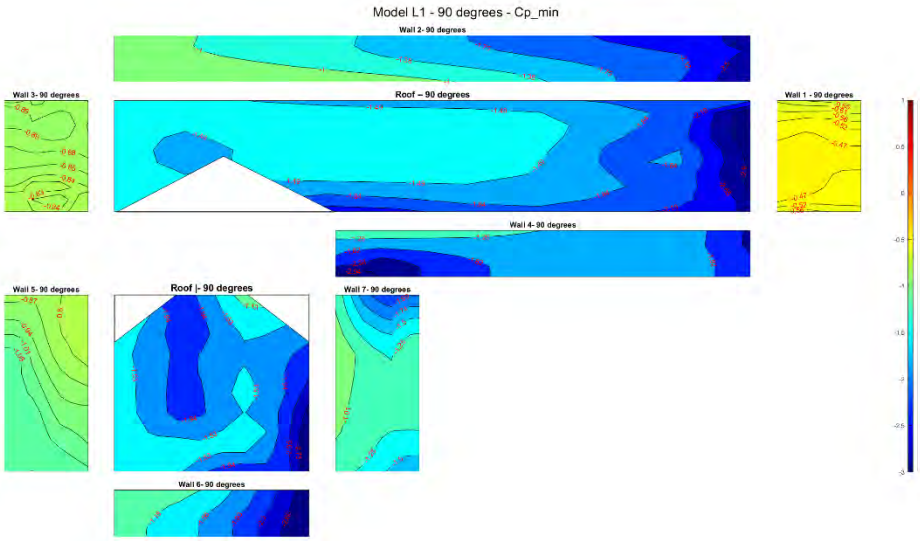

B 31. Minimum peak Cp at 90 degrees for model L

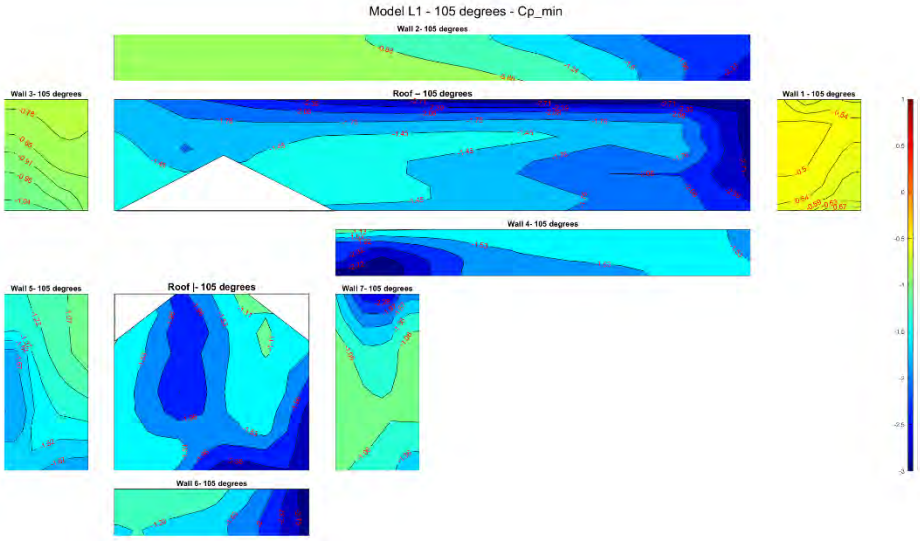

B 32. Minimum peak Cp at 105 degrees for model L

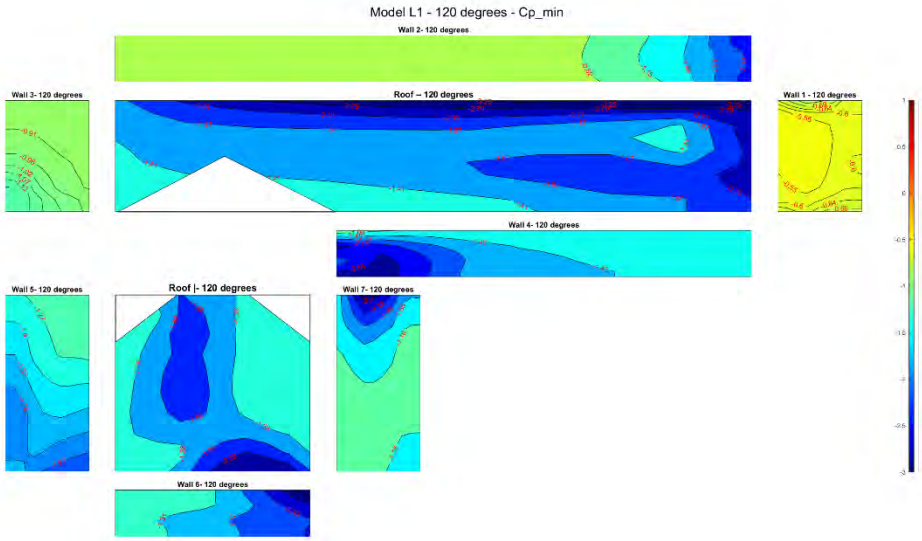

B 33. Minimum peak Cp at 120 degrees for model L

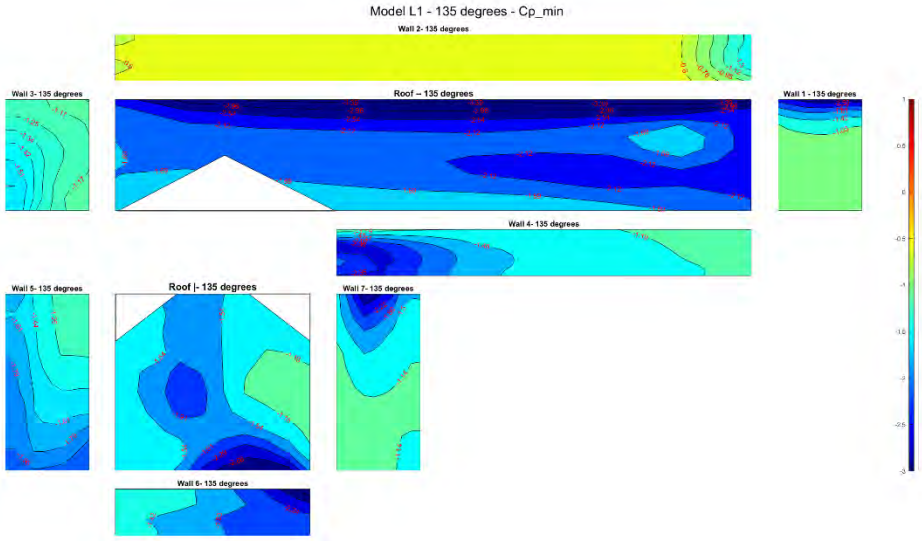

B 34. Minimum peak Cp at 135 degrees for model L

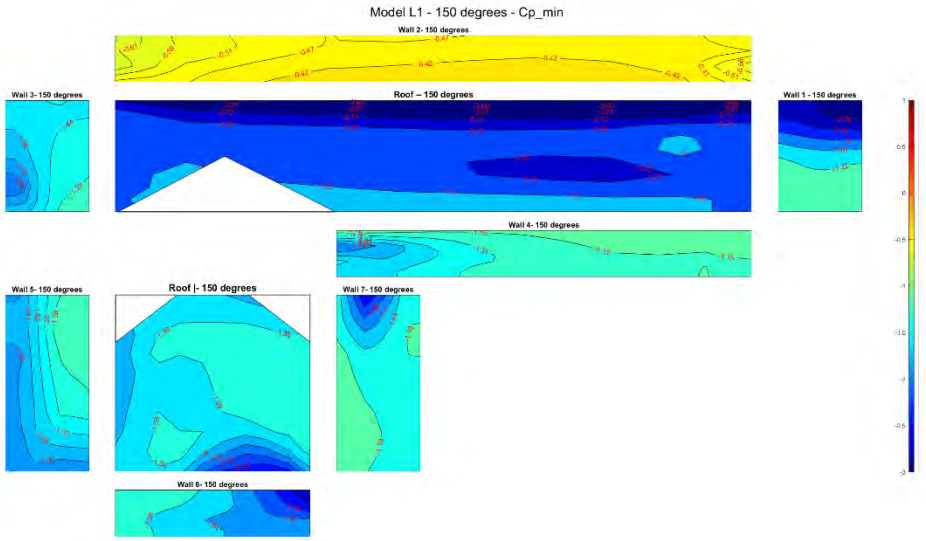

B 35. Minimum peak Cp at 150 degrees for model L

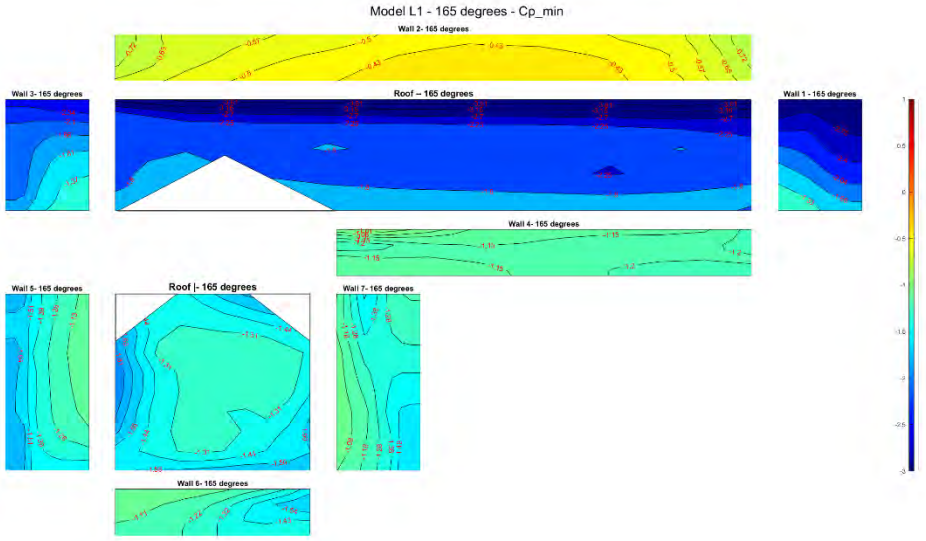

B 36. Minimum peak Cp at 165 degrees for model L

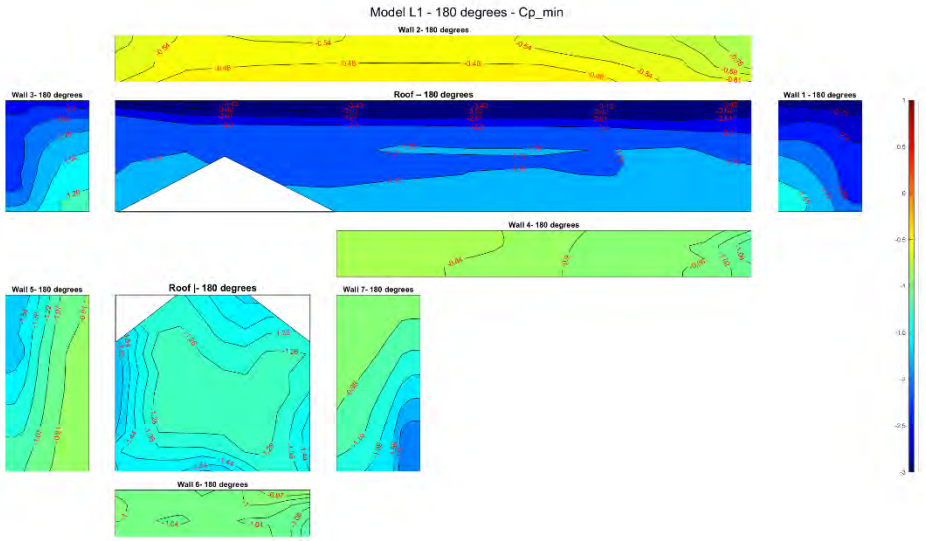

B 37. Minimum peak Cp at 180 degrees for model L

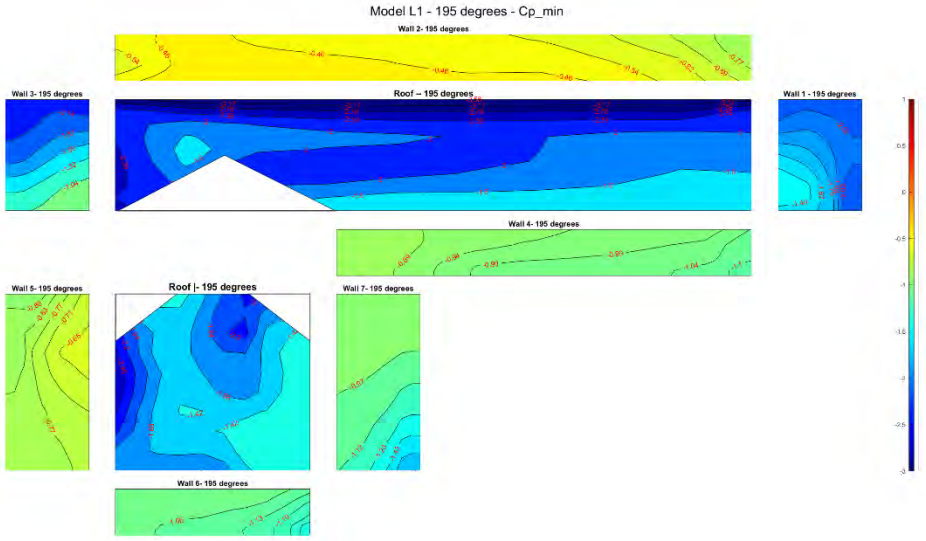

B 38. Minimum peak Cp at 195 degrees for model L

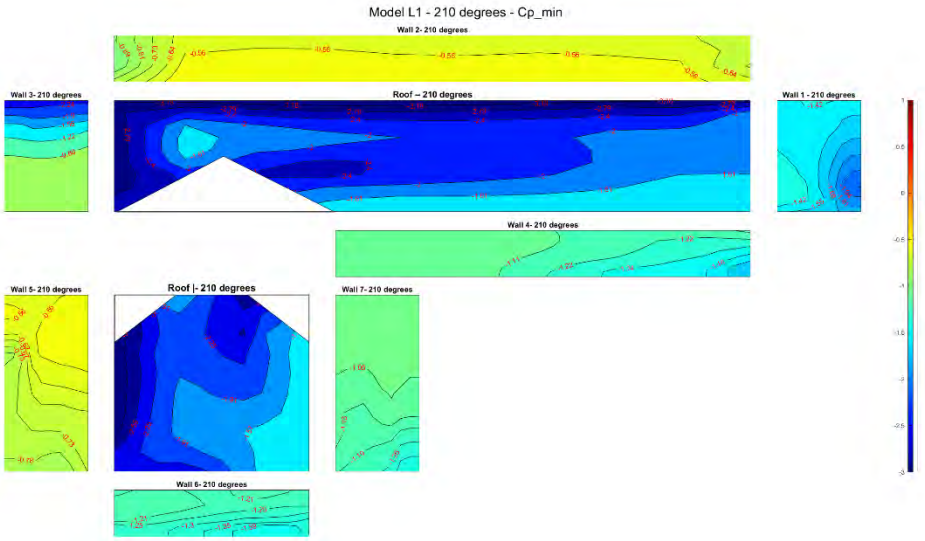

B 39. Minimum peak Cp at 210 degrees for model L

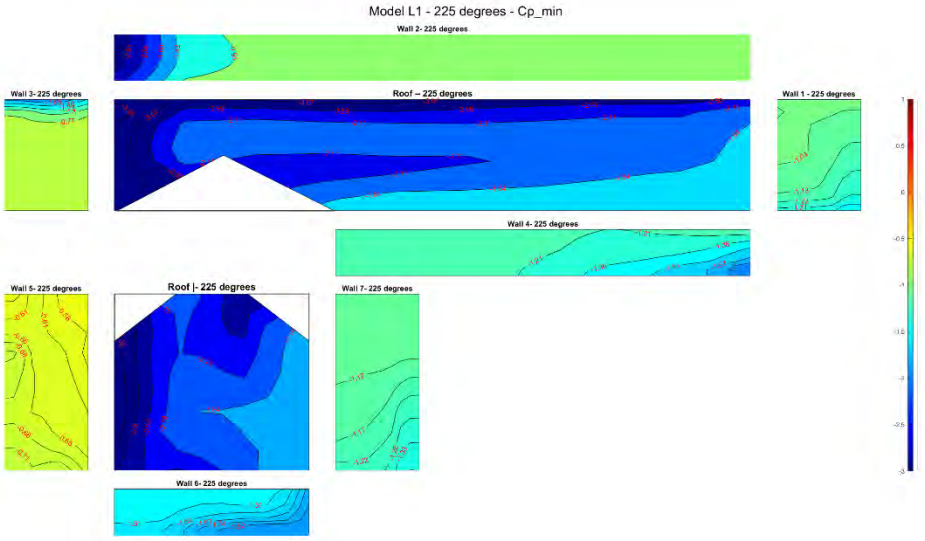

B 40. Minimum peak Cp at 225 degrees for model L

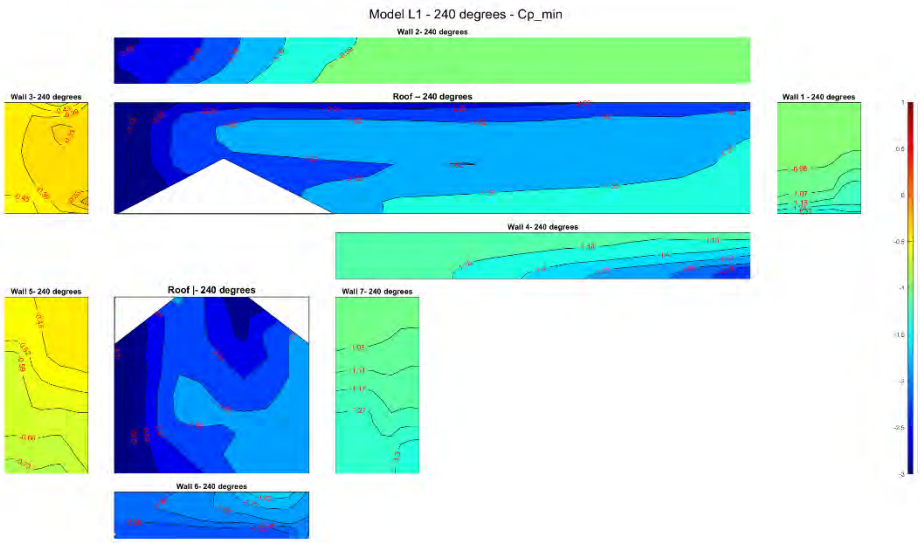

B 41. Minimum peak Cp at 240 degrees for model L

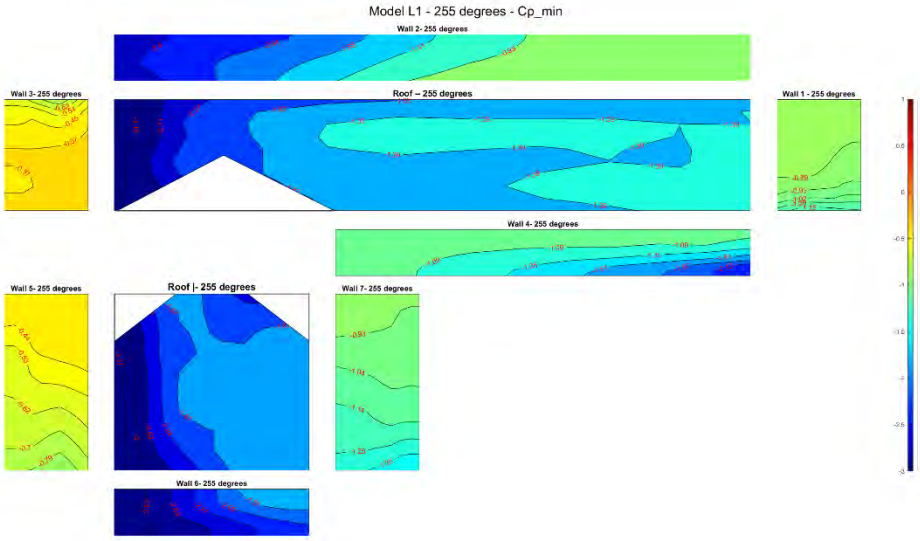

B 42. Minimum peak Cp at 255 degrees for model L

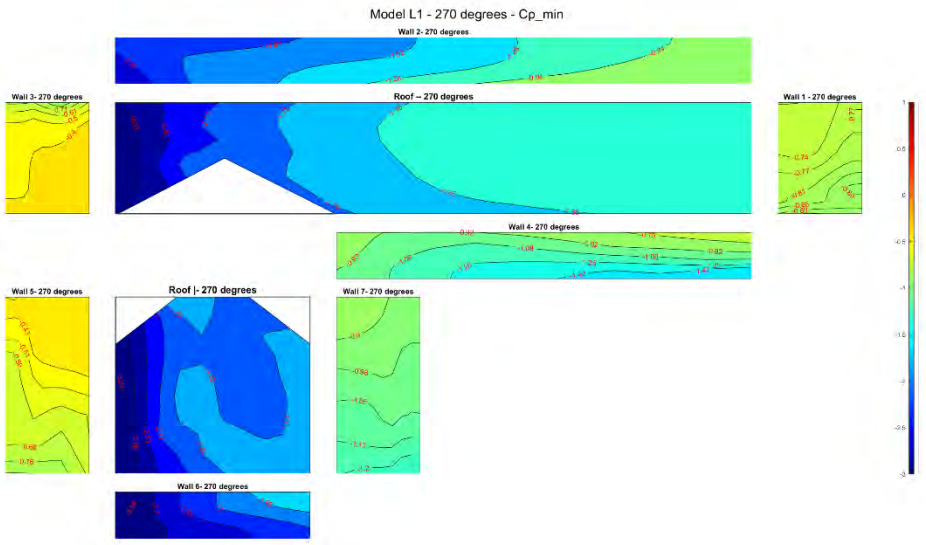

B 43. Minimum peak Cp at 270 degrees for model L

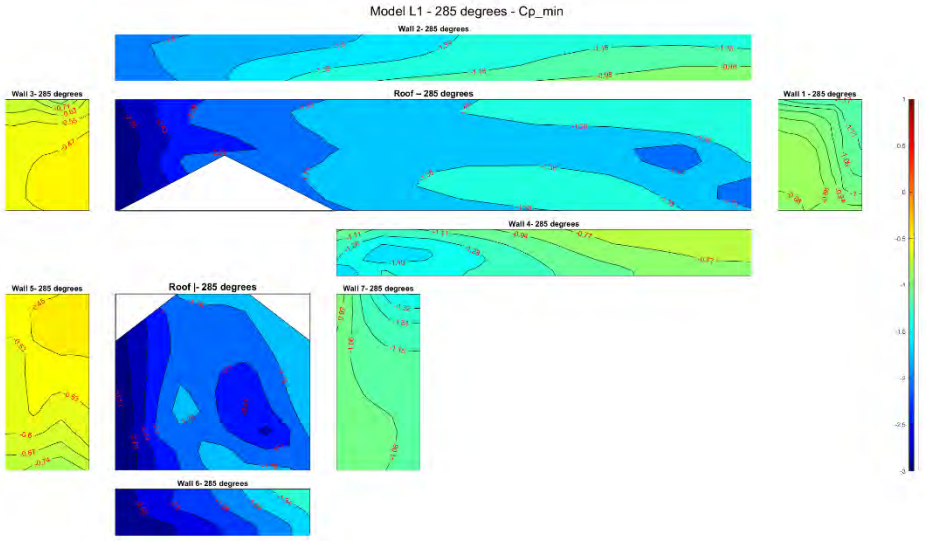

B 44. Minimum peak Cp at 285 degrees for model L

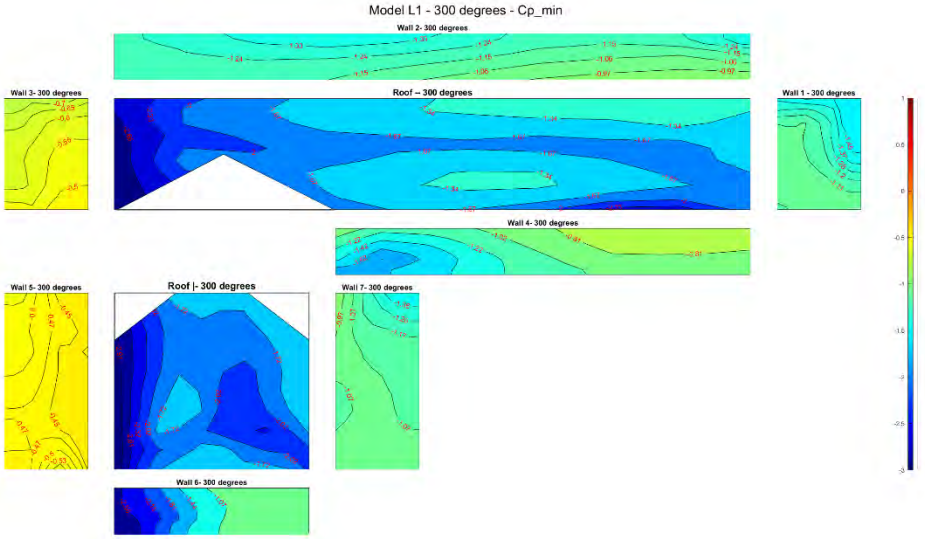

B 45. Minimum peak Cp at 300 degrees for model L

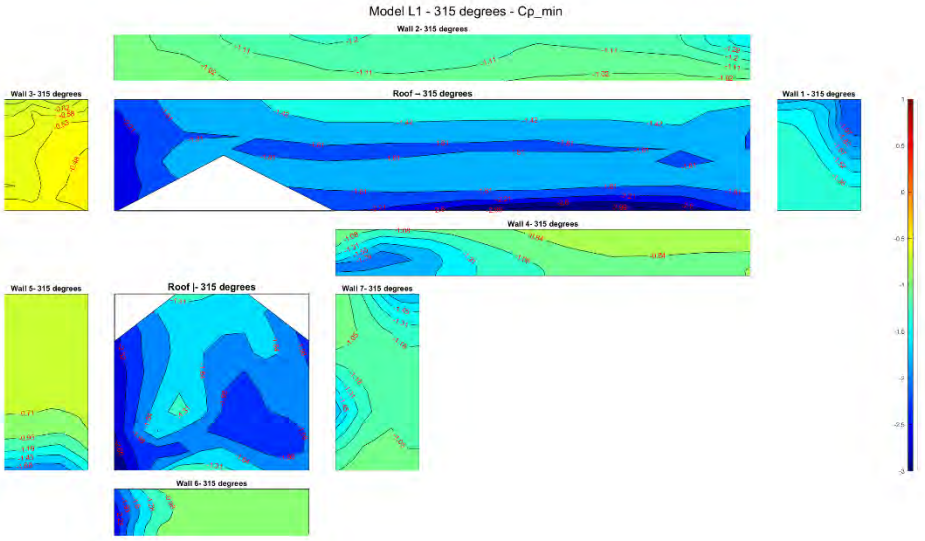

B 46. Minimum peak Cp at 315 degrees for model L

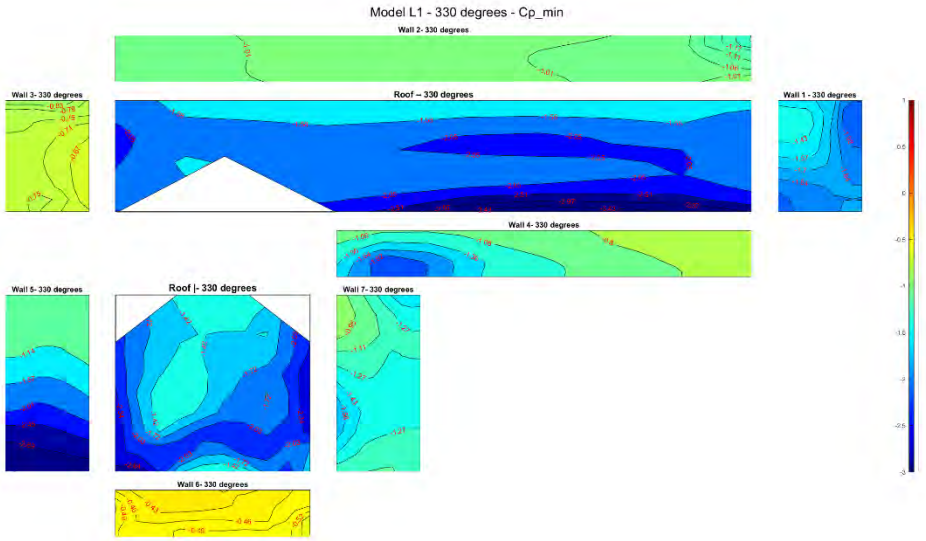

B 47. Minimum peak Cp at 330 degrees for model L

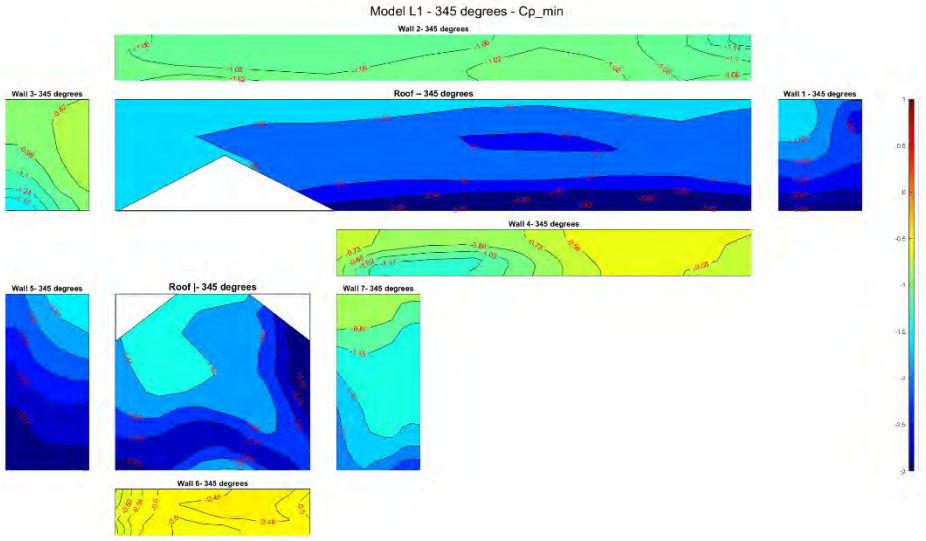

B 48. Minimum peak Cp at 345 degrees for model L

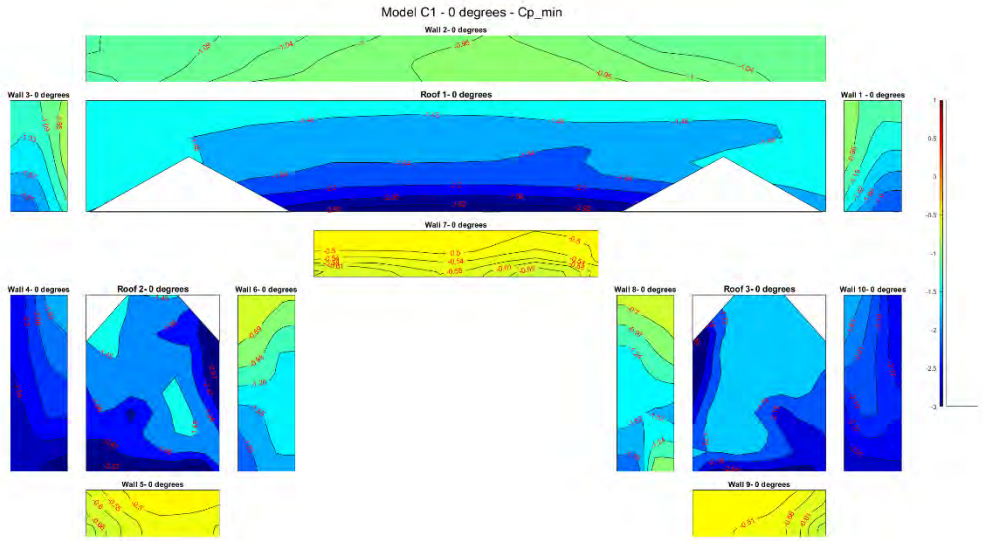

B 49. Minimum peak Cp at 0 degrees for model C

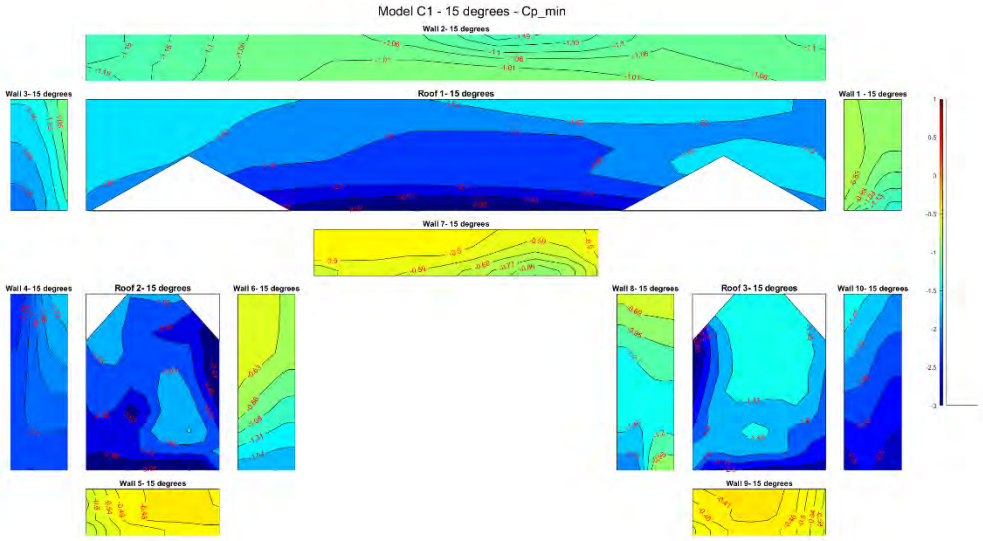

B 50. Minimum peak Cp at 15 degrees for model C

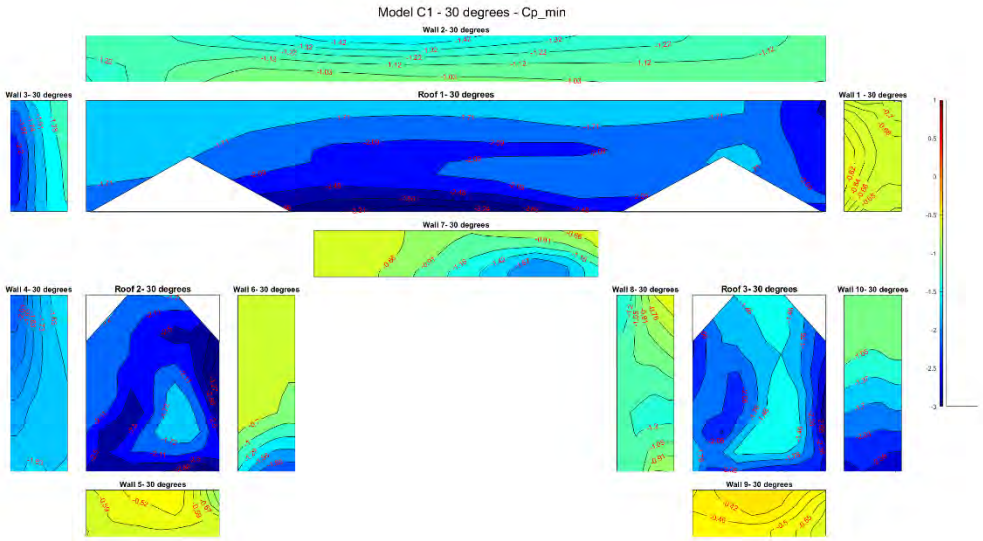

B 51. Minimum peak Cp at 30 degrees for model C

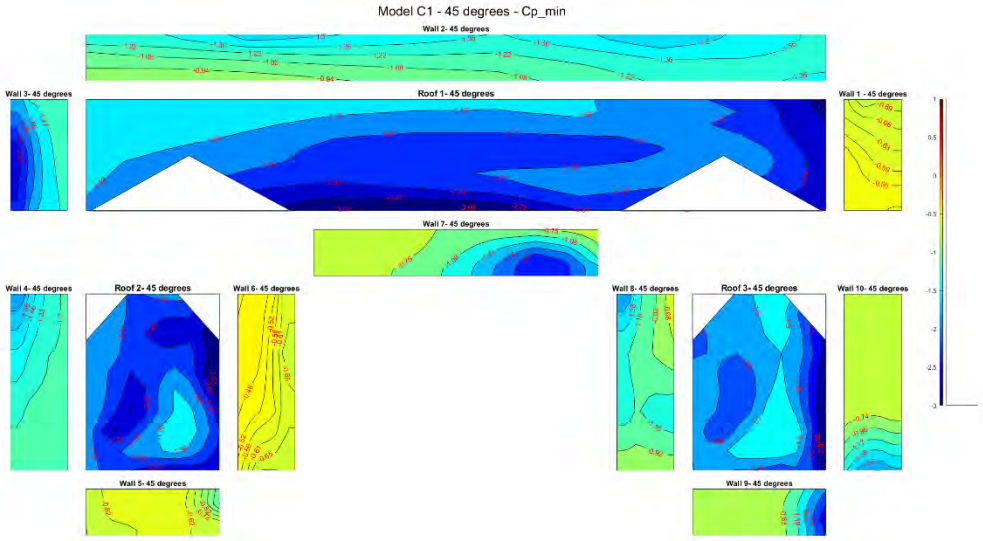

B 52. Minimum peak Cp at 45 degrees for model C

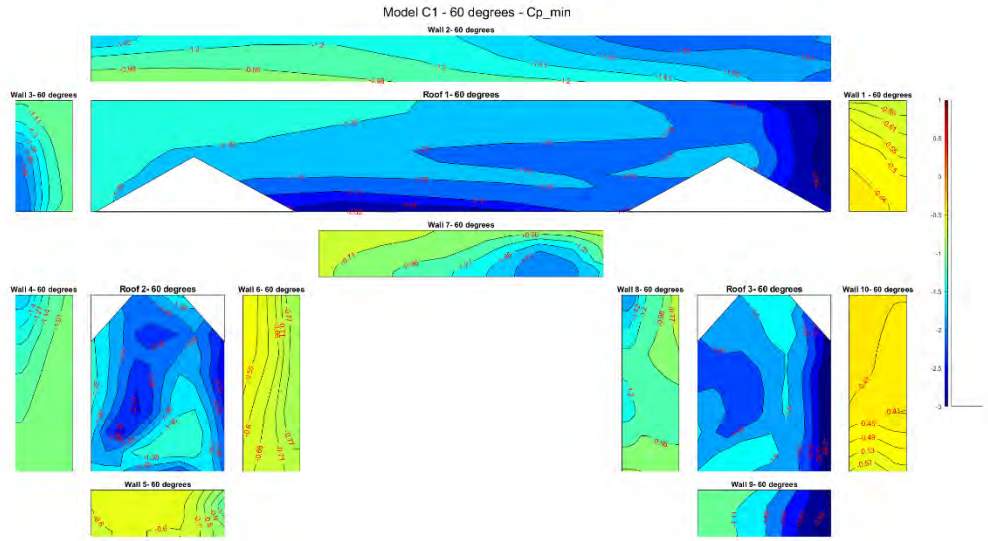

B 53. Minimum peak Cp at 60 degrees for model C

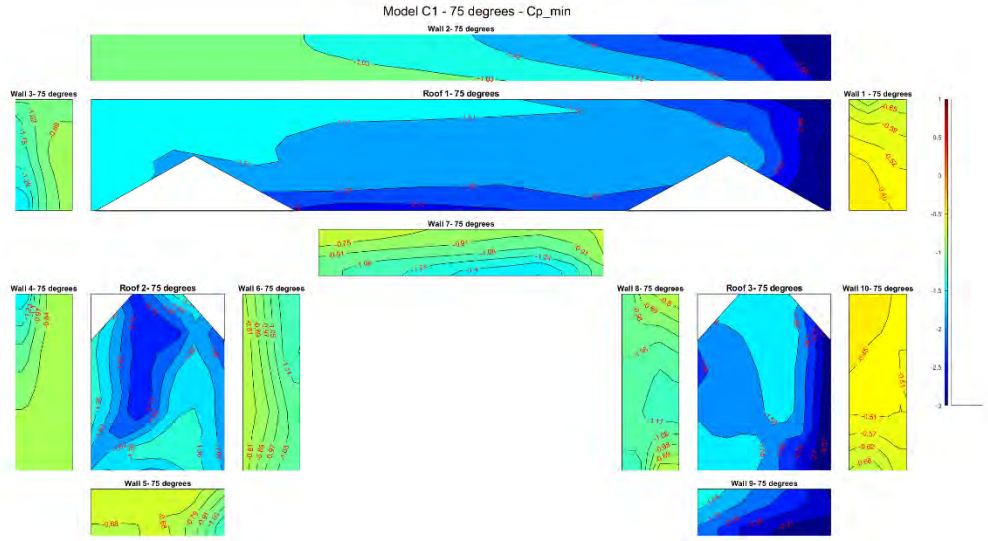

B 54. Minimum peak Cp at 75 degrees for model C

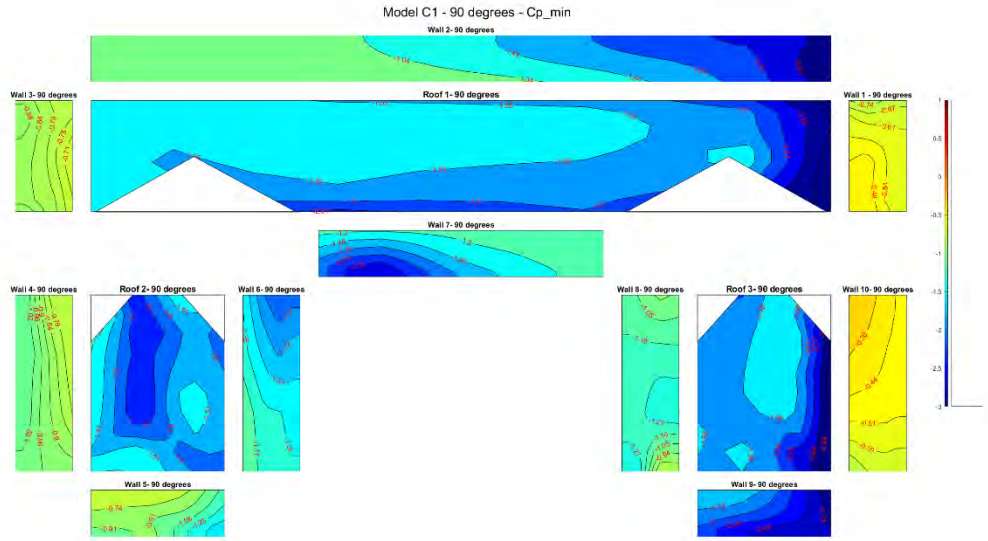

B 55. Minimum peak Cp at 90 degrees for model C

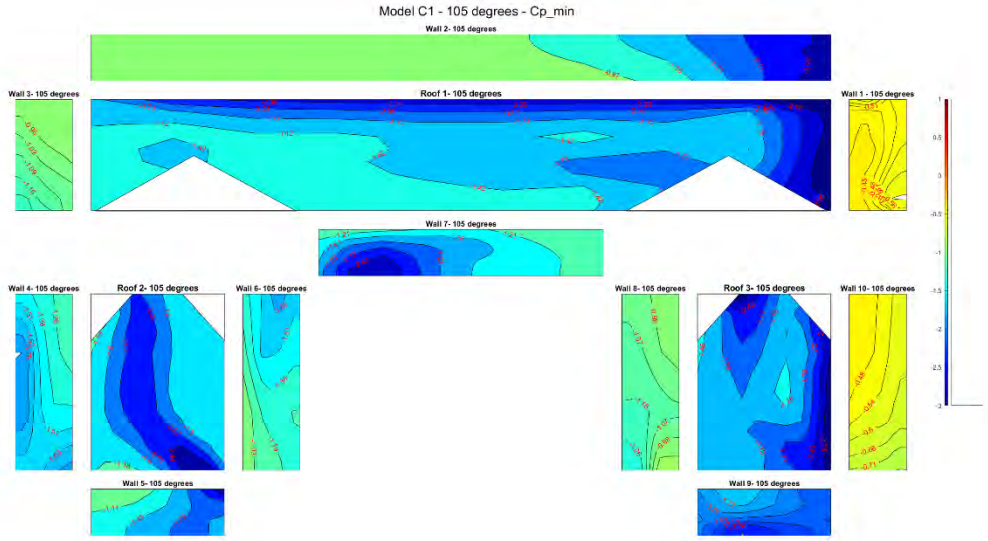

B 56. Minimum peak Cp at 105 degrees for model C

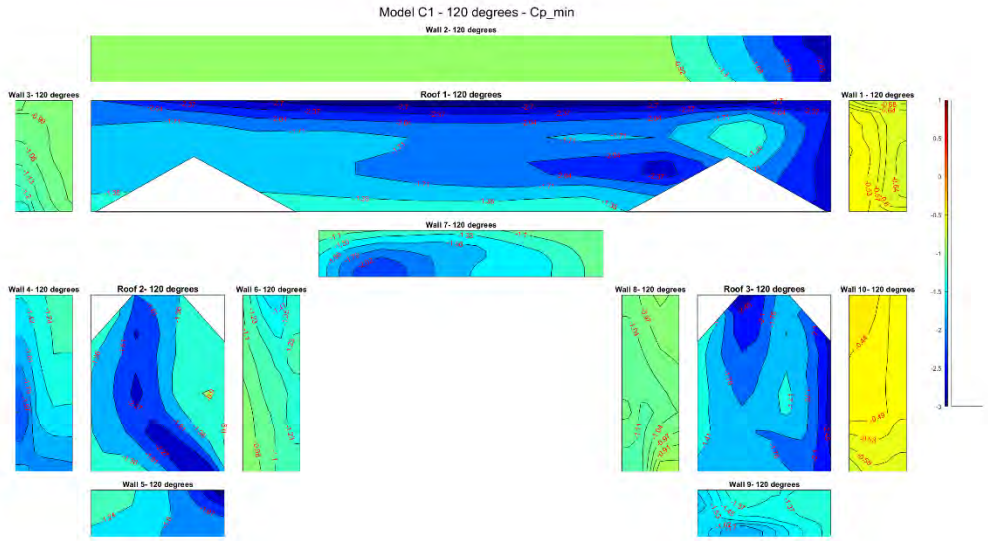

B 57. Minimum peak Cp at 120 degrees for model C

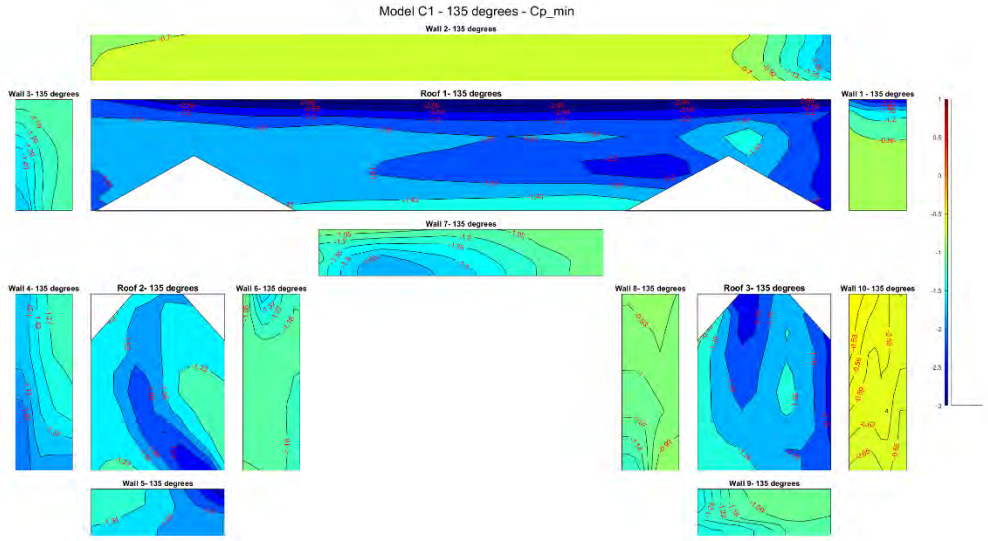

B 58. Minimum peak Cp at 135 degrees for model C

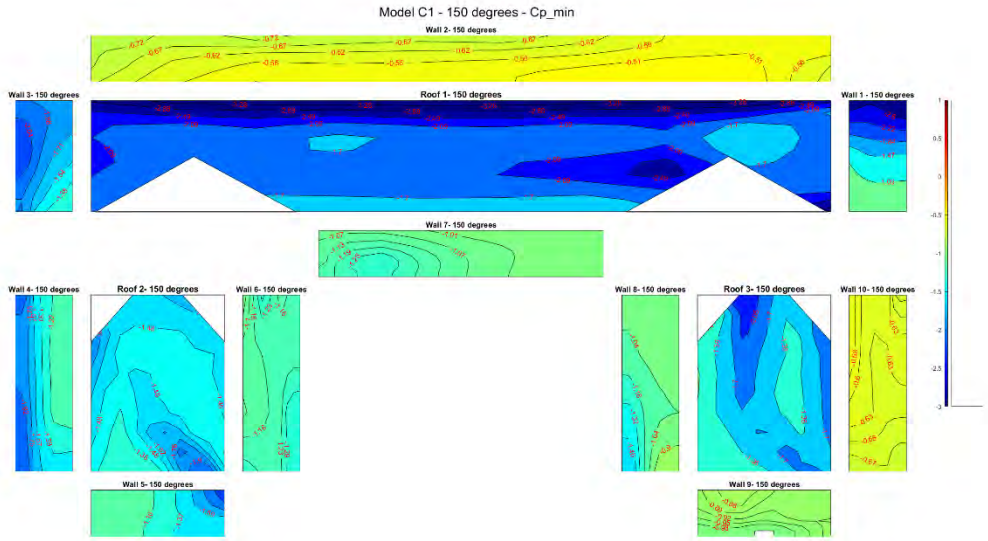

B 59. Minimum peak Cp at 150 degrees for model C

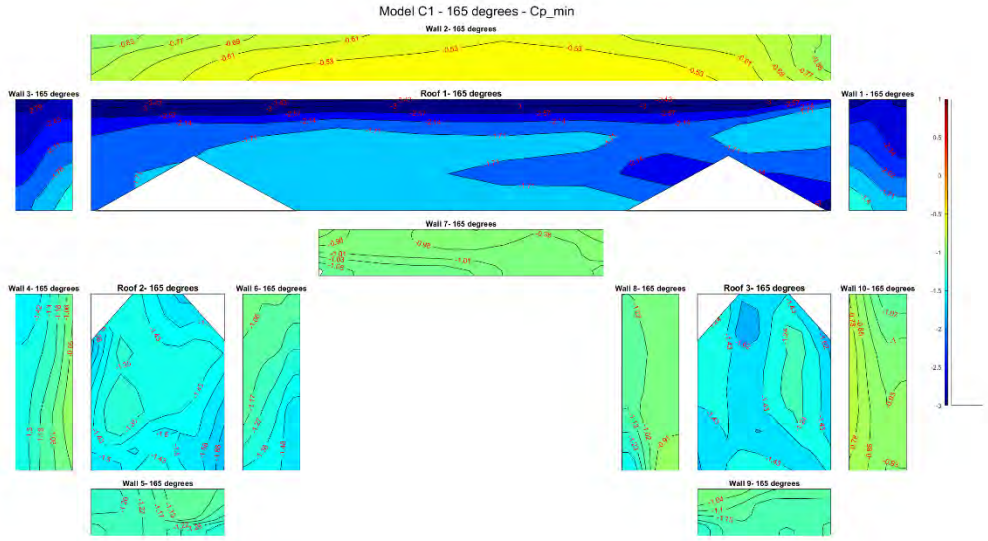

B 60. Minimum peak Cp at 165 degrees for model C

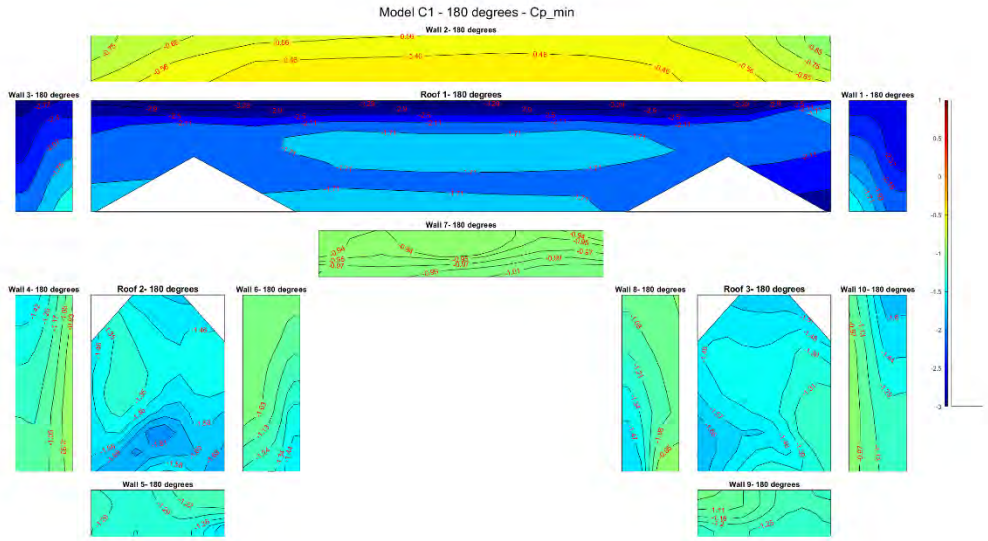

B 61. Minimum peak Cp at 180 degrees for model C

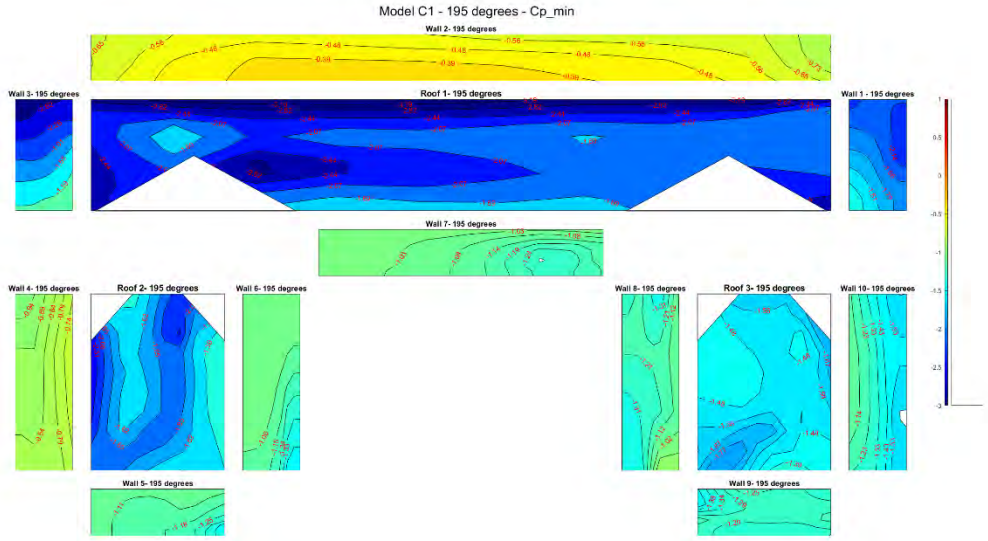

B 62. Minimum peak Cp at 195 degrees for model C

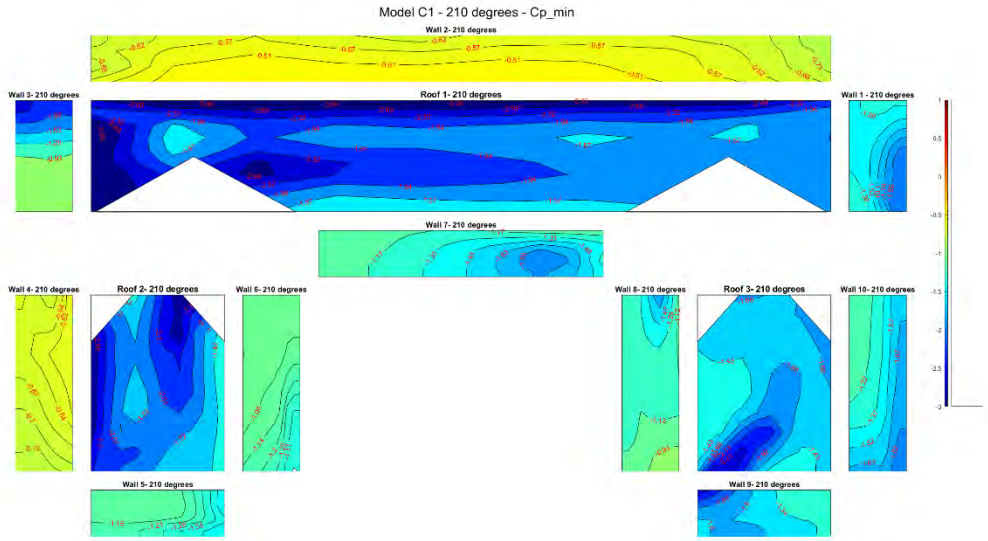

B 63. Minimum peak Cp at 210 degrees for model C

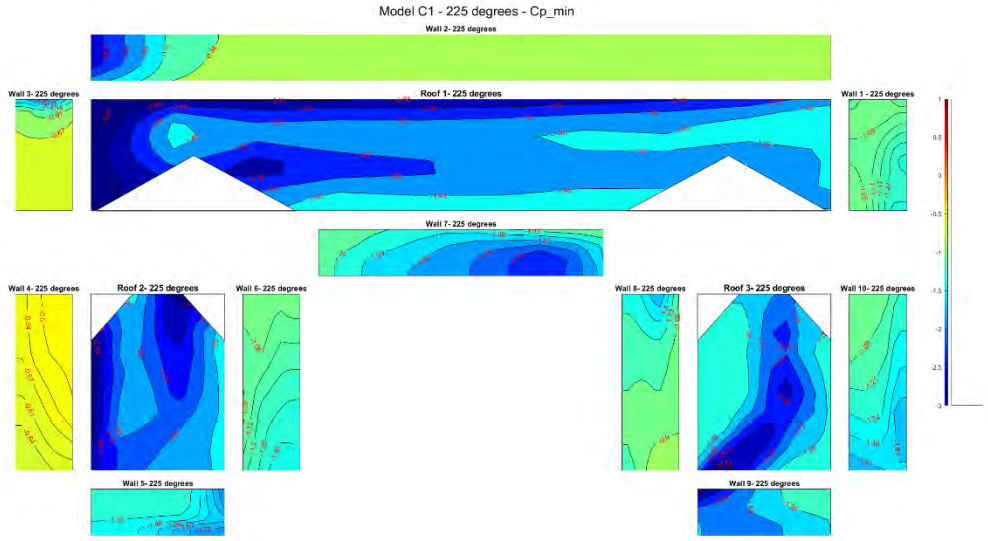

B 64. Minimum peak Cp at 225 degrees for model C

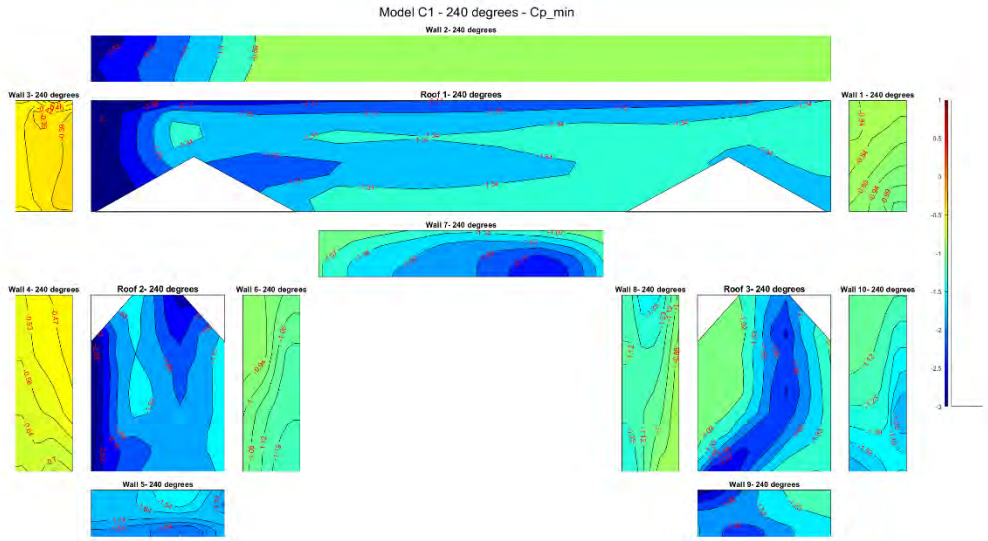

B 65. Minimum peak Cp at 240 degrees for model C

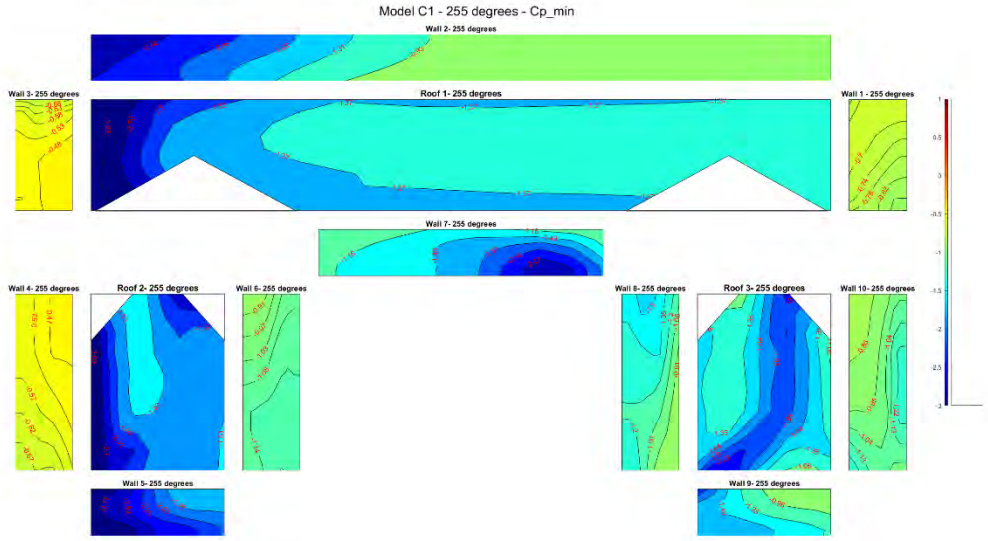

B 66. Minimum peak Cp at 255 degrees for model C

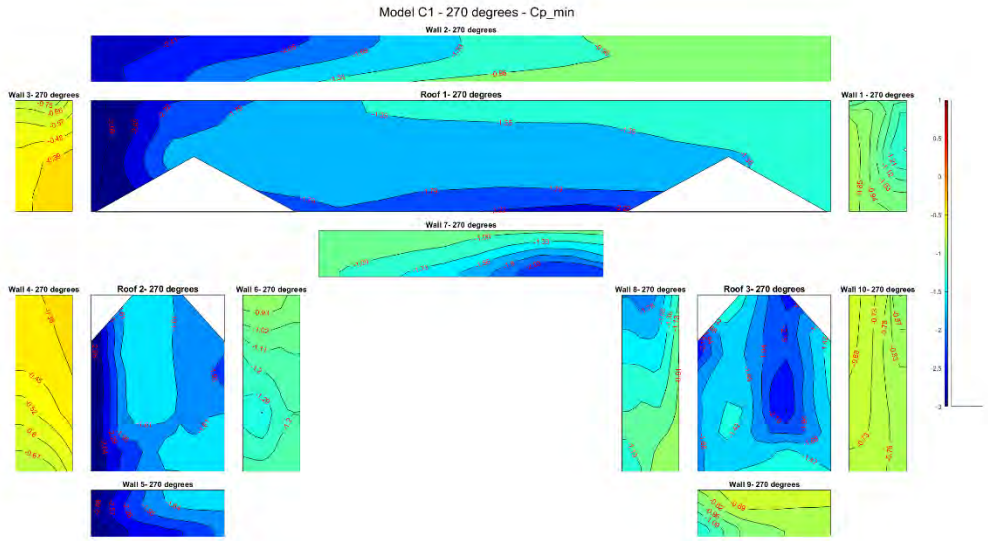

B 67. Minimum peak Cp at 270 degrees for model C

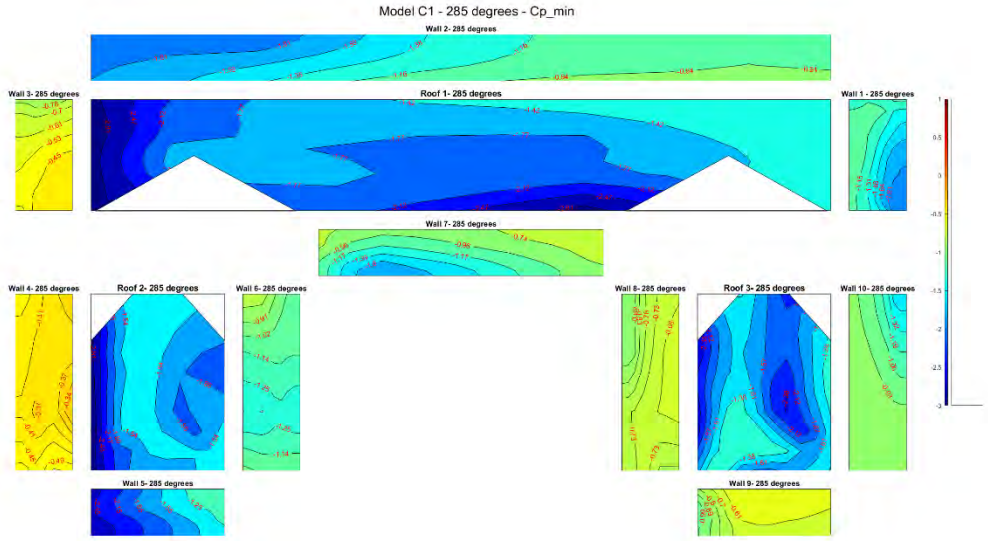

B 68. Minimum peak Cp at 285 degrees for model C

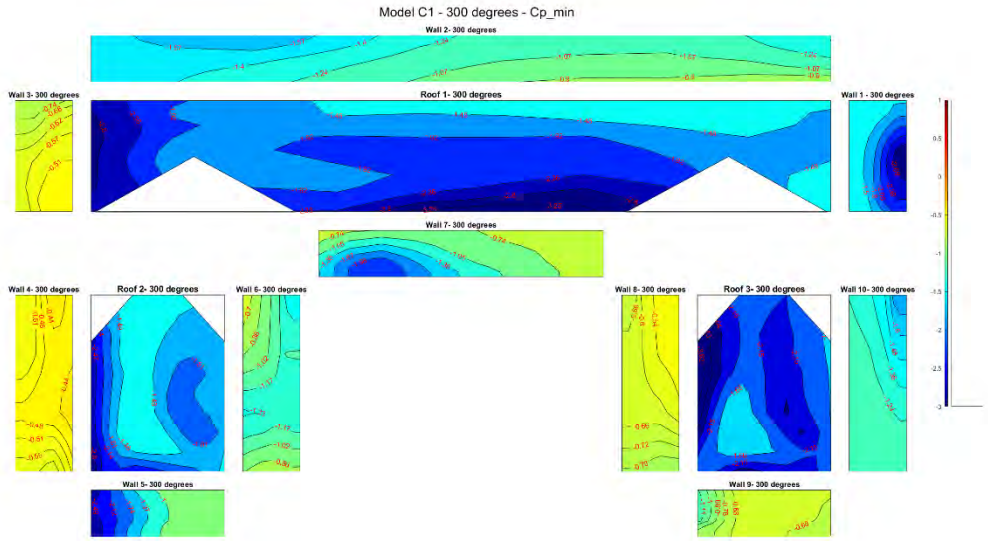

B 69. Minimum peak Cp at 300 degrees for model C

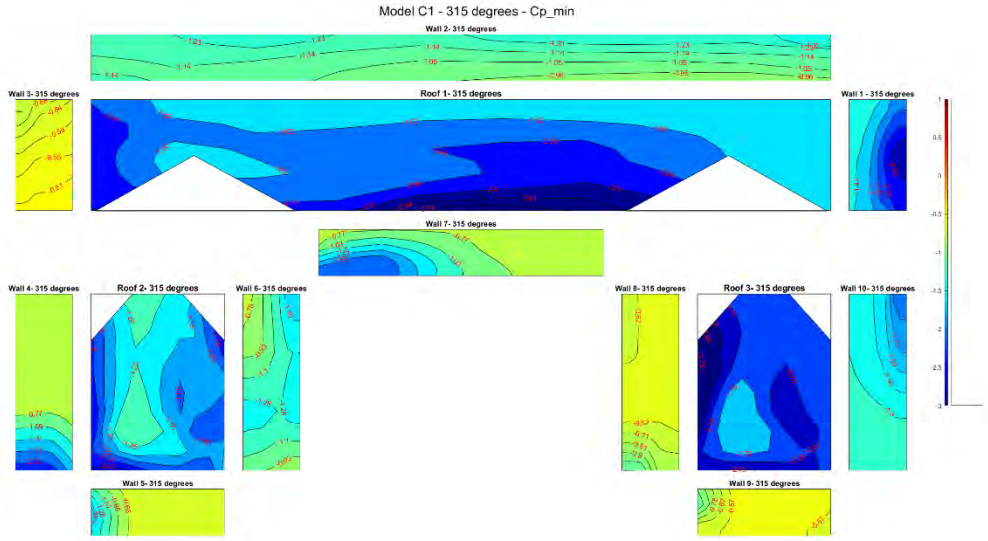

B 70. Minimum peak Cp at 315 degrees for model C

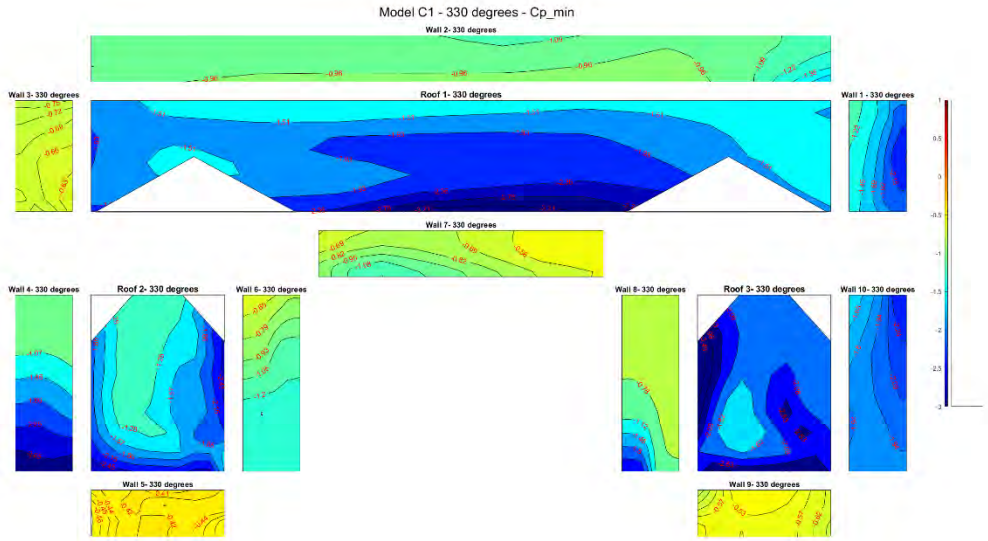

B 71. Minimum peak Cp at 330 degrees for model C

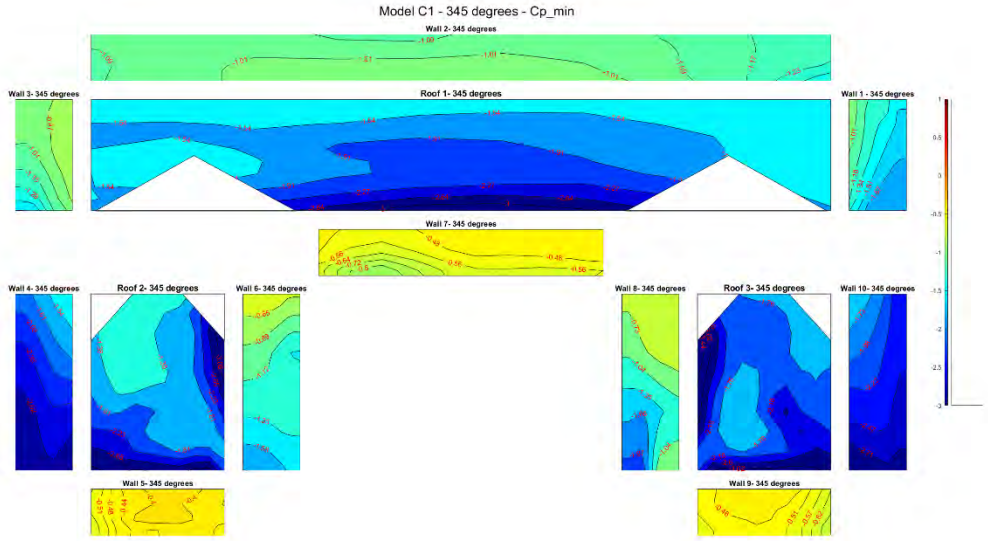

B 72. Minimum peak Cp at 345 degrees for model C

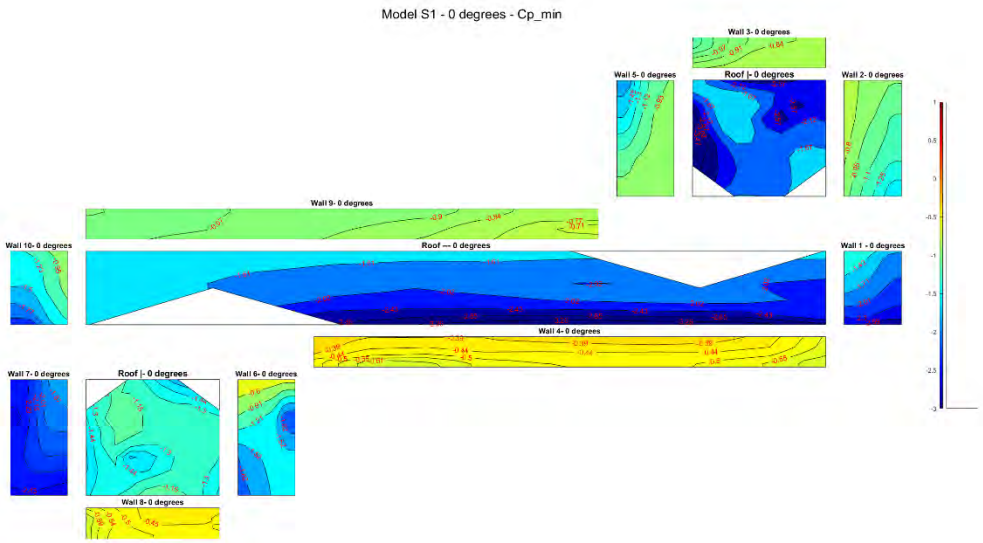

B 73. Minimum peak Cp at 0 degrees for model S

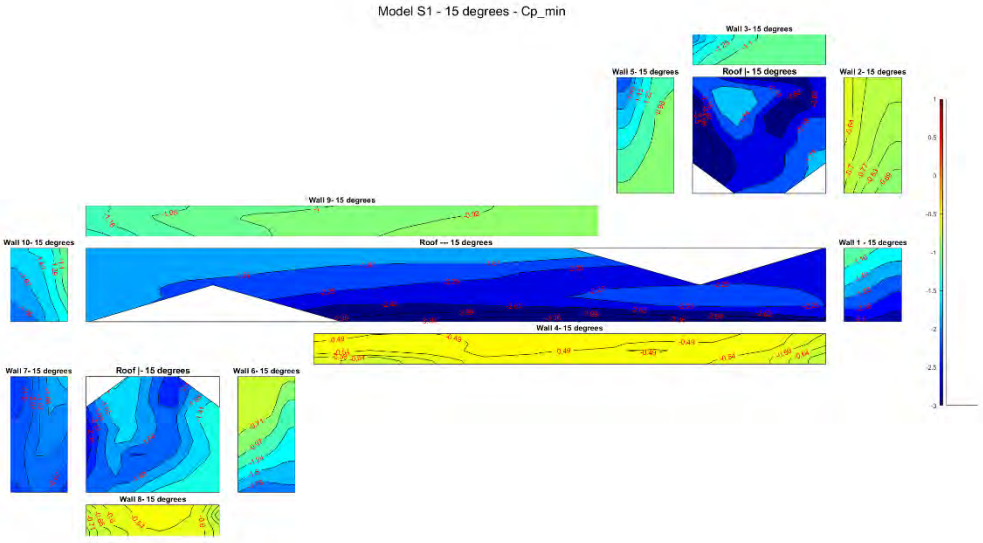

B 74. Minimum peak Cp at 15 degrees for model S

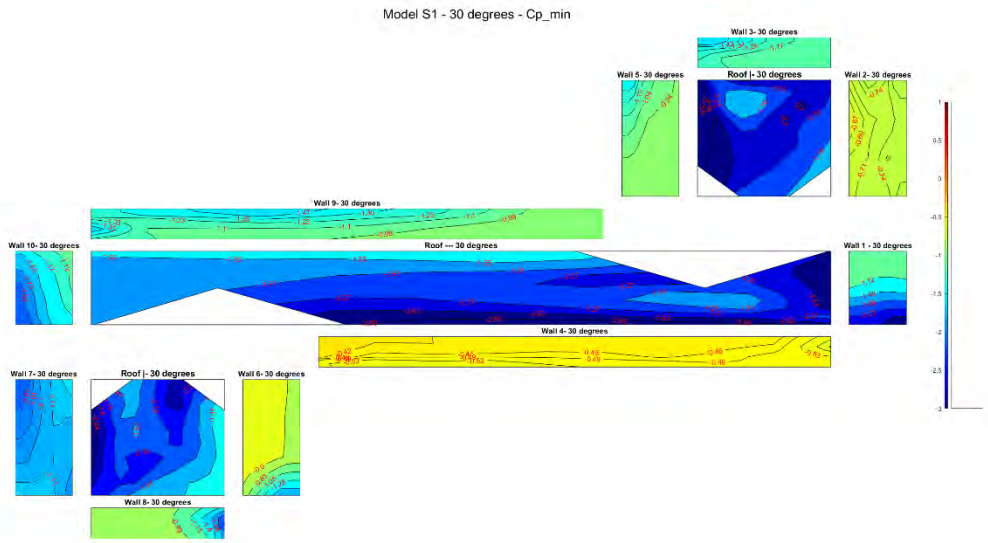

B 75. Minimum peak Cp at 30 degrees for model S

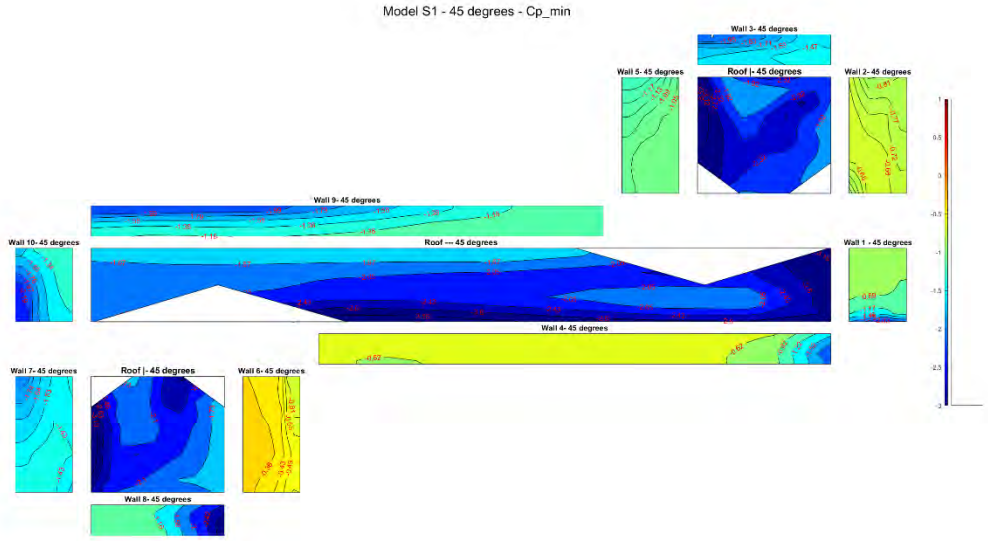

B 76. Minimum peak Cp at 45 degrees for model S

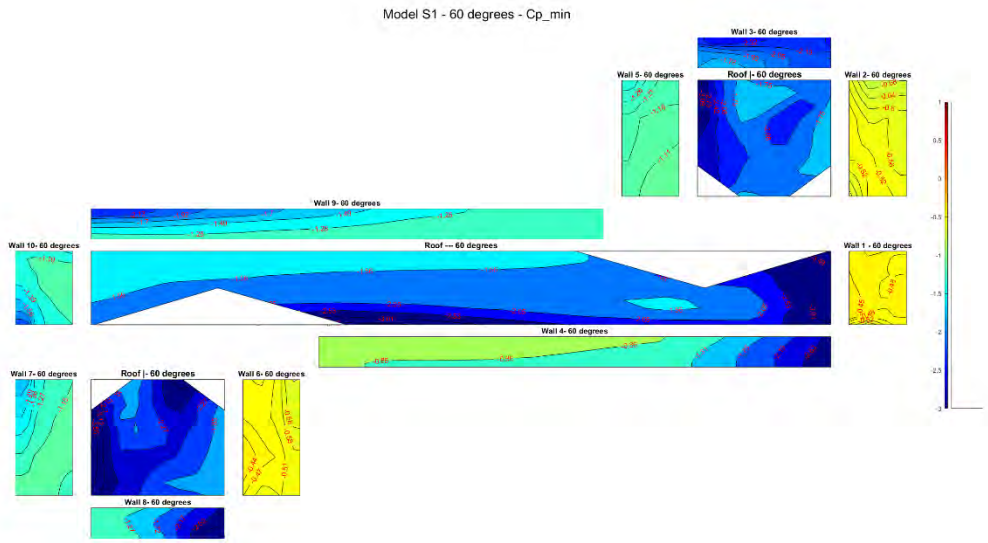

B 77. Minimum peak Cp at 60 degrees for model S

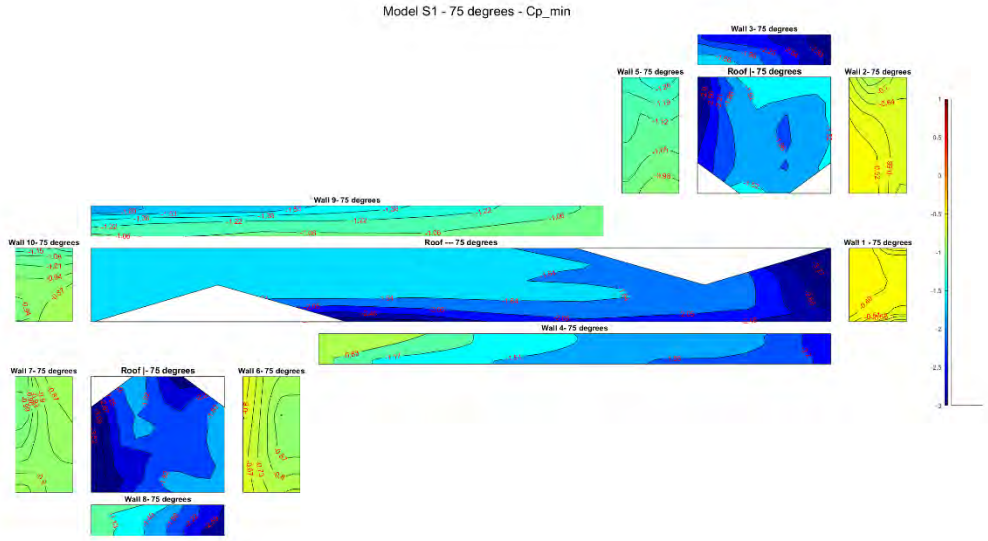

B 78. Minimum peak Cp at 75 degrees for model S

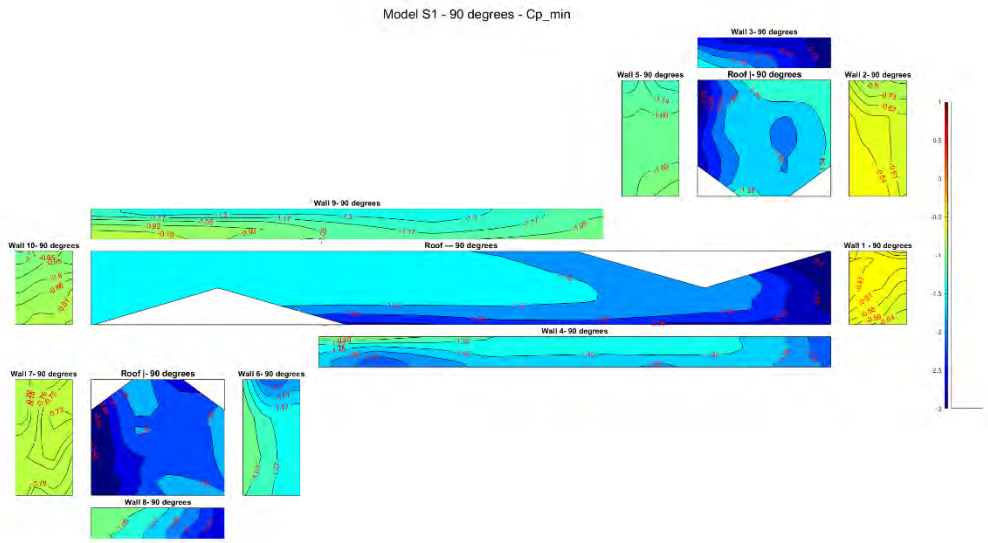

B 79. Minimum peak Cp at 90 degrees for model S

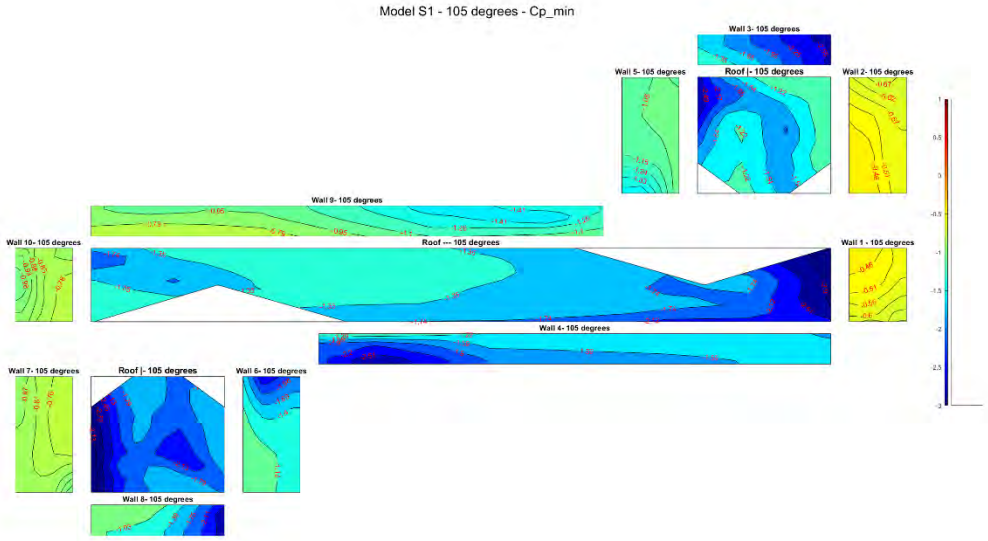

B 80. Minimum peak Cp at 105 degrees for model S

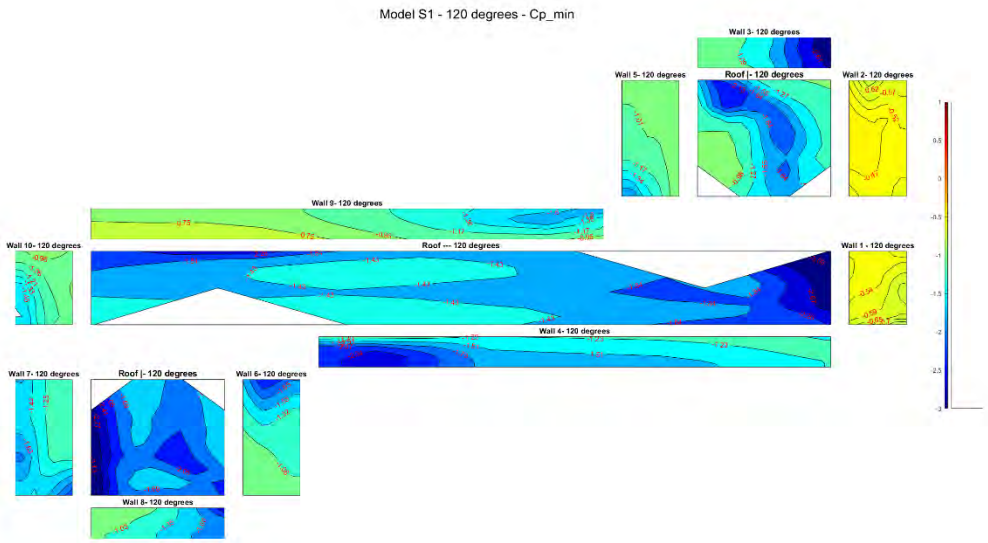

B 81. Minimum peak Cp at 120 degrees for model S

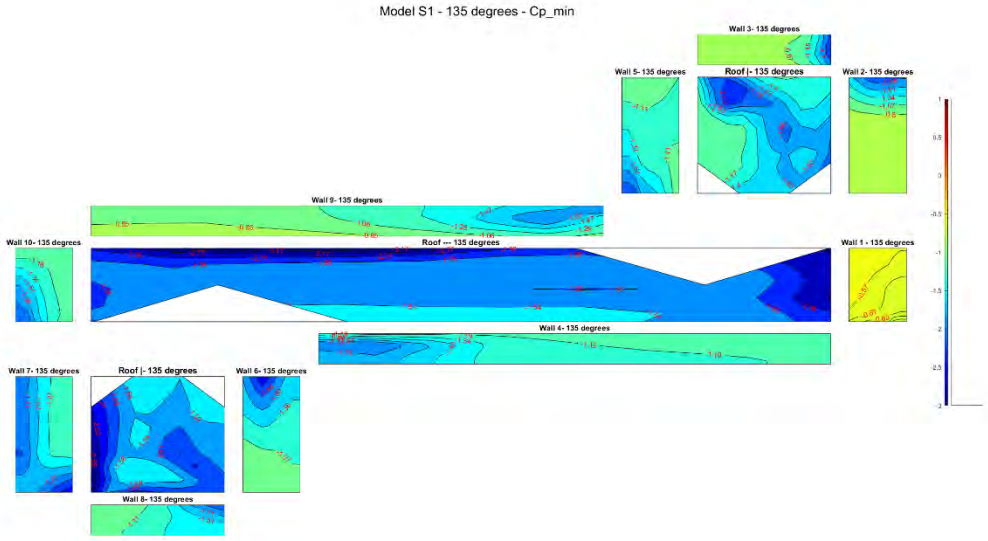

B 82. Minimum peak Cp at 135 degrees for model S

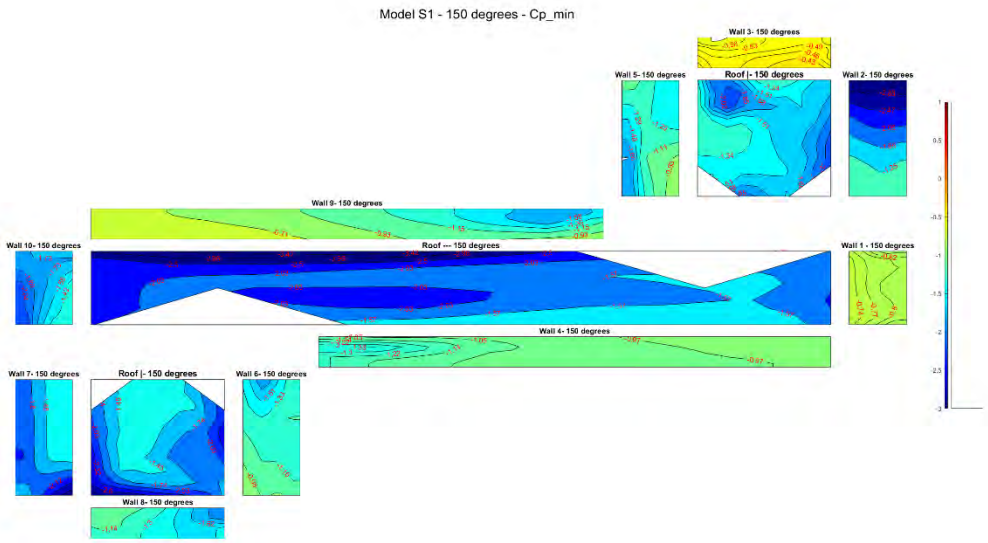

B 83. Minimum peak Cp at 150 degrees for model S

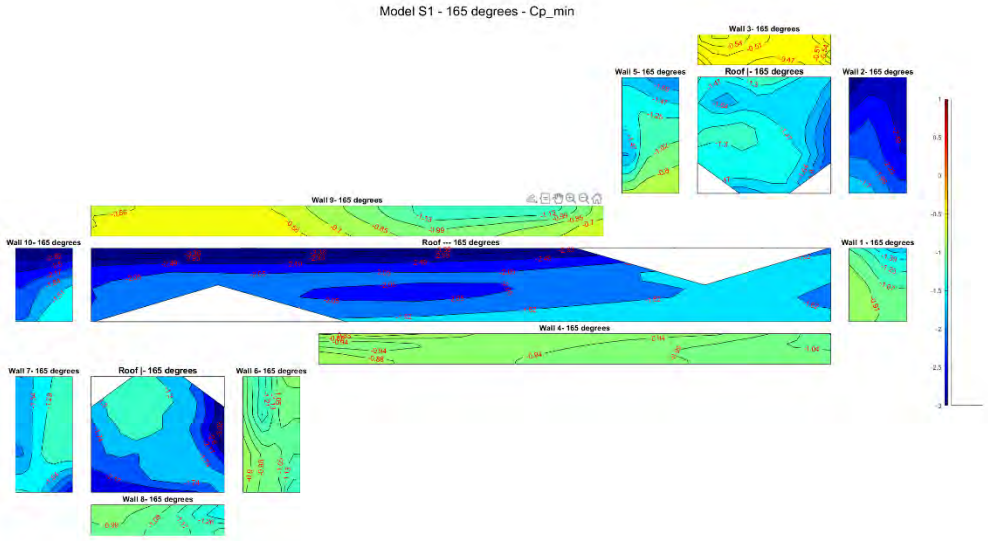

B 84. Minimum peak Cp at 165 degrees for model S

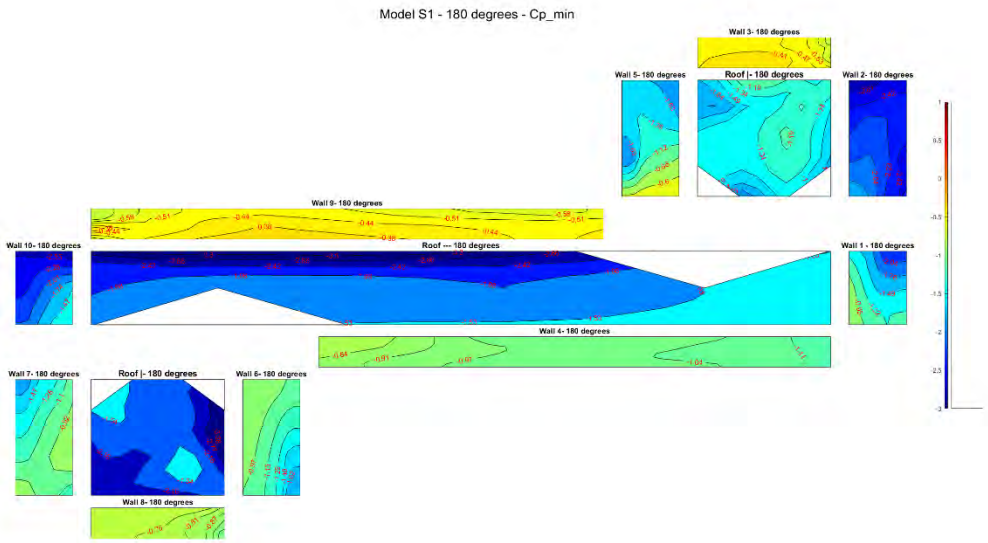

B 85. Minimum peak Cp at 180 degrees for model S

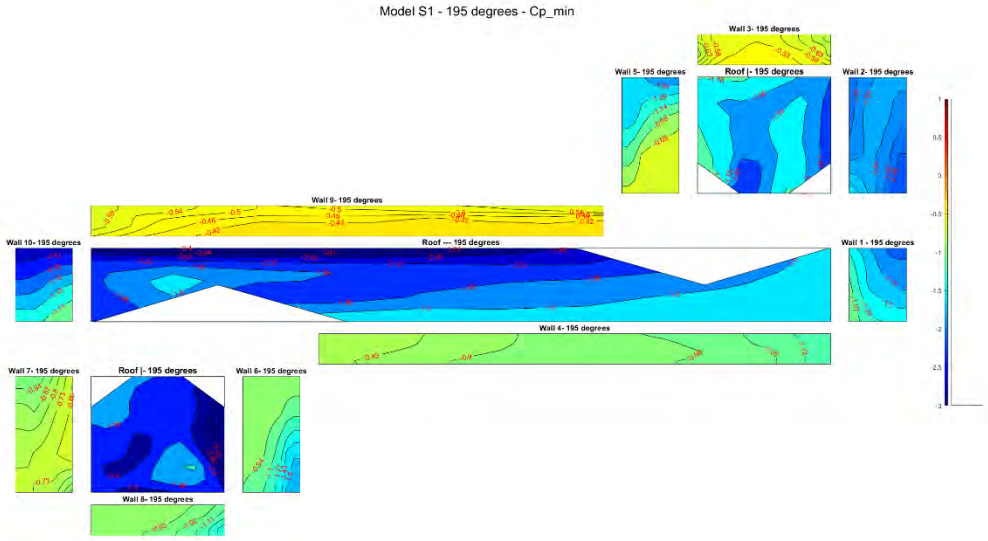

B 86. Minimum peak Cp at 195 degrees for model S

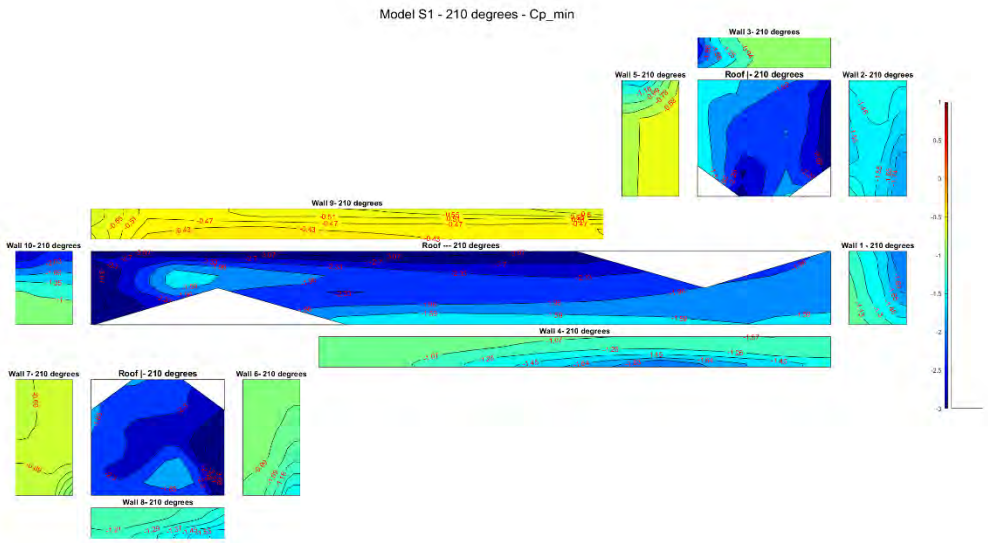

B 87. Minimum peak Cp at 210 degrees for model S

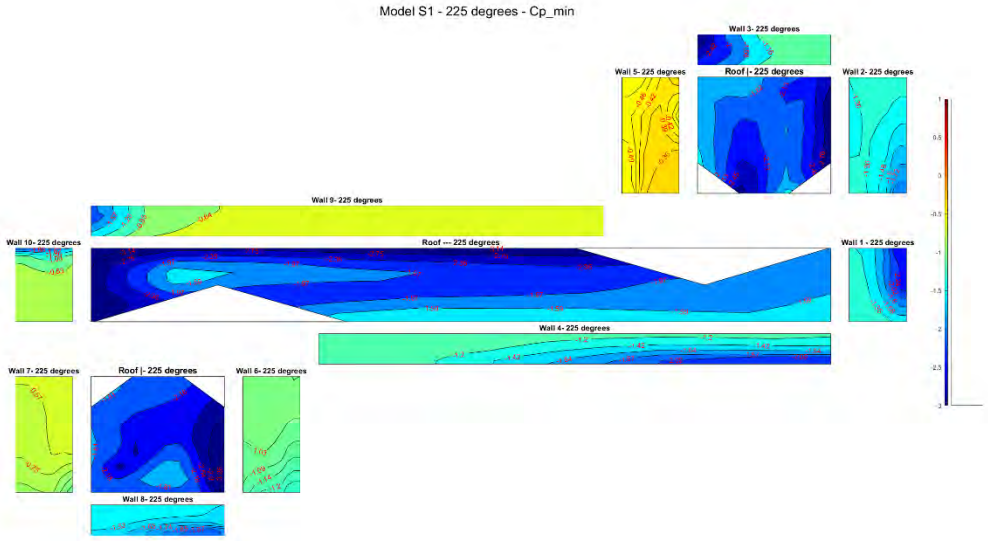

B 88. Minimum peak Cp at 225 degrees for model S

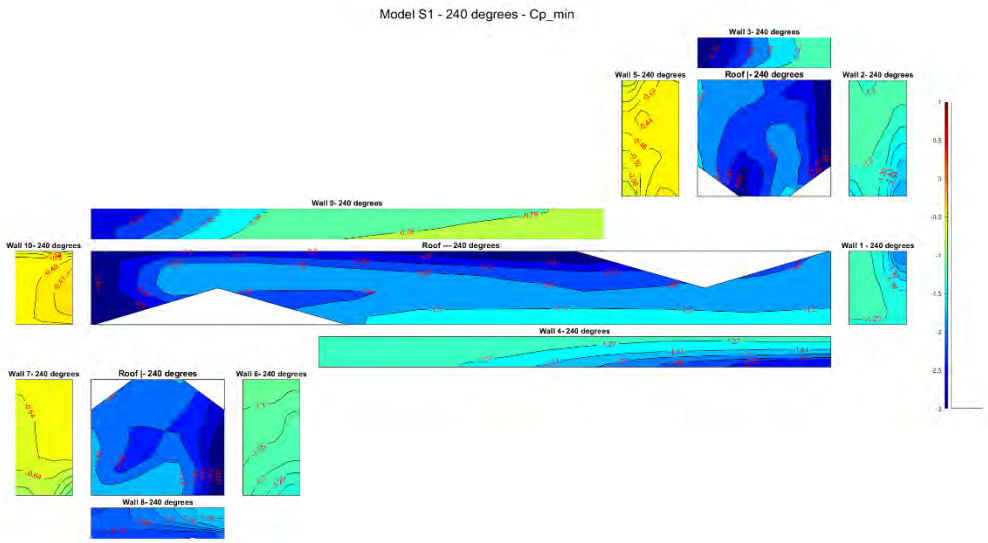

B 89. Minimum peak Cp at 240 degrees for model S

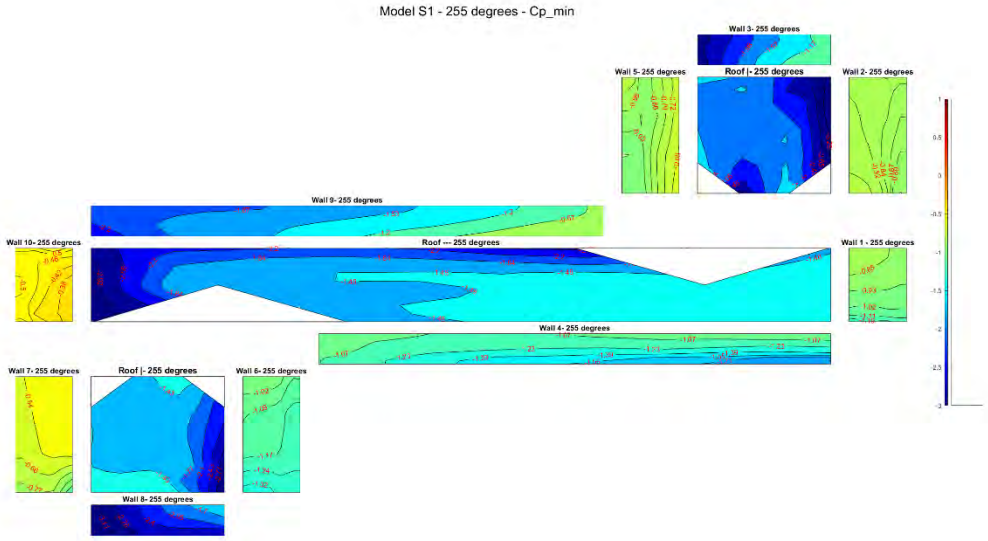

B 90. Minimum peak Cp at 255 degrees for model S

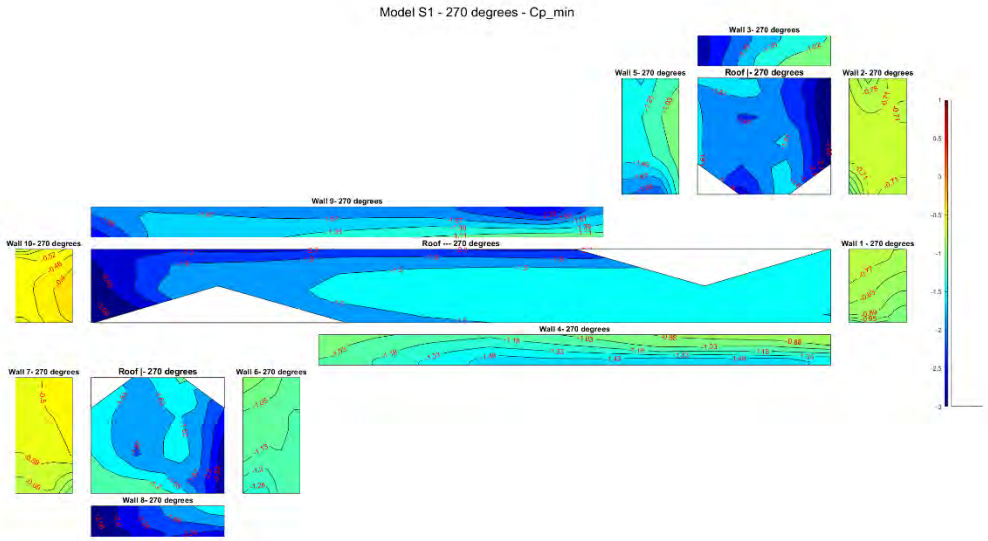

B 91. Minimum peak Cp at 270 degrees for model S

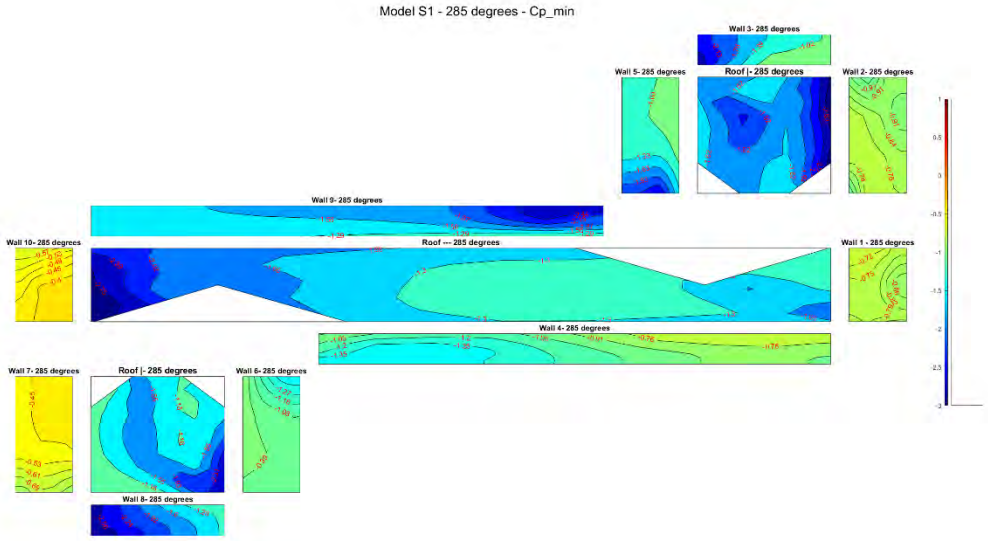

B 92. Minimum peak Cp at 285 degrees for model S

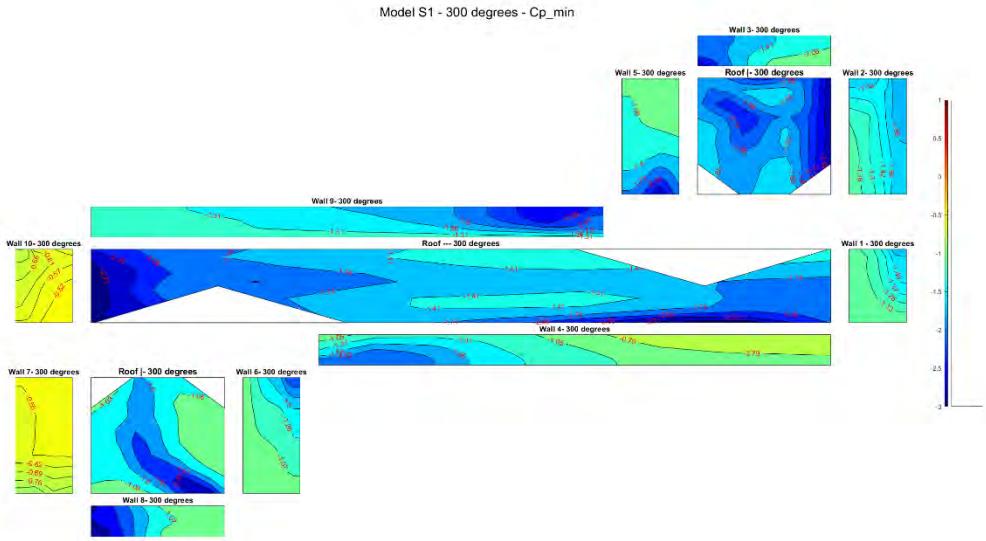

B 93. Minimum peak Cp at 300 degrees for model S

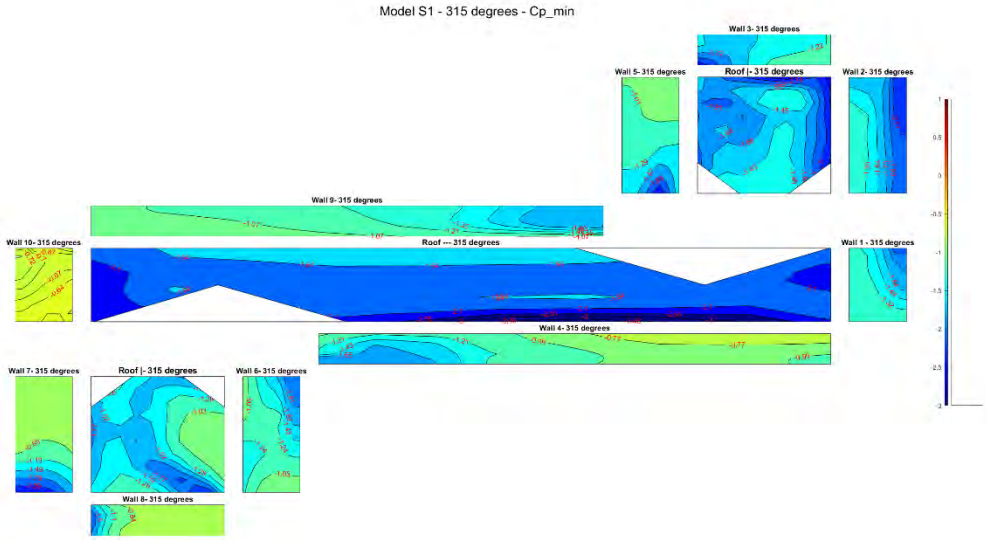

B 94. Minimum peak Cp at 315 degrees for model S

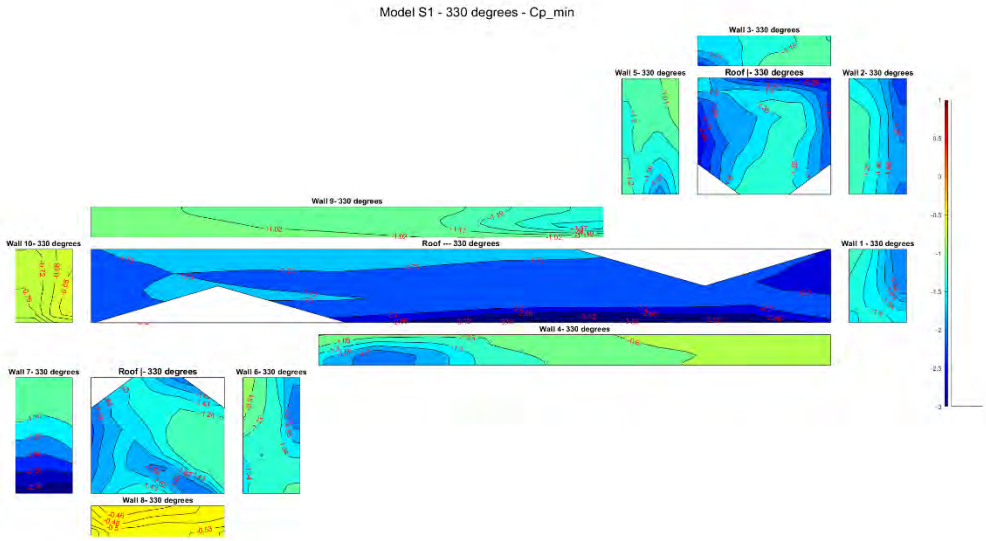

B 95. Minimum peak Cp at 330 degrees for model S

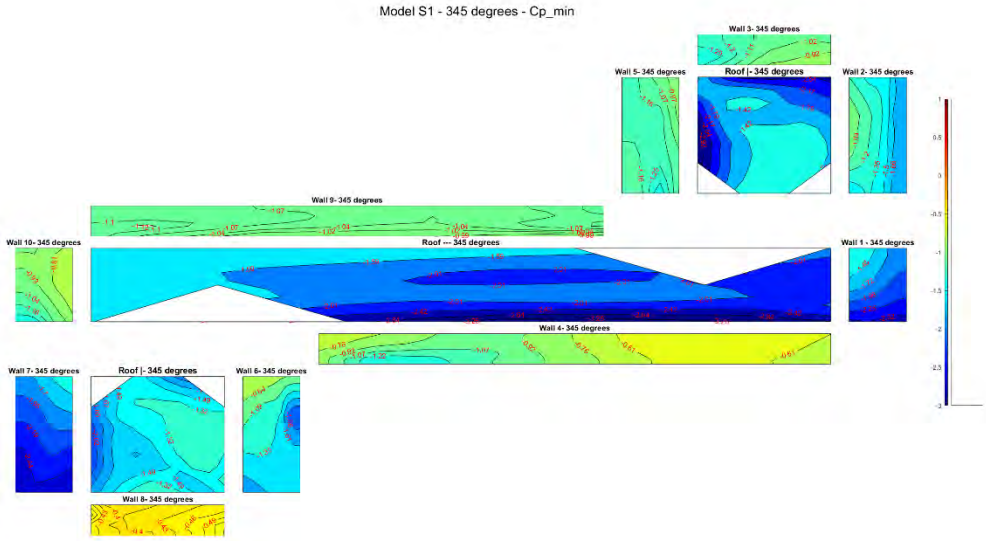

B 96. Minimum peak Cp at 345 degrees for model S

A Resource for the State of Florida

SECTION 5

Development of an Integrated Storm Tide and Freshwater Flooding Model Phase 4

A Report Submitted to:
The State of Florida Division of Emergency Management

Prepared By:
Dr. Yuepeng Li
Dr. Qiang Chen

Graduate Student
Linlin Zhou

The International Hurricane Research Center (IHRC)
Florida International University

July 30, 2021

Executive Summary

In the previous phases, IHRC developed the prototype SSFOF (Storm Surge and Freshwater Overland Flooding) model which can simulate the compound effect of tide, storm surge and rainfall runoff during hurricane impact. The SSFOF model has been proven to be stable, robust, and efficient, and is one of the most advanced full-physics Nonlinear Shallow Water Equation (NSWE) based depth-averaged storm surge models. Previous reports have focused on applying the SSFOF model to large domain simulations covering particularly South Florida and North Florida regions. While a large computational domain at region scale is necessary for storm surge simulations, local geometrical and bathymetric characteristics may be compromised in those simulations, due to the limitations of current computational capacity.

In this phase, the study was focused on a relatively local area around the Panama City FL, whose boundary is delineated according to the HU-8 watershed boundary dataset. This study investigates the hurricane induced compound storm surge and rainfall runoff flooding impact on the Panama City area. The simulations include not only a historical hurricane event Michael (2018) with measured NEXRAD (The Next Generation Weather Radar) rainfall data, but also synthetic hurricanes in combination with synthetic rainfall amount and duration, since Hurricane Michael (2018) is surge dominated.

The deliverables for the 2020-21 research period included:
1. The riverine flooding module was built in the current SSFOF model, and a fine grid covering Panama City was generated.
2. A more reliable and updated digital elevation data set, The Continuously Updated Digital Elevation Model (CUDEM) - 1/9 Arc-Second Resolution (3 meters), was collected and employed into the current model, to replace 5 meters Lidar Digital Elevation Model (DEM) data covering the North Florida region from U.S. Geological Survey (USGS) or Florida Geographic Data Library (FGDL).
3. The population in the originally proposed study region Panhandle and Apalachicola bay is generated, and the adjacent rivers and stream were resolved.
4. With the newly generated grid, recent historical hurricanes Michael (2018) was simulated. Since Ivan (2004) didn't have significant impact to Panama City, three synthetic hurricanes simulation are performed with different moving speed and landfall locations.
5. Current model has the ability to simulate the storm surge induced by wind, astronomical tide, rainfall runoff, and riverine flooding simultaneously. The compound flooding of storm surge, tide, and rainfall runoff at the Panama City area are investigated, using historical Hurricane Michael (2018) and synthetic hurricane events.

In detail, a nesting technique was developed into the model to provide the boundary conditions at the shoreline, which are the water level and the flow velocity interpolated from the pre-computed storm surge results in large domains. The rainfall data is applied during the local domain computation, and the riverine flooding due to rainfall are directly resolved through applying a refined grid along the rivers instead of using upstream river discharge boundary conditions. The Continuously Updated Digital Elevation Model (CUDEM) - 1/9 Arc-Second

Resolution (3 meters) Bathymetric-Topographic Tiles that is being developed by NOAA's National Centers for Environmental Information (NCEI) were been employed for the bathymetry and topography.

The finest grid resolution of the local computational domain is at the order of 50 m, particularly around the Panama City, coastal areas, and major rivers. An enhanced data map of the Manning coefficients representing the effects of different land covers on the flooding has been generated using the same approach as previously reported. Also for the rainfall runoff module, the same Curve Number (CN) based approach is employed and a data map of the CNs has been produced. The rainfall data associated with Hurricane Michael (2018) is downloaded from the NEXRAD database and interpolated onto the local computational grid through Python scripts.

In general, it is found that heavy rainfall (20 inches in 1 day) during extreme rainfall dominated scenarios would cause significant flooding both in the Panama City and around the Deer Point Lake areas to the north of the city. It is also confirmed that a larger rainfall rate would lead to higher maximum inundation depth. If Michael (2018) made landfall at the west side of the city, much severer storm surge could occur around the city. If a hurricane forwarding speed was also reduced by half, the peak water level caused by storm surge could increase by approximately 30% at the Deer Point Lake areas. Simulations have also been carried out by replacing the original rainfall amount of Michael (2018) with a much severer rainfall (20 inches in 1 day). The results show that such rainfall could increase the peak water level by nearly 35%, depending on the location and the time period of rainfall. On the other hand, when shifting the track of Michael (2018) to the west side of the Panama City, the same extreme rainfall amount would prolong the flooding time period by days but would not increase the peak water levels significantly. In both cases, it is concluded that estimating the compound rainfall and storm surge flooding through simple superposition would cause significant errors.

1. Background

When hurricanes make landfall, they pose great threats of both inland flooding caused by intense rainfall and coastal inundation due to storm surge. The coastal flooding can be surge dominated (Michael 2018), rainfall dominated (Allison 2001, Harvey 2017, and Barry 2019), or caused by the compound effects of rainfall and storm surge (Florence 2018 and Ike 2008). This compound flooding could lead to severer inundation extent and time duration than any of the above-mentioned single effect, hence requiring more attention from scientists, engineers, and policy makers (Resio & Westerink, 2008; Torres et al., 2015; Gori et al., 2020). At the estuary area, the heavy rainfall could also cause riverine flooding. According to Kumbier et al. (2018), neglecting riverine contributions would underestimate the extent of coastal flooding by 30%, based on a storm event along the coast of Australia. Other studies also draw similar conclusions regarding the effect of riverine flooding, ranging from minimal impacts (Torres et al., 2015) to severe impacts (Silva-Araya et al., 2018). Bilskie & Hagen (2018) pointed out that the compound flooding cannot be estimated by simple superposition of water levels of surge and inland flooding. It thus remains a challenge to understand and quantify the compound effects of rainfall runoff and storm surge.

For numerical modeling of such compound effect, previous studies often employ loose coupling between different numerical models. For example, Gori et al. (2020) applied a high-resolution hydraulic model (HEC-RAS) to simulate such compound effect at the Cape Fear River Estuary, NC, for which the downstream boundary conditions at the coastline was generated by utilizing the hydrodynamic model Advanced CIRCulation (ADCIRC), the upstream boundary condition was generated by using the empirical rainfall-runoff model HEC-HMS, together with measured river discharges, and for the computational domain radar rainfall data were also applied directly. This loose coupling approach is necessary since ADCIRC cannot directly handle coastal rainfall (Yin et al., 2016; Gori et al., 2020). However, the loosely coupled model method could cause numerical difficulties and errors, since different grid resolution, time step, and numerical schemes are utilized in many different models. In order to mitigate these difficulties, IHRC developed a combined storm surge and overland flooding model, SSFOF (Storm Surge and Freshwater Overland Flooding), to reduce the number of models needed for coupling.

The previous developments and applications of the SSFOF model are mainly focused on the flat and low-lying South Florida region, where the flooding caused by the upstream heavy rainfall accumulating from surrounding watersheds and flowing to the downstream is not significant and therefore is omitted in the numerical simulations. However, for the North Florida coastal zone, there are regions with highlands upstream, such as Ochlockonee River, Choctawhatchee River, and Apalachicola River. The compound effects of rainfall runoff induced flooding and storm surge may be dominating in certain scenarios. Therefore, the answers to the following questions are desirable: 1) how much overland flood extend and depth would be if only heavy rainfall occurs? 2) how more intensive the storm surge would be if a hurricane like Michael (2018) shifted its track or reduced its moving speed? 3) if a hurricane like Michael (2018) with much heavier rainfall makes landfall at the same or different locations, how much flood extend and depth would be

due to the compound effect? and how this compound flooding change if the time pace of storm surge and rainfall varies? This study aims to address these questions using the SSFOF model.

2. Objectives

First, a local computational domain centered at the Panama City FL is established whose boundary is delineated based on the HU-8 watershed boundary. The Panama City is a large city with large population and is catastrophically damaged when Hurricane Michael (2018) made landfall. Michael (2018) made landfall with a relatively fast forwarding speed (approximately 27 km/h) and the landfall location is slightly to the east of the Panama City, both of which would lead to relatively weak storm surges in the Panama City area according to Zhang et al. (2012). The total rainfall around the Panama City area during Hurricane Michael (2018) is approximately 7 to 10 inches (https://www.weather.gov/tae/, accessed 07/12/2021), which is also relatively small compared to heavy rainfall dominated hurricanes events (Pathak, 2001). Therefore, it is important to understand the threats of storm surge and rainfall to the Panama City area when these hurricane conditions change, such as those mentioned in the above questions. For the current study, a high-resolution local computational grid has been generated rather than using the previous regional and relatively coarse North Florida Mesh developed at Phase 3 of this project. Nevertheless, the downstream boundary conditions along the coastline for the local computational domain is extracted from the results of the previous regional North Florida domain, through a newly developed nesting technique in the SSFOF model. Second, while rainfall and storm surge are included as external input data for the numerical model, the riverine flooding due to heavy rainfall upstream is directly resolved by the model itself via extended fine grid and high-resolution topographic data along the major rivers, rather than through developing external numerical models for coupling. Finally, the numerical simulations were designed to cover storm surge dominated, heavy rainfall dominated, and combined rainfall and storm surge dominated scenarios, in order to understand the compound effects of storm surge and rainfall runoff.

3. Numerical model setup

Fig. 1 shows the study area centered at the Panama City, FL, with the boundary of the computational domain delineated based on the HU-8 watershed boundary (https://apps.nationalmap.gov/downloader/#/ accessed 07/06/2021). The current study focuses on the simulation of Hurricane Michael (2018) (see the track in Fig. 1). Michael (2018) was very powerful and destructive; it was the first Category 5 hurricane to impact Florida since Hurricane Andrew in 1992. Michael (2018) reached peak winds of approximately 160 mph just before making landfall near Mexico Beach on October 10. Being close to the eye of Michael (2018) at landfall, the Panama City was significantly impacted. However, the city was at the west side of the track where the storm surge may be weak. Therefore, the current study also investigates the scenarios of synthetic hurricanes whose track were generated by directly shifting the track of Michael (2018) to the west such that the Panama City is approximately at the maximum wind band during landfall (see the synthetic track in Fig. 1). Fig. 1 also depicts the location of the NOAA tide gauges and a number of test sites, at which the water levels may be affected by both storm surge and rainfall runoff.

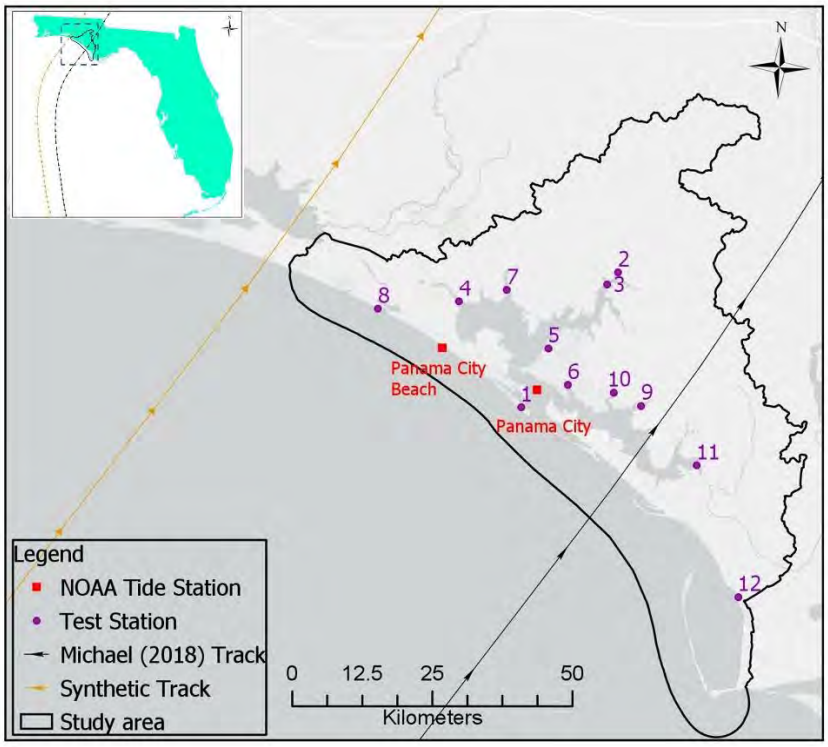

Fig. 1 The study area, hurricane tracks and measurement locations.

Fig. 2 presents the newly generated computational grid for the Panama City area. The grid consists of approximately 470,000 nodes and 940,000 triangular elements, with a grid resolution varying from nearly 600 m in the downstream ocean side to 50 m along the coastline, in the Panama City, and along major rivers.

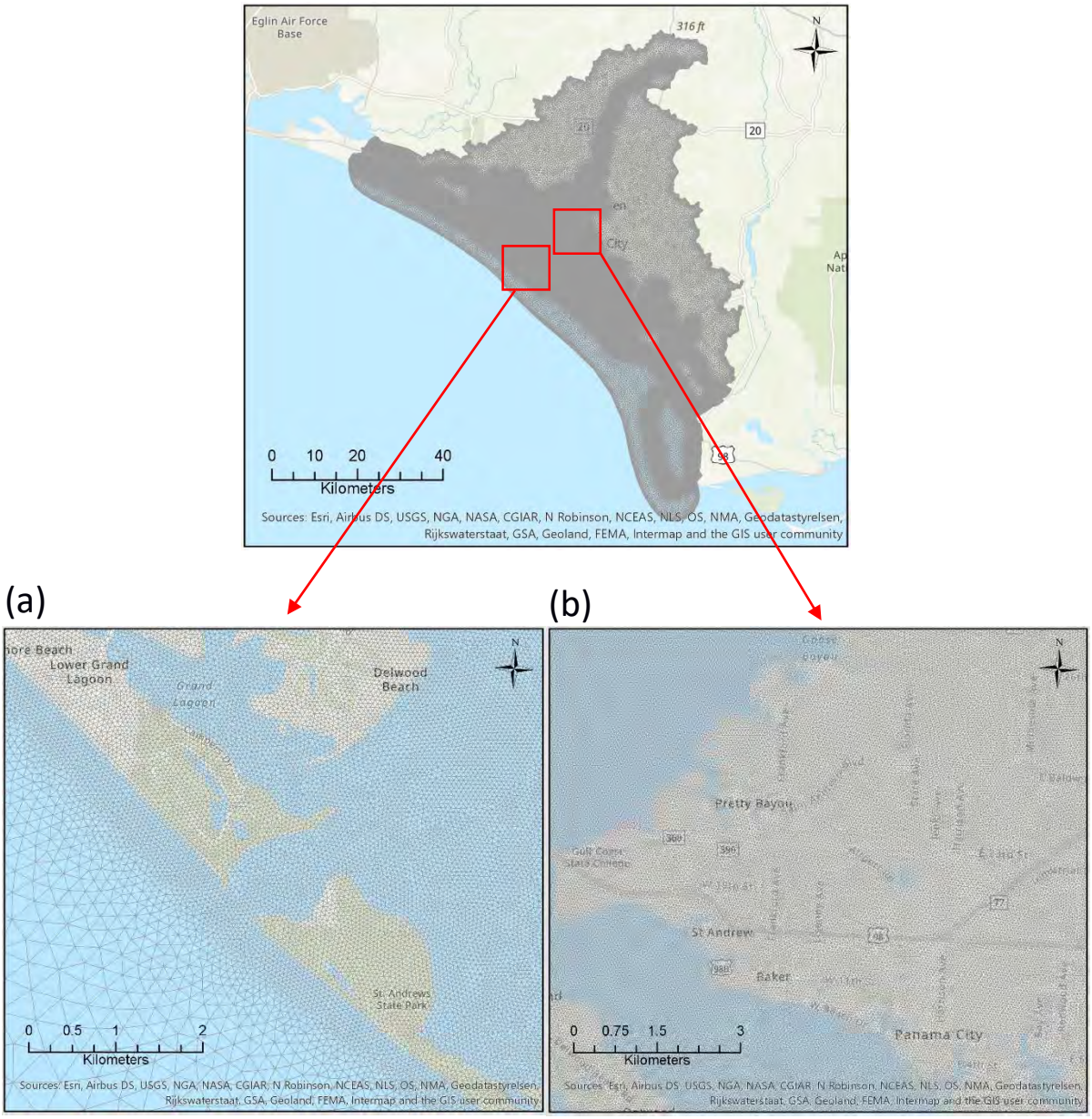

Fig. 2 The computational grid (upper panel) and zoomed in views at (a) the outlet of Saint Andrew Bay and (b) Panama City.

Fig. 3 shows the bottom elevation interpolated on the gird (referred to NAVD88), which makes use of the Continuously Updated Digital Elevation Model (CUDEM) - 1/9 Arc-Second Resolution Bathymetric-Topographic Tiles that is being developed by NOAA's national Centers for Environmental Information (NCEI). The Florida Geographic Data Library (FGDL) 5-m DEM data were employed for the elevation above water (https://www.fgdl.org/metadataexplorer/explorer.jsp) and where the 1/9 Arc-Second Resolution Bathymetric-Topographic Tiles data is not available.

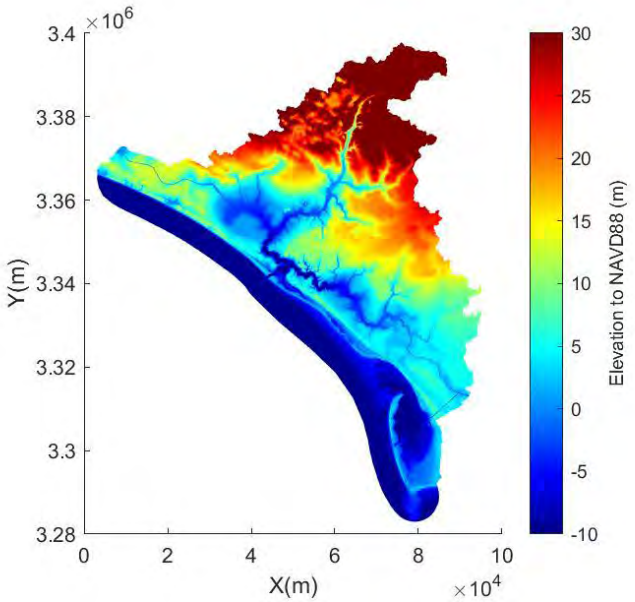

Fig. 3 Interpolated bathymetry and topography on the computational grid (referenced to the NAVD88 vertical datum).

The Manning friction coefficient (Fig. 4) was set to 0.02 in water areas, and for the wet areas and dry land the Manning coefficient was calculated based on the National Land Cover Dataset (NCLD) 2006, using the method described in Zhang et al. (2012). Details of this method has been described in the previous Phase 1 and Phase 2 reports and are not repeated here.

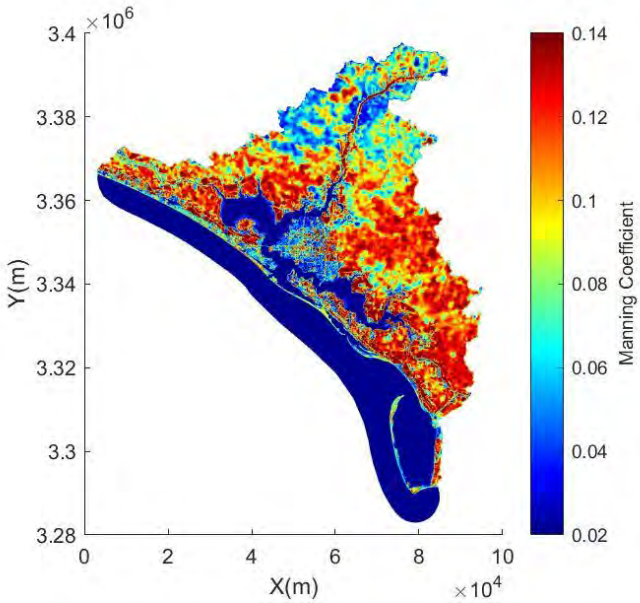

Fig. 4 The calculated Manning coefficients on the computational grid.

The current study employs the empirical Curve Number (CN) based approach developed by Soil Conservation Services (SCS) for the rainfall runoff estimation. The CN method uses soil, land use, and antecedent moisture parameters to estimate a curve number that ranges in value from 0 to 100 (see Fig. 5). Higher CN values indicate areas with a higher potential for runoff generation during a rainfall event. Details of the implementation of the CN rainfall runoff module within the SSFOF model can be found in the previous Phase 1 and Phase 2 reports and are not repeated in this report.

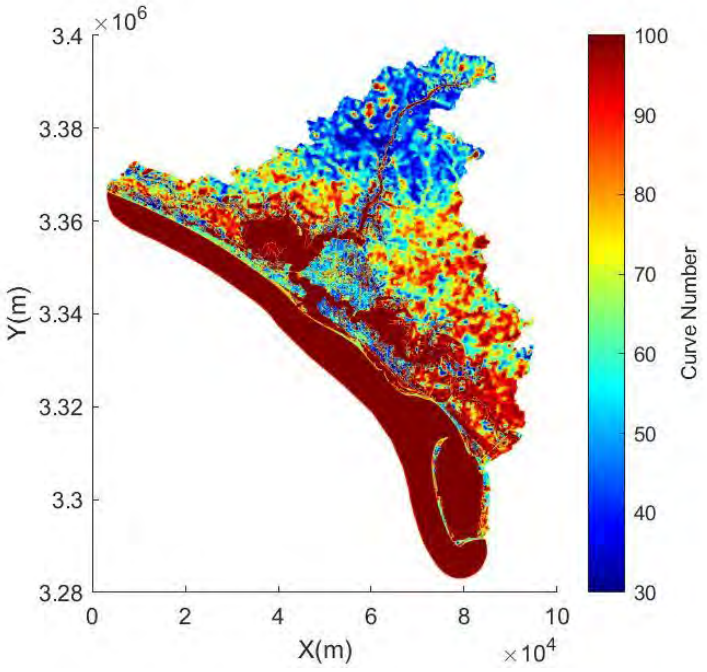

Fig. 5 The calculated Curve Numbers on the computational grid.

The current study employs both hypothetical rainfall and the measured rainfall data according to the test cases under consideration. For the simulation of historical hurricane events, the measured rainfall data from the NEXRAD (Next Generation Radar) database managed by the U.S. National Weather Service of NOAA were employed. NEXRAD is placed at seven locations in Florida (i.e., Eglin Air Force Base, Tallahassee, Jacksonville, Melbourne, Tampa, Miami, and Key West), covering the entire state (https://www.ncdc.noaa.gov/nexradinv/map.jsp). For this project, the Tallahassee NEXRAD station data L3[N1P]-One Hour Precipitation (PPS) (16 Level/230 KM) data were downloaded and interpolated onto the computational grid through Python scripts. Fig. 6 shows snapshots of the interpolated rainfall data on the computational grid at various time instants.

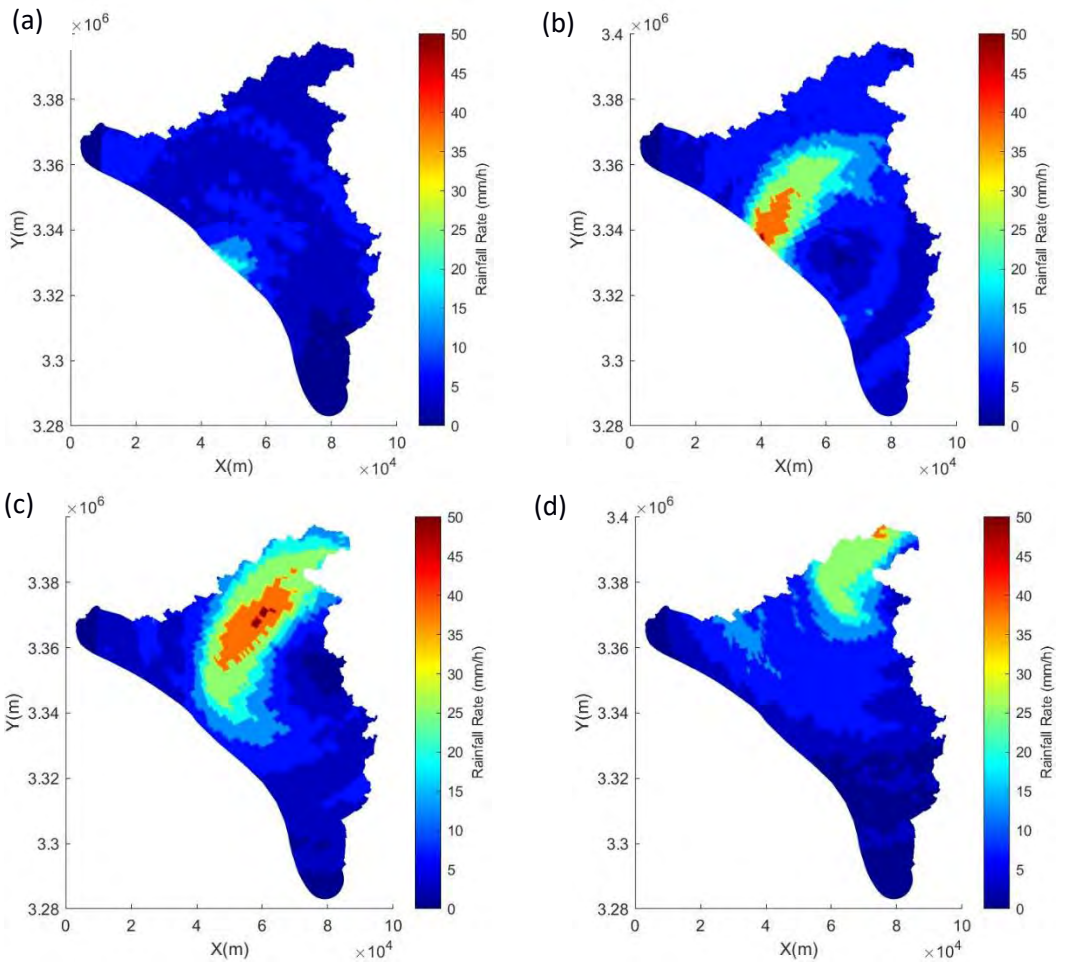

Fig. 6 The interpolated rainfall rate (mm/hour) on the computational grid at (a) 18:00, (b) 19:00, (c) 20:00, and (d) 21:00 October 10 2018.

The wind field was computed using the SLOSH parametric wind model (Jelesnianski et al., 1992), which has been added to the SSFOF model at the Phase 1 stage of this project. A brief description of the SLOSH wind model can be found in the Phase 1 report.

The boundary conditions for the downstream boundary located within the nearshore area are extracted, via a nesting technique, from the regional domain storm surge results, which are obtained by computations using the same setup and regional grid as those presented in the Phase 3 report. More specifically, the time series of the free surface and the flow velocity at each of the boundary nodes (of the current local computational domain) were interpolated from the large domain results. It is noted that the tidal effects were included in the regional domain modeling, hence are reflected in the local domain results through the boundary condition enforcement. Fig. 7 presents the comparison of the time history of the free surface at the two NOAA tide gauge stations between the large (external) domain and the local small (internal) domain results, for the storm surge simulation during Hurricane Michael (2018). The nesting configuration

implemented in the current study enables a good repeat of the pattern of the large domain results in the small domain, despite some minor discrepancies due likely to the difference between the grid resolutions. The current local computational grid has a much higher spatial resolution compared to the large domain grid employed for the Phase 3 study of this project.

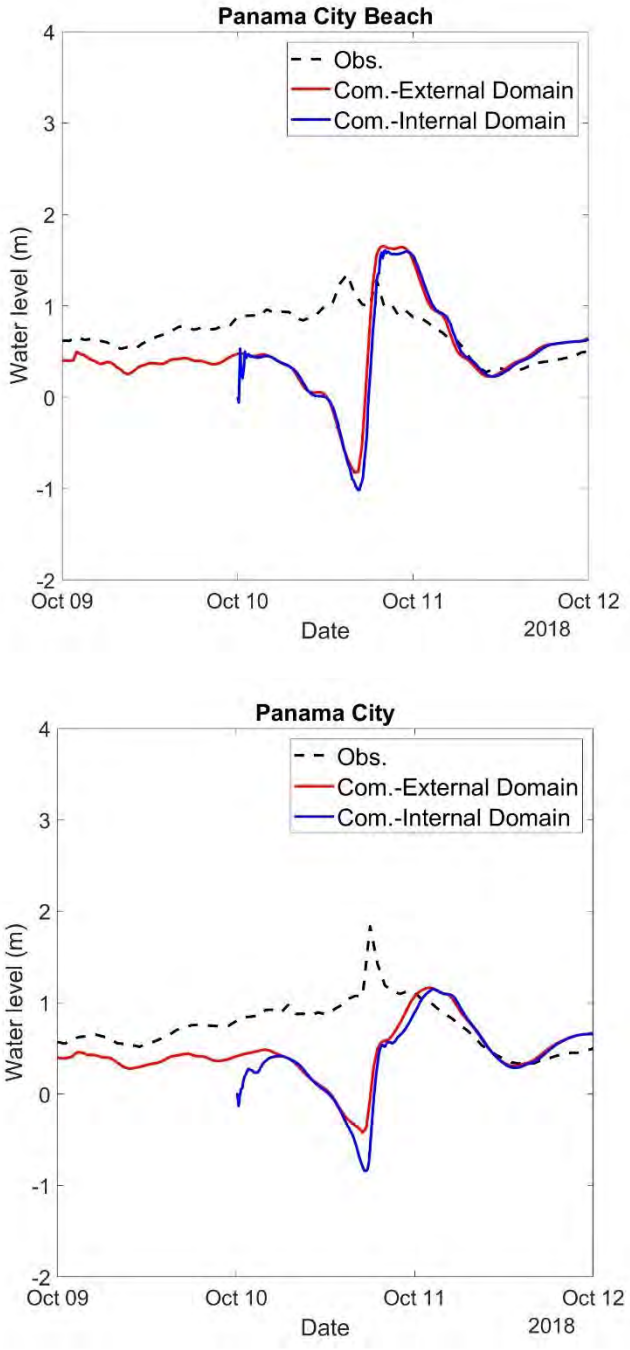

Fig. 7 Comparison between the large (external) domain and the small (internal) domain results for the free surface elevations at the NOAA tide gauges (see Fig. 1).

4. Results and Discussions

4.1 Effect of rainfall duration on overland flooding

In the Phase 2 report of this project, it is demonstrated, through a sensitive study of different rainfall scenarios in the Downtown Miami Basin, that in general larger amount of rainfall will lead to higher inundation depth and extents. However, it remains interesting to see how the duration of rainfall affects the overland flooding, if the total amount of rainfall is unchanged. The rainfall amount caused by Hurricane Michael (2018) is relatively small (about 7 to 10 inches) compared to extreme historical events (> 20 inches) according to Pathak (2001). In this section, in order to identify the most vulnerable areas within the study area to freshwater overland flooding caused by hurricane induced rainfall, three hypothetical rainfall scenarios are investigated. For the three cases, a total rainfall amount of 20 inches is applied directly on each grid cell of the computational domain, but has a duration of 1 day, 2 days, and 3 days, respectively. In other words, in test case 1, the total rainfall amount is 20 inches, and this amount of rainfall is averaged in 1 day; therefore, the rainfall rate is roughly 22 mm per hour. In test cases 2 and 3, the same amount of rainfall is completed within 2 days and 3 days, with a rainfall rate of 11 and 7 mm per hour, respectively. In all cases, the rainfall starts at the beginning of the simulations, which are set to 10 October 2018 00:00:00, and the simulations last for 3 days. It is noted that storm surge has not been included in these test cases.

Fig. 8 shows the comparison for the computed maximum inundation depth, which is defined as the maximum value of the increased water level as the simulation progresses. In general, it appears that the shorter the duration of rainfall, the higher the maximum inundation depth, particularly around the river mouths such as the Bear Creek, when the total rainfall amount is fixed. Fig. 9 presents the comparison for the time history of the water level amongst the three cases. It is noticed that at Stations 1, 8 and 12, which are located at the shoreline, the effect of rainfall on inundation is minor, whereas at Stations 2, 3, 9, 10, and 11, which are located at the river mouths, rainfall effect is significant. Moreover, the comparison of water level time history at those river mouth stations confirms the above observation that when the same amount of rainfall occurs in a shorter period of time, a higher inundation depth is likely to happen.

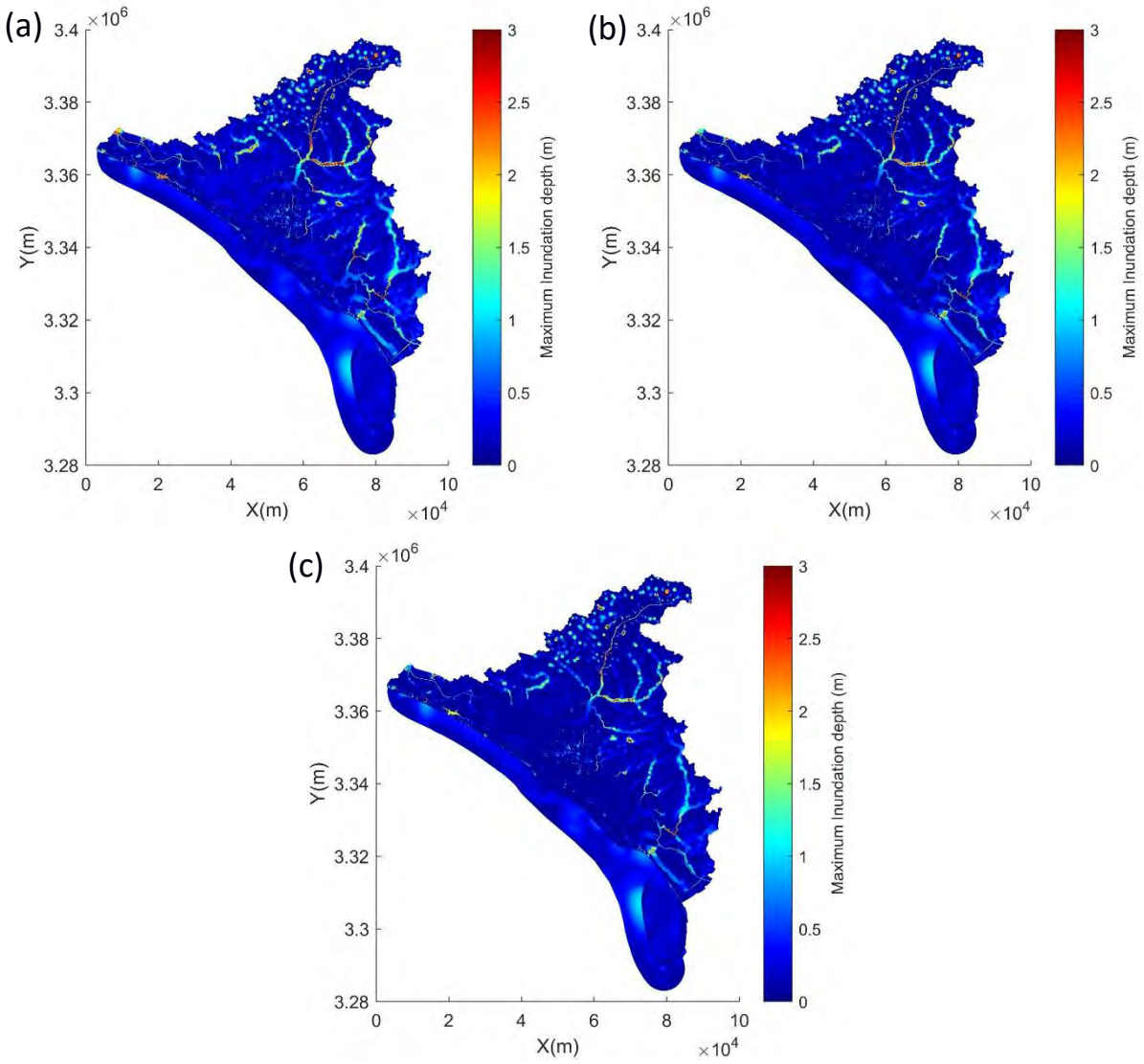

Fig. 8 The computed maximum inundation depth for the three hypothetical rainfall events: (a) total rainfall = 20 inches, duration = 1 day; (b) total rainfall = 20 inches, duration = 2 days; (c) total rainfall = 20 inches, duration = 3 days.

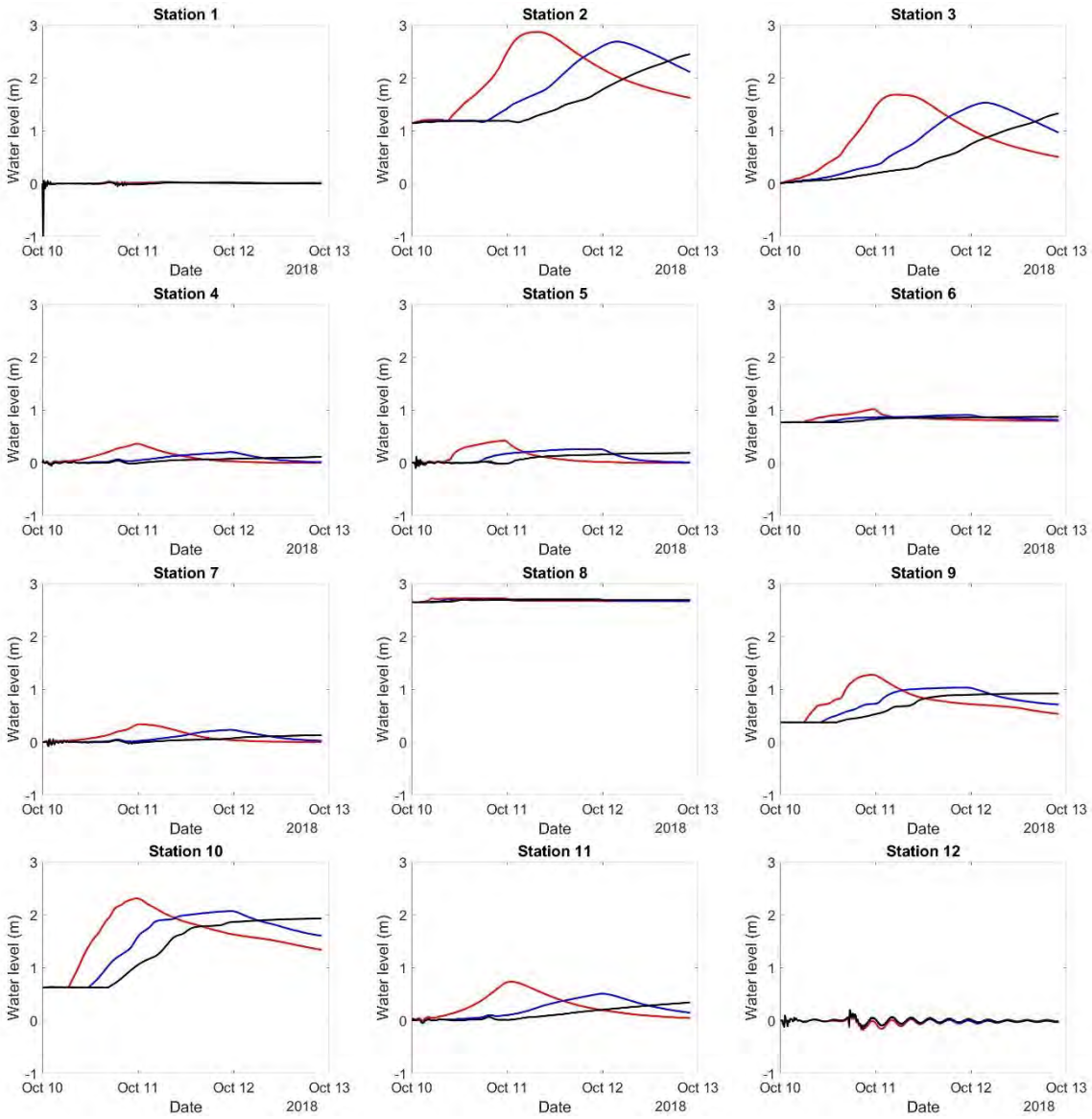

Fig. 9 Comparison for the time histories of the water levels (referenced to NAVD88) at the test locations (see Fig. 1) amongst the three hypothetical rainfall events. Red line: total rainfall = 20 inches, duration = 1 day; Blue line: total rainfall = 20 inches, duration = 2 days; Black line: total rainfall = 20 inches, duration = 3 days.

4.2 Effects of hurricane moving speed and track location on storm surge

In addition to Hurricane Michael (2018), numerical simulations have also been carried out for synthetic hurricane events, which include: Synthetic 1) all the features of Hurricane Michael (2018) are kept except that the moving speed of the hurricane at landfall has been reduced by half from approximately 27 km/h to 13.5 km/h, Synthetic 2) all the features of Hurricane Michael

(2018) are kept except that the track of Michael (2018) has been shifted nearly 74 km to the west (see Fig. 1), and Synthetic 3) the moving speed of the hurricane defined in Synthetic 2 is reduced by half at landfall and all other features are kept unchanged. These synthetic hurricanes are specifically designed to cause more significant storm surge impact on the Panama City area. It is noted that no rainfall effect is considered in this section.

Fig. 10 presents the computed maximum inundation depths for the four hurricane scenarios (Hurricane Michael (2018) plus the three synthetic hurricane events). It is seen from Fig. 10(a) and (b) that for Hurricane Michael (2018) and Synthetic 1, the maximum storm surge occurs around the Mexico Beach area and inside the Saint Joseph Bay, while for Synthetic 2 and Synthetic 3, the maximum storm surge happens at the west around the Panama City Beach area (Fig. 10(c) and (d)). In terms of the effect of the reduced hurricane forwarding speed, it is seen from Fig. 10(a) and (b) that as the hurricane forwarding speed decreases, the maximum inundation depth increases, as the wind has more time to push water into the Saint Joseph Bay. In contrast, from Fig. 10(c) and (d) that the reduction of the forwarding speed contributes less to the maximum inundation depth increase along the shoreline area, compared to the previous case. The could be due to that for Synthetic 2, the wind contribution to storm surge has already reached a balance; hence increasing the wind action time would not significantly increase the storm surge height along the shoreline area. However, this is not the case for the Deer Point Lake area (north to the Panama City), where the slower Synthetic 3 causes much higher maximum inundation depth than Synthetic 2, which is confirmed from the time history of water level comparison presented in Fig. 11 (Stations 2 and 3). In particular, at Station 12, it is noticed that reducing the hurricane forwarding speed of Michael (2018) by half leads to an increase of the peak water level by 34%. At Station 2, the peak water level increase due to this moving speed reduction on Synthetic 2 hurricane event is around 33%.

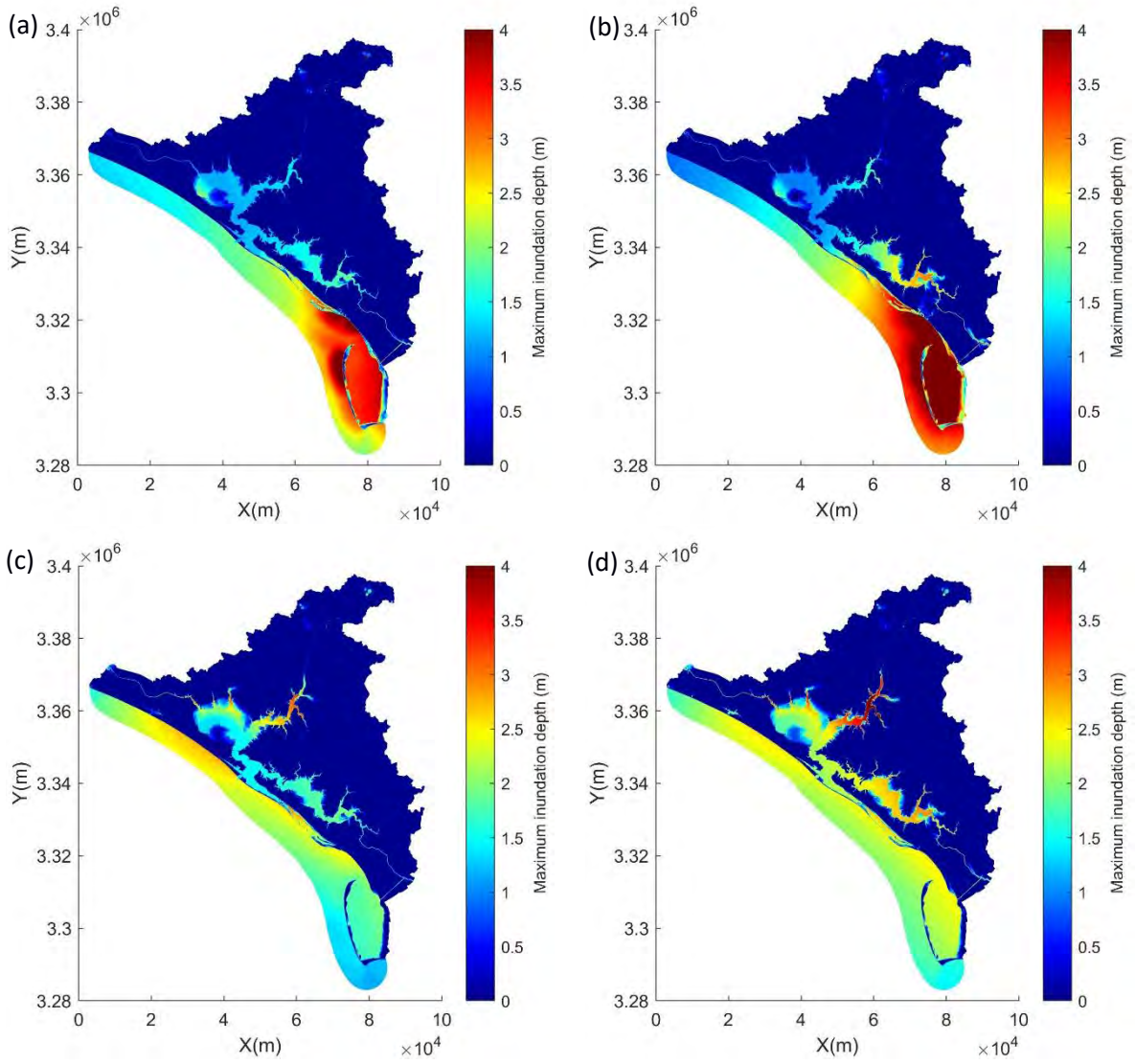

Fig. 10 The computed maximum inundation depth for (a) Hurricane Michael (2018), (b) Synthetic 1, (c) Synthetic 2, and (d) Synthetic 3.

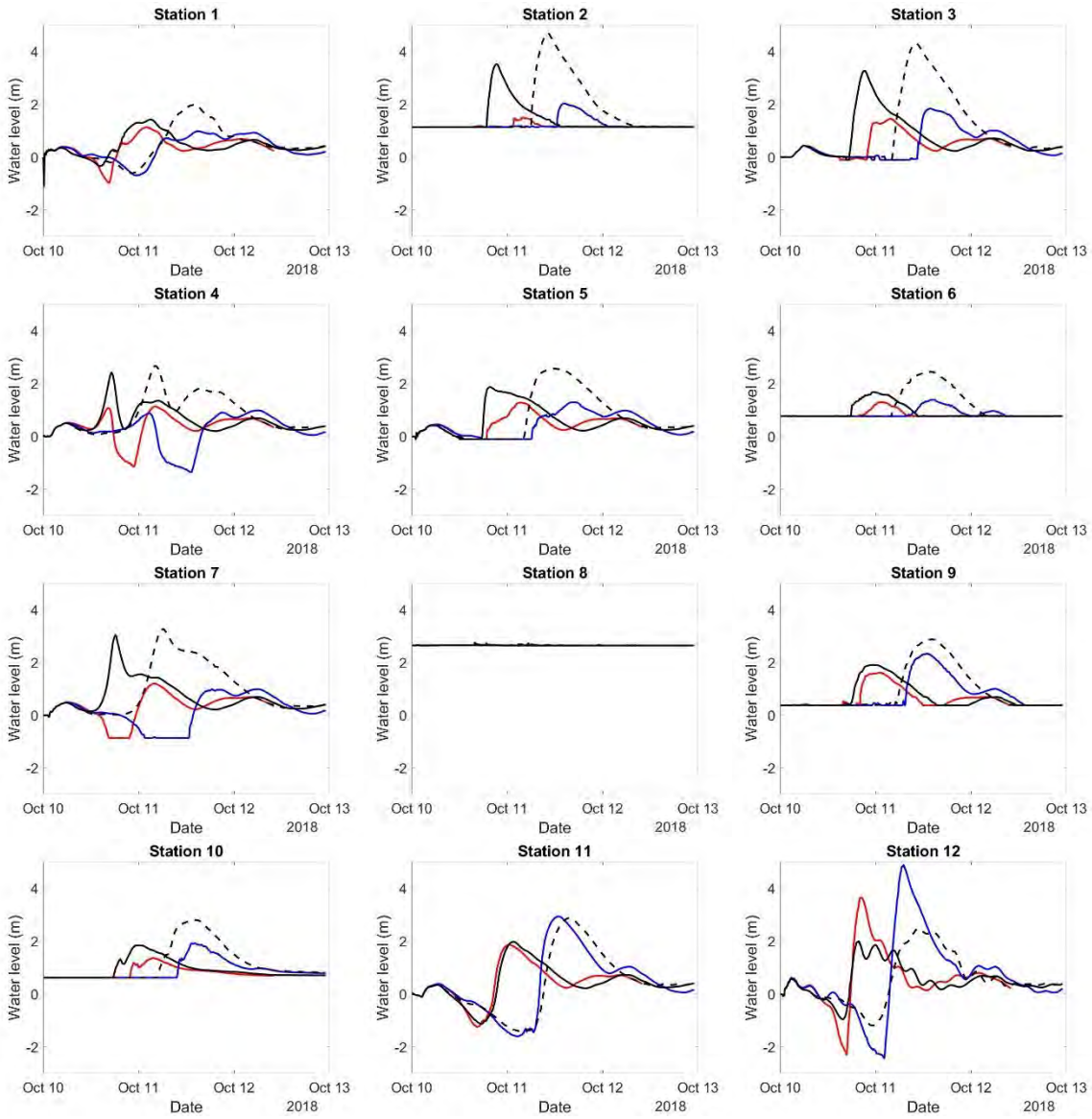

Fig. 11 Comparison for the time histories of the water levels (referenced to NAVD88) at the test locations (see Fig. 1) amongst Hurricane Michael (2018) and the three synthetic hurricanes. Red line: Hurricane Michael (2018), Blue line: Synthetic 1 — Michael (2018) with reduced forwarding speed at landfall, Black line: Synthetic 2 — shifted Michael (2018) track to the west, and Black dashed line: Synthetic 3 — Synthetic 2 with reduced forwarding speed at landfall.

4.3 Compound effect of storm surge and rainfall runoff

Fig. 12 presents the comparison for the computed maximum inundation depth of Hurricane Michael (2018), with and without the rainfall data obtained through the NEXRAD database applied in the simulation. Fig. 13 shows the comparison of the time history of the water level for the two cases at the test sites (see location in Fig. 1). The numerical results in general show that the rainfall effect induced by Hurricane Michael (2018) is minor, compared to the storm tide.

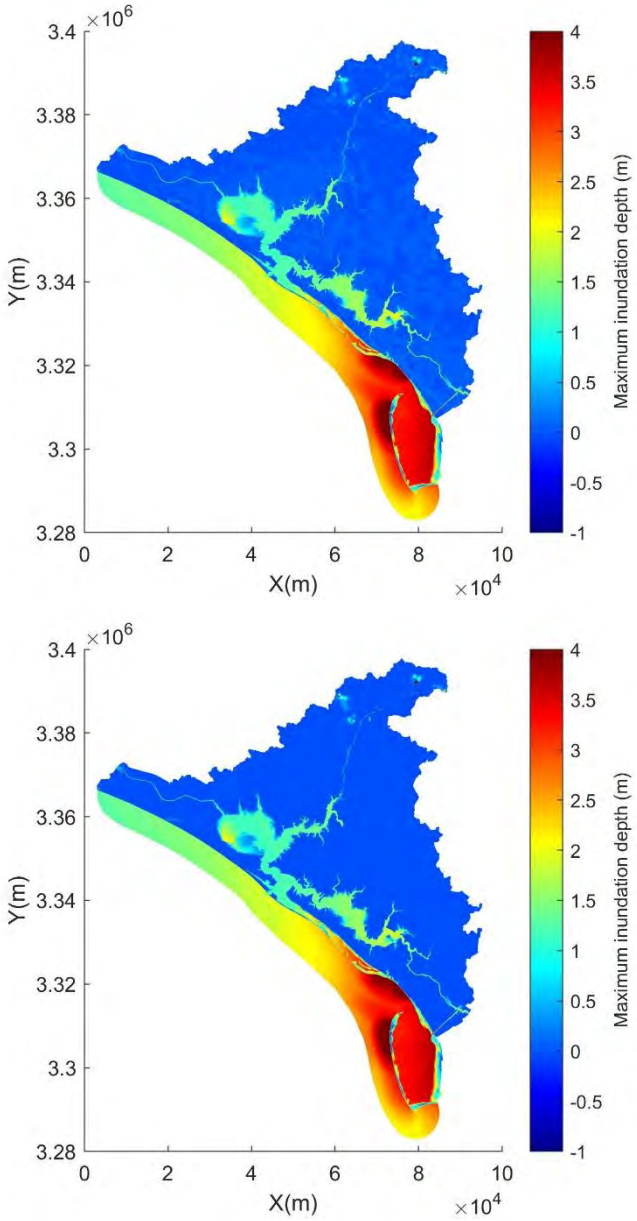

Fig. 12 The computed maximum inundation depth for Hurricane Michael (2018) with (upper panel) and without (lower panel) rainfall obtained from the NEXRAD database (see Fig. 6).

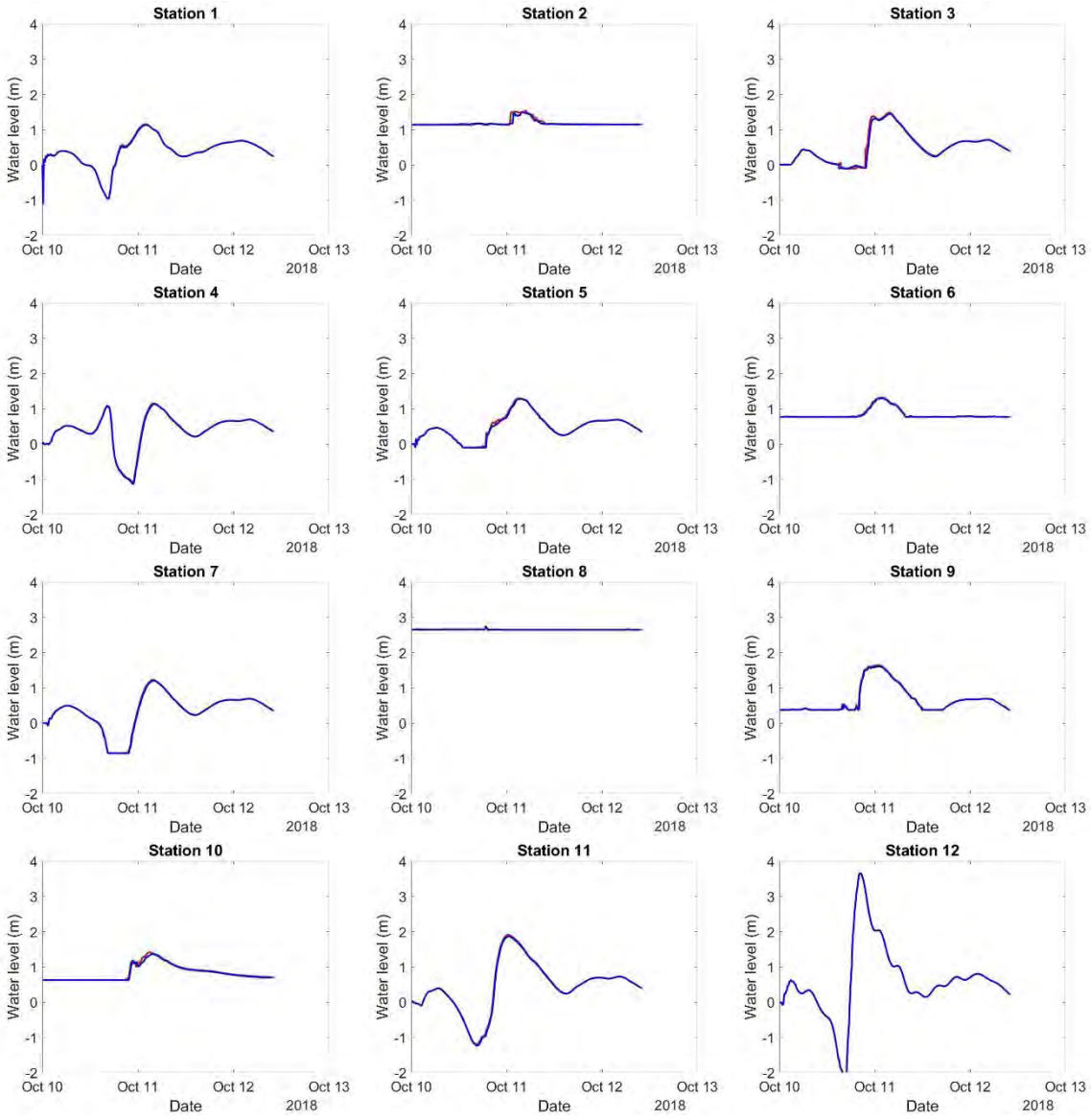

Fig. 13 Comparison for the time histories of the water levels (referenced to NAVD88) at the test locations (see Fig. 1) between Hurricane Michael (2018) with and without the NEXRAD rainfall data. Red line: with rainfall, and Blue line: without rainfall.

In order to investigate the potential compound effect of storm tide and rainfall runoff, three hypothetical rainfall scenarios are simulated in combination with the storm tide caused by Hurricane Michael (2018). In particularly, the rainfall scenarios all have a total rainfall amount of 20 inches and a duration of 1 day, but differ in the starting time, which are 00:00:00, 12:00:00, and 24:00:00 10 October 2018, respectively. Fig. 14 shows the computed maximum inundation depths for the three test cases for comparison, and Fig. 15 presents the comparison for the time histories of the water levels at the test sites. It is clear that at Stations 1, 8, and 12, located along

the shoreline, the water level is surge dominated, whereas at Stations 2 and 10, the water level appears to be rainfall dominated, and other locations exhibit the compound effect of storm surge and rainfall. From Stations 3, 4, 7, 9, and 11, it appears that in the test case where rainfall starts at 00:00:00 10 October 2018, the rainfall induced flooding coincides with storm tide, which leads to much more significant flooding, that neither storm tide nor rainfall runoff alone can fully explain. Take Station 3 as an example, the rainfall runoff induced inundation depth increase accounts for approximately 36% of the overall inundation depth (~ 2.35 m) at the peak water level time. However, it should be noted that the compound inundation depth at Station 3 does not equal to the simple addition of the rainfall alone and storm surge alone inundation depths (which are approximately 1.65 m and 1.5 m, respectively; see Fig. 9 and Fig. 13). This confirms the conclusion drawn by Bilskie & Hagen (2018) that the compound flooding cannot be estimated by simple superposition of water levels of surge and inland flooding.

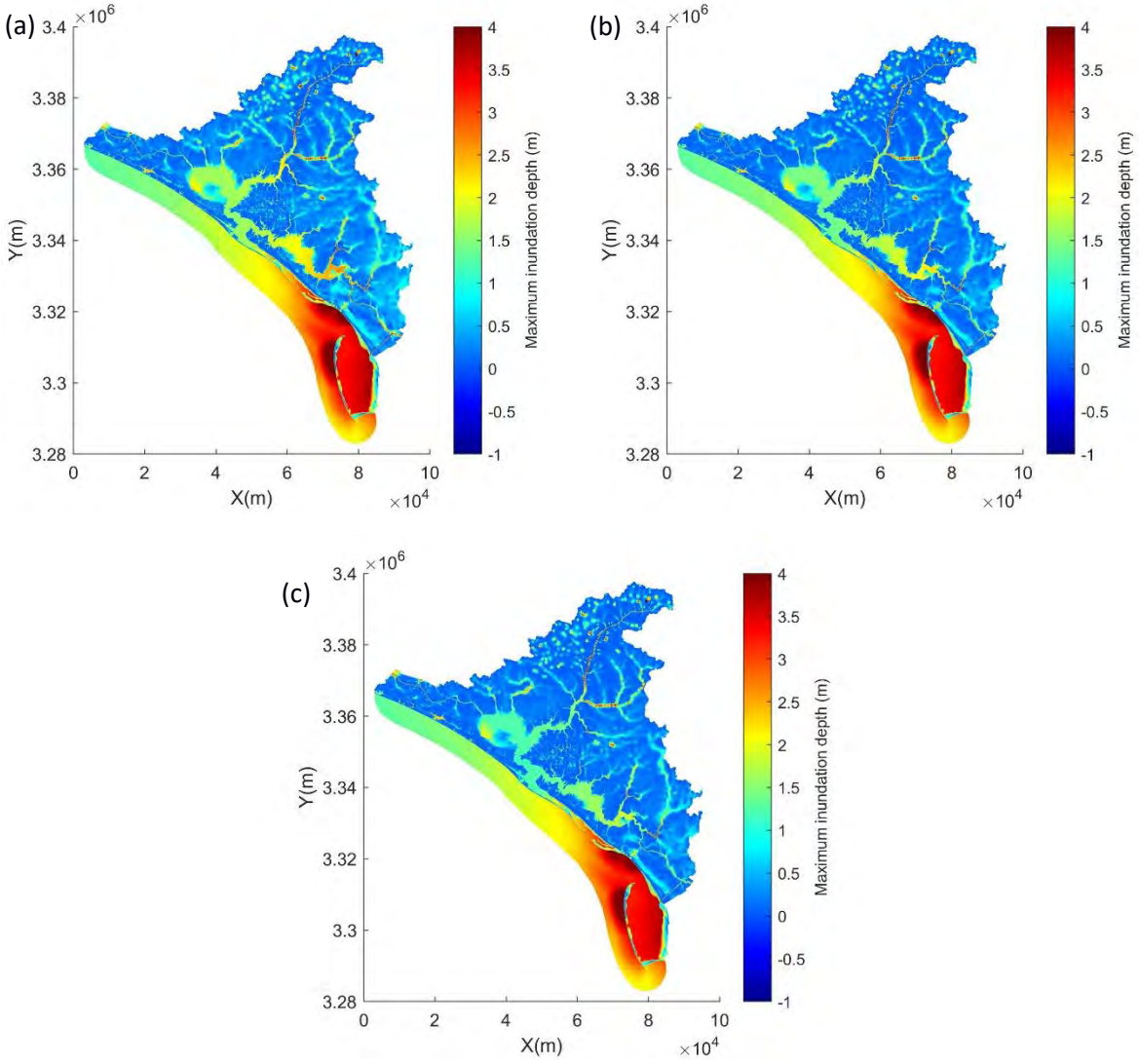

Fig. 14 The computed maximum inundation depth for Hurricane Michael (2018), with the rainfall amount of 20 inches and duration of 1 day, that starts at (a) 00:00 10 October, (a) 12:00 10 October, and (a) 00:00 11 October.

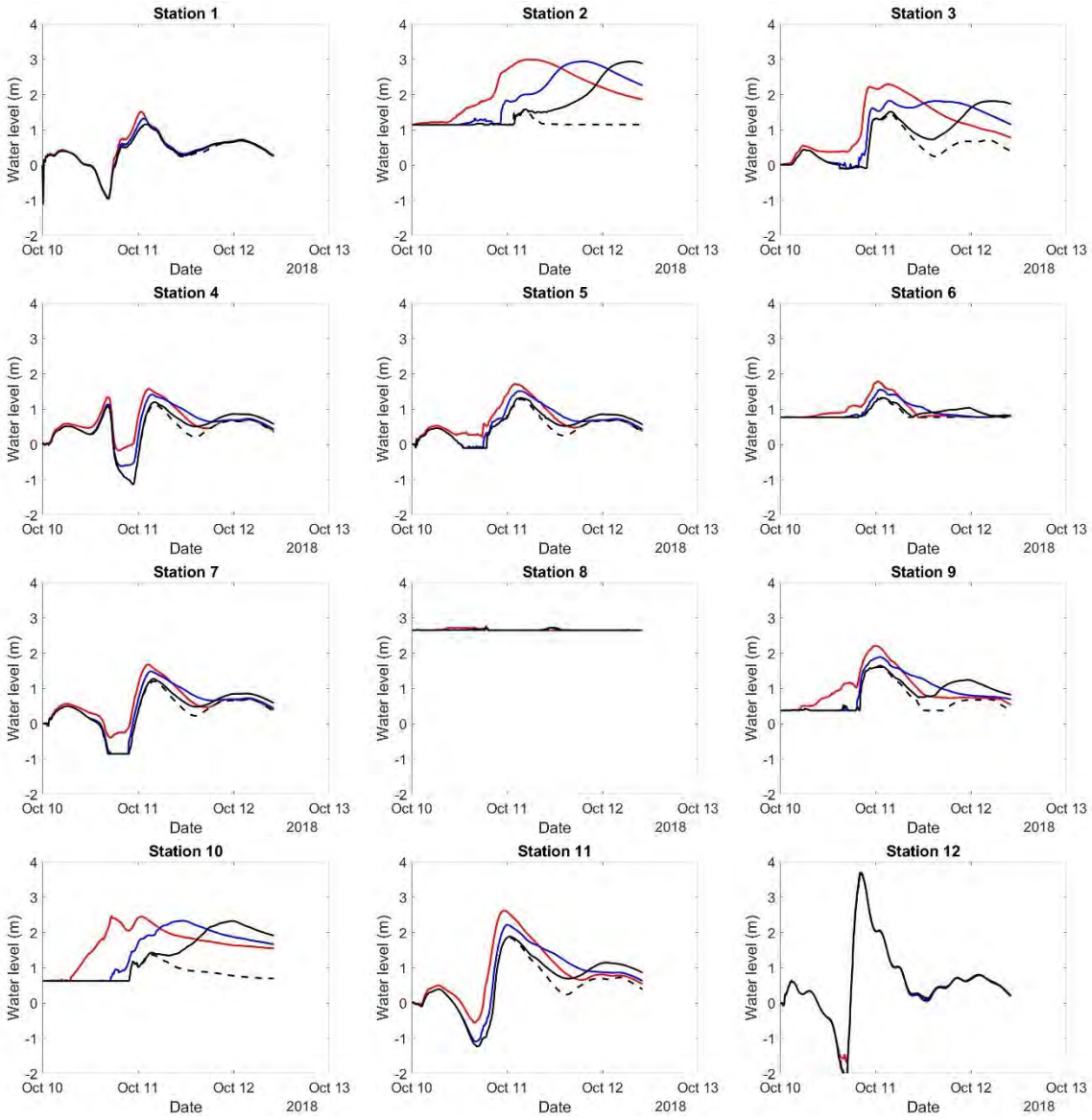

Fig. 15 Comparison for the time histories of the water levels (referenced to NAVD88) at the test locations (see Fig. 1) for Hurricane Michael (2018) with the rainfall amount of 20 inches and duration of 1 day, that starts at 00:00 10 October (the red line), 12:00 10 October (the blue line), and 00:00 11 October (the black line). The black dashed line represents the case without rainfall.

As the worst case scenario, this study also carried out simulations of Synthetic 3 hurricane with the same three rainfall events as above. As seen from Fig. 10(d), Synthetic 3 hurricane event results in significant storm surge around the Panama City, particularly in the Deer Point Lake to the north and in the East Bay to the east, which are both heavily affected by the rainfall as seen in the standalone rainfall test results from Fig. 8(a). Fig. 16 and Fig. 17 show the computed

maximum inundation depth and the time histories of the water levels at the test sites, respectively. In general, it may be seen that the contributions from rainfall, despite being very significant in rainfall standalone tests (e.g., a maximum of approximately 1.6 m inundation depth at Station 2, see Fig. 9), to the peak water levels are less significant than those in the above Michael (2018) test cases. This is probably due to 1) the storm surge induced by Synthetic 3 hurricane is significantly larger than that by Michael (2018) around the Panama City; hence a surge dominated scenario, and 2) the peaks of the rainfall flooding (of all three rainfall cases) do not coincide with those of the storm surge at the test sites. However, it is clear from Stations 2, 3, 9, and 10 from Fig. 17 that the rainfall runoff in all cases has resulted in prolonged time duration of flooding by days.

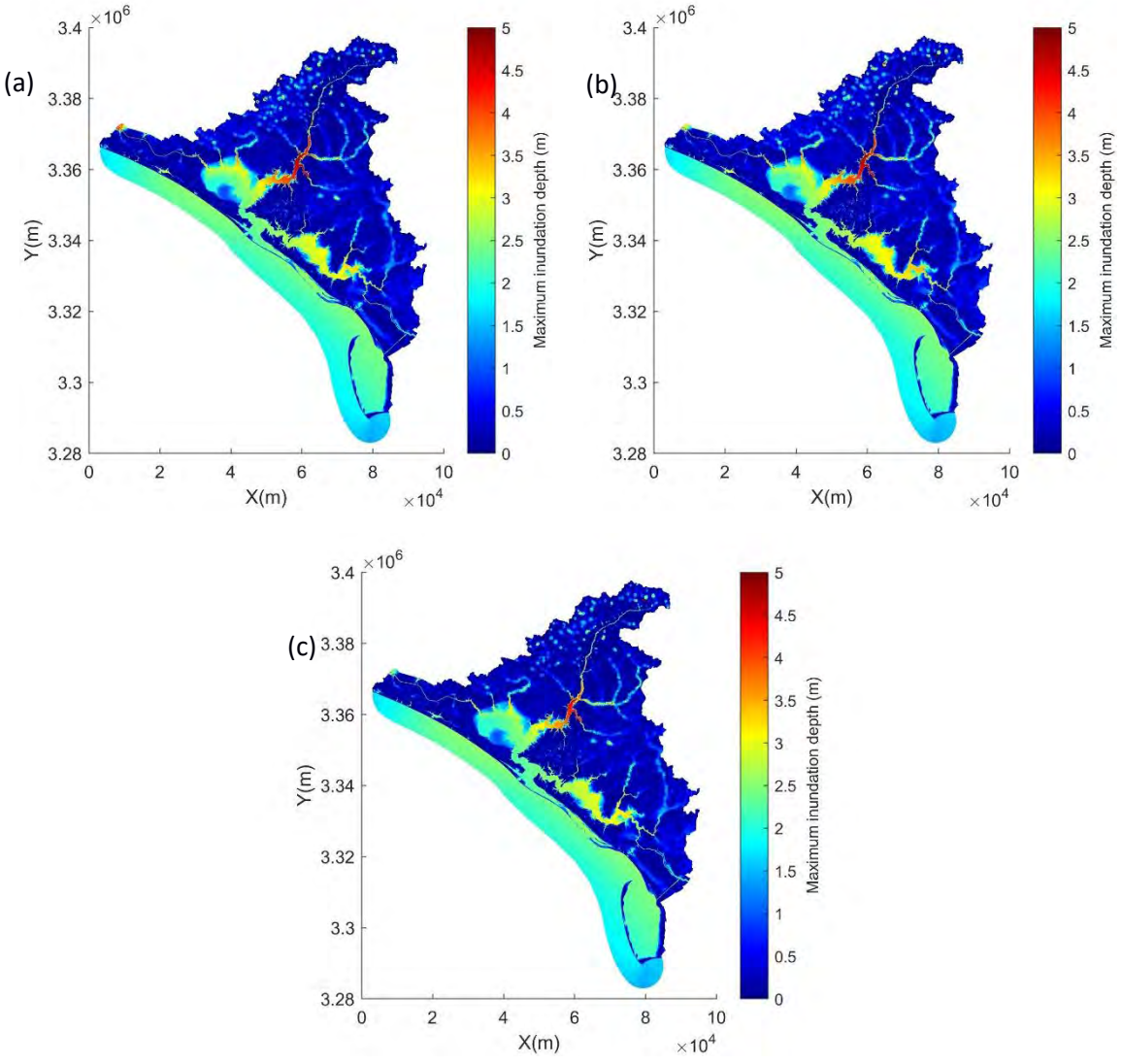

Fig. 16 The computed maximum inundation depth for Synthetic 3 Hurricane, with the rainfall amount of 20 inches and duration of 1 day, that starts at (a) 00:00 10 October, (a) 12:00 10 October, and (a) 00:00 11 October.

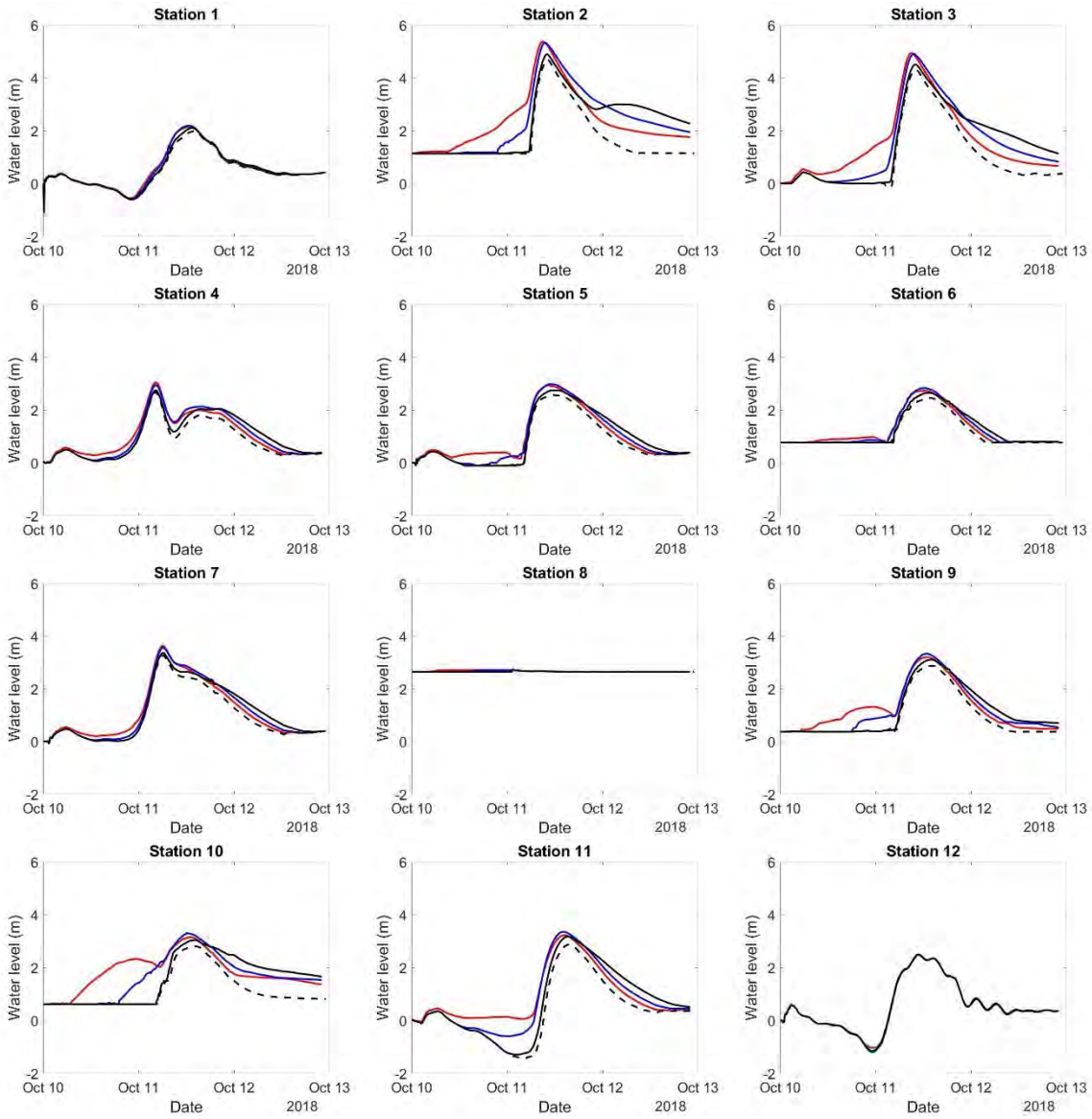

Fig. 17 Comparison for the time histories of the water levels (referenced to NAVD88) at the test locations (see Fig. 1) for Synthetic 3 Hurricane with the rainfall amount of 20 inches and duration of 1 day, that starts at 00:00 10 October (the red line), 12:00 10 October (the blue line), and 00:00 11 October (the black line). The black dashed line represents the case without rainfall.

5. Conclusions and Recommendations

This study has demonstrated that the SSFOF model is capable of simulating extreme compound flooding due to storm surge, tide, and rainfall runoff. A nesting technique was newly developed into the model to provide the boundary conditions at the shoreline, which enables the use of local refined computation grid to resolve detailed bathymetry and topography, with good

reproduction of storm surge signal that is pre-computed using a regional but relatively coarse grid. The riverine flooding due to rainfall runoff is directly resolved through applying a refined grid along the rivers instead of using upstream river discharge boundary conditions, for which measurement data are not always available in specific areas. This also eliminates the numerical difficulty and errors caused by coupling different numerical models, in order to provide the upstream boundary conditions.

This study investigated the hurricane induced compound storm tide and rainfall runoff flooding impact on the Panama City area. The simulations include not only history hurricane event Michael (2018) with measured NEXRAD rainfall data, but also synthetic hurricanes in combination with synthetic rainfall amount and duration, since Hurricane Michael (2018) is surge dominated. In general, heavy rainfall (20 inches in 1 day) during extreme hurricane scenarios would cause significant flooding both in the Panama City and around the Deer Point Lake areas to the north of the city. It is also confirmed that a larger rainfall rate would lead to higher maximum inundation depth. If Michael (2018) made landfall at the west side of the city, much severer storm surge could occur around the city (Fig. 10), with reduced hurricane forwarding speed by half further increasing the peak water level by approximately 30% at the Deer Point Lake areas. Simulations that replace the original rainfall amount of Michael (2018) with a much severer rainfall of 20 inches in just 1 day show that the rainfall could increase the peak water level by nearly 35%, depending on the location and the time period of rainfall. On the other hand, with the Synthetic 3 slow moving hurricane event, the same extreme rainfall amount would prolong the flooding time duration by days but would not increase the peak water levels significantly. Whatever the circumstance may be, it is certain that estimating the compound rainfall runoff and storm surge flooding through simple superposition would cause significant errors.

For future work, either in the same or in other study areas within Florida, it will be beneficial to further develop the wind field generation module within the SSFOF model. Currently, this is based on the SLOSH parametric wind model. However, it is desirable that the model can read in temporal and spatial varying wind data provided by meteorology models such as HWRF (The Hurricane Weather Research and Forecasting). This is because wind field is the key drive for storm surge models; this capability will certainly improve the simulation results. Secondly, the CN based rainfall runoff approach currently implemented in the SSFOF model provides a reliable first approximation. However, an improvement would certainly be useful is to consider an infiltration model based on the modified Green & Ampt approach (Triadis and Broadbridge, 2010).

Reference

Bilskie, M. V., & Hagen, S. C. (2018). Defining flood zone transitions in low-gradient coastal regions. *Geophysical Research Letters*, 45, 2761– 2770.

Gori, A., Lin. N., and Smith J. (2020) Assessing Compound Flooding from Landfalling Tropical Cyclones on the North Carolina Coast. *Water Resources Research,* Volume 56, Issue 4, 1-21.

Kumbier, K., Carvalho, R. C., Vafeidis, A. T., & Woodroffe, C. D. (2018). Investigating compound flooding in an estuary using hydrodynamic modelling: A case study from the Shoalhaven River, Australia. *Natural Hazards and Earth System Sciences*, 18, 463–477.

Resio, D. T., & Westerink, J. J. (2008). Modeling the physics of storm surges. *Physics Today*, 61, 33– 38.

Silva-Araya, W., Santiago-Collazo, F., Gonzalez-Lopez, J., & Maldonado-Maldonado, J. (2018). Dynamic modeling of surface runoff and storm surge during hurricane and tropical storm events. *Hydrology*, 5, 13.

Torres, J. M., Bass, B., Irza, N., Fang, Z., Proft, J., Dawson, C., Kiani, M., & Bedient, P. (2015). Characterizing the hydraulic interactions of hurricane storm surge and rainfall-runoff for the Houston-Galveston region. *Coastal Engineering*, 106, 7–19.

Yin, J., Lin, N., & Yu, D. (2016). Coupled modeling of storm surge and coastal inundation: A case study in New York City during Hurricane Sandy. *Water Resources Research*, 52, 8685–8699.

Zhang, K., Liu, H., Li, Y., Xu, H., Shen, J., Rhome, J. and Smith III, T.J., 2012. The role of mangroves in attenuating storm surges. *Estuarine, Coastal and Shelf Science*, *102*, pp.11-23.

Pathak C. S. 2001, Frequency analysis of daily rainfall maxima for central and south Florida. Tech. Publ. EMA390, South Florida Water Management District West Palm Beach, FL.

Jelesnianski, C.P., Chen, J. and Shaffer, W.A., 1992. SLOSH: Sea, lake and overland surges from hurricanes, NOAA, Washington, D.C.

Triadis, D. and Broadbridge, P., 2010. Analytical model of infiltration under constant concentration boundary conditions, *Water Resources Research*, 46, W03526.

A Resource for the State of Florida

SECTION 6

Improving individual preparedness for hurricanes: Lessons to be learned from longitudinal survey data collected from Florida

(Presented as two separate reports)

A Report Submitted to:
The State of Florida Division of Emergency Management

Prepared By:
Jeffrey Czajkowski, Ph.D
W. J. Wouter Botzen, Ph.D
Peter J. Robinson, Ph.D
Max Tesselaar, Ph.D
Juan Zhang, Ph.D.

National Association of Insurance Commissioners (NAIC)
The International Hurricane Research Center (IHRC)
Florida International University

July 30, 2021

Improving individual preparedness for hurricanes: Lessons to be learned from longitudinal survey data collected from Florida - Hurricane preparedness and insurance uptake in Florida during Hurricane Eta as well as at the start of the 2021 hurricane season

W. J. Wouter Botzen[1,2,3], Max Tesselaar[1], Peter J. Robinson[1], Juan Zhang[4], Jeffrey Czajkowski[4]

[1] Department of Environmental Economics, Institute for Environmental Studies, VU University Amsterdam, The Netherlands.

[2] Utrecht University School of Economics (U.S.E.), Utrecht University, Utrecht, The Netherlands.

[3] Risk Management and Decision Processes Center, The Wharton School, University of Pennsylvania, Philadelphia, USA.

[4] Center for Insurance Policy and Research, National Association of Insurance Commissioners, Kansas City, Missouri, USA.

Date: July 27, 2021

Executive summary

This study is part of a multi-year research effort on hurricane preparedness by coastal residents in Florida which aims to give insights into determinants of hurricane preparedness behavior. In order to design policies to improve disaster preparedness we need to have a better understanding of individual decision making during a threat of a disaster as well as in its aftermath, and in particular obtain insights into why some people are well prepared and others not, which may be related to behavioral characteristics, like risk perceptions. However, most studies of individual natural disaster risk perceptions and their relation to risk reduction activities rely on cross-sectional data that is collected at one point in time after the disaster has occurred, while risk perceptions and preparedness activities evolve over time. Therefore, we collected data on risk perceptions and preparations in real-time during the 2020 hurricane season and under the direct threat of impacts from flooding and wind from Hurricane Eta to gain insights into how households prepare, take risk reduction measures, evacuate and/or have insurance, and study the factors that explain these decisions. Moreover, we conducted a follow up survey of the same households six months after the storm and coinciding with the beginning of the 2021 hurricane season to examine how preparedness activities, risk perceptions, and other factors that drive disaster preparedness have changed over time. While the real-time survey provides an important and relatively unique understanding of preparation activities during the heightened threat of the hurricane, the follow-up survey provides a

longitudinal view of preparation activities that is critical to understanding factors which drive these activities, given that risk perceptions and preparedness activities evolve over time especially in the wake of events – including record breaking near-miss storms and pandemics. Based on these insights we draw lessons for improving individual preparedness for future hurricanes.

Specifically, we address results obtained from a survey conducted on November 10th and 11th of 2020, shortly before hurricane Eta made landfall near Cedar Key in Florida, and a survey conducted between May 26th and June 7th 2021, at the start of the 2021 hurricane season. We are interested in the drivers of insurance uptake and whether risk reduction effort is a substitute or a complement to insurance uptake, i.e. whether there is moral hazard or advantageous selection concerning flood insurance in Florida. Moreover, we examine how individual intentions to evacuate for a storm threat are influenced by concerns about becoming infected by COVID-19. Finally, since in the U.S., there is no one "base policy" for property insurance that can cover all disaster perils, homeowners need to acquire a significant amount of information and knowledge to understand their homeowner's insurance policies and make informed decisions about their coverage options including separate polices, deductibles, and coverage limits. Consequently, we also demonstrate the complexity of property insurance in the U.S. and understand the difference in the determinants of insurance coverage purchase by various policyholder types through statistical analyses of the identified policyholder type data.

In particular, using the real-time survey conducted just ahead of what was Hurricane Eta's impact we are able to address a particular research gap on the relationship between flood insurance coverage and the implementation of emergency preparedness measures. As these measures are applied shortly before or during immediate hurricane threats, preferences for taking emergency measures may differ compared to a low-threat situation. We find advantageous selection for both emergency and ex ante flood risk reduction measures for both surveys, meaning that individuals with flood insurance coverage are more likely to engage in these risk reduction activities, which is in contrast to results found in an earlier study using survey data obtained during a low-risk situation in New York city. Furthermore, we find that advantageous selection is largely driven by high levels of perceived worry about flood damage as well as perceived social norms for uptake of insurance and risk reduction measures. By focusing on survey respondents that are particularly cautious or uncautious we find that the former are more likely to worry about flooding, have experience with flooding, and perceive a social norm for preparedness, whereas uncautious individuals are less likely to have experience with flooding and perceive a lower social norm for preparedness. These results suggest that uptake of both insurance and risk reduction measures can

be improved by raising awareness of flood risk and social norms. Flood awareness can be improved by communicating flood probabilities and consequences through advertisement campaigns, while social norms may be enhanced by giving households information on disaster preparedness by others and signaling that this is the proper thing to do.

The U.S. 2020 hurricane season was extraordinary because of a record number of named storms coinciding with the COVID-19 pandemic. This study draws lessons on how individual hurricane preparedness is influenced by the additional risk stemming from a pandemic, which turns out to be a combination of perceptions of flood and pandemic risks that have opposite effects on preparedness behavior. Our statistical analyses investigating the factors influencing evacuation intentions during Hurricane Eta in November 2020 show that older individuals are less likely to evacuate under a voluntary order, because they are more concerned about the consequences of becoming infected by COVID-19. Our results of our survey in June 2021 at the start of the 2021 hurricane season point towards similar impacts of COVID-19 risk perceptions on evacuation intentions. Although the effect of COVID-19 on evacuation intention has become slightly smaller, it is still an issue for the 2021 hurricane season despite lower COVID-19 infections and hospitalization compared with 2020 due to the ongoing vaccination campaign.

We discuss the implications of our findings on evacuation intentions for risk communication and emergency management policies. Examples during the COVID-19 pandemic are: including COVID-19 mitigation measures in hurricane preparedness kits, such as hand sanitizer and mouth masks, abiding by social distancing rules during an evacuation, and planning ahead to identify safe evacuation locations. Moreover, government agencies can send more tailored communication messages to older people to alleviate their concerns over COVID-19 or improve their flood risk perceptions. Emergency management policies should create safe evacuation shelters where COVID-19 risks are well controlled and communicate their COVID-19 measures to the public to increase people's confidence in shelters' safety.

In terms of the analysis of the various policyholder type decisions, we find that the determinants of insurance coverage purchase of different policyholder types are different. This is because policyholders' demand for different types of insurance policies can be a different function of their locations, demography, house characteristics, risk perceptions, etc. For example, we find that the mandated purchase of an NFIP flood policy is not driven by the value of building and contents, the demographic characteristics, and the individuals' financial difficulty due to COVID-19, whereas these factors can impact the voluntary purchase of flood insurance. Having a basement positively affects the voluntary purchase of private flood insurance products and negatively impacts the voluntary purchase of an NFIP policy

because the NFIP policy does not cover the contents in the basement. The purchase of windstorm coverage is driven by different factors than flood insurance. Being a homeowner significantly increases the probability of having windstorm coverage. The objective windstorm risk has a strong and positive relation with windstorm coverage, and the effect is stronger for the wind-only policy type. Compared to the standard market buyers, the residual market buyers of wind coverage are more significantly and positively affected by the experience of having trouble getting or renewing the wind insurance due to an increase in disaster activities.

The statistical analyses of different types of policyholders' hurricane insurance purchase determinants can help public policy officials to better understand the incentives of different policyholder types to purchase insurance and come up with policies that better target specific types of homeowners. Although our data and analysis are limited to Florida, the results could be relevant and informative to all coastal states that aim to increase the uptake rate of insurance coverage.

1. Introduction

Tropical storms and hurricanes are the most costly natural disasters in Florida and other US states bordering the Gulf of Mexico. Climate change may increase the severity of these storms in the future (Marsooli et al., 2019), which highlights the need to improve preparedness for hurricanes to limit their future costs. Most damage during a hurricane or tropical storm occurs as a result of powerful winds and flooding, both due to large amounts of rainfall and high storm surges at sea. Households can limit potential property damage caused by flooding and windstorms by implementing risk reduction measures. Such measures range from structural alterations to the property, such as home-elevation or applying flood-proof floors, to emergency preparation measures taken during an immediate threat of a hurricane, which includes installing window shutters and sandbags, and moving belongings to higher floors. Households can also limit morbidity and mortality impacts to flooding and windstorms through evacuation Besides physical preparation for storms and hurricanes, households can choose to purchase insurance coverage to offset flood- and windstorm risk which offers financial protection thereby transferring the risk.

It is important, considering the increasing intensity of hurricanes, that existing properties at risk of these storms are well-prepared for heavy winds and floods. Besides limiting reconstruction costs of damaged property, the mitigation of risk can limit the macroeconomic shock that may occur in the aftermath of the disaster (Botzen et al., 2019). Moreover, insurance coverage against wind- and flood risk enhances the financial security of individuals, which is found to aid recovery in the wake of a disaster (Waugh and Smith, 2006). For governments too it is beneficial when private households implement risk reduction measures and purchase insurance coverage, as it limits the potential amount of disaster aid provided by governments in the wake of a hurricane.

Although it may be in their interest to implement hurricane risk reduction measures and purchase insurance coverage, individuals may refrain from doing so. This can have a wide range of situational causes, including the costs of risk-reduction measures or insurance, or the expectation of government aid (Bubeck et al., 2012). But also behavioral motives can be a source, including low coping appraisals, such as perceived effectiveness and perceived self-efficacy of risk-reduction measures (Bubeck et al., 2012), or risk misperception (Kunreuther and Pauly, 2004). Besides these root causes for low insurance uptake and lacking risk reduction effort, individuals that are insured may feel further dissuaded to implement risk reduction measures, as potential damage will be reimbursed. This negative effect of insurance, known as moral hazard, is found in a wide range of insurance applications. On the contrary, advantageous selection

arises in some cases, where insured individuals, often because they are more risk averse or wealthy, are more likely to also implement risk reduction measures (de Meza and Webb, 2001).

The frequency and economic costs associated with natural disasters have been increasing over time in the United States. For many of these events, the amount of property damages caused by natural disasters has not been covered by homeowner's property insurance, which is known as the insurance protection gap. In the U.S., there is no one "base policy" for property insurance that can cover all disaster perils.1 Instead, policyholders need to purchase an additional endorsement or even a separate insurance policy to cover certain natural disasters, such as floods and windstorms. Moreover, the coverage that is purchased for natural disasters typically comes with separate deductibles and coverage limits. Consequently, homeowners need to acquire a significant amount of information and knowledge to understand their homeowner's insurance policies and make informed decisions about their coverage options.

In this study we attempt to shed light on behavioral, personal and socio-demographic factors that influence the decision to implement ex ante risk reduction measures, take emergency preparation measures, and obtain flood- or wind insurance coverage. More specifically, we are interested in how risk preferences and emergency preparations differ when the threat of a hurricane is looming, compared to a situation when no hurricane is forecasted in the near future. Especially regarding emergency preparation measures, which have to be applied shortly before a storm strikes, preferences may change just prior to its expected impact. This is because individuals may feel less inclined to think of emergency preparation measures when there is no imminent danger, whereas ex ante risk reduction measures and insurance coverage need to be arranged well-before a hurricane occurs.

This may, moreover, give interesting insights into moral hazard or advantageous selection, behavioral phenomenon where individuals become more and less careful respectively after obtaining insurance coverage. A previous study by Botzen et al. (2019) found that the application of ex ante risk reduction measures and emergency measures differs for insured individuals. Whereas ex ante risk reduction measures, which have to be implemented before a threatening storm arises, are compatible with insurance coverage, emergency risk reduction measures, which have to be implemented right before the storm is expected, are found to be substitutes to insurance coverage. However, stated preferences for implementing emergency measures may be different at a time of low threat compared to a situation where hurricane impact is imminent. Therefore, in this study we seek to advance upon the results by

[1] There may be comprehensive policies that include added-on endorsements to cover the disaster perils.

Botzen et al. (2019), by exploring household behavior with respect to risk reduction measures in a high-threat situation and compare this behavior in a situation without a direct threat of a hurricane. Note that initial analysis from Hudson et al. (2017) found evidence of advantageous selection in the purchase of flood insurance and other risk reduction measures in surveys that measured preparation during the direct threat of a hurricane.

Furthermore, this study examines how evacuation intentions are influenced by individual concerns about COVID-19. This is important because many individuals may be less likely to evacuate during a storm threat when they are concerned about COVID-19 infections, given that when people evacuate to hotels or shelters proper social distancing may not be possible. Insights into the influence of pandemics on hurricane preparedness can provide relevant information for risk communication and emergency management policies.

Another goal of this study is to demonstrate the complexity of property insurance in the U.S. and understand the difference in the determinants of insurance coverage purchase by various policyholder types through statistical analyses of the identified policyholder type data. We use a decision tree to show the multiple decisions (the black box) that homeowners need to consider while purchasing property insurance. Homeowners can end up being different types of policyholders depending on where they purchased the insurance and what type of policy they purchased. Individuals may be mandated to have flood insurance. Currently, the major underwriter of flood insurance is the NFIP, but there are private flood insurance products underwritten by private insurers. For flood insurance, we identify four types of policyholders -- *mandatory NFIP, mandatory private insurer, voluntary NFIP, voluntary private insurer*. Windstorm peril is mainly covered by the homeowners' insurance, but in certain areas, the insurers may choose to exclude the windstorm peril and the policyholders must purchase a wind endorsement or a separate wind-only policy to obtain the wind coverage. The wind-only policy is provided mainly through the state-run program (also known as the residual market). We have four types of wind policyholder types -- *homeowners' insurance from a private insurer, homeowners' insurance from Citizens, wind-only coverage from a private insurer, wind-only policy from Citizens.*

We find that the determinants of insurance coverage purchase of different policyholder types are different. This is because policyholders' demand for different types of insurance policies can be a different function of their locations, demography, house characteristics, risk perceptions, etc. For example, we find that the mandated purchase of an NFIP flood policy is not driven by the value of building and contents, the demographic characteristics, and the individuals' financial difficulty due to COVID-19, whereas these

factors can impact the voluntary purchase of flood insurance. Having a basement positively affects the voluntary purchase of private flood insurance products and negatively impacts the voluntary purchase of an NFIP policy because the NFIP policy does not cover the contents in the basement. The purchase of windstorm coverage is driven by different factors than flood insurance. Being a homeowner significantly increases the probability of having windstorm coverage. The objective windstorm risk is a strong and positive factor, and the effect is stronger for the wind-only policy type. Compared to the standard market buyers, the residual market buyers of wind coverage are more significantly and positively affected by the experience of having trouble getting or renewing the wind insurance due to an increase in disaster activities.

The statistical analyses on different types of policyholders' hurricane insurance purchase behavior can help public policy officials better understand the incentives of different policyholder types to purchase insurance and come up with policies that better target specific types of homeowners. Although our data and analysis are limited to Florida, the results could be relevant and informative to all coastal states that aim to increase the uptake rate of hurricane insurance coverage.

This study is part of a multi-year research effort on hurricane preparedness in Florida for which previous data was collected in August 2019 during Hurricane Dorian, February 2020 shortly after Dorian, and June 2020 at the start of the 2020 hurricane seasons (Botzen et al., 2020a, 2020b). This report specifically includes results of two additional survey data collections. To obtain relevant data that captures behavior and emergency preparation in a high-threat situation, a survey was applied to households in the Gulf coast of Florida on November 10th and 11th 2020, a day before hurricane Eta made landfall at Cedar Key. Besides real-time survey questions, which intend to capture variables such as worry about flood- or wind damage, subjective risk perceptions, and emergency preparations, the survey contained questions to measure wind- or flood insurance uptake, the application of ex ante risk reduction measures, evacuation intentions, and personal and socio-demographic variables. Moreover, another survey was conducted in the Gulf and Atlantic coasts of Florida from May 26th until June 7th 2021 to examine hurricane preparedness at the start of the hurricane season.

In order to design policies to improve disaster preparedness we need to have a better understanding of individual decision making during a threat of a disaster as well as in its aftermath, and in particular obtain insights into why some people are well prepared and others not, which may be related to behavioral characteristics, like risk perceptions. However, most studies of individual natural disaster risk perceptions and their relation to risk reduction activities rely on cross-sectional data that is collected at one point in

time after the disaster has occurred, while risk perceptions and preparedness activities evolve over time. While the Hurricane Eta real-time survey provides an important and relatively unique understanding of preparation activities during the heightened threat of the hurricane, the follow-up survey at the beginning of the 2021 hurricane season provides a longitudinal view of preparation activities that is critical to understanding factors which drive these activities, given that risk perceptions and preparedness activities evolve over time especially in the wake of events – including record breaking near-miss storms and pandemics. Based on these insights we draw lessons for improving individual preparedness for future hurricanes.

2. The development of hurricane Eta

The 2020 hurricane season produced a record-breaking 30 named storms, of which 13 became hurricanes, including six major hurricanes (NOAA, 2020). This extremely active hurricane season was already predicted beforehand, as Atlantic sea surface temperatures were above-average, combined with a strong west African monsoon and the climatic phenomenon La Niña (NOAA, 2020). Florida was surprisingly spared from direct landfall of hurricanes, although several storms did make landfall there. Hurricane Eta approached Florida from Central America, where it caused severe damage, but decreased in power on the way and made landfall on the Florida Keys on November 8th as a tropical storm with maximum sustained winds of 100km/h (65mph) (Insurancejournal.com, 2020). After reentering the Gulf of Mexico it regained power, becoming a category 1 hurricane, and veered back towards Tampa Bay on November 11th, where heavy rains and a powerful storm surge caused significant damage. On November 12th Eta, albeit reduced to a tropical storm with maximum sustained winds of 85 km/h (50mph), made landfall for the second time in Florida, this time in Cedar Key. Although no deaths were reported as a consequence of the storm, estimated direct damage to structures exceeds $1.1 billion, of which insurance firms cover approximately half (*AON*, 2020). Figure 1, below, exhibits the track of hurricane Eta and it's development in terms of strength classifications.

Figure 1: Final track of hurricane/storm Eta. Source: (weather.com, 2020)

3. Survey method

An online survey was conducted on November 10th and 11th 2020 on households spread across the Gulf coast of Florida. As can be seen in Figure 2 below, most survey responses were located close to the Tampa bay area, which was where hurricane Eta was projected to make landfall on November 12th. In total, the survey received 844 responses.

Figure 2: Location of respondents to the survey conducted in November 2020.

Another online survey was conducted among households living along the Gulf and Atlantic coasts of Florida from May 26th until June 7th 2021 to examine hurricane preparedness at the start of the hurricane season. In total, 1245 respondents completed the survey which were located in the areas shown in Figure 3.

Figure 3: Location of respondents to the survey conducted in May and June 2021.

Table 1 shows sample characteristics per conducted survey. Survey 1 refers to the August 2019 survey conducted during Hurricane Dorian, Survey 2 is a follow-up survey conducted among part of the same respondents in February 2020, and Survey 3 is the survey that was conducted in June 2020. The focus of this report is on Surveys 4 and 5 that were conducted in November 2020 during hurricane Eta and May and June of 2021 at the start of the 2021 hurricane season. An interesting difference with the earlier surveys is that Survey 4 is conducted in the Gulf coast of Florida, whereas earlier surveys were taken on the Atlantic coast of the state. This is done because no major hurricane was threatening the Atlantic coast of Florida in 2020, which was a requirement to gain insight into household risk preferences and decision making under a looming threat. As the Gulf coast did experience a threat of a hurricane in November 2020, the target location of the survey was shifted there. From the sample characteristics it can be seen that there are no major socio-demographic differences between Survey 4 respondents and those in earlier surveys, except that the average age in Surveys 3 and 4 is significantly lower than in the first two surveys.

Survey 5, conducted in the period of May 26th until June 7th 2021, was taken with households spread all across Florida, as can be seen in Figure 3. This survey is meant to capture behavior regarding risk reduction measures, insurance uptake and behavioral factors prior to the hurricane season. Therefore, we chose to sample an approximately evenly spread sample across Florida. There are in total 1245 responses to the survey, which are most responses out of all five surveys conducted. In Table 1 it can be seen that regarding

the sample characteristics there are no remarkable differences between Survey 5 and earlier surveys. Table 2 gives the definition of variables that were based on the survey questions and will be used in the statistical analyses reported in the subsequent section.

Table 1: Sample characteristics per survey

	Survey 1 (n=871)	Survey 2 (n=255)	Survey 3 (n=600)	Survey 4 (n=844)	Survey5 (n=1245)
Gender					
Female	452 (52%)	128 (50%)	393 (66%)	575 (68%)	797(64%)
Male	416 (48%)	126 (49%)	199 (33%)	262 (31%)	448(36%)
Missing	3 (0.3%)	1 (0.4%)	8 (1.3%)	7 (1%)	0
Age (years)					
Mean (SD)	62 (± 17)	62 (± 17)	48 (± 17)	47 (± 18)	50 (± 19)
Missing	62 (7.1%)	15 (5.9%)	12 (2.0%)	0	0
Education level					
Some high school	23 (3%)	7 (3%)	13 (2%)	26 (3%)	44 (4%)
High school graduate	130 (15%)	26 (10%)	104 (17%)	216 (26%)	310 (25%)
Some college	170 (20%)	52 (20%)	159 (26%)	243 (29%)	325 (26%)
College graduate	325 (37%)	96 (38%)	214 (36%)	254 (30%)	376 (30%)
Post graduate	201 (23%)	72 (28%)	105 (18%)	100 (12%	174 (14%)
Missing	22 (2.5%)	2 (0.8%)	5 (0.8%)	5 (0.6%)	16 (1%)
Income (x $1,000)					
Mean (SD)	84 (± 48)	84 (± 46)	74 (± 47)	Categorical	Categorical
Missing	208 (23.9%)	56 (22.0%)	43 (7.2%)	31 (3.6%)	51 (4%)
Home value (x $1,000)					
Mean (SD)	370 (± 260)	370 (± 240)	300 (± 210)	Categorical	Categorical
Missing	138 (15.8%)	24 (9.4%)	108 (18.0%)	152 (18%)	214 (17%)

Table 2: Coding of variables used in our regression models

Variable	Coding
Voluntary uptake	*"Did you purchase flood insurance because it was mandatory?"* 0 = Yes; 1 = No
Mandatory uptake	*"Did you purchase flood insurance because it was mandatory?"* 0 = No; 1 = Yes
Number of emergency measures	The sum of emergency measures implemented by a respondent, including the installation of window protection and shields or sandbags, and moving belongings to less flood prone parts of the house.
Number of ex ante risk reduction measures	The sum of ex ante risk reduction measures applied by a respondent, including home elevation; flood-proof paint or coating; a sump pump and/or a drainage system; flood-resistant building materials; water-resistant floor; and the installation of electrical and central heating systems above potential flood levels.
Premium discount for flood risk mitigation*	*"Did you receive a premium discount on your flood insurance for taking any of these (the above flood risk mitigation) measures?"* 1 = Yes, 0 = No

Window protection	*"Did you implement the following measures to reduce the windstorm damages to your home? Window protection such as shutters, plywood panels, or hurricane proof glass."* 1 = Yes (in or before 2021), 0 = No (plan to do in 2021 or not plan to do)
Roof retrofit*	*"Did you implement the following measures to reduce the windstorm damages to your home? Roof construction that meets the 2001 Florida Building Code such as roof covering, roof-deck attachment, and roof-to-wall connection."* 1 = Yes (in or before 2021), 0 = No (plan to do in 2021 or not plan to do)
Hip roof*	*"Did you implement the following measures to reduce the windstorm damages to your home? Hip roof, i.e., roof sloping down to meet all your outside walls (like a pyramid)."* 1 = Yes (in or before 2021), 0 = No (plan to do in 2021 or not plan to do)
Premium discount for wind risk mitigation*	*"Did you receive a premium discount on your windstorm insurance coverage for taking any of these measures?"* 1 = Yes, 0 = No
Experience with flooding	*"How many times has your current household previously been affected by floods caused by natural disasters while you were living there?"* Written response
Worry about flooding	*"I am worried about the danger of a flood at my current residence."* 1 = strongly disagree to 5 = strongly agree
Perceived flood impact	*"What would it cost to repair the damage to your home and its contents if your home did flood?"* 0 = "Less than $10,000"; 6 = *"$200,000 or more"*
Perceived flood probability	*"What is your best estimate of how often a flood will occur at your home?"* categorical, 1 = less often than 1/1,000 years to 7 = more often than 1/10 years
Worry about windstorm*	*"I am worried about the danger of a windstorm at my current residence."* 1 = strongly disagree to 5 = strongly agree
Perceived wind impact*	*"What would it cost to repair the damage to your home and its contents if your home did suffer a windstorm?"* 0 = "Less than $10,000"; 6 = *"$200,000 or more"*
Trust in government flood policies	*"How much do you trust the ability of government officials to limit flood risk where you live, for example by maintaining levees and enforcing building codes? Do you:"* 0 = "*Not trust them at all"* to 3 = "*Trust them completely*"
Risk taking/aversion	*"Using a 10-point scale, where 0 means you are not willing to take any risks and 10 means you are very willing to take risks, what number reflects how much risk you are willing to take?"* For risk aversion, the inverse is taken, i.e. 0 = 10 and 10 = 0
Internal locus of control	*"Using a 10-point scale, where 0 means you have no control and 10 means you have complete control, what number reflects how much control you think you have over how your life turns out?"* scale from 0 to 10
Social norm for insurance uptake	*"Most people who are important to me would think that someone in my situation ought to purchase flood insurance."* 0 = "*Strongly disagree"* to 4 = "*Strongly agree"*
Social norm for risk reduction measures	*"Most people who are important to me would think that someone in my situation ought to take measures to reduce flood risk to one's home."* 0 = "*Strongly disagree"* to 4 = "*Strongly agree"*
Regret of no insurance	*"I would regret not purchasing flood insurance coverage if a flood were to occur next year."* 1=Strongly disagree to 5=Strongly agree
Regret of having insurance	*"I would regret purchasing flood insurance coverage if no flood were to occur next year."* 1=Strongly disagree to 5=Strongly agree
House owner	0 if respondent rents his/her house; 1 if respondent is a property owner
Value of home building	*"What is approximately the current market value of your home?"* 1=Less than $100k to 8=$800k or more
Value of home content	*"What is approximately the value of your home contents?"* 0 = "*Less than $5000*" to 7 = "*$75,000 or more"*
Length of residence	*"How long have you lived in your home (in years)?"*
Underfloor basement	*"Does your home have a basement, cellar or crawlspace?"* 1 = Yes for basement, 0 = No basement
Age	*"How old are you?"* in years
Education	*"What is your highest completed level of education?"* 1 = some high school to 5 = post graduate
Income	*"Which of the following describes your total household income for 2019 before taxes?"* 1 = less than $10,000 to 6 = $125,000 or more
Gender	*Was the respondent male of female?* female = 1, male = 0

Voluntary evacuation intention	*"Please tell me if you are extremely likely, likely, somewhat likely or not at all likely to evacuate to a safer place this hurricane season if a voluntary evacuation were to be ordered for your county."* 1= not at all likely to 4 = extremely likely
Perceived coronavirus infection probability	"*How likely do you think it is that you will personally be infected by the coronavirus?"* 1 = very unlikely to 5 = very likely
Concern about COVID-19	*"The probability of being infected by the coronavirus is so low that I am not concerned about its consequences."* 1 = strongly agree to 5 = strongly disagree (higher numbers indicate more concern)
Financial difficulty due to COVID-19	*"Did you experience any financial difficulties as a result of the coronavirus that prevented you from purchasing insurance for your home?"* 1 = Yes, 0 = No
Trouble purchasing flood insurance*	*"Have you had trouble getting or renewing your flood insurance because of natural disasters in the past?"* 1 = Yes, 0 = No
Trouble purchasing homeowners insurance*	*"Have you had trouble getting or renewing your homeowners insurance because of natural disasters in the past?"* 1 = Yes, 0 = No
InWindonly_territory	Identify whether the respondent's home is located within the Florida Citizens Coastal Account Area (wind-only policy eligible area) based on the latitude and longitude of their home. 1 = Yes, 0 = No

*: These questions were only included in the fifth survey.

4. Analysis of Insurance Purchases, Risk Reduction & Evacuation Intentions

4.1. Results of relations between insurance purchases and risk reduction

4.1.1 Results of relations between insurance purchases and risk reduction activities in Survey 4

In this section the results of the survey analysis with respect to risk reduction activities and insurance purchases is presented. First, we show the general survey outcomes regarding insurance uptake and risk reduction measures, after which we discuss a regression analysis of the impact of various explanatory variables on the purchases of flood insurance. Within the regression analysis, interaction effects that determine under what conditions we find either a positive or negative relation between the taking of insurance and other preparedness measures are also examined.

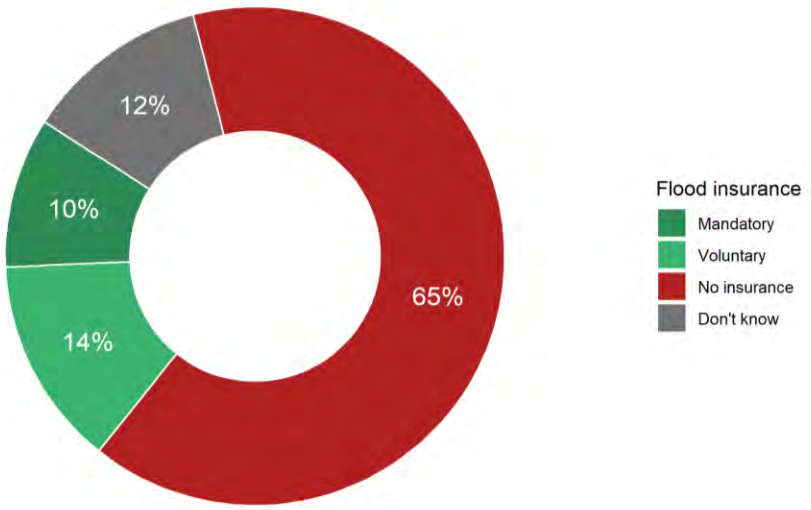

Figure 4: Flood insurance uptake of survey respondents differentiated for mandatory and voluntary uptake during Hurricane Eta (Survey 4 in November 2020).

In Figure 4, it can be seen that the majority of survey respondents have no insurance for flood damage to their homes or home contents during Hurricane Eta (Survey 4 in November 2020). Of the 24% of surveyed individuals that have flood insurance, 10% stated to be mandated to have coverage because they live in a special flood hazard zone. In the US, flood coverage is mandatory for households living in a high-risk floodplain (usually where a flood occurs at least once every 100 years) (FEMA.org, 2020).

We are interested in how the uptake of risk reduction measures differs between insured and not-insured households. Of particular interest is how this difference is affected by the looming threat of a hurricane. For example it may be expected that risk perceptions that can trigger risk reduction activities are higher in this scenario compared to a situation without immediate danger. Figure 5 and 6, below, show the percentage of respondents with voluntary and mandatory insurance, and no insurance, that take specific ex ante risk reduction measures and emergency preparation measures respectively. Ex ante risk reduction measures are defined here as measures that are taken well in advance of a direct hurricane threat, which are usually structural adjustments to a building, such as applying flood proof coating on walls. Emergency preparation measures are defined here as measures that are applied during or shortly before a direct hurricane threat, such as moving expensive furniture above potential flood water levels. The stars indicate the level of statistical significance of chi-square tests performed to assess the differences in applied risk reduction measures between the groups of people with, and without, flood insurance coverage.

For almost all of the ex ante risk reduction measures in Figure 5 it can be seen that the differences between the two insured groups and the non-insured group are statistically significant. Only for the measure “pump and drainage” the difference in implementation is insignificant between voluntarily insured and non-insured households. For the emergency preparation measures plotted in Figure 6 the same effect is observed, which already suggests that the results from the current real-time survey differ from the survey results in Botzen et al. (2019), who find that ex ante risk reduction measures are complements to flood insurance, while emergency preparation measures are substitutes. In addition, it can be seen that both emergency preparation measures and ex ante risk reduction measures are generally applied more by households for whom insurance is mandatory compared to voluntary. This could be due to higher flood risk of individuals in the former compared to the latter group.

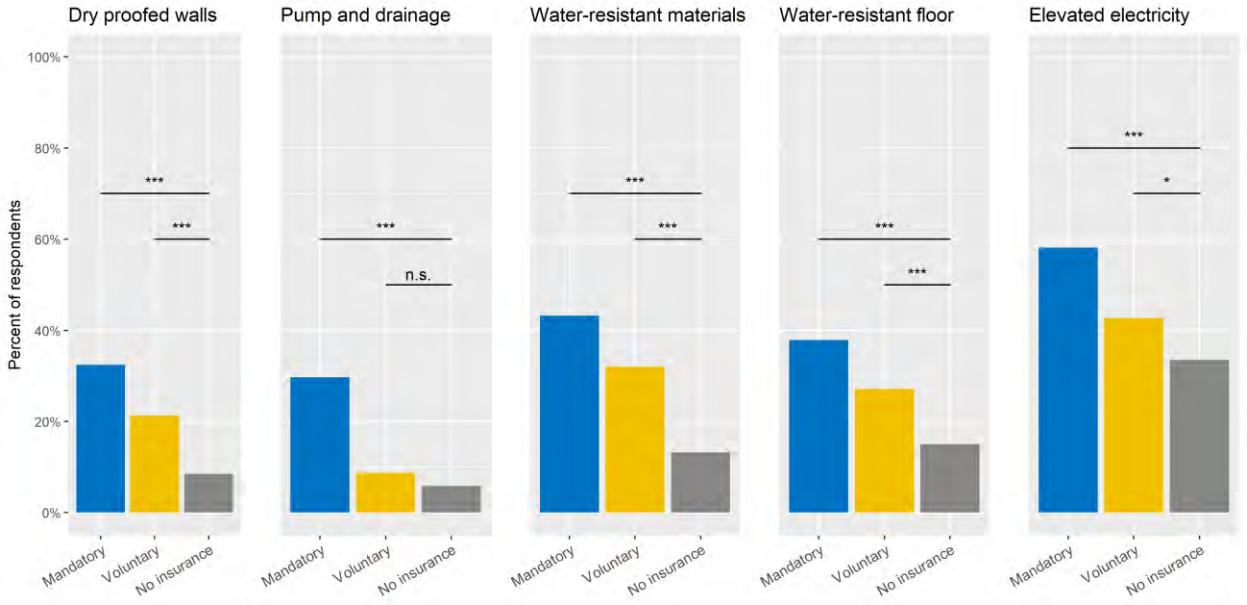

Figure 5: Percentage of voluntarily and mandatorily insured, and not-insured respondents who implement specific ex ante risk reduction measures in Survey 4. The stars indicate the level of significance of a chi-square test between the two insured groups and the not-insured group. (*=10%, **=5%, ***=1%)

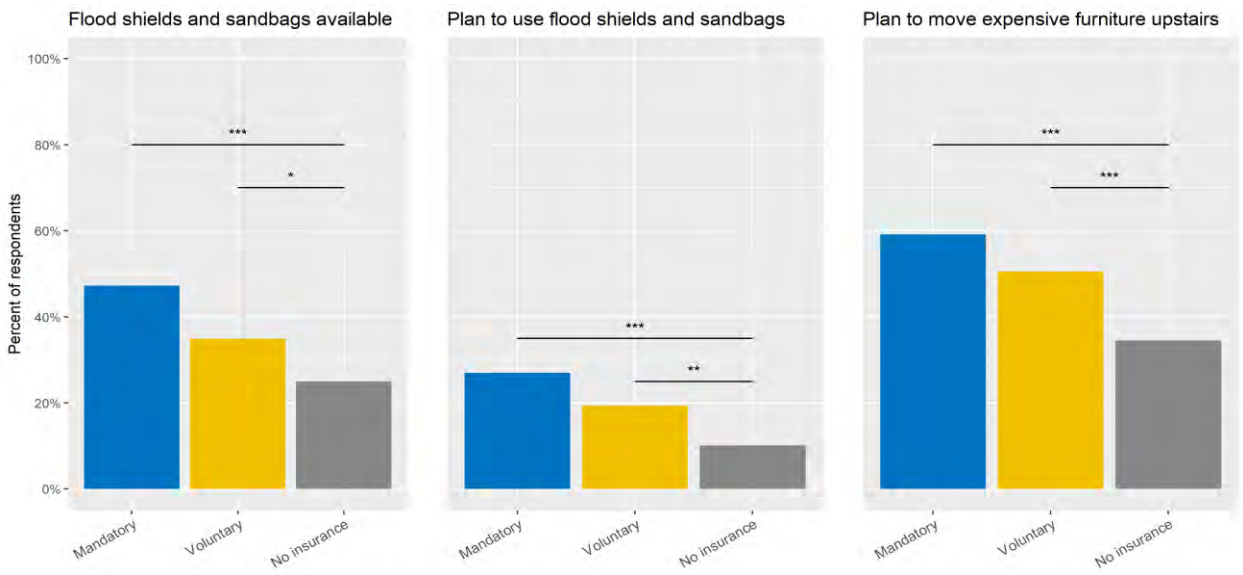

Figure 6: Percentage of voluntarily and mandatorily insured, and not-insured respondents who implement specific emergency risk reduction measures in Survey 4. The stars indicate the level of significance of a chi-square test between the two insured groups and the not-insured group. (*=10%, **=5%, ***=1%)

In the previous figures we observed higher uptake of both ex ante risk reduction and emergency preparation measures for insured compared to uninsured households, in the real-time survey shortly before hurricane Eta made landfall. Next, we apply a regression analysis to gain a more detailed understanding of why individuals choose to purchase insurance and whether there is indeed advantageous selection after controlling for several behavioral, personal and socio-demographic characteristics.

In Table 3 we show the marginal effects and significance levels of these variables on the decision to purchase voluntary flood insurance. We include variables to the model in a stepwise manner in order to detect whether e.g., a possibly significant relation between the taking of preparedness measures and insurance purchase can be explained by other factors. In the first model we test the effect of the number of ex ante risk reduction and emergency measures on the decision to purchase flood insurance. The number of ex ante measures is the sum of the measures included in Figure 5 that a household has implemented. Similarly, the number of emergency measures equals the sum of those presented in Figure 6 that a household has implemented. The probit results for model 1 indicate a positive impact of the number of emergency measures on the decision to purchase flood insurance, which is significant at the 1% level. No significant effect is found for the number of ex ante measures, which can be explained by substantial correlation between the number of emergency and ex ante risk reduction measures (correlation = 0.47; $p < 0.01$). For this reason, ex ante risk reduction measures is not included in the Table

3. This suggests advantageous selection for emergency measures, where households that implemented more emergency measures are more likely to also have flood insurance.

In the second probit model we introduce several personal variables and find positive effects for the level an individual worries about flooding and the perceived flood impact, both significant at a 1% level. The Pseudo R^2 increases considerably to 16%, suggesting that after these variables are controlled for, more variation in the voluntary purchase of flood insurance is explained. After introducing behavioral characteristics in the 3rd model, we find a strong positive effect of the social norm for insurance uptake on the decision to purchase flood insurance, significant at the 1% level. A significant Sobel test suggests that the effect of emergency preparedness measures may be mediated by the perceived social norm for insurance uptake. That is, people who take more emergency preparedness measures are more likely to perceive a strong social norm for insurance uptake. A linear regression of the amount of implemented emergency measures on the experienced social norm for insurance uptake suggests that this effect is indeed positive (0.3) and significant ($p < 0.01$). In addition, once the impact of the social norm on insurance purchase is controlled for, the previously significant effect of emergency measures on insurance uptake is no longer significant. Overall, this suggests that the impact of emergency measures on insurance uptake is an indirect effect, mediated by social norms (Baron and Kenny, 1986).

In the 4th model we introduce housing characteristics, which reveals a highly significant positive effect of the declared value of home contents on insurance uptake ($p < 0.01$). In the 4th model the perceived flood impact no longer has a significant effect, which can be explained by these two variables being strongly correlated (0.57; $p < 0.01$). Also, a significant Sobel test suggests that home contents mediates this relationship, perhaps because respondents that expect a higher flood impact also have a higher home content value. Finally, in the 5th model we introduce socio-demographic variables, but find no significant effects there. The Pseudo R^2 of 34% in the final model means that a considerable proportion of the variation in voluntary flood insurance purchase can be explained with our observed variables.

Table 3: Probit regression results of variables of influence on the decision to purchase flood insurance in Survey 4

	Voluntary coverage				
	(1)	(2)	(3)	(4)	(5)
Constant	-1.293***	-2.108***	-2.547***	-3.105***	-3.334***
	(0.100)	(0.302)	(0.582)	(0.754)	(0.881)

Number of emergency measures	0.351*** (0.071)	0.361*** (0.099)	0.262** (0.120)	0.204 (0.128)	0.206 (0.141)
Worry about flooding		0.284*** (0.072)	0.151* (0.087)	0.215** (0.089)	0.233** (0.093)
Experience with flooding		-0.009 (0.043)	-0.033 (0.050)	-0.019 (0.062)	-0.008 (0.062)
Perceived flood impact		0.180*** (0.042)	0.183*** (0.047)	0.016 (0.071)	-0.001 (0.071)
Trust in government flood policies		-0.095 (0.107)	-0.054 (0.123)	-0.033 (0.117)	-0.011 (0.118)
Risk aversion			0.004 (0.046)	-0.002 (0.049)	-0.002 (0.053)
Social norm for insurance uptake			0.497*** (0.114)	0.479*** (0.104)	0.474*** (0.113)
Internal locus of control			-0.048 (0.042)	-0.069 (0.051)	-0.076 (0.049)
House owner				0.156 (0.290)	0.170 (0.297)
Value of home content				0.264*** (0.066)	0.260*** (0.073)
Years of residence				-0.001 (0.010)	0.001 (0.011)
Gender					-0.261 (0.232)
Education					0.095 (0.132)
Income					-0.028 (0.107)
age					0.005 (0.008)
Log likelihood	-247.1	-156.8	-134.8	-112.8	-109.8
Pseudo R(McFadden)	0.047	0.162	0.266	0.324	0.338
Observations	558	373	364	326	322
Note:					*p**p***p<0.01

In Table 4, the probit regression output of variables of influence on mandatory insurance uptake is presented. Although these respondents indicated that flood insurance is mandatory for them, which is likely because they live in a 1/100 year floodplain and flood insurance is mandatory for federally backed mortgages, the actual uptake in areas where insurance is mandatory in Florida is estimated at 47% (Lingle

and Kousky, 2018). This means that the uptake requirement is not very well enforced, and that insurance uptake is still a decision for many households, which may to some extent be explained by behavioral and socio-demographic characteristics. This analysis is important to gain insight into the behavior of insured individuals regarding risk-reduction measures. However, the results may differ considerably from those presented in Table 3, as mandatorily insured individuals may apply risk reduction measures for different reasons than those insured voluntarily, for example, because of higher flood risk, pressure from insurers or governments, or to receive a premium discount.

The number of emergency measures implemented does not significantly impact mandatory insurance uptake in a regression model together with ex ante risk reduction measures. Both emergency and ex ante risk reduction measures show positive and significant results when separately put into the regression models. Therefore, it is likely that ex ante risk reduction measures mediates the relationship between emergency measures and mandatory insurance, which is confirmed by a Sobel test ($p < 0.01$). As the effect of ex ante risk reduction measures on mandatory insurance uptake is more consistently significant, we chose to exclude emergency measures from the models in Table 4. The positive effect of ex ante risk reduction measures shown in the table indicates that mandatory insurance uptake and ex ante risk reduction behavior is complementary, which is in line with previous studies regarding this topic (Botzen et al., 2019; Hudson et al., 2017; Mol et al., 2020). Next, we find that the declared level of worry about flooding has a positive impact on mandatory insurance uptake, which is significant only in model 2 ($p < 0.01$). A significant Sobel test of the perceived social norm for insurance uptake on the impact of worry about flooding on insurance uptake reveals that this variable mediates this relationship. What this suggests is that respondents that worry more about flood damage also experience a social norm to take insurance more strongly. The level of perceived social norm for insurance uptake shows, similar to the models for voluntary flood insurance uptake, consistently strong positive impacts that are significant at the 1%-level.

The results presented in Tables 3 and 4 suggest that, when comparing households with voluntary and mandatory coverage, there are different variables that drive a household to obtain insurance coverage. For both types of insurance coverage we observe advantageous selection to an extent, where insured individuals also choose to implement risk reduction measures. Next, we try to derive the characteristics of individuals that choose both to insure and implement risk reduction measures.

Table 4: Probit regression results of variables of influence on mandatory flood insurance uptake in Survey 4

	Mandatory coverage				
	(1)	(2)	(3)	(4)	(5)
Constant	-1.755*** (0.142)	-2.746*** (0.447)	-3.856*** (0.841)	-4.571*** (1.001)	-4.550*** (1.117)
Number of ex-ante measures	0.451*** (0.062)	0.425*** (0.083)	0.358*** (0.097)	0.383*** (0.114)	0.430*** (0.112)
Worry about flooding		0.300*** (0.094)	0.137 (0.107)	0.149 (0.112)	0.122 (0.117)
Experience with flooding		0.009 (0.055)	-0.013 (0.044)	-0.017 (0.045)	-0.046 (0.053)
Perceived flood impact		0.045 (0.055)	0.071 (0.061)	-0.039 (0.086)	-0.033 (0.097)
Trust in government flood policies		0.185 (0.157)	0.156 (0.194)	0.285* (0.160)	0.299* (0.161)
Risk aversion			-0.046 (0.047)	-0.045 (0.051)	-0.044 (0.058)
Social norm for insurance uptake			0.598*** (0.124)	0.582*** (0.139)	0.615*** (0.145)
Internal locus of control			0.025 (0.061)	0.018 (0.068)	0.022 (0.072)
House owner				0.239 (0.316)	0.231 (0.395)
Value of home content				0.166* (0.088)	0.184 (0.113)
Years of residence				0.001 (0.019)	0.003 (0.022)
Gender					0.329 (0.312)
Education					-0.136 (0.191)
Income					0.040 (0.194)
age					-0.005 (0.010)
Log likelihood	-117.7	-76.4	-64.1	-56.1	-54.5
Pseudo R(McFadden)	0.202	0.277	0.389	0.426	0.44
Observations	376	255	251	228	225

Note: *p **p ***p<0.01

For the regression analysis of interaction effects, presented in Table 5, we constructed a regression model using variables that are statistically significant in an individual interaction analysis. That is, only variables are included that are significant in an interaction model with three variables, insurance uptake, risk reduction measures and the variable of interest. The size of the interaction models is limited in order to reduce the threat of multicollinearity, and also because conditional effects are difficult to detect in complex interaction analyses due to issues of statistical power (Aguinis, 1995). Moreover, the interactions regarding risk reduction measures differ between the types of insurance coverage. Considering this, we observe positive interaction effects with "worry about flooding" ($p < 0.1$) and "education" ($p < 0.05$) for the mandatory uptake model. Essentially, how this can be interpreted is that individuals who indicate to worry more about flooding are more likely to have both ex ante risk reduction measures and mandatory insurance. The same applies to individuals with a higher completed level of education. In the voluntary insurance model, the experienced level of social norm to implement risk reduction measures is found to positively interact ($p < 0.01$). This means that individuals who indicate to experience a higher social norm for risk reduction measures are more likely to implement emergency preparation measures and take voluntary insurance. We chose to include social norm for risk reduction measures here because it shows the strongest interaction effect. Moreover, a Cronbach's alpha of 0.83, comparing with social pressure for insurance uptake solely, suggests that these variables measure largely the same feature.

Table 5: Probit regression of interactions in Survey 4

	Mandatory coverage (1)	Voluntary coverage (2)
Constant	-1.446*** (0.371)	-1.461*** (0.209)
number of ex-ante measures implemented	-0.082 (0.215)	
Worry about flooding	0.114 (0.118)	
Education	-0.240* (0.136)	
Ex ante measures x Worry about flooding	0.099* (0.056)	
Ex ante measures x Education	0.146** (0.064)	
Number of emergency measures implemented		-0.272 (0.184)
Social norm for risk reduction measures		0.110 (0.090)
Emergency measures x Social norm for risk reduction measures		0.206*** (0.068)
Log likelihood	-107.4	-224.1
Pseudo R(McFadden)	0.27	0.105
Observations	374	536

Note: $^{*}p$ $^{**}p$ $^{***}p<0.01$

The interaction effects shown in Table 5 are visualized as margin plots in Figures 7 and 8 below. In the first figure it is shown that higher levels of worry about flooding are associated with a higher impact of taking ex-ante risk reduction measures on mandatory insurance uptake. In other words, as insurance uptake is mandatory for these respondents, a higher level of worry about flooding drives the decision to implement risk reduction measures for insured individuals. In Figure 8 it can be seen that the social norm for flood preparedness positively impacts the coefficient of emergency preparedness measures on voluntary insurance uptake. The coefficient becomes positive for social pressure levels after 3, which means that respondents are more likely to take both emergency measures and insurance when they perceive social pressure to do this (values 0, 1, and 2, mean no social norm is experienced).

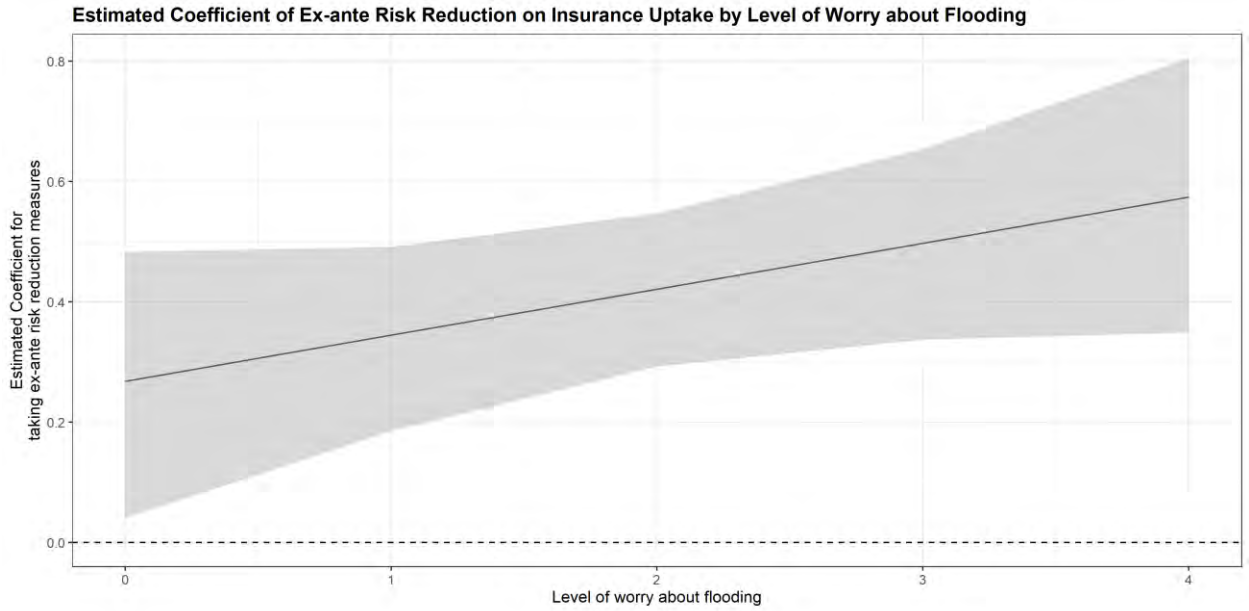

Figure 7: Margin plot of the interaction effect between the level of worry about flooding and taking ex ante risk reduction measures on mandatory insurance uptake in Survey 4.

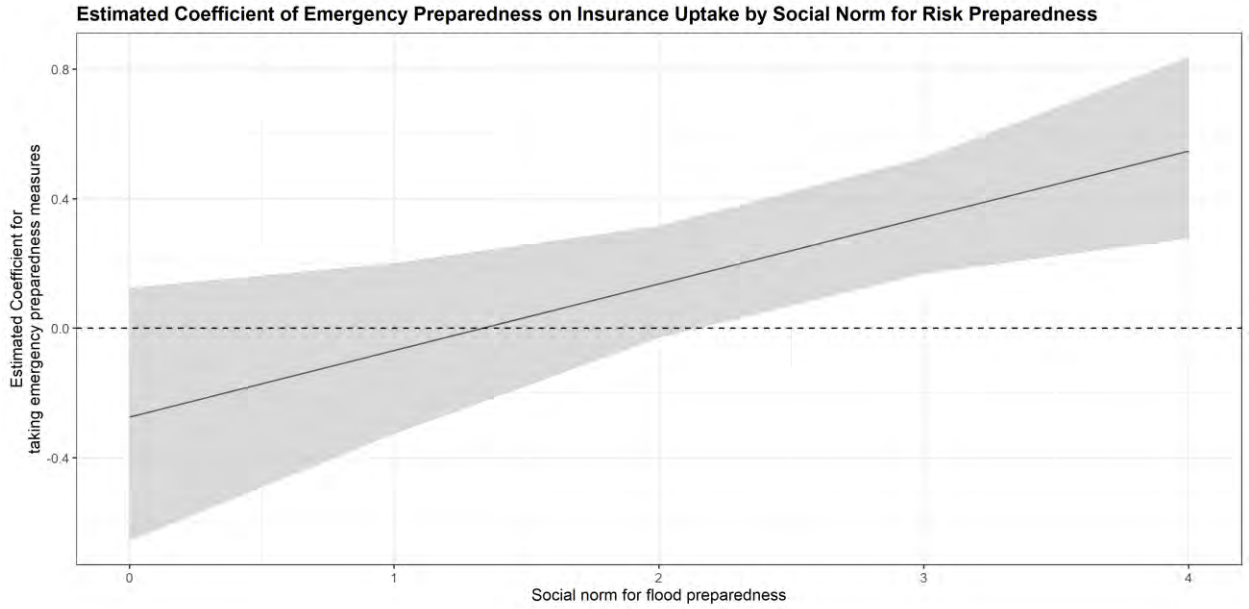

Figure 8: Margin plot of the interaction effect between the level of social pressure for flood preparedness and taking emergency measures on voluntary insurance uptake in Survey 4.

Finally, in Table 6 we examine the sources of advantageous selection for individuals that can be classified as extremely cautious and uncautious. This approach is based on a technique introduced in Mol et al. (2020). For this, we categorize a respondent as "cautious" if they are insured and have taken more than the 3rd quartile of risk reduction measures (both ex ante and emergency measures). A respondent is "uncautious" if she/he has not insured and has taken no risk reduction measures. Table 6 presents the probit regression results with the two subgroups as dependent variables and several variables that show significant results in earlier regression models as independent variables. The reference category in model 1 comprises of all respondents that are not classified as "cautious", meaning everyone that does not have flood insurance in addition to at least 2 risk reduction measures. In model 2 the reference category includes everyone that has flood insurance or applied at least one risk reduction measure. From the table it can be seen that worry about flooding is positive and significant ($p < 0.05$) for cautious individuals, which suggests that cautious respondents worry more about flooding. Worry about flooding is negative for uncautious individuals, however this result is not significant. Cautious respondents are more likely to have experience with flooding ($p < 0.1$), while uncautious ones are less likely to have experienced flooding ($p < 0.05$). Moreover, cautious respondents generally perceive a high level of social norms for both insurance uptake and risk reduction measures ($p < 0.01$), whereas uncautious ones are less likely to perceive this ($p < 0.01$). Furthermore, uncautious individuals are more likely to be tenants ($p < 0.01$); their home content

is likely to be less valuable than cautious respondents ($p < 0.05$); and they are more likely to be female ($p < 0.05$).

Table 6: Probit regression of cautious and uncautious types in Survey 4.

	cautious (1)	uncautious (2)
Constant	-3.198*** (0.671)	0.500 (0.575)
Worry about flooding	0.163** (0.075)	-0.088 (0.075)
Experience with flooding	0.027* (0.016)	-0.135** (0.060)
Perceived flood probability	0.039 (0.057)	0.008 (0.048)
Trust in government flood policies	-0.015 (0.105)	-0.120 (0.091)
Risk aversion	-0.006 (0.035)	0.091*** (0.033)
Social norms uptake and DRR	0.477*** (0.084)	-0.210*** (0.074)
Internal locus of control	0.008 (0.042)	-0.011 (0.037)
House owner	0.351 (0.254)	-0.523*** (0.186)
Value of home content	0.076 (0.059)	-0.108** (0.043)
Years of residence	0.002 (0.006)	0.005 (0.006)
Gender (1=female)	-0.407** (0.177)	0.330** (0.154)
Education	0.023 (0.104)	-0.055 (0.079)
Income	0.010 (0.085)	-0.074 (0.072)
age	-0.001 (0.006)	0.004 (0.005)
Log likelihood	-147.9	-212
Pseudo R(McFadden)	0.233	0.181
Observations	450	450
Note:		*p**p***p<0.01

4.1.2 Results of relations between insurance purchases and risk reduction activities in Survey 5

In this section we present the results of influencing factors on flood insurance purchases using the 5th survey, which was taken prior to the 2021 hurricane season from May 26th until June 7th. In this survey, 51% of respondents reported to have no flood insurance, whereas 14% and 19% of respondents have mandatory and voluntary insurance, respectively. A further 16% do not know their flood insurance status. These results are different to the data collected during survey 4, where less respondents reported to hold flood coverage. However, both surveys find that of those who hold flood insurance, most do so on a voluntary basis rather than because it is mandatory.

The analysis presented in this section essentially repeats the steps presented in section 4.1.1., which facilitates a comparison of factors influencing flood insurance demand and risk reduction effort between a high- and low-threat situation. Especially regarding emergency preparation measures, such as the willingness to apply sandbags or relocate expensive belongings to higher parts of the house, we may observe different behavior in data obtained during low threat of hurricanes, as these measures are generally implemented shortly before a hurricane is expected. Also, as the previous hurricane threat was already some time ago, individuals may be less aware of flood risk, which may explain a lower willingness to apply emergency preparation measures. For this reason, instead of the observed advantageous selection in Survey 4, it is possible we may observe moral hazard regarding emergency measures in Survey 5, as was reported in Botzen et al. (2019). Furthermore, we are interested to observe whether there are considerable differences between the two surveys regarding psychological factors that drive moral hazard or advantageous selection. These results may be useful to enhance overall flood risk preparedness, for example, by targeting information campaigns to population groups with low risk flood risk awareness. Since flood insurance uptake and ex ante risk reduction measures are generally purchased or implemented at times of lower threat, we do not expect to observe considerable differences between Surveys 4 and 5 in this respect.

Figures 9 and 10, below, show that uptake of ex ante risk reduction and emergency measures is generally higher for insured compared to uninsured respondents. The difference between the insured groups and the not-insured group is confirmed with significant chi-square tests ($p < 0.01$) for all individual measures. Since Survey 5 was taken during a period of low hurricane threat, we did not include the question whether a respondent has applied sandbags or flood shields, as was done in Survey 4 and shown in Figure 6. Except for more and higher degrees of significance using the Survey 5 data, there are no notable differences with the results of Survey 4, presented in Figures 5 and 6.

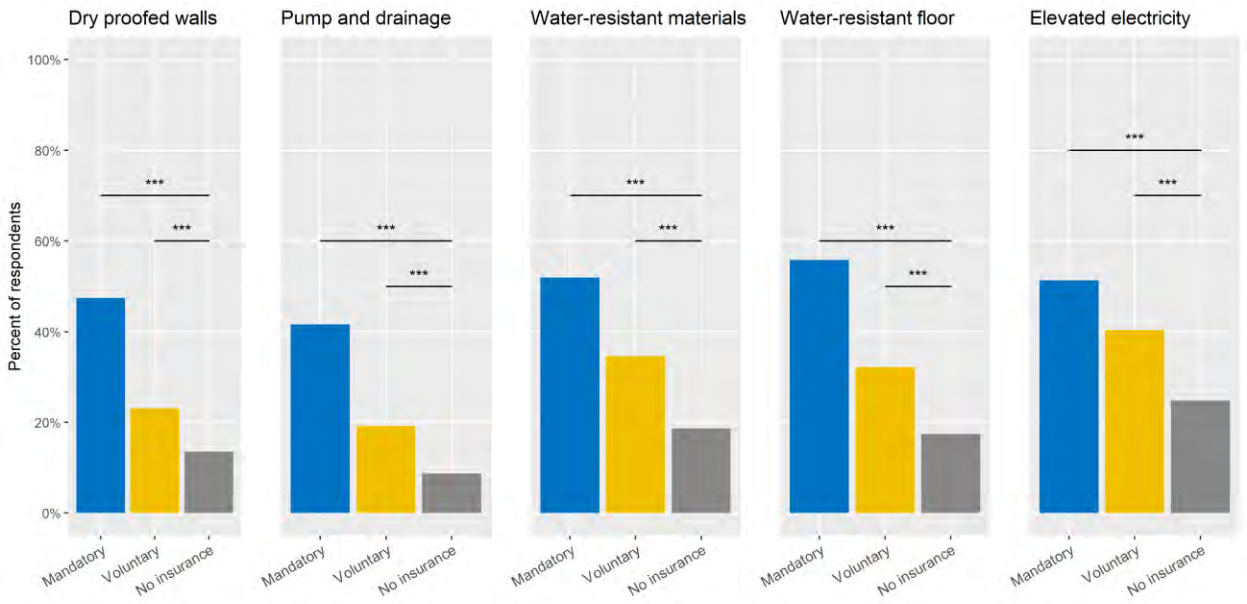

Figure 9: Percentage of voluntarily and mandatorily insured, and not-insured respondents who implement specific ex ante risk reduction measures in Survey 5. The stars indicate the level of significance of a chi-square test between the two insured groups and the not-insured group. (*=10%, **=5%, ***=1%)

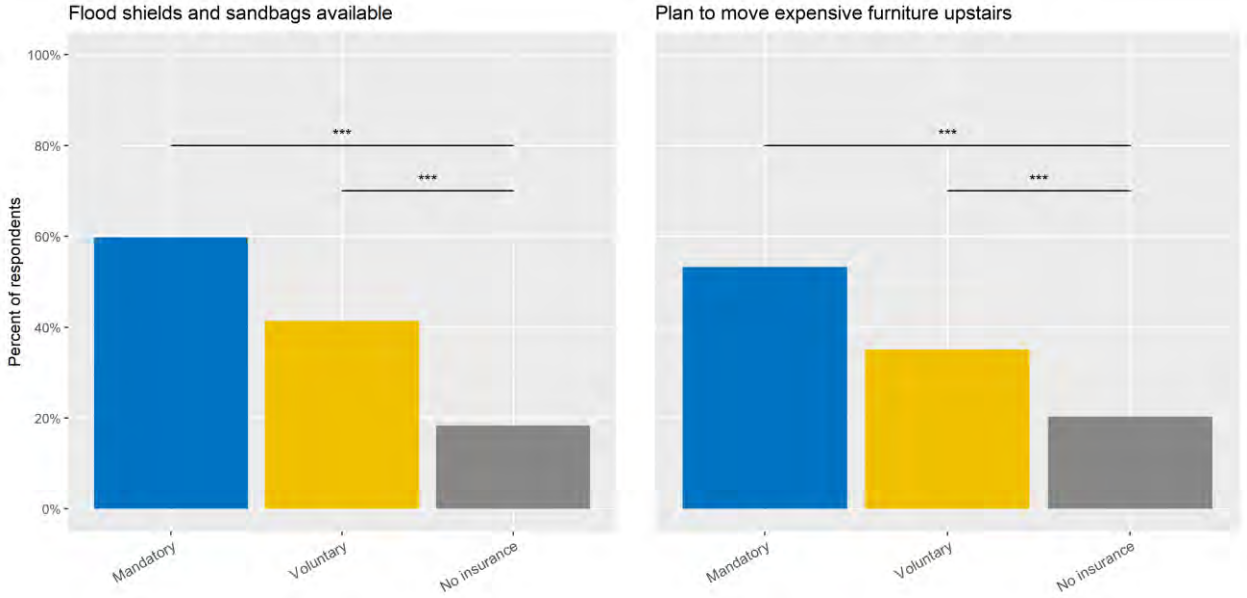

Figure 10: Percentage of voluntarily and mandatorily insured, and not-insured respondents who implement specific emergency risk reduction measures in Survey 5. The stars indicate the level of significance of a chi-square test between the two insured groups and the not-insured group. (*=10%, **=5%, ***=1%)

Next, we seek to observe causal relationships of several variables on voluntary insurance uptake using probit models, which is shown in Table 7. For this, we introduce variables in a step-wise manner, identical to what is done in Table 3. We observe a consistently positive and significant impact of the number of

emergency measures implemented on voluntary insurance uptake. This effect reduces in strength when introducing more variables and the significance becomes slightly less ($p < 0.05$) in Model 5. Similar as in the approach applied for Survey 4, the impact of ex ante risk reduction measures is left out in this model as it does not show significant results, which can be largely attributed to high and significant correlation between this measures and emergency preparedness measures (0.81; $p < 0.01$). The positive effect we observe for emergency preparation measures on insurance uptake indicates that this is complementary to insurance uptake. Therefore, the fact that this survey was taken during a period of low risk of hurricanes does not seem to affect the observation that insured respondents are more willing to take emergency preparedness measures than uninsured respondents.

Further significant variables of influence on voluntary insurance uptake includes the perceived level of worry about flooding, which is significant only in Model 2 ($p < 0.01$). Similar to the analysis of Survey 4, the significance of this effect diminishes when the perceived social norms for insurance uptake are introduced in Models 3 to 5. This can be explained by a positive and significant causal effect of perceived social norms on worry about flooding (0.46; $p < 0.01$) and a significant Sobel test ($p < 0.01$), which suggests that the former mediates the relationship between worry about flooding on insurance uptake. In other words, respondents that worry about flooding generally perceive a social norm for insurance uptake, which, in turn, incentivizes individuals to purchase flood insurance. Perceived flood impact is another influencing factor for insurance uptake, which declines in effect size and significance after introducing more independent variables. The observed positive effect suggests that respondents who perceive a higher impact of flooding are generally more likely to purchase flood insurance.

Table 7: Probit regression results of variables of influence on the decision to purchase flood insurance in survey 5

	Voluntary coverage				
	(1)	(2)	(3)	(4)	(5)
Constant	-0.877***	-1.520***	-2.061***	-2.256***	-2.338***
	(0.065)	(0.204)	(0.383)	(0.416)	(0.472)
Number of emergency measures	0.308***	0.238***	0.172***	0.189***	0.174**
	(0.048)	(0.058)	(0.066)	(0.069)	(0.071)
Worry about flooding		0.166***	0.061	0.038	0.035
		(0.054)	(0.061)	(0.064)	(0.066)
Experience with flooding		0.309	0.161	0.010	-0.011
		(0.197)	(0.212)	(0.246)	(0.251)
Perceived flood impact		0.151***	0.140***	0.077*	0.063
		(0.030)	(0.033)	(0.040)	(0.040)

Trust in government flood policies		0.009 (0.074)	-0.033 (0.080)	0.017 (0.086)	0.015 (0.087)
Risk aversion			-0.028 (0.028)	-0.029 (0.029)	-0.029 (0.030)
Social norm for insurance uptake			0.460*** (0.064)	0.475*** (0.068)	0.472*** (0.069)
Internal locus of control			0.003 (0.031)	-0.012 (0.034)	-0.015 (0.035)
House owner				0.075 (0.191)	0.039 (0.200)
Value of home content				0.085** (0.038)	0.057 (0.042)
Years of residence				0.006 (0.006)	0.008 (0.006)
Gender					0.030 (0.137)
Education					0.031 (0.069)
Income					0.098 (0.069)
age					-0.001 (0.005)
Log likelihood	-428.1	-318.4	-276.3	-251.8	-250.2
Pseudo R(McFadden)	0.046	0.089	0.177	0.185	0.19
Observations	769	569	547	496	496
Note:					*p**p***p<0.01

The probit regression output for variables influencing mandatory insurance uptake is shown in Table 8. For mandatory insurance coverage we found that the willingness to apply emergency measures is insignificant, which is why it is not included in the models presented in Table 8. Main differences between these results and those of Survey 4, shown in Table 4, include a more consistently significant effect found for the perceived level of worry about flooding; significant effects found for experience with flooding and perceived flood impact in models 2 and 3; a significant positive effect observed for whether a respondent is a house owner compared to a tenant ($p < 0.05$); a negative effect for the age of the respondent ($p < 0.01$). Similar to the results for voluntary insurance uptake, shown in Table 7, the mediating effect of social norms for insurance uptake on the effect of perceived worry about flooding on insurance uptake results in a large decline of the effect size of worry about flooding in Models 3 to 5. The positive impact of the

number of ex ante risk reduction measures on mandatory insurance uptake ($p < 0.01$) suggests that also in Survey 5 we observe that these are complementary.

Table 8: Probit regression results of variables of influence on the decision to purchase mandatory flood insurance in survey 5

	Mandatory coverage				
	(1)	(2)	(3)	(4)	(5)
Constant	-1.291*** (0.078)	-2.078*** (0.236)	-2.618*** (0.429)	-2.740*** (0.497)	-2.333*** (0.584)
Number of ex-ante measures	0.340*** (0.032)	0.248*** (0.042)	0.223*** (0.047)	0.241*** (0.052)	0.212*** (0.053)
Worry about flooding		0.315*** (0.063)	0.177*** (0.068)	0.177** (0.076)	0.148* (0.082)
Experience with flooding		0.497*** (0.184)	0.272 (0.198)	0.179 (0.215)	0.123 (0.219)
Perceived flood impact		0.075** (0.036)	0.082** (0.039)	0.048 (0.049)	0.065 (0.051)
Trust in government flood policies		0.069 (0.091)	0.007 (0.099)	0.056 (0.108)	0.056 (0.112)
Risk aversion			-0.044 (0.033)	-0.061* (0.036)	-0.037 (0.035)
Social norm for insurance uptake			0.496*** (0.089)	0.538*** (0.101)	0.568*** (0.103)
Internal locus of control			-0.001 (0.034)	-0.027 (0.035)	-0.012 (0.035)
House owner				0.437** (0.216)	0.523** (0.229)
Value of home content				-0.027 (0.044)	-0.040 (0.049)
Years of residence				0.009 (0.007)	0.015** (0.007)
Gender					-0.144 (0.168)
Education					-0.056 (0.095)
Income					0.095 (0.086)
age					-0.015*** (0.005)
Log likelihood	-315.3	-227.2	-193.4	-172.9	-166.8
Pseudo R(McFadden)	0.154	0.231	0.326	0.345	0.365

Observations	715	527	509	460	459
Note:					*p**p***p<0.01

Table 9 shows results of an interaction analysis, which is applied to identify behavioral or socio-demographic variables that drive advantageous selection of insurance uptake and risk reduction measures. Similar as in Table 5, we limit the assessment of interaction effects to variables that show significant results in individual interaction models. Using the data obtained in Survey 5, we find only positive significant interaction results for the perceived level of worry about flooding and the effect of ex ante risk reduction measures and mandatory insurance uptake (p < 0.05). This result suggests that individuals that worry more about flooding are more likely to have both flood insurance and take ex ante risk reduction measures. Concerning the advantageous selection of voluntary insurance uptake and the willingness to apply emergency preparation measures, we do not find any significant variables that explain this observation. In Table 9 we show the impact of perceived social norms for risk reduction measures, as was done in Table 5, however the interaction analysis shows non-significant results. This suggests that, unlike in a high-threat situation, perceived social norms for risk reduction measures do not drive advantageous selection in the low-threat situation during which Survey 5 was taken.

Table 9: Probit regression of interactions

	Mandatory coverage (1)	Voluntary coverage (2)
Constant	-1.651*** (0.146)	-1.561*** (0.164)
Number of ex-ante measures implemented	0.168** (0.076)	
Worry about flooding	0.230*** (0.068)	
Ex ante measures x Worry about flooding	0.059** (0.030)	
Number of emergency measures implemented		0.784*** (0.278)
Social norm for risk reduction measures		0.361*** (0.070)
Emergency measures x Social norm for risk reduction measures		-0.152 (0.109)
Log likelihood	-286.5	-387.6
Pseudo R(McFadden)	0.215	0.081
Observations	705	721
Note:		*p**p***p<0.01

The interaction effect of the perceived worry about flooding on ex ante risk reduction measures and mandatory insurance uptake is visualized as a margin plot in Figure 11. The plot is almost identical to the margin plot of the same interaction effect shown in Figure 7, except for a slightly lower estimated coefficient. As the interaction effect with perceived social norms is insignificant, this relationship is not shown in a margin plot.

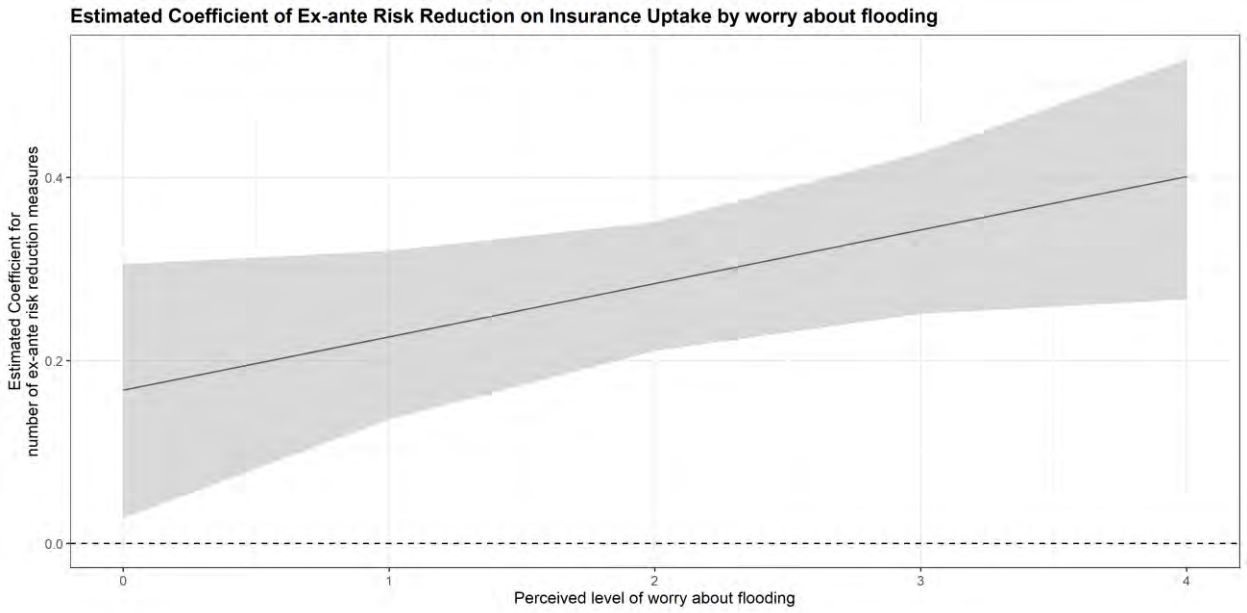

Figure 11: Margin plot of the interaction effect of the perceived level of worry about flooding on taking ex ante risk reduction measures and mandatory insurance uptake in Survey 5.

Finally, Table 10 shows the variables influencing whether respondents can be considered "cautious" or "uncautious". These stylized groups are derived similar as was done for the analysis of Survey 4 in Table 6. Using the results presented in Table 10 we can observe several variables that partly determine whether a respondent has insurance coverage and implemented several risk reduction or emergency preparation measures. These individuals, defined as "cautious", generally have more experience with flooding ($p < 0.05$); experience higher social norms for insurance uptake and risk reduction measures ($p < 0.01$); are more likely to be home owners ($p < 0.01$); have a higher level of completed education ($p < 0.05$); and are likely to be younger ($p < 0.01$). On the contrary, respondents that have no insurance coverage and no risk reduction or emergency preparedness measures implemented, and are consequently defined as "uncautious", generally are less likely to have experienced flooding ($p < 0.01$); have less trust in government flood policies ($p < 0.01$); are more risk averse ($p < 0.05$); perceive lower social norms for insurance uptake and risk reduction measures ($p < 0.01$); are more likely to be tenants ($p < 0.01$); have a lower value of home content ($p < 0.05$); and are older ($p < 0.01$).

Table 10: Probit regression of cautious and uncautious types

	cautious (1)	uncautious (2)
Constant	-1.694*** (0.489)	0.747** (0.367)
Worry about flooding	0.059 (0.064)	-0.040 (0.057)
Experience with flooding	0.329** (0.147)	-0.508*** (0.179)
Perceived flood probability	0.016 (0.041)	-0.066* (0.037)
Trust in government flood policies	0.075 (0.072)	-0.179*** (0.066)
Risk aversion	-0.050* (0.028)	0.051** (0.023)
Social norms uptake and DRR	0.317*** (0.069)	-0.267*** (0.060)
Internal locus of control	-0.002 (0.031)	0.008 (0.026)
House owner	0.488*** (0.168)	-0.580*** (0.146)
Value of home content	0.048 (0.032)	-0.080** (0.032)
Years of residence	-0.009 (0.006)	0.004 (0.005)
Gender (1=female)	-0.109 (0.123)	-0.033 (0.114)
Education	0.129** (0.062)	-0.083 (0.059)
Income	-0.045 (0.055)	-0.093* (0.054)
age	-0.014*** (0.004)	0.016*** (0.003)
Log likelihood	-304.6	-373.1
Pseudo R(McFadden)	0.176	0.2
Observations	749	749
Note:		*p**p***p<0.01

4.2. Results of evacuation intentions and COVID-19 risk perceptions

4.2.1. Evacuation intentions during Hurricane Eta (survey 4)

When respondents to our real-time survey during the threat of Hurricane Eta were asked when they were going to evacuate to a safer place, 35% answered this is very unlikely, 27% answered unlikely, 10% answered likely, and only 6% answered very likely. These results for evacuation during Hurricane Eta are reported in Tables 11 and 12. The ordered probit model results in Table 11 show that evacuation intentions are negatively related to age (model 1), of which the significance declines to marginally significant in model 2 when risk perceptions are added. These findings show that evacuation intentions are negatively related to concern about the consequences of becoming infected by COVID-19, and positively related to flood risk perceptions. Furthermore, although the sign of the coefficient estimate on the length of residence is negative, the coefficient estimate is not significant in Table 11. Whereas, the

perceived coronavirus infection probability is significantly positively related to evacuation intentions, which may be due to people with higher intentions to evacuate perceiving that they are more likely to become infected by COVID-19 in the event that an evacuation is in fact ordered.[2]

Moreover, the mediation analysis results in Table 12 show that a large proportion of the relationship between age and voluntary evacuation intentions (42%) is explained by concern about the consequences of becoming infected by COVID-19 and worry about flooding. However, worry about flooding is only a statistically significant mediator without other control variables added to the model. Length of residence is also an insignificant mediator in Table 12 which is expected given the lack of significance of this variable in Table 11. Note that these findings corroborate the findings of survey 3 that was conducted in June 2020, i.e., older individuals are less likely to evacuate under a voluntary order, because they are more concerned about the consequences of becoming infected by COVID-19 and less worried about flooding (Botzen et al., 2020).

Table 11: Ordered probit model of variables of influence on voluntary evacuation intentions during Hurricane Eta (based on the November 2020 survey). An ordered probit model is used to account for the ordinal nature of the dependent variable (1= not at all likely to 4 = extremely likely to evacuate).

	Coefficients model 1	*Coefficients model 2*
Socio-demographics		
Age	-0.017***	-0.006*
	(0.00)	(0.00)
Gender (1 = female)	0.003	0.038
	(0.10)	(0.12)
Education	-0.018	-0.075
	(0.05)	(0.06)
Income	-0.053	-0.021
	(0.04)	(0.04)
Length of residence		-0.001
		(0.01)
Flood risk perceptions		
Perceived flood probability		0.071*
		(0.04)
Worry about flooding		0.324***
		(0.05)
COVID-19 perceptions		
Perceived coronavirus infection probability		0.195***
		(0.05)
Concern about COVID-19		-0.187***

[2] We estimated the models again without perceived coronavirus infection probability to mitigate problems stemming from reverse causality. The conclusions remain the same.

	Coefficients model 1	*Coefficients model 2*
		(0.05)
Observations	603	455
Log likelihood	-689.4	-464.2
Pseudo R^2	0.032	0.131

Notes: $^{***}p < 0.01$; $^{**}p < 0.05$; $^{*}p < 0.1$. Standard errors are shown in between parentheses below the coefficients.

Table 12: Decomposition of the total effect of age on voluntary evacuation during Hurricane Eta into direct and indirect effects via concern about COVID-19, worry about flooding and length of residence using the ordered probit model (based on the November 2020 survey)

	Without control variables	**Including control variables**
Total effect	-0.017*** (0.003)	-0.011*** (0.003)
Direct effect	-0.010*** (0.003)	-0.006* (0.004)
Indirect effect	-0.007*** (0.002)	-0.005*** (0.002)
via concern about COVID-19	-0.001** (0.001)	-0.003*** (0.001)
via worry about flooding	-0.006*** (0.001)	-0.002 (0.001)
via length of residence	-0.000 (0.001)	-0.000 (0.001)
Mediation percentage	42.36	42.04
via concern about COVID-19	7.11	26.82
via worry about flooding	32.56	14.34
via length of residence	2.68	0.89
Observations	600	455

Notes:
***Significant at 1%; **Significant at 5%; *Significant at 10%.
Coefficient estimates are provided with standard errors in parentheses.
Control variables are: female, education, income, perceived flood probability and perceived coronavirus infection probability.

4.2.2. Evacuation intentions after Hurricane Eta (survey 5)

We repeated the same analyses of evacuation intentions after Hurricane Eta during the start of the 2021 hurricane season using our June 2021 survey data (survey 5). These results are shown in Table 13. Overall the Table 11 and 13 results for voluntary evacuation intentions are very similar before and after Hurricane Eta. In particular, age is a significant negative determinant of evacuation intentions. Once risk perceptions are added to the model (model 2) the coefficient estimate on age is lower in absolute terms and becomes marginally significant – so some of the impact of age on intentions is explained by these risk perceptions variables. The signs and significance of coefficient estimates for the risk perceptions indicators are also very similar before and after Eta (model 2).

There are some similarities and differences regarding the mediation results which are reported in Table 14 for the June 2021 survey 5. The three variables: "concern about COVID-19", "worry about flooding" and "length of residence" mediate between 42 and 46 percent of the relationship between age and voluntary intentions to evacuate across both surveys. The percentage mediated by "concern about COVID-19" is lower (perhaps concern about COVID-19 is becoming a less important reason for older people not

to evacuate over time, e.g. because they are more likely to be vaccinated in the second survey). Worry about flooding remains a significant mediator. Age and worry are negatively correlated (Spearman's rho = -0.301; p-value = 0.000). Overall we conclude from the survey 5 results that concern over COVID-19 is still an obstacle for evacuation in the 2021 hurricane season, although its importance has declined compared with situation in November 2020 as may be expected given lower risks from COVID-19.

Table 13: Ordered probit model of variables of influence on voluntary evacuation intentions after Hurricane Eta using survey 5 data. An ordered probit model is used to account for the ordinal nature of the dependent variable (1= not at all likely to 4 = extremely likely to evacuate).

	Coefficients model 1	*Coefficients model 2*
Socio-demographics		
Age	-0.011***	-0.004*
	(0.00)	(0.00)
Gender (1 = female)	0.127*	0.100
	(0.07)	(0.08)
Education	-0.022	-0.018
	(0.03)	(0.04)
Income	0.022	0.019
	(0.03)	(0.03)
Length of residence		-0.007*
		(0.00)
Flood risk perceptions		
Perceived flood probability		0.048*
		(0.03)
Worry about flooding		0.215***
		(0.04)
COVID-19 perceptions		
Perceived coronavirus infection probability		0.107***
		(0.04)
Concern about COVID-19		-0.082**
		(0.03)
Observations	1123	820
Log likelihood	-1491.8	-1047.2
Pseudo R^2	0.016	-1047.2

Notes: $^{***}p < 0.01$; $^{**}p < 0.05$; $^{*}p < 0.1$. Standard errors are shown in between parentheses below the coefficients.

Table 14. Decomposition of the total effect of age on voluntary evacuation after Hurricane Eta into direct and indirect effects via concern about COVID-19, worry about flooding and length of residence using the ordered probit model (survey 5 data)

	Without control variables	**Including control variables**
Total effect	-0.012*** (0.002)	-0.008*** (0.002)
Direct effect	-0.007*** (0.002)	-0.004* (0.002)
Indirect effect	-0.006*** (0.001)	-0.004*** (0.001)

via concern about COVID-19	-0.000 (0.000)	-0.001** (0.000)
via worry about flooding	-0.005*** (0.001)	-0.002*** (0.000)
via length of residence	-0.001 (0.001)	-0.001* (0.001)
Mediation percentage	45.65	45.35
via concern about COVID-19	0.76	11.07
via worry about flooding	38.34	19.49
via length of residence	6.55	14.78
Observations	1059	820

Notes:
***Significant at 1%; **Significant at 5%; *Significant at 10%.
Coefficient estimates are provided with standard errors in parentheses.
Control variables are: female, education, income, perceived flood probability and perceived coronavirus infection probability.

5. Analysis of Insurance Purchases by Policyholder Type

This section presents the decision tree models and the empirical analysis of the insurance purchase behavior by various policyholder types. In Section 4.1, we examine the relationship between insurance purchases and risk reduction activities. In this section, we differ our analysis by policyholder type, and we examine all potential determinants of insurance coverage purchase for each policyholder type. Our analysis in this section is based on the responses of Surveys 4 and 5 which included detailed questions about individuals' insurance decisions.

5.1 Decision Trees and Policyholder Types

We use a decision tree for purchasing flood insurance and windstorm coverage to demonstrate the complexity of property insurance. The decision tree shows the process that leads to different policyholder types. The root and branch nodes represent a decision, and the end nodes show the outcomes (i.e., choice sets). The outcomes show the different policyholder types that we examine in the quantitative analysis using our survey data. One thing to note is that consumers often use an agent to purchase insurance. Consumers may not consciously make the decisions in the decision tree because the agent can collect their information and help them determine the appropriate coverage. However, we still want to use the decision tree to explain the process behind the policy chosen by an agent or a consumer. The complexity of the process also indicates the opacity of the property insurance and the substantial knowledge that consumers need to acquire to understand their insurance policy. Also, we do not distinguish admitted and non-admitted carriers because "where to purchase the insurance" often depends on the agent and is not up to a policyholder's choice. If the agent can write in both the standard and the non-admitted market, the policyholder is likely to choose the insurer based on the price.

5.1.1 Flood Insurance Decision Tree

Flooding is the costliest natural disaster in the U.S.; however, flood peril is not covered by a standard homeowners insurance policy. Homeowners need to purchase a separate flood insurance policy to obtain coverage. Moreover, homeowners located in high-risk flood areas with mortgages from government-backed lenders are required to have flood insurance (FEMA, n.d.).[3] The high-risk flood area is also called the Special Flood Hazard Area (SFHA), with a 1-in-100 year flood probability.[4] Homeowners without the mandatory requirement, such as those living in moderate- to low-risk flood areas, can voluntarily choose to purchase flood insurance.

Most flood insurance is provided through the National Flood Insurance Program (NFIP), which is a federal program and administered by the Federal Emergency Management Agency (FEMA). Only property owners in the participating communities can purchase an NFIP policy. There are approximately 23,000 NFIP participating communities nationwide; only 9 communities in Florida do not participate.[5] Homeowners living in non-participating communities must purchase a private flood insurance product that is designed and underwritten by a private insurance company. The private flood insurance product can be a stand-alone flood policy or an endorsement of the homeowners' insurance.[6]

Owners of high-value homes may want to purchase a private flood insurance product to obtain additional coverage beyond the NFIP policy. The NFIP policy has coverage limits of $250,000 for the building and $100,000 for the building contents. In comparison, private flood insurance products have much higher coverage limits, along with some additional benefits, such as more deductible choices, a shorter waiting period, and fewer underwriting questions. In sum, for a mandated flood insurance purchase (top branch of the decision tree), homeowners may have three options to obtain flood coverage: an NFIP policy plus a private flood insurance policy for additional coverage, a sole NFIP policy, or a sole private flood insurance policy.

[3] The federal banking regulators have allowed for either a NFIP policy or a private flood insurance, and a rule on acceptance of private flood was finalized in 2019. However, Federal Housing Administration (FHA) regulations currently do not allow FHA-insured properties to purchase private flood insurance to fulfill the mandatory requirement.

[4] High-risk flood areas begin with the letters A or V on the FEMA flood maps. Moderate- to low-risk flood areas are designated with the letters B, C, and X on the FEMA flood maps. More than 40% of all NFIP flood claims come from outside of high-risk food areas between 2015 and 2019 (FEMA, 2020).

[5]The numbers of Florida are obtained from the Community Status Book, retrieved October 5, 2020 from https://www.fema.gov/national-floodinsurance-program-community-status-book.

[6] Alternatively, homeowners may have a flood endorsement onto a dwelling fire policy.

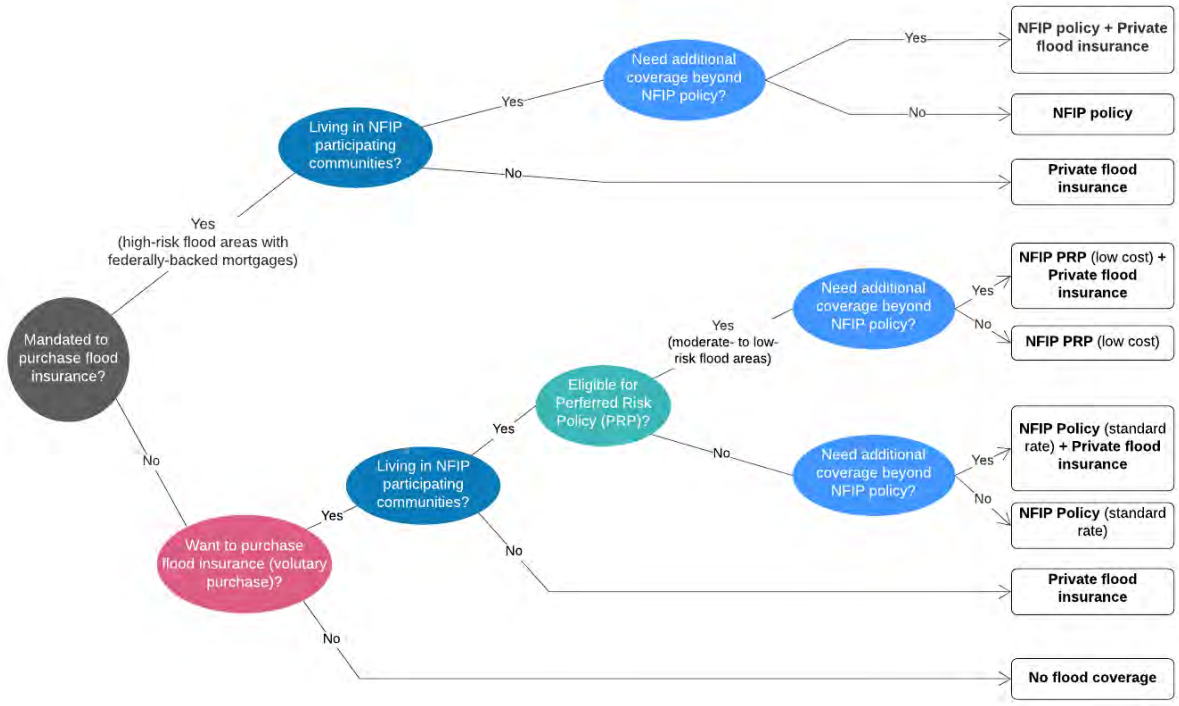

Note: FHA-insured properties mandated to have flood insurance but not located in the NFIP participating communities cannot purchase private flood insurance to fulfill the requirement at this stage. Insurance regulators have been working to change the rule.

Figure12: Flood Insurance Decision Tree in Florida

For a voluntary flood insurance purchase (bottom branch of the decision tree), homeowners living in the NFIP participating communities can buy an NFIP policy. Homeowners located in moderate- to low-risk flood areas (non-SFHA areas, Zone B, C, or X) are eligible for a Preferred Risk Policy (PRP), which has the same coverage as a standard-rated NFIP policy but charges a lower cost.[7] Similarly, policyholders with a voluntary purchase can add a private flood insurance policy for additional coverage. In sum, there are five options for homeowners who purchase flood insurance voluntarily: an NFIP PRP plus a private flood insurance policy, an NFIP standard-rated policy plus a private flood insurance policy, a sole NFIP PRP policy, a sole NFIP standard-rated policy, and a sole private flood insurance policy.

[7] More policy information regarding PRPs is available at https://www.fema.gov/pdf/nfip/manual201105/content/09_prp.pdf.

5.1.2 Windstorm Coverage Decision Tree

Windstorm peril is typically covered by the standard homeowners (HW) multi-peril insurance policy except in some wind-prone areas. The windstorm loss in some coastal states is subject to a separate deductible. There are three types of wind deductibles:

- Hurricane deductible applies to windstorm damages caused by a named hurricane.
- Named-Storm deductible is less restrictive than Hurricane deductible and additionally applies to damages caused by named tropical storms that are not a hurricane when making landfall.
- Windstorm deductible is the broadest type and applies to windstorm damages from any source.

Based on the III (2020) and CIPR website, 19 states and the District of Columbia currently have a hurricane or named storm deductible in place.[8] Unlike the NFIP flood policy, homeowners insurance is specific to states because different states can employ different triggers and amounts for windstorm deductibles. The residual markets in different states may also have different eligibility requirements, policies, programs, and management rules. We focus on the decision-making process in Florida because our survey data do not cover other states.

In Florida, homeowners living in coastal areas may not find a standard HW multi-peril insurance policy from a private insurer or can only find coverage with extremely high premiums. In this case, homeowners can turn to the Citizens Property Insurance Corporation (Citizens), the residual market and last resort of high-risk homeowners.[9] A homeowner is eligible for a Citizens policy if one of the following criteria is met: (1) no comparable private-market offers of coverage are received, or (2) comparable private-market offers of coverage are received, but the premiums are more than 15 percent higher than a comparable Citizens policy.

Another situation is that, in some high-risk regions, private insurers can exclude the windstorm peril from the coverage. According to the Florida Statute s. 627.712(1), admitted insurers are required to offer windstorm coverage in the base policy except in areas covered by the Citizens Coastal Account. The Citizens Coastal Account, formerly known as High Risk Account, is for wind-only and multi-peril policies

[8] More detailed information is available at https://www.agordon.com/blog/bid/163479/wind-deductible-vs-hurricane-vs-named-storm-deductibles and CIPR website https://content.naic.org/cipr_topics/topic_hurricane_deductibles.htm.
[9] Citizens was established by the Florida Legislature in 2002 when the state combined two separate high-risk insurance pools – the Florida Windstorm Underwriting Association and the Florida Residential Property & Casualty Joint Underwriting Association. Company website is https://www.citizensfla.com/insurance-101.

for personal residential, commercial residential, and commercial nonresidential risks located in eligible coastal high-risk areas, i.e., in areas that were defined on January 1, 2002, to be eligible for coverage by the Florida Windstorm Underwriting Association. Surplus line underwriters are not subject to the s. 627.712(1).

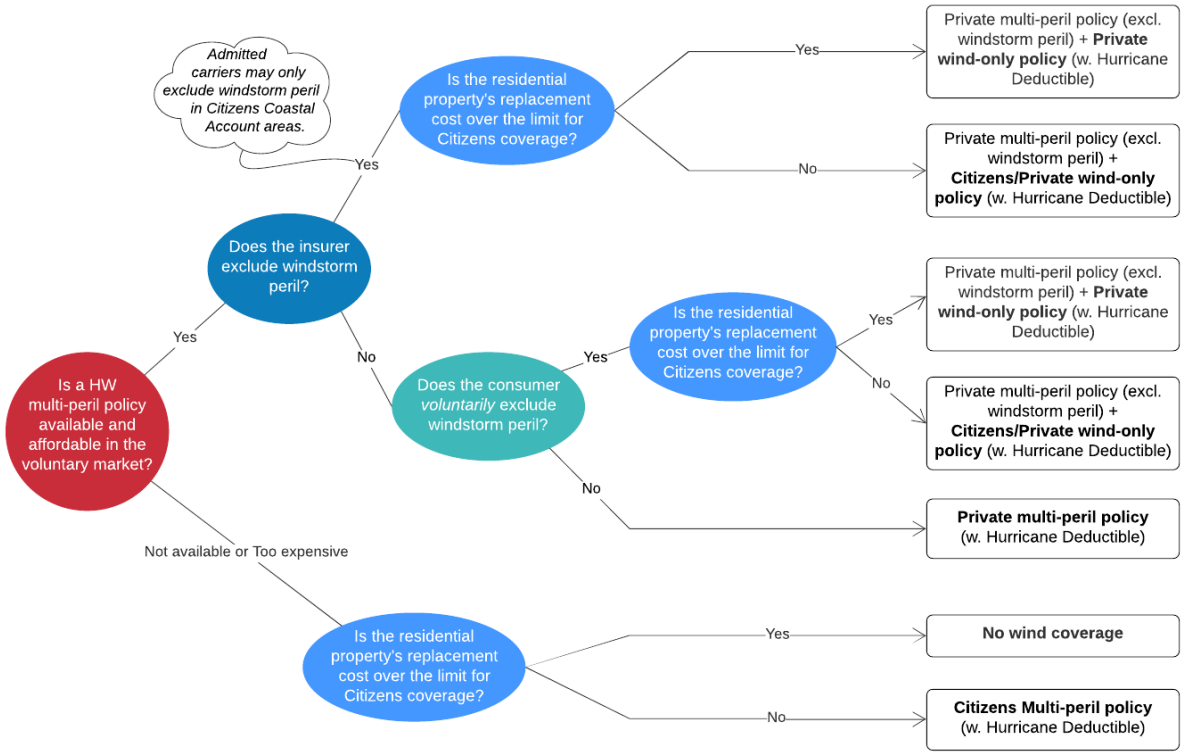

Note: The voluntary/private market includes admitted carriers and surplus line (i.e., non-admitted) underwriters. The replacement cost limit for the Citizens coverage is $0.7 million in Florida except in Miami-Dade and Monroe counties, where the limit rises to $1 million. A private wind-only policy in the end nodes can be a separate wind-only policy or an endorsement for windstorm damages onto the base policy.

Figure 13: Windstorm Coverage Decision Tree in Florida

When the windstorm peril is excluded, homeowners can purchase a wind-only policy from Citizens covering only damages from hail and windstorms. Only properties in areas within the boundaries of the Citizens Coastal Account are eligible for Citizens wind-only policies. On the demand side, the policyholders may voluntarily exclude the windstorm peril and purchase a wind-only policy if the latter is a cheaper option.

High-value properties are ineligible to obtain coverage from Citizens and thus, must purchase coverage from private insurers. Effective January 1, 2017, house units with a replacement cost of $0.7 million or over are not eligible for any coverage by the Citizens (the replacement cost limit is $1 million in Miami-Dade and Monroe counties).[10] In Florida, a few private insurers provide a wind-only policy or an endorsement for windstorm damages.[11] When the windstorm peril is excluded from the base policy, the high-value houses must find wind-only coverage from these private insurers.

In Florida, both HW multi-peril insurance and wind-only insurance have a Hurricane deductible that applies to wind damages caused by a named hurricane. A Hurricane deductible can be either a flat amount of $500 or 2%, 5%, or 10% of the home's total insured value. The $500 flat deductible is only available for certain types of policies, such as homes with a total insured value of less than $100,000. The Hurricane deductible applies only once during a hurricane season.[12] In sum, policyholders in Florida may have four options to obtain windstorm coverage: a standard homeowners' multi-peril policy from a private insurer, a homeowners' multi-peril policy from Citizens, and a private homeowners' multi-peril policy excluding windstorm peril plus a Citizens wind-only policy, and a private homeowners' multi-peril policy excluding windstorm peril plus a private wind-only policy.

In Florida, there are several programs to help homeowners access the state's increasingly expanding insurance market. The Clearinghouse program established by Citizens helps policyholders with no option other than Citizens to shop around and find better property coverage from private insurers. Policyholders are not eligible for Citizens if a comparable offer of coverage is received through the Clearinghouse with a premium less than 15 percent higher than the Citizens premium. The Homeowners Rate Comparison Tool (CHOICES) on the Florida Office of Insurance Regulation (OIR) website[13] provides users the average rate quotes for three coverage examples and the user's county from various insurance companies (including Citizens). The quotes reflect the most recent rate filings approved by the OIR office. The Florida

[10] Based on the s. 627.351(6)(a)3.d., effective January 1, 2017, a structure that has a dwelling replacement cost of $700,000 or more, or a single condominium unit that has a combined dwelling and contents replacement cost of $700,000 or more, is not eligible for coverage by the corporation. Such dwellings insured by the corporation on December 31, 2016, may continue to be covered by the corporation until the end of the policy term. Rules and processes were revised in December 2019; see details at Citizens website.

[11] There are around 10 private insurers that sell wind-only policies in Florida, according to our talk with the Florida OIR staff.

[12] When homeowners incur wind losses under the second hurricane, the deductible of the second claim will be either the remainder of the unused hurricane deductible or the AOP deductible, whichever is greater. See more details at the Florida's Chief Financial Officer's website.

[13] The CHOICES system is for four types of insurance including homeowners at https://www.floir.com/choices.aspx.

Market Assistance Plan (FMAP), run by Citizens, is a free and online referral service that matches property owners with agents who believe they can help the property owners find private-market coverage.

Under Florida law, policyholders can obtain premium discounts for implementing certain types of mitigation measures. The first layer discount is for new building codes and eligible for houses built after 2001 or houses built before 2001 but with an updated roof construction that meets the 2001 Florida Building Code. The second layer discount only applies to the hurricane-wind portion of the premium. It includes two types of wind mitigation measures -- securing the roof and protecting windows from flying debris.[14]

5.2 Measures of Policyholder Types and Method

5.2.1 Measures of Policyholder Types

Based on the survey questions, we have mandatory vs. voluntary purchase of flood insurance. The mandatory and voluntary flood insurance purchase can be further distinguished by where the individuals obtain the insurance -- NFIP policy vs. private flood insurance. The flood policyholders are primarily measured by four *mutually exclusive* types – *mandatory NFIP, mandatory private insurer, voluntary NFIP, voluntary private insurer*. For each group, the zero value is always no flood coverage.

The table below shows the frequency and percentage of different types of flood insurance policyholders. For both Surveys 4 and 5, we have slightly more voluntary purchase of flood insurance than mandatory purchase. About 10% of respondents in Survey 4 and 11% of respondents in Survey 5 purchased a private flood product. The NAIC report[15] showed that the private flood premiums written was 8% of the total flood premiums written in Florida in 2018. We have a slightly higher percentage of private flood buyers possibly because our sample limits to coastal counties.

Table 15: Distribution of Flood Policyholder Types

Flood PH Types	Definition	Survey 4		Survey 5	
		Freq.	Percent	Freq.	Percent
mandatory NFIP	mandated to purchase flood insurance, and only purchased the NFIP policy	46	6%	79	8%

[14]To learn more about wind mitigation discount, see Form OIR-B1-1655 from Florida OIR available at https://www.floir.com/siteDocuments/OIR-B1-1655.pdf.

[15] National Association of Insurance Commissioners (NAIC), December 2019, "Considerations for State Insurance Regulators in Building the Private Flood Insurance Market."

mandatory private insurer	mandated to purchase flood insurance, and purchased a private flood product	28	4%	60	6%
voluntary NFIP	voluntarily chose to purchase flood insurance, and only purchased the NFIP policy	62	8%	70	7%
voluntary private insurer	voluntarily chose to purchase flood insurance, and purchased a private flood product	41	6%	108	11%
none	no flood insurance	567	76%	690	69%
Subtotal		**744**	**100%**	**1,007**	100%
*don't know**	don't know if have a flood policy	91		171	
	with flood insurance but don't know insurance type (mandatory or not / insurance provider)	9		67	
Total		**844**		**1,245**	

*The data of respondents who don't know any needed information are not used in the analysis due to lack of information.

Based on our survey questions, in Survey 4, the wind coverage buyers can be divided into two types – obtaining wind coverage from the homeowners' insurance (*homeowners' insurance*) or from a wind-only policy (*wind-only policy*). There are 331 respondents whose homeowners insurance covered the windstorm peril and 34 respondents who had to obtain windstorm coverage through a wind-only policy.

In Survey 5, we asked the policyholder type question separately for individuals who purchased wind coverage from private insurers and from the Florida Citizens. Therefore, there are four types of wind policyholder types for Survey 5 -- *homeowners' insurance from a private insurer, homeowners' insurance from Citizens, wind-only coverage from a private insurer, wind-only policy from Citizens*.

The table below shows the frequency and percentage of different types of wind insurance policyholders. The majority of policyholders (47% in Survey 4 and 45% in Survey 5) obtained their wind coverage through their homeowners' insurance policy. Only 10% or fewer respondents purchased a wind-only policy.

Table 16: Distribution of Wind Policyholder Types

Wind PH Types	**Definition**	**Survey 4**		**Survey 5**	
		Freq.	**Percent**	**Freq.**	**Percent**
homeowners' insurance from a private insurer	coverage through a homeowners' insurance policy from private insurers	331	47%	309	33%
homeowners' insurance from Citizens	coverage through a homeowners' insurance policy from Florida Citizens			112	12%
wind-only coverage from a private insurer	coverage through a wind-only policy (or wind endorsement) from private insurers	34	5%	73	8%
wind-only policy from Citizens	coverage through a wind-only policy from Florida Citizens			15	2%
none	no wind coverage	341	48%	435	46%

Subtotal		**706**	**100%**	**944**	**100%**
*don't know**	don't know if have a flood policy	138		253	
	with wind insurance but don't know insurance type (insurance provider / coverage type)			48	
Total		**844**		**1,245**	

*The data of respondents who don't know any needed information are not used in the analysis due to lack of information.

5.2.2 Other Survey Variables

To study the insurance purchase behavior, we control for the variables including demographic factors, house characteristics, flood risk perception, wind risk perceptions (only in Survey 5), the regret of having or not having flood insurance, the social norm of buying flood insurance, the mitigation measures taken, the premium discount for implementing measures (only in Survey 5), the trouble obtaining insurance due to disaster activities (only in Survey 5), the financial difficulty of purchasing insurance due to COVID-19, and the trust in the government's ability to limit flood risk.

The summary statistics of variables are displayed in the tables below. The overall flood insurance uptake rate increases to 36% in Survey 5 from 25% in Survey 4. The overall wind insurance uptake rate increases to 56% in Survey 5 from 52% in Survey 4. The means of the influencing factors are similar between Surveys 4 and 5. The length of residence is winsorized at the 1% and 99% levels to reduce the effect of extreme values that are likely typing errors.

Table 17: Summary Statistics of Variables

	Survey 4		**Survey 5**	
	N	mean	N	mean
Insurance uptake:				
Flood policy	753	0.247	1,074	0.358
Wind policy	706	0.517	992	0.561
Influencing factors:				
Worry about flooding	839	2.712	1,210	2.756
Perceived flood probability	676	0.105	974	0.0895
Perceived flood impact	674	3.714	971	3.821
Worry about windstorm			1,208	3.475
Perceived wind impact			980	3.789
Trust in government flood policies	796	2.734	1,137	2.553
Number of ex ante risk reduction measures	844	1.315	1,245	1.530
Window protection	794	0.486	1,245	0.516
Roof retrofit			1,245	0.561
Hip roof			1,245	0.425

Premium discount for flood risk mitigation			739	0.108
Premium discount for wind risk mitigation			804	0.267
Trouble purchasing flood insurance			1,245	0.142
Trouble purchasing homeowners insurance			1,245	0.153
Internal locus of control	835	7.404	1,229	7.206
Risk taking	838	5.827	1,228	5.818
Regret of no insurance	795	3.551	1,142	3.613
Regret of having insurance	807	2.984	1,152	2.941
Social norm for insurance uptake	790	3.108	1,140	3.111
Financial difficulty due to COVID-19	844	0.217	1,060	0.208
Age	832	46.73	1,245	49.66
Education	839	3.222	1,229	3.265
Income	813	3.480	1,194	3.626
Female	837	0.687	1,245	0.640
Value of home building	692	3.251	1,031	3.596
Value of home content	716	4.581	1,058	4.757
House owner	814	0.649	1,190	0.703
Length of residence	814	9.026	1,178	11.09
Underfloor basement	844	0.0403	1,245	0.0739
InWindonly_territory	844	0.0533		

5.2.3 Regression Method of Insurance Purchases by Policyholder Type

The regression model in general is:

$$insurance\ purchase_i = f(\boldsymbol{\beta_1 demographic}_i + \boldsymbol{\beta_2 house}_i + \boldsymbol{\beta_3 risk\ perception}_i + \boldsymbol{\beta_4 measures}_i + \boldsymbol{\beta_5 psychology}_i + \boldsymbol{\beta_6 other}_i + \epsilon_i)$$

where *i* indices survey respondents. The dependent variable is either the dummy variable for the overall insurance update or the categorical variable for various policyholder types. Depending on the dependent variable, the regression model $f()$ is also different. On the right-hand side, we include independent variables for demographic factors (e.g., age, female, education, income), house characteristics (e.g., home value, contents value, length of residence, underfloor basement), risk perceptions (e.g., worry, damage estimated), measures taken and the associated premium discount, psychology factors (e.g., internal locus of control, risk-taking, regret, social norm), and other factors (e.g., trust in government's ability, financial difficulty due to COVID-19). ϵ_i is the error term.

We first examine the overall insurance uptake, i.e., whether the respondent has any types of flood or wind insurance coverage. The dependent variable is the insurance uptake dummy variable, which is 1 if the

respondent has purchased the insurance policy and 0 otherwise. As the dependent variable is a dummy variable, a Probit regression model is used.

Next, we examine the insurance purchase behavior by different PH types. For flood insurance, we firstly compare the mandatory vs. voluntary types of buyers. We expect that the demographic factors, house characteristics, and risk perception are more likely to affect voluntary purchase than mandatory purchase. The dependent variable is still the insurance uptake dummy and thus we still use a Probit regression model. The mandatory vs. voluntary types of buyers can link back to the decision tree as follows:

- *flood insurance*: 1= with any type of flood policy, 0 = no flood coverage
- *flood insurance mandatory*: 1 = mandatory purchase of flood insurance (top branch of the decision tree), 0 = no flood coverage
- *flood insurance voluntary*: 1 = voluntary purchase of flood insurance (bottom branch of the decision tree), 0 = no flood coverage

We conduct a more detailed analysis of the flood policyholder types by examining the four mutually exclusive groups. In this case, we can compare the mandatory flood purchase of the private flood product vs. the NFIP policy; the same for the voluntary purchase. When we look at the four flood policyholder types, we consider each group against the no flood coverage group and use a multinomial Probit model. The dependent variable has five outcomes, and each of them can link back to the decision tree as follows:

- Outcome 1: None = no flood coverage (end node 9); base outcome
- Outcome 2: mandated purchase and buying only NFIP policies (end node 2)
- Outcome 3: mandated purchase and buying private flood product (end nodes 1 & 3)
- Outcome 4: voluntary purchase and buying only NFIP policies (end nodes 5 & 7)
- Outcome 5: voluntary purchase and buying private flood product (end nodes 4, 6, 8)

For the windstorm coverage, there are two policyholder types in Survey 4 and four policyholder types in Survey 5. The dependent variable of Survey 4 has three outcomes:

- Outcome 1: None = no wind coverage (end node 6); base outcome
- Outcome 2: wind coverage through homeowners' multi-peril insurance (end nodes 5 & 7)
- Outcome 3: wind coverage through a wind-only policy (end nodes 1-4)

The dependent variable of Survey 5 has five outcomes:

- Outcome 1: None = no wind coverage (end node 6); base outcome
- Outcome 2: wind coverage through homeowners' multi-peril insurance from private insurers (end node 5)

- Outcome 3: wind coverage through a wind endorsement or a wind-only policy from private insurers (end nodes 1-4)
- Outcome 4: wind coverage through homeowners' multi-peril insurance from Florida Citizens (end node 7)
- Outcome 3: wind coverage through a wind-only policy from Florida Citizens (end nodes 2 & 4)

Since the dependent variable is a categorical variable, we use a multinomial Probit model, with the base outcome being the no wind coverage group.

5.3 Empirical Results of Insurance Purchases by Policyholder Type

For the discussions below about our survey results, we consider a factor statistically significant at or above the 95th confidence level.

5.3.1 Results of Overall Insurance Uptake

The table below shows the results of the Probit model on the overall uptake of flood insurance. The effect of income is reversed after we add in the value of the home and contents. It becomes insignificant when risk perception, mitigation, and psychology variables are incorporated. The value of contents has a statistically significant and positive impact on the flood insurance purchase, whereas the value of home building does not make a difference. Having a basement can increase the probability of flood insurance purchase, but the effect is insignificant after the mitigation variable is controlled. Only the flood risk perception measured by the worry about flooding has a significant and positive impact on the probability of purchasing flood coverage. The estimated flood probability or the perceived flood damage have no impact.

The regret of having no flood insurance when flooded and the high social norm of purchasing flood insurance both lead to an increased probability of purchasing flood insurance. As we expected, the financial difficulty of buying insurance due to COVID-19 reduces the likelihood of flood insurance purchases. The number of ex-ante mitigation measures that individuals have taken positively relates to the flood insurance purchase, suggesting no evidence for adverse selection. The results of this table are in general consistent with the earlier results presented in Section 4.1.

Table 18: Probit Model of Overall Flood Insurance Uptake (Survey 4)

	(1) flood insurance purchase	(2) flood insurance purchase	(3) flood insurance purchase	(4) flood insurance purchase

Age	0.000	-0.000	0.001	0.001
	(0.001)	(0.001)	(0.001)	(0.001)
Education	0.027	0.041*	0.023	0.005
	(0.017)	(0.021)	(0.022)	(0.022)
Income	0.037***	-0.037**	-0.037*	-0.025
	(0.013)	(0.019)	(0.021)	(0.022)
Female	-0.009	-0.022	-0.074*	-0.054
	(0.034)	(0.039)	(0.042)	(0.041)
House owner		0.077	0.036	0.008
		(0.051)	(0.055)	(0.053)
Value of home building		0.011	-0.001	-0.020
		(0.014)	(0.015)	(0.016)
Value of home content		0.043***	0.043***	**0.039*** **
		(0.011)	(0.013)	(0.012)
Length of residence		-0.002	-0.002	-0.001
		(0.002)	(0.002)	(0.002)
Underfloor basement		0.213***	0.154**	0.132
		(0.081)	(0.077)	(0.085)
Worry about flooding			0.098***	**0.044** **
			(0.016)	(0.018)
Perceived flood probability			-0.151	-0.137
			(0.121)	(0.117)
Perceived flood impact			0.023*	0.015
			(0.013)	(0.012)
Risk taking				-0.001
				(0.009)
Internal locus of control				-0.011
				(0.010)
Regret of no insurance				**0.056*** **
				(0.020)
Regret of having insurance				-0.027
				(0.017)
Social norm for insurance uptake				**0.104*** **
				(0.020)
Number of ex ante risk reduction measures				**0.027** **
				(0.013)
Financial difficulty due to COVID-19				**-0.125** **
				(0.055)
Trust in government flood policies				-0.020
				(0.025)
Observations	726	558	452	418

Note: Robust standard errors in parentheses. *** p<0.01, ** p<0.05, * p<0.1. The table reports average marginal effects.

The table below shows the results of the Probit model on the overall uptake of windstorm coverage. Similar to the results of flood insurance, the effect of income diminishes when we add in the value of the home and contents. Owning a home significantly increases the probability of having windstorm coverage, possibly because most homeowners buy property insurance for their homes but many tenants don't purchase renters' insurance. The properties located within the Florida Citizens' coastal account boundaries are more likely to have windstorm insurance coverage than those located outside of the coastal account areas. This indicates that individuals in high-risk wind areas may be more concerned about windstorm damage and are more active in getting insurance protection than those not located in high-risk wind areas. Implementing window protection against wind damages positively impacts the purchase of windstorm coverage, but the effect is marginally significant. Like flood insurance, we don't find evidence of adverse selection for wind insurance either.

Table 19: Probit Model of Overall Wind Coverage Uptake (Survey 4)

	(1) wind coverage purchase	(2) wind coverage purchase	(3) wind coverage purchase
Age	0.004***	0.002	0.002
	(0.001)	(0.001)	(0.001)
Education	-0.008	-0.036*	-0.031
	(0.019)	(0.022)	(0.022)
Income	0.100***	0.030	0.027
	(0.013)	(0.020)	(0.021)
Female	-0.038	-0.033	-0.026
	(0.038)	(0.043)	(0.043)
House owner		0.228***	**0.217*** **
		(0.051)	(0.053)
Value of home building		0.015	0.012
		(0.015)	(0.016)
Value of home content		0.018	0.014
		(0.012)	(0.012)
Length of residence		-0.003	-0.003
		(0.002)	(0.002)
InWindonly_territory			**0.271*** **
			(0.090)
Risk taking			0.006
			(0.009)
Internal locus of control			0.013
			(0.010)
Window protection			0.072*
			(0.041)

Financial difficulty due to COVID-19			-0.034
			(0.055)
Observations	679	528	518

Note: Robust standard errors in parentheses. *** p<0.01, ** p<0.05, * p<0.1. The table reports average marginal effects.

The results of the overall flood insurance update for Survey 5 are different from the results for Survey 4 to some extent. The value of home building becomes a significant and positive factor for flood insurance purchase whereas the value of contents no longer makes a difference. Also, only the flood risk perception measured by the estimated flooding probability (1 in X years) positively affects the likelihood of flood insurance purchase, but the impact is statistically weak.

The common determinants between Surveys 4 and 5 are the regret of having no flood insurance when flooded, the social norm of purchasing flood insurance (similar to section 4.1), the number of ex-ante measures implemented (similar to section 4.1), and the financial difficulty due to the pandemic. They have a similar impact on the overall flood insurance uptake for Surveys 4 and 5.

Table 20: Probit Model of Overall Flood Insurance Uptake (Survey 5)

	(1) flood insurance purchase	(2) flood insurance purchase	(3) flood insurance purchase	(4) flood insurance purchase
Age	-0.002**	-0.003***	-0.001	-0.002
	(0.001)	(0.001)	(0.001)	(0.002)
Education	0.017	0.010	0.012	0.042*
	(0.015)	(0.017)	(0.019)	(0.023)
Income	0.067***	-0.002	0.005	-0.015
	(0.012)	(0.017)	(0.020)	(0.023)
Female	0.016	-0.002	-0.010	0.016
	(0.030)	(0.034)	(0.038)	(0.045)
House owner		0.021	0.027	0.010
		(0.048)	(0.055)	(0.066)
Value of home building		0.061***	0.051***	**0.033****
		(0.011)	(0.013)	(0.016)
Value of home content		0.009	-0.002	-0.011
		(0.010)	(0.012)	(0.014)
Length of residence		0.001	0.002	0.001
		(0.002)	(0.002)	(0.002)
Underfloor basement		0.028	-0.010	-0.132*
		(0.063)	(0.068)	(0.075)

Worry about flooding			0.063***	0.016
			(0.017)	(0.021)
Perceived flood probability			0.258**	0.258*
			(0.114)	(0.136)
Perceived flood impact			0.016	0.009
			(0.012)	(0.013)
Risk taking				0.013
				(0.010)
Internal locus of control				0.008
				(0.011)
Regret of no insurance				**0.049****
				(0.023)
Regret of having insurance				-0.017
				(0.018)
Social norm for insurance uptake				**0.115*****
				(0.020)
Number of ex ante risk reduction measures				**0.025****
				(0.012)
Premium discount for flood risk mitigation				0.076
				(0.069)
Trouble purchasing flood insurance				0.027
				(0.071)
Financial difficulty due to COVID-19				**-0.184*****
				(0.065)
Trust in government flood policies				0.029
				(0.027)
Observations	1,054	836	661	446

Note: Robust standard errors in parentheses. *** p<0.01, ** p<0.05, * p<0.1. The table reports average marginal effects.

For Survey 5, the factors that determine the overall wind coverage update are also different. Age becomes a significant and positive factor. Being a homeowner still positively affects the wind coverage update, but the effect is marginally significant. We asked about the wind risk perceptions in Survey 5. The worry about windstorms does significantly increase the wind coverage uptake. Getting a premium discount for implementing mitigation measures also increases individuals' incentive to purchase windstorm coverage. Having had trouble getting or renewing the windstorm insurance due to increased disaster activities leads to a higher incentive of purchasing windstorm coverage. Like Survey 4, the financial difficulty for purchasing insurance due to COVID-19 negatively impacts the wind coverage uptake.

Table 21: Probit Model of Overall Wind Coverage Uptake (Survey 5)

	(1) wind coverage purchase	(2) wind coverage purchase	(3) wind coverage purchase	(4) wind coverage purchase
Age	0.005***	0.003***	0.003***	**0.004*** **
	(0.001)	(0.001)	(0.001)	(0.001)
Education	0.010	-0.007	-0.011	0.009
	(0.016)	(0.017)	(0.018)	(0.020)
Income	0.078***	-0.001	0.003	-0.017
	(0.012)	(0.016)	(0.017)	(0.019)
Female	-0.021	-0.047	-0.049	0.013
	(0.032)	(0.034)	(0.036)	(0.039)
House owner		0.157***	0.143***	0.087*
		(0.045)	(0.046)	(0.052)
Value of home building		0.035***	0.025**	0.005
		(0.012)	(0.012)	(0.013)
Value of home content		0.019*	0.004	-0.010
		(0.010)	(0.011)	(0.012)
Length of residence		-0.001	-0.001	-0.002
		(0.002)	(0.002)	(0.002)
Worry about windstorm			0.070***	**0.062*** **
			(0.015)	(0.017)
Perceived wind impact			0.034***	0.009
			(0.010)	(0.011)
Risk taking				-0.005
				(0.008)
Internal locus of control				0.013
				(0.009)
Window protection				-0.006
				(0.041)
Roof retrofit				0.068
				(0.045)
Hip roof				0.049
				(0.041)
Premium discount for wind risk mitigation				**0.163*** **
				(0.043)
Trouble purchasing homeowners insurance				**0.114** **
				(0.054)
Financial difficulty due to COVID-19				**-0.159*** **
				(0.050)
Observations	967	775	697	526

Note: Robust standard errors in parentheses. *** p<0.01, ** p<0.05, * p<0.1. The table reports average marginal effects.

5.3.2 Results by Flood Policyholder Types

Next, we look at the determinants of flood and hurricane insurance purchase across various policyholder types. The table below displays the Probit model regression results for the mandatory vs. voluntary flood insurance purchase. We find that demographic and house characteristics and flood risk perceptions, including age, gender, and the existence of a basement, the value of building and contents, and the worry about flooding, affect the voluntary flood insurance purchase but do not significantly impact the mandatory purchase. This is true for both Surveys 4 and 5.

Both mandatory and voluntary flood insurance purchases are positively affected by the social norm of purchasing flood insurance. The mandatory-type purchase is distinctly affected by the regret of having no coverage when flooded and the number of ex-ante mitigation measures taken. The voluntary-type purchase is additionally affected by the financial difficulty due to COVID-19.

Table 22: Probit Model of Mandatory vs. Voluntary Flood Insurance Purchases

	Survey 4		**Survey 5**	
	mandatory flood purchase	voluntary flood purchase	mandatory flood purchase	voluntary flood purchase
Age	-0.001	**0.003****	-0.003*	-0.001
	(0.001)	(0.001)	(0.001)	(0.002)
Education	-0.004	0.008	0.025	0.043*
	(0.019)	(0.021)	(0.023)	(0.024)
Income	-0.012	-0.027	-0.010	-0.007
	(0.019)	(0.021)	(0.023)	(0.023)
Female	0.013	**-0.085****	-0.005	0.012
	(0.037)	(0.036)	(0.042)	(0.049)
House owner	0.017	0.009	0.057	-0.041
	(0.044)	(0.050)	(0.060)	(0.076)
Value of home building	-0.008	-0.017	0.025	**0.033****
	(0.014)	(0.014)	(0.016)	(0.016)
Value of home content	0.017*	**0.043*****	-0.016	-0.002
	(0.010)	(0.011)	(0.014)	(0.015)
Length of residence	0.000	-0.003*	0.002	0.000
	(0.002)	(0.002)	(0.002)	(0.002)
Underfloor basement	0.007	**0.204*****	-0.099	**-0.193****
	(0.064)	(0.077)	(0.065)	(0.086)
Worry about flooding	0.017	**0.040****	0.040*	-0.003
	(0.015)	(0.016)	(0.021)	(0.023)
Perceived flood probability	-0.005	-0.186*	0.167	0.192
	(0.090)	(0.105)	(0.115)	(0.153)

Perceived flood impact	0.013	0.003	-0.006	0.019
	(0.010)	(0.012)	(0.013)	(0.013)
Risk taking	-0.004	0.005	0.007	0.013
	(0.007)	(0.009)	(0.009)	(0.011)
Internal locus of control	0.005	-0.011	0.013	0.000
	(0.009)	(0.009)	(0.010)	(0.012)
Regret of no insurance	**0.048*** **	0.033*	**0.073*** **	0.012
	(0.017)	(0.017)	(0.022)	(0.024)
Regret of having insurance	-0.005	-0.029*	-0.004	-0.026
	(0.016)	(0.015)	(0.018)	(0.019)
Social norm for insurance uptake	**0.059*** **	**0.080*** **	**0.093*** **	**0.106*** **
	(0.018)	(0.019)	(0.021)	(0.022)
Number of ex ante risk reduction measures	**0.043*** **	-0.013	**0.027** **	0.013
	(0.010)	(0.013)	(0.012)	(0.013)
Premium discount for flood risk mitigation			0.103*	-0.073
			(0.060)	(0.083)
Trouble purchasing flood insurance			0.044	-0.040
			(0.062)	(0.077)
Financial difficulty due to COVID-19	-0.076*	-0.104*	-0.098*	**-0.255*** **
	(0.044)	(0.055)	(0.058)	(0.070)
Trust in government flood policies	0.015	-0.034	0.023	0.017
	(0.023)	(0.023)	(0.027)	(0.031)
Observations	340	360	335	342

Note: Robust standard errors in parentheses. *** p<0.01, ** p<0.05. The table reports average marginal effects.

The major research question is to understand how the determinants of insurance coverage purchase varies across different flood policyholder types. The table below shows the Multinomial Probit model results across the four types of flood policyholders for Survey 4.

Some factors that are not significant at the aggregated level of flood insurance purchase may become significant for specific policyholder types because these factors only affect these types of policyholders. For example, having a basement does not affect the overall flood insurance uptake but positively affects the voluntary purchase of private flood insurance products. This may be explained by the fact that the NFIP policy does not cover the contents in the basement so that individuals must obtain the basement coverage from a private flood insurance policy. Being a female reduces the probability of voluntarily purchasing an NFIP policy but doesn't affect the other three types. The internal locus of control negatively impacts the voluntary purchase of the private flood insurance product. This group of policyholders has

the lightest pressure on purchasing flood insurance because they are not mandated, and their communities may not participate in the NFIP. As a result, if their purchase behavior may be negatively impacted when they perceive that they have strong control over the result of life events.

Some factors have different impacts on the four types of flood policyholders. The value of contents positively impacts all but the type of mandatory NFIP purchase. The worry about flooding and the financial pressure due to COVID-19 do not impact the type of mandatory NFIP purchase either. When individuals are mandated to purchase flood insurance and buy an NFIP policy, they could be insensitive to the home/contents value, their flood risk perceptions, and their financial issues. The number of ex-ante mitigation measures implemented only affects the purchase likelihood of the mandatory private product type. The trust in the government's ability to deal with flood risk positively impacts the mandatory purchase of an NFIP policy and negatively impacts the voluntary purchase of an NFIP policy. The individuals who are not mandated to buy flood insurance may have a lower incentive to purchase flood insurance if the local government is effectively dealing with the flood events.

Regarding other factors, the social norm of purchasing flood insurance is the only factor that has the same (positive) impact on all flood policyholder types. Both the mandatory and the voluntary purchase of an NFIP policy are affected by the regret of having no flood insurance when flooded. The voluntary purchase of a private flood product is negatively affected by the regret of having flood insurance when there was no flood.

Table 23: Multinomial Probit Model of Flood Insurance Purchase by Policyholder Types (Survey 4)

	none (base)	mandatory purchase of NFIP	mandatory purchase of a private product	voluntary purchase of NFIP	voluntary purchase of a private product
Age		0.004	-0.023*	0.016*	0.017*
		(0.010)	(0.013)	(0.009)	(0.010)
Education		0.232	-0.020	0.096	-0.057
		(0.149)	(0.186)	(0.161)	(0.147)
Income		-0.122	-0.170	-0.157	-0.151
		(0.154)	(0.155)	(0.146)	(0.154)
Female		0.344	-0.170	**-0.542****	-0.514*
		(0.318)	(0.374)	(0.268)	(0.309)
House owner		0.109	0.378	0.372	-0.231
		(0.405)	(0.420)	(0.360)	(0.396)
Value of home building		0.089	**-0.334****	-0.199*	-0.026
		(0.098)	(0.130)	(0.105)	(0.108)
Value of home content		0.006	**0.337*****	**0.288*****	**0.213*****

	(0.093)	(0.098)	(0.080)	(0.082)
Length of residence	0.009	-0.069*	-0.020	-0.015
	(0.016)	(0.036)	(0.014)	(0.016)
Underfloor basement	-61.191	0.334	0.928	**1.359****
	(0.000)	(0.468)	(0.630)	(0.540)
Worry about flooding	-0.042	**0.370*****	**0.319****	0.180
	(0.156)	(0.130)	(0.130)	(0.115)
Perceived flood probability	0.344	-0.051	-1.226	-0.737
	(1.009)	(0.754)	(0.814)	(0.586)
Perceived flood impact	-0.008	0.181*	0.003	0.102
	(0.088)	(0.098)	(0.088)	(0.088)
Risk taking	0.012	-0.056	0.040	0.009
	(0.058)	(0.075)	(0.070)	(0.059)
Internal locus of control	0.090	0.047	-0.015	**-0.136****
	(0.070)	(0.092)	(0.071)	(0.065)
Regret of no insurance	**0.415*****	0.206	**0.403*****	0.132
	(0.136)	(0.191)	(0.117)	(0.149)
Regret of having insurance	**-0.292****	0.261*	-0.142	**-0.256****
	(0.138)	(0.141)	(0.104)	(0.126)
Social norm for insurance uptake	**0.474*****	**0.422****	**0.562*****	**0.485*****
	(0.142)	(0.166)	(0.152)	(0.167)
Number of ex ante risk reduction measures	0.115	**0.609*****	-0.084	0.003
	(0.099)	(0.113)	(0.091)	(0.092)
Financial difficulty due to COVID-19	-0.668	**-0.916****	**-1.043****	-0.235
	(0.413)	(0.358)	(0.408)	(0.394)
Trust in government flood policies	**0.356****	-0.167	**-0.416****	-0.025
	(0.159)	(0.231)	(0.184)	(0.186)
Observations	413	413	413	413

Note: Robust standard errors in parentheses. *** p<0.01, ** p<0.05. This table reports log-odds ratios.

The Multinomial Probit model results across flood policyholder types for Survey 5 have some similar patterns. The difference mainly arises from the different factors of flood insurance uptake for Surveys 4 and 5.

Like Survey 4, we observe that having a basement negatively impacts the voluntary purchase of an NFIP policy. Individuals must obtain basement coverage from a private flood insurance product. The only common factor for all flood policyholder types is the social norm of purchasing flood insurance. The mandated purchase of an NFIP policy is not driven by the value of building and contents, the demographic characteristics, and the individuals' financial difficulty. However, the worry about flooding has a significant

and positive effect on the type of mandatory NFIP purchase for Survey 5. The regret of having no flood insurance affects both the mandatory and voluntary purchases of the NFIP policy.

Table 24: Multinomial Probit Model of Flood Insurance Purchase by Policyholder Types (Survey 5)

	none (base)	mandatory purchase of NFIP	mandatory purchase of a private product	voluntary purchase of NFIP	voluntary purchase of a private product
Age		-0.001	**-0.020****	-0.009	-0.005
		(0.008)	(0.010)	(0.009)	(0.009)
Education		0.194	0.064	0.016	**0.269****
		(0.149)	(0.144)	(0.133)	(0.120)
Income		0.020	-0.053	-0.003	-0.099
		(0.130)	(0.139)	(0.132)	(0.115)
Female		0.050	-0.073	-0.072	0.049
		(0.263)	(0.260)	(0.256)	(0.240)
House owner		-0.072	0.327	0.378	-0.496
		(0.354)	(0.398)	(0.447)	(0.361)
Value of home building		0.147	0.150*	**0.395*****	0.018
		(0.099)	(0.087)	(0.096)	(0.080)
Value of home content		-0.141*	-0.095	-0.075	0.079
		(0.076)	(0.087)	(0.079)	(0.074)
Length of residence		0.024*	-0.002	-0.005	0.003
		(0.013)	(0.013)	(0.015)	(0.012)
Underfloor basement		-0.653*	-0.862*	**-0.870****	-0.631
		(0.380)	(0.454)	(0.437)	(0.467)
Worry about flooding		**0.321*****	0.164	0.181	-0.110
		(0.119)	(0.126)	(0.116)	(0.115)
Perceived flood probability		0.451	0.586	**1.591****	0.447
		(0.680)	(0.666)	(0.778)	(0.797)
Perceived flood impact		-0.085	0.020	0.095	0.084
		(0.085)	(0.080)	(0.073)	(0.070)
Risk taking		0.079	-0.004	-0.066	0.101*
		(0.060)	(0.050)	(0.061)	(0.056)
Internal locus of control		0.063	0.066	**0.228*****	-0.065
		(0.060)	(0.063)	(0.073)	(0.060)
Regret of no insurance		**0.552*****	0.160	**0.376*****	-0.086
		(0.187)	(0.130)	(0.126)	(0.113)
Regret of having insurance		0.007	-0.147	-0.073	-0.100
		(0.097)	(0.104)	(0.108)	(0.096)
Social norm for insurance uptake		**0.432*****	**0.593*****	**0.342****	**0.447*****
		(0.140)	(0.147)	(0.141)	(0.112)
Number of ex ante risk reduction measures		**0.228*****	0.092	0.056	0.062
		(0.075)	(0.075)	(0.075)	(0.064)
Premium discount for		0.228	0.629	-0.534	0.220

flood risk mitigation				
	(0.369)	(0.389)	(0.492)	(0.371)
Trouble purchasing flood insurance	0.377	0.362	0.344	-0.827*
	(0.337)	(0.404)	(0.440)	(0.462)
Financial difficulty due to COVID-19	-0.321	**-0.937****	-0.760*	**-1.231*****
	(0.313)	(0.406)	(0.452)	(0.383)
Trust in government flood policies	0.250	-0.164	0.083	0.010
	(0.172)	(0.158)	(0.142)	(0.156)
Observations	428	428	428	428

Note: Robust standard errors in parentheses. *** p<0.01, ** p<0.05. This table reports log-odds ratios.

5.3.3. Results by Wind Policyholder Types

For the windstorm insurance purchase, the wind-only policy type tends to be riskier than the homeowners' insurance type. The factor of being located in the high-wind risk areas (Citizen wind-only territory) positively affects the insurance uptake of both types but has a larger impact on the wind-only policy type. Being a homeowner positively affects the wind coverage uptake through the homeowners' insurance. Income positively affects the likelihood of purchasing the wind-only policy. Having financial difficulty due to COVID-19 positively affects the wind-only policy type possibly due to the outlier effect. The wind-only policy type only has 34 respondents. The positive effect of financial difficulty due to COVID-19 may be biased for this small sample.

Table 25: Multinomial Probit Model of Wind Coverage Purchase by Policyholder Types (Survey 4)

	none (base)	homeowners' insurance	wind-only policy
Age		0.010*	-0.012
		(0.006)	(0.010)
Education		-0.097	-0.212
		(0.092)	(0.161)
Income		0.069	**0.372****
		(0.086)	(0.149)
Female		-0.114	-0.115
		(0.181)	(0.291)
House owner		**1.055*****	-0.036
		(0.238)	(0.313)
Value of home building		0.025	0.157
		(0.065)	(0.109)
Value of home content		0.085*	-0.117*
		(0.050)	(0.067)
Length of residence		-0.014	0.012

	(0.009)	(0.014)
InWindonly_territory	**0.878****	**1.969*****
	(0.371)	(0.477)
Risk taking	0.018	0.066
	(0.037)	(0.062)
Internal locus of control	0.071*	-0.021
	(0.042)	(0.078)
Window protection	0.279	0.239
	(0.175)	(0.285)
Financial difficulty due to COVID-19	-0.408*	**0.935*****
	(0.233)	(0.333)
Observations	518	518

Note: Robust standard errors in parentheses. *** p<0.01, ** p<0.05. This table reports log-odds ratios.

For Survey 5, we can divide each of the previous two wind policyholder types into two categories based on where the individuals purchased the coverage. Compared to the type of homeowners' insurance from a private insurer, the other three types tend to be riskier customers. As a result, the right three types, except the type of homeowners' insurance from a private insurer, have an increased probability of purchasing windstorm coverage if they have had trouble getting or renewing the wind insurance due to an increase in disaster activities.

Similar to Survey 4, being a homeowner increases the wind coverage uptake in the form of homeowners' insurance from private insurers. Like the overall wind coverage uptake results, the new factors in Survey 5, the worry about windstorms, the premium discount for implementing mitigation measures, and the financial difficulty due to COVID-19 significantly, affect most or all wind policyholder types. The insurance purchase from private insurers is especially affected by higher age. The high-risk type of purchasing the wind-only policy from Citizens is distinctly driven by the usage of the hip roof.

Table 26: Multinomial Probit Model of Wind Coverage Purchase by Policyholder Types (Survey 5)

	none (base)	homeowners' insurance from a private insurer	wind-only coverage from a private insurer	homeowners' insurance from Citizens	wind-only policy from Citizens
Age		**0.022*****	**0.026*****	0.008	-0.017
		(0.006)	(0.007)	(0.008)	(0.012)
Education		-0.050	0.110	0.049	0.526*
		(0.103)	(0.108)	(0.120)	(0.285)
Income		-0.098	-0.047	-0.049	-0.369*
		(0.098)	(0.108)	(0.120)	(0.213)

Female	-0.191	0.100	0.292	**1.184****
	(0.199)	(0.226)	(0.235)	(0.500)
House owner	**0.810*****	-0.056	0.391	0.328
	(0.285)	(0.325)	(0.322)	(0.536)
Value of home building	0.041	0.023	0.006	-0.056
	(0.069)	(0.073)	(0.079)	(0.166)
Value of home content	-0.040	-0.053	-0.060	-0.046
	(0.062)	(0.067)	(0.070)	(0.155)
Length of residence	**-0.020****	-0.001	0.005	**-0.076****
	(0.010)	(0.010)	(0.011)	(0.031)
Worry about windstorm	**0.285*****	**0.245****	**0.427*****	0.176
	(0.090)	(0.100)	(0.129)	(0.188)
Perceived wind impact	0.043	0.069	0.021	-0.140
	(0.057)	(0.066)	(0.069)	(0.148)
Risk taking	-0.028	-0.057	0.032	0.190*
	(0.043)	(0.045)	(0.053)	(0.113)
Internal locus of control	**0.148*****	0.020	0.042	-0.032
	(0.051)	(0.047)	(0.058)	(0.081)
Window protection	-0.084	0.045	0.004	-0.448
	(0.211)	(0.238)	(0.259)	(0.623)
Roof retrofit	0.297	0.411	-0.058	-0.443
	(0.228)	(0.267)	(0.298)	(0.581)
Hip roof	0.067	0.170	0.373	**1.494****
	(0.211)	(0.233)	(0.276)	(0.707)
Premium discount for wind risk mitigation	**0.824*****	**0.726*****	**0.559****	**1.285*****
	(0.229)	(0.248)	(0.267)	(0.477)
Trouble purchasing homeowners insurance	0.145	**0.690****	**0.647****	**1.391*****
	(0.282)	(0.289)	(0.295)	(0.525)
Financial difficulty due to COVID-19	**-0.700*****	**-0.705****	**-0.705****	-0.408
	(0.271)	(0.305)	(0.289)	(0.480)
Observations	503	503	503	503

Note: Robust standard errors in parentheses. *** p<0.01, ** p<0.05. This table reports log-odds ratios.

6. Discussion and conclusions

Inadequate insurance coverage and disaster preparation are major obstacles for society to deal with increasing risk posed by hurricanes. Surrounded by seas and regularly impacted by hurricanes, Florida is extremely vulnerable to flood and wind damage. Although it has the highest flood insurance market penetration rate in the US (35% NFIP and 3% private sector policies in 2018), there is still a considerable coverage gap (Lingle and Kousky, 2018). Besides insurance coverage to limit the financial vulnerability of households to hurricane damage, by implementing risk-reduction measures households can to a certain extent prevent damage. With climate change causing rising sea-temperatures and a higher intensity of

hurricanes in the US (Marsooli et al., 2019), it becomes increasingly important that the uptake of both these measures rises.

By conducting and analyzing two surveys of households in Florida, in this study we sought to explore motives and characteristics of households with regard to the uptake of flood insurance and risk reduction measures during the direct threat of Hurricane Eta in November 2020 and in June 2021 at the start of the hurricane season. Moreover, the decision to apply emergency preparation measures such as sandbags, flood shields, or moving expensive belongings to less flood prone parts of the house, was of particular interest. The reason for the particular interest in studying this behavior in both surveys is that households may behave differently in situations when a threat is looming compared to when there is no perceived threat of a hurricane. Therefore, the drivers of the uptake of emergency measures in a situation with no threat may be different, as these measures have to be implemented shortly before a hurricane is projected to make impact which may depend on individual risk perceptions at that time.

Using multiple regression models, in this study we find that insurance uptake and the application of ex ante risk reduction measures, as well as emergency preparation measures, are complementary to flood insurance uptake. This is in contrast to results found by Botzen et al. (2019) for a sample of household in New York City, who conclude advantageous selection for ex ante risk reduction measures, which have to be implemented well before a hurricane strikes, while moral hazard was found for emergency preparation, meaning these measures are substitutes to flood insurance. A feasible explanation for this difference is that there was no immediate threat of flooding at the time data was collected in Botzen et al. (2019), which may suggest that individuals have less incentive to prepare to limit potential damage. One finding that may explain the higher uptake of emergency measures for insured households is that individuals that take both measures indicated to perceive a social norm to do this. Consequently, individuals that take neither of these measures state to perceive no such norm. Advantageous selection for ex ante risk reduction measures seems to be largely driven by the perceived level of worry about flooding, as well as education. Furthermore, by categorizing respondents as cautious when they take insurance and multiple risk reduction measures, and uncautious when they take none, we find that cautious individuals are more likely to worry about flooding, have experience with flooding, and perceive a social norm. Uncautious individuals indicate to not experience any of these.

The applied statistical method for the 4th survey data, collected before hurricane Eta, is replicated for the data collected in the 5th survey, which was completed before the 2021 hurricane (26th of May until 7th June). This was done to observe potential changes in the driving factors of emergency preparedness

measures and to test whether advantageous selection regarding emergency preparedness measures that was found in Survey 4 still holds under a low-threat situation. As the previous hurricane threat was already some time ago, individuals may be less aware of flood risk, which may explain a lower willingness to apply emergency preparedness measures. Contrary to these prospects, the results of Survey 5 largely substantiate those of Survey 4. We find ex ante risk reduction- and emergency preparedness measures to be complementary to insurance uptake. Significant psychological and socio-economic variables that drive insurance uptake are also approximately similar. Some differences include that homeowners are found to be significantly more likely to have insurance and older respondent are less likely to have insurance. Besides this, some effect sizes are found to be higher using the 5th survey data, and significance levels also tend to be slightly higher. Unlike in Survey 4, we find no significant interaction effects that explain the observed advantageous selection regarding emergency preparedness measures and insurance uptake.

Because the uptake of flood insurance and risk reduction measures are complements in our dataset, we conclude that moral hazard is not an issue with individuals that are currently insured. This finding suggests there are opportunities for stimulating the taking of risk reduction measures by policyholders through flood and windstorm insurance, for example by offering premium discounts to policyholders who take risk reduction measures, or information provision by insurers (Botzen, 2021). As we find advantageous selection to be largely driven by social norms and concern about flooding, an approach to increase the uptake of both measures is to raise these perceptions. Concern about flooding can be enhanced by raising flood risk awareness through, for example, advertisement campaigns. Communication on flood risk should not solely focus on giving information about flood probabilities through the FEMA flood zone classification, but also stress potential consequences. Moreover, framing flood-probabilities over longer time horizons, such as 40 years, may have the effect that people pay more attention to the risk (Bradt, 2019). Social norms for uptake of insurance and risk reduction measures can be strengthened by making it clear whether others in the neighborhood have taken these measures if the majority have done so. The NFIP has already taken such action through the Community Rating System (CRS), where households can reduce their flood insurance premium by taking certain communal actions to reduce flood risk. Perhaps, this can be improved by triggering social norms for disaster preparation, for instance by giving households information on disaster preparedness by others and signaling that this is the right thing to do (Mol et al., 2021).

With regards to evacuation intentions, the results of our surveys of coastal residents in Florida conducted in November 2020 and the start of the 2021 hurricane season show that hurricane preparedness is

affected by the pandemic. Older people, who are more concerned about the consequences of becoming infected by COVID-19, state lower evacuation intentions. This is apparent from evacuation intentions elicited at the end of the hurricane season during the threat of Hurricane Eta as well as at the start of the 2021 hurricane season, although this effect has become slightly smaller. This influence of COVID-19 on evacuation should be taken into account by policies aimed at improving hurricane preparedness during a pandemic with a disease for which older people are more vulnerable. Adequate risk communication could be an important component of adaptation strategies to improve individual hurricane preparedness. For instance, our analyses of hurricane preparedness activities during Hurricane Dorian showed that risk awareness was an important driver of these activities (Botzen et al. 2020). Our survey at the start of the hurricane season reveals that risk communication by state governments, insurers, and insurance regulators reached a large number of respondents.[16] Given the large influence of COVID-19 on evacuation intentions, it is critical to refocus risk communication activities in times when the hurricane season coincides with a pandemic towards ensuring that people can safely evacuate by minimizing health risks. Examples during the COVID-19 pandemic are: including COVID-19 mitigation measures in hurricane preparedness kits, such as hand sanitizer and mouth masks, abiding by social distancing rules during an evacuation, and planning ahead to identify safe evacuation locations. Moreover, governments and agencies can send more tailored communication messages to older people to alleviate their concerns over COVID-19 or improve their flood risk perceptions. Emergency management policies should create safe evacuation shelters where COVID-19 risks are well controlled and communicate their COVID-19 measures to the public to increase people's confidence in shelters' safety.

We also conducted regression models to analyze the determinants of insurance coverage purchase of different policyholder types because homeowners may exhibit a distinct demand function for a specific insurance policy depending on their locations, home characteristics, and other perceptions. We use a decision tree to illustrate the complex insurance purchase process and show how individuals can end up being different policyholder types. Through the regression analyses, we find that some factors that are not significant at the aggregated level of insurance purchase may become significant for specific policyholder types. For example, having a basement does not affect the overall flood insurance uptake but positively affects the voluntary purchase of private flood insurance products (Survey 4) or negatively impacts the voluntary purchase of an NFIP policy (Survey 5). This may be explained by the fact that the

[16] Approximately 50% consulted information from these agencies to prepare for the hurricane season.

NFIP policy does not cover the contents in the basement so that individuals must obtain the basement coverage from a private flood insurance policy.

Many factors have different impacts on the four types of flood policyholders. For both Surveys 4 and 5, the mandated purchase of an NFIP policy is not driven by the value of building and contents, the demographic characteristics, and the individuals' financial difficulty due to COVID-19, whereas these factors can impact the voluntary purchase of flood insurance. When individuals are mandated to purchase flood insurance, they could be insensitive to the home/contents value and their financial issues. For Survey 4, the trust in the government's ability to deal with flood risk positively impacts the mandatory purchase of an NFIP policy and negatively impacts the voluntary purchase of an NFIP policy. The individuals who are not mandated to buy flood insurance may have a lower incentive to purchase flood insurance if the local government is effectively dealing with the flood events. The number of ex-ante mitigation measures implemented only affects the likelihood of mandatory insurance purchase. For both Surveys 4 and 5, the social norm of purchasing flood insurance is the only factor that has the same (positive) impact on all flood policyholder types.

We find different determinants for the purchase of windstorm coverage. Being a homeowner significantly increases the probability of having windstorm coverage especially for the homeowners' insurance type. This may be because many tenants do not purchase renters' insurance. The objective windstorm risk is a strong factor that positively affects the purchase of windstorm insurance coverage, and the effect is stronger for the wind-only policy type. Individuals in high-risk wind areas may be more concerned about the windstorm damage and more actively purchase insurance protection. Compared to the type of homeowners' insurance from a private insurer, the residual market buyers tend to be riskier customers and, as a result, have an increased probability of purchasing windstorm coverage if they have had trouble getting or renewing the wind insurance due to an increase in disaster activities (Survey 5). The type of purchasing a wind-only policy from Citizens is distinctly and positively driven by the usage of the hip roof and the only type that is not affected by the financial difficulty due to COVID-19. In Survey 5, the premium discount for wind mitigation measures is the only factor that affects all four types of wind policyholders.

As property insurance is complex in the U.S., the decision trees reveal the hidden information behind the insurance purchase process and help readers better understand the flood and hurricane insurance decisions and the resulting policyholder types. The regression results of various policyholder types' insurance purchase behavior may shed light on the policies reinforcing the availability of flood and hurricane insurance. Through this study, public policy officials may better understand the incentives of

different policyholder types to purchase insurance and make policies that better target different types of homeowners.

Bibliography

Aguinis, H., 1995. Statistical power problems with moderated multiple regression in management research. Journal of Management 21, 1141–1158. https://doi.org/10.1016/0149-2063(95)90026-8

AON (2020). Global Catastrophe Recap: November 2020. Available online at: http://thoughtleadership.aon.com/documents/20201210_analytics-if-november-global-recap.pdf (last accessed 2 July 2021).

Baron, R.M., Kenny, D.A., 1986. The moderator–mediator variable distinction in social psychological research: Conceptual, strategic, and statistical considerations. Journal of Personality and Social Psychology 51, 1173–1182. https://doi.org/10.1037/0022-3514.51.6.1173

Blackwell, J., 2020. Record-breaking Atlantic hurricane season draws to an end [WWW Document]. NAtional Oceanic and Atmospheric Administration. URL https://www.noaa.gov/media-release/record-breaking-atlantic-hurricane-season-draws-to-end (accessed 5.27.21).

Botzen, W.J.W., 2021. Economics of Insurance Against Natural Disaster Risks, in: Oxford Research Encyclopedia of Environmental Science. Oxford University Press. https://doi.org/10.1093/acrefore/9780199389414.013.712

Botzen, W.J.W., Kunreuther, H., Michel-Kerjan, E., 2019. Protecting against disaster risks: Why insurance and prevention may be complements. J Risk Uncertain 59, 151–169. https://doi.org/10.1007/s11166-019-09312-6

Botzen, W.J.W., Mol, J.M., Robinson, P.J., Zhang, J., Czajkowski, J., 2020. Individual Hurricane Preparedness During the COVID-19 Pandemic: Insights for Risk Communication and Emergency Management Policies. SSRN Journal. https://doi.org/10.2139/ssrn.3699277

Botzen, W. J. W., Robinson, P.J., Mol, J.M., Czajkowski, J., 2020. Improving individual preparedness for natural disasters: Lessons learned from longitudinal survey data collected from Florida during and after Hurricane Dorian. Institute for Environmental Studies - Vrije Universiteit, Amsterdam.

Bradt, J., 2019. Comparing the effects of behaviorally informed interventions on flood insurance demand: an experimental analysis of 'boosts' and 'nudges.' Behav. Public Policy 1–31. https://doi.org/10.1017/bpp.2019.31

Bubeck, P., Botzen, W.J.W., Aerts, J.C.J.H., 2012. A Review of Risk Perceptions and Other Factors that Influence Flood Mitigation Behavior: Review of Flood Risk Perceptions. Risk Analysis 32, 1481–1495. https://doi.org/10.1111/j.1539-6924.2011.01783.x

de Meza, D., Webb, D.C., 2001. Advantageous Selection in Insurance Markets. The RAND Journal of Economics 32, 249. https://doi.org/10.2307/2696408

FEMA (July 2020). Special Flood Hazard Area (SFHA). Available online at: https://www.fema.gov/glossary/special-flood-hazard-area-sfha (last accessed 2 July 2021).

Federal Emergency Management Agency (FEMA). (n.d.). *National Flood Insurance Program*. Retrieved February 24, 2021, from https://www.fema.gov/flood-insurance.

Federal Emergency Management Agency (FEMA). (2020). *Flood Insurance: One Small Action Can Protect You From A Huge Problem*. Retrieved from https://agents.floodsmart.gov/sites/default/files/preferred-risk-policy-homeowners-renters_fact-sheet_jul20.pdf.

Hudson, P., Wouter Botzen, W.J., Czajkowski, J., Kreibich, H., 2017. Moral Hazard in Natural Disaster Insurance Markets: Empirical Evidence from Germany and the United States. Land Economics 93, 179–208. https://doi.org/10.3368/le.93.2.179

Hurricane Eta Drenches Central America, Then Meansers Toward Florida [WWW Document], 2020. . Weather.com. URL https://weather.com/storms/hurricane/news/2020-11-12-tropical-storm-eta-landfall-florida-southeast-flooding-rain (accessed 5.31.21).

Insurance Information Institute (III). (2020). *Background on: Hurricane and windstorm deductibles*. Retrieved October 5, 2020, from https://www.iii.org/article/background-on-hurricane-and-windstorm-deductibles.

Insurance Journal (14 December 2020). With Economic Damages of $9B, Hurricanes Eta and Iota Topped Off Record Year. Available online at: https://www.insurancejournal.com/news/international/2020/12/14/593841.htm (last accessed 2 July 2021).

Kunreuther, H., Pauly, M., 2004. Neglecting Disaster: Why Don't People Insure Against Large Losses? Journal of Risk and Uncertainty 28, 5–21. https://doi.org/10.1023/B:RISK.0000009433.25126.87

Lingle, B., Kousky, C., 2018. FLORIDA'S PRIVATE RESIDENTIAL FLOOD INSURANCE MARKET. Risk Management and Decision Processes Center, University of Pennsylvania.

Marsooli, R., Lin, N., Emanuel, K., Feng, K., 2019. Climate change exacerbates hurricane flood hazards along US Atlantic and Gulf Coasts in spatially varying patterns. Nat Commun 10, 3785. https://doi.org/10.1038/s41467-019-11755-z

Mol, J.M., Botzen, W.J.W., Blasch, J.E., 2020. Behavioral motivations for self-insurance under different disaster risk insurance schemes. Journal of Economic Behavior & Organization 180, 967–991. https://doi.org/10.1016/j.jebo.2018.12.007

Mol, J.M., Botzen, W.J.W., Blasch, J.E., Kranzler, E.C., Kunreuther, H.C., 2021. All by myself? Testing descriptive social norm-nudges to increase flood preparedness among homeowners. Behav. Public Policy 1–33. https://doi.org/10.1017/bpp.2021.17

Waugh, W.L., Smith, R.B., 2006. Economic Development and Reconstruction on the Gulf After Katrina. Economic Development Quarterly 20, 211–218. https://doi.org/10.1177/0891242406289287

Appendix

End of Hurricane Season Survey

(Survey 4, October 2020)

Q1 Are you taking this survey at your home?

□ 1 Yes

□ 2 No

[IF THE ANSWER IS 1, THEN SKIP TO QUESTION 2]

Q1a In which of the following counties do you live?

□ 1 Brevard County

□ 2 Broward County

□ 3 Duval County

□ 4 Flagler County

□ 5 Indian River County

□ 6 Martin County

□ 7 Miami-Dade County

□ 8 Monroe County

□ 9 Nassau County

□ 10 Palm Beach County

□ 11 St. John's County

□ 12 St. Lucie County

□ 13 Volusia County

□ 14 Osceola County

□ 15 Seminole County

□ 16 Orange County

□ 17 Okeechobee County

□ 18 Polk County

□ 19 Highlands County

□ 20 Alachua County

□ 21 Other: _____

Q1b Do you live in a Special Flood Hazard area (SFHA), i.e., an area with a 1-percent annual chance of flooding?

□ 1 Yes

□ 2 No

□ 3 Don't know

Q1c What is your street address?

……

□ Rather not say

Q1d What is your zip-code?

……

□ Rather not say

We will next ask a few questions about your general attitudes and preferences.

Q2 Using a 10-point scale, where 0 means you have no control and 10 means you have complete control, what number reflects how much control you think you have over how your life turns out?

Control Score ____

□ Don't know

Q3 Using a 10-point scale, where 0 means you are not willing to take any risks and 10 means you are very willing to take risks, what number reflects how much risk you are willing to take?

Risk Score ____

□ Don't know

Q4 When it comes to financial decisions, how would you assess your willingness to give up something today in order to benefit from that in the future?

Please use a scale from 0 to 10, where 0 means you are "completely unwilling to give up something today" and a 10 means you are "very willing to give up something today". You can also use the values in-between to indicate where you fall on the scale.

Score ____

□ Don't know

Q5 Using a 10-point scale, where 0 means totally unhappy and 10 means totally happy, how satisfied are you with your life as a whole?

Happiness Score ____

□ Don't know

Q6 To what extent do you think it is important to do things for the benefit of others and society even if they have some costs to you personally?

□ 1 Very much so

□ 2 To some extent

□ 3 Only a little

□ 4 Not at all

□ 5 Don't know

We will now ask a few questions about flood risks. Please keep in mind that we are talking here about **floods caused by natural disasters**.

Q7 Please tell me if you strongly agree, agree, neither agree nor disagree, disagree or strongly disagree with the following: I am worried about the danger of a flood at my current residence.

□ 1 Strongly agree

□ 2 Agree

□ 3 Neither agree nor disagree

□ 4 Disagree

□ 5 Strongly disagree

□ 6 Not sure

Q8 What is your best estimate of how often a flood will occur at your home?

□ 1 More often than 1 in 10 years

□ 2 Exactly 1 in 10 years

□ 3 Between 1 in 10 years and 1 in 100 years

□ 4 Exactly 1 in 100 years

□ 5 Between 1 in 100 years and 1 in 1000 years

□ 6 Exactly 1 in 1000 years

□ 7 Less often than 1 in 1000 years

□ 8 Not sure

[IF THE ANSWER IS 2, 4, 6 or 8, THEN SKIP TO QUESTION 9]

[IF THE ANSWER IS 1, THEN SKIP TO QUESTION 8a]

[IF THE ANSWER IS 3, THEN SKIP TO QUESTION 8b]

[IF THE ANSWER IS 5, THEN SKIP TO QUESTION 8c]

[IF THE ANSWER IS 7, THEN SKIP TO QUESTION 8d]

Q8a So you expect that a flood occurs at your home more often than 1 in 10 years. What is your best estimate of how often a flood will occur at your home? Once every (HOW MANY) years?

…….. years

□ Don't know

Q8b So you expect that a flood occurs at your home between 1 in 10 years and 1 in 100 years. What is your best estimate of how often a flood will occur at your home? Once every (HOW MANY) years?

…….. years

□ Don't know

Q8c So you expect that a flood occurs at your home between 1 in 100 years and 1 in 1000 years. What is your best estimate of how often a flood will occur at your home? Once every (HOW MANY) years?

…….. years

□ Don't know

Q8d So you expect that a flood occurs at your home less often than 1 in 1000 years. What is your best estimate of how often a flood will occur at your home? Once every (HOW MANY) years?

…….. years

□ Never

□ Don't know

Q9 Please tell me if you strongly agree, agree, neither agree nor disagree, disagree or strongly disagree with the following: The probability of flooding is so low that I am not concerned about the consequences of a flood.

- □ 1 Strongly agree
- □ 2 Agree
- □ 3 Neither agree nor disagree
- □ 4 Disagree
- □ 5 Strongly disagree
- □ 6 Not sure

Q10 What would it cost to repair the damage to your home and its contents if your home did flood?

- □ 1 Less than $10,000
- □ 2 $10,000 to $24,999
- □ 3 $25,000 to $44,999
- □ 4 $45,000 to $74,999
- □ 5 $75,000 to $124,999
- □ 6 $125,000 to $199,999
- □ 7 $200,000 or more
- □ 8 Don’t know

Q11 In the next 10 years will climate change increase or decrease the risk of your home flooding or will it have no impact?

- □ 1 Increase greatly
- □ 2 Increase slightly
- □ 3 No impact

□ 4 Decrease slightly

□ 5 Decrease greatly

□ 6 Not sure

Q12 Have you heard about any tropical storms or hurricanes currently active that could pose a threat to your home?

□ 1 Yes

□ 2 No

[IF THE ANSWER IS 2, THEN SKIP TO QUESTION 21]

Q13 What is the first letter of this tropical storm or hurricane?

Letter _____

□ Don't know

Q14 The last you heard, was it a tropical storm or a hurricane?

□ 1 Tropical Storm

□ 2 Hurricane

□ 3 Don't know

[IF THE ANSWER IS 1 OR 3, THEN SKIP TO QUESTION 16]

Q15 Hurricanes are rated on a five category scale, where Category 1 is the weakest and Category 5 is the strongest. The last you heard, what was the category of the hurricane that's out there now?

□ 1 Category 1

□ 2 Category 2

□ 3 Category 3

□ 4 Category 4

□ 5 Category 5

□ 6 Don't know

Q16 How certain are you that the area where you are living will be affected by this storm?

□ 1 You are certain that your area will be affected

□ 2 You think your area will be affected, but you are not sure

□ 3 You don't think your area will be affected, but you are not sure

□ 4 You are certain that your area will not be affected

□ 5 Don't know

Q17 Please tell me if you strongly agree, agree, neither agree nor disagree, disagree or strongly disagree with the following: I am worried about the storm causing damage to my home or home contents.

□ 1 Strongly agree

□ 2 Agree

□ 3 Neither agree nor disagree

□ 4 Disagree

□ 5 Strongly disagree

□ 6 Not sure

Q18 Please tell me whether you are currently very likely, likely, unlikely or very unlikely to evacuate to a safer place.

□ 1 Very likely

□ 2 Likely

□ 3 Unlikely

□ 4 Very unlikely

□ 5 Don't know

Q19 Which of the following channels is your primary source to stay updated about the storm?

□ 1 Facebook

□ 2 Twitter

□ 3 Instagram

□ 4 Other internet sites

□ 5 Face-to-face communication

□ 6 TV

□ 7 Radio

□ 8 Other: …….

Q20 Did you share any information on social media about the storm?

□ 1 Yes

□ 2 No

□ 3 Don't know

Q21 How much do you trust the ability of government officials to limit flood risk where you live, for example by maintaining levees and enforcing building codes? Do you:

□ 1 Trust them completely

□ 2 Trust them somewhat

□ 3 Not trust them very much

□ 4 Not trust them at all

□ 5 Don't know

Q22 Are you aware of what letter storm we are on for the 2020 hurricane season?

Letter _____

□ Don't know

Q23 Was the hurricane activity of 2020 above or below the average of the past 30 years?

□ 1 Above average

□ 2 Average

□ 3 Below average

□ 4 Don't know

Q24 How effective do you think the response from the federal organization FEMA has been this hurricane season compared with the previous year?

□ 1 Much more effective

□ 2 More effective

□ 3 Just as effective

□ 4 Less effective

□ 5 Much less effective

□ 6 No idea

Q25 How effective do you think the response from your state government has been this hurricane season compared with the previous year?

□ 1 Much more effective

□ 2 More effective

□ 3 Just as effective

□ 4 Less effective

□ 5 Much less effective

□ 6 No idea

Q26 Did you take any of the following measures to prepare for this year's hurricane season? Select all that apply.

□ 1 Create a home inventory, i.e., create a list of your home contents

□ 2 Know your insurer contact information

□ 3 Gather other important documents

□ 4 Put together a hurricane preparedness kit

□ 5 None

Q27 Did you receive or consult any information about how to prepare for this hurricane season from your insurance company, insurance regulator, state government, or other agency? Select all that apply.

□ 1 No

□ 2 Yes, from my insurance company

□ 3 Yes, from my insurance regulator

□ 4 Yes, from my state government

□ 5 Yes, from another agency: _____

Q28 Please tell me if you strongly agree, agree, neither agree nor disagree, disagree or strongly disagree with the following: The coronavirus has disrupted my preparations for this year's hurricane season.

□ 1 Strongly agree

□ 2 Agree

□ 3 Neither agree nor disagree

□ 4 Disagree

□ 5 Strongly disagree

□ 6 Not sure

Q29 Are there any potential obstacles which may prevent you from evacuating during the threat of a hurricane? Select all that apply.

□ 1 Not owning a car

□ 2 Disability

□ 3 Job requirements

□ 4 Material possessions

□ 5 Stubborn family members

□ 6 No place to go

□ 7 Unable to pay for hotel costs

□ 8 A pet

□ 9 Staying in home to prevent coronavirus infections

□ 10 Other: ……

□ 11 No potential obstacles

Now I will ask a few questions about flood and windstorm insurance. Please keep in mind that we are talking here about insurance against natural disasters.

Q30 Flood risk is not covered in standard homeowners insurance policies, but a separate policy covering flood risk can be purchased from the National Flood Insurance Program (NFIP) or from a private company. Did you purchase such a separate flood insurance policy?

□ 1 Yes

□ 2 I plan to buy it in the next year

□ 3 No

□ 4 Don't know

[IF THE ANSWER IS 2, 3 or 4, THEN SKIP TO QUESTION 31]

Q30a Did you purchase flood insurance because it was mandatory?

□ 1 Yes

□ 2 No

□ 3 Don't know

Q30b How much is your flood insurance deductible for the building and for the building contents?

Building: $_____

Building contents: $_____

□ Don't know

Q30c As an alternative to the NFIP flood insurance policy, property owners may purchase a **private flood insurance product** as a stand-alone policy or as an endorsement to the homeowners insurance policy. Did you purchase any type of private flood insurance product?

□ 1 Yes

□ 2 No

[IF THE ANSWER IS 2, THEN SKIP TO QUESTION 31]

Q30d What are your reasons for purchasing a private flood insurance product? Select all that apply.

□ 1 I couldn't obtain flood insurance from the NFIP

□ 2 The NFIP flood insurance coverage is NOT enough to cover my losses

□ 3 The rate of the private flood insurance policy is cheaper than that of the NFIP policy

□ 4 The deductible or coverage choices of the private flood insurance policy are more flexible than the NFIP policy

□ 5 The underwriting process of the private flood insurance policy is simpler and quicker than the NFIP policy

□ 6 Other reason: _____

□ 7 Don't know

Q31 Windstorm damage is typically covered by standard homeowners insurance policies. Alternatively, a wind-only insurance policy is available in certain areas of Florida and covers solely damages from hail and windstorms.

Do you have insurance coverage that would pay for wind damages to your home and possessions?

□ 1 Yes, from a homeowners insurance policy

□ 2 Yes, from a wind-only insurance policy

□ 3 I plan to buy it in the next year

□ 4 No

□ 5 Not sure

[IF THE ANSWER IS 3, 4 or 5, THEN SKIP TO QUESTION 32]

Q31a Did you use any of the state information programs when you looked for windstorm insurance coverage? Select all that apply.

□ 1 Clearinghouse program

□ 2 Market Assistance Plan (FMAP)

□ 3 Homeowners Rate Comparison Tool (CHOICES)

□ 4 Other_____

□ 5 No

□ 6 Don't know

Q31b Both the homeowners and the wind-only insurance policies have a separate Hurricane Deductible for wind damages caused by hurricanes. How much is your Hurricane Deductible?

□ 1 A flat amount of $500

□ 2 2% of total insured value

□ 3 5% of total insured value

□ 4 10% of total insured value

□ 5 Don't know

Q31c Did you receive a premium discount for any mitigation activities that limit damage from wind? Select all that apply.

□ 1 Shutters to protect windows and doors from windborne debris

□ 2 Hip Roof (sloped on all four sides like a pyramid)

□ 3 Roof construction that meets the 2001 Florida Building Code

□ 4 Other_____

□ 5 No

□ 6 Don't know

Next, you will read actions that reduce flood or wind risk to your home. Please tell me if each has been implemented in your house.

Q32 Does your home have any sort of window protection such as shutters, plywood panels, or hurricane proof glass?

□ 1 Yes

□ 2 No

□ 3 Don't know

[IF THE ANSWER IS 2 or 3, THEN SKIP TO QUESTION 33]

Q32a Is the window protection:

□ 1 Permanent

□ 2 Temporary and it is in place now

□ 3 Temporary, but it is not in place now

□ 4 Don't know

Q33 Have you elevated your lowest floor above the expected flood level?

□ 1 Yes

□ 2 No

□ 3 Don't know

Q34 Do you have metal or wood flood shields or sand bags available?

□ 1 Yes

□ 2 No

□ 3 Don't know

[IF THE ANSWER IS 2 or 3, THEN SKIP TO QUESTION 35]

Q34a Did you install them to prepare for the coming storm, or do you plan to do this?

□ 1 I have installed them

□ 2 I am planning to install them

□ 3 I am not planning to install them

□ 4 Don't know

Q35 Have you sprayed or coated outside walls to waterproof them?

□ 1 Yes

□ 2 No

□ 3 Don't know

Q36 Have you installed a sump pump and/or a drainage system?

□ 1 Yes

□ 2 No

□ 3 Don't know

Q37 Have you used flood-resistant building materials?

□ 1 Yes

□ 2 No

□ 3 Don't know

Q38 Have you installed a water-resistant floor?

□ 1 Yes

□ 2 No

□ 3 Don't know

Q39 Have you installed electrical and central heating systems above potential flood levels?

□ 1 Yes

□ 2 No

□ 3 Don't know

Q40 Have you kept or moved expensive furniture or contents out of flood-prone parts of your home? Or do you plan to?

□ 1 Yes, I did

□ 2 I plan to

□ 3 No

□ 4 Don't know

Q41 Did you take any other measures to reduce flood or storm damage to your home?

□ 1 Yes, specify ……

□ 2 No

Q42 Did you receive any insurance premium discounts for implementing measures that reduce flood damage?

□ 1 Yes

□ 2 No

□ 3 Don't know

Q43 How effective do you think the following actions are in protecting your home and its contents against flooding?

	Very effective	Somewhat effective	Somewhat not effective	Not at all effective	Not sure
Elevating the lowest floor of your home					
Preventing flood waters from entering your home by using metal or wood water shields or sand bags, or installing a sump pump or drainage system					
Limiting damage once water enters your home by using flood-resistant building materials, installing a water-resistant floor, or installing electrical and central heating systems above potential flood levels					

Q44 To what extent are you or a member of your household able, to actually carry out these measures?

	Definitely able	Possibly able	Possibly not able	Definitely not able	Not sure
Elevating the lowest floor of your home					
Preventing flood waters from entering your home by using metal or wood water shields or sand bags, or installing a sump pump or drainage system					
Limiting damage once water enters your home by using flood-resistant building materials, installing a water-resistant floor, or installing electrical and central					

heating systems above potential flood levels					

Q45 Suppose that your current home will be flooded in the future. Do you expect that the federal government will compensate you for at least part of your flood damage?

□ 1 Definitely

□ 2 Probably

□ 3 Probably not

□ 4 Definitely not

□ 5 Don't know

[IF THE ANSWER IS 3, 4 or 5, THEN SKIP TO QUESTION 46]

Q45a What is the percentage of the total damage you expect to get back from the government?

□ 1 Less than 20%

□ 2 21% to 40%

□ 3 41% to 60%

□ 4 61% to 80%

□ 5 More than 80%

□ 6 Don't know

Q46 How many times has your current household previously been affected by floods caused by natural disasters while you were living there?

Times ____

□ Don't know

Please tell me if you strongly agree, agree, neither agree nor disagree, disagree or strongly disagree with the following statements:

Q47 I am confident that a flood insurance policy would pay out in the event of a flood.

- □ 1 Strongly agree
- □ 2 Agree
- □ 3 Neither agree nor disagree
- □ 4 Disagree
- □ 5 Strongly disagree
- □ 6 Not sure

Q48 I would regret not purchasing flood insurance coverage if a flood were to occur next year.

- □ 1 Strongly agree
- □ 2 Agree
- □ 3 Neither agree nor disagree
- □ 4 Disagree
- □ 5 Strongly disagree
- □ 6 Not sure

Q49 I would regret purchasing flood insurance coverage if no flood were to occur next year.

- □ 1 Strongly agree
- □ 2 Agree
- □ 3 Neither agree nor disagree
- □ 4 Disagree
- □ 5 Strongly disagree
- □ 6 Not sure

Q50 Most people who are important to me would think that someone in my situation ought to purchase flood insurance.

- □ 1 Strongly agree
- □ 2 Agree
- □ 3 Neither agree nor disagree
- □ 4 Disagree
- □ 5 Strongly disagree
- □ 6 Not sure

Q51 Most people who are important to me would think that someone in my situation ought to take measures to reduce flood risk to one's home.

- □ 1 Strongly agree
- □ 2 Agree
- □ 3 Neither agree nor disagree
- □ 4 Disagree
- □ 5 Strongly disagree
- □ 6 Not sure

These next questions are about your opinions related to the coronavirus.

Q52 How likely do you think it is that you will personally be infected by the coronavirus in the near future?

- □ 1 Very likely
- □ 2 Likely
- □ 3 Not likely/not unlikely

□ 4 Unlikely

□ 5 Very unlikely

□ 6 Not sure

Q53 Suppose you became infected by the coronavirus. How ill do you expect to get from the virus?

□ 1 Extremely ill

□ 2 Very ill

□ 3 Quite ill

□ 4 A little bit ill

□ 5 Not ill at all

□ 6 Not sure

Q54 Suppose you became infected by the coronavirus. What financial consequences do you expect for you personally from this infection, for example due to medical costs or income loss?

□ 1 Very high financial costs

□ 2 High financial costs

□ 3 Moderate financial costs

□ 4 Low financial costs

□ 5 No financial costs

□ 6 Not sure

Q55 Please tell me if you strongly agree, agree, neither agree nor disagree, disagree or strongly disagree with the following: The probability of being infected by the coronavirus is so low that I am not concerned about its consequences.

□ 1 Strongly agree

□ 2 Agree

□ 3 Neither agree nor disagree

□ 4 Disagree

□ 5 Strongly disagree

□ 6 Not sure

Q56 Has your household incurred any expenses as a result of the coronavirus because of loss of employment or other income, temporary leave, or medical expenses? Select all that apply.

□ 1 Yes, because of loss of employment

□ 2 Yes, because of temporary leave

□ 3 Yes, because of loss of other income

□ 4 Yes, because of medical expenses

□ 5 No

[IF THE ANSWER IS 5, THEN SKIP TO QUESTION 57]

Q56a Did you experience any financial difficulties as a result of the coronavirus that prevented you from purchasing flood insurance, windstorm insurance or other protection measures?

□ 1 Yes

□ 2 No

Q57 Please tell me if you strongly agree, agree, neither agree nor disagree, disagree or strongly disagree with the following: I am worried about becoming infected by the coronavirus.

□ 1 Strongly agree

□ 2 Agree

□ 3 Neither agree nor disagree

□ 4 Disagree

□ 5 Strongly disagree

□ 6 Not sure

Q58 Have you personally been infected by the coronavirus?

□ 1 Yes for certain, but I was not tested

□ 2 Yes for certain because it was confirmed by test results

□ 3 I think so, but I am not fully certain about this

□ 4 No

□ 5 No idea

[IF THE ANSWER IS 4 or 5, THEN SKIP TO QUESTION 59]

Q58a How ill did you get from the (possible) infection with the coronavirus?

□ 1 Extremely ill

□ 2 Very ill

□ 3 Quite ill

□ 4 A little bit ill

□ 5 Not ill at all

□ 6 Not sure

Q59 Has one of your household members, close relatives or close friends been infected by the coronavirus?

□ 1 Yes for certain, but they were not tested

□ 2 Yes because it was confirmed by test results

□ 3 I think so, but I am not fully certain about this

□ 4 No

□ 5 No idea

[IF THE ANSWER IS 3, 4 or 5, THEN SKIP TO QUESTION 60]

Q59a Did one of your household members, close relatives or close friends get hospitalized or die as a result of a coronavirus infection?

□ 1 Yes, they were hospitalized due to a coronavirus infection

□ 2 Yes, they died due to a coronavirus infection

□ 3 No

□ 4 Don't know

Q60 Please tell me if you strongly agree, agree, neither agree nor disagree, disagree or strongly disagree with the following: I am worried about the consequences of the current economic situation.

□ 1 Strongly agree

□ 2 Agree

□ 3 Neither agree nor disagree

□ 4 Disagree

□ 5 Strongly disagree

□ 6 Not sure

Q61 How would you grade how much you trust the government in terms of how it is dealing with the coronavirus pandemic? Please grade on a scale from 0 to 10, where 0 means 'no trust at all' and 10 means 'trust completely'.

Score ____

□ Don't know

Q62 Have you taken any of the following actions to understand and prevent the coronavirus? Please tick all that apply.

□ 1 Check the statistics of infection cases and deaths

□ 2 Follow CDC or other public health institutes on social media for guidelines and news

□ 3 Actively seek out information from friends and family

□ 4 Wear a mask in public settings

□ 5 Keep social distancing

□ 6 Clean hands frequently with soap or a hand sanitizer

□ 7 Clean and disinfect frequently touched objects and surfaces daily

□ 8 Avoid close contact with people who are sick

□ 9 Self-quarantine when having symptoms and self-isolation when being infected

□ 10 None of these

Q63 How much do you feel you understand the government's strategy to deal with the coronavirus pandemic?

□ 1 Very much so

□ 2 To some extent

□ 3 Only a little

□ 4 Not at all

□ 5 Don't know

Q64 To what extent do you think scientists have a good understanding of the coronavirus?

□ 1 Very much so

□ 2 To some extent

□ 3 Only a little

□ 4 Not at all

□ 5 Don’t know

Q65 To what extent do you feel that the personal actions you are taking to try to limit the spread of coronavirus make a difference?

□ 1 Very much so

□ 2 To some extent

□ 3 Only a little

□ 4 Not at all

□ 5 Don’t know

Q66 To what extent do you feel the actions that the government is taking to limit the spread of coronavirus make a difference?

□ 1 Very much so

□ 2 To some extent

□ 3 Only a little

□ 4 Not at all

□ 5 Don’t know

Q67 How old are you?

…….Years

□ Rather not say

Q68 What is your highest completed level of education?

□ 1 Some high school

□ 2 High school graduate

□ 3 Some college

□ 4 College graduate

□ 5 Post graduate

□ 6 Rather not say

Q69 Which of the following ranges best describes your total yearly household income before taxes?

□ 1 Less than $10,000

□ 2 $10,000 to $24,999

□ 3 $25,000 to $44,999

□ 4 $45,000 to $ 74,999

□ 5 $75,000 to $124,999

□ 6 $125,000 or more

□ 7 Don't know

Q70 What is approximately the current market value of your home?

□ 1 Less than $100,000

□ 2 $100,000 to $149,999

□ 3 $150,000 to $199,999

□ 4 $200,000 to $ 299,999

□ 5 $300,000 to $399,999

□ 6 $400,000 to $599,999

□ 7 $600,000 to $799,999

□ 8 $800,000 or more

□ 9 Don't know

Q71 What is approximately the value of your home contents?

□ 1 Less than $5,000

□ 2 $5,000 to $9,999

□ 3 $10,000 to $14,999

□ 4 $15,000 to $ 24,999

□ 5 $25,000 to $34,999

□ 6 $35,000 to $49,999

□ 7 $50,000 to $74,999

□ 8 $75,000 or more

□ 9 Don't know

Q72 Does your home have a basement, cellar or crawlspace?

□ 1 Basement/cellar

□ 2 Crawlspace

□ 3 None of these

□ 4 Don't know

Q73 Which of the following types of structures do you live in?

□ 1 Mobile or Manufactured home

□ 2 Detached single family home

□ 3 Duplex or triplex home

□ 4 Multi-family building - 4 stories or less (Apartment/condo)

□ 5 Multi-family building - more than 4 stories (Apartment/condo)

□ 6 Apartment, at floor(s)……..

□ 7 Don't know

[IF THE ANSWER IS 1 or 2, THEN SKIP TO QUESTION 74]

Q73a Does the part of the building you occupy include the ground floor level?

- □ 1 Yes
- □ 2 No
- □ 3 Rather not say

Q74 How many floors does the house (or apartment) that you occupy have?

…….. floors

□ Rather not say

Q75 How many square feet is your house (or apartment)?

- □ 1 1 to 499 square feet
- □ 2 500 to 999 square feet
- □ 3 1,000 to 1,499 square feet
- □ 4 1,500 to 1,999 square feet
- □ 5 2,000 to 2,499 square feet
- □ 6 2,500 square feet or more
- □ 7 Don't know

Q76 Approximately what year was your home built?

Year:.....

□ Don't know

Q77 Do you rent or own your home?

- □ 1 Renter
- □ 2 Property owner
- □ 3 Other, specify: ……..
- □ 4 Rather not say

Q78 How long have you lived in your home (in years)?

Years:……

□ Rather not say

Q79 How would you describe your political affiliation?

- □ 1 Strong Democrat
- □ 2 Democrat
- □ 3 Lean Democrat
- □ 4 Independent/other
- □ 5 Lean Republican
- □ 6 Republican
- □ 7 Strong Republican
- □ 8 Rather not say

Q80 How would you describe your political ideology?

- □ 1 Strongly liberal
- □ 2 Liberal
- □ 3 Weakly liberal

□ 4 Middle of the road

□ 5 Weakly conservative

□ 6 Conservative

□ 7 Strongly conservative

□ 8 Rather not say

Q81 Are you male or female?

□ 1 Male

□ 2 Female

□ 3 Rather not say

Other things to be included:

Date and time……

Latitude: …….

Longitude: …….

Beginning of Hurricane Season Survey

(Survey 5, June 2021)

Q1 Are you taking this survey at your home?

□ 1 Yes

□ 2 No

[IF THE ANSWER IS 1, THEN SKIP TO QUESTION 2]

Q1a In which of the following counties do you live?

□ 1 Brevard County

□ 2 Broward County

□ 3 Duval County

□ 4 Flagler County

□ 5 Indian River County

□ 6 Martin County

□ 7 Miami-Dade County

□ 8 Monroe County

□ 9 Nassau County

□ 10 Palm Beach County

□ 11 St. John's County

□ 12 St. Lucie County

□ 13 Volusia County

□ 14 Osceola County

□ 15 Seminole County

□ 16 Orange County

□ 17 Okeechobee County

□ 18 Polk County

□ 19 Highlands County

□ 20 Alachua County

□ 21 Other: _____

Q1b What is your 5-digit zip-code?

……

□ Rather not say

Q2 Do you live in a Special Flood Hazard Area (SFHA), i.e., Zone A and V, or an area with a 1-percent annual chance of flooding?

□ 1 Yes

□ 2 No

□ 3 Don't know

Next, we will ask a few questions about your general attitudes and preferences.

Q3 Using a 10-point scale, where 0 means you have no control and 10 means you have complete control, what number reflects how much control you think you have over how your life turns out?

Control Score ____

□ Don't know

Q4 Using a 10-point scale, where 0 means you are not willing to take any risks and 10 means you are very willing to take risks, what number reflects how much risk you are willing to take?

Risk Score ____

□ Don't know

Q5 When it comes to financial decisions, how would you assess your willingness to give up something today in order to benefit from that in the future?

Please use a scale from 0 to 10, where 0 means you are "completely unwilling to give up something today" and a 10 means you are "very willing to give up something today". You can also use the values in-between to indicate where you fall on the scale.

Score ____

□ Don't know

Q6 Using a 10-point scale, where 0 means totally unhappy and 10 means totally happy, how satisfied are you with your life as a whole?

Happiness Score ____

□ Don't know

We will now ask a few questions about your risk perceptions. Please keep in mind that we are talking here about **floods and windstorms caused by natural disasters such as a tropical storm or a hurricane**.

Q7 Please tell me if you strongly agree, agree, neither agree nor disagree, disagree or strongly disagree with the following: I am worried about the danger of a flood at my current residence.

□ 1 Strongly agree

□ 2 Agree

□ 3 Neither agree nor disagree

□ 4 Disagree

□ 5 Strongly disagree

□ 6 Not sure

Q8 What is your best estimate of how often a flood will occur at your home?

□ 1 More often than 1 in 10 years

□ 2 Exactly 1 in 10 years

□ 3 Between 1 in 10 years and 1 in 100 years

□ 4 Exactly 1 in 100 years

□ 5 Between 1 in 100 years and 1 in 1000 years

□ 6 Exactly 1 in 1000 years

□ 7 Less often than 1 in 1000 years

□ 8 Not sure

[IF THE ANSWER IS 2, 4, 6 or 8, THEN SKIP TO QUESTION 9]

[IF THE ANSWER IS 1, THEN SKIP TO QUESTION 8a]

[IF THE ANSWER IS 3, THEN SKIP TO QUESTION 8b]

[IF THE ANSWER IS 5, THEN SKIP TO QUESTION 8c]

[IF THE ANSWER IS 7, THEN SKIP TO QUESTION 8d]

Q8a So you expect that a flood occurs at your home more often than 1 in 10 years. What is your best estimate of how often a flood will occur at your home? Once every (HOW MANY) years?

…….. years

□ Don't know

Q8b So you expect that a flood occurs at your home between 1 in 10 years and 1 in 100 years. What is your best estimate of how often a flood will occur at your home? Once every (HOW MANY) years?

…….. years

□ Don't know

Q8c So you expect that a flood occurs at your home between 1 in 100 years and 1 in 1000 years. What is your best estimate of how often a flood will occur at your home? Once every (HOW MANY) years?

…….. years

□ Don't know

Q8d So you expect that a flood occurs at your home less often than 1 in 1000 years. What is your best estimate of how often a flood will occur at your home? Once every (HOW MANY) years?

…….. years

□ Never

□ Don't know

Q9 Please tell me if you strongly agree, agree, neither agree nor disagree, disagree or strongly disagree with the following: The probability of flooding is so low that I am not concerned about the consequences of a flood.

□ 1 Strongly agree

□ 2 Agree

□ 3 Neither agree nor disagree

□ 4 Disagree

□ 5 Strongly disagree

□ 6 Not sure

Q10 What would it cost to repair the damage to your home and its contents if your home did flood?

□ 1 Less than $10,000

□ 2 $10,000 to $24,999

□ 3 $25,000 to $44,999

□ 4 $45,000 to $74,999

□ 5 $75,000 to $124,999

□ 6 $125,000 to $199,999

□ 7 $200,000 or more

□ 8 Don't know

Q11 Please tell me if you strongly agree, agree, neither agree nor disagree, disagree or strongly disagree with the following: I am worried about the danger of a windstorm at my current residence.

□ 1 Strongly agree

□ 2 Agree

□ 3 Neither agree nor disagree

□ 4 Disagree

□ 5 Strongly disagree

□ 6 Not sure

Q12 Please tell me if you strongly agree, agree, neither agree nor disagree, disagree or strongly disagree with the following: The probability of windstorm is so low that I am not concerned about the consequences of a windstorm.

□ 1 Strongly agree

□ 2 Agree

□ 3 Neither agree nor disagree

□ 4 Disagree

□ 5 Strongly disagree

□ 6 Not sure

Q13 What would it cost to repair the damage to your home and its contents if your home did suffer a windstorm?

- □ 1 Less than $10,000
- □ 2 $10,000 to $24,999
- □ 3 $25,000 to $44,999
- □ 4 $45,000 to $74,999
- □ 5 $75,000 to $124,999
- □ 6 $125,000 to $199,999
- □ 7 $200,000 or more
- □ 8 Don't know

Q14 In the next 10 years will climate change increase or decrease the risk to your home due to flooding and hurricanes?

- □ 1 Increase greatly
- □ 2 Increase slightly
- □ 3 No impact
- □ 4 Decrease slightly
- □ 5 Decrease greatly
- □ 6 Not sure

Q15 Are you aware whether the 2020 hurricane season's activities (i.e., tropical storms, hurricanes) were above or below the average of the past 30 years?

- □ 1 Above average
- □ 2 Average
- □ 3 Below average

□ 4 Don’t know

Q16 Are you aware whether the 2021 hurricane season is forecasted to be above or below the average of the past 30 years with regards to hurricane activities?

□ 1 Above average

□ 2 Being average

□ 3 Below average

□ 4 Don’t know

Q17 How much do you trust the ability of government officials to limit flood risk where you live, for example by maintaining levees and enforcing building codes?

□ 1 Trust them completely

□ 2 Trust them somewhat

□ 3 Not trust them very much

□ 4 Not trust them at all

□ 5 Don’t know

Q18 How effective do you think the response from the federal organization FEMA will be if a severe hurricane will hit Florida this hurricane season compared with the previous year?

□ 1 Much more effective

□ 2 More effective

□ 3 Just as effective

□ 4 Less effective

□ 5 Much less effective

□ 6 No idea

Q19 How effective do you think the response from your state government will be if a severe hurricane will hit Florida this hurricane season compared with the previous year?

□ 1 Much more effective

□ 2 More effective

□ 3 Just as effective

□ 4 Less effective

□ 5 Much less effective

□ 6 No idea

Q20 Did you take any of the following measures to prepare for the 2021 hurricane season? Select all that apply.

□ 1 Create a home inventory, i.e., create a list of your home contents

□ 2 Know your insurer contact information

□ 3 Gather other important documents

□ 4 Put together a hurricane preparedness kit

□ 5 None

Q21 Did you receive or consult any information about how to prepare for the 2021 hurricane season from your insurance company, insurance regulator, state government, or other agency? Select all that apply.

□ 1 No

□ 2 Yes, from my insurance company

□ 3 Yes, from my insurance regulator

□ 4 Yes, from my state government

□ 5 Yes, from another agency: _____

Q22 Please tell me if you are extremely likely, likely, somewhat likely or not at all likely to evacuate to a safer place this hurricane season if a mandatory evacuation were to be ordered for your county.

- □ 1 Extremely likely
- □ 2 Likely
- □ 3 Somewhat likely
- □ 4 Not at all likely
- □ 5 Not sure

Q23 Please tell me if you are extremely likely, likely, somewhat likely or not at all likely to evacuate to a safer place this hurricane season if a voluntary evacuation were to be ordered for your county.

- □ 1 Extremely likely
- □ 2 Likely
- □ 3 Somewhat likely
- □ 4 Not at all likely
- □ 5 Not sure

Q24 Are there any potential obstacles which may prevent you from evacuating during the threat of a hurricane? Select all that apply.

- □ 1 Not owning a car
- □ 2 Disability
- □ 3 Job requirements
- □ 4 Material possessions
- □ 5 Stubborn family members
- □ 6 No place to go
- □ 7 Unable to pay for hotel costs

□ 8 A pet

□ 9 Staying in home to prevent coronavirus infections

□ 10 Other: ……

□ 11 No potential obstacles

Next, we will ask a few questions about your insurance coverage. Please keep in mind that we are talking here about **insurance against natural disasters**.

Q25 Did you have insurance coverage for flood risk?

Please note that most homeowners insurance policies DO NOT cover flood risk.

□ 1 Yes

□ 2 No, I plan to buy it in the next year

□ 3 No

□ 4 Don't know

[IF THE ANSWER IS 2, 3 or 4, THEN SKIP TO QUESTION 25g]

Q25a Did you purchase flood insurance because it was mandatory?

□ 1 Yes

□ 2 No

□ 3 Don't know

Q25b Flood insurance can be purchased from the federal National Flood Insurance Program (NFIP). Alternatively, a private flood insurance product can be bought that is offered by the private insurers other than the NFIP.

Did you purchase a policy from the National Flood Insurance Program (NFIP) or from the private insurance market?

□ 1 I purchased flood coverage from the National Flood Insurance Program (NFIP)

□ 2 I purchased flood coverage from the private insurance market

□ 3 Not sure

[IF THE ANSWER IS 1 or 3, THEN SKIP TO QUESTION 25d]

Q25c What are your reasons for purchasing a private flood insurance product? Select all that apply.

□ 1 I couldn't obtain flood insurance from the NFIP

□ 2 The NFIP flood insurance coverage is NOT enough to cover my losses

□ 3 The private flood insurance is cheaper than the NFIP policy

□ 4 The private flood insurance has more flexible coverage and deductible choices than the NFIP policy

□ 5 The private flood insurance has a simpler and quicker underwriting process than the NFIP policy

□ 6 Other reason, specify _____

□ 7 Don't know

Q25d How much is your flood insurance deductible for the building?

□ 1 Less than $1,000

□ 2 $1,000 to $2,000

□ 3 $2,001 to $5,000

□ 4 $5,001 to $10,000

□ 5 More than $10,000

□ 6 I don't know

Q25e How much is your flood insurance deductible for the building contents?

□ 1 Less than $1,000

□ 2 $1,000 to $2,000

□ 3 $2,001 to $5,000

□ 4 $5,001 to $10,000

□ 5 More than $10,000

□ 6 I don't know

Q25f Approximately how much is your annual flood insurance premium?

□ 1 Less than $1,000 per year

□ 2 $1,000 to $2,000 per year

□ 3 $2,001 to $4,000 per year

□ 4 More than $4,000 per year

□ 5 Don't know

Q25g Have you had trouble getting or renewing your flood insurance because of natural disasters in the past?

□ 1 Yes

□ 2 No

Q26 Do you have insurance coverage for windstorm damages?

Please note that most homeowners insurance policies DO cover windstorm damages.

□ 1 Yes

□ 2 No, I plan to buy it in the next year

□ 3 No

□ 4 Not sure

[IF THE ANSWER IS 2, 3 or 4, THEN SKIP TO QUESTION 26f]

Q26a Where did you obtain your windstorm insurance coverage?

□ 1 From a private insurance company

□ 2 From the Citizens Property Insurance Corporation (state-run insurance program)

□ 3 Don't know

[IF THE ANSWER IS 1, THEN SKIP TO QUESTION 26b]

[IF THE ANSWER IS 2, THEN SKIP TO QUESTION 26c]

[IF THE ANSWER IS 3, THEN SKIP TO QUESTION 26d]

Q26b If you obtained your coverage from a private insurer, which type of insurance did you have as the windstorm coverage?

□ 1 Homeowners insurance policy

□ 2 Wind endorsement to the existing homeowners insurance policy

□ 3 Wind-only policy

□ 4 Don't know

[FOR ANY ANSWER, SKIP TO QUESTION 26d]

Q26c If you obtained your coverage from the Citizens, which type of insurance did you have as the windstorm coverage?

□ 1 Homeowners insurance policy

□ 2 Wind-only policy

□ 3 Don't know

Q26d In Florida, all types of wind insurance coverage apply a Hurricane Deductible to wind damages caused by named hurricanes. How much is your Hurricane Deductible?

□ 1 A flat amount of $500

□ 2 2% of total insured value

□ 3 5% of total insured value

□ 4 10% of total insured value

□ 5 Other, specify _____

□ 6 Don't know

Q26e Approximately how much is your annual homeowners insurance premium (including wind endorsement or wind-only policy)?

□ 1 Less than $1,000 per year

□ 2 $1,000 to $2,000 per year

□ 3 $2,001 to $4,000 per year

□ 4 More than $4,000 per year

□ 5 Don't know

Q26f Have you had trouble getting or renewing your homeowners insurance because of natural disasters in the past?

□ 1 Yes

□ 2 No

Q27 In general, what is your role in choosing the insurance for your home?

□ 1 I am the sole decision maker

□ 2 I used an agent to help make the decision

□ 3 I completely relied on the agent's advice

□ 4 Don't apply – I don't have any insurance for my home

[IF THE ANSWER IS 4, THEN SKIP TO QUESTION 28]

Q27a Did you experience any financial difficulties as a result of the coronavirus that prevented you from purchasing insurance for your home?

□ 1 Yes

□ 2 No

Next, you will read actions that reduce flood or wind risk to your home. Please tell us if each has been implemented in your house.

Q28 Did you implement the following measures to reduce the windstorm damages to your home?

	Yes, in 2021	Yes, before 2021	No, I plan to do it in 2021	No, I do not plan to do it
Roof construction that meets the 2001 Florida Building Code such as roof covering, roof-deck attachment, and roof-to-wall connection				
Window protection such as shutters, plywood panels, or hurricane proof glass				
Hip roof, i.e., roof sloping down to meet all your outside walls (like a pyramid)				

Q29 Did you receive a premium discount on your windstorm insurance coverage for taking any of these measures? If yes, please specify for which measure(s).

□ 1 Yes, specify_____

□ 2 No

□ 3 Don't apply – I didn't implement any of these measures or have insurance

Q30 Did you implement the following measures to reduce the flood damages to your home?

	Yes, in 2021	Yes, before 2021	No, I plan to do it in 2021	No, I do not plan to do it
Elevating the lowest floor of your home				
Having metal or wood flood shields or sand bags available				
Spraying or coating outside walls to waterproof them				
Installing a sump pump and/or a drainage system				
Using flood-resistant building materials				
Installing a water-resistant floor				
Installing electrical and central heating systems above potential flood levels				
Keeping or moving expensive furniture or contents out of flood-prone parts of your home				

Q31 Did you receive a premium discount on your flood insurance for taking any of these measures? If Yes, please specify for which measure(s).

□ 1 Yes, specify_____

□ 2 No

□ 3 Don't apply – I didn't implement any of these measures or have insurance

Q32 How effective do you think the following measures are in protecting your home and its contents against flooding?

	Very effective	Somewhat effective	Somewhat not effective	Not at all effective	Not sure
Elevating the lowest floor of your home					
Preventing flood waters from entering your home by using metal or wood water shields or sand bags,					

or installing a sump pump or drainage system					
Limiting damage once water enters your home by using flood-resistant building materials, installing a water-resistant floor, or installing electrical and central heating systems above potential flood levels					

Q33 To what extent are you or a member of your household able to actually carry out these measures?

	Definitely able	Possibly able	Possibly not able	Definitely not able	Not sure
Elevating the lowest floor of your home					
Preventing flood waters from entering your home by using metal or wood water shields or sand bags, or installing a sump pump or drainage system					
Limiting damage once water enters your home by using flood-resistant building materials, installing a water-resistant floor, or installing electrical and central heating systems above potential flood levels					

Q34 Suppose that your current home will be flooded in the future. Do you expect that the federal government will compensate you for at least part of your flood damage?

□ 1 Definitely

□ 2 Probably

□ 3 Probably not

□ 4 Definitely not

□ 5 Don't know

Q35 Has your current household previously suffered damage to your home or contents due to flood or wind?

□ 1 Yes, flood damage

□ 2 Yes, wind damage

□ 3 Yes, both flood and wind damage

□ 4 No

□ 5 Don't know

Please tell me if you strongly agree, agree, neither agree nor disagree, disagree or strongly disagree with the following statements:

Q36 I am confident that a flood insurance policy would pay out in the event of a flood.

□ 1 Strongly agree

□ 2 Agree

□ 3 Neither agree nor disagree

□ 4 Disagree

□ 5 Strongly disagree

□ 6 Not sure

Q37 I would regret not purchasing flood insurance coverage if a flood were to occur next year.

□ 1 Strongly agree

□ 2 Agree

□ 3 Neither agree nor disagree

□ 4 Disagree

□ 5 Strongly disagree

□ 6 Not sure

Q38 I would regret purchasing flood insurance coverage if no flood were to occur next year.

□ 1 Strongly agree

□ 2 Agree

□ 3 Neither agree nor disagree

□ 4 Disagree

□ 5 Strongly disagree

□ 6 Not sure

Q39 Most people who are important to me would think that someone in my situation ought to purchase flood insurance.

□ 1 Strongly agree

□ 2 Agree

□ 3 Neither agree nor disagree

□ 4 Disagree

□ 5 Strongly disagree

□ 6 Not sure

Q40 Most people who are important to me would think that someone in my situation ought to take measures to reduce flood risk to one's home.

□ 1 Strongly agree

□ 2 Agree

□ 3 Neither agree nor disagree

□ 4 Disagree

□ 5 Strongly disagree

□ 6 Not sure

These next questions are about your opinions related to the coronavirus.

Q41 How likely do you think it is that you will personally be infected by the coronavirus in the near future?

□ 1 Very likely

□ 2 Likely

□ 3 Not likely/not unlikely

□ 4 Unlikely

□ 5 Very unlikely

□ 6 Not sure

Q42 Suppose you became infected by the coronavirus. How ill do you expect to get from the virus?

□ 1 Extremely ill

□ 2 Very ill

□ 3 Quite ill

□ 4 A little bit ill

□ 5 Not ill at all

□ 6 Not sure

Q43 Suppose you became infected by the coronavirus. What financial consequences do you expect for you personally from this infection, for example due to medical costs or income loss?

□ 1 Very high financial costs

□ 2 High financial costs

□ 3 Moderate financial costs

□ 4 Low financial costs

□ 5 No financial costs

□ 6 Not sure

Q44 Please tell me if you strongly agree, agree, neither agree nor disagree, disagree or strongly disagree with the following: The probability of being infected by the coronavirus is so low that I am not concerned about its consequences.

□ 1 Strongly agree

□ 2 Agree

□ 3 Neither agree nor disagree

□ 4 Disagree

□ 5 Strongly disagree

□ 6 Not sure

Q45 Has your household incurred any expenses as a result of the coronavirus because of loss of employment or other income, temporary leave, or medical expenses? Select all that apply.

□ 1 Yes, because of loss of employment

□ 2 Yes, because of temporary leave

□ 3 Yes, because of loss of other income

□ 4 Yes, because of medical expenses

□ 5 No

Q46 Please tell me if you strongly agree, agree, neither agree nor disagree, disagree or strongly disagree with the following: I am worried about becoming infected by the coronavirus.

□ 1 Strongly agree

□ 2 Agree

□ 3 Neither agree nor disagree

□ 4 Disagree

□ 5 Strongly disagree

□ 6 Not sure

Q47 Please tell me if you strongly agree, agree, neither agree nor disagree, disagree or strongly disagree with the following: I am worried about the consequences of the current economic situation.

□ 1 Strongly agree

□ 2 Agree

□ 3 Neither agree nor disagree

□ 4 Disagree

□ 5 Strongly disagree

□ 6 Not sure

Q48 How would you grade how much you trust the government in terms of how it is dealing with the coronavirus pandemic? Please grade on a scale from 0 to 10, where 0 means 'no trust at all' and 10 means 'trust completely'.

Score ____

□ Don't know

Q49 How old are you?

…….Years

□ Rather not say

Q50 What is your highest completed level of education?

□ 1 Some high school

□ 2 High school graduate

□ 3 Some college

□ 4 College graduate

□ 5 Post graduate

□ 6 Rather not say

Q51 Which of the following ranges best describes your total yearly household income before taxes?

□ 1 Less than $10,000

□ 2 $10,000 to $24,999

□ 3 $25,000 to $44,999

□ 4 $45,000 to $ 74,999

□ 5 $75,000 to $124,999

□ 6 $125,000 or more

□ 7 Don't know

Q52 What is approximately the current market value of your home?

□ 1 Less than $100,000

□ 2 $100,000 to $149,999

□ 3 $150,000 to $199,999

□ 4 $200,000 to $ 299,999

□ 5 $300,000 to $399,999

□ 6 $400,000 to $599,999

□ 7 $600,000 to $799,999

□ 8 $800,000 or more

□ 9 Don't know

Q53 What is approximately the value of your home contents?

□ 1 Less than $5,000
□ 2 $5,000 to $9,999
□ 3 $10,000 to $14,999
□ 4 $15,000 to $ 24,999
□ 5 $25,000 to $34,999
□ 6 $35,000 to $49,999
□ 7 $50,000 to $74,999
□ 8 $75,000 or more
□ 9 Don't know

Q54 Does your home have a basement, cellar or crawlspace?

□ 1 Basement/cellar
□ 2 Crawlspace
□ 3 None of these
□ 4 Don't know

Q55 Which of the following types of structures do you live in?

□ 1 Single family home
□ 2 Apartment at floor(s) number……
□ 3 Other……
□ 4 Don't know

[IF THE ANSWER IS 4, THEN SKIP TO QUESTION 56]

Q55a Does the part of the building you occupy include the ground floor level?

□ 1 Yes

□ 2 No

□ 3 Rather not say

Q56 How many floors does the house (or apartment) that you occupy have?

…….. floors

□ Rather not say

Q57 How many square feet is your house (or apartment)?

□ 1 1 to 499 square feet

□ 2 500 to 999 square feet

□ 3 1,000 to 1,499 square feet

□ 4 1,500 to 1,999 square feet

□ 5 2,000 to 2,499 square feet

□ 6 2,500 square feet or more

□ 7 Don't know

Q58 Approximately what year was your home built?

Year:.....

□ Don't know

Q59 Do you and your family rent or own your home?

- □ 1 Renter
- □ 2 Property owner
- □ 3 Other, specify: ……..
- □ 4 Rather not say

Q60 How long have you lived in your home (in years)?

Years:……

□ Rather not say

Q61 How would you describe your political affiliation?

- □ 1 Strong Democrat
- □ 2 Democrat
- □ 3 Lean Democrat
- □ 4 Independent/other
- □ 5 Lean Republican
- □ 6 Republican
- □ 7 Strong Republican
- □ 8 Rather not say

Q62 How would you describe your political ideology?

- □ 1 Strongly liberal
- □ 2 Liberal
- □ 3 Weakly liberal

□ 4 Middle of the road

□ 5 Weakly conservative

□ 6 Conservative

□ 7 Strongly conservative

□ 8 Rather not say

Q63 Are you male or female?

□ 1 Male

□ 2 Female

□ 3 Rather not say

Other things to be included:

Date and time……

Latitude: …….

Longitude: …….

Individual Hurricane Evacuation Intentions During the COVID-19 Pandemic: Insights for Risk Communication and Emergency Management Policies

W. J. Wouter Botzen[a,b,c,*], Jantsje M. Mol[a,d], Peter J. Robinson[a], Juan Zhang[e], Jeffrey Czajkowski[e]

[a] Institute for Environmental Studies, Vrije Universiteit, 1081 HV, Amsterdam, The Netherlands.

[b] Utrecht University School of Economics (U.S.E.), Utrecht University, The Netherlands.

[c] Risk Management and Decision Processes Center, The Wharton School, University of Pennsylvania, Philadelphia, USA.

[d] Center for Research in Experimental Economics and Political Decision Making (CREED), University of Amsterdam, The Netherlands.

[e] Center for Insurance Policy and Research, National Association of Insurance Commissioners (NAIC), USA

* Email: wouter.botzen@vu.nl

Date of this version: 13 April 2021.

Abstract

The U.S. 2020 hurricane season was extraordinary because of a record number of named storms coinciding with the COVID-19 pandemic. This study draws lessons on how individual hurricane preparedness is influenced by the additional risk stemming from a pandemic, which turns out to be a combination of perceptions of flood and pandemic risks that have opposite effects on preparedness behavior. We conducted a survey in early June 2020 of 600 respondents in flood-prone areas in Florida to obtain insights into households' risk perceptions and preparedness for the upcoming hurricane season under COVID-19. The results show that concerns over COVID-19 dominated flood risk perceptions and negatively impacted people's evacuation intentions. Whereas hotel costs were the main obstacle to evacuating during Hurricane Dorian in 2019 in the same geographic study area, the main evacuation obstacle identified in the 2020 hurricane season is COVID-19. Our statistical analyses investigating the factors influencing evacuation intentions show that older individuals are less likely to evacuate under a voluntary order, because they are more concerned about the consequences of becoming infected by COVID-19. We observe similar findings based on a real-time survey we conducted in Florida with another group of respondents under the threat of Hurricane Eta at the end of the hurricane season in November 2020. We discuss the implications of our findings for risk communication and emergency management policies that aim to improve hurricane preparedness when dealing with additional health risks such as a pandemic, a situation that may be exacerbated under the future climate.

Keywords: COVID-19, evacuation, hurricane preparedness, pandemic, risk perception.

Declarations

Funding: This research was funded by the State of Florida Division of Emergency Management.

Conflicts of interest/Competing interests: The authors have no conflicts of interest to declare.

Availability of data and material: The data used in this research are confidential.

Code availability: Not applicable.

1. Introduction

It has been projected that climate change may increase the risks of flooding due to sea-level rise and a possible increase in the severity of hurricanes (IPCC 2014). Therefore, adaptation policies such as purchasing insurance, taking risk reduction measures, and evacuating from a storm and flood threat, should focus on improving individual preparedness for hurricanes to limit their destructive impacts. However, experience during the 2020 hurricane season shows that a pandemic may hamper hurricane preparedness, especially concerning evacuation. For instance, during the threat of Hurricanes Laura and Hanna in the United States, it was expected that those who did evacuate could cause a surge in COVID-19 cases with preparations for the pandemic leading to transport disruptions and difficulties in providing adequate shelter accommodation (Schulz et al. 2020). Moreover, many individuals may be less likely to evacuate during a storm threat when they are concerned about COVID-19 infections, given that when people evacuate to hotels or shelters proper social distancing may not be possible. Previous studies have in fact shown that without the COVID-19 pandemic, natural disasters have already resulted in further spreading of infectious diseases attributed to the crowding of people, for example, in shelters (Ivers and Ryan 2006; Lemonick 2011; Shukla et al. 2018).

Insights into the influence of pandemics on hurricane preparedness can provide relevant information for risk communication and emergency management policies, because pandemics are likely to occur more often in our globalized economy (Philips et al. 2020). Moreover, climate change may exacerbate the risks of certain infectious diseases in addition to increasing the frequency and severity of extreme weather (IPCC 2014). Furthermore, hurricane-prone states in the U.S. may still be dealing with ongoing issues stemming from COVID-19 during the 2021 hurricane season which at the time of this writing is less than three months away. Hence, lessons can be drawn for natural disaster risk management strategies from the 2020 hurricane season with record-breaking hurricane activity (NOAA 2020) that coincided with a pandemic. To our knowledge, this study is one of the first empirical analysis that draws lessons on how hurricane preparedness is influenced by a pandemic.

A similar recent study to ours is Collins et al. (2021), who conducted a survey of about 7,000 households in Florida and found that these individuals were less likely to evacuate to a shelter in the 2020 hurricane season with COVID-19 compared with the pre-COVID-19 situation. Collins et

al. (2021) further found that most of their respondents felt that being in a shelter during COVID-19 times posed a higher risk than enduring a hurricane in their home, highlighting the important role COVID-19 may play in individuals evacuation decisions. We conducted a survey around the same time in June 2020 in Florida to examine individuals' general evacuation intentions at the start of the hurricane season, irrespective of whether this is to a shelter or some other place. In particular, we examine how evacuation intentions are independently influenced by flood risk perceptions and COVID-19 risk perceptions using regression and mediation analyses that we employ to further our understanding of how a person's socio-demographic profile can influence evacuation intentions through these perceptions. This moves beyond the simple descriptive analyses by Collins et al. (2021). We also assess evacuation obstacles during the COVID-19 pandemic and how these compare to the 2019 hurricane season without COVID-19 that we collected using an earlier survey conducted in the same sample areas in February 2020. Moreover, we collected similar data at the end of the hurricane season using a real-time survey that was conducted when Hurricane Eta approached Florida in November 2020. This additional data allows us to examine if we find a similar influence of COVID-19 on evacuation intentions at the beginning and the end of the hurricane season.

In this paper, specific attention is paid to older people who may be more vulnerable to both low rates of evacuation and becoming very ill due to the coronavirus (Meng et al. 2020). A review by Huang et al. (2016) of actual evacuation studies found that 41% reported a significantly negative correlation between age and evacuation, while the other 59% reported a non-significant correlation. A number of factors can cause a negative relation between age and evacuation, e.g., lack of mobility, pre-existing health conditions, limited social networks, low income, and poor vision and hearing (Cohen and Mulvaney, 2005; Rosenkoetter et al. 2007; Smith et al. 2009; Nakanishi et al. 2019; Dostal, 2015). We study whether concerns about the consequences of becoming infected by COVID-19 are an additional barrier to evacuation for older people, who are also more likely to experience adverse health impacts from hurricanes (Jenkins et al. 2007). This focus is relevant since Collins et al. (2021) found that older people were more likely to believe that the threat of COVID-19 in shelters is more dangerous than the threat of a hurricane.

Based on the survey that we conducted in early June 2020 of 600 respondents residing within coastal regions of Florida, our results show that when it comes to the factors that influence

evacuation intentions, flood risk perceptions are overshadowed by perceived risks related to COVID-19. Moreover, the main obstacle to evacuating during a storm threat changed from hotel costs in the 2019 hurricane season to COVID-19 in the 2020 hurricane season. In particular, older people are less likely to evacuate due to deeper concerns about the consequences of becoming infected by COVID-19. We draw several implications from these findings for risk communication and emergency management policies that should be part of a broader adaptation strategy to limit impacts from future hurricanes. Our policy implications link to hurricane preparedness guidance with COVID-19 considerations that have been issued by various organizations and federal agencies, such as the American Red Cross (2020) and FEMA (2020), and state and local governments (NAIC/CIPR Research Library 2020).

2. Survey of coastal residents in Florida

This study is primarily based on a survey we conducted in early June 2020 of 600 respondents of coastal residents in Florida. The survey aimed to obtain insights into individual risk perceptions and hurricane preparedness for a hurricane season under a pandemic. The survey was conducted online using a representative sample of households living in the same areas as respondents to previous surveys we conducted in both August 2019 as well as February 2020 to analyse evacuation behaviour related to Hurricane Dorian.[1] Figure 1 shows the location of respondents in our June 2020 survey in blue dots. The sample was randomly drawn by a specialized survey company from an online consumer panel of residents in areas that were forecasted by the National Hurricane Center to be potentially hit by Hurricane Dorian in 2019. Although Hurricane Dorian eventually did not make landfall in Florida in 2019, it was a major threat when it approached the Florida coasts with winds speeds up to category 5. We sampled these areas for our June 2020 survey since they faced a substantial hurricane risk, and residents of these areas have likely recently considered evacuation. Moreover, this allows for a comparison of evacuation obstacles between a pre-pandemic hurricane season (February 2020 survey) and a post-pandemic hurricane survey (June 2020 survey) using households' responses in the same areas.

[1] See Botzen et al. (2020) for the results of the August 2019 and February 2020 surveys (available on request). The February 2020 survey was completed by 255 respondents using a combination of phone and online questionnaires.

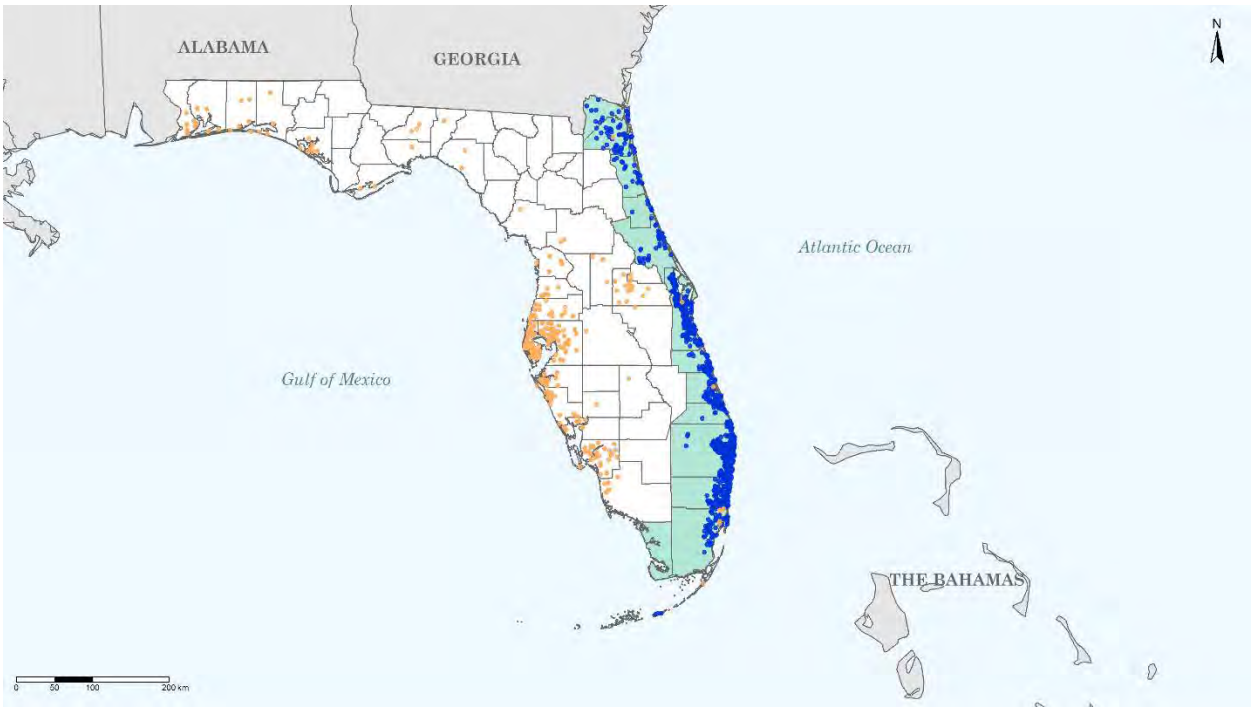

Figure 1. Locations of respondents in Florida to our surveys conducted in February 2020 (in blue dots), June 2020 (in green counties) and November 2020 (in orange dots)

The average age of respondents in our June 2020 survey is 48 years, with an average household income of $74,546 per year before taxes[2], and 66% are female. Respondents reported their highest level of education as follows: some high school (2%), high school graduate (17%), some college (26%), college graduate (36%), and post graduate (18%). Compared with the sample of the February 2020 survey, respondents to the June 2020 survey are 14 years younger on average, which may be explained by the data collection method. Older people are perhaps less likely to participate in online surveys than phone surveys. The February 2020 survey collected a significant portion of responses through phone questionnaires.

Moreover, we collected similar data on evacuation intentions and influencing factors at the end of the hurricane season using a real-time survey that was conducted when Hurricane Eta approached

[2] We converted the income categories to a continuous variable using the midpoint method. For example, the category $100,000 to $149,999 was recoded as 125,000. The number reported here is the average of this continuous variable.

Florida in November 2020. Although Eta approached the U.S. as a hurricane, it was downgraded to a tropical storm when it made landfall in Florida on November 7 and again on November 12 and caused flooding in various areas. Total U.S. losses of Eta amounted to about $1.1bn (Aon, 2020). This survey was completed by 844 respondents between 10 and 11 November before the second landfall of Eta. Figure 1 shows the location of our November 2020 survey respondents in orange dots. The sample was drawn by a specialized survey company and includes areas of the coast that could be impacted by wind and flooding caused by Eta. The average age of respondents in our November 2020 survey is 47 years, with an average household income of $40,134 per year before taxes[3], and 69% are female. Respondents reported their highest level of education as follows: some high school (3%), high school graduate (26%), some college (29%), college graduate (30%), and post graduate (12%). Compared with the June 2020 survey, our respondents to the November 2020 survey have a lower income and education level, but are similar in terms of age and gender.

Table 1 defines the variables used in our statistical analyses. To elicit these variables, respondents faced several questions in relation to: their risk perceptions associated with flooding and COVID-19, voluntary evacuation intentions, trust in the government response to COVID-19, as well as age, education, income, home value, whether the respondent is a homeowner, length of residence and gender. The overall selection of these questions allows us to identify to what extent perceptions of COVID-19 hamper evacuation, controlling for other potential determinants of evacuation, such as perceptions of the primary threat posed by a hurricane to households, i.e. flooding, and their socio-demographic profile. Our focus on risk perceptions is motivated by economic and psychological theories of individual decision-making under risk that point towards the important role of risk perceptions or threat appraisals in individual protective behaviours. Examples are Subjective Expected Utility Theory and Protection Motivation Theory (e.g., Botzen et al. 2015; Bubeck et al. 2012).

Flood risk perceptions were elicited according to both qualitative and quantitative measures. The quantitative question displayed probability answer options on a logarithmic scale, which has been

[3] See footnote 2.

shown to perform well in terms of eliciting low likelihood risks (Woloshin et al. 2000; de Bruin et al. 2011). Moreover, concern about the consequences of flooding and worry about the danger of a flood at respondents' homes were asked using items adopted from some previous studies (Robinson and Botzen 2018; 2019; Botzen et al. 2015).

Concern and worry related to COVID-19 were elicited on similar formats as those related to flooding. A qualitative measure was also selected for the perceived COVID-19 infection probability, given the expected difficulty that respondents may have with attaching a numeric probability to the likelihood of becoming infected with the novel coronavirus.[4] Furthermore, at the time we conducted our survey in early June, COVID-19 had mainly caused high infections in areas other than Florida, such as New York.[5] Nevertheless, our respondents were highly concerned about the consequences of becoming infected by COVID-19 (see Section 3), which makes it relevant to examine how coronavirus risk perceptions influence evacuation intentions. The expectation of the level of illness respondents would experience upon falling ill from COVID-19 was asked on a qualitative response scale. In addition, trust in the government response to COVID-19 was elicited following a similar format to how general trust in people is determined in the European Social Survey (ESS) on an eleven-point scale.

Our main outcome variable, voluntary evacuation intention, was asked on a qualitative ordinal response scale. Therefore we treat this intention as an ordinal dependent variable in our statistical analyses, using ordered probit models. This method accounts for the ordinal nature of intentions, avoids having predicted probabilities that fall outside the unit interval (Cameron and Trivedi 2005), and makes no assumptions regarding the interval distances between answer options (Liddell and Kruschke 2018). As an aside, we do not dichotomize this ordinal variable as this would discard potentially useful data and reduce statistical power (Fitzsimons 2008). However, whether respondents identify COVID-19 as an obstacle for evacuation is treated as a dichotomous variable in our analyses because respondents answered this question on a dichotomous scale (yes or no). For this reason, a binary probit model is used to examine factors of influence on whether COVID-

[4] This issue is less likely for the probability of flooding, given that respondents may be aware of this probability according to FEMA flood zone maps (https://msc.fema.gov/portal/home).
[5] https://covid.cdc.gov/covid-data-tracker/#trends_dailytrendscases

19 is identified as an obstacle to evacuation. The exact way in which we derived the variables in Table 1 can be found in the Supplementary Information.

Table 1. Coding of variables used in our regression models

Variable	Coding
Worry about flooding	*"I am worried about the danger of a flood at my current residence."* 1 = strongly disagree to 5 = strongly agree
Perceived flood probability	*"What is your best estimate of how often a flood will occur at your home?"* categorical, 1 = less often than 1/1,000 years to 7 = more often than 1/10 years
Concern about flooding	*"The probability of flooding is so low that I am not concerned about the consequences of a flood."* 1 = strongly agree to 5 = strongly disagree (higher numbers indicate more concern)
Age	*"How old are you?"* in years
Education	*"What is your highest completed level of education?"* 1 = some high school to 5 = post graduate
Income	*"Which of the following describes your total household income for 2019 before taxes?"* 1 = less than $10,000 to 6 = $125,000 or more
Home value	*"What is approximately the current market value of your home?"* 1 = less than $100,000 to 8 = $800,000 or more
Home owner	*"Do you rent or own your home?"* 1 = home owner, 0 = rent (or other)
Length of residence	*"How long have you lived in your home (in years)?"*
Gender	*Was the respondent male of female?* female = 1, male = 0
Voluntary evacuation intention	*"Please tell me if you are extremely likely, likely, somewhat likely or not at all likely to evacuate to a safer place this hurricane season if a voluntary evacuation were to be ordered for your county."* 1= not at all likely to 4 = extremely likely
Perceived coronavirus infection probability	"*How likely do you think it is that you will personally be infected by the coronavirus?"* 1 = very unlikely to 5 = very likely
Concern about COVID-19	*"The probability of being infected by the coronavirus is so low that I am not concerned about its consequences."* 1 = strongly agree to 5 = strongly disagree (higher numbers indicate more concern)
Expect to get ill from COVID-19	*"Suppose you became infected by the coronavirus. How ill do you expect to get from the virus?"* 1 = not ill at all to 5 = extremely ill
Worry about COVID-19	*"I am worried about becoming infected by the coronavirus."* 1 = strongly disagree to 5 = strongly agree
Trust government response COVID-19	*"How would you grade how much you trust the government in terms of how it is dealing with the coronavirus pandemic?"* 0 = no trust at all to 10 = trust completely

3. Individual perceptions of flood and COVID-19 risks at the start of the 2020 hurricane season

A comparison of perceptions of COVID-19 and hurricane-related risks shows that perceptions of COVID-19 risks at the start of the 2020 hurricane season exceed those of flood risks. For example,

more people are worried or strongly worried about COVID-19 risks (63%) than about flood risks (33%), as Figure 2 illustrates. Moreover, only 21% disagree and 7% strongly disagree with the statement, "The probability of flooding is so low that I am not concerned about the consequences of a flood." These percentages are 28% and 30%, respectively, for a similar statement about the consequences of being infected by the coronavirus. Individuals not only worry about the negative consequences of COVID-19, but also perceive high infection risks. For instance, 34% of respondents believe that it is likely or very likely they will become infected by COVID-19, and 39% expect to become very ill or extremely ill, once infected. More than half of the sample already experienced expenses because of COVID-19, mainly due to a loss of income. The vast majority of respondents (81%) are worried about the current economic situation.[6] Previous research has shown that feelings towards risks are likely to affect how people prepare for a disaster. Examples are worry about the consequences of a hazard or perceptions about whether or not the probability of experiencing a threat is high enough to trigger concern (Kunreuther and Pauly 2018; Botzen et al. 2019). In summary, our survey results indicate that the start of the 2020 hurricane season is dominated by concerns about COVID-19, which can influence hurricane preparedness activities.

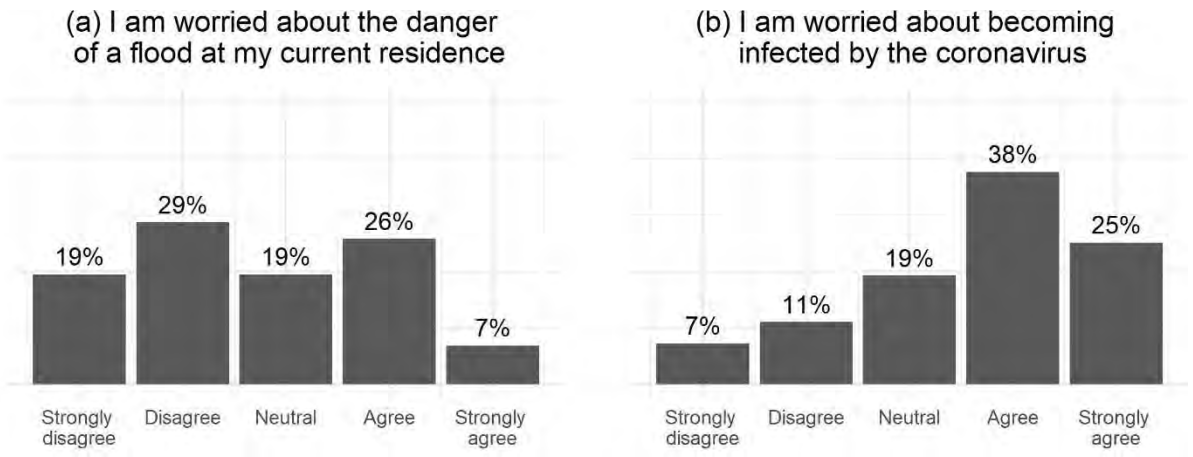

Figure 2. Responses to statements about worry of flooding (panel a) and COVID-19 (panel b) (based on the June 2020 survey).

[6] This variable is not further used in the analysis since worry about the economic situation is unlikely to influence evacuation intentions, but it does highlight that individuals are highly concerned about the impacts of COVID-19, which also encompasses its economic consequences.

4. Evacuation intentions

4.1. Evacuation intentions at the start of the 2020 hurricane season

When being asked about intentions to evacuate to a safer place under a voluntary evacuation order at the start of the hurricane season, 39% of respondents answer that it is likely or extremely likely they would evacuate (see Table 2).

Table 2. Please tell me if you are extremely likely, likely, somewhat likely or not at all likely to evacuate to a safer place this hurricane season if a voluntary evacuation were to be ordered for your county (based on the June 2020 survey).

	Evacuation intentions
Not at all likely	37%
Somewhat likely	25%
Likely	24%
Extremely likely	15%

Descriptive statistics and regression analyses of factors influencing evacuation intentions indicate that concern about COVID-19 is the most important obstacle for evacuation during the 2020 hurricane season. Both of our surveys in February and June 2020 contained a question about the obstacles for evacuation during a hurricane threat. More respondents indicated at least one potential obstacle in the June survey than in the February survey (75% versus 56%). The inability to pay for hotel costs was the most frequently mentioned obstacle during Hurricane Dorian (by 26% of the February 2020 survey respondents who had an obstacle). However, as Figure 3 illustrates, hotel costs dropped to the number four obstacle during the 2020 hurricane season, although the percentage of respondents who list hotel costs as an obstacle remains stable at 26%.

Instead, COVID-19 was mentioned the most frequently, by almost half of the respondents to the June survey who expected to experience any obstacles.

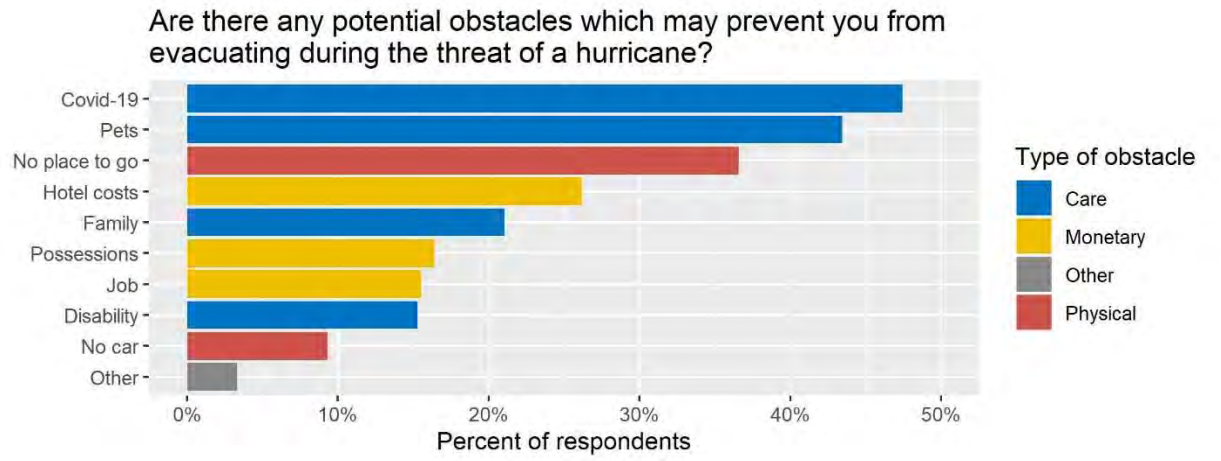

Figure 3. Percent of respondents who answered obstacles for evacuation, by obstacle (based on the June 2020 survey).

Note: Sample includes only respondents who reported at least one obstacle.

We conducted a probit model analysis to examine in more detail how COVID-19 risk perceptions relate to people identifying COVID-19 as an obstacle, while controlling for socio-demographic characteristics and flood risk perceptions. The results in Table 3 show that reporting COVID-19 as an obstacle for evacuation is positively and significantly related to the degree of worry about COVID-19 risk and concern about the consequences of becoming infected by COVID-19. In other words, high individual perceptions of COVID-19 risks are an important driver of viewing COVID-19 as an obstacle for evacuation.

Table 3. Binary probit model results of variables of influence on answering COVID-19 as an evacuation obstacle (based on the June 2020 survey). A probit model is used to account for the binary nature of the dependent variable (1 = reported COVID-19 as an obstacle for evacuation, 0 = otherwise).

	Marginal effects
Socio-demographics	
Age	0.001
	(0.002)
Gender (1 = female)	-0.003
	(0.055)
Education	0.031
	(0.030)
Income	-0.051**
	(0.025)
Length of residence	-0.003
	(0.003)
Home value	0.037**
	(0.017)
Flood risk perceptions	
Worry about flooding	0.045*
	(0.026)
Concern about flooding	-0.036
	(0.024)
COVID-19 perceptions	
Trust government response COVID-19	0.002
	(0.009)
Concern about COVID-19	0.087***
	(0.024)
Worry about COVID-19	0.086***
	(0.028)
Expect to get ill from COVID-19	0.004
	(0.024)
Observations	398
Log likelihood	-241.639
Pseudo R^2	0.087

Notes: ***p < 0.01; **p < 0.05; *p < 0.1. Standard errors are shown in between parentheses below the marginal effects.

We conduct a series of statistical analyses to examine how evacuation intentions under a voluntary order depend on socio-demographic characteristics and perceptions of the hurricane and COVID-19 risks. An ordered probit model of the intentions to evacuate voluntarily with only socio-demographic characteristics as explanatory variables finds that older people are significantly less likely to evacuate (Table 4).[7] As a next step, we add perceptions of the hurricane and COVID-19 risks and length of residence as explanatory variables to the model to examine whether the significant relationship between age and intentions to evacuate still holds once these explanatory variables are controlled for. We find that the likelihood of voluntary evacuation significantly

[7] The main results in Table 4 and Tables 5, 6 and 7 shown below are robust to including age as a dummy variable that represents people of age 65 and higher, which is the age group that is likely to experience more severe health consequences from infection by COVID-19.

increases with worry about flooding[8], but significantly declines with concern about the consequences of becoming infected by COVID-19 and the length of residence (Table 4).[9] Moreover, the independent effect of age on intentions to evacuate voluntarily becomes insignificant, indicating that the significant negative effect of age in the first model is an indirect effect, perhaps driven by perceptions of flood and COVID-19 risks as well as the length of residence. This result is examined in more detail using a mediation model (Table 5).[10]

Table 4. Ordered probit model of variables of influence on voluntary evacuation intentions (based on the June 2020 survey). An ordered probit model is used to account for the ordinal nature of the dependent variable (1= not at all likely to 4 = extremely likely to evacuate).

	Coefficients model 1	*Coefficients model 2*
Socio-demographics		
Age	-0.010***	-0.003
	(0.003)	(0.004)
Gender (1 = female)	-0.247**	-0.196
	(0.102)	(0.123)
Education	0.093*	0.118*
	(0.053)	(0.068)
Income	-0.008	-0.004
	(0.038)	(0.048)
Length of residence		-0.016**
		(0.007)
Flood risk perceptions		
Perceived flood probability		0.008
		(0.039)
Worry about flooding		0.259***
		(0.062)
COVID-19 perceptions		
Perceived coronavirus infection probability		0.092*
		(0.050)
Concern about COVID-19		-0.143***
		(0.047)

[8] Worry about the danger of a flood at the current residence of respondents is a stronger predictor of voluntary evacuation intentions than concern about the consequences of flooding. The latter consequences are likely to be broader than those experienced at one's home (and include other things like the consequences of economic disruption elsewhere due to flooding) which are expected to drive a person's evacuation intentions.

[9] We examine concern about COVID-19 rather than worry about COVID-19 here because we expect that older people are less likely to evacuate due to their concerns about the consequences of becoming infected by COVID-19, given that these are generally more severe for aged individuals.

[10] We also find that older individuals are less likely to state that they intend to evacuate if there is a mandatory evacuation order, but this is not due to perceptions related to COVID-19 and flooding. However, this may be due to other issues like poor mobility and health, or limited social networks, which we do not capture in the survey.

	Coefficients model 1	*Coefficients model 2*
Observations	519	362
Log likelihood	-682.4	-443.6
Pseudo R^2	0.017	0.081

Notes: $^{***}p < 0.01$; $^{**}p < 0.05$; $^{*}p < 0.1$. Standard errors are shown in between parentheses below the coefficients.

Table 5 displays the total effect of age on voluntary evacuation, divided into a direct and indirect effect via concern about the consequences of becoming infected by COVID-19, worry about flooding, and length of residence. Overall, the total effect shows that older individuals have lower evacuation intentions. Controlling for concern about the consequences of becoming infected by COVID-19, worry about flooding, and length of residence leaves an insignificant direct effect of age. The indirect effect, which is the share of the relationship between age and voluntary evacuation that can be attributed to perceptions of COVID-19 and flood risks and length of residence, is explained by the coefficient estimate -0.007 (p-value < 0.01). Between 60% and 73% (depending on included control variables) of the relationship between age and voluntary evacuation is explained by concern about the consequences of becoming infected by COVID-19, worry about flooding, and length of residence.[11] The two risk perception variables are statistically significant and explain a larger proportion of the relationship than the length of residence.

Table 5. Decomposition of the total effect of age on voluntary evacuation into direct and indirect effects via concern about COVID-19, worry about flooding and length of residence using the ordered probit model (based on the June 2020 survey)

	Without control variables	**Including control variables**
Total effect	-0.012*** (0.003)	-0.010*** (0.004)
Direct effect	-0.005 (0.003)	-0.003 (0.004)
Indirect effect	-0.007*** (0.001)	-0.007*** (0.002)
via concern about COVID-19	-0.001** (0.001)	-0.003** (0.001)
via worry about flooding	-0.004*** (0.001)	-0.003*** (0.001)
via length of residence	-0.001* (0.001)	-0.001 (0.001)
Mediation percentage	59.57	72.51
via concern about COVID-19	12.73	27.96
via worry about flooding	35.88	33.35
via length of residence	10.95	11.20
Observations	527	362

Notes:
***Significant at 1%; **Significant at 5%; *Significant at 10%.
Coefficient estimates are provided with standard errors in parentheses.
Control variables are: female, education, income, perceived flood probability and perceived coronavirus infection probability.

[11] Correlation analyses show that a higher age is associated with higher concern about COVID-19 and length of residence, but a lower worry about flooding.

309

310 *4.2. Evacuation intentions during Hurricane Eta*

311 When respondents to our real-time survey during the threat of Hurricane Eta were asked when they
312 were going to evacuate to a safer place, 35% answered this is very unlikely, 27% answered
313 unlikely, 10% answered likely, and only 6% answered very likely. We repeated the same analyses
314 of evacuation intentions at the start of the 2020 hurricane season (that were reported in Tables 4
315 and 5) for evacuation intentions during Hurricane Eta, which hit Florida at the end of the hurricane
316 season in November 2020. These results for evacuation during Hurricane Eta are reported in Tables
317 6 and 7. The ordered probit model results in Table 6 confirm our previous findings that evacuation
318 intentions are negatively related to age (model 1), of which the significance declines to marginally
319 significant in model 2 when risk perceptions are added. These findings again show that evacuation
320 intentions are negatively related to concern about the consequences of becoming infected by
321 COVID-19, and positively related to flood risk perceptions. Furthermore, although the sign of the
322 coefficient estimate on the length of residence is the same in Table 6 as Table 4, this estimate is
323 not significant in Table 6. Whereas, the perceived coronavirus infection probability is significantly
324 positively related to evacuation intentions, which may be due to people with higher intentions to
325 evacuate perceiving that they are more likely to become infected by COVID-19 in the event that
326 an evacuation is in fact ordered.[12]

327 Moreover, the mediation analysis results in Table 7 confirm that the main pattern of findings that
328 were reported in Table 5 for evacuation intentions at the start of the hurricane season also hold for
329 evacuation intentions among a separate sample who faced Hurricane Eta. More specifically, a large
330 proportion of the relationship between age and voluntary evacuation intentions (in this case 42%)
331 is explained by concern about the consequences of becoming infected by COVID-19 and worry
332 about flooding. However, worry about flooding is only a statistically significant mediator without
333 other control variables added to the model. Length of residence is also an insignificant mediator
334 in Table 7 which is expected given the lack of significance of this variable in Tables 5 and 6.

335

[12] We estimated the models again without perceived coronavirus infection probability to mitigate problems stemming from reverse causality. The conclusions remain the same.

Table 6. Ordered probit model of variables of influence on voluntary evacuation intentions during Hurricane Eta (based on the November 2020 survey). An ordered probit model is used to account for the ordinal nature of the dependent variable (1= not at all likely to 4 = extremely likely to evacuate).

	Coefficients model 1	*Coefficients model 2*
Socio-demographics		
Age	-0.017***	-0.006*
	(0.00)	(0.00)
Gender (1 = female)	0.003	0.038
	(0.10)	(0.12)
Education	-0.018	-0.075
	(0.05)	(0.06)
Income	-0.053	-0.021
	(0.04)	(0.04)
Length of residence		-0.001
		(0.01)
Flood risk perceptions		
Perceived flood probability		0.071*
		(0.04)
Worry about flooding		0.324***
		(0.05)
COVID-19 perceptions		
Perceived coronavirus infection probability		0.195***
		(0.05)
Concern about COVID-19		-0.187***
		(0.05)
Observations	603	455
Log likelihood	-689.4	-464.2
Pseudo R^2	0.032	0.131

Notes: $^{***}p < 0.01$; $^{**}p < 0.05$; $^{*}p < 0.1$. Standard errors are shown in between parentheses below the coefficients.

Table 7 Decomposition of the total effect of age on voluntary evacuation during Hurricane Eta into direct and indirect effects via concern about COVID-19, worry about flooding and length of residence using the ordered probit model (based on the November 2020 survey)

	Without control variables	**Including control variables**
Total effect	-0.017*** (0.003)	-0.011*** (0.003)
Direct effect	-0.010*** (0.003)	-0.006* (0.004)
Indirect effect	-0.007*** (0.002)	-0.005*** (0.002)
via concern about COVID-19	-0.001** (0.001)	-0.003*** (0.001)
via worry about flooding	-0.006*** (0.001)	-0.002 (0.001)
via length of residence	-0.000 (0.001)	-0.000 (0.001)
Mediation percentage	42.36	42.04
via concern about COVID-19	7.11	26.82
via worry about flooding	32.56	14.34

via length of residence	2.68	0.89
Observations	600	455

Notes:
***Significant at 1%; **Significant at 5%; *Significant at 10%.
Coefficient estimates are provided with standard errors in parentheses.
Control variables are: female, education, income, perceived flood probability and perceived coronavirus infection probability.

5. Policy implications and conclusion

The 2020 storm season, in which a record-breaking active hurricane season coincided with a pandemic, may be viewed as a learning experiment for risk communication and emergency management strategies that aim to limit hurricane impacts when more severe hurricanes in the future occur simultaneously with other health emergencies, such as a pandemic. Importantly, it is quite possible that hurricane-prone states in the U.S. may still be dealing with ongoing issues stemming from COVID-19 during the 2021 hurricane season which at the time of this writing is less than three months away. Indeed the results of our surveys of coastal residents in Florida conducted at the start and the end of the 2020 hurricane season show that hurricane preparedness is affected by the pandemic. The start of the 2020 hurricane season is dominated by concerns over COVID-19, which is an obstacle for evacuation. Moreover, older people, who are more concerned about the consequences of becoming infected by COVID-19, state lower evacuation intentions. This is apparent from evacuation intentions elicited among a sample at the start of the 2020 hurricane season, and confirmed by a real-time survey we conducted among another independent sample of respondents residing in the same state at the end of the hurricane season during the threat of Hurricane Eta. This should be taken into account by policies aimed at improving hurricane preparedness during a pandemic with a disease for which older people are more vulnerable. The majority of previous studies on evacuation that were not conducted during a pandemic did not observe a significant influence of age (Baker 1991; Sorensen 2000; Burnside et al. 2007; Meyer et al. 2018). Findings of a negative age effect by some (Huang et al. 2016) have been attributed to low mobility, poor health, limited social networks, and low income, as well as the length of residence (Morss et al. 2016). Our survey results show that evacuation behavior is different when a hurricane season coincides with a pandemic, because we observe a negative effect of age on evacuation intentions that is mainly caused by concerns over COVID-19 and worry about flooding. This is in line with findings by Collins et al. (2021) that older people were more likely to believe that the threat of COVID-19 in shelters is more dangerous than the threat of a hurricane.

Adequate risk communication could be an important component of adaptation strategies to improve individual hurricane preparedness. For instance, our analyses of hurricane preparedness activities during Hurricane Dorian showed that risk awareness was an important driver of these activities (Botzen et al. 2020). Our survey at the start of the hurricane season reveals that risk communication by state governments, insurers, and insurance regulators reached a large number of respondents.[13] Given the large influence of COVID-19 on evacuation intentions during the 2020 hurricane season, it is critical to refocus risk communication activities in times when the hurricane season coincides with a pandemic towards ensuring that people can safely evacuate by minimizing health risks. Examples during the COVID-19 pandemic are: including COVID-19 mitigation measures in hurricane preparedness kits, such as hand sanitizer and mouth masks, abiding by social distancing rules during an evacuation, and planning ahead to identify safe evacuation locations.

Moreover, governments and agencies can send more tailored communication messages to older people to alleviate their concerns over COVID-19 or improve their flood risk perceptions. Emergency management policies should create safe evacuation shelters where COVID-19 risks are well controlled and communicate their COVID-19 measures to the public to increase people's confidence in shelters' safety. Moreover, our results show that the experience of living in a hurricane-prone area as proxied by the length of residence reduces evacuation intentions at the start of the hurricane season, which may be due to the experience of false alarms and near misses, such as Hurricane Dorian. Communication policies should stress that each storm is different, and the possibility of a direct hit by the next one should be taken seriously.

References

American Red Cross (2020). *Preparing for Disaster During COVID-19*. https://www.redcross.org/content/dam/redcross/get-help/pdfs/Preparing_for_Disasters_during_COVID-19_04282020.pdf

AON (2020). *Global Catastrophe Recap.* November 2020. http://thoughtleadership.aon.com/documents/20201210_analytics-if-november-global-recap.pdf

[13] Approximately 50% consulted information from these agencies to prepare for the hurricane season.

401 Baker, E.J. (1991). Hurricane evacuation behavior. *International Journal of Mass Emergencies*
402 *and Disasters*, 9(2): 287-310.
403 Botzen, W.J.W., Kunreuther, H.C., Czajkowski, J., de Moel, H. (2019). Adoption of individual
404 flood damage mitigation measures in New York City: An extension of Protection
405 Motivation Theory. *Risk Analysis*, 39(10): 2143-2159.
406 Botzen, W.J.W., Kunreuther, H., Michel-Kerjan, E. (2015). Divergence between individual
407 perceptions and objective indicators of tail risks: Evidence from floodplain residents in
408 New York City. *Judgment and Decision Making*, 10(4): 365-385.
409 Botzen, W.J.W., Robinson, P.J., Mol, J.M., Czajkowski, J. (2020). *Improving individual*
410 *preparedness for natural disasters: Lessons learned from longitudinal survey data*
411 *collected from Florida during and after Hurricane Dorian.* Report for The State of Florida
412 Division of Emergency Management.
413 Bubeck, P., Botzen, W.J.W., Aerts, J.C.J.H. (2012). A review of risk perceptions and other factors
414 that influence flood mitigation behavior. *Risk Analysis*, 32(9): 1481-1495.
415 Burnside, R. De Mond Shondell, M., Rivera, J.D. (2007). The impact of information and risk
416 perception on the hurricane evacuation decision-making of greater New Orleans residents.
417 *Sociological Spectrum*, 27(6): 727-740.
418 Cameron, A.C., Trivedi, P.K. (2005). *Microeconometrics: Methods and applications*. Cambridge
419 University Press.
420 Cohen, S.S., Mulvaney, K. (2005). Field observations: Disaster medical assistance team response
421 for Hurricane Charley, Punta Gorda, Florida, August 2004. *Disaster Management &*
422 *Response*, 3(1): 22-27.
423 Collins, J., Polen, A., McSweeney, K., Colón-Burgos, D., Jernigan, I. (2021). Hurricane risk
424 perceptions and evacuation decision making in the age of COVID-19. *Bulletin of the*
425 *American Meteorological Society*. DOI:10.1175/BAMS-D-20-0229.1
426 de Bruin, W.B., Parker, A.M., Maurer, J. (2011). Assessing small non-zero perceptions of chance:
427 The case of H1N1 (swine) flu risks. *Journal of Risk and Uncertainty*, 42(2): 145-159.
428 Dostal, P.J. (2015). Vulnerability of urban homebound older adults in disasters: A survey of
429 evacuation preparedness. *Disaster Medicine and Public Health Preparedness*, 9(3): 301-
430 306.

FEMA (2020). *COVID-19 Pandemic Operational Guidance for the 2020 Hurricane Season*. US Department of Homeland Security FEMA. https://www.fema.gov/sites/default/files/2020-07/fema-2020-hurricane-pandemic-plan_english.pdf

Fitzsimons, G.J. (2008). Editorial: A death to dichotomizing. *Journal of Consumer Research*, 35(1): 5-8.

Jenkins, P., Laska, S., Williamson, G. (2007). Connecting future evacuation to current recovery: Saving the lives of older people in the next catastrophe. *Generations*, 31(4): 49-52.

Huang, S-K., Lindell, M.K., Prater, C.S. (2016). Who leaves and who stays? A review and statistical meta-analysis of hurricane evacuation studies. *Environment and Behavior*, 48(8): 991-1029.

IPCC. (2014). *Climate change 2014: Impacts, adaptation, and vulnerability. Contribution of Working Group II to the Fifth Assessment Report of the Intergovernmental Panel on Climate Change.* Cambridge: Cambridge University Press.

Ivers, L. C., Ryan, E.T. (2006). Infectious diseases of severe weather-related and flood related natural disasters. *Current Opinion in Infectious Diseases*, 19(5): 408- 56.

Kunreuther, H., Pauly, M. (2018). Dynamic insurance decision making for rare events: The role of emotions. *The Geneva Papers on Risk and Insurance-Issues and Practice*, 43(2): 335–355.

Lemonick, D. M. (2011). Epidemics after natural disasters. *American Journal of Clinical Medicine*, 8(3): 144-152.

Liddell, T.M., Kruschke, J.K. (2018). Analyzing ordinal data with metric models: What could possibly go wrong?. *Journal of Experimental Social Psychology*, 79: 328-348.

Meng, Y., Wu, P., Lu, W., Liu, K., Ma, K., Huang, L., Cai, J., Zhang, H., Qin, Y., Sun, H., Ding, W. (2020). Sex-specific clinical characteristics and prognosis of coronavirus disease-19 infection in Wuhan, China: A retrospective study of 168 severe patients. *PLoS Pathogens*, 16(4).

Meyer, M.A., Mitchell, B., Purdum, J.C., Breen, K., Iles, R.L. (2018). Previous hurricane evacuation decisions and future evacuation intentions among residents of southeast Louisiana. *International Journal of Disaster Risk Reduction*, 31: 1231-1244.

Morss, R.E., Demuth, J.L., Lazo, J.K., Dickinson, K., Lazrus, H., Morrow, B.H. (2016). Understanding public hurricane evacuation decisions and responses to forecast and warning messages. *Weather Forecast*, 31(2): 395-417.

Nakanishi, H., Black, J., Suenaga, Y. (2019). Investigating the flood evacuation behaviour of older people: A case study of a rural town in Japan. *Research in Transportation Business & Management*, 30.

NAIC/CIPR Research Library (2020). Disaster Preparedness & COVID-19. *Regulator Insight* August 2020. https://content.naic.org/sites/default/files/inline-files/Regulator%20Insight%20-Disaster%20Preparedness%20and%20COVID-19_3.pdf

NOAA (2020). Record-Breaking Atlantic Hurricane Season Draws to An End. 24 November 2020. https://www.noaa.gov/media-release/record-breaking-atlantic-hurricane-season-draws-to-end

Philips, C.A., Caldas, A., Cleetus, R., Dahl, K.A., Declet-Barreto, J., Licker, R., Merner, L.D., Ortiz-Partida, J.P., Phelan, A.L., Spanger-Siegfried, E., Talati, S., Trisos, C.H., Carlson, C.J. (2020). Compound climate risks in the COVID-19 pandemic. *Nature Climate Change*, 10: 586–588.

Robinson, P.J., Botzen, W.J.W. (2018). The impact of regret and worry on the threshold level of concern for flood insurance demand: Evidence from Dutch homeowners. *Judgment and Decision Making*, 13(3): 237-245.

Robinson, P.J., Botzen, W.J.W. (2019). Determinants of probability neglect and risk attitudes for disaster risk: An online experimental study of flood insurance demand among homeowners. *Risk Analysis*, 39(11): 2514-2527.

Rosenkoetter, M.M., Covan, E.K., Cobb, B.K., Bunting,S., Weinrich, M. (2007). Perceptions of older adults regarding evacuation in the event of a natural disaster. *Public Health Nursing*, 24(2): 160-168.

Schultz, J.M., Kossin, J.P., Ali, A., Borowy, V., Fugate, C., Espinel, Z., Galea, S. (2020). Superimposed threats to population health from Tropical Cyclones in the prevaccine era of COVID-19. *The Lancet Planetary Health*, 4: e506–e508.

Shukla, M.A., Woc-Colburn, L., Weatherhead, J. E. (2018) Infectious diseases in the aftermath of hurricanes in the United States. *Current Tropical Medicine Reports*, 5: 217–223.

491 Smith, S.M., Tremethick, M.J., Johnson, P., Gorski, J. (2009). Disaster planning and response:
492 Considering the needs of the frail elderly. *International Journal of Emergency*
493 *Management*, 6(1): 1-13.
494 Sorensen, J.H. (2000). Hazard warning systems: Review of 20 years of progress. *Natural Hazards*
495 *Review*, 1(2): 119-125.
496 Woloshin, S., Schwartz, L.M., Byram, S., Fischhoff, B., Welch, H.G. (2000). A new scale for
497 assessing perceptions of chance: A validation study. *Medical Decision Making*, 20(3): 298-
498 307.

Supplementary Information

Worry about flooding

Please tell me if you strongly agree, agree, neither agree nor disagree, disagree or strongly disagree with the following: "I am worried about the danger of a flood at my current residence."

- □ Strongly agree
- □ Agree
- □ Neither agree nor disagree
- □ Disagree
- □ Strongly disagree
- □ Not sure

Perceived flood probability

What is your best estimate of how often a flood will occur at your home?

- □ More often than 1 in 10 years
- □ Exactly 1 in 10 years
- □ Between 1 in 10 years and 1 in 100 years
- □ Exactly 1 in 100 years
- □ Between 1 in 100 years and 1 in 1000 years
- □ Exactly 1 in 1000 years
- □ Less often than 1 in 1000 years
- □ Not sure

Concern about flooding

Please tell me if you strongly agree, agree, neither agree nor disagree, disagree or strongly disagree with the following: "The probability of flooding is so low that I am not concerned about the consequences of a flood."

- □ Strongly agree
- □ Agree
- □ Neither agree nor disagree
- □ Disagree
- □ Strongly disagree
- □ Not sure

Voluntary evacuation intention

Please tell me if you are extremely likely, likely, somewhat likely or not at all likely to evacuate to a safer place this hurricane season if a voluntary evacuation were to be ordered for your county.

- □ Extremely likely
- □ Likely
- □ Somewhat likely
- □ Not at all likely
- □ Not sure

Obstacles to evacuation

Are there any potential obstacles which may prevent you from evacuating during the threat of a hurricane? Select all that apply.

- □ Not owning a car
- □ Disability
- □ Job requirements
- □ Material possessions
- □ Stubborn family members
- □ No place to go
- □ Unable to pay for hotel costs
- □ A pet
- □ Staying in home to prevent coronavirus infections
- □ Other: _____
- □ No potential obstacles

Perceived coronavirus infection probability

How likely do you think it is that you will personally be infected by the coronavirus?

- □ Very likely
- □ Likely
- □ Not likely/not unlikely
- □ Unlikely
- □ Very unlikely
- □ Not sure

Concern about COVID-19

Please tell me if you strongly agree, agree, neither agree nor disagree, disagree or strongly disagree with the following: “The probability of being infected by the coronavirus is so low that I am not concerned about its consequences.”

- □ Strongly agree
- □ Agree
- □ Neither agree nor disagree
- □ Disagree
- □ Strongly disagree
- □ Not sure

Expect to get ill from COVID-19

Suppose you became infected by the coronavirus. How ill do you expect to get from the virus?

- □ Extremely ill
- □ Very ill
- □ Quite ill
- □ A little bit ill
- □ Not ill at all
- □ Not sure

Worry about COVID-19

Please tell me if you strongly agree, agree, neither agree nor disagree, disagree or strongly disagree with the following: “I am worried about becoming infected by the coronavirus.”

- □ Strongly agree
- □ Agree
- □ Neither agree nor disagree
- □ Disagree
- □ Strongly disagree
- □ Not sure

Trust government response COVID-19

How would you grade how much you trust the government in terms of how it is dealing with the coronavirus pandemic? Please grade on a scale from 0 to 10, where 0 means ‘no trust at all’ and 10 means ‘trust completely’.

Score _____

Age

How old are you?

Age _____

Education

What is your highest completed level of education?

□ Some high school

□ High school graduate

□ Some college

□ College graduate

□ Post graduate

□ Refused

Income

Which of the following ranges best describes your total household income for 2019 before taxes?

□ Less than $10,000

□ $10,000 to $24,999

□ $25,000 to $44,999

□ $45,000 to $ 74,999

□ $75,000 to $124,999

□ $125,000 or more

□ Don't know

□ Refused

Home value

What is approximately the current market value of your home?

□ Less than $100,000

□ $100,000 to $149,999

□ $150,000 to $199,999

□ $200,000 to $ 299,999

□ $300,000 to $399,999

□ $400,000 to $599,999

□ $600,000 to $799,999

□ $800,000 or more

☐ Don’t know

☐ Refused

Home owner

Do you rent or own your home?

☐ Renter

☐ Property owner

☐ Other: _____

☐ Refused

Length of residence

How long have you lived in your home (in years)?

_____

Gender

Are you male or female?

☐ Male

☐ Female

☐ Refused

A Resource for the State of Florida

SECTION 6

Education and Outreach Programs to Convey the Benefits of Various Hurricane Loss Mitigation Devices and Techniques

A Report Submitted to:
The State of Florida Division of Emergency Management

Prepared By:
Erik Salna

The International Hurricane Research Center (IHRC)
Florida International University

July 30, 2021

Executive Summary:

The FIU International Hurricane Research Center developed and coordinated education and outreach activities to build on the foundation of previous work under this grant and showcased the hurricane-loss mitigation objectives of the HLMP.

For the 2020-2021 performance period, the below mentioned educational partnerships, community events, and outreach programs were developed:

Wall of Wind Mitigation Challenge (WOW! Challenge): Friday, March 26th, 2021
(Due to COVID-19, Miami-Dade County Public Schools requested the competition be done virtually.)
The International Hurricane Research Center (IHRC), located on the campus of Florida International University (FIU), has developed the Wall of Wind Mitigation Challenge (WOW! Challenge), a judged competition for South Florida high school students. As the next generation of engineers to address natural hazards and extreme weather, this STEM education event features a competition between high school teams to develop innovative wind mitigation concepts and real-life human safety and property protection solutions. The mitigation concepts are tested live at the FIU NHERI Wall of Wind (WOW) Experimental Facility (EF), located on FIU's Engineering Campus.

- The objective for the 2021 Wall of Wind Mitigation Challenge was for students to design a wind mitigation solution to reduce the impact of wind scour on a building's flat roof.
- Each student team was supplied with a model flat roof and their wind mitigation solution had to prevent gravel on the roof from being blow away by hurricane-force winds.
- The student teams prepared three components for the competition: a physical test, an oral presentation, and a written technical paper.
- The competition included teams from five South Florida high schools.
- *First Place* was awarded to G. Holmes Braddock Senior High School.
- *Second Place* was awarded to Miami Coral Park Senior High School.
- *Third Place* was awarded to MAST Academy.
- A complete scoring summary can be found on the following link: https://www.ihrc.fiu.edu/wp-content/uploads/2021/07/2021_WOW_CHALLENGE_RESULTS_SUMMARY.pdf

Media exposure resulted in great positive visibility in the community for the IHRC, FIU and FDEM's message of mitigation:

- FIU News: https://news.fiu.edu/2021/virtual-wall-of-wind-challenge-inspires-high-school-students-to-tackle-real-world-problems?utm_source=Newsletter&utm_medium=Email&utm_campaign=FIU%20Newsletter

Eye of the Storm (Science, Mitigation & Preparedness) In-Person Event: May 15th, 2021
The Museum of Discovery & Science (MODS), located in Fort Lauderdale, FL, assisted the IHRC in planning, coordinating and facilitating this free admission public education event that

showcased special hands-on, interactive activities and demonstrations teaching hurricane science, mitigation and preparedness.

- For this year's onsite, in-person Eye of the Storm, the Museum of Discovery and Science (MODS) in Fort Lauderdale had COVID-19 protocols in place for all staff, partners, vendors, participants, volunteers, and public: Healthy Scientists Make Healthy Choices Protocol | MODS.
- A record 3,750 visitors attended Eye of the Storm, showcasing special interactive activities and demonstrations teaching hurricane science, mitigation and preparedness.
- A Participant Post Survey showed 62.16% of respondents increased their knowledge about wind engineering and mitigating hurricane damage and 67.57% will be taking steps to mitigate hurricane damage.

Media exposure resulted in great positive visibility in the community for the IHRC, FIU and FDEM's message of mitigation.

- FIU News Website "University helps community prepare for hurricane season," June 7, 2021.

NOAA Hurricane Awareness Tour: Cancelled due to COVID-19.

Get Ready, America! The National Hurricane Survival Initiative: Cancelled due to lack of sponsorships.

Education and Outreach Programs:

Wall of Wind Mitigation Challenge (WOW! Challenge): Friday, March 26th, 2021

COVID-19:
Due to COVID-19, Miami-Dade County Public Schools requested the Wall of Wind Challenge be done virtually.

Overview:
The International Hurricane Research Center (IHRC), located on the campus of Florida International University (FIU), has developed the Wall of Wind Mitigation Challenge (WOW! Challenge), a judged competition for South Florida high school students. As the next generation of engineers to address natural hazards and extreme weather, this STEM education event features a competition between high school teams to develop innovative wind mitigation concepts and real-life human safety and property protection solutions. The student teams prepare three components for the competition: a physical test, an oral presentation, and a written technical paper. The mitigation concepts are tested live at the FIU NSF-NHERI Wall of Wind (WOW) Experimental Facility (EF), located on FIU's Engineering Campus.

The WOW! Challenge requires problem solving, teamwork, and creativity, and it includes aspects of science, technology, engineering, mathematics, architectural design, and business entrepreneurship. The high school students are inspired to pursue STEM education and careers in wind engineering and hurricane mitigation. The competition has real world applications and

benefits society as a whole by developing hurricane mitigation techniques that can lead to enhanced human safety, property loss reduction, insurance cost reduction, and a culture of hurricane preparedness. There is no other competition like it in the entire country, and it's a once in a lifetime opportunity for the high school students – *an experience they never forget*.

2021 Wall of Wind Mitigation Challenge:
The objective for the 2021 Wall of Wind Mitigation Challenge was for students to design a wind mitigation solution to reduce the impact of wind scour on a building's flat roof. Each student team was supplied with a model flat roof and their wind mitigation solution had to prevent gravel on the roof from being blow away by hurricane-force winds. For the competition, the flat roofs were attached to a building model representing a one-story building and then tested by the FIU NSF-NHERI Wall of Wind Experimental Facility to evaluate their effectiveness of the wind mitigation solution.

The wind mitigation solution could be created by:

1. Constructing a parapet on the roof.
2. Constructing and attaching a mitigation device along the upper edges of the building's walls.
3. Constructing and attaching a mitigation device along the perimeter of the roof
4. Any combination of options (1) and (2) and (3)

Teams from five South Florida high schools participated in the competition. They were from Miami Coral Park Senior High School, MAST Academy, Booker T. Washington High School, G. Holmes Braddock High School and Florida Christian School.

An informational virtual Zoom workshop detailing the 2021 WOW! Challenge was provided for the five teams before the actual competition. The virtual workshop PowerPoint was made available on the WOW! Challenge web page. All of the details of the rules and guidelines for the three required components are also found on the WOW! Challenge web page located at: http://www.ihrc.fiu.edu/outreach-education/wall-of-wind-challenge/.

The Physical Test Description:

- Each team was able to watch their flat roof get tested on a live Zoom link.
- Physical tests occurred on a uniform cube (3ft x 3ft x 3ft). These cubes represented a building with a flat roof.
- Teams were provided with the top portion of the cube (3ft x 3ft x 0.5ft), which represented the flat roof, on which they attached their wind mitigation solution (see Figure 1).
- Gravel was applied on top of the flat roof. As already stated, the objective was to reduce the amount of scour on the flat roof.
- As shown shaded in green in Figure 2, the restrictions for the wind mitigation solutions if using a solid parapet, were to be no more than 1½ inches tall and ¾ inch thick. This parapet could be made out of any material.
- There was no restriction as to what could be placed in the area that extended 2¼ inches out of the top outer corner of the parapet and 6 inches below this same point. Any material could be used here. This area is shaded in black in Figure 2.

- In the 3” by 6” area above the area shaded in red, any material used was required to be 40% porous or greater. Proof of porosity was required. This area is shaded in red on Figure 2.
- Any type of non-hazardous material was allowed and considered acceptable for designing the wind mitigation solution, given that the solution complied with the construction guidelines. Some common examples of acceptable materials included (but not limited to) wood, foam, plastic, metal, white glue, super glue, and epoxy.
- No material that extended outwards from the walls were to be used to decorate the building models. Paint, stickers, etc. were acceptable. The flat roof was not to be tampered with in any way.

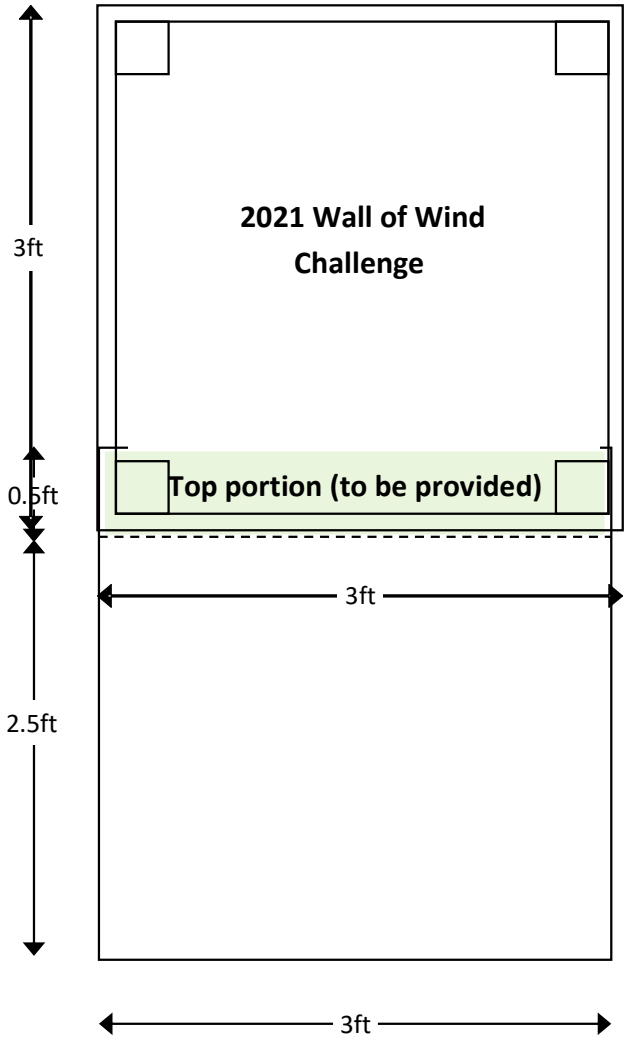

Figure 1. Top and side views of the test cube representing a building with a flat roof.

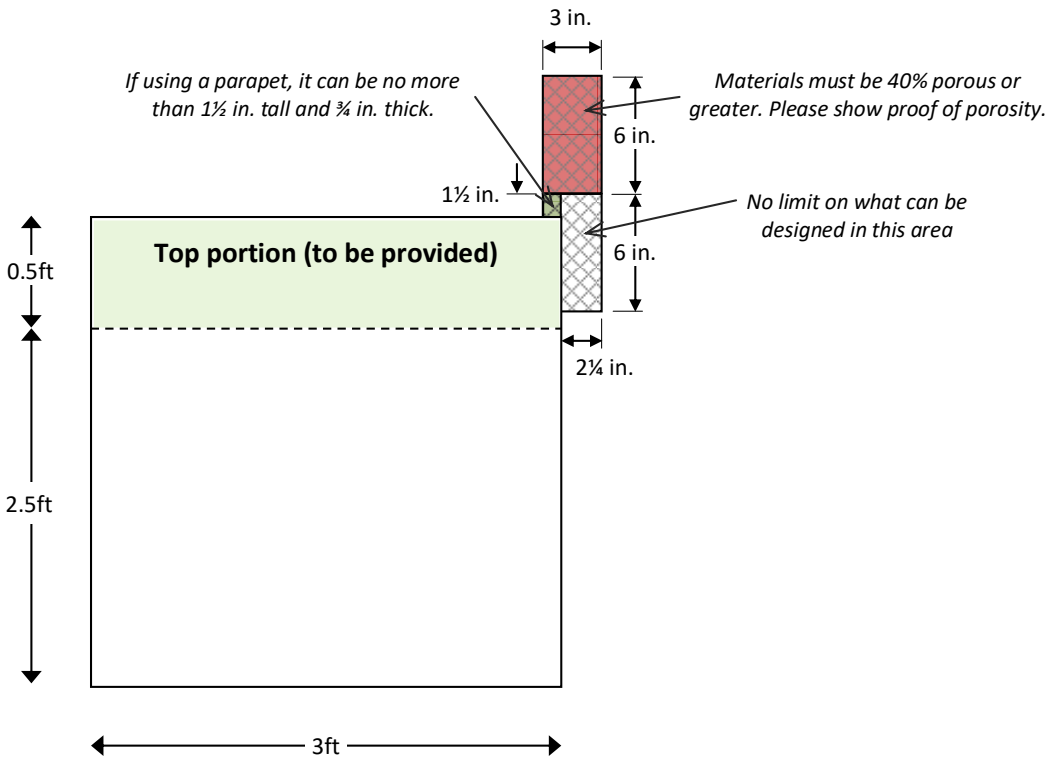

Figure 2. Design parameters for the flat roof and wind mitigation solution.

The Oral Presentation Description:

- Oral presentations were done virtually by a recorded Zoom video and judged by the IHRC NSF-NHERI Wall of Wind faculty and research team.
- Oral presentations were to be no more than 7 minutes.

Oral presentations and written technical papers had to include these items:

- Effectively communicate some scientific process or analysis involved with the development of their wind mitigation solution for their flat roof, including the 40% porosity requirement.
- What is hurricane wind mitigation?
- What is the importance of hurricane wind mitigation?
- How is hurricane wind mitigation being addressed with your flat roof?
- In addition to wind engineering, presentations could also include disciplines such as architecture, business, economics, finance, marketing, geosciences, insurance, political science, sociology, and urban planning.

All three required components of the competition were judged and scored by the IHRC NSF-NHERI Wall of Wind faculty and research team.

The judges were:

- Amal Elawady, PhD, Assistant Professor, Department of Civil & Environmental Engineering, College of Engineering and Computing, International Hurricane Research Center, Extreme Events Institute, Florida International University
- Ioannis Zisis, PhD, Assistant Professor, Dept. of Civil & Environ. Engineering, Co-Director, Lab. Wind Engineering Research, Extreme Events Institute, Florida International University
- Steven W. Diaz, PhD, PE, Program Director/Site Operations Manager, NSF-NHERI Wall of Wind Experimental Facility, International Hurricane Research Center, Extreme Events Institute, Florida International University
- Walter Conklin, B.S., Laboratory and Health and Safety Manager, NSF-NHERI Wall of Wind Experimental Facility, International Hurricane Research Center, Extreme Events Institute, Florida International University
- James Erwin, M.S., NSF-NHERI Wall of Wind Research Specialist II, International Hurricane Research Center, Extreme Events Institute, Florida International University
- Roy Liu-Marques, M.S., Project Engineer, NSF-NHERI Wall of Wind Experimental Facility, International Hurricane Research Center, Extreme Events Institute, Florida International University
- Dejiang Chen, Ph.D., Research Specialist, NSF-NHERI Wall of Wind Experimental Facility, International Hurricane Research Center, Extreme Events Institute, Florida International University
- Erik Salna, M.S., Associate Director for Education and Outreach, International Hurricane Research Center, Extreme Events Institute, Florida International University

The scores from the judges for all three required components were added up for a cumulative total and used to determine the top three teams; the final results were as follows:

- *First Place* was awarded to G. Holmes Braddock Senior High School.
- *Second Place* was awarded to Miami Coral Park Senior High School.
- *Third Place* was awarded to MAST Academy.

A complete scoring summary can be found on the following link:
https://www.ihrc.fiu.edu/wp-content/uploads/2021/07/2021_WOW_CHALLENGE_RESULTS_SUMMARY.pdf

Once again the Wall of Wind Mitigation Challenge was supported by local media. This media exposure resulted in great positive visibility in the community for the IHRC, FIU and FDEM's message of mitigation. The following media representative participated:

- FIU News: https://news.fiu.edu/2021/virtual-wall-of-wind-challenge-inspires-high-school-students-to-tackle-real-world-problems?utm_source=Newsletter&utm_medium=Email&utm_campaign=FIU%20Newsletter

The Wall of Wind Mitigation Challenge received positive feedback from the teachers and students.

Booker T. Washington Senior High School:

- *"The FIU WOW challenge this year has truly been a great rewarding experience for my students. During this unprecedented time when all things are scaled back, the FIU Wall*

of Wind Challenge provided our MDCPS students the opportunity to put into physical practice all the concepts they are learning in their hybrid virtual and physical STEM classes during this 2020-2021 pandemic school year. Through the FIU Wall of Wind Challenge we are moving on STEM wise. NOT even Covid-19 can stop us now. Go BTW Tornadoes - Go FIU Wall of Wind Challenge." Mr. Bidokwu D.O, Chemistry, Physics and Engineering Teacher, Booker T. Washington Senior High School

Florida Christian School:

- *"Thank you FIU for the Challenge. It was a great learning experience. South Florida really needs these real life experiences. The Challenge helped my students to bond together and become a better team. It was a great hands-on application to our Physics Honors Class."* Lisa Pericles, Science Department Chairperson, Florida Christian School

G. Holmes Braddock Senior High School:

- *"The Wall of Wind Challenge was a great experience for me. The hard work led me to get closer with my classmates as we all collectively set ourselves towards the same goal. The Challenge allowed me to learn a lot of new information about wind mitigation that I previously did not know. I'm grateful for the experience that the Wall of Wind Challenge gave me and I would totally recommend it to anyone who is considering partaking."* Bryan Pacheco, Senior
- *"The Wall of Wind Challenge was a great way for my students to get hands on exposure to solving real-life problems. My students and I enjoyed the experience, and they learned a lot about wind mitigation. Overall, this was an amazing educational experience."* Lacey Simpson, Science Department, G. Holmes Braddock Senior High School

MAST Academy:

- *"Thank you for giving me the opportunity to participate in this challenge. I am not a person that collaborates with others much because I don't feel comfortable, however, this experience made me feel different. The WOW challenge gave insight of the career path I'd like to take in the future - engineer."* Anthony Delgado, Freshman
- *"This was a great experience for students to work on life skills such as teamwork, critical thinking, creativity and most important problem-solving. I noticed how members of the team came out of their comfort zone. Thank you again for the opportunity to participate in this challenge and for your time. The award is truly beautiful, and my students were so excited about it. This challenge definitely helps them build confidence in themselves."* Ms. Alvarez, Biology Instructor, MAST Academy

Miami Coral Park Senior High School:

- *"The Wall of Wind Challenge offered me an opportunity to gain insight in the field of wind engineering which has sparked an interest that I did not know I had. This challenge has become a memorable learning experience that I hope to carry on in the future."* Jenna Silvera, Junior
- *"A one of a kind experience."* Anaya Brooks, Sophomore
- *"Engineers like to solve problems and as a young woman, I am inspired by the several challenges of high-speed wind mitigation to be solved with Solidworks simulations and a*

well-designed constructive model with breathable screens. This allowed me to learn more about multiple weather patterns in Miami and encouraged me to pursue a career as a civil engineer." Angelica Verity, Senior

- *"The Wall of Wind Challenge has not only helped me grow as a leader in a group but attempt to work better in a group with people that have different interests in the many fields of engineering. Because of this year's challenge, it has helped me with improving my skills in leadership and teamwork in the field of architecture."* Elizabeth Miqueo, Senior
- *"This competition is one of my favorites! The excitement builds up from the anxiety of testing your project in the Wall of Wind. To the surprise of the results. You can watch the video replay over and over and never get tired of it."* Charlie Delahoz, Engineering/Architecture Magnet Teacher, Miami Coral Park Senior High School

NHERI Wall of Wind (WOW) Experimental Facility (EF):

- *"The virtual Wall of Wind Challenge is a platform to educate high school students in our community with regards to wind engineering and how to conceive and validate wind mitigation concepts. This event informs students about the importance of mitigation and prepares them as future leaders in disaster mitigation. These young students get motivated in joining STEM careers and possibly enrolling at FIU with the dream of performing Wall of Wind research and imparting resilience to our coastal communities."* Arindam Gan Chowdhury, PhD, Professor, Dept. of Civil & Environ, Engineering PI and Director, NHERI Wall of Wind (WOW) Experimental Facility (EF), Co-Director, Lab. Wind Engineering Research, Extreme Events Institute, Florida International University

Each high school team received a flat roof.

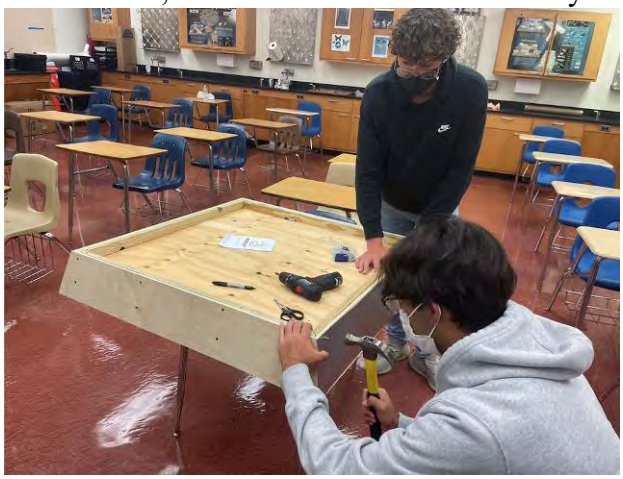

G. Holmes Braddock working on their roof.

Booker T. Washington working on their roof.

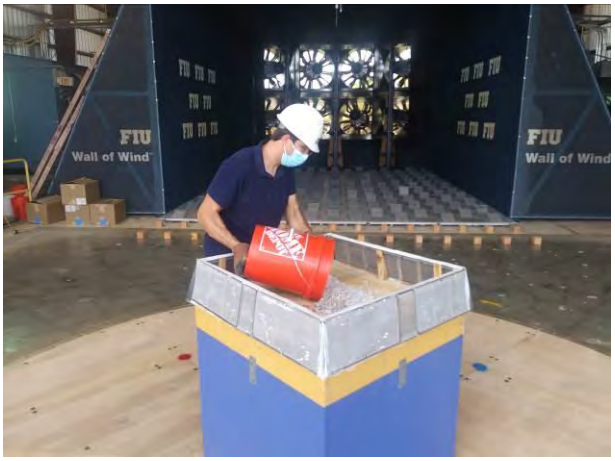

Placing gravel on roof for Wall of Wind test.

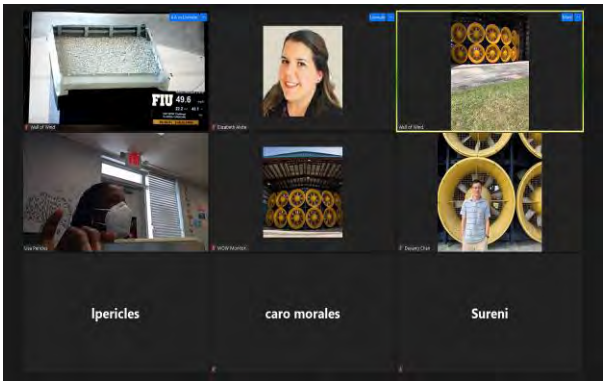

Florida Christian School live Zoom test.

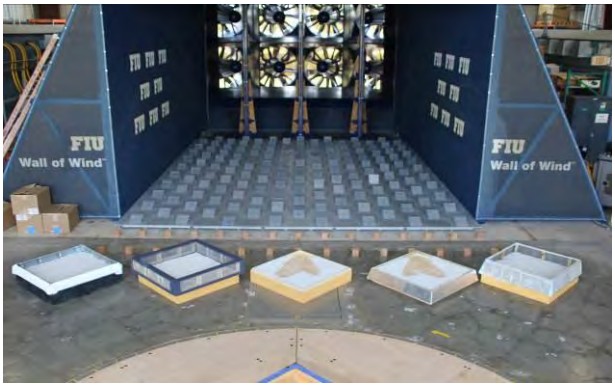

Rooftops in Wall of Wind Challenge.

1st Place Roof: G. Holmes Braddock Sr. H.S.

2nd Place Roof: Miami Coral Park Sr. H.S.

3rd Place Roof: MAST Academy

1st Place Team: G. Holmes Braddock Sr. H.S.

2nd Place Team: Miami Coral Park Sr. H.S.

3rd Place Team: MAST Academy

Eye of the Storm (Science, Mitigation & Preparedness) Event: May 15th, 2021

COVID-19:
For this year's onsite, in-person Eye of the Storm, the Museum of Discovery and Science (MODS) in Fort Lauderdale had COVID-19 protocols in place for all staff, partners, vendors, participants, volunteers, and public: Healthy Scientists Make Healthy Choices Protocol | MODS

Overview:
The Museum of Discovery & Science (MODS), located in Fort Lauderdale, FL, assisted the IHRC in planning, coordinating and facilitating this free admission public education event.
A record 3,750 visitors attended Eye of the Storm, showcasing special interactive activities and demonstrations teaching hurricane science, mitigation and preparedness. This included special learning activities for parents and children providing family fun throughout the day.

Key Messages:
1. Know Your Risk
2. Know Your Evacuation Zone
3. Complete Your Hurricane Plan
4. Address Any Special Needs
5. Assemble Your Supply Kit
6. Prepare Your Pets
7. Get an Insurance Check-Up
8. Protect Your Home
9. Help Your Neighbor

This collaborative community education outreach project partnered the IHRC with the Florida Division of Emergency Management, Broward County Emergency Management, City of Fort Lauderdale Emergency Management, NOAA's National Hurricane Center, and NOAA's Miami Office of the National Weather Service. Great support was provided by many community organizations, including Florida Power & Light and the International Hurricane Protection Association (IHPA) and local media. Due to COVID-19, several partners participated remotely through live Zoom presentations.

Media Release: https://eei.fiu.edu/wp-content/uploads/2021/05/2021_EOTS_Release_FINAL.pdf

Eye of the Storm Activities:
Special interactive exhibits and demonstrations included:

- IHPA Live Air Cannon Demonstrations Showing Debris Impact of Shutters and Windows
- How the Weather Works Interactive Weather Education Activities
- Weather Jeopardy Game
- TV Hurricane Broadcast Center
- Live Tropical Weather Briefing by NOAA's National Hurricane Center
- FIU NSF-NHERI Wall of Wind Exhibit
- Live MODS Live Weather Science Demonstrations
- Special Showings of Built to Last? Resilience Documentary in IMAX Theater

Various distinguished hurricane experts participated:

- Daniel Brown, Senior Hurricane Specialist, NOAA's National Hurricane Center (by live Zoom)
- John Cangialosi, Hurricane Specialist, NOAA's National Hurricane Center (by live Zoom)
- Robert Molleda, Warning Coordination Meteorologist, National Weather Service-Miami (by live Zoom)

Special guests:

- Broward County CERT Teams

Special live interactive theater presentations:

- Tsunami Tim Live Weather Education Theater Shows
- How The Weather Works Live Theater Show

Assessment Activities:
Participant Post Survey

- 879 unique email addresses
- 204 recipients opened the email (24% open rate)
- 43 recipients clicked on the link (21% click rate)
- 37 responses collected (86% response rate of the clicks)
- 0 skipped questions

Four Survey Questions:

1. Did you attend the 2021 Eye of the Storm event?
2. To what extent did this event increase your knowledge about how wind engineering can mitigate hurricane damage?
3. To what extent are you interested in learning more about wind engineering?
4. To what extent will you be taking to steps to mitigate hurricane damage to your property?

Positive Results:

- 97.3% Attended the Event
- 62.16% Increased Their Knowledge About Wind Engineering and Mitigating Hurricane Damage
- 37.84% Would Like to Learn More About Wind Engineering
- 67.57% Will Be Taking Steps to Mitigate Hurricane Damage

Message Board #1 During Eye of the Storm at MODS:

- What did you learn today about protecting your home from hurricanes?
- Key responses were, “hurricane shutters are important” and “tape on windows doesn’t work against a storm.”

Message Board #1 During Eye of the Storm at MODS

Message Board #2 During Eye of the Storm at MODS:

- Would you like to study wind engineering? (Definitely, maybe, don't know, definitely not)
- Many positive responses.

Public Relations Campaign Summary facilitated by MODS:

- Media Pickup: 53
- Circulation: 121,298,810+

Media Coverage:
The Eye of the Storm received great coverage by the local South Florida media. This resulted in great positive visibility in the community for IHRC, FIU and FDEM's message of hurricane preparedness and mitigation:

- *The Boca Raton Observer*, "Explore the Eye of the Storm at the Museum of Discovery & Science," April 20, 2021. The website has a circulation of 27,700.
- Florida International University's International Hurricane Research Center, Florida Division of Emergency Management and the Museum of Discovery and Science Announce Eye of the Storm Event, May 3, 2021.
- South Florida Sun-Sentinel.com, "Community and Entertainment Events," May 9, 2021. The website has a circulation of 220,000.
- WPTV, "Explore the Eye of the Storm at the Museum of Discovery & Science," The website has a circulation of 2,120.
- Sun-sentinel.com, "Sunday calendar: Community and entertainment events starting May 9," May 7, 2021. The website has a circulation of 220,000.
- Go Riverwalk newsletter, "Eye of the Storm," May 12, 2021. The newsletter has a circulation of 10,000.
- Go Riverwalk website, "Explore Eye of the Storm," May 12, 2021. The website has a circulation of 15,300.
- NewsRadio WIOD, "Explore Eye of the Storm," May 12, 2021. The website has a circulation of 15,000.
- Sun-sentinel.com, "Explore the Eye of the Storm at the Museum of Discovery & Science," May 15, 2021. The website has a circulation of 4,850,000.
- The Published Reporter, "Explore the Eye of the Storm at the Museum of Discovery & Science," May 15, 2021. The website has a circulation of 22,000.
- South Florida Reporter, "Explore the Eye of the Storm at the Museum of Discovery & Science," May 15, 2021. The website has a circulation of 22,000.
- 99JAMZ, "Explore the Eye of the Storm at the Museum of Discovery & Science," May 15, 2021. The website has a circulation of 5,250.
- Local10.com, "Explore the Eye of the Storm at the Museum of Discovery & Science," May 15, 2021. The website has a circulation of 4,750,000.
- SpinGo, "Explore the Eye of the Storm at the Museum of Discovery & Science," May 15, 2021. The website has a circulation of 44,500.
- Miami on the Cheap, "Explore the Eye of the Storm at the Museum of Discovery & Science," May 15, 2021. The website has a circulation of 112,000.

- Evensi, "Explore the Eye of the Storm at the Museum of Discovery & Science," May 15, 2021. The website has a circulation of 95,800.
- Sailboat Bend - Parkbench, "Explore the Eye of the Storm at the Museum of Discovery & Science," May 15, 2021. The website has a circulation of 197,000.
- EventCrazy, "Explore the Eye of the Storm at the Museum of Discovery & Science," May 15, 2021. The website has a circulation of 234,000.
- Yelp, "Explore the Eye of the Storm at the Museum of Discovery & Science," May 15, 2021. The website has a circulation of 16,000,000.
- Stay Happening, "Explore the Eye of the Storm at the Museum of Discovery & Science," May 15, 2021. The website has a circulation of 2,980,000.
- FIU News Website "FIU hosts congressional briefing on preparing communities for hurricane season," June 1, 2021. The website has a monthly circulation of 432,330.
- FIU News Website "University helps community prepare for hurricane season," June 7, 2021. The website has a monthly circulation of 432,330.

2020 Virtual Eye of the Storm:
The 2020 virtual Eye of the Storm, the 12-episode "evergreen" video series, was re-promoted in conjunction with the Eye of the Storm in-person event on May 15th.

All the videos are listed on the MODS virtual Eye of the Storm web-page:
https://mods.org/?page_id=16093
All the videos are also listed on the following MyFloridaCFO web-page: Plan Prepare Protect: Are You Disaster Ready? Eye of the Storm Videos (myfloridacfo.com)

The virtual Eye of the Storm has resulted in a hugely successful digital marketing campaign and has expanded the reach and impact beyond South Florida to other states on the Gulf of Mexico and the U.S. eastern seaboard at risk of a hurricane landfall. Social media channels have included Facebook, Twitter, Instagram, LinkedIn and YouTube.

Update as of July 15th:
Digital Marketing Campaign Summary for 2020 Virtual Eye of the Storm:
- Views: 872,280+
- Impressions: 7,825,145+
- Engagements and Clicks: 62,850+
- Hours Watched: 5,413+

Top Target Audience Demographics
- Gender: 56.8% Female, 43.2% Male
- Age: 47.9% between the ages of 25 - 44

Top Locations
- Puerto Rico: 64.2%
- Florida: 48.9%
- Texas: 23.6%
- Louisiana: 4.4%
- Virginia: 1.7%
- North Carolina: 1.4%

- South Carolina: 1.2%

Fort Lauderdale CERT and SWAT Vehicles

Live Weather Safety Theater Shows

FIU Wall of Wind Exhibit

NOAA-NHC (by live mobile Zoom robot)

Broward County Emergency Management

Creating Hurricane Storm Cloud

Broward County Humane Society

Live Air Cannon Missile Demonstrations

Mitigation Education: Simpson Strong-Tie

Mitigation Education: Atlantic Shutters

Families Building Houses for Wind Testing

Interactive Weather Experiments

American Red Cross (by live Zoom)

Fort Lauderdale CERT Team

A Resource for the State of Florida

HURRICANE LOSS REDUCTION FOR HOUSING IN FLORIDA

FINAL REPORT
For the Period October 23, 2019 to March 31, 2021

A Research Project Funded by:
The State of Florida Division of Emergency Management
Through Contract #DEM-HL00031-B0053

Prepared by
The International Hurricane Research Center (IHRC)
Florida International University (FIU)

April 15, 2021

Final Report

Table of Contents

Section 1
Executive Summary

Six major efforts were identified by the International Hurricane Research Center (IHRC) for the Hurricane Loss Mitigation Program (HLMP) Fiscal Year 2019-2020. A No Cost Extension (NCE) was received through March 2021 as several programs were impacted by the COVID-19 pandemic. Funding was dedicated to areas of structural mitigation analysis, integrated flood modeling analysis, and education and outreach. In keeping with the comprehensive agenda of the research topics for this project, the IHRC organized a multidisciplinary team of researchers, students and support staff to complete the stated objectives. The following is a summary of research findings:

Research Area 1: Experimental and Analytical Assessment of Effects of Leakage around Doors, Windows, and Other Openings on Internal Pressures in Residential Buildings (PI: Dr. Arindam Gan Chowdhury)

Background air leakage is common in residential buildings due to the typical materials and installation techniques involved in constructing building envelope components such as walls, doors, and windows. Moreover, the porosity created by cracks and deficiencies around doors and windows as well as openings at soffits, utility ducts, and vents may lead to further air leakage. To assess the internal pressures generated due to air leakage, experimental testing has been carried out at the NSF NHERI Wall of Wind Experimental Facility (WOW EF) at Florida International University (FIU) on a large-scale building model with a gable roof. Different leakage areas were modeled on a wall of the test building to simulate the effects of various deficiencies and defects. In addition, different wind speeds and defect aspect ratios were considered to investigate the Reynolds number (Re) effect on the internal pressure. Results of experimental testing showed that the internal pressure increased with the increase in leakage area. The experimental results were compared with internal pressure coefficients provided by ASCE 7-16 for an enclosed building. It was shown that ASCE7-16 underestimated peak internal pressures for all leakage configurations except the background leakage case. The new knowledge is expected to be used

for the enhancement of the Florida Public Hurricane Loss Model (FPHLM). Improved estimation of peak internal pressures and their use in risk modeling (such as by the FPHLM) may lead to significantly improved models. Such models can be used to inform designs and retrofitting techniques to reduce damage and property losses during extreme wind events, which will positively impact the economy of the State of Florida and increase the safety of its residents. The test-based findings may also be used to enhance wind load provisions in standards and codes (e.g. ASCE 7 Standard and Florida Building Code). The enhanced provisions will lead to informed resilient designs to protect buildings and the residents in the State of Florida and across the U.S.

Research Area 2: Numerical and Experimental Investigation to Codify Wind Pressure Distribution of Elevated House (PI: Dr. Amal Elawady)

During recent hurricane seasons, varying levels of damage have occurred on elevated structures located in vulnerable coastal regions. The damage observations were primarily linked to wave and wind actions on the structure. The wind velocity increase and the presence of the air gap beneath the building affect the resulting wind pressure on the building surfaces. The affected houses have different geometries, including the number of stories, the stilt heights and the building aspect ratio. Therefore, more investigation is needed to provide a comprehensive methodology to predict wind loads acting on elevated houses. This will reduce the failure probability and hence increase the structural reliability and safety of buildings located in coastal communities. To establish a database of wind loading parameters on elevated structures, an ongoing study is being conducted at FIU to assess the performance of various shapes of elevated house. The current Phase 3 research includes an experimental test performed at the Wall of Wind (WOW) Experimental Facility on a large scale single-story elevated house with different stilt heights: 0 ft, 7 ft, 12 ft, and 17 ft. In addition, several numerical simulations were done of a full-scaled elevated house with different stilt heights and different aspect ratio. A 7 ft stilt case including stairs was also numerically simulated to find out the effect of stairs on the wind flow characteristics.

The results showed that the pressure coefficient was higher in case of the single-story elevated house. Most of the noticeable differences occurred in the 16.8in (7 ft full-scale) stilt case. High suction pressures were seen along both the top and bottom edges of the sidewalls when the model was elevated above ground level. For the floor surface, the densified pressure tap distribution showed the pressure variation around the stilts in the two cases. A region of high suction pressure beneath the model occurred due to the vortices present at the oblique wind angles. These regions were larger in the single-story case compared to the two-story case. The experimental data obtained from the various cases of elevated houses were used to perform numerical simulations. The recorded wind velocity, turbulence intensity, and pressure time histories aided the choice for the boundary condition criteria of the computational domain. In

addition, the pressure distribution of the experimentally tested cases was used to validate the outcome of the numerical calculations.

The numerical simulation showed that the resulting local mean pressure coefficients were significantly higher for larger aspect ratio. The mean wind force on windward wall was found to be increasing rapidly with the increase of the stilt height or the aspect ratio. For instance, at oblique wind direction, the force ratio of the 17 ft stilt case windward wall reached to be triple its correspondent in the on-ground case. However, the side walls didn't experience a noticeable change. It was observed in the floor surface that the main reason of the pressure coefficient increase with stilt height is the oblique wind flow, which causes a high suction around the model stilts. The total shear force acting on the foundation showed a considerable increase as the stilt height increases, while the total vertical force dropped by elevating the house due to the presence of a new force on the floor. The overturning moment increased tremendously in larger stilt cases. The overturning moment increase was not as significant by increasing the aspect ratio, but the vertical force increase was considerable for larger aspect ratio cases. The flow streamlines inside the computational domain showed that the flow separation region increased as the stilt height increases. However, the flow separation region decreased by increasing the model aspect ratio. In the small stilt cases, the wind speed increased beneath the building floor due to venture effect through the airgap. A flow circulation of air took place between the two intermediate columns. This clarify the reason behind the high negative pressure around the model stilts. There was a slight reduction of the mean pressure coefficient in all surfaces of the elevated house with stairs except for the floor surface which showed a considerable reduction of the wind pressure. The total force acting on the elevated house (including wind load on the stairs) did not experience a noticeable change. The force share of the stairs was large and it should be considered in the design work.

For future studies, it is recommended to monitor the wind velocity beneath the house in smaller stilt cases as it leads to the occurrence of several damages. The observed increase in the mean pressure coefficient emphasizes the need to investigate the effect of changing the building aspect ratio. The observed increase in the vertical, shear forces and the overturning moments acting on the building foundations due to aspect ratio and stilt height increase, should also be taken into

consideration in the future design of elevated houses. The commonly used configuration of stairs did not show a noticeable change on the resulting pressure and it can be excluded from experimental testing to reduce time and cost.

Research Area 3: Codification Wind-induced Loads on Irregular Shaped Buildings (PI: Dr. Ioannis Zisis)

Extreme wind events impact the United States on an annual basis. These events have been responsible for numerous fatalities and yearly loses of $34 billion dollars in the residential sector. Considerable research has been performed to mitigate the impact of such events, however, a significant portion of the investigations has been directed towards mid- and high-rise structures, while the effect of residential building shape on the overall pressure distributions has been somewhat overlooked. The current wind load provisions provide information on the design of residential structures; however, these provisions have been developed by results obtained from regular shaped studies in the late 70's and improved by several other field and wind tunnel studies since then. With the advancement of technology and building techniques, the shapes of the residential structures have become much more complex than rectangles and squares. This report presents findings on the wind-induced effect on residential buildings with irregular plans and flat roofs.

The first task of this investigation was to identify common irregular shapes that structures may take. This was done by taking multiple satellite images of residential areas and identifying the shapes that were more common. The next task was to construct and test the building models at the Wall of Wind Experimental Facility at FIU, to assess the effect of building shape on the overall pressure distribution. Four irregular shaped modes, (shapes T, L and C) were constructed and tested. In parallel with the above tasks, the team designed and constructed a small-scale Atmospheric Boundary Layer (ABL) Wind Tunnel (WT) that is to be used in the next set of tests (DEM 2020-2021 cycle). The findings include mean and peak pressure coefficient contour plots along with area averaging envelope curves that provide information for the preliminary comparison with the current wind standards. Overall, the findings indicate that there is an increase of the pressures/suctions experienced by structures with irregular plan shapes. This is especially true in internal corners where high suction zones appear to develop due to complex

flow separation events. The database will be available for public use through the National Science Foundation (NSF) funded DesignSafe-CI domain.

Research Area 4: Development of integrated storm tide and freshwater flooding model Phase 3 (PI: Dr. David Kelly and Dr. Yuepeng Li)

During Phase 3 (2019-2021) the development of the SSFOF (Storm Surge and Freshwater Overland Flooding) model, based on the open-source TELEMAC modelling suite continued. In the previous 2017-2018 Phase 1 and 2019-2020 Phase 2 reports, IHRC developed the prototype SSFOF model which can simulate the compound effect of tide, storm surge and rain-fall run-off during hurricane impact. The SSFOF model was proven to be stable, robust, and efficient, and is one of the most advanced full-physics Nonlinear Shallow Water Equation (NSWE) based depth-averaged storm surge models. In the previous phases, the applications of the SSFOF model were focused on South Florida and adjacent coasts and open oceans using both historic and synthetic hurricanes. High resolution basins resolving small-features such as rivers, canals, streams, levees, dams, high ways, and major roads in Miami-Dade County, for example, have been developed to achieve better understanding of the county's vulnerability to storm surge and freshwater overland flooding. In this phase, investigations on hurricane impact to the North Florida region, as well as Lake Okeechobee, have been conducted with the SSFOF model. Moreover, the SSFOF model was further developed to include a full 3D model that is capable of modelling saltwater intrusion due to storm surges and tides.

The North Florida mesh was generated to cover the whole northwest coastline of Florida, where the Continuously Updated Digital Elevation Model (CUDEM) - 1/9 Arc-Second Resolution Bathymetric-Topographic Tiles that is being developed by NOAA's national Centers for Environmental Information (NCEI) have been employed for the bathymetry and topography. The finest grid resolution, however, was limited to the order of 100 m due to the relatively large basin. The storm surges caused by Hurricanes Hermine (2016) and Michael (2018) were simulated with result validation using NOAA tide gauges and USGS High Water Marks.

For Lake Okeechobee investigation, an independent new mesh was generated rather than using the previous South Florida mesh. Researchers determine that a high resolution mesh with spacing

around the Herbert Hoover Dike (HHD) at 10 meters was applicable, due to the Lake Okeechobee Composite Bathymetry 2014 SFWMD 5-ft database. Four historic hurricanes, including Frances (2004), Wilma (2005), Matthew (2016), and Irma (2017), have been used for case studies. Simulation results have been verified using the gauge measurements from the DBHYDRO database managed by SFWMD.

The newly added 3D model for saltwater intrusion modeling under hurricane conditions was developed and tested in a qualitative manner (no validation was conducted at this development stage). Saltwater intrusion modeling inside and around the outlet of Miami River under Hurricane Irma (2017) impact was conducted as an example test. A new mesh with grid resolution of approximately 10 meters was generated around the Miami River outlet. The result shows a high impact of saltwater intrusion inside Miami River due to Irma (2017); the salt water can travel upstream as far as 4 km. The stratification of salinity was also observed at locations around the river outlet.

Phase 3 has again demonstrated that the SSFOF model is robust, efficient and comprehensive with great potential for new functionalities. The model can forecast and hindcast hurricane-induced inundation extent, maximum flooding depth, duration of the flooding, water velocity and salinity at given locations. With new innovations, the SSFOF model can become a reliable tool at either regional or local scales.

Research Area 5: Investigation and Incorporation of WOW testing outputs in the Florida Public Hurricane Loss Model (PI: Jean-Paul Pinelli (Florida Institute of Technology; Kurt Gurley (University of Florida))

The Florida Public Hurricane Loss Model (FPHLM) is a risk hazard model that is updated periodically as new information is discovered regarding the performance of residential construction in hurricane winds. For the current performance period, three tasks were proposed to investigate the possible incorporation of recent FIU Wall of Wind (WOW) experimental outcomes within the FPHLM.

Results of roof to wall connection (R2WC) uplift research carried out at the WOW were compared to the current uplift model employed by the FPHLM. The primary finding to date is that the current FPHLM method to load R2WC using component and cladding loading and tributary area is supported by the WOW findings, while the specific load values and distribution with location warrants additional consideration.

Non-breach related leakage paths (defects) have long been incorporated in the FPHLM to account for water ingress, but the influence of such paths on internal pressure is not yet well understood nor implemented in the FPHLM. The WOW sequence of tests on internal pressure due to varying controlled aperture sizes provided an initial benchmark to develop an internal pressure model that is sensitive to both approach wind direction and defect size. Preliminary simulations indicate a potentially significant influence on FPHLM loss outputs that requires further model development.

Ongoing WOW research concerning pressure loads on non-rectangular building plans offers a potentially significant expansion to the library of rectangular models currently employed in the FPHLM. As of the end of this performance period, results of the WOW research are not far enough advanced to determine whether non-rectangular models should be developed for the FPHLM.

Research Area 6 Education and Outreach Programs to Convey the Benefits of Various Hurricane Loss Mitigation Devises and Techniques (PI: Erik Salna)

The FIU International Hurricane Research Center (IHRC) developed and coordinated education and outreach activities to build on the foundation of previous work under this grant and showcased the hurricane-loss mitigation objectives of the HLMP.

For the 2019-20 performance period, the below mentioned educational partnerships, community events, and outreach programs were developed:

Wall of Wind Mitigation Challenge (WOW! Challenge): Cancelled due to COVID-19.

The following was completed before the COVID-19 pandemic closed FIU and Miami-Dade County Public Schools campuses and both went to virtual and remote operations.

- Wall of Wind Research team determined the Challenge would focus on wind mitigation solutions for a flat roof.
- Conducted Wall of Wind Challenge information workshop on February 21st, 2020.
- Registered 9 high school teams for the Challenge which was scheduled for April 24th, 2020 at FIU.
- Rooftops for each team were constructed. It was decided that the 2021 competition would employ the same challenge and the rooftops would be used the following year under the FY 2020-2021 contract.

Hurricane STEM Science, Mitigation and Preparedness Education Learning Modules (6th Grade and High School): March 31st, 2021

A contract modification was executed with the Division when the Wall of Wind Mitigation Challenge was cancelled due to COVID-19. Funds were rededicated to create virtual hurricane learning modules for 6th grade and high school classrooms. The learning modules teach students about hurricane STEM science, mitigation, preparedness, and wind engineering. They also teach about emergency management and the role it plays in the community during a threatening hurricane. The learning modules were developed with the guidance of Miami-Dade County Public Schools (M-DCPS) and available as an educational resource for all teachers.

- IHRC Teacher Resources: http://www.ihrc.fiu.edu/outreach-education/teachers/education-learning-module/
- M-DCPS Department of Science (modules under the outreach tab): M-DCPS District - Science Department (dadeschools.net)

Eye of the Storm (Science, Mitigation & Preparedness) at the Museum of Discovery and Science in Fort Lauderdale: Cancelled due to COVID-19.

Due to COVID-19 the Museum of Discovery and Science (MODS) had to close and the Eye of the Storm Event at the museum was cancelled.

Virtual Eye of the Storm: June 30th, 2020

When the Eye of the Storm Event at the Museum of Discovery and Science (MODS) was cancelled due to COVID-19, a contract modification was executed with the Division and funds were rededicated towards a virtual event. The virtual Eye of the Storm is a 12-episode video series (10-12 minutes each) that educates people about hurricanes and emergency management and connects them with inspiring science.

All the videos are listed on the MODS Virtual Eye of the Storm web-page: https://mods.org/events/eyeofthestorm/

All the videos are also listed on the following MyFloridaCFO web-page: Plan Prepare Protect: Are You Disaster Ready? Eye of the Storm Videos (myfloridacfo.com)

"This video series is a great way to learn about hurricane preparedness and prepare for all possible impacts before a storm makes landfall," said FDEM Deputy Director Kevin Guthrie. "The division is proud to sponsor this informative series so we can help educate all Floridians on how to stay safe before, after and during a hurricane. We look forward to our continued partnership with the International Hurricane Research Center as we continue through the 2020 Atlantic Hurricane Season."

The virtual Eye of the Storm resulted in a hugely successful digital marketing campaign and expanded the reach and impact beyond South Florida to other states on the Gulf of Mexico and the U.S. eastern seaboard at risk of a hurricane landfall.

Digital Marketing Campaign Total Numbers for 12 Videos (The numbers will keep growing because the videos are evergreen.)

- Impressions: 7,054,250+
- Views: 586,320+
- Engagements and Clicks: 23,515+
- Hours Watched: 3,700+

Hurricane Mitigation & Preparedness at FIU: June 30th, 2020

IHRC shared the virtual Eye of the Storm 12-episode video series with the FIU faculty, staff and 55,000 plus students. This was facilitated through the FIU social media channels of LinkedIn, Facebook, and Twitter. IHRC partnered with the FIU Office of Emergency Management and the FIU Division of External Relations and Social Media.

NOAA Hurricane Awareness Tour: Cancelled due to COVID-19.

Get Ready, America! The National Hurricane Survival Initiative: Cancelled due to lack of sponsorships.

A Resource for the State of Florida

SECTION 2
EXPERIMENTAL AND ANALYTICAL ASSESSMENTS OF EFFECTS OF LEAKAGE AROUND DOORS, WINDOWS, AND OTHER OPENINGS ON INTERNAL PRESSURES IN RESIDENTIAL BUILDINGS.

FINAL REPORT
(Period: 2019-2020)

A Research Project Funded by:
The State of Florida Department of Emergency Management

Prepared by
Dr. Arindam Gan Chowdhury
Dr. Amal Elawady
Dr. Changda Feng
Dr. Dejiang Chen

Graduate Students
Ziad Azzi
Krishna Sai Vutukuru

Executive Summary

Background air leakage is common in residential buildings due to the typical materials and installation techniques involved in constructing building envelope components such as walls, doors, and windows. Moreover, the porosity created by cracks and deficiencies around doors and windows as well as openings at soffits, utility ducts, and vents may lead to further air leakage. To assess the internal pressures generated due to air leakage, experimental testing has been carried out at the NSF NHERI Wall of Wind Experimental Facility (WOW EF) at Florida International University (FIU) on a large-scale building model with a gable roof. Different leakage areas were modeled on a wall of the test building to simulate the effects of various deficiencies and defects. In addition, different wind speeds and defect aspect ratios were considered to investigate the Reynolds number (Re) effect on the internal pressure. Results of experimental testing showed that the internal pressure increased with the increase in leakage area. The experimental results were compared with internal pressure coefficients provided by ASCE 7-16 for an enclosed building. It was shown that ASCE7-16 underestimated peak internal pressures for all leakage configurations except the background leakage case. The new knowledge is expected to be used for the enhancement of the Florida Public Hurricane Loss Model (FPHLM). Improved estimation of peak internal pressures and their use in risk modeling (such as by the FPHLM) may lead to significantly improved models. Such models can be used to inform designs and retrofitting techniques to reduce damage and property losses during extreme wind events, which will positively impact the economy of the State of Florida and increase the safety of its residents. The test-based findings may also be used to enhance wind load provisions in standards and codes (e.g. ASCE 7 Standard and Florida Building Code). The enhanced provisions will lead to informed resilient designs to protect buildings and the residents in the State of Florida and across the U.S.

1. Introduction and Background

During extreme wind events, such as hurricanes, the inflow of wind through openings and defects could contribute to the development of high internal pressures that, combined with the external pressures, significantly increase the wind loads (Holmes & Cermak, 1980). Further, deficiencies and openings in the building's envelope can cause water intrusion induced by wind-driven rain that may damage the interior content. This problem can be further exacerbated during a hurricane if the building envelope is compromised by wind-borne debris. In addition to the internal pressure

buildup in response to wind-induced external pressure fluctuations, several other factors can affect the magnitude of internal pressures: the size and location of leakage, the wind direction, the upstream flow turbulence, the building's internal volume and compartmentalization, and the flexibility of the structure (Ho et al., 2005; Holmes & Cermak, 1980; Liu & Saathoff, 1982; Vickery, 1986; Womble et al., 1995).

The design wind loads on a building envelope consist of a combination of external and internal pressures, resulting in net pressures. Several experimental studies have been performed in boundary layer wind tunnels (BLWTs) to investigate the external building aerodynamics. In addition to the external pressures, internal pressures can contribute to a significant portion of the total wind load depending on the opening size and location, the shape of the building, and other aerodynamic factors (Holmes & Cermak, 1980; Irwin & Sifton, 1998; Sharma & Richards, 2003, 2005; Stathopoulos et al., 1979). Though several studies have been conducted to investigate the effect of openings on internal pressures (Aynsley et al., 1977; Ginger et al., 1997; Kopp et al., 2008; Oh et al., 2007; Stathopoulos et al., 1979; Tecle et al., 2015; Woods & Blackmore, 1995; Wu et al., 1998), limited research has been carried out to assess the internal pressures due to leakage and defects. For example, Kandola (1978) conducted a wind-tunnel investigation on a simple cubical model to study the effect of outside wall leakage on internal pressures. It has been found that the internal pressures are highly dependent on the leakage characteristics as well as the direction of the approaching wind. For instance, the author observed that the internal pressures tend to increase with the increase of the leakage ratio and their magnitude becomes negative as the wind direction changes from 0° to 90°. Stathopoulos et al. (1979) carried out BLWT experiments to investigate the impact of wall porosity on mean and fluctuating internal pressures in a nominally sealed building and a building with a range of openings. The authors reported that the internal pressure is uniform throughout the building's interior, and its magnitude does not depend on the measurement point.

The objective of the current study is to assess the wind-induced internal pressure changes due to air leakage through pre-existing wall deficiencies and gaps in a residential building. To achieve this objective, experimental testing has been carried out at the NSF NHERI Wall of Wind Experimental Facility (WOW EF) at Florida International University (FIU) on a large-scale building model with a gable roof.

2. Methodology

2.1. *Wall of Wind Facility*

Experimental testing has been carried out at the NHERI WOW EF at FIU. The 12-fan WOW is a full- and large-scale testing facility, capable of generating wind speeds up to 157 mph (70 m/s) and turbulence characteristics similar to those recorded in Category 5 hurricanes on the Saffir-Simpson scale (Chowdhury et al., 2017). **Figure 1** shows the 12-fan WOW system. The flow field of the WOW is conditioned with spires and roughness elements (see **Figure 2**) that help generate Atmospheric Boundary Layer (ABL) wind flows under various terrain conditions. In addition, the facility is equipped with a turntable that allows testing for different wind directions.

Figure 1. 12-fan Wall of Wind System, Florida International University

Figure 2. Spires and Floor Roughness Elements

2.2. *Building Model and Instrumentation*

A large-scale gable-roof building model was tested under simulated winds generated by the 12-fan WOW. The model was constructed with stick-built framing and plywood sheathing. The full-scale test specimen had approximate dimensions of 109 × 97 × 113 in (L × W × H), and a gable roof (3:12 slope) with approximately 12 in overhangs extending from all sides of the base building. For the current research, the testing was conducted with exposed plywood sheathing on the walls. Before testing, all gaps and nail holes in the plywood sheathing were filled with a gunnable sealant material, and the model was painted to protect the exposed plywood sheathing. The building model retained interior drywall and also had an attic space that was separated from the main room volume by a ceiling made from plywood. The building model did not have any soffit vents installed underneath the roof overhangs.

The building model was constructed with two window openings: one located on a gable end wall at the north, and the other located on a non-gable wall at the west. An access door is located on the remaining non-gable wall at the east. For the current research, the desired wall deficiencies and gaps were modeled by creating controlled openings in the north gable-end window region. The existing window assembly was removed and new 2x4 wood framing was installed around the interior perimeter of the window opening. Pieces of plywood sheathing were cut to size and secured to the new wood framing with wood screws to create a simulated "leakage area, A_L". A leakage ratio R (in %), representing the ratio of A_L to the wall area A_w, is defined by Eq. (1**)**.

$$R\ (\%) = \frac{A_L}{A_W} \times 100 = \frac{w_L \times\ h_L}{(w_W \times h_W) + (0.5 \times w_W \times\ h_g)} \times 100 \qquad (1)$$

where w_L and h_L are the width and height of the leakage area, respectively. The width and height of the wall with the simulated leakage area are w_w and h_w, respectively. The height of the gable wall triangle is h_g. **Figure 3** shows a representation of the leakage area simulated in the window of the gable-end wall. **Figure 4** shows the building model mounted on the WOW turntable.

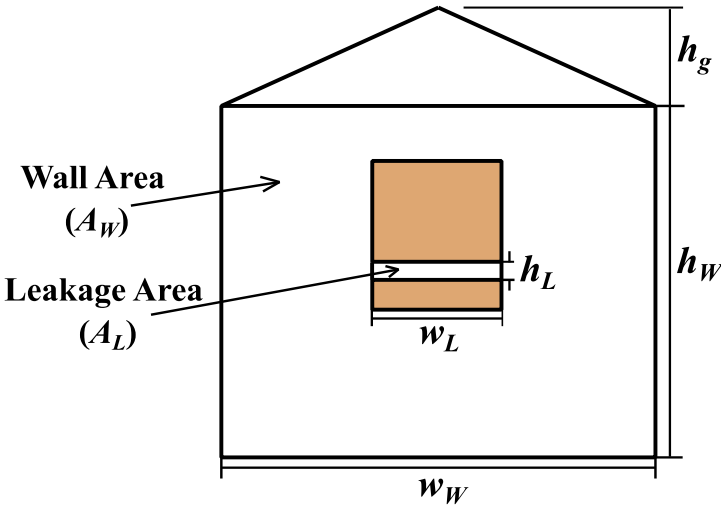

Figure 3. Representation of the simulated leakage area

Figure 4. Building model mounted on the WOW turntable

To measure the internal pressures, a total of 22 pressure taps were installed throughout the building's interior, as shown in **Figure 5**.

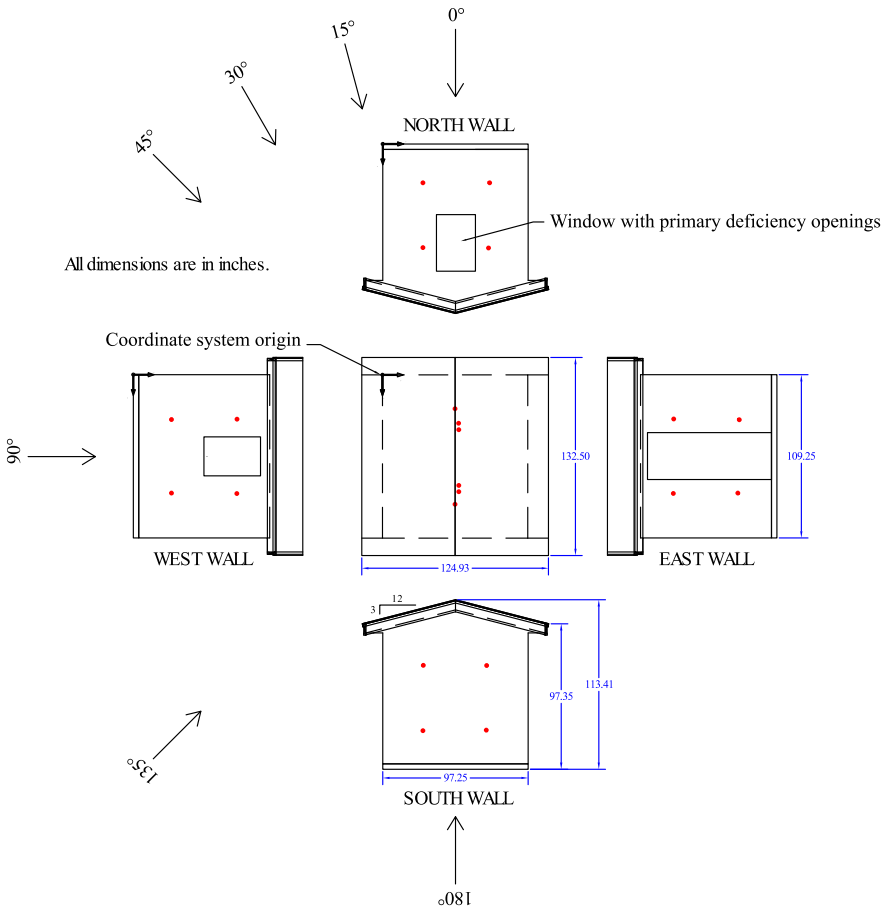

Figure 5. Internal pressure tap layout

Four taps were installed on the interior side of each wall, two taps were installed on the ceiling facing into the main room volume, two taps were installed within the attic space, and two taps were installed at approximately the mid-height of the main room volume. The pressure taps were connected to a ZOC33/DSM4000 Scanivalve data acquisition system, which sampled pressures at a rate of 520 Hz. A tubing transfer function was used to correct the collected pressure data for distortion effects introduced by the tubing length (Irwin et al., 1979).

2.3.*Testing Protocol*

The building model was tested at 40% and 60% throttle of the WOW full wind speed capacity, corresponding to one-minute mean wind speeds U_{mean} of 25 m/s (57 mph) and 39 m/s (87 mph) at a mean roof height ($H = 2.8$ m or 9 ft), respectively. The corresponding 3-sec gust wind speeds U_{3sec} above open terrain for the same building height are 32 m/s (73 mph) and 50 m/s (111 mph), respectively. The wind speed data were recorded at a sampling rate of 2500 Hz for a one-minute

duration using Turbulent Flow Instrumentation cobra probes located at the mean roof height. The model specimen was placed on the turntable and tests were conducted for seven wind directions: 0°, 15°, 30°, 45°, 90°, 135°, and 180°, as shown in **Figure 6**. The 0° wind direction refers to the direction where the leakage is located on the windward wall.

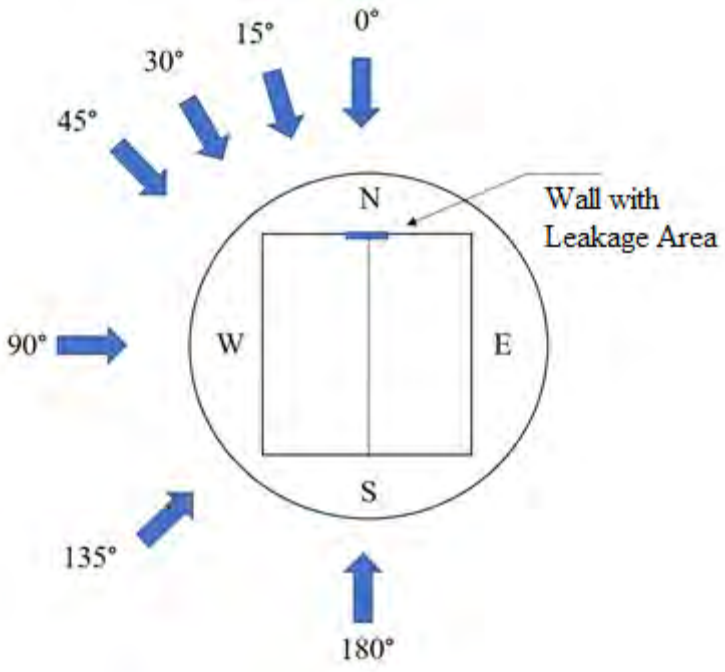

Figure 6. Wind directions

Various leakage ratios R ranging between 0 and 0.5% were considered for experimental testing, based on deficiency areas adopted in the Florida Public Hurricane Loss Model (Chen et al., 2004) that are derived from effective air leakage areas provided in Chapter 26, Table 1 of ASHRAE (2001). Internal pressure time histories were recorded for a 60-sec duration at each tested case. In addition to wind speed, wind direction, and wall leakage ratio, two other secondary factors were considered during the experimental testing: the aspect ratio and the number of defects. The aspect ratio of defects was varied (i.e., rectangle versus square) to investigate the possibility of a Reynolds number effect on the internal pressures (**Fig. 7**). The number of defects (i.e., defect on one wall versus two walls) was also varied to investigate the effect of having a single leakage area on a windward wall or two simultaneous leakage areas on the windward wall and sidewalls, as shown in **Figure 8.**

a) Rectangle b) Square

Figure 7. Building model with different defect geometries

Figure 8. Building model with two simultaneous defects

Table 1 summarizes the testing protocol. It should be noted that test cases 1 and 2, corresponding to $R = 0\%$, were used to measure the background leakage of the building model. Thus, to evaluate the effect of leakage due to defects in the building's wall, the internal pressure measured in the presence of background leakage (test cases 1 and 2) was deducted from the values obtained for all test cases.

Test #	Throttle (%)	U_{mean} (mph)	Leakage Ratio R (%)	Defect Aspect Ratio	Number of Defects	Wind direction (deg)
1	40	57	0	Rectangle	One	0:15:45, 45:45:180
2	60	87	0	Rectangle	One	0:15:30
3	40	57	0.025	Rectangle	One	0:15:45, 45:45:180
4	40	57	0.05	Rectangle	One	0:15:45, 45:45:180

5	40	57	0.075	Rectangle	One	0:15:45, 45:45:180
6	40	57	0.10	Rectangle	One	0:15:45, 45:45:180
7	40	57	0.10	Square	One	0:15:30
8	40	57	0.10	Rectangle	Two	0:15:45, 45:45:180
9	60	87	0.10	Rectangle	One	0:15:30
10	40	57	0.15	Rectangle	One	0:15:45, 45:45:180
11	40	57	0.2	Rectangle	One	0:15:45, 45:45:180
12	40	57	0.3	Rectangle	One	0:15:45, 45:45:180
13	40	57	0.4	Rectangle	One	0:15:45, 45:45:180
14	40	57	0.5	Rectangle	One	0:15:45, 45:45:180
15	40	57	0.5	Square	One	0:15:30
16	60	87	0.5	Rectangle	One	0:15:30

Table 1. Testing protocol

2.4. *Data Analysis*

The wind-induced internal pressure time history measured by each pressure tap was collected during the experimental testing. The instantaneous internal pressure coefficient C_{p_i} is defined in Eq. (2) as:

$$C_{P_i}(t) = \frac{P_i(t)}{\frac{1}{2}\rho U_{mean}^2} \tag{2}$$

where P_i is the internal pressure, ρ is the air density, and U_{mean} is the 60-sec mean wind speed at the mean roof height. The mean internal pressure coefficient $C_{P,mean}$ was calculated from each time history sample. The root-mean-square (RMS) of internal pressure coefficient $C_{P,RMS}$ was also calculated for each pressure tap and can be defined as:

$$C_{P,RMS} = \sqrt{\frac{1}{N}\sum_{i=1}^{N}\left(C_{P_i} - C_{P,mean}\right)^2} \tag{3}$$

where *N* represents the number of data points in the pressure time history. Peak internal pressure coefficients $C_{P,peak}$, normalized by the 3-sec dynamic pressure, were estimated for a one-hour storm duration using extreme value analysis (using Fisher Tippet fit) with a 78% probability of non-exceedance. The fit parameters were estimated by Lieblein's best linear unbiased estimation (BLUE) method (Lieblein, 1974).

Advantages of full- or large-scale wind tunnel testing of low-rise buildings are reducing scaling effects from larger-sized models and avoiding Reynolds number dissimilarity between the model and prototype building. However, one challenge that the full-scale wind tunnel testing encounters is the insufficient low-frequency eddies in the simulated flow due to the size limitations imposed by the wind tunnel test section. **Figure 9a** shows the wind flow power spectral density (PSD) of WOW at the mean roof height with a mean wind speed U_{mean} of 25 m/s (57 mph) and turbulence intensity I_u of 6%. The simulated wind flow PSD of WOW is compared to the full-scale spectrum from ESDU item 85020 (ESDU, 2001) with a roughness length $z_0 = 0.02$ m (open-terrain exposure). It is noted that the high-frequency component of the turbulence spectrum is fully simulated at WOW, whereas the low-frequency part is missing compared to its full-scale counterpart. **Figure 9b** shows the normalized mean wind speed and turbulence intensity profiles of the WOW, where U_{ref} refers to the mean wind speed at the mean roof height H_{ref}.

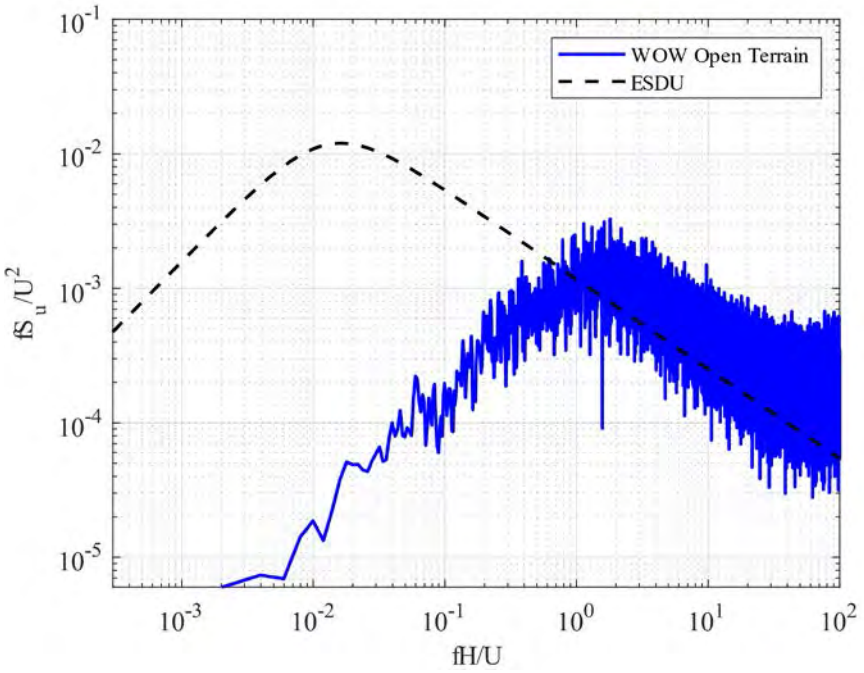

(a) Normalized power spectral density of the longitudinal velocity fluctuations

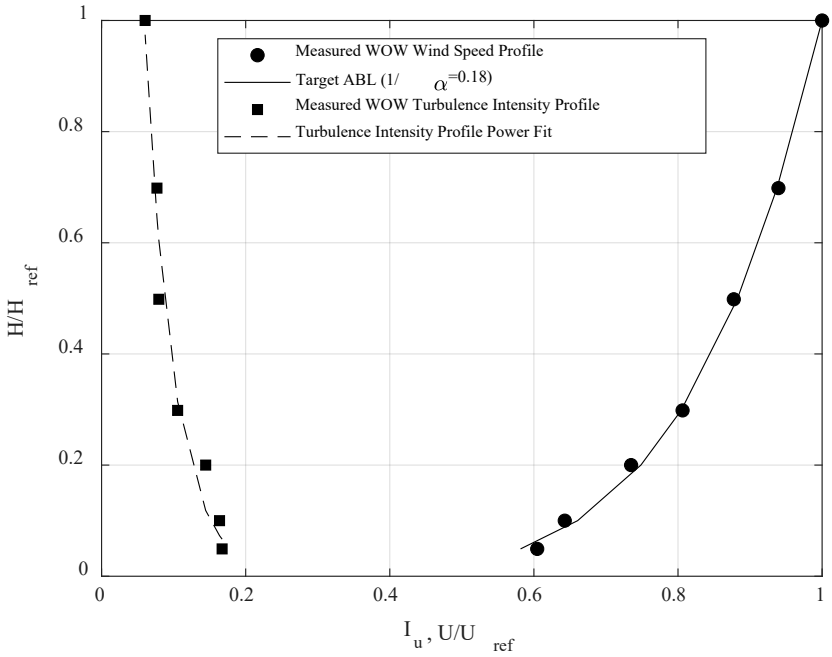

(b) Normalized mean wind speed and turbulence intensity profiles of WOW

Figure 9. WOW open-terrain wind flow condition

In this study, the partial turbulence simulation (PTS) approach was used to analytically incorporate the effects of the missing low-frequency turbulence in the fluctuating wind-induced internal pressure coefficients measured at the WOW. The PTS approach is based on the quasi-steady assumption to correct the peak pressure coefficients in the post-test numerical analysis with the consideration of the missing low-frequency turbulence. The accuracy of the PTS method was previously validated in Mooneghi et al. (2016) and Moravej (2018) by comparing peak pressure coefficients obtained at the WOW, corrected by PTS, with the field measurements of the Silsoe cube building (Richards & Hoxey, 2012) and the Texas Tech University (TTU) building (Levitan & Mehta, 1992a, 1992b).

3. Results and Discussion

3.1. *Uniformity of Wind-induced Internal Pressure Coefficients*

Time histories of internal pressures C_{pi} were collected using 22 pressure taps (PTs). To investigate whether the internal pressures at different locations throughout the building interior are uniform or not, C_{pi} from two distinct pressure taps were chosen for comparison. For instance, test cases 6 and 14 with 0° and 90° wind directions were considered. C_{pi} from two pressure taps installed on

the windward and leeward walls were compared for the different configurations, as shown in **Figures 10** and **11**.

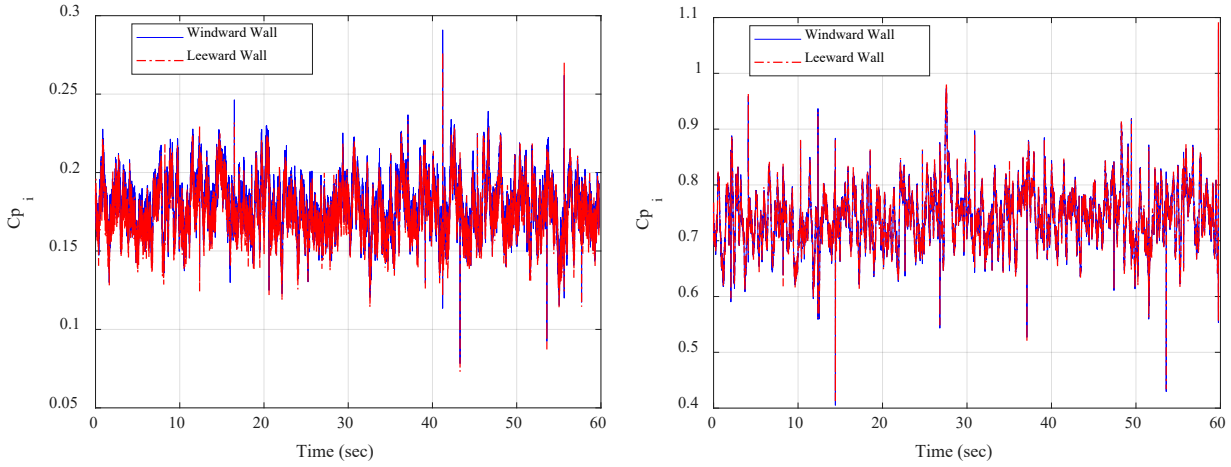

a) $R = 0.1\%$ b) $R = 0.5\%$

Figure 10. C_{pi} time histories for 0° wind direction

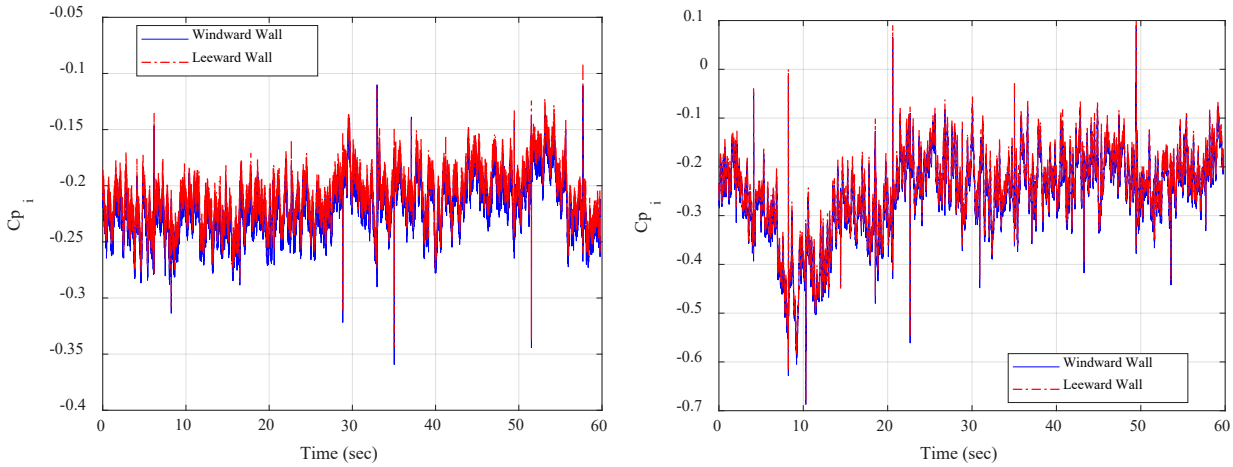

a) $R = 0.1\%$ b) $R = 0.5\%$

Figure 11. C_{pi} time histories for 90° wind direction

Table 2 summarizes the statistical parameters of each time history sample. The highest differences between $C_{pi,mean}$, $C_{pi,RMS}$, and $C_{pi,peak}$ on the windward and leeward walls for all configurations were found to be 4.67%, 2%, and 4.18%, respectively.

Table 2. C_{pi} statistical parameters for the windward and leeward walls

	0° Wind Direction					
Leakage Ratio	R = 0.1%			R = 0.5%		
PT Location	$C_{pi,mean}$	$C_{pi,RMS}$	$C_{pi,peak}$	$C_{pi,mean}$	$C_{pi,RMS}$	$C_{pi,peak}$
Windward Wall	0.178	0.017	0.291	0.742	0.049	1.078
Leeward Wall	0.175	0.017	0.283	0.742	0.050	1.089
Difference (%)	1.68	0	2.75	0	2.00	1.01
	90° Wind Direction					
Leakage Ratio	R = 0.1%			R = 0.5%		
PT Location	$C_{pi,mean}$	$C_{pi,RMS}$	$C_{pi,peak}$	$C_{pi,mean}$	$C_{pi,RMS}$	$C_{pi,peak}$
Windward Wall	-0.219	0.024	-0.359	-0.257	0.083	-0.687
Leeward Wall	-0.209	0.024	-0.344	-0.245	0.083	-0.686
Difference (%)	4.56	0	4.18	4.67	0	0.15

Hence, it can be concluded that the internal pressure may be considered to act uniformly throughout the building's interior and its magnitude does not depend on the spatial measurement point. These observations are in line with those reported by Stathopoulos et al. (1979) and Wu et al. (1998). Based on the uniformity of C_{pi}, the statistical parameters (i.e., $C_{pi,mean}$, $C_{pi,RMS}$, $C_{pi,peak}$), presented in the following sub-sections of this report, are averaged between the 22 pressure taps for each test case.

3.2. *Statistics of the Internal Pressure Coefficients*

3.2.1. Background Leakage Effects

Background leakage in buildings can be caused by poor airtightness of walls, doors, windows, door-wall interfaces, window-wall interfaces, soffits, utility ducts, and vents. To investigate the effect of background leakage on internal pressure coefficient, experimental testing was conducted on a fully enclosed building with a 0% wall leakage ratio and subjected to two different mean wind speeds: 57 mph and 87 mph. **Figures 12a** and **12b** show $C_{pi,mean}$ and $C_{pi,RMS}$ for three wind directions: 0°, 15°, and 30°. It was observed that the closed building experiences negative mean internal pressures, which have the largest magnitude for 0° wind direction ($C_{pi,mean}$ = -0.12). For 15° and 30° wind directions, no significant change in $C_{pi,mean}$ was detected ($C_{pi,mean}$ = -0.09). The $C_{pi,RMS}$ values were the largest for 0° wind direction, but still with a relatively small magnitude

($C_{pi,RMS}$ = 0.015). The estimated and corrected $C_{pi,peak}$ values, shown in **Figures 12c** and **12d**, agreed well with the general trend described for $C_{pi,mean}$ and $C_{pi,RMS}$, with the largest values of about -0.15 and -0.18 respectively, detected for 0° wind direction. The obtained statistical parameters for 0% wall leakage ratio, corresponding to a background leakage, were used to adjust the obtained C_{pi} values for different leakage ratios ranging between 0.1% and 0.5%, as will be discussed in the following sub-sections. Overall, the internal pressure for the background leakage case is negative and small in magnitude with limited variation with the change of wind direction. These observations are consistent with the findings of Bodhinayake et al. (2017).

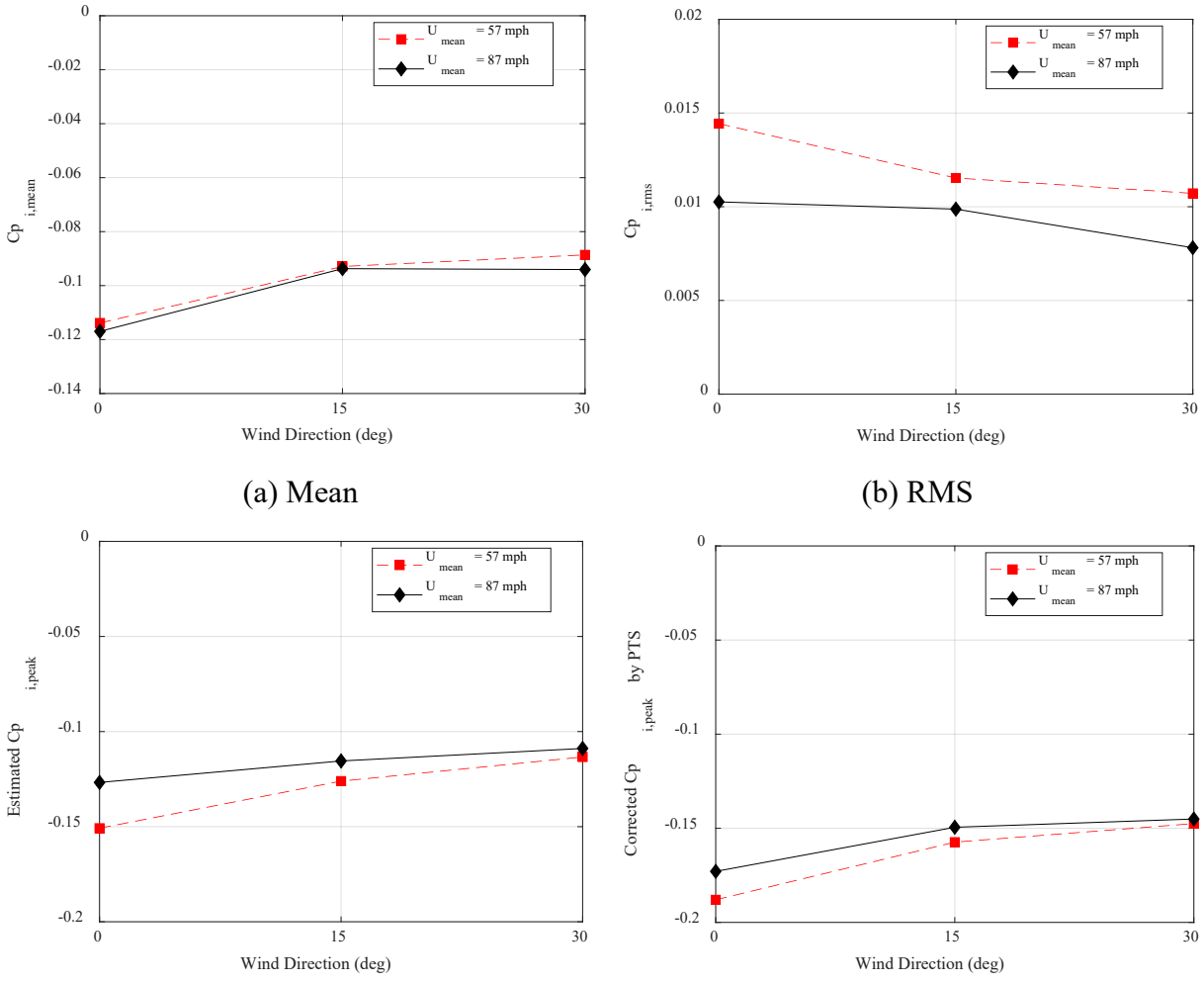

Figure 12. $C_{pi,mean}$, $C_{pi,RMS}$, and $C_{pi,peak}$ for the background leakage case

3.2.2. Wall Leakage Effects

To investigate the effect of wall leakage on the internal pressure in a nominally sealed building, a total of 9 test cases were considered for wind directions ranging between 0° and 180°. Moreover, defects were modeled on a gable-end wall with leakage ratios R ranging between 0.025% and 0.5%. **Figure 13** shows $C_{pi,mean}$, $C_{pi,RMS}$, and $C_{pi,peak}$ for the considered test cases. It can be seen that the largest magnitude of positive $C_{pi,mean}$ was observed to occur for all considered leakage ratios when wind flow impacted the building model with 0° wind direction (e.g., +0.75 for R = 0.5%). This might be attributed to the location of defects on the windward wall. For wind directions ranging between 0° and 90°, positive $C_{pi,mean}$ values started decreasing until suction developed at 90° (-0.2 for R = 0.5%) when the defects are located on the sidewall. A decrease in the magnitude of suction was noticed when the wind direction varied between 90° and 180° until it reached its smallest $C_{pi,mean}$ values for 180° wind direction (i.e., defects are on the leeward wall). These observations are in line with the findings of Bodhinayake et al. (2017), Oh et al. (2007), and Kopp et al. (2008).

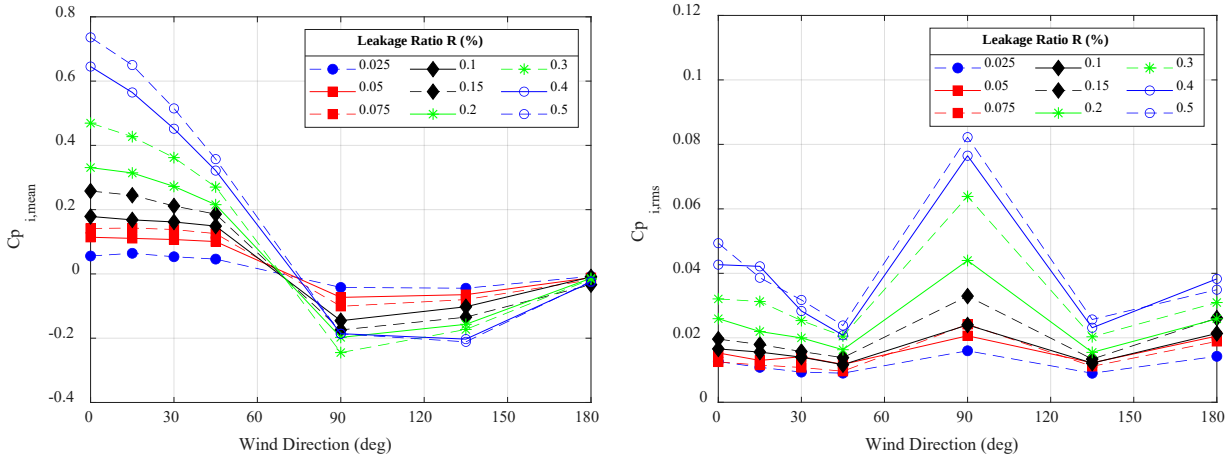

a) Mean b) RMS

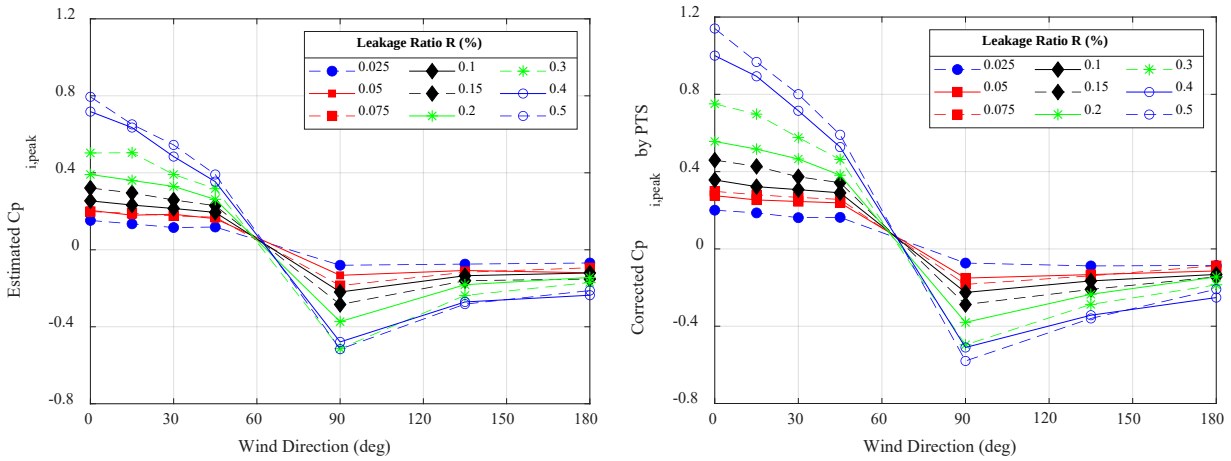

(a) Estimated (b) Corrected

Figure 13. $C_{pi,mean}$, $C_{pi,RMS}$, and $C_{pi,peak}$ for U_{mean} of 57 mph and different leakage ratios

The $C_{pi,mean}$ values follow an increasing trend as the wall leakage ratio increases. For instance, the largest $C_{pi,mean}$ magnitude for any given wind direction was observed for $R = 0.5\%$, and the smallest magnitude was observed for R = 0.025%. Such a trend was detected for all wind directions; however, it was shown to be more pronounced for a 0° wind direction where $C_{pi,mean}$ is about 93% higher for $R = 0.5\%$ than that for $R = 0.025\%$. It is interesting to note that the effect of wall leakage ratio on $C_{pi,mean}$ is less pronounced for 180° wind direction.

The $C_{pi,RMS}$ results demonstrated an increasing trend between 0° to 90° for any given leakage ratio, and a symmetric decreasing trend between 90° and 180°. The largest $C_{pi,RMS}$ values were found to occur for 90° (e.g., $C_{pi,RMS}$ = +0.08 for $R = 0.5\%$). For all wind directions, $C_{pi,RMS}$ values increased as the leakage ratio increased. **Figures 13c** and **13d** show the estimated $C_{pi,peak}$ and their corresponding corrected values by PTS. The peak values exhibited a similar trend to that observed for $C_{pi,mean}$ for all test cases. For instance, the largest magnitude of positive estimated and corrected $C_{pi,peak}$ was observed at a wind direction of 0° for all considered leakage ratios (e.g., $C_{pi,peak}$ = +0.8 and +1.2 for $R = 0.5\%$). Also, suction developed at 90° ($C_{pi,peak}$ = -0.5 and -0.6 for $R = 0.5\%$) when the defects are located on the sidewall and decreased when the wind direction was closer to 180°. It was also observed that the estimated and corrected $C_{pi,peak}$ values increased as the leakage ratio increased for all wind directions. These trends agree well with the observations of Ginger et al. (1997), where it was found that the mean and fluctuating internal pressure coefficients increase with increasing windward/leeward open-area ratio.

3.2.3. Reynolds Number Effects

To investigate the Reynolds number (*Re*) effects on the internal pressure of the building model, different wind speeds (i.e., 57 mph and 87 mph) and defect aspect ratios (i.e., rectangle and square) were considered. **Figure 14** shows a comparison between the internal pressure statistics for two different mean wind speeds U_{mean} and a rectangular defect. No significant change was observed when the building model with a given leakage ratio was impacted with two different wind speeds. However, the internal pressure coefficients for any given wind speed increased when the leakage ratio increased from 0.1 to 0.5%. For instance, the $C_{pi,mean}$, $C_{pi,RMS}$, and $C_{pi,peak}$ values for $R = 0.5\%$ and 0° wind direction were about 70% higher than those obtained for $R = 0.1\%$. Hence, it was noted that the leakage ratio has a significant effect on the internal pressure, but the effect of wind speed was shown to be less significant.

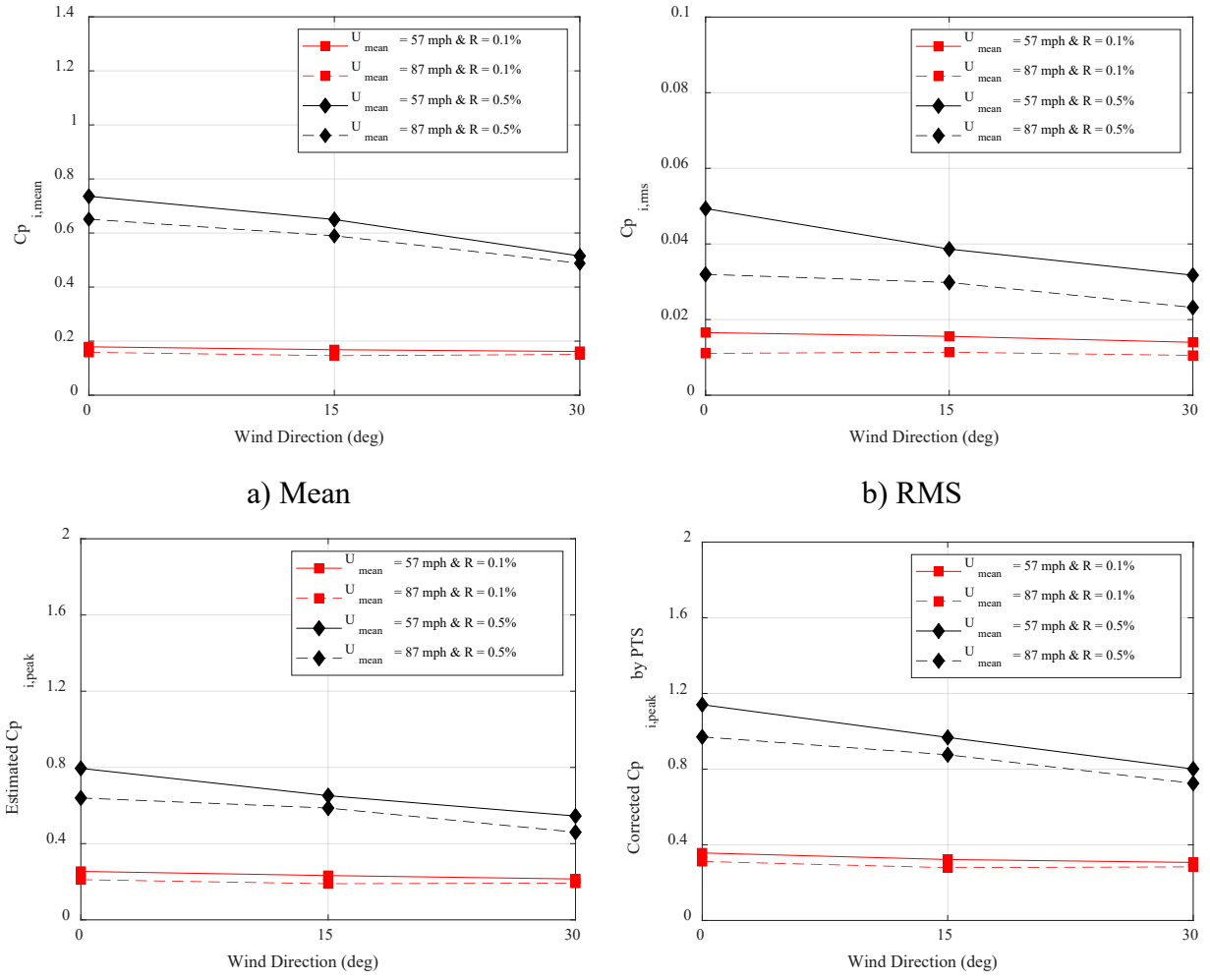

Figure 14. $C_{pi,mean}$, $C_{pi,RMS}$, and $C_{pi,peak}$ for different rectangular defects and wind speeds

Figure 15 shows a comparison of the internal pressure statistics for two different leakage and aspect ratios for U_{mean} of 57 mph. It was observed that there is no significant difference in the obtained $C_{pi,mean}$, $C_{pi,RMS}$, and $C_{pi,peak}$ values for a given leakage ratio of a rectangle and square defects. However, when the leakage ratio increased from 0.1 to 0.5%, the obtained internal pressure coefficients for the two aspect ratios increased by about 70%. Hence, it was noted that the leakage ratio has a significant effect on the internal pressure, but the effect of the defect's aspect ratio was shown to be less significant. To summarize, the internal pressure tends to be affected significantly by the leakage ratio in contrast to the Reynolds number effect or defect configuration (rectangular versus square) which may not play a significant role.

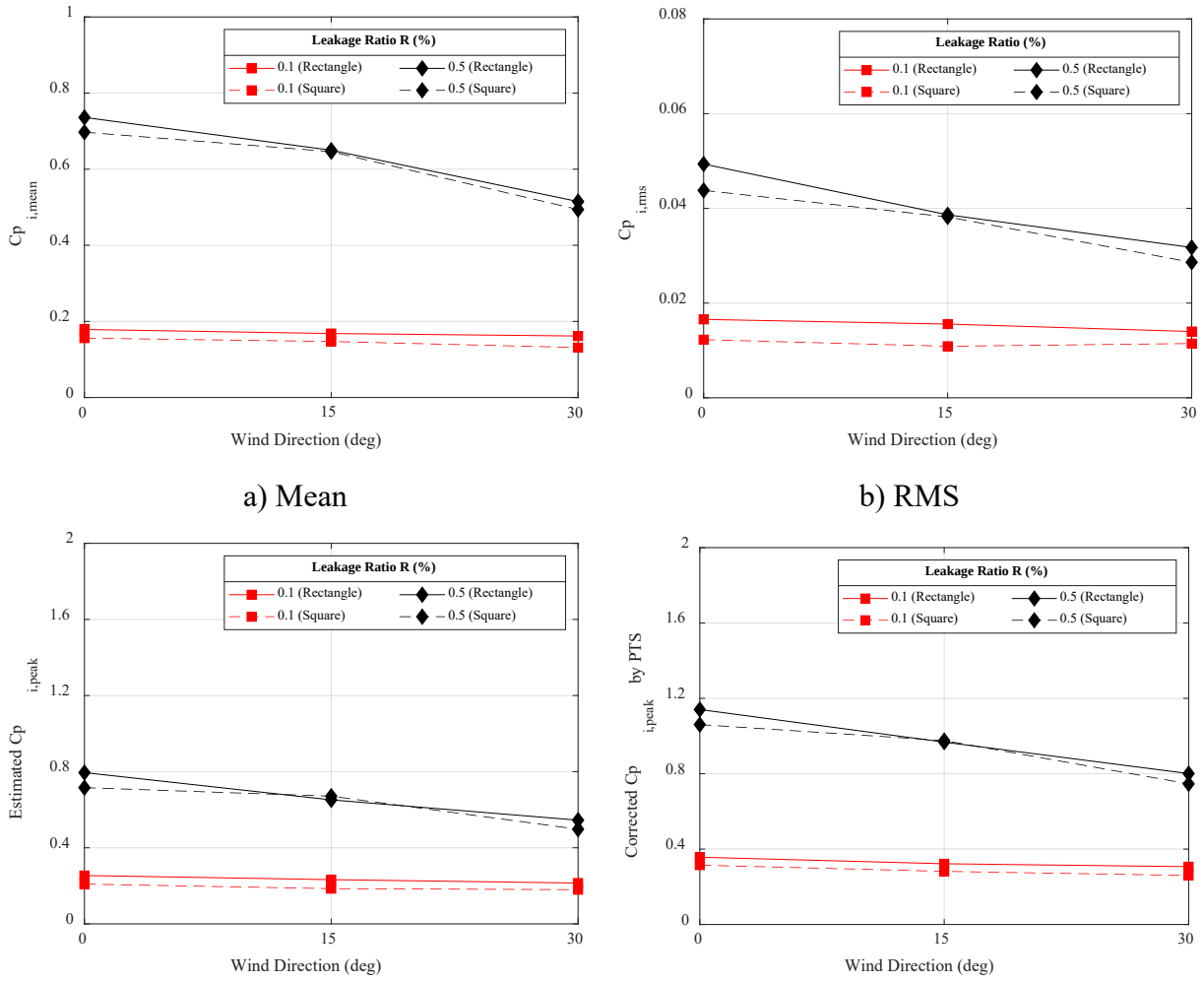

Figure 15. $C_{pi,mean}$, $C_{pi,RMS}$, and $C_{pi,peak}$ for U_{mean} of 57 mph and different geometries

3.2.4. Number of Openings Effects

Since it is not uncommon for a building to have multiple defects during extreme wind events, test case 8 was designed to account for simultaneous defect locations. For this purpose, in addition to the defects modeled on a gable-end wall, similar defects were modeled on a side wall to study the effects on internal pressures (**Fig. 8**). A comparison was made between the internal pressure statistics for a leakage ratio of 0.1% on a single wall and for a total leakage ratio of 0.2% on two simultaneous walls (i.e., R = 0.1% for each wall), as shown in **Figure 16**. It was observed that the $C_{pi,mean,}$ and $C_{pi,peak}$ values are lower in the presence of two simultaneous defects than that of a single defect in the building model for 0° and 15° wind directions. However, the model with a single defect experienced lower $C_{pi,mean,}$ and $C_{pi,peak}$ values for wind directions between 15° and 90°. As expected, due to symmetry, a $C_{pi,mean}$ of +0.08 and $C_{pi,peak}$ of +0.2 were observed for the two defects case when the wind directions were 0 and 90°. When the wind direction varied between 90 and 180°, the internal pressure started decreasing until suction developed at 180°, leading to negative $C_{pi,mean,}$ and $C_{pi,peak}$ values of -0.1 and -0.18, respectively. For $C_{pi,RMS}$, no significant difference was noticed between the two test cases.

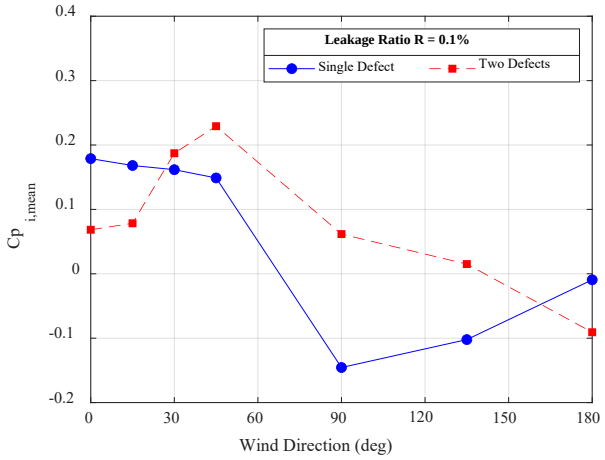

a) Mean

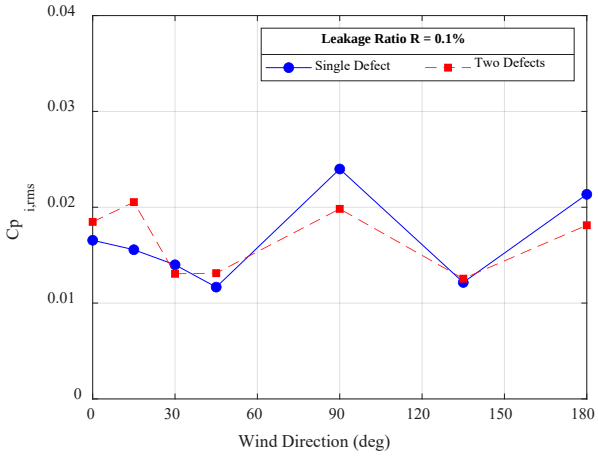

b) RMS

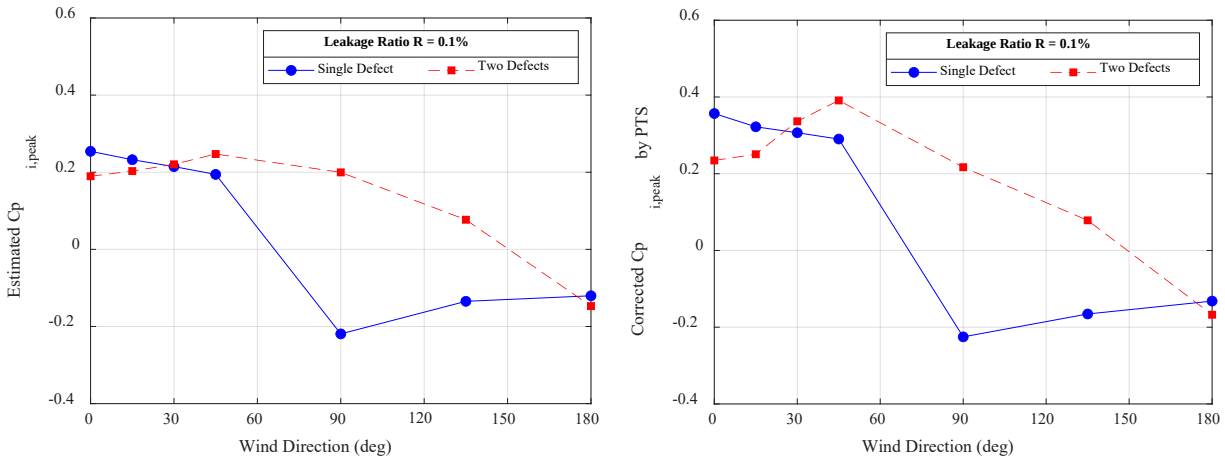

c) Estimated d) Corrected

Figure 16. $C_{pi,mean}$, $C_{pi,RMS}$, and $C_{pi,peak}$ for U_{mean} of 57 mph and different number of defects

3.3. Comparison of experimental results with ASCE7-16

The ASCE7-16 provisions on internal pressure suggest that a building can be classified into one of the four enclosure categories: enclosed, partially enclosed, open, and partially open. Enclosed buildings are defined as having the opening area in a wall that receives positive external pressure less than the smaller of 0.01 times the wall's gross area and 4 ft^2 (0.37 m^2). For partially enclosed buildings, they satisfy the following two conditions: (1) the total area of openings in a wall that receives positive external pressure exceeds the sum of the areas of openings in the balance of the building envelope (walls and roof) by more than 10%, and (2) the total area of openings in a wall that receives positive external pressure exceeds 0.37 m^2 or 1% of the area of that wall, whichever is smaller, and the percentage of openings in the balance of the building envelope does not exceed 20%. Open buildings are defined as having each wall at least 80% open. A building that does not comply with enclosed, partially enclosed, or open classifications is considered as partially open. For the building model considered in this study, the largest leakage area corresponding to R = 0.5% is $A_L = 0.03$ m^2 (0.33 ft^2). According to the ASCE7-16's definition of building enclosure, the building model is classified as enclosed and $GC_{pi} = \pm 0.18$ should be used.

As discussed in Section 3.4 of this report, the corrected $C_{pi,peak}$ values by PTS were normalized by the 3-sec dynamic pressure and estimated for a one-hour storm duration. The WOW experimental results (i.e., $C_{pi,peak}$) were compared with the ASCE7-16 provided internal pressure values (i.e., GC_{pi}) for the critical wind direction of 0°, as shown in **Figure 17**.

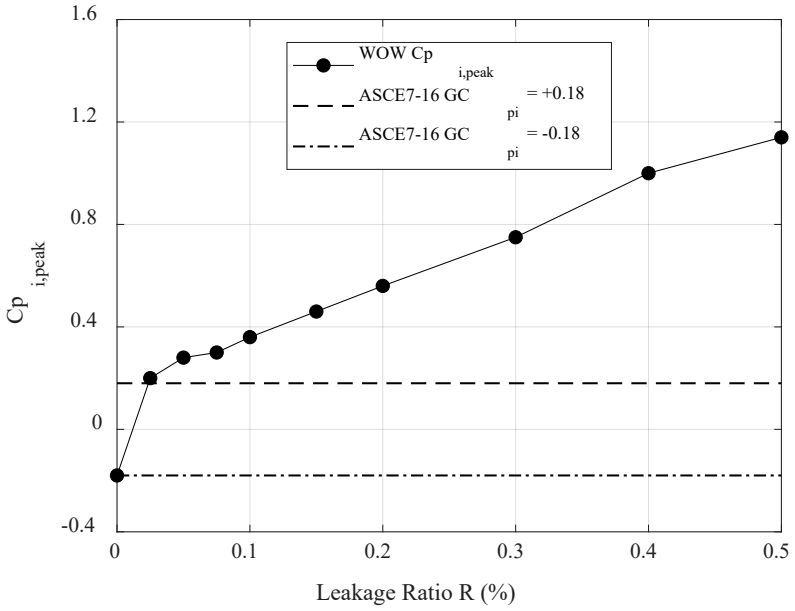

Figure 17. Comparison of $C_{pi,peak}$ for 0° wind direction with ASCE7-16

The results presented in **Figure 17** suggest that ASCE7-16 underestimates peak internal pressures for the leakage ratios considered in this study. For instance, the results from R = 0.5% experiments indicated $C_{pi,peak}$ values about 84% higher than GC_{pi} given in ASCE7-16 for an enclosed building. For R = 0% (background leakage), the experimental results $C_{pi,peak}$ of -0.19 compared well with the ASCE7-16 GC_{pi} for an enclosed building, with only a 5% difference.

4. Conclusion

Consideration of internal pressures has significant importance while assessing overall wind loading on buildings subjected to major wind events such as hurricanes. This study aimed to investigate the effect of wall defects on internal pressure – a topic that was not carefully investigated till date. To achieve this goal, experimental testing has been performed at the WOW EF at FIU on a gable-roofed building with different wall defects. Several leakage configurations and wind directions were considered for experimental testing and internal pressures were measured for each test case. The Reynolds number (Re) effect was studied by modeling two different leakage aspect ratios (rectangle and square) and two different wind speeds. Besides studying the effect of a single defect on the internal pressure, the effect of simultaneous defects modeled on two walls of the building model was also considered.

The following points summarize the key findings of this study:

- The internal pressure coefficient was found to be uniform throughout the building interior and its magnitude did not depend on the location of measurement point.
- The internal pressure coefficient for the background leakage case was negative and small in magnitude with limited variation with the wind direction.
- The largest positive mean and peak internal pressure coefficients were observed when the defects were located on the windward wall. Suction developed when the defects were on the sidewall.
- The mean and peak internal pressure coefficients followed an increasing trend as the leakage ratio increased for any given wind direction.
- The internal pressure was significantly affected by the leakage ratio in contrast to the Reynolds number effect which may not play a significant role.
- ASCE 7-16 internal pressure coefficients for an enclosed building underestimated the peak internal pressures measured for all leakage configurations except the background leakage case.

The key findings of this study are expected to provide useful insights into the effect of wall defects on internal pressure. The new knowledge is expected to be used to enhance the Florida Public Hurricane Loss Model (FPHLM). The improved models can be used to inform designs and retrofitting techniques to mitigate damage and property losses during extreme wind events, which will positively impact the economy of the State of Florida and increase the safety of its residents. The test-based findings may also be used to enhance wind load provisions pertaining to internal pressure in standards and codes, such as ASCE 7 Standard and Florida Building Code. The enhanced provisions will lead to informed resilient designs to protect buildings and the residents in the State of Florida and across the U.S. Future studies should focus on correlation of leakage effects to overall wind loading. Risk assessments using vulnerability and fragility modeling should be also conducted using the FPHLM.

5. References

American Society of Heating, Refrigerating and Air-Conditioning Engineers. (2001). *2001 ASHRAE handbook: Fundamentals.* ASHRAE.

Aynsley, R., Melbourne, W., & Vickery, B. (1977). *Architectural Aerodynamics*. Applied Science: London.

Bodhinayake, G. G., Ginger, J. D., & Henderson, D. J. (2017). *External and Internal Pressure Fluctuations on Industrial-Type Buildings*. 9th Asia-Pacific Conference on Wind Engineering, Auckland, New Zealand.

Chen, S.-C., Gulati, S., Hamid, S., Huang, X., Luo, L., Morisseau-Leroy, N., Powell, M. D., Zhan, C., & Zhang, C. (2004). A Web-based Distributed System for Hurricane Occurrence Simulation. *Software: Practice and Experience*, *34*(6), 549–571.

Chowdhury, A. G., Zisis, I., Irwin, P., Bitsuamlak, G., Pinelli, J.-P., Hajra, B., & Moravej, M. (2017). Large-Scale Experimentation Using the 12-Fan Wall of Wind to Assess and Mitigate Hurricane Wind and Rain Impacts on Buildings and Infrastructure Systems. *Journal of Structural Engineering*, *143*(7). https://doi.org/04017053.

ESDU. (2001). *Characteristics of the Atmospheric Boundary Layer, Part II: Single Point Data for Strong Winds (Neutral Atmosphere)* (Item 85020). Engineering Sciences Data Unit.

Ginger, J. D., Mehta, K. C., & Yeatts, B. B. (1997). Internal pressures in a low-rise full-scale building. *Journal of Wind Engineering and Industrial Aerodynamics*, *72*, 163–174. https://doi.org/10.1016/S0167-6105(97)00241-9

Ho, T. C. E., Surry, D., Morrish, D., & Kopp, G. A. (2005). The UWO contribution to the NIST aerodynamic database for wind loads on low buildings: Part 1. Archiving format and basic aerodynamic data. *Journal of Wind Engineering and Industrial Aerodynamics*, *93*(1), 1–30. https://doi.org/10.1016/j.jweia.2004.07.006

Holmes, J. D., & Cermak, J. E. (1980). Mean and fluctuating internal pressures induced by wind. *Proc., 5th Int. Conf. on Wind Engineering*, 435–450.

Irwin, P., Cooper, K. R., & Girard, R. (1979). Correction of distortion effects caused by tubing systems in measurements of fluctuating pressures. *Journal of Wind Engineering and Industrial Aerodynamics*, *5*(1), 93–107. https://doi.org/10.1016/0167-6105(79)90026-6

Irwin, P., & Sifton, V. (1998). Risk considerations for internal pressures. *Journal of Wind Engineering and Industrial Aerodynamics*, *77–78*, 715–723. https://doi.org/10.1016/S0167-6105(98)00186-X

Kandola, B. S. (1978). Wind effects on buildings with varying leakage characteristics—Wind-tunnel investigation. *Journal of Wind Engineering and Industrial Aerodynamics*, *3*(4), 267–284. https://doi.org/10.1016/0167-6105(78)90033-8

Kopp, G. A., Oh, J. H., & Inculet, D. R. (2008). Wind-Induced Internal Pressures in Houses. *Journal of Structural Engineering*, *134*(7), 1129–1138. https://doi.org/10.1061/(ASCE)0733-9445(2008)134:7(1129)

Levitan, M. L., & Mehta, K. C. (1992a). Texas Tech field experiments for wind loads part 1: Building and pressure measuring system. *Journal of Wind Engineering and Industrial Aerodynamics*, *43*(1), 1565–1576. https://doi.org/10.1016/0167-6105(92)90372-H

Levitan, M. L., & Mehta, K. C. (1992b). Texas tech field experiments for wind loads part II: Meteorological instrumentation and terrain parameters. *Journal of Wind Engineering and Industrial Aerodynamics*, *43*(1), 1577–1588. https://doi.org/10.1016/0167-6105(92)90373-I

Lieblein, J. (1974). *Efficient methods of extreme-value methodology* (NBS IR 74-602). National Bureau of Standards. https://doi.org/10.6028/NBS.IR.74-602

Liu, H., & Saathoff, P. (1982). Internal pressure and building safety. *J. Struct. Div.*, *108*(10), 2223–2234.

Mooneghi, M. A., Irwin, P., & Chowdhury, A. G. (2016). Partial turbulence simulation method for predicting peak wind loads on small structures and building appurtenances. *Journal of Wind Engineering and Industrial Aerodynamics*, *157*, 47–62. https://doi.org/10.1016/j.jweia.2016.08.003

Moravej, M. (2018). Investigating Scale Effects on Analytical Methods of Predicting Peak Wind Loads on Buildings. *FIU Electronic Theses and Dissertations*. https://doi.org/10.25148/etd.FIDC006834

Oh, J. H., Kopp, G. A., & Inculet, D. R. (2007). The UWO contribution to the NIST aerodynamic database for wind loads on low buildings: Part 3. Internal pressures. *Journal of Wind Engineering and Industrial Aerodynamics*, *95*(8), 755–779. https://doi.org/10.1016/j.jweia.2007.01.007

Richards, P. J., & Hoxey, R. P. (2012). Pressures on a cubic building—Part 1: Full-scale results. *Journal of Wind Engineering and Industrial Aerodynamics*, *102*, 72–86. https://doi.org/10.1016/j.jweia.2011.11.004

Sharma, R. N., & Richards, P. J. (2003). The influence of Helmholtz resonance on internal pressures in a low-rise building. *Journal of Wind Engineering and Industrial Aerodynamics*, *91*(6), 807–828. https://doi.org/10.1016/S0167-6105(03)00005-9

Sharma, R. N., & Richards, P. J. (2005). Net pressures on the roof of a low-rise building with wall openings. *J. Wind Eng. Ind. Aerodyn.*, 25.

Stathopoulos, T., Surry, D., & Davenport, A. G. (1979). Internal pressure characteristics of low-rise buildings due to wind action. In *Wind Engineering* (pp. 451–463). Elsevier. https://doi.org/10.1016/B978-1-4832-8367-8.50047-4

Tecle, A. S., Bitsuamlak, G. T., & Chowdhury, A. G. (2015). Opening and Compartmentalization Effects of Internal Pressure in Low-Rise Buildings with Gable and Hip Roofs. *Journal of Architectural Engineering*, *21*(1), 04014002. https://doi.org/10.1061/(ASCE)AE.1943-5568.0000101

Vickery, B. J. (1986). Gust-factors for internal-pressures in low rise buildings. *Journal of Wind Engineering and Industrial Aerodynamics*, *23*, 259–271. https://doi.org/10.1016/0167-6105(86)90047-4

Womble, J., Yeatts, B. B., Cermak, J. E., & Mehta, K. C. (1995). Internal wind pressures in a full and small-scale building. *Proc., 9th Int. Conf. on Wind Engineering*, 1079–1090.

Woods, A. R., & Blackmore, P. A. (1995). The effect of dominant openings and porosity on internal pressures. *Journal of Wind Engineering and Industrial Aerodynamics*, *57*(2–3), 167–177. https://doi.org/10.1016/0167-6105(95)00003-A

Wu, H., Stathopoulos, T., & Saathoff, P. (1998). *Wind-induced internal pressure revisited: Low-rise buildings*. Structural Engineers World Congress, San Francisco, CA, U.S.A.

A Resource for the State of Florida

SECTION 3
NUMERICAL AND EXPERIMENTAL INVESTIGATION TO CODIFY WIND PRESSURE DISTRIBUTION OF ELEVATED HOUSES

FINAL REPORT
For the Period 2019-2020

A Research Project Funded by:
The State of Florida Department of Emergency Management

Prepared by
Dr. Amal Elawady
Dr. Arindam Chowdhury

Graduate Students
Nourhan Abdelfatah

Executive Summary

During recent hurricane seasons, varying levels of damage have occurred on elevated structures located in vulnerable coastal regions. The damage observations were primarily linked to wave and wind actions on the structure. The wind velocity increase and the presence of the air gap beneath the building affect the resulting wind pressure on the building surfaces. The affected houses have different geometries, including the number of stories, the stilt heights and the building aspect ratio. Therefore, more investigation is needed to provide a comprehensive methodology to predict wind loads acting on elevated houses. This will reduce the failure probability and hence increase the structural reliability and safety of buildings located in coastal communities. To establish a database of wind loading parameters on elevated structures, an ongoing study is being conducted at FIU to assess the performance of various shapes of elevated house. The current Phase 3 research includes an experimental test performed at the Wall of Wind (WOW) Experimental Facility on a large scale single-story elevated house with different stilt heights: 0 ft, 7 ft, 12 ft, and 17 ft. In addition, several numerical simulations were done of a full-scaled elevated house with different stilt heights and different aspect ratio. A 7 ft stilt case including stairs was also numerically simulated to find out the effect of stairs on the wind flow characteristics.

The results showed that the pressure coefficient was higher in case of the single-story elevated house compared to an on-ground counterpart. Most of the noticeable differences occurred in the 16.8in (7 ft full-scale) stilt case. High suction pressures were seen along both the top and bottom edges of the sidewalls when the model was elevated above ground level. For the floor surface, the densified pressure tap distribution showed the pressure variation around the stilts in the two cases. A region of high suction pressure beneath the model occurred due to the vortices present at the oblique wind angles. These regions were larger in the single-story case compared to the two-story case. The experimental data obtained from the various cases of elevated houses were used to perform numerical simulations. The recorded wind velocity, turbulence intensity, and pressure time histories aided the choice for the boundary condition criteria of the computational domain. In addition, the pressure distribution of the experimentally tested cases was used to validate the outcome of the numerical calculations.

The numerical simulation showed that the resulting local mean pressure coefficients were significantly higher for larger aspect ratio. The mean wind force on windward wall was found to be increasing rapidly with the increase of the stilt height or the aspect ratio. For instance, at oblique wind direction, the force ratio of the 17 ft stilt case windward wall reached to be triple its correspondent in the on-ground case. However, the side walls didn't experience a noticeable change. It was observed in the floor surface that the main reason of the pressure coefficient increase with stilt height is the oblique wind flow, which causes a high suction around the model stilts. The total shear force acting on the foundation showed a considerable increase as the stilt height increases, while the total vertical force dropped by elevating the house due to the presence of a new force on the floor. The overturning moment increased tremendously in larger stilt cases. The increase in the overturning moment was not as significant when increasing the aspect ratio. However, the increase of the overall vertical force was considerable for larger aspect ratio cases. The flow streamlines inside the computational domain showed that the flow separation region increased as the stilt height increases. However, the flow separation region decreased by increasing the model aspect ratio. In the small stilt cases, the wind speed increased beneath the building floor due to venture effect through the airgap. A flow circulation of air took place between the two intermediate columns. This clarify the reason behind the high negative pressure around the model stilts. There was a slight reduction of the mean pressure coefficient in all surfaces of the elevated house with stairs except for the floor surface which showed a considerable reduction of the wind pressure. The total force acting on the elevated house (including wind load on the stairs) did not experience a noticeable change. This can be attributed to the presence of wind force acting on the stairs which implies the need to quantify it in the design process.

For future studies, it is recommended to monitor the wind velocity beneath the house in smaller stilt cases as it leads to the occurrence of several damages. The observed increase in the mean pressure coefficient emphasizes the need to investigate the effect of changing the building aspect ratio. The observed increase in the vertical, shear forces and the overturning moments acting on the building foundations due to aspect ratio and stilt height increase, should also be taken into consideration in the future design of elevated houses.

Introduction and Background

The coastline of the United States is home to approximately 40% of the population (NOAA, 2018). This poses significant infrastructure risks to coastal communities because structures built near shorelines are vulnerable to strong windstorms and flooding hazards. Elevating houses along shorelines is one common strategy to avoid flooding from ocean waves. However, damage studies in the wake of recent hurricanes demonstrate the vulnerability of elevated houses. During the 2017 hurricane season, the United States sustained impacts from multiple hurricanes (Harvey, Irma, and Maria), which resulted in insurance claims greater than $265 billion (Cangialosi et al., 2018); (Blake and Zelinsky, 2018); and (Pasch et al., 2019). In 2018, Hurricane Michael affected 50,000 structures in the Florida Panhandle, southwest Georgia, and southeast Alabama (NOAA, 2018). Figure I-1 shows observed damage due to wind and wave action caused by hurricane Michael's impact at Mexico Beach, FL. The two wooden buildings in the figure have experienced wall and roof damages due to wind action, and floor damage due to wave action.

Figure I-1 Single-story houses elevated by 8 ft and 9 ft (wall, roof and floor damages) Hurricane Michael (2018) Mexico beach, Florida (Alipour et al., 2018).

Hurricane Michael's landfall near Mexico Beach, FL, impacted the region with wind speeds of 157 mph, and storm surge exceeding 6 ft (Alipour et al., 2018). As of June 2019, the total insured losses in Florida alone exceeded $7.2 billion USD (Artemis, 2019). Most recently, in 2019, Hurricane Dorian, which hit the Bahamas, resulted in insured losses of about $6.5 billion (Newmark, 2019). Figure I-2 shows the roof and wall damage on a two-story elevated house located in Marsh Harbour Bahamas during hurricane Dorian.

Figure I-2 Two-story elevated house after hurricane Dorian.

Available wind loading information on elevated structures are limited. An experimental study was conducted by Homes (1994) to compare a 1:50 scale elevated house with an on-ground case. The Atmospheric Boundary Layer (ABL) flow modeled rural terrain. The results showed an increase of mean pressure coefficients on the wall surface for all the tested wind directions. However, the study was not able to present peak pressure values as the results showed discrepancies between the values measured using the 1:100 scale model compared to these measured for the 1:50 scale model. The author claimed that the reason is the effect of Reynolds Number (Re) scaling effects.

Damage observations following hurricanes Irma (2017), Michael (2018), and Dorian (2019) all indicate a need to conduct more research to better understand the wind flow on elevated structures. This study should not be limited to changing elevation heights only. Damage observations from these storms indicated much variability in the geometry of residences constructed on stilts in coastal regions, such as single-, two-, and three-story buildings were all impacted by these storms. Building aspect ratios also varied throughout the impacted regions. Finally, it was observed for most of the affected houses that the main stairs were severely damaged. Figure I-3, I-4 and I-5 show various building geometries that sustained damage during hurricane Michael.

Figure I-3 Two-story houses elevated by 8 ft (wall, roof and stairs damages) Hurricane Michael (2018) Mexico beach, Florida (Alipour et al., 2018)

Figure I-4 Coastal house elevated by 7 ft with aspect ratio > 2 severely damaged Hurricane Michael (2018) in Florida

Fully destroyed stairs **Minor damages in stairs**

Figure I-5 Different cases of elevated houses with external stairs elevated by 8 ft Hurricane Michael (2018) Mexico beach, Florida (NSF, 2019).

Preliminary research to determine the aerodynamic wind loading on elevated homes was conducted at the Wall of Wind (WOW) Engineering Facility (EF) at Florida International

University (FIU) in 2017 (Chowdhury et al., 2017). In Phase 1, a large-scale wind test was performed to determine the aerodynamic force and moment coefficients for a representative elevated building. The study considered a single-story low-rise gable roof residential structure with full-scale exterior dimensions of 28.75 × 21 × 12.5 ft (L × W × H). The home's roof pitch was sloped 4:12, or approximately 18° relative to the horizontal. The building was standing on 4 large columns and tested for on-ground and at three different full-scale elevation heights: 2 ft, 7 ft, and 12 ft. A Phase 2 experimental study was conducted in 2018 to assess wind effects on two-story elevated houses (Elawady et al., 2019). This study focused more on the wind pressure distribution on a two-story building's surfaces. During Phase 2, the full-scale height of the tested model was 21.5 ft. The pressure taps were densified to present the pressure distribution at the floor edges, around the model stilts and the effect of adding intermediate columns at the center of the model's longer walls. The second phase gave a better understanding of the pressure distribution and how the cladding could be affected by the variation of the stilt height and changing the location and number of columns. These interesting results showed the necessity of comparing those results with a similar single-story building.

For Phase 3, the current phase, the research is divided into three partitions:

- First, an experimental test was conducted at the WOW on a single-story building with a 14 ft building height standing on six columns. The 1:5 scaled model was tested for an on-ground baseline case, and then elevated to three different full-scale elevation heights: 7 ft, 12 ft, and 17 ft to compare against the two-story phase two testing. Compared to the model tested in phase one (Chowdhury et al., 2017), the current model has a densified pressure tap distribution, and different eave heights, column sizes, number of columns, and location of columns. This report presents a comparison of the resulting pressure distribution of the current single-story model with the two-story house previously tested in phase two.
- Second, a numerical analysis of the single-story house was attempted using Computational Fluid Dynamics (CFD). The CFD scope of work starts with a validation study to compare the data extracted from the CFD simulation with experimental observations obtained from the measurements in phase two. The full-scale two-story model simulated using CFD is evaluated by comparing the resulting mean pressure coefficients, and local forces on building surfaces with the predicted loads determined from the experimental methods in

phase two. Thereafter, a parametric study was conducted using the Reynolds-averaged Navier–Stokes equations (RANS) model with several objectives: (1) investigate the characteristics of wind flow surrounding the building for various geometrical configurations, and (2) assess wind actions on elevated structures and their variations with the building stilt height and aspect ratio. This study can help in identifying the geometrical controlling parameters and therefore, facilitate the codifying of the results. In addition, the CFD study enables the identification of the most critical configurations and geometrical range for future experimental studies.

- Third, a numerical study of a full-scale model was performed with adding external stairs. The aim was to check the necessity of including stairs during the experimental testing of elevated houses. As shown in figure I-5, significant damage may occur on the building stairs. In this partition, a 7 ft elevated single-story house is simulated with and without stairs. The stairs location is chosen to match one common configuration adopted for coastal houses. The results will be used to determine if the stairs significantly affect the wind loading beneath an elevated house. Further, this study presents the wind force acting on the stairs compared to the total wind force acting on the building.

1. Experimental test to compare the resulting pressure coefficient of the single-story and two-story elevated house models.

1.1 Methodology

In the current project phase, a large-scale wind test was conducted on a single-story elevated house. The building full scale dimensions were chosen to be 28.75 × 21 × 14 ft (L × W × H) with gable roof inclined by 18° above the horizontal. Compared to the two-story elevated house previously tested in 2019 (Elawady et al., 2019), the difference in the current configuration is the building height. To investigate the aerodynamics effects of different stilt elevations, the experimental models in both cases were affixed to four different full-scale equivalent column heights: 0 ft, 7 ft, 12 ft, and 17 ft. These cases simulate a ground-level building, two commonly reported cases in the available hurricane damage observation reports , and the highest elevation recommended by (FEMA, 2009).

1.1.1 Wall of Wind facility

The Wall of Wind (WOW) is a full- and large-scale testing facility located at Florida International University (FIU). The WOW system is a 12-fan array that can generate wind speeds and turbulence characteristics similar to those observed during tropical cyclones.

A view of the exhaust side of the 12-fan system is shown in Figure 1-1. Turbulence and boundary layer characteristics are generated using a set of triangular spires and roughness elements that are attached to the floor as shown in the figure. To produce a free-stream wind speed profile resembling the open terrain Atmospheric Boundary Layer (ABL) conditions, the automatic floor roughness elements were tilted to an angle of 25° above the horizontal and the triangular spires were adjusted to an opening angle of 45°. The WOW is equipped with a series of Turbulent Flow Instrumentation cobra probes, which resolve 3-dimensional velocity components of the free-stream wind field at heights

Figure 1-1 Flow management box inside WOW experimental facility

corresponding to the mean roof height of the elevated building model for all test cases. Reference wind speeds were collected with the WOW fans operating at 40% throttle. This throttle rate was chosen to optimize testing without exceeding the measurement range of the pressure scanner instrumentation installed within the building model.

1.1.2 Model description

A large-scale wind tunnel model of the case study residential structure was constructed using a length scale of 1:5, yielding model dimensions of 69 × 50.4 × 33.6 in (L × W × H) and equivalent stilt heights of 0.0 in, 16.8 in, 28.8 in, and 40.8 in for the four test cases. The wind tunnel model was constructed from clear 9-mm thick polycarbonate sheets installed onto a wooden frame structure constructed from nominal 2×4 lumber stock. The model stilts were cut to length from 4×4 lumber stock. Figure 1-2 show images of the four different stilt cases installed on the WOW turntable. Table 1-1 summarizes all the tested model configurations in the current experimental work, as well as the previous 2-story testing configurations, which will be referred to later for comparison purposes.

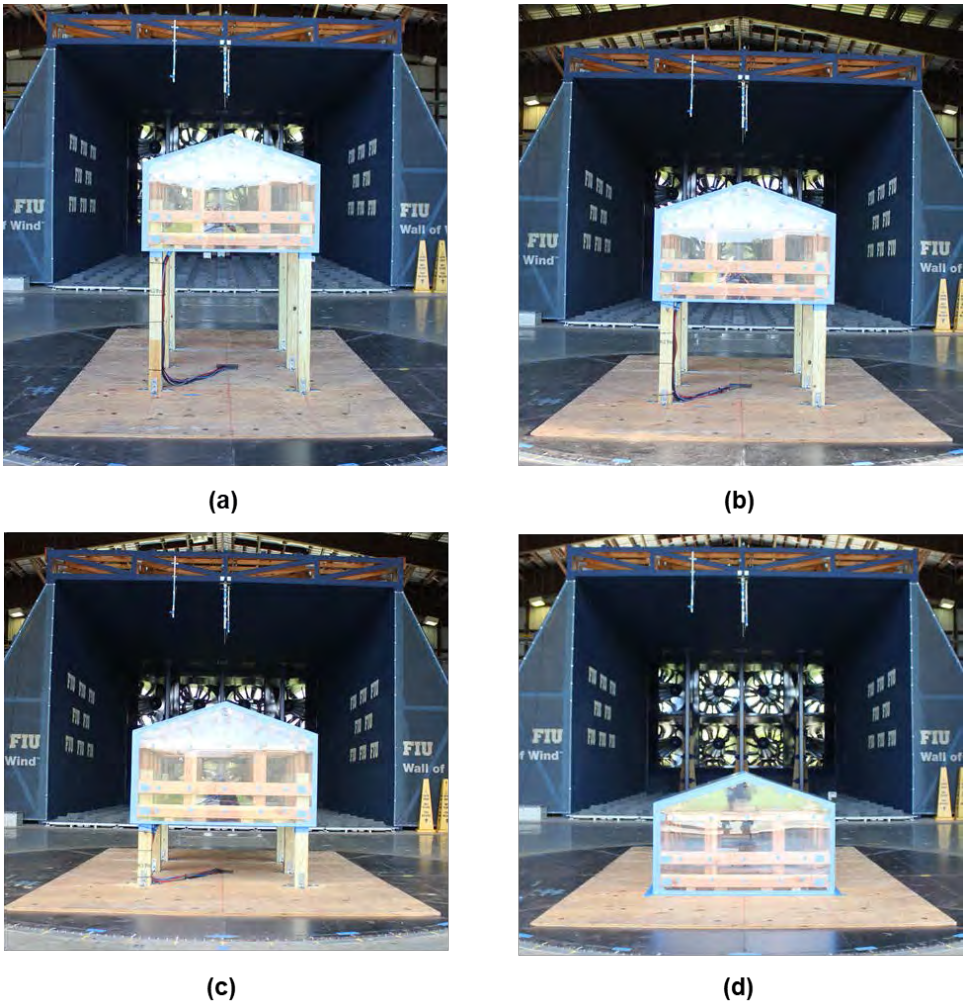

Figure 1-2 Test model installed on WOW turntable at different stilt heights (a) 1s-00.0in (b) 1s-16.8in (c) 1s-28.8in (d) 1s-40.8in

Table 1-1 Summary of stilt house test models

Model name	1s-00.0in	1s-16.8in	1s-28.8in	1s-40.8in	2s-00.0in	2s-16.8in	2s-28.8in	2s-40.8in
Number of stories	1				2			
Roof mean height (in)	29.4	46.2	58.2	70.2	47.4	64.2	76.2	88.2

During the Phase 3 experiments, the single-story building model was instrumented with 262 total pressure taps to capture the aerodynamic pressure distribution on the roof, wall, and floor surfaces. Based on experience gained during the Phase 1 testing, improvements were made to the Phase 2 and 3 test setups to precisely monitor the pressure distribution, especially on the floor surface in the vicinity of the stilts. Due to the building's geometric symmetry, the pressure taps were located on the roof, wall, and floor surfaces of only one quarter of the model, as shown in Figure 1-3. The distribution of pressure taps was as follows: 72 pressure taps on

the roof surface, with their distribution relatively densified near the corners and the ridgeline; 79 taps on two wall surfaces, and they were densified along the model edges; 111 pressure taps on the floor surface, with spacing densified around the corner and middle silts. Figure 1-3 shows the general pressure tap locations. Figure 1-4 highlights the orientation of the pressure taps with respect to the WOW wind flow. Appendix A includes detailed drawings with dimensions of the tap locations. The current test procedures for the single-story elevated house were chosen to match the Phase 2 test setup.

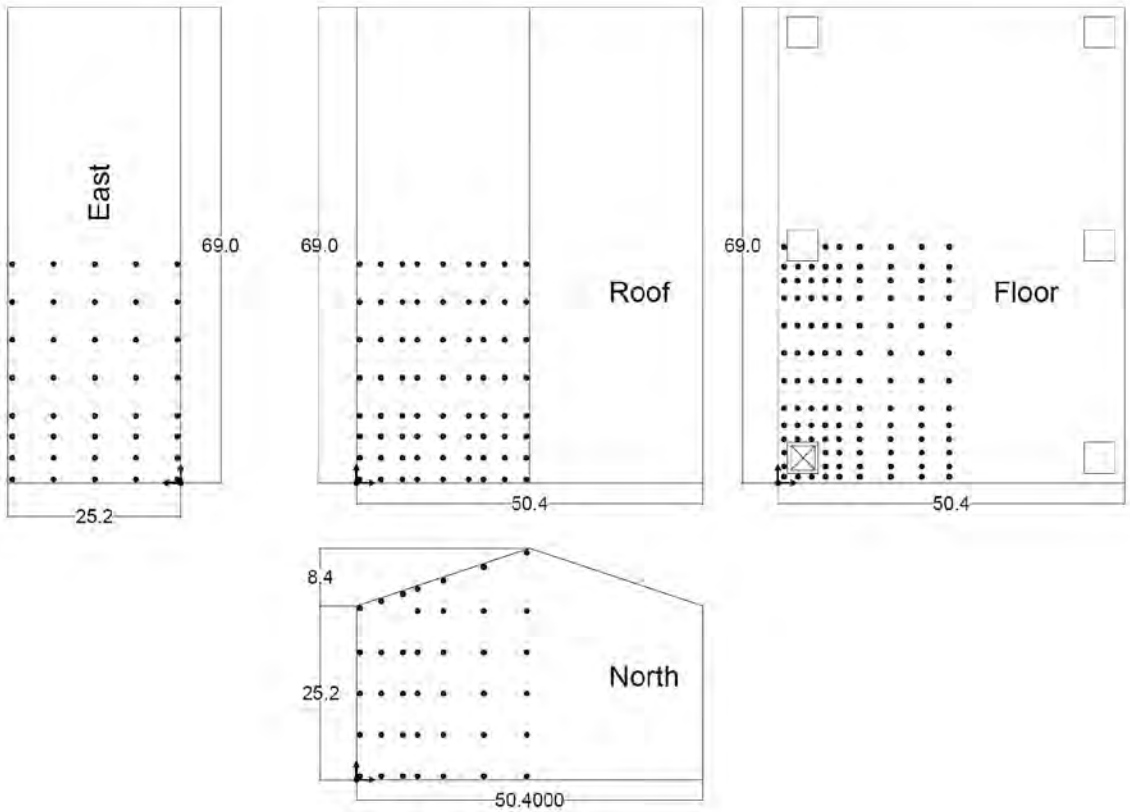

Figure 1-3 1:5 Scaled elevated house outer dimensions and tap location (Dimensions in inches)

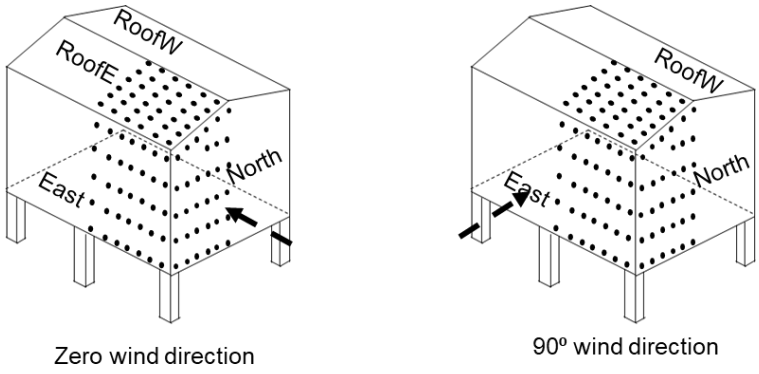

Figure 1-4 Stilt house model testing orientation with respect to wind direction (3D View)

The pressure taps were connected to a total of six Scanivalve ZOC33 pressure scanners to acquire the high-resolution time histories for this study. Experimental pressure measurements were recorded for wind directions ranging from 0° to 360° at 5° intervals for each of the four test cases. For each wind direction, pressure data was recorded at a rate of 520 Hz/channel for a 60 s duration. The measured time histories were used to investigate the overall pressure distributions on the elevated houses and to determine the localized cladding loads. It should be noted that the test model's floor panel was installed only during the elevated test cases; the floor was removed when the model was tested at ground level since there was no air flow beneath the building during that case. As a result, floor pressure data was not reported for the 0.0-in stilt height test case. The model description on the two-story elevated house has been explained in details in the published report (Elawady et al., 2019).

1.2 Data analysis

As shown in Figure 1-5, cobra probes were adjusted at the mean roof height of each stilt case to record the wind velocity fluctuation. The cobra probes collected wind speed data at a sampling frequency of 2,500 Hz for a duration of 180 sec. For building model pressure distributions, the Scanivalve ZOC33s recorded pressure data at a rate of 520 Hz/channel for a 60 s duration at each wind direction. As recommended by (Irwin et al., 1979), a transfer function was applied to the measured pressure time histories to eliminate the distortion effect caused by the pressure tubes' length. Mean, maximum, and minimum pressure coefficients were derived from the experimental data to provide an insight about wind actions on the building's outer envelope. Pressure coefficients were determined according to Equation 1:

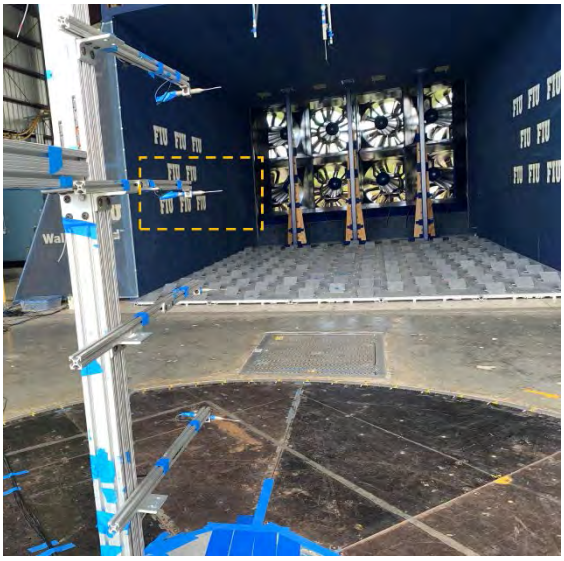

Figure 1-5 Cobra probes fixed at the model location over the turn table

$$C_P = \frac{P}{\frac{1}{2}\rho U^2} \quad (1)$$

The mean wind speed (U) was measured at the mean roof height for each stilt height of the single- and two-story models. P is the measured pressure, and ρ is the density of air.

1.3 Results

1.3.1 Local Mean Pressure Coefficient Distribution: Comparison between single-story and two-story elevated house.

The recorded pressure time histories were used to calculate the mean and peak pressure coefficients (C_{pmean} , C_{pmin} , and C_{pmax}). For both single-story and two-story building models, the pressure coefficient was calculated using the wind velocity at the mean roof height of each stilt case. The aim is to present a comparison between the single-story elevated model tested recently versus the two-story model cases previously tested in Phase 2. This comparison includes the on-ground case and three elevated conditions. Figures 1-6 and 1-7 show the case of wind acting parallel to the ridge (0º wind direction) for the 0, 16.8 and 28.8 in, and 40.8 in stilt heights, respectively. For the roof surface, there is a 17% increase of the C_{pmean} in the single-story cases. This increase is noticed as well at the higher edge of the side walls. By comparing the relation between different stilts, the C_{pmean} at the roof surface of the on-ground case (1s-00.0in) is higher than the elevated case (1s-16.8in) by 30%. However, the corresponding cases in the two-story model, showed an increase of 11%. For the elevated cases, there is no considerable change in the C_{pmean}. At the windward walls, the positive C_{pmean} distribution looked similar for both cases with almost the same range. For the floor surface, C_{pmean} values were similar for the single-story cases. In the 1s-16.8in case, higher suction pressures are noticeable around the stilts on the floor surface; the 1s-16.8in case showed approximately 25% higher suction pressures than 2s-16.8in case.

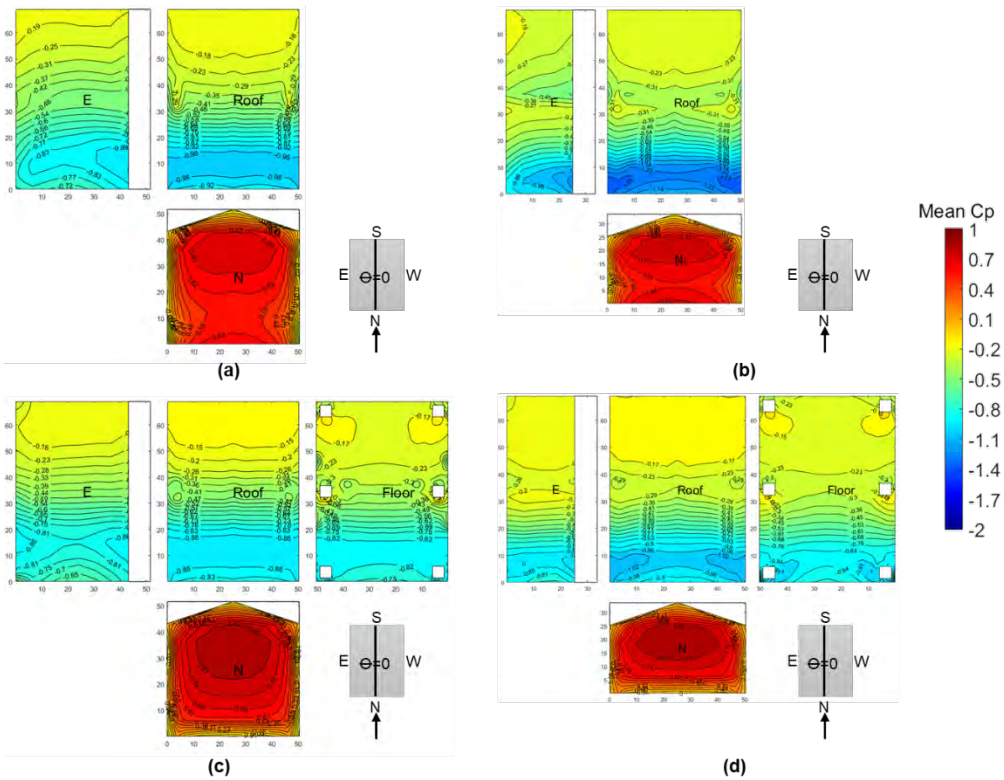

Figure 1-6 Observed $C_{p\,mean}$ for 0° wind angle (a) 2s-00.0in (b) 1s-00.0in (c) 2s-16.8in (d) 1s-16.8in

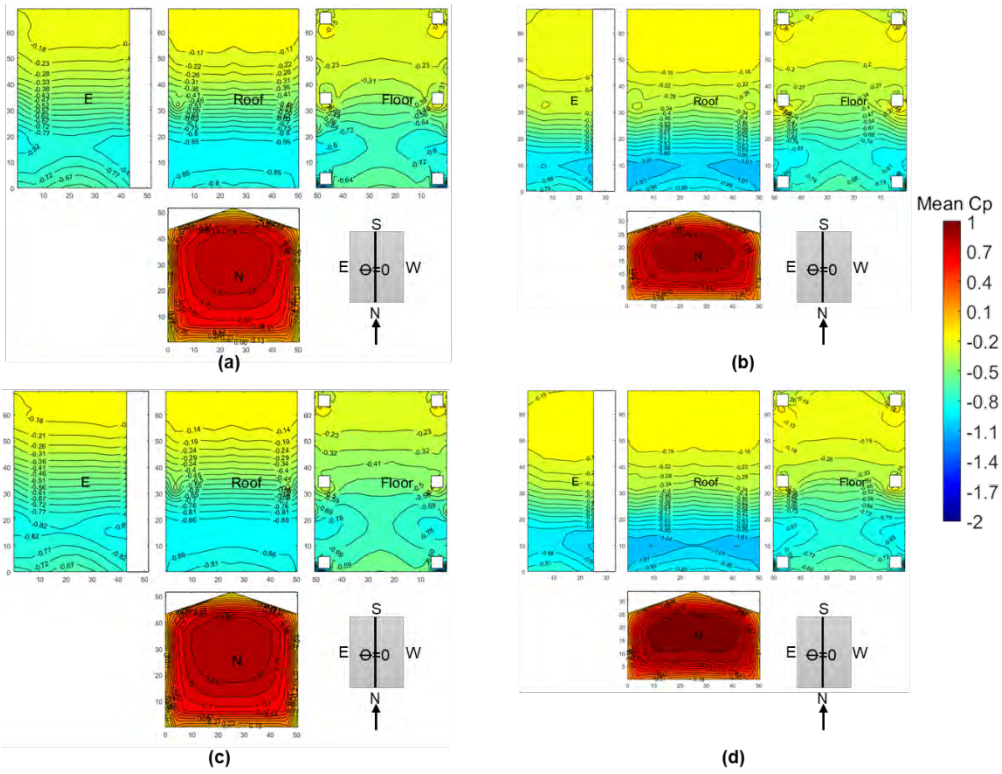

Figure 1-7 Observed $C_{p\,mean}$ for 0° wind angle (a) 2s-28.8in (b) 1s-28.8in (c) 2s-40.8in (d) 1s-40.8in

For the case of wind acting at a 45º angle, Figures 1-8 and 1-9 show that the floor surface experienced higher suction in the single-story case. Suction regions were located around the columns and they were more apparent around the intermediate column in 1s-28.8in, and 1s-40.8in cases. Both single- and two-story cases follow the same trend as $C_{p,mean}$ increasing with increasing stilt height above the ground. At the roof surface, the negative $C_{p,mean}$ values are also higher in magnitude for the single-story cases; a trend in roof suction pressures is not noticeable as the stilt height increases. Figures 1-10 and 1-11 show the case of wind acting perpendicular to the ridge (90º wind direction) for the 0, 16.8in, 28.8in, and 40.8in stilt heights, respectively. For the roof surface, the observed difference is opposite to what noticed in the 0º wind direction. The two-story case $C_{p,mean}$ is higher, and the pressure coefficient distribution is different. These figures reveal that the flow separation and reattachment occur with different shapes, and the vortices formed above the roof surface have a different size. The walls experience higher suction in the single-story case. There is not much difference in the observed $C_{p,mean}$ at the floor surface of the 28.8 in and 40.8 in stilt cases. However, there is a 20% increase of $C_{p,mean}$ in the 1s-16.8in stilt case with high observed suction around the intermediate column.

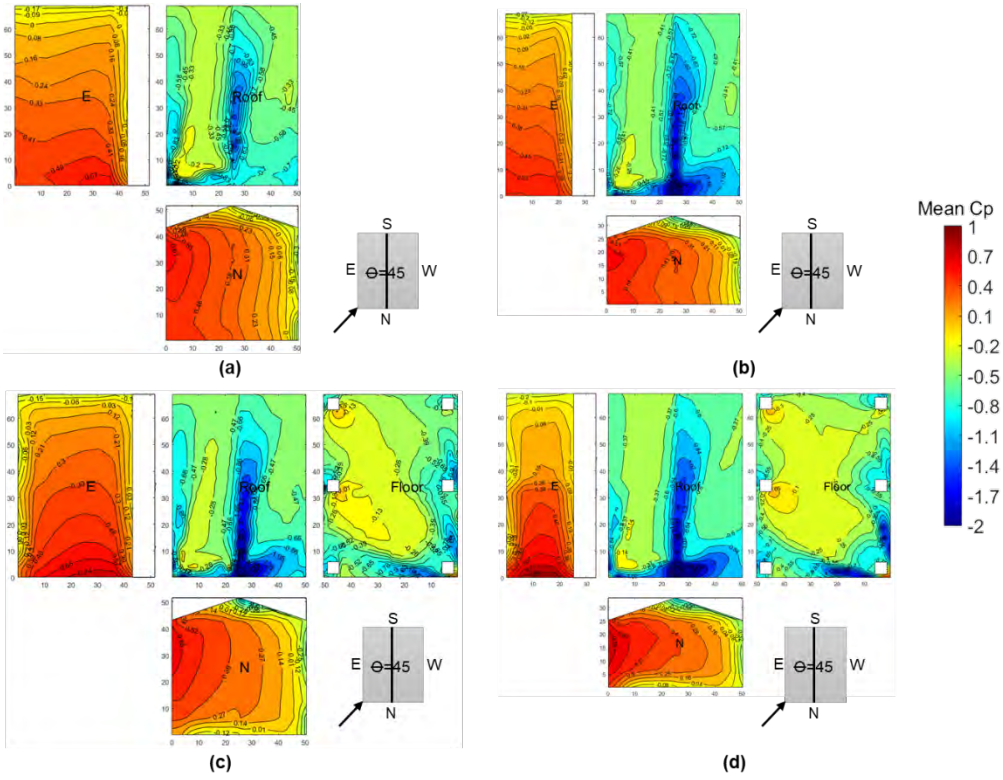

Figure 1-8 Observed $C_{p\ mean}$ for 45° wind angle (a) 2s-00.0in (b) 1s-00.0in (c) 2s-16.8in (d) 1s-16.8in

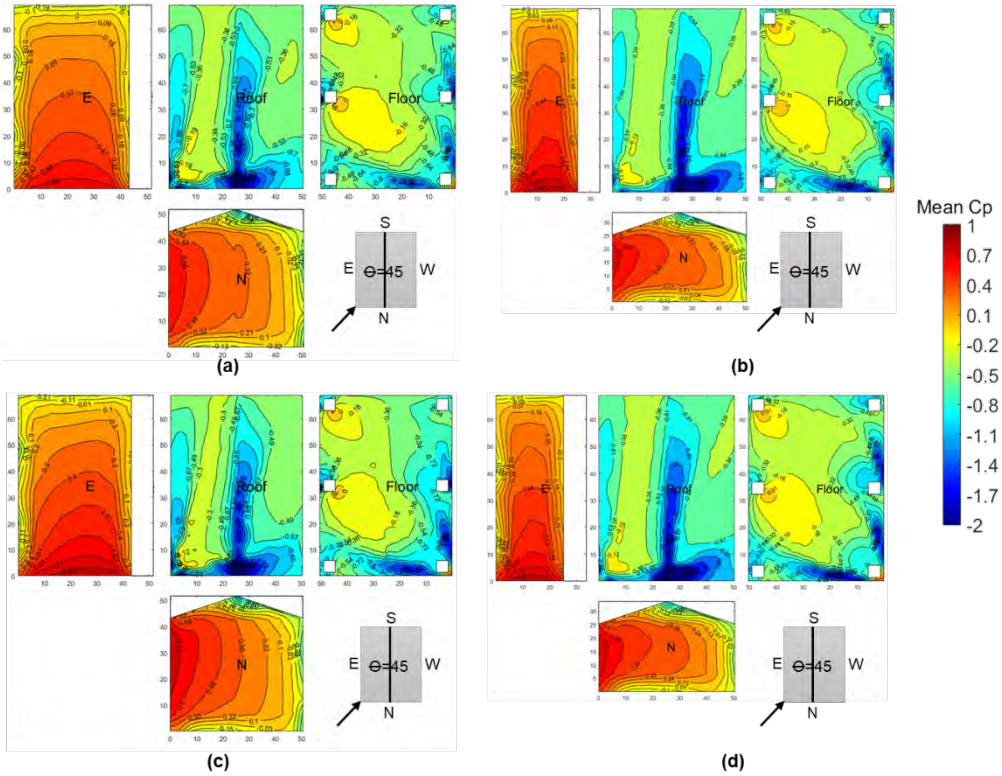

Figure 1-9 Observed $C_{p\ mean}$ for 45° wind angle (a) 2s-28.8in (b) 1s-28.8in (c) 2s-40.8in (d) 1s-40.8in

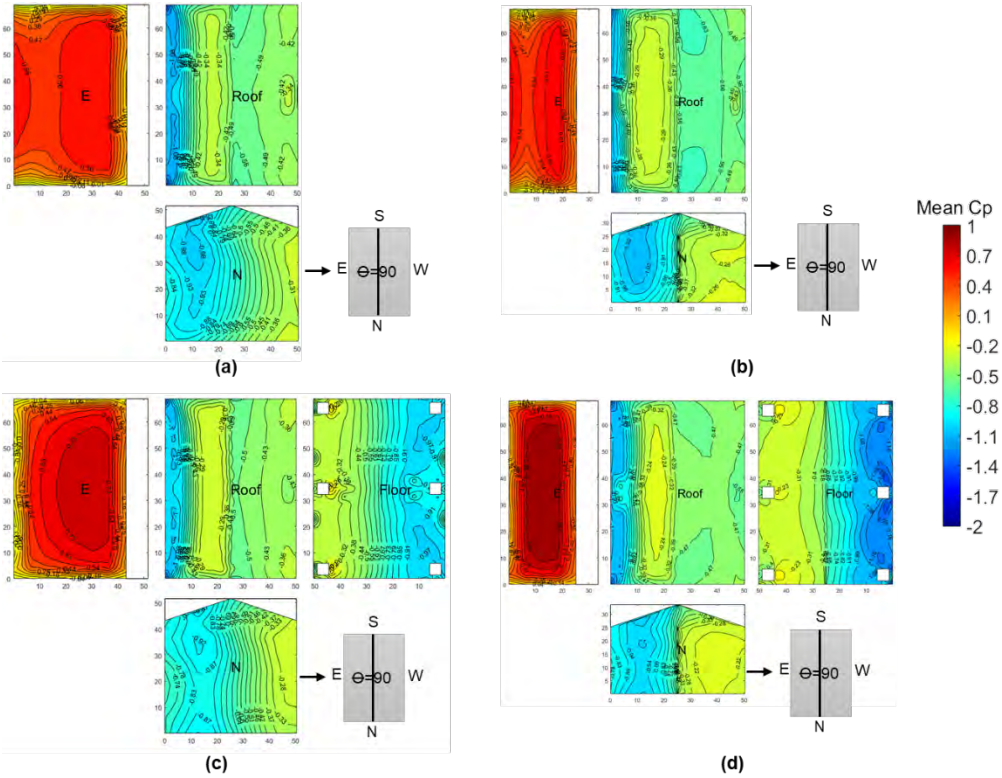

Figure 1-10 Observed $C_{p\ mean}$ for 90° wind angle (a) 2s-00.0in (b) 1s-00.0in (c) 2s-16.8in (d) 1s-16.8in

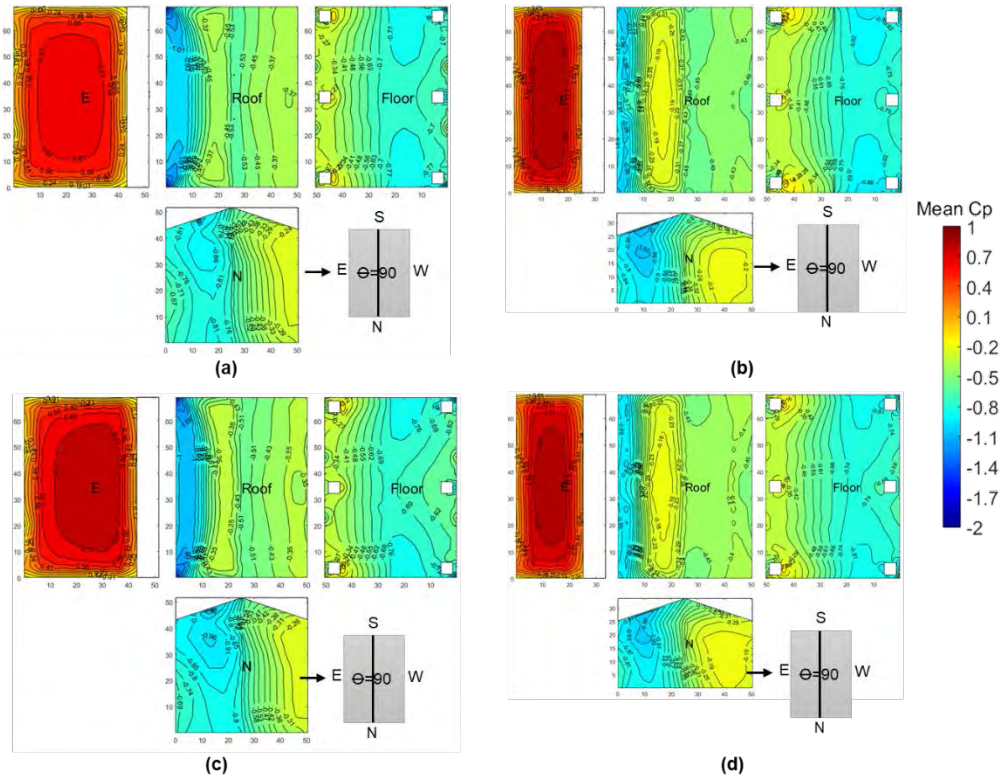

Figure 1-11 Observed $C_{p\ mean}$ for 90° wind angle (a) 2s-28.8in (b) 1s-28.8in (c) 2s-40.8in (d) 1s-40.8in

1.3.2 Local peak pressure coefficient for all wind directions compared to the two-story case.

This section presents a general comparison between the single- and two-story elevated houses for all wind directions. The observed peak pressure coefficient values for all angles were exported and the maximum local values are presented in Figures 1-12 and 1-13 for each stilt case. For the North and East walls, the contour plots reveal that the $C_{p,max}$ values tend to decrease slightly as the stilt height increases. For the on-ground case, there is a 30% increase in the $C_{p,max}$ values in the 1s-00.0in case when compared to 1s-16.8in case. On the other hand, there is only 10% increase in the $C_{p,max}$ values in the 2s-00.0in case when compared to 2s-16.8in case. The single-story elevated cases show that the $C_{p,max}$ values are 23% higher than the two-story case.

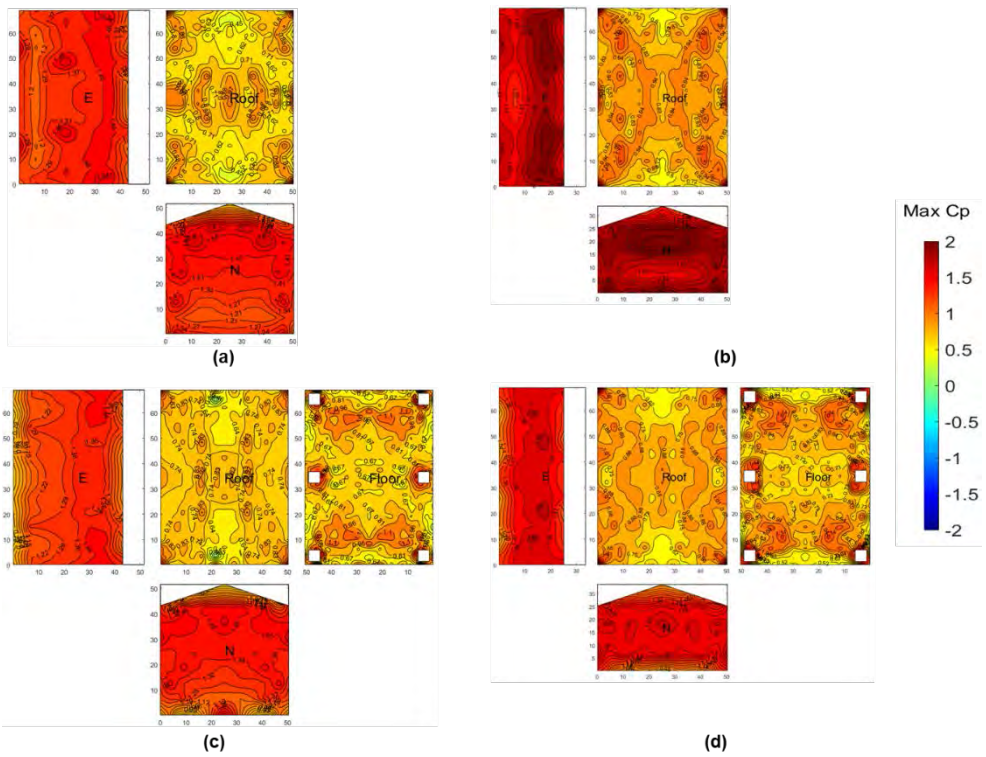

Figure 1-12 Peak observed $C_{p\,max}$ among all wind directions (a) 1s-00.0in (b) 2s-00.0in (c) 1s-16.8in (d) 2s-16.8in

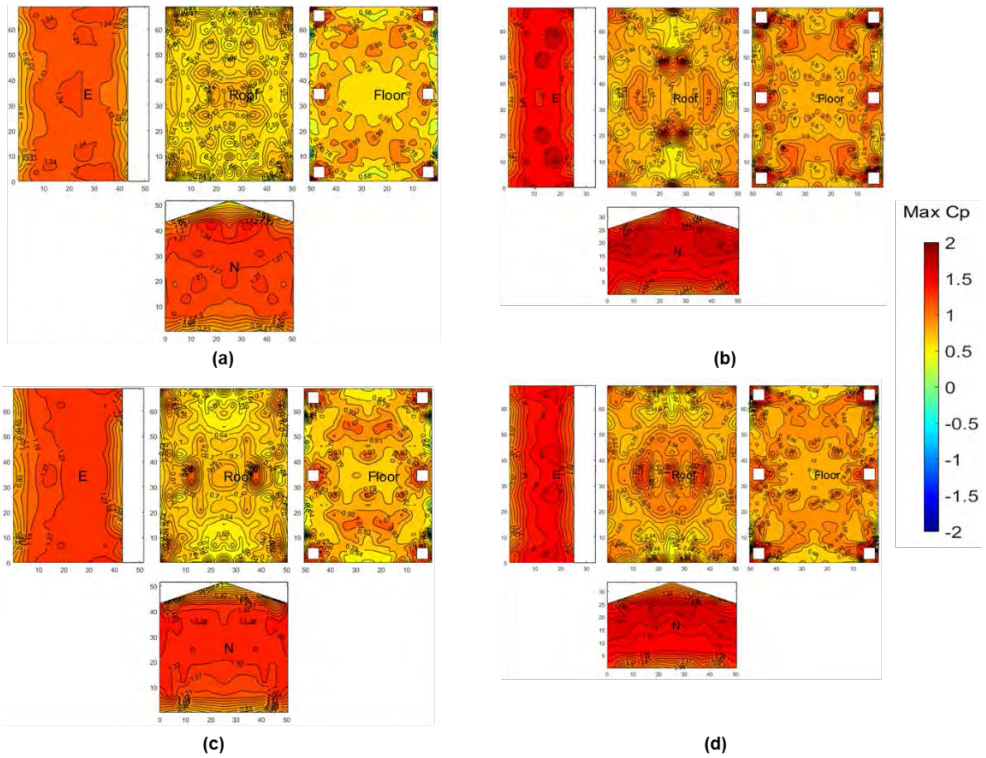

Figure 1-13 Peak observed $C_{p\,max}$ among all wind directions (a) 2s-28.8in (b) 1s-28.8in (c) 2s-40.8in (d) 1s-40.8in

The minimum observed pressure coefficient for each wind direction, $C_{p,min}$, was calculated for each pressure tap. The largest magnitude observed $C_{p,min}$ values for all angles were exported and the results are presented in Figures 1-14 and 1-15 for each stilt case. These results indicate the highest suction pressures exist near the roof and wall edges and along the roof ridgeline. For both single- and two-story cases, the $C_{p,min}$ at the roof surface does not show trend with increasing stilt height. However, by comparing the two cases together, the single-story is significantly higher than the two-story case. For the floor surface, a concentration of high negative pressure is located around the building stilts. As the stilt height increases, the area of the negative pressure region increases. The observed negative pressure is more than 20% higher in the single-story case compared to the two-story case.

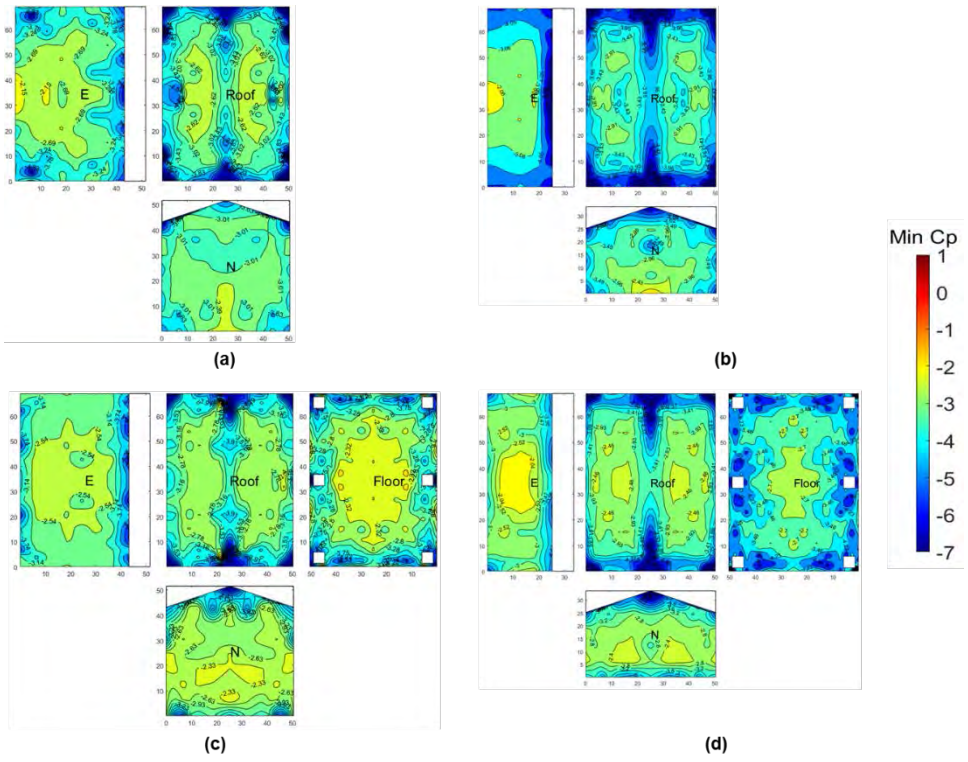

Figure 1-14 Peak observed $C_{p\,max}$ among all wind directions (a) 2s-00.0in (b) 1s-00.0in (c) 2s-16.8in (d) 1s-16.8in

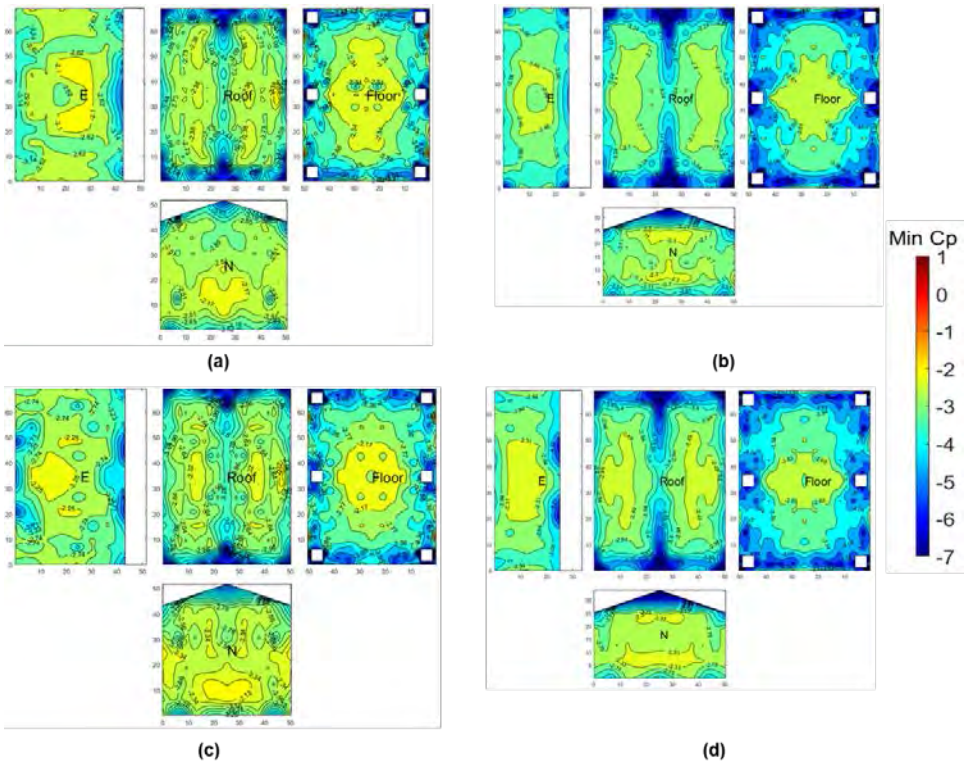

Figure 1-15 Peak observed $C_{p\,max}$ among all wind directions (a) 2s-28.8in (b) 1s-28.8in (c) 2s-40.8in (d) 1s-40.8in

Several "slices" of the building models were chosen at the roof and floor surface to clarify the $C_{p,min}$ variation for each stilt case. Figure 1-16 shows the pressure taps along each slice chosen. The $C_{p,min}$ variations versus distance are plotted in Figure 1-17 for the single-story case and Figure 1-18 for the two-story case. As shown, the high suction at the roof surface is located near the ridge and roof edges. The graphs show that the pressures along roof Slice 1 are nearly twice the magnitude as the values of roof slice 2. By comparing the current results with the two-story case, the $C_{p,min}$ along the edges is 25% higher in the single-story case. This percentage increases as the stilt height increase until it reaches 40% in the 40.8in stilt case. This is due to the slight decrease of $C_{p,min}$ in the single-story cases. Floor slice 1 is located beside the corner stilt column as shown in Figure 1-16, and the graphs in Figure 1-17 show that the magnitude of the pressure coefficients increase between distances ranging from 0 to 5 inches away from the building edge, which represents the column's location on the model. The $C_{p,min}$ values then stabilize as the distance continues approaching the center of the floor, beyond the stilt column location. A similar pattern was also observed for the two-story case, however the $C_{p,min}$ values were 35% lower near the stilts on the two-story model. At the mid

span, the $C_{p,min}$ ranges between -4 and -5 for the single-story case, while it ranges between -3 and -4 for the two-story case. As an overall observation, the floor surface's minimum pressure coefficient is nearly 25% lower in case of the two-story model compared to the single-story model.

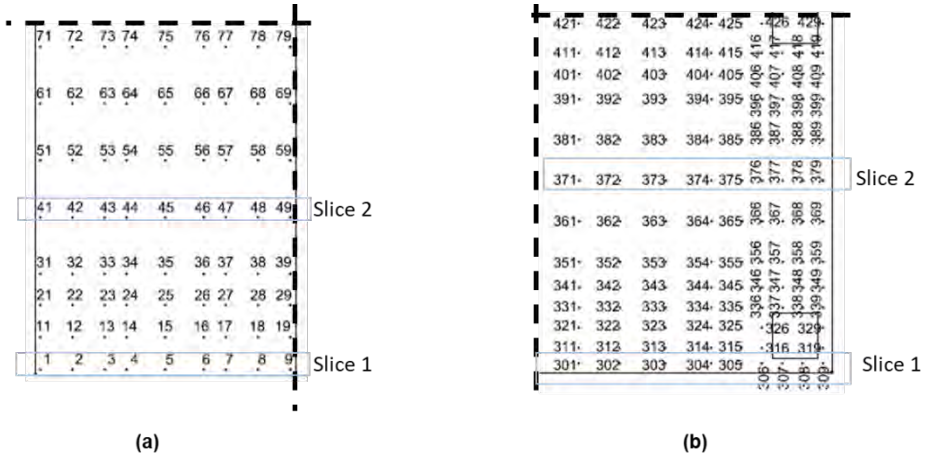

Figure 1-16 Pressure taps used for analysis of peak observed $C_{p,min}$ variation with distance

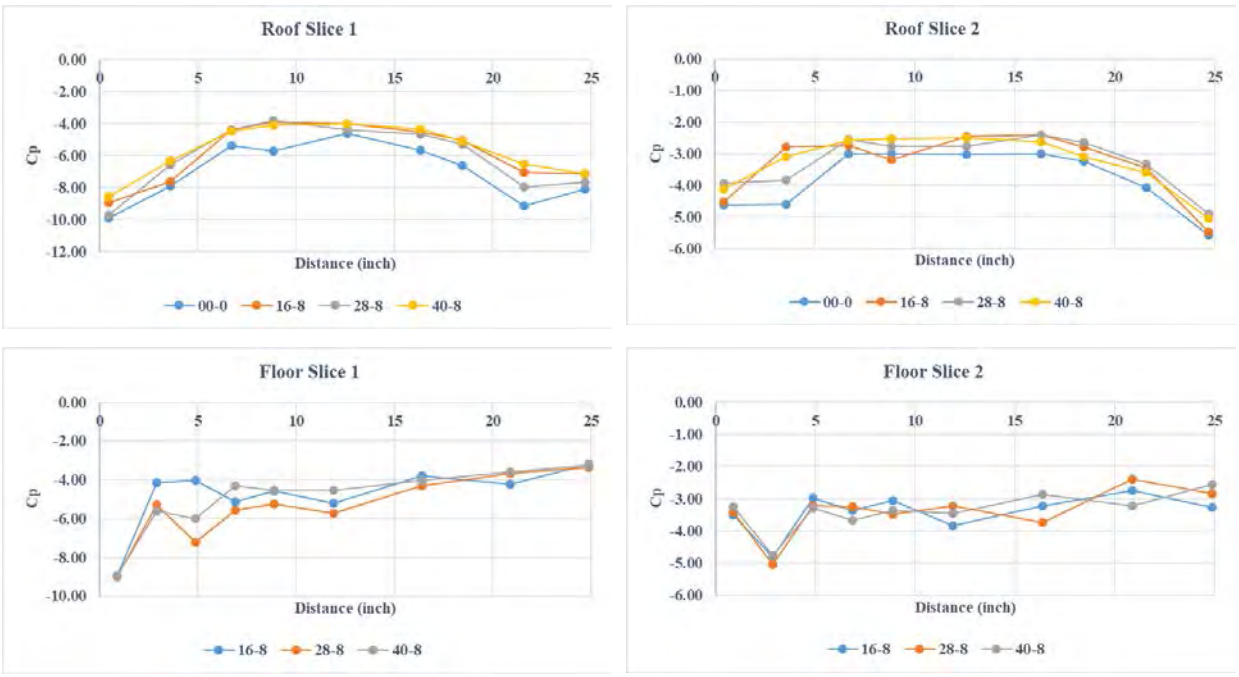

Figure 1-17 Peak observed $C_{p,min}$ along each slice of the Roof and Floor surfaces of the single-story model

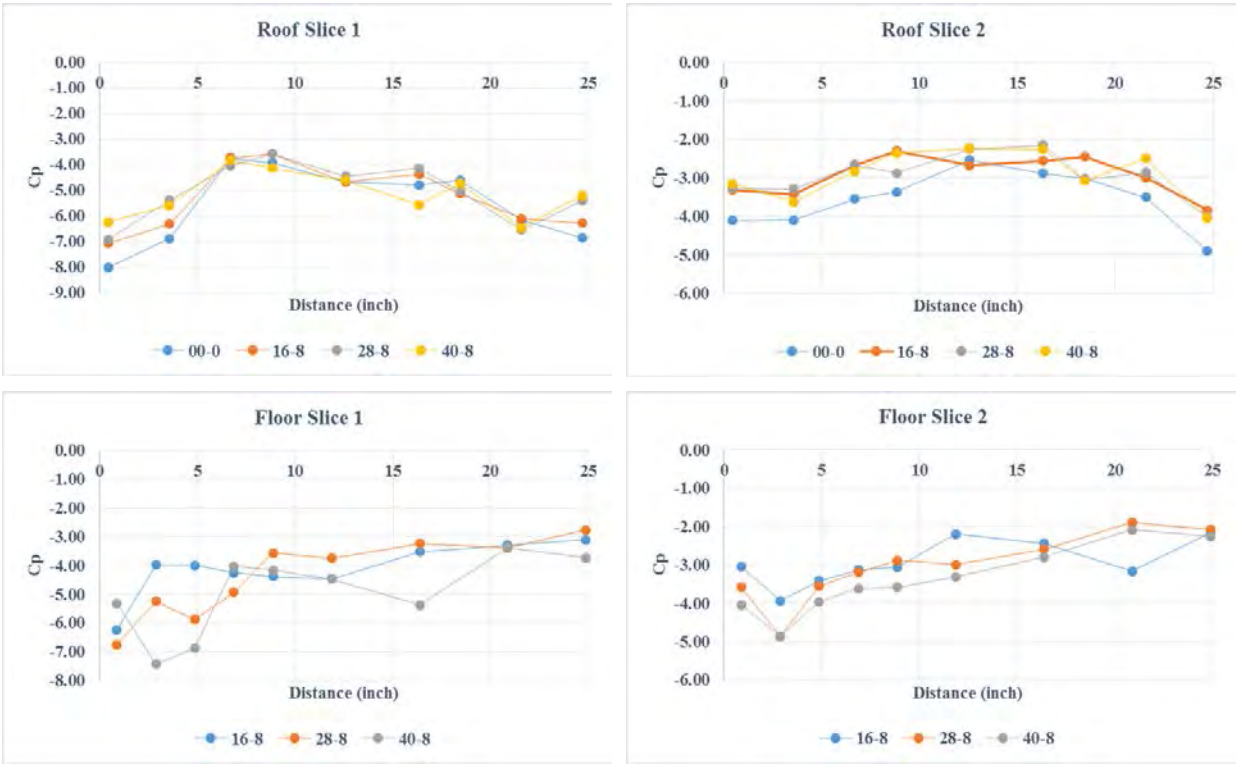

Figure 1-18 Peak observed $C_{p,min}$ along each slice of the Roof and Floor surfaces of the two-story model

1.4 Conclusion and Discussion

Coastal structures are vulnerable to strong windstorms and flooding hazards. Elevating houses to avoid flooding cannot be the sole solution to maintain building safety and resiliency since wind effects cannot be ignored. During recent hurricanes, several elevated houses experienced severe damage due to the combined effects of wind and water acting on the structure. The high wind velocity and the aerodynamic flow patterns affect the wind load characteristics. However, the design of coastal houses relies on the same engineering principles as on-ground buildings. Preliminary studies were conducted in 2017 and 2018 to determine the aerodynamic wind loading on elevated homes. In the current phase of this ongoing research effort, an experimental test was conducted at the WOW facility on a single-story building having an equivalent full-scale height of 14 ft and standing on 6 columns. The 1:5 scale model was tested for an on-ground configuration, and three different full-scale stilt elevation heights: 7 ft, 12 ft, and 17 ft. Compared to the single-story model previously tested in phase one, the single-story model investigated in this current study had a different pressure tap distribution, eave height, column size, column number, and column location. The model was instrumented with 262 pressure taps to capture the fluctuating pressure distributions on the roof, wall, and floor surfaces.

The results showed that the pressure coefficient was higher in the single-story elevated house. Most of the noticeable differences occurred in the 16.8in (7 ft full-scale) stilt case. The roof surface of the single-story house experiences higher uplift pressures along the roof edges. There were no noticeable changes in the negative pressure coefficient on walls. High suction pressures were seen along both the top and bottom edges of the sidewalls when the model was elevated above ground level. However, positive values were higher in the on-ground single-story model. For the floor surface, the densified pressure tap distribution showed the pressure variation around the stilts in the two cases. A region of high suction pressure beneath the model occurred due to the vortices' presence at the oblique wind angles. This region is larger in the single-story testing specimen compared to the two-story testing specimen.

The experimental data obtained from the various cases of elevated houses described in this section were used to perform numerical simulations, outlined in the next part of this report. The recorded wind velocity, turbulence intensity, and pressure time histories aided the choice

for the boundary condition criteria of the computational domain. In addition, the pressure distribution of the experimentally tested cases were used to validate the outcome of the numerical calculations. The next part of the report will present a comparison between numerical and experimental results. Then, the relation between the stilt height, aspect ratio and the resulting wind loads will be determined. A case study including stairs were presented to find out the effect of stairs on the wind flow characteristics.

2. Development and Validation of a Computational Fluid Dynamics (CFD) Model of Elevated Houses

Computational Fluid Dynamics (CFD) is a numerical approach that can be used to simulate the airflow around bluff bodies. This is done by applying the equations of fluid motion at discrete points through the studied fluid field. This can be accomplished by using various types of turbulence models. Compared to experimental wind tests, CFD methods provide a wide range of output data which describes the airflow characteristics and the resulting wind loads. CFD is also distinguished by its ability to simulate different flow turbulence characteristics, atmospheric boundary layer profiles, and various building geometries at a low cost compared to conventional wind tunnel testing (Murakami, 1998). To successfully simulate a wind tunnel test using CFD, it is important to accurately define a large enough domain size, good quality mesh size, precise boundary conditions, and the proper discretization methods. The cost factor is also important as the most precise CFD model can take years to develop and analyze. Several studies available in the literature discuss the effect of those parameters and how to maintain the model size to provide accurate results at a reasonable cost (Blocken et al., 2007; Chaudhari, 2012; Mochida et al., 2006; Näslund et al., 2001; Patel et al., 2007; Salim, 2009; Soe and Khaing, 2017).

In this project, the full-scale (prototype) size of the tested on-ground and elevated models were simulated using CFD with Reynolds-Averaged Navier-Stokes (RANS) equations. The RANS model is a sufficiently accurate and economic CFD technique that can be used to represent wind tunnel experiments (Franke et al., 2007).

First, a validation study was done by comparing the data extracted from the CFD simulation with what was obtained from the two-story experimental work in phase two. The full-scale

two-story model simulated using CFD was evaluated by comparing the resulting mean pressure coefficient, and local forces on the building surfaces with their corresponding values predicted by the 1:5 scale model tested at the WOW facility. Thereafter, a parametric study was conducted using the RANS model with two objectives: (1) investigate the characteristics of wind flow surrounding the building for various geometrical configurations, and (2) assess wind actions on elevated structures and their variations with the building stilt height and aspect ratio. This study can help in identifying the controlling geometrical parameters and, therefore, facilitate the codification of the results. In addition, the CFD study will enable the most critical configurations and geometrical range to be identified for future experimental studies.

2.1 Numerical model

The numerical simulation was achieved using the prototype dimensions of the elevated houses tested in the experimental program. Figure 2-1 shows the typical shape of the simulated model and coordinate system used through the numerical analysis. To insure the quality of the numerical simulation, a validation study was done first on the two story model tested in phase two (Elawady et al., 2019). The full-scale model is 28.75 × 21 × 21.5 ft (L × W × H) with gable roof angle 18º and placed at four different elevations 0 ft, 7 ft, 12 ft, and 17 ft. The CFD simulation was done for three wind directions; 0º, 45º, and 90º (i.e. 0º wind flow at Y-dir. and 90º wind flow at X-dir.). Next, same data setup and boundary conditions were used to simulate the full-scale size of the tested model in the current phase in WOW. From these simulations, parametric study was done to show the relation of the resulting wind load with the model stilt height and aspect ratio. The studied stilt heights ranges between 0 ft and 16 ft stilts with 2 ft increment. And the aspect ratio ranges between 1 and 2.5 with 0.25 increment. RANS simulation is widely used to study the aerodynamics of low-rise buildings. Therefore, this model was chosen for the current numerical study. The turbulent model named RNG k-ε was used to perform the simulation. Where, k is the turbulent kinetic energy, and ε is the turbulent dissipation rate. The RNG k-ε turbulence model shows a good performance in the literature (Jeong et al., 2002; Tominaga et al., 2015). This model can moderately predict and enhance the turbulent kinetic energy.

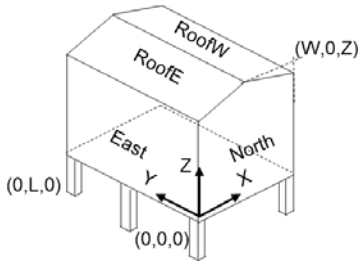

Figure 2-1 Full-scale elevated house schematic and the global axis

2.2 Computational domain and mesh criteria

As recommended by (Franke et al., 2007), the domain dimensions were chosen to avoid any external effect by means of the domain walls. As recommended the distance between the tested model and the inlet should be less than 6H, where H is the total height of the building. As shown in Figure 2-2, this distance was taken as 5H which is equivalent to the turn table location from the flow management box in Wall of Wind. The height of the computational domain was taken 7H to take the stilt height into account. The length behind the building till the outlet was taken 15 H. The adopted dimensions allows the blockage to be less than 5% and does not affect the test results (Choi and Kwon, 1998). A structured tetrahedral grid was constructed, and the resolution was determined after performing grid-sensitivity analyses. To precisely simulate the flow separation, reattachment points and vortices, the number of cells inside the domain reached up to 6 million cells, y+ was kept through the range (30-300) which is recommended for the current model type (Franke et al., 2007).

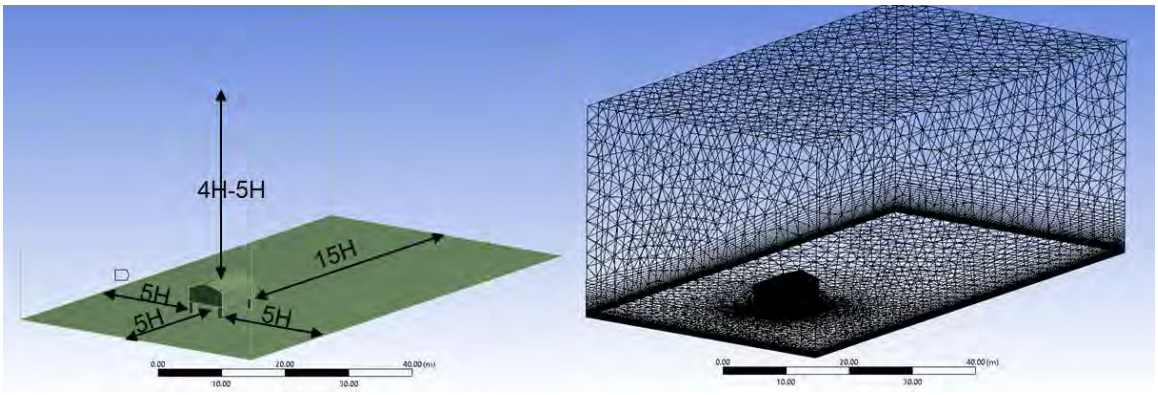

Figure 2-2 Full-scale single-story elevated house inside the wind flow domain and domain meshing

2.3 Boundary conditions and solver settings

To simulate real conditions of an open terrain category, all the boundary conditions were calculated precisely to describe the ABL and its characteristics. At the upwind boundary, the wind profile logarithmic law was used to define the mean wind velocity U change with height z which is equivalent to the experimental study as well. Using the appropriate friction velocity (u^*), von Karman constant (κ=0.4), and roughness length (z_0 =0.08m) same as for WOW conditions, the mean win velocity U was defined using equation (2). Figure 2-3 shows the wind profile inside the computational domain compared to the recorded mean wind speed inside WOW facility. Where U_{ref} is the mean wind speed at the reference height (Z_{ref}) which is 10m height in Full-scale and 2m height inside WOW.

$$U(z) = \frac{u^*}{\kappa} \ln \frac{z+z_0}{z_0} \tag{2}$$

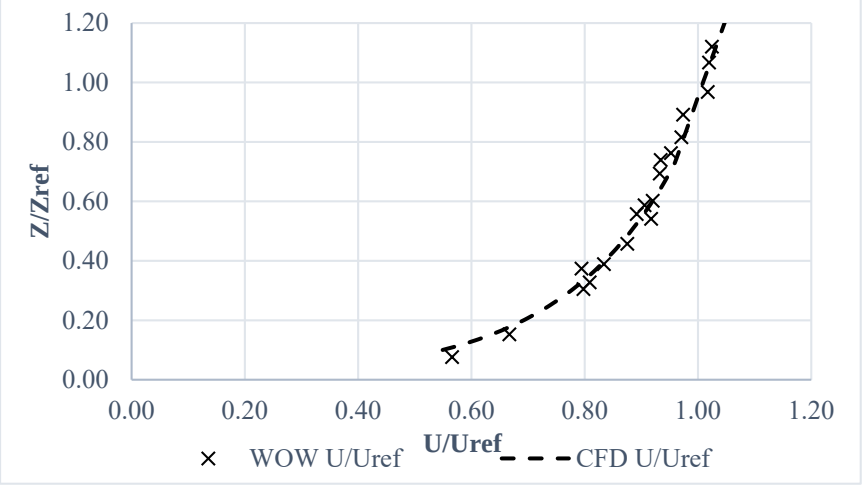

Figure 2-3 Wind flow ABL inside the computational domain compared to WOW

The model turbulence was defined using RNG k-ε model, the turbulent kinetic energy (k) defines the wind turbulence (I_u) using equation (3&4), where Cμ is the turbulence model constant and taken as 0.09 (Gorlé et al., 2009). The turbulent dissipation rate (ε) was calculated using equation (5) as recommended by Richards and Hoxey, (1993)

$$K(z) = \frac{{u*}^2}{\sqrt{C_\mu}} \tag{3}$$

$$K(z) = \frac{(Iu\ U)^2}{2} \tag{4}$$

$$\varepsilon(z) = \frac{u*^3}{\kappa(z+z_0)} \quad (5)$$

To avoid any external effect of the domain walls which confines the simulated building, all the outer surfaces were defined as slip walls. The domain ground was defined as rough wall. The roughness length was defined using input values; roughness height (C_s), roughness constant (K_s=0.5) and calculated using equation (6) (Blocken et al., 2007).

$$C_s = \frac{9.793\, z_0}{K_s} \quad (5)$$

ANSYS FLUENT 19.0 commercial software was used for the current simulation. Naiver Stokes and continuity equations were solved using the control volume method. The computational equations were discretized using a second-order upwind scheme with standard pressure interpolation. The SIMPLE algorithm was used for pressure velocity coupling. In order to reduce computational errors or uncertainties, a range of 10^{-4} to 10^{-7} was applied for the scaled residuals.

2.4 Simulation Results

2.4.1 Validation of CFD model using the two-story experimental results

In this section the two-story elevated house numerical model was evaluated by comparing it with the WOW model. Figures 2-4, 2-5, & 2-6 show the comparison between the mean pressure coefficient pressure (C_{pmean}) distribution using CFD with their correspondent from WOW for the 7ft stilt case. The figures reveal the good agreement between the two methods. In case of wind acting at 0º direction, the roof and floor surfaces experiences higher suction at the windward region where the wind separation occur. The floor surface of the CFD model shows that the peak suction region is generally around the column and decreases at the midspan. The agreement is better in the side (East) walls. The windward wall of the CFD model experiences higher pressure at the middle than that for the WOW model. But the difference does not exceed 7%. In case of 90º wind direction, the resulting C_{pmean} matches well at the roof, windward wall, and floor surfaces. However, the floor surface of the CFD model experiences higher suction at the intermediate column. This observation did not happen in the two-story case tested inside WOW, but it was noticed in the single-story case illustrated in the first section of this report. In oblique wind direction, CFD results agree with the experimental results showing that higher suction takes place on the floor surface around the model stilts.

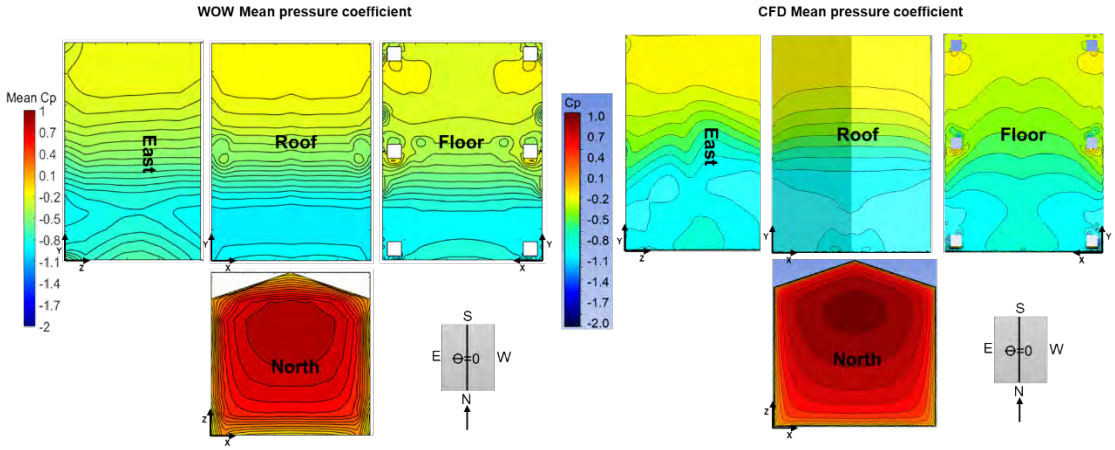

Figure 2-4 Local mean pressure coefficient of two-story 7 ft elevated case CFD vs WOW 0º wind direction

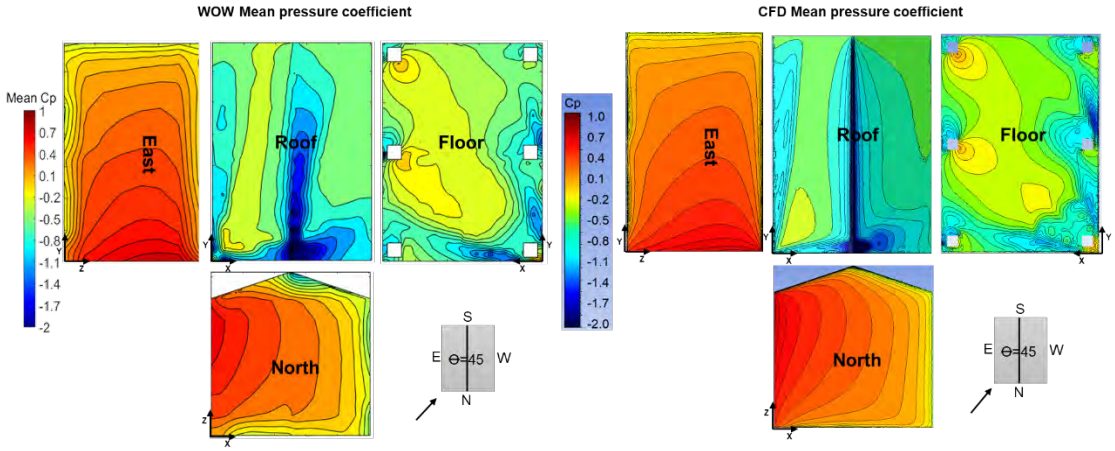

Figure 2-5 Local mean pressure coefficient of two-story 7 ft elevated case CFD vs WOW 45º wind direction

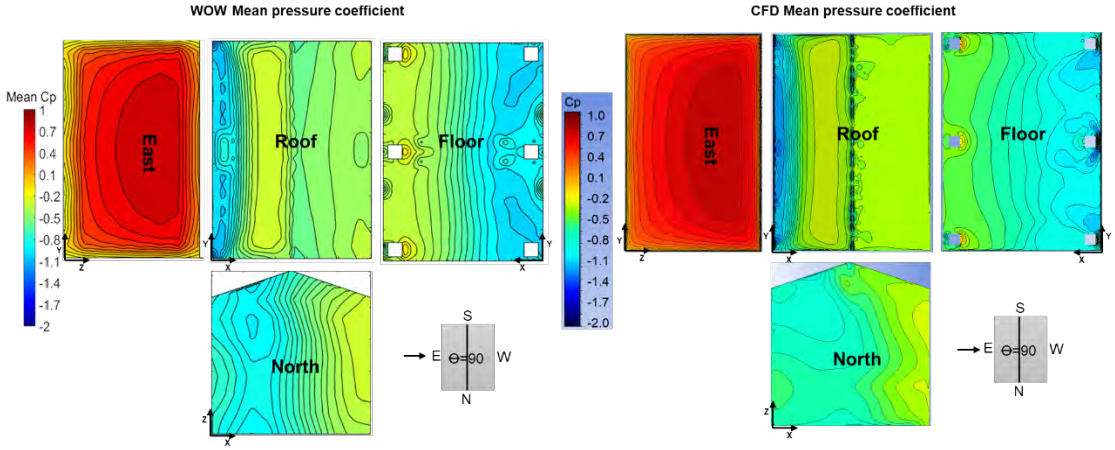

Figure 2-6 Local mean pressure coefficient of two-story 7 ft elevated case CFD vs WOW 90º wind direction

Several slices were taken, as shown in Figure 2-7 to present more detailed comparison between the two methods. Figures 2-8 and 2-9 show the plot of mean pressure coefficient variation with model length for the 7 ft stilt case. Those figures reveal the agreement between the experimental and numerical results. According to figure 2-1, for wind moving at Y-direction, figure 2-8 shows that the agreement is good especially for the windward, side wall, and floor surfaces. For wind moving at X-direction, figure 2-8 shows a high suction region beside the intermediate column. This is observed also in Figure 2-6. Generally, the graph drawings show that the difference between the two methods does not exceed 10%.

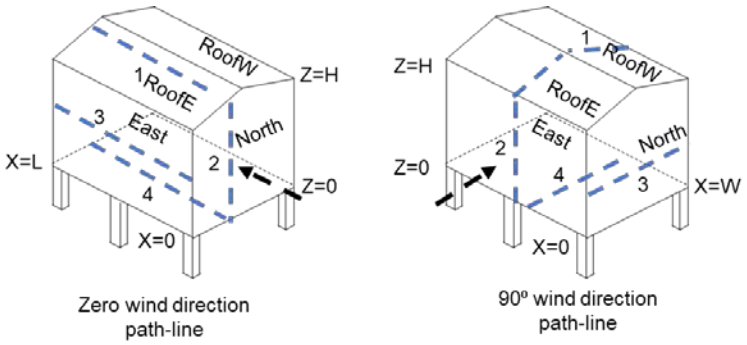

Figure 2-7 Full-scale elevated house path-lines for different wind flow directions

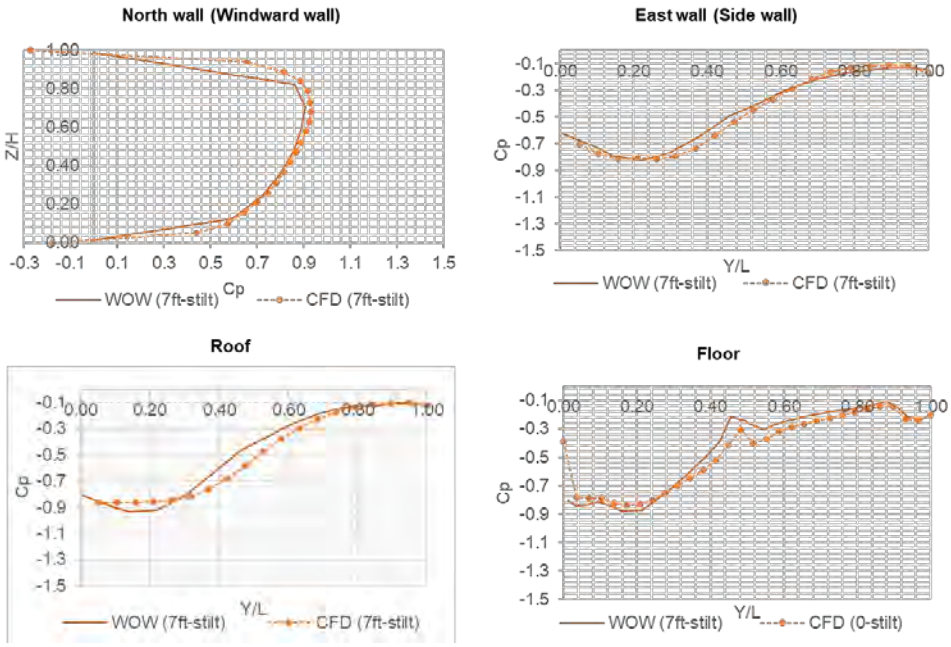

Figure 2-8 Local mean pressure coefficient at different path-lines of two-story 7 ft elevated case CFD vs WOW 0º wind direction

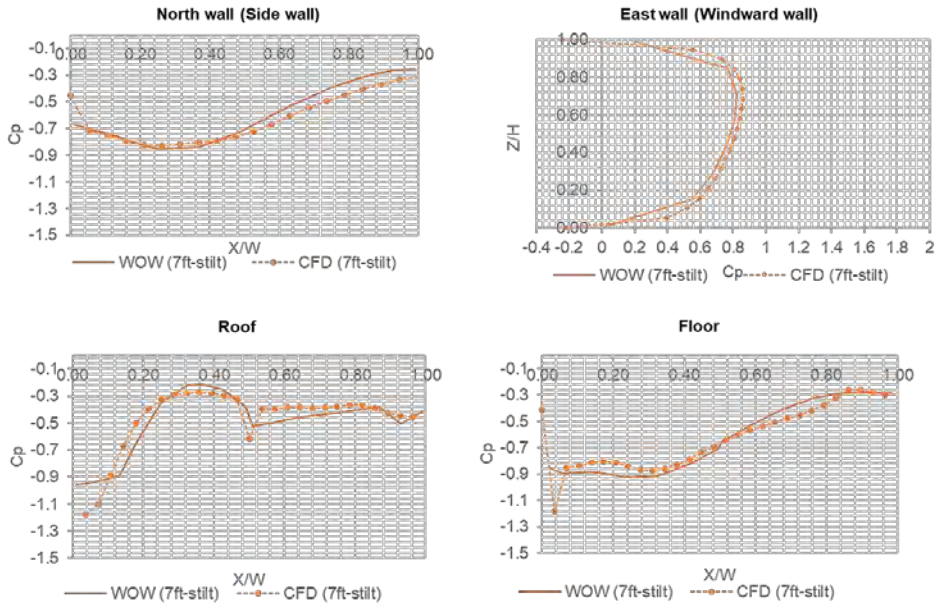

Figure 2-9 Local mean pressure coefficient at different path-lines of two-story 7 ft elevated case CFD vs WOW 90º wind direction

Finally, the comparison of the resulting average pressure coefficient (C_p) of each stilt case with WOW results. CFD positive pressure coefficient is around 7% higher than WOW for the windward wall. There is a 3% difference at the East wall and roof surfaces. CFD values are 6% higher for the floor surface. The deviation between CFD and WOW is very narrow and acceptable. Average pressure coefficient comparison for 45º and 90º wind angles are provided in Appendix B. This takes us forward to the next step of doing a parametric study using the same boundary conditions.

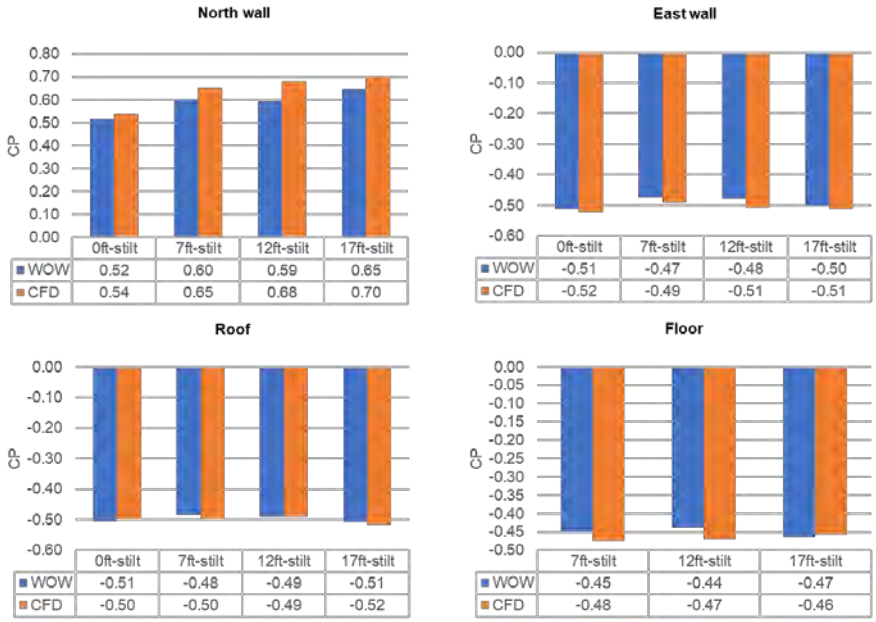

Figure 2-10 Mean pressure coefficient of each surface of two-story 7 ft elevated case CFD vs WOW 0º wind direction

2.4.2 Parametric Study to Evaluate Wind Pressure on Elevated Structures using CFD Methods

a- Wind pressure data

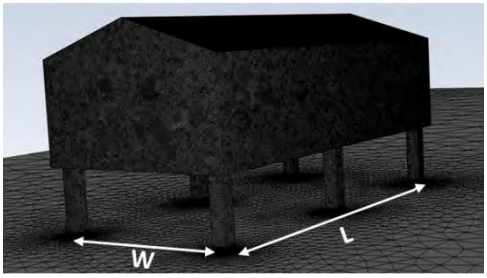

Figure 2-11 7 ft elevated house after increasing the model aspect ratio

By using CFD techniques, the simulation of the full-scale elevated house can provide a wide range of information about the wind flow characteristics and its effect on the model. As mentioned in the introduction, the parametric study covers two variables; stilt height, and the aspect ratio. The contour line plots provided in this section are for two different aspect ratios (A=1&2.5) and same stilt height (St=7 ft). It is worth mentioning that the aspect ratio (A) was increased by increasing the building length (L) as shown in Figure 2-11. As shown in Figure 2-12, by comparing the two aspect ratio cases, the high suction region occurs along the same length for two cases. The floor surface distribution is affected by the aspect ratio increase in a similar trend like the walls and roof surface. For wind acting at 0º direction, the region of wind separation and high suction is at the first quarter of the building. The floor area experiences less wind suction in case of A=2.5 but the suction is similar around the columns. However, by checking Figure 2-14 for the 90º

wind direction, the suction occurring around the columns in the windward region of the floor surface is significantly higher in case of A=2.5. This increase is more noticeable at the intermediate column. The roof surface windward side experiences higher suction in case of A=2.5. The same observations occur with the 45º wind angle for negative pressure value unlike the positive pressure area which look the same for the three wind cases.

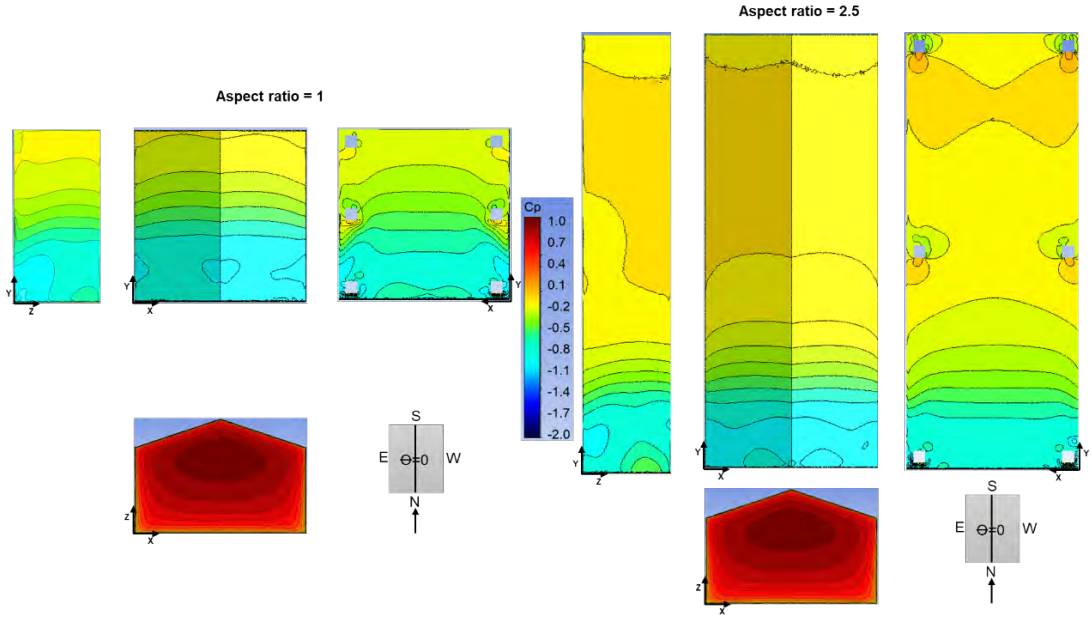

Figure 2-12 Mean pressure coefficient of single-story 7 ft elevated case with A=1&2.5 and 0º wind direction

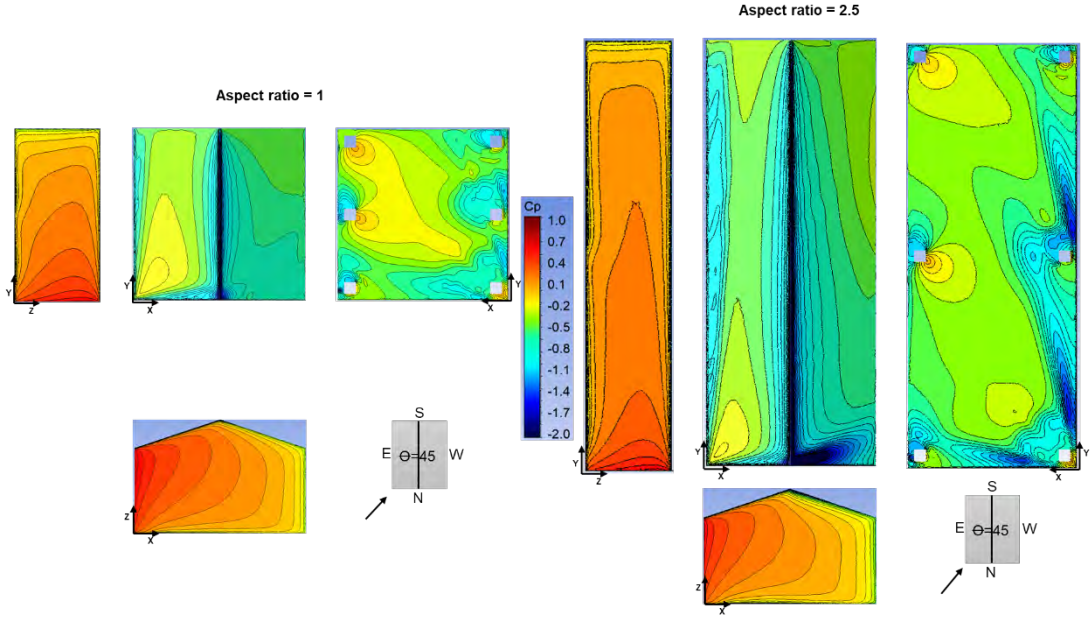

Figure 2-13 Mean pressure coefficient of single-story 7 ft elevated case with A=1&2.5 and 45º wind direction

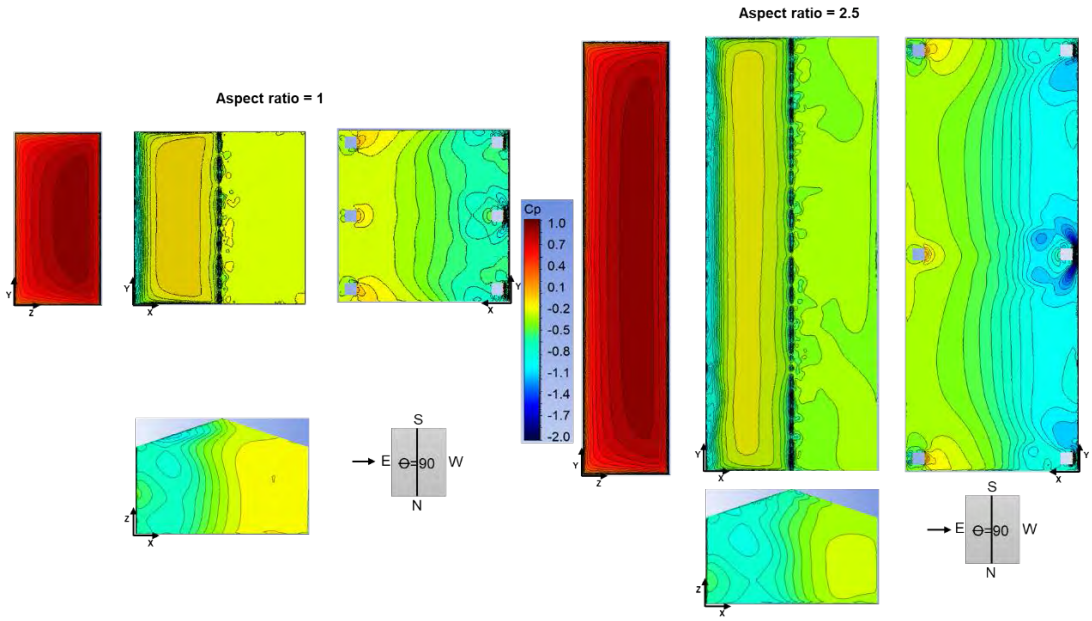

Figure 2-14 Mean pressure coefficient of single-story 7 ft elevated case with A=1&2.5 and 90º wind direction

For each surface of the model, the wind force was calculated then normalized with respect to the wind force of its correspondent in the on-ground case except for the floor surface the wind force was normalized with respect to the 2 ft stilt case. Then, the relationship of the resulting force ratio with the stilt height was drawn as shown in Figure 2-15. Similarly, the normalized force relationship with the aspect ratio was drawn as shown in Figure 2-16. As illustrated in Figure 2-7 for wind acting at zero direction, it hits the North wall. In that case, the wind force on the North wall increases rapidly with the stilt height; for every 2 ft stilt height the total force increases by around 10% till the force doubles when the stilt height is 16 ft. And this can be observed also with the East wall for 90º wind direction. At oblique direction, the force ratio becomes triple for 17 ft stilt case. However, when those walls are aligned with the wind direction, they don't experience a noticeable change. For the roof surface, at 45º and 90º wind directions, after elevating the house 2 ft upward the force value drops to 80% then it increases gradually to be higher by 15% than the on-ground case. At 0º wind directions, after elevating the house 2 ft upward the force on the roof surface drops to 95% then it increases gradually till it becomes higher by 40% than the on-ground case. For the floor surface, the first region of the graph, from 0 to 2 ft, has no data because this surface started to appear from the 2 ft stilt case, therefore, other forces of larger stilts are normalized with respect to this case. In case of 45º wind direction, the total vertical force increases by 30% for 17 ft stilt case. In the

two other wind directions, the total force decreases, compared to the 2 ft stilt, till the 7 ft stilt case then it increases till it becomes 10% higher than the smallest stilt case. This observation gives an indication that the increase of the negative pressure region at the floor surface is mainly due to the suction occurring around silts columns by the act of oblique wind flow. This was also concluded from the experimental test of the single-story elevated house.

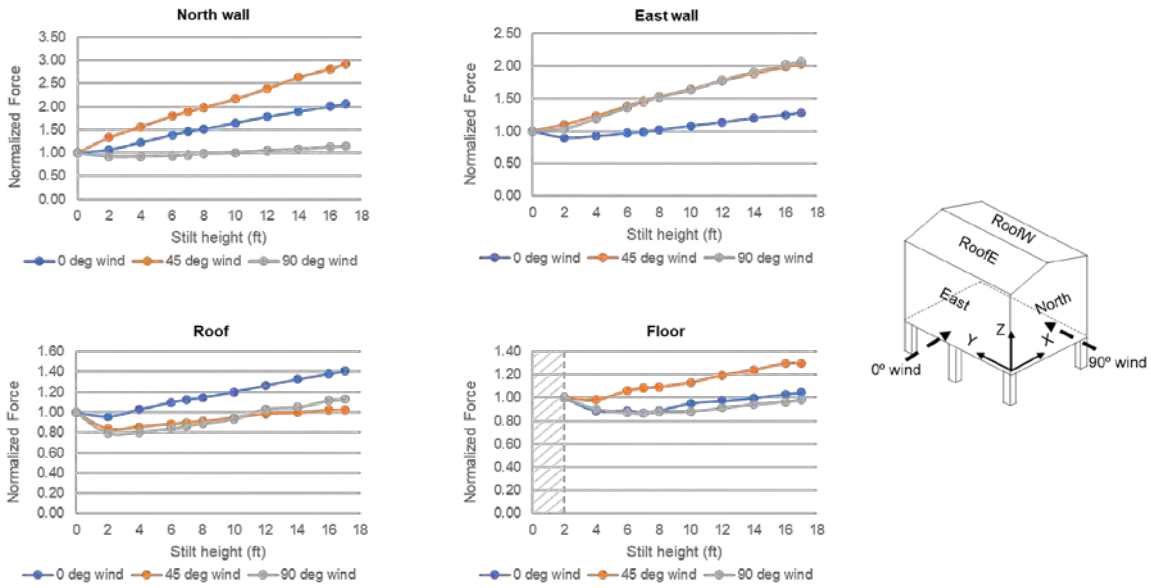

Figure 2-15 Relation between the average pressure coefficient of each model surface and the stilt height

The force increase is noticed also by increasing the model aspect ratio. By normalizing the resulting force on each face using the model with A=1 as a reference, a significant increase of the force ratio occurs specially in the floor and roof surfaces. The building windward walls experience a noticeable increase in the positive wind force (ex. North wall for wind angle 0º) and reaches up to 40% in case of A=2.5. This increase is higher for the East wall due to the wall area increase. At 90º wind direction, there is around 80% increase in the wind for every 0.25 increase in the aspect ratio. For the roof and floor surface, the vertical force in case of A=2.5 is found to be 5 time the vertical force in case of A=1. Zero wind direction graph shows clearly the slight change of the acting wind force on the side walls, roof, and the floor like what observed from the contour plots.

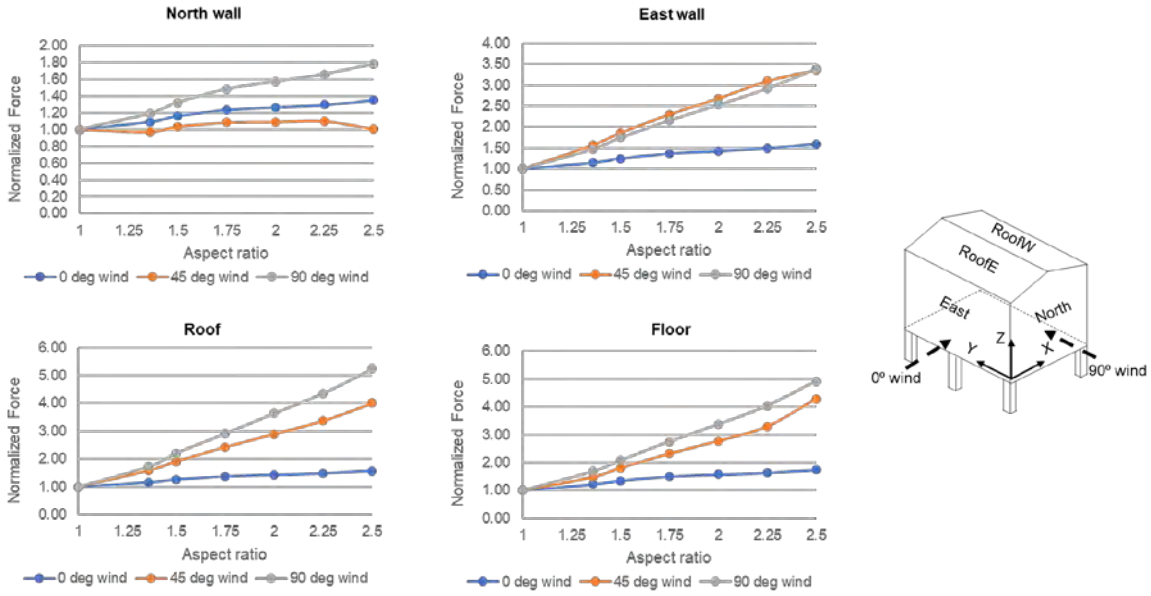

Figure 2-16 Relation between the average pressure coefficient of each model surface and the aspect ratio

b- Total force and Overturning moment

Investigating the total resulting forces on the building foundation is an important objective of the current study. This section presents the effect of changing the stilt height and aspect ratio on the total uplift, shear force, and the overturning moments. Figure 2-17 and 2-18 show the total force and overturning moment acting on the model foundations. By changing the model stilts, the normalized forces were calculated by dividing the stilt case total force and the on-ground case total force. Force direction was named according to the building axis shown in figure 2-1. It should be noted that the following graphs presents only the forces at the longitudinal direction of the wind flow or the vertical direction. The lateral wind forces are very small (ex. F_x in case of wind acting at zero direction), so the normalized force appears in the graph to be zero. From figure 2-17, there is a noticeable increase of the total shear forces F_x and F_y in case of wind acting at angle 90º and 0º respectively. And the total force in case of 17 ft stilt reached 2.5 times the on-ground case. Figure 2-17 shows lower values of vertical forces in the elevated case due to the presence of a new force acting downward on the floor surface. Negative ratio in case of 90º wind direction indicate that the force acting on the floor surface is larger than that for the roof surface and vice versa. The overturning moment resulting from the wind flow drops at 2 ft stilt case then increases tremendously as shown in the figure. Zero wind angle which hits the North wall cause a 450% increase in the resulting moment on the 17 ft stilt case, while 90º wind angle that hits the East and roof surfaces causes

800% increase. Similar observation can be seen in Figure 2-18 but the percentage of the moment increase is not as large as the stilt height effect. For instance, M_y increases by 250% in case of A=2.5. However, the vertical force is increasing with the aspect ratio increase to reach 350% in case of A=2.5. Therefore, the resulting increase of the shear and overturning moment on the building foundation is very large and should be taken into consideration in the future design of elevated houses. And the increase of the vertical force due to the aspect ratio increase is considerable as well. Monitoring the flow streamlines inside the computational domain could provide us with the explanation of the occurring differences due to the stilt and aspect ratio variation.

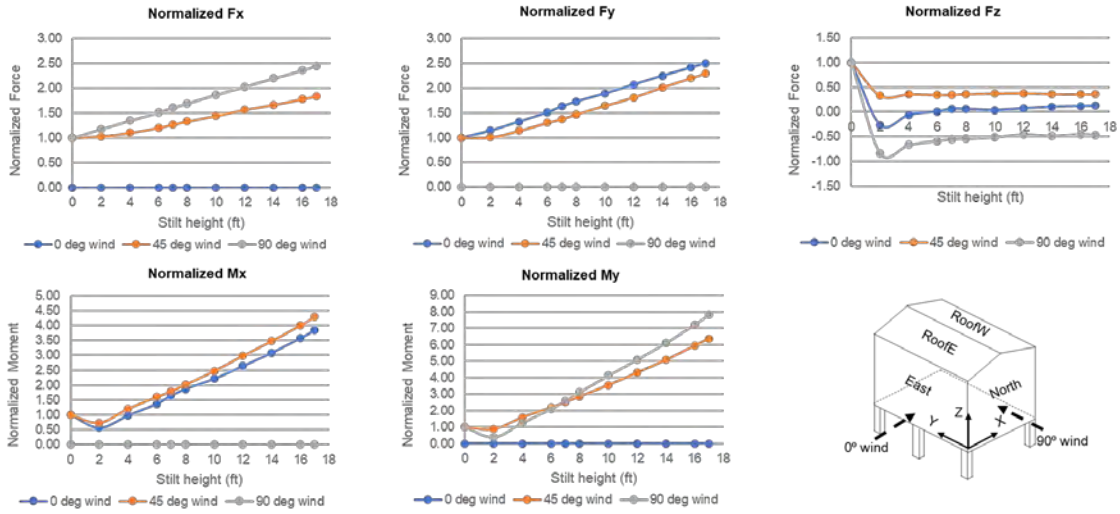

Figure 2-17 Relation between normalized wind forces on each surface of single-story elevated house and the stilt height

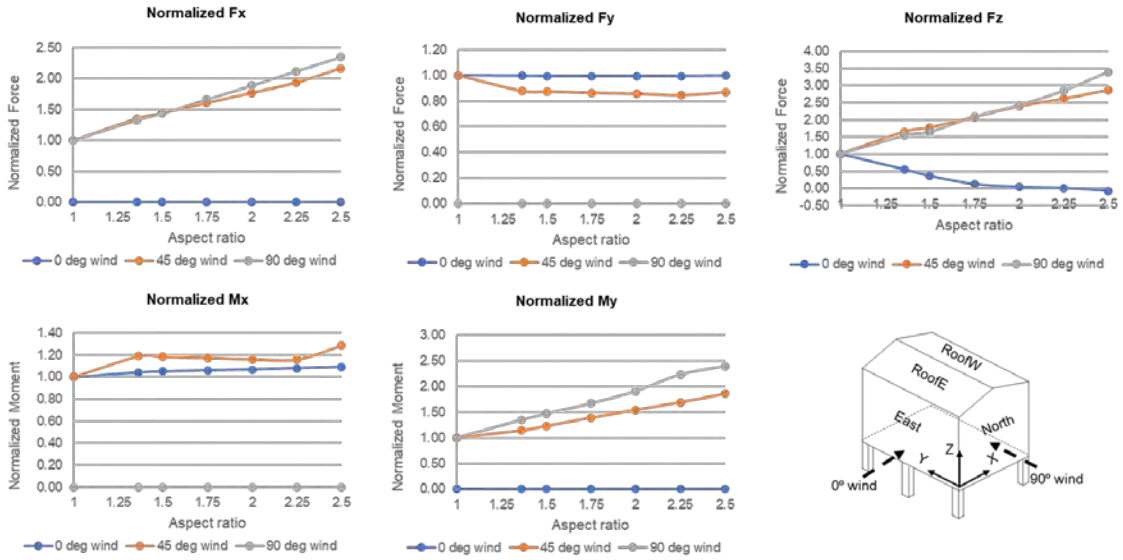

Figure 2-18 Relation between normalized wind forces on each surface of single-story elevated house and the aspect ratio

2.4.3 Air flow characteristics around the single-story elevated building

The final objective of the current parametric study is to present the air flow path lines in various simulated cases. This would help to understand the effect of the model aerodynamics affect the air flow and the resulting wind loads. Figure 2-19 shows the air flow streamlines of the on-ground, and other three different elevated cases (4ft, 10ft, and 14ft). The domain section is taken at the middle of the computational domain showing the wind flow at Y-dir. (i.e. along the ridge line). The figure shows that above the model roof the flow separation distances increases as the stilt height increase and a vortex starts to occur in 10 ft and 14 ft stilt cases. Beneath the model floor the separation area increases, and a vortex starts to appear in the 14 ft stilt case. In addition, higher wind speed appears in the airgap of the lower stilt cases. At the 4 ft stilt case the wind speed increases beneath the building floor. This phenomenon is known as Venturi effect. This is an important observation as it justifies the reason of the damages encountered below coastal house during wind incidents. At the wake, two vortices took place beside the leeward wall and they started to affect the floor surface too in the higher stilt cases. Figure 2-20 shows the streamlines in case of wind acting at 90º angle (perpendicular to the roof ridge). The figure shows the circulation of air that takes place

between the two intermediate columns. This clarify the reason behind the high negative pressure around the model stilts.

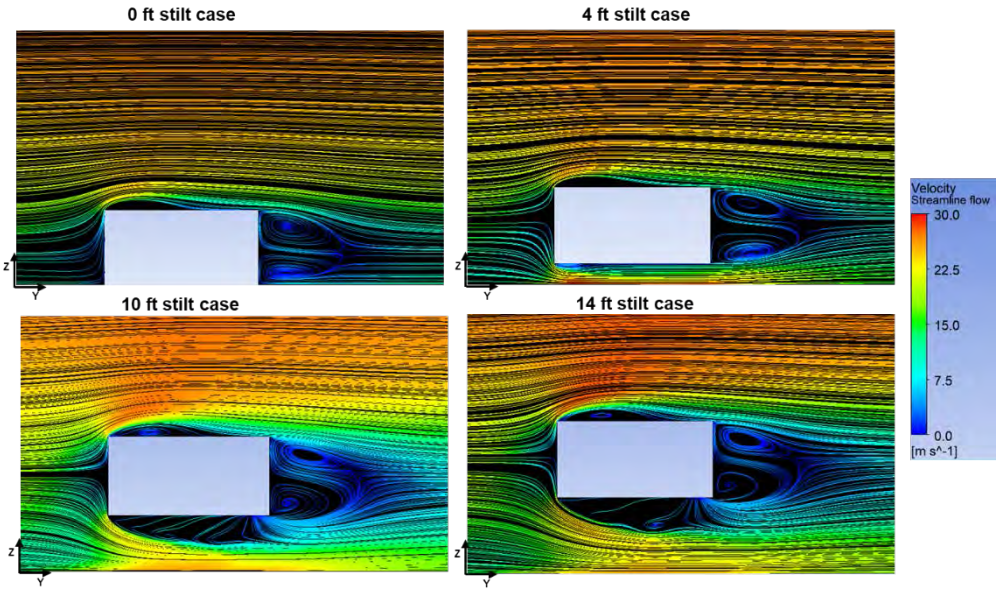

Figure 2-19 Air flow streamlines at the midsection of the computational domain for different stilt height under 0º wind direction

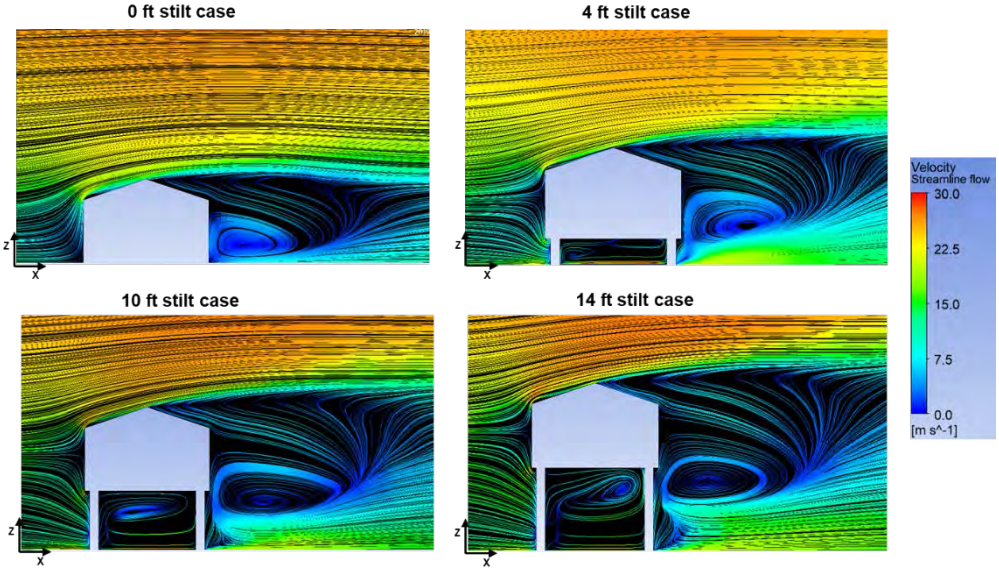

Figure 2-20 Air flow streamlines at the midsection of the computational domain for different stilt height under 90º wind direction

By increasing the house length, the vortex at the wake starts to increase and turned to be one instead of two. This affects the resulting suction on the leeward wall. Figure 2-21 shows that

the distance prior flow reattachment to the roof surface slightly increases as the aspect ratio increases. This increase is negligible as it didn't cause much difference in the high suction region as shown in figure 2-12. Below the model floor, for A=1, the flow reattached at the end of the floor surface (i.e. L=W). When A=1.5, the flow reattached at the middle (i.e. L=0.75W). So, as the aspect ratio increases the separation distance decreases.

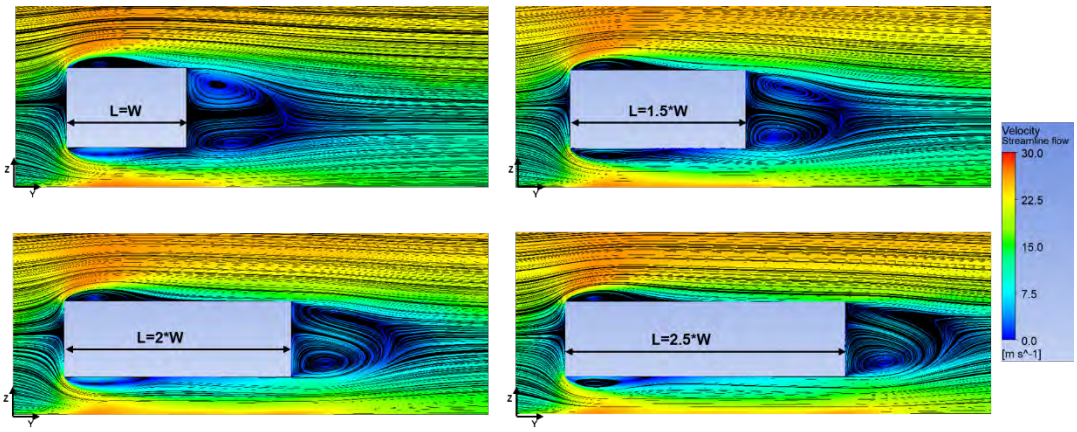

Figure 2-21 Air flow streamlines at the midsection of the computational domain for different aspect ratio under 0º wind direction

2.5 Investigating the effect of adding stairs to an elevated house using CFD

As mentioned in the introduction, a single-story elevated house with external stairs was simulated using CFD technique. The aim is to compare the resulting wind force with the same building but without attached stairs then check if the presence of external stairs affects the air flow and the resulting wind load. This numerical simulation was done on a full-scale 7 ft elevated house with the same dimensions, roof angle, and boundary conditions as the parametric study. The computational domain dimensions and the mesh size were considered based on the CFD model developed for the no-stairs case. However, the mesh size was reduced along the stairs due to the complicity of its geometry. The same solver setting was used in this simulation as well. Figure 3-1 shows the model configuration which was simulated and tested at three wind directions; 0º, 45º, and 90º.

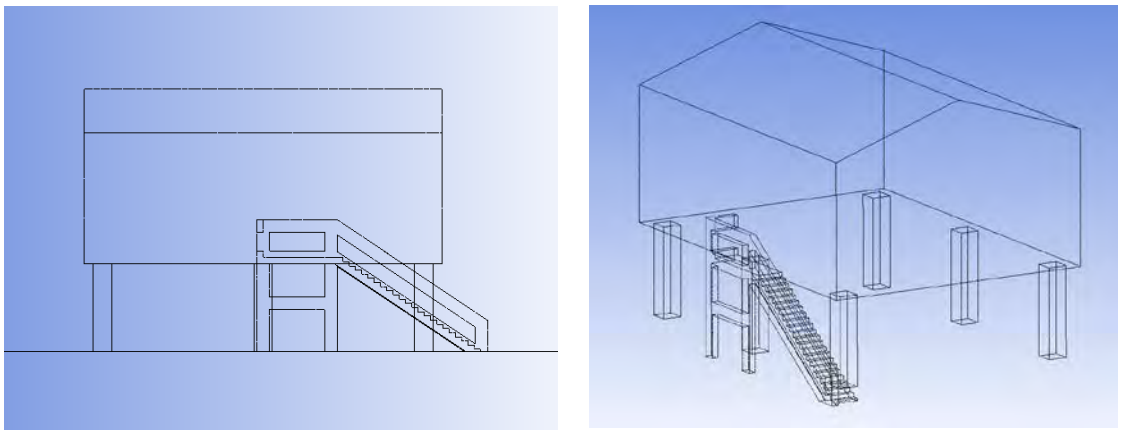

Figure 3-1 Gable roof house drawing elevated by 7 ft with stairs

2.5.1 Simulation Results

a- Contour plots of the mean pressure coefficient

As shown in Figure 3-2, there are some deviation of the mean pressure coefficient distribution on the right figure due to the presence of the stairs. There is a slight reduction of the C_{pmean} in case of the house with stairs. This difference is noticeable only at the floor surface; the pressure coefficient is much lower especially at the leeward part. The same reduction can be seen in the other two wind cases in figures 3-3 and 3-4. Both roof and floor surfaces experiences lower negative pressure. These observations reveal that there is no need to add the stairs in the experimental studies as it does not cause a noticeable effect and it does not increase the wind loads on the house.

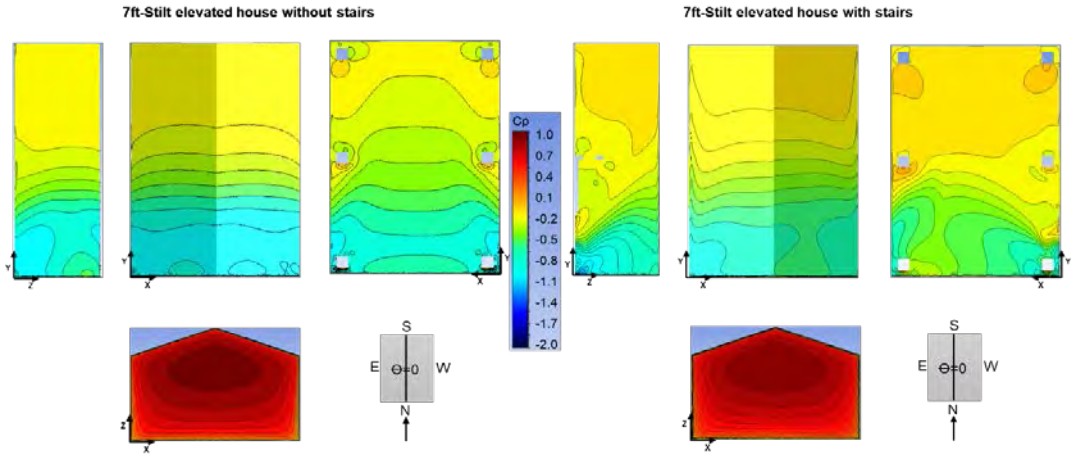

Figure 3-2 Mean pressure coefficient of single-story 7 ft elevated case with and without stairs under 0º wind direction

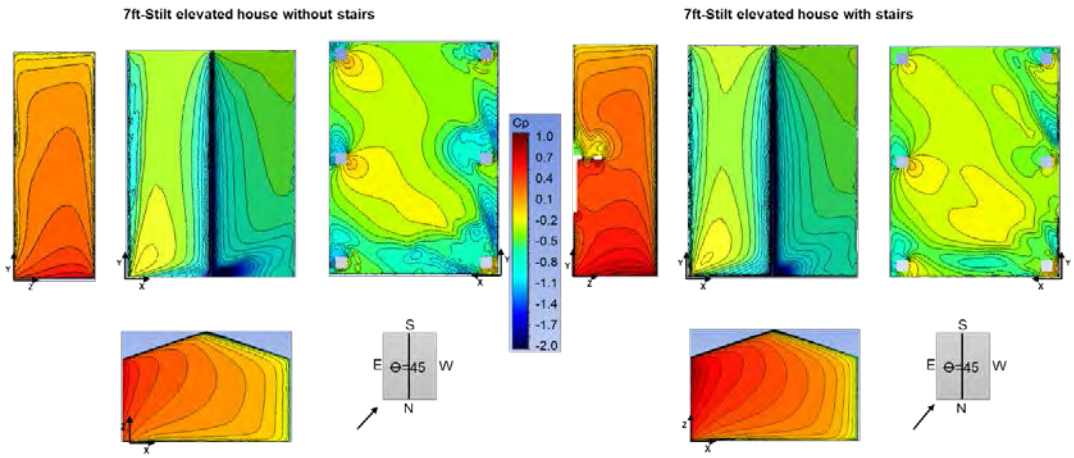

Figure 3-3 Mean pressure coefficient of single-story 7 ft elevated case with and without stairs under 45º wind direction

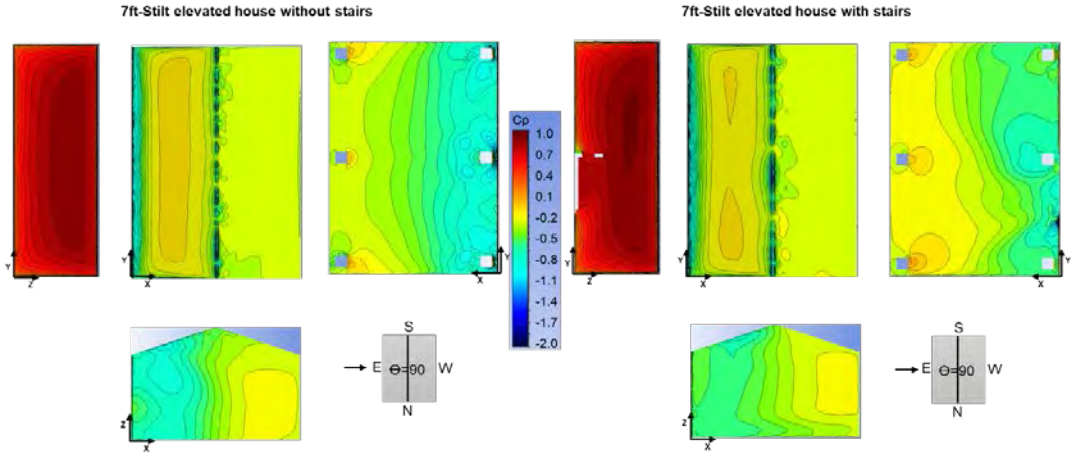

Figure 3-4 Mean pressure coefficient of single-story 7 ft elevated case with and without stairs under 90º wind direction

b- The effect of the building stairs on the average pressure coefficient

By comparing the average pressure coefficients (C_p), figure 3-5 shows that there is not much difference between the two cases. For 0º and 45º wind directions, after adding external stairs, the negative C_p value on the building roof and walls is lower by around 7% and 5% respectively. However, the positive C_p value is higher by 7%. The C_p reduction in the floor surface is considerable (35%) as concluded from the contour plots. Table 3-1 shows the wind force acting on the elevated house in case of adding or without stairs. It reveals that the total force acting on the elevated house (including wind load on the stairs) did not experience noticeable change. The force share of the stairs was 5%, 15%, and 13% for 0º, 45º, and 90º

respectively. These are considerable values that should be taken into account in the future design of stairs.

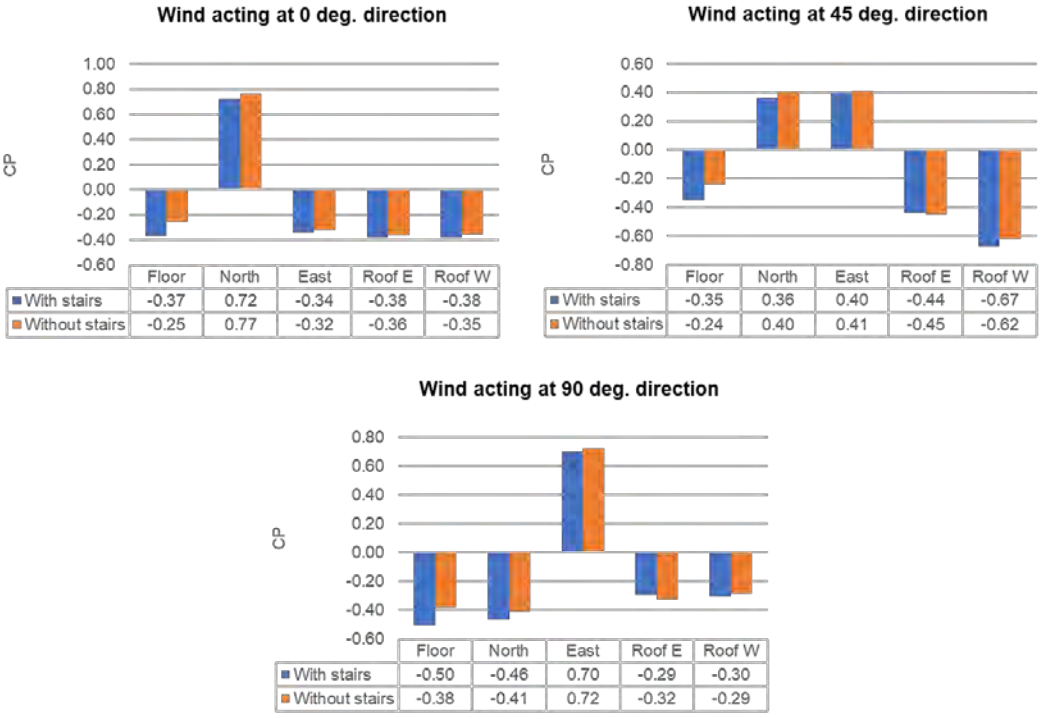

Figure 3-5 Mean pressure coefficient of each surface of single-story 7 ft elevated case without stairs vs with stairs

Table 3-1 Total force acting on elevated house and the external stairs

Wind direction	Global forces (Newton)											
	without stairs			with stairs								
				Model			Stairs			Total		
	Fx	Fy	Fz	Fx	Fy	Fz	Fx	Fy	Fz	Fx	Fy	Fz
0	-10	7855	368	51	7461	1761	353	392	-239	404	7853	1522
45	-9913	6712	3704	-8460	5920	4926	-1114	978	-2	-9574	6898	4925
90	-10250	37	-3297	-9055	-57	-1338	-1137	-51	3	-10192	-109	-1335

2.6 Summary and Discussion

The current project aimed to perform a parametric study using CFD on a full-scale (prototype) on-ground and elevated houses. RNG k-ε turbulent model was used to solve the current numerical simulation. First, a validation study was done to evaluate the data extracted from the CFD simulation using the experimental work results of the two-story case tested last year. Thereafter, the parametric study was conducted using the same boundary conditions and solver type to investigate the characteristics of wind flow surrounding the building for various geometrical configurations and to assess wind actions on elevated structures and their variations with the building stilt height and aspect ratio. The CFD study will enable the most critical configurations and geometrical range to be identified for future experimental studies.

The resulting local mean pressure coefficients were similar for different aspect ratios of the elevated house in case of wind acting parallel to the roof ridge. However, for 45º and 90º wind directions, the suction occurring in the roof surface and around the stilts in the floor surface was significantly higher for larger aspect ratio. After calculating the total forces acting on each surface, the mean positive wind force on windward walls was found to be increasing rapidly with increase of the stilt height or the aspect ratio. At oblique wind direction, the force ratio of the 17 ft stilt case windward wall reached to be triple its correspondent in the on-ground case. But side walls didn't experience a noticeable change. It was observed also that in the floor surface the main reason of the pressure coefficient increase with stilt height is the oblique wind flow which caused the high suction around the model stilts. The total shear force acting on the foundation showed a considerable increase as the stilt height increase. While the total vertical force dropped by elevating the house due to the presence of a new force on the floor. The overturning moment increased tremendously; 0º wind caused a 450% increase in the largest stilt case while 90º wind caused 800% increase. For larger aspect ratio, the overturning moment increased by 250 when A=2.5 and the vertical force increased by 350%. The flow streamlines inside the computational domain showed that the flow separation region increased as the stilt height increased. However, the flow separation region decreased by increasing the model aspect ratio. In the small stilt cases, the wind speed increased beneath the building floor due to venture effect through the airgap. A flow circulation of air took place between the two intermediate columns. This clarify the reason behind the high negative pressure around the model stilts. There was a slight reduction of the mean pressure coefficient in all surfaces of the

elevated house with stairs except for the floor surface which showed a considerable reduction of the wind pressure in case of adding stairs. The total force acting on the elevated house (including wind load on the stairs) did not experience a noticeable change. The force share of the stairs was large and should be considered in the future design work.

In conclusion future research should consider the following recommendations and instruction:
:

- Wind velocity beneath the house floor is higher in smaller stilt cases so it needs to be monitored as it leads to the occurrence of several damages.
- The observed increase in the mean pressure coefficient emphasis the need to study the effect of changing the building aspect ratio.
- The resulting increase of the shear forces and the overturning moments, due to stilt height increase, acting on the building foundations is significantly large and should be taken into consideration in the future design of elevated houses.
- The increase of the total vertical force, due to aspect ratio increase, acting on the foundations is noticeable and should be taken into consideration.
- The commonly used configuration of stairs did not cause noticeable effect on the resulting pressure and it can be excluded from experimental testing to reduce time and cost.

References

Alipour, A., Aly, A.M., Davis, B.M., Soto, M.G., Kijewski-Correa, T., Lenjani, A., Lichty, B., Miner, N., Roueche, D.B., Salman, A., Smith, D.J., Sutley, E., 2018. Hurricane Michael preliminary virtual assessment team (p-vat) report.

Artemis, 2019. Hurricane Michael loss creeps to $7.2bn, but 17,347 claims still open 1–2.

Blake, E.S., Zelinsky, D.A., 2018. National Hurricane Center Tropical Cyclone Report, Hurricane Harvey 1–77.

Blocken, B., Stathopoulos, T., Carmeliet, J., 2007. CFD simulation of the atmospheric boundary layer: wall function problems. Atmos. Environ. 41, 238–252. https://doi.org/10.1016/j.atmosenv.2006.08.019

Cangialosi, J.P., Latto, A.S., Berg, R., 2018. National Hurricane Center Tropical Cyclone Report: Huricane Irma. Natl. Huricane Cent. 1–111. https://doi.org/10.1097/TA.0000000000002006

Chaudhari, A., 2012. Large Eddy Simulation for Large Eddy Simulation for Atmospheric Boundary Layer (ABL). Presentation 24.

Choi, C.-K., Kwon, D.K., 1998. Wind tunnel blockage effects on aerodynamic behavior of bluff body. Wind Struct. An Int. J. 1, 351–364. https://doi.org/10.12989/was.1998.1.4.351

Chowdhury, A.G., Irwin, P., Azzi, Z., Sayyafi, E.A., 2017. Holistic Testing to Determine the Efficacy of a Retrofit Technique for Residential Buildings and Assessing the Aerodynamics of Elevated Home. https://doi.org/10.13140/RG.2.2.29597.82400

Elawady, A., Chowdhury, A.G., Abdelfatah, N., Erwin, J., 2019. Large-scale testing investigation to assess elevated houses aerodynamics.

FEMA, 2009. Recommended Residential Construction for Coastal Areas: Building on Strong and Safe Foundations. http://fema.gov/library/viewRecord.do?id=1853.

Franke, J., Hellsten, A., Schlünzen, H., Carissimo, B., 2007. Best Practice Guideline for the CFD Simulation of Flows in the Urban Environment. COST action 732, 51.

Gorlé, C., Beeck, J., Rambaud, P., 2009. RANS CFD modeling of particle dispersion behind a rectangular building in the atmospheric boundary layer. 5th Eur. African Conf. Wind Eng. EACWE 5, Proc.

Irwin, H.P.A.H., Cooper, K.R., Girard, R., 1979. Correction of distortion effects caused by tubing systems in measurements of fluctuating pressures. J. Wind Eng. Ind. Aerodyn. 5, 93–107. https://doi.org/https://doi.org/10.1016/0167-6105(79)90026-6

Jeong, U.Y., Koh, H.-M., Lee, H.S., 2002. Finite element formulation for the analysis of turbulent wind flow passing bluff structures using the RNG k−ε model. J. Wind Eng. Ind. Aerodyn. 90, 151–169. https://doi.org/https://doi.org/10.1016/S0167-6105(01)00190-8

Mochida, A., Tominaga, Y., Yoshie, R., 2006. AIJ Guideline for Practical Applications of CFD to Pedestriau Wind Environment around Buildings, in: The Fourth International Symposium on Computational Wind Egineering (CWE2006). pp. 533–536. https://doi.org/http://dx.doi.org/10.1016/j.jweia.2008.02.058

Murakami, S., 1998. Overview of turbulence models applied in CWE–1997. J. Wind Eng. Ind. Aerodyn. 74–76, 1–24. https://doi.org/https://doi.org/10.1016/S0167-6105(98)00004-X

Näslund, E., Hellström, P.M., Kral, J.G., 2001. The Gut and Food Intake: An Update for Surgeons, Journal of Gastrointestinal Surgery. https://doi.org/10.1016/S1091-255X(01)80095-0

Newmark, C., (RMS), 2019. Hurricane Dorian Insured Losses in Caribbean from Wind, Storm-Surge. https://insurancejournal.com/news/international/2019/09/10/539310.htm.

NOAA, 2018. National Oceanic and Atmospheric Administration, Office for Coastal Management.

NSF, 2019. The National Science Foundation (NSF), Network, and Structural Extreme Events Reconnaissance (StEER), Fulcrum App. https://web.fulcrumapp.com.

Pasch, R.J., Penny, A.B., Berg, R., 2019. National Hurricane Center Tropical Cyclone Report, Hurricane Maria 16–30.

Patel, R., Ramani, S., Murakami, S., Mochida, A., Hayashi, Y., Sakamoto, S., 2007.

Determination of Optimum Domain Size for 3D Numerical Simulation in ANSYS CFX. Int. J. Innov. Res. Sci. Eng. Technol. (An ISO Certif. Organ. 3297, 4671–4679. https://doi.org/10.15680/IJIRSET.2015.0406126

Richards, P.J., Hoxey, R.P., 1993. Appropriate boundary conditions for computational wind engineering models using the k-ϵ turbulence model. J. Wind Eng. Ind. Aerodyn. 46–47, 145–153. https://doi.org/https://doi.org/10.1016/0167-6105(93)90124-7

Salim, S.M., 2009. □Wall Y+ Strategy for Dealing with Wall-bouded Turbulent Flows II. https://doi.org/10.1.1.149.722

Soe, T.M., Khaing, S.Y., 2017. Comparison of Turbulence Models for Computational Fluid Dynamics Simulation of Wind Flow on Cluster of Buildings in Mandalay. Int. J. Sci. Res. Publ. 7, 337–350.

Tominaga, Y., Akabayashi, S., Kitahara, T., Arinami, Y., 2015. Air flow around isolated gable-roof buildings with different roof pitches: Wind tunnel experiments and CFD simulations. Build. Environ. 84, 204–213. https://doi.org/https://doi.org/10.1016/j.buildenv.2014.11.012

Appendix A

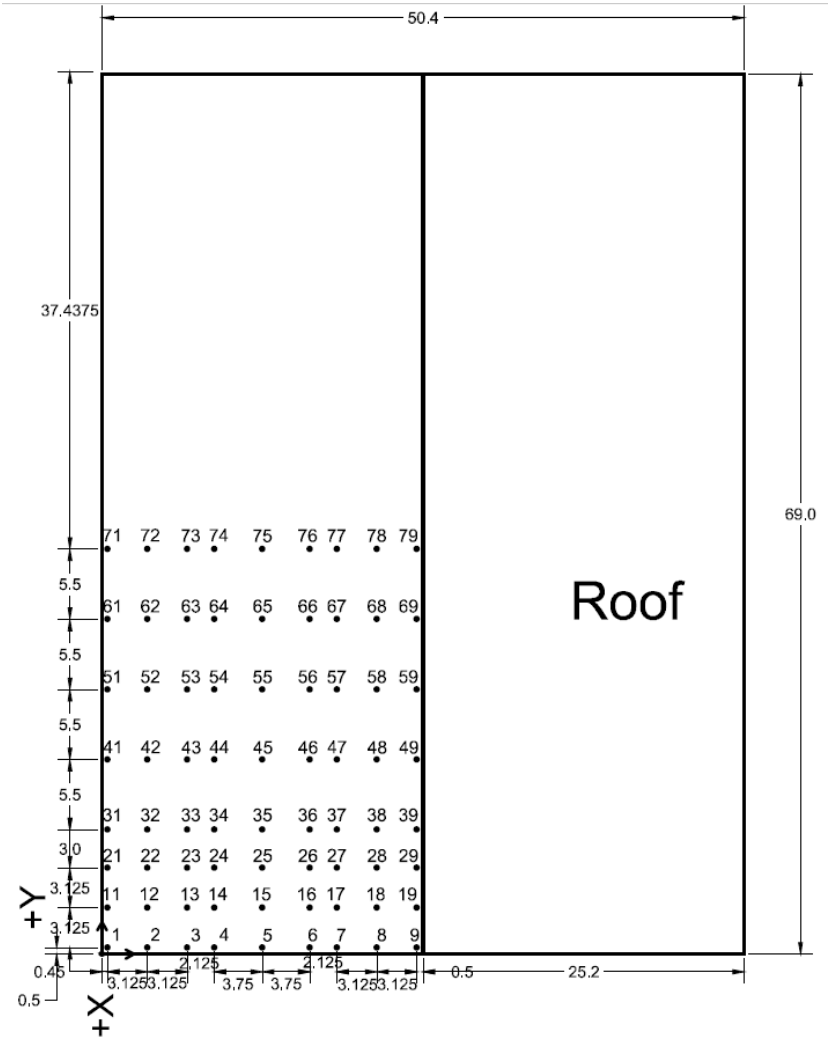

Figure A-1 Pressure Tap Layout on 1:5 Scale Model: Roof Surface

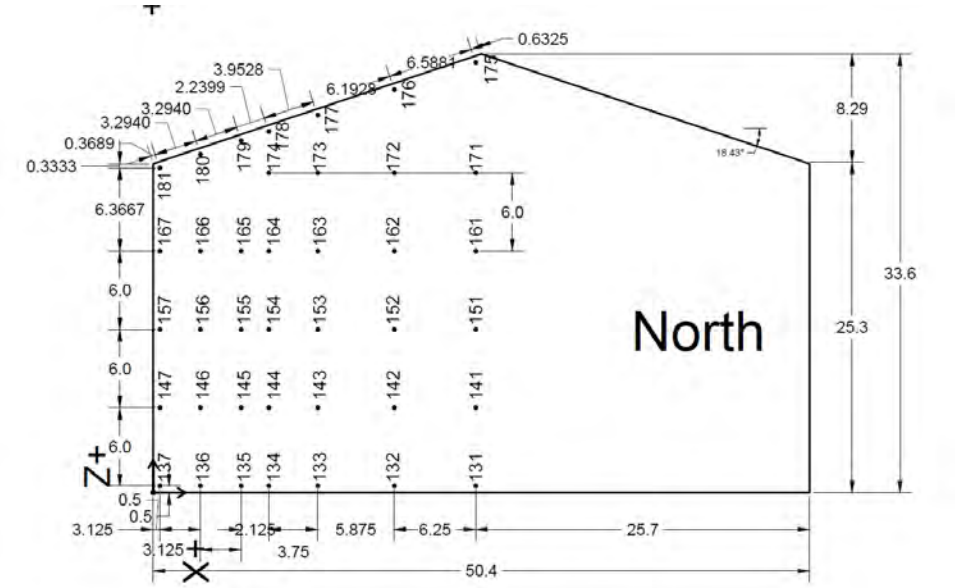

Figure A-2. Pressure Tap Layout on 1:5 Scale Model: North Wall

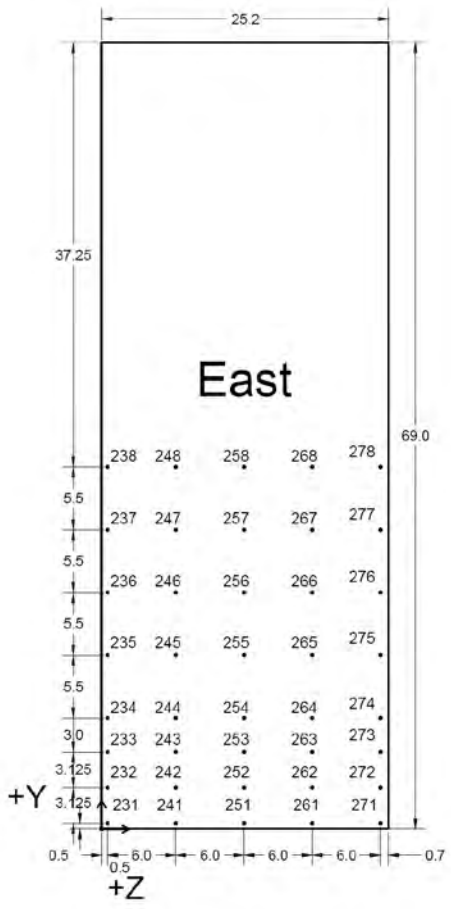

Figure A-3. Pressure Tap Layout on 1:5 Scale Model: East Wall

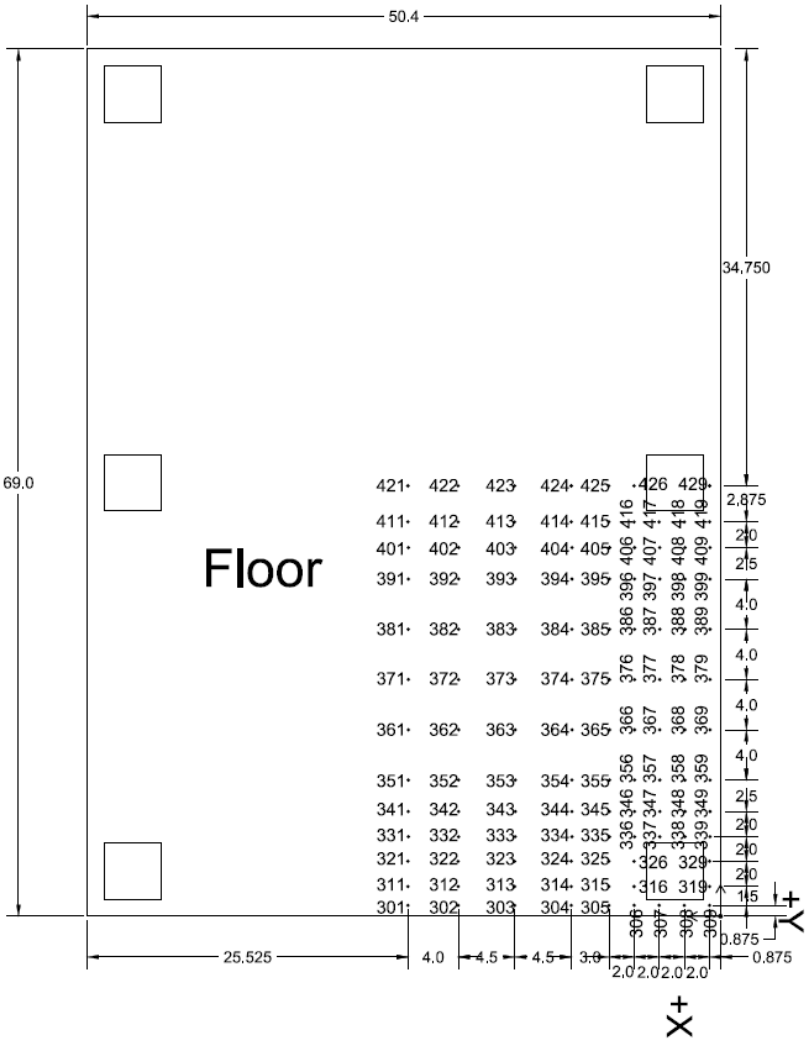

Figure A-4. Pressure Tap Layout on 1:5 Scale Model: Floor Surface

Appendix B

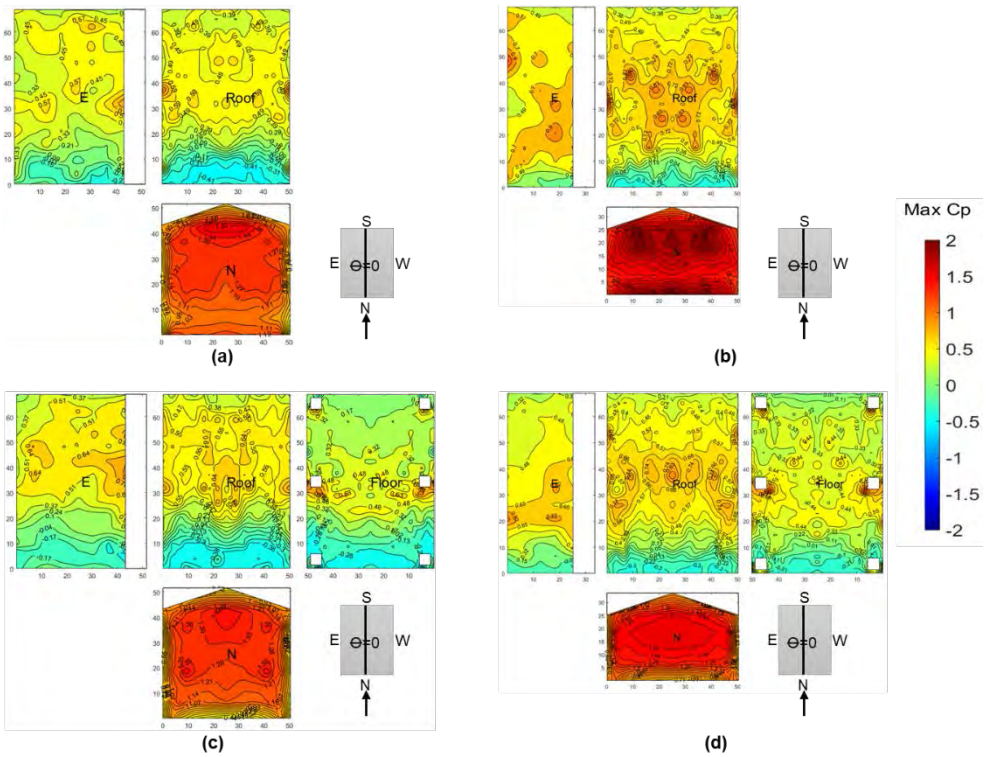

Figure B-1. Observed $C_{p\,max}$ for 0° wind angle (a) 1s-00.0in (b) 2s-00.0in (c) 1s-16.8in (d) 2s-16.8in

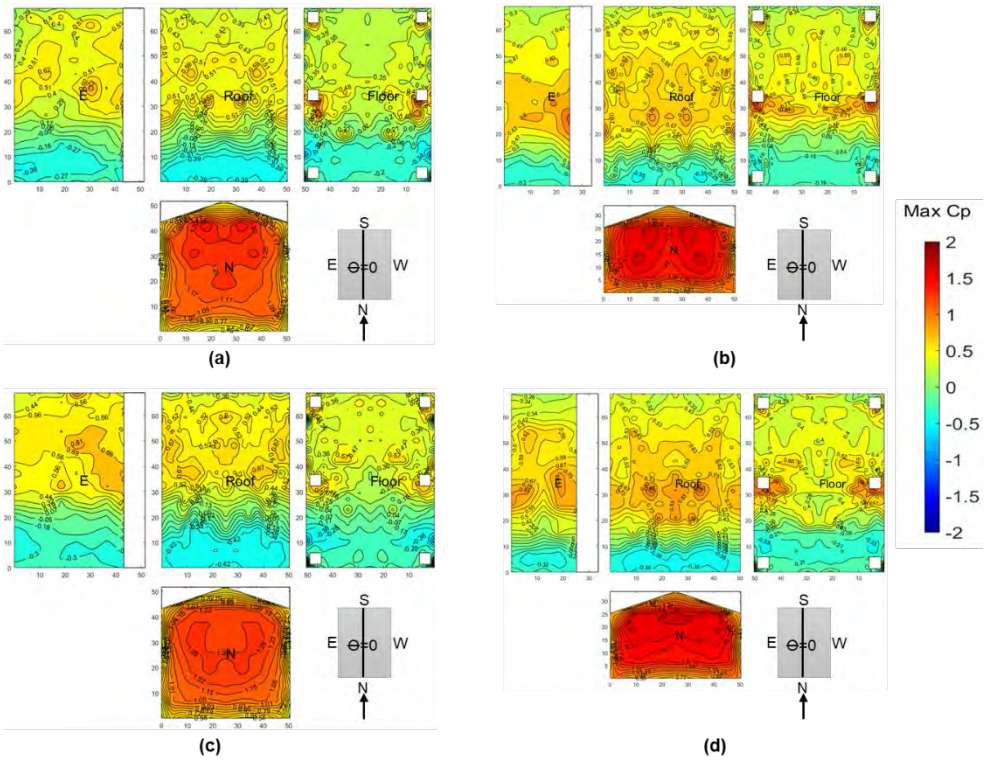

Figure B-2. Observed $C_{p\,max}$ for 0° wind angle (a) 2s-28.8in (b) 1s-28.8in (c) 2s-40.8in (d) 1s-40.8in

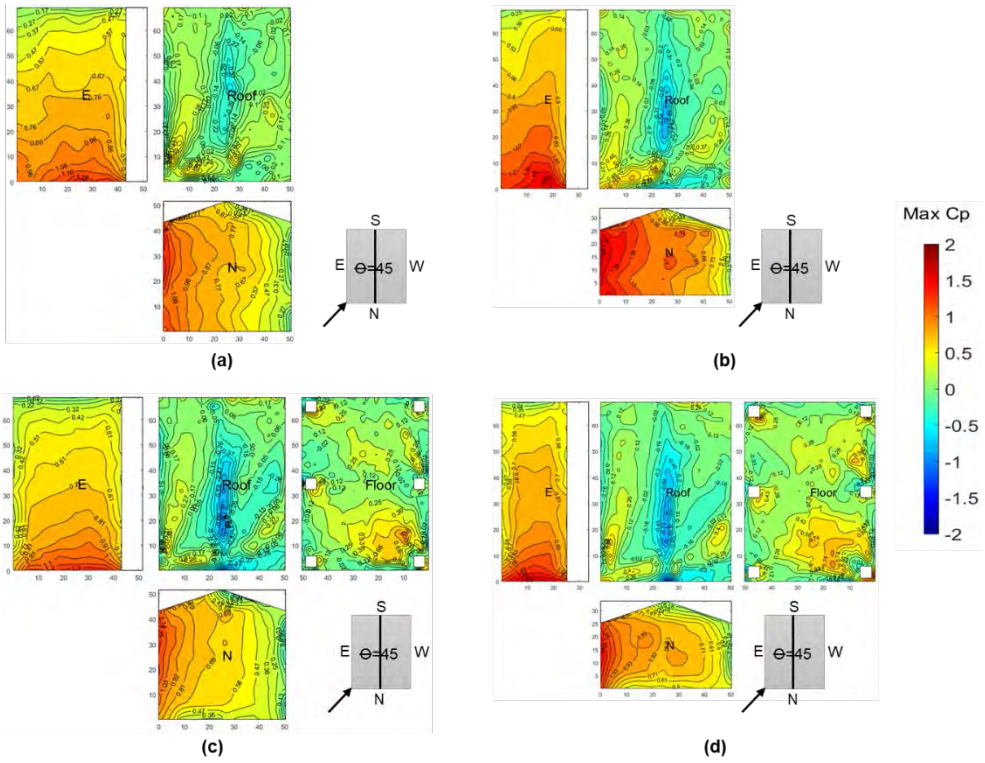

Figure B-3. Observed $C_{p\,max}$ for 45° wind angle (a) 2s-00.0in (b) 1s-00.0in (c) 2s-16.8in (d) 1s-16.8in

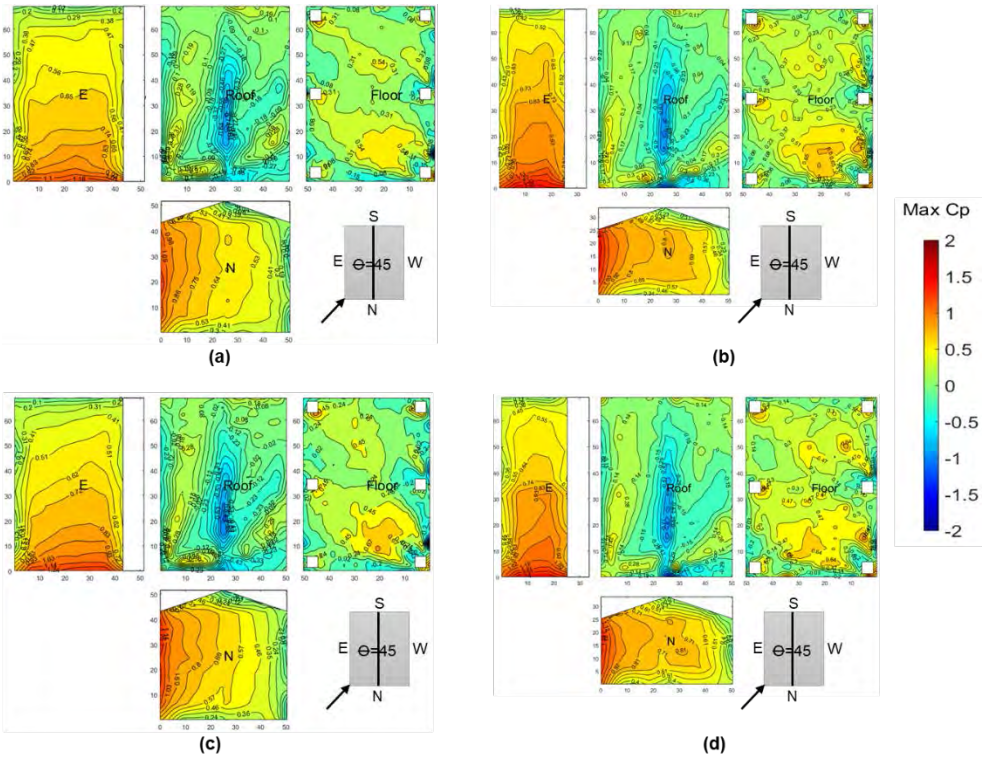

Figure B-4. Observed $C_{p\,max}$ for 45° wind angle (a) 2s-28.8in (b) 1s-28.8in (c) 2s-40.8in (d) 1s-40.8in

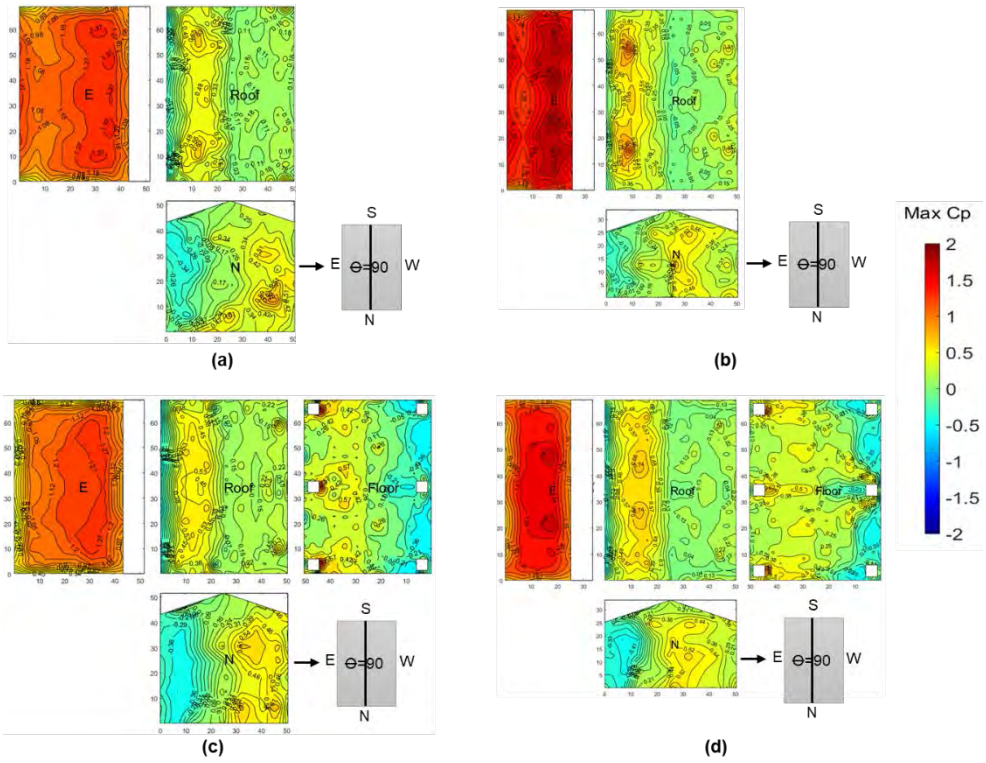

Figure B-5. Observed $C_{p\,max}$ for 90° wind angle (a) 1s-00.0in (b) 2s-00.0in (c) 1s-16.8in (d) 2s-16.8in

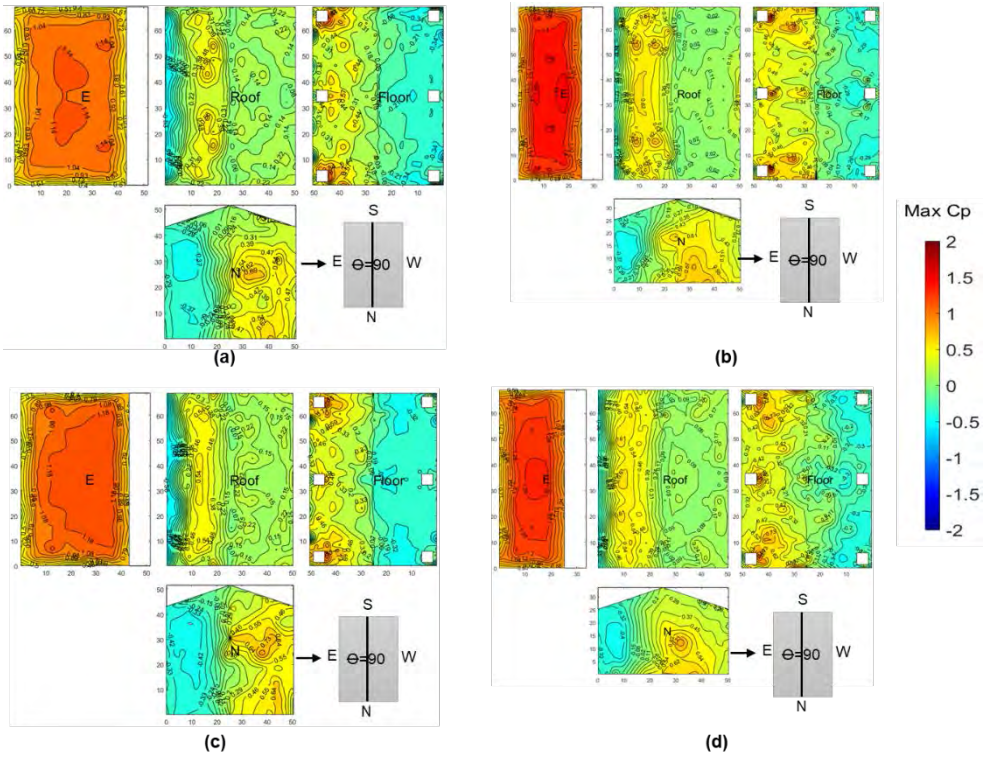

Figure B-6. Observed $C_{p\,max}$ for 90° wind angle (a) 2s-28.8in (b) 1s-28.8in (c) 2s-40.8in (d) 1s-40.8in

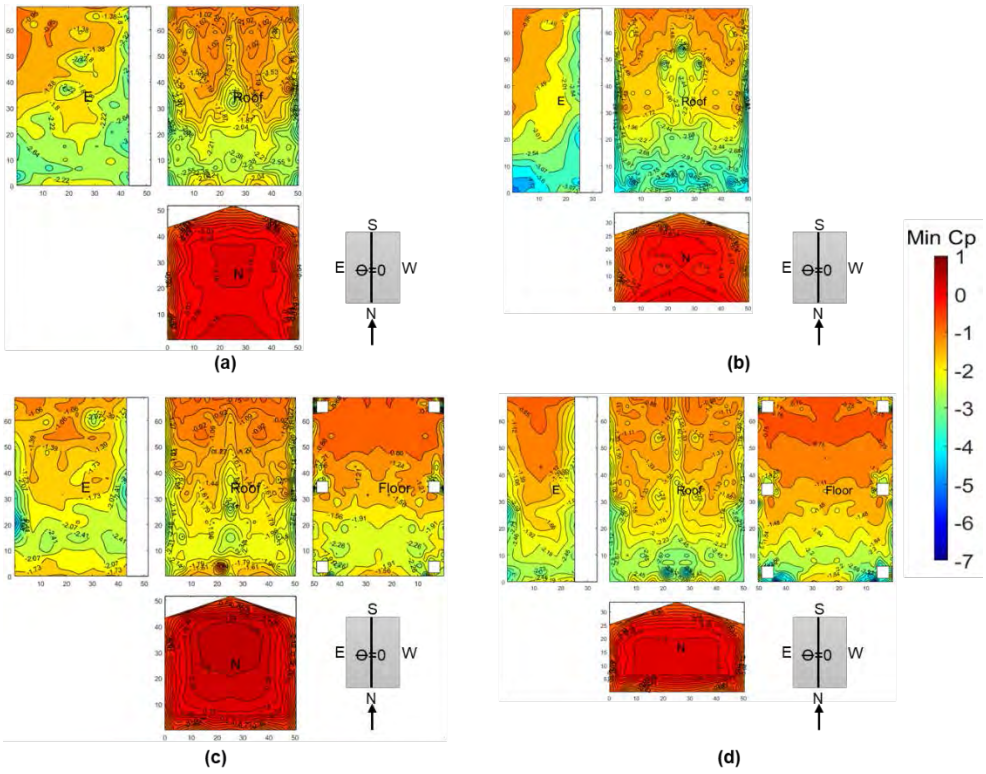

Figure B-7. Observed $C_{p\,min}$ for 0° wind angle (a) 2s-00.0in (b) 1s-00.0in (c) 2s-16.8in (d) 1s-16.8in

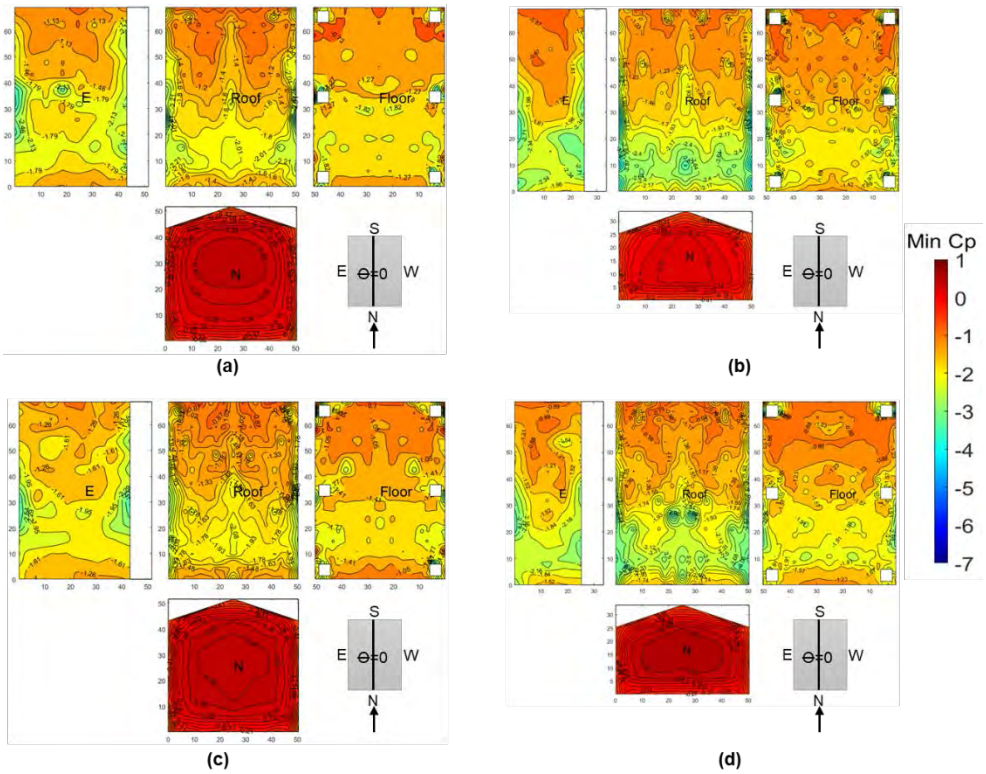

Figure B-8. Observed $C_{p\,min}$ for 0° wind angle (a) 2s-28.8in (b) 1s-28.8in (c) 2s-40.8in (d) 1s-40.8in

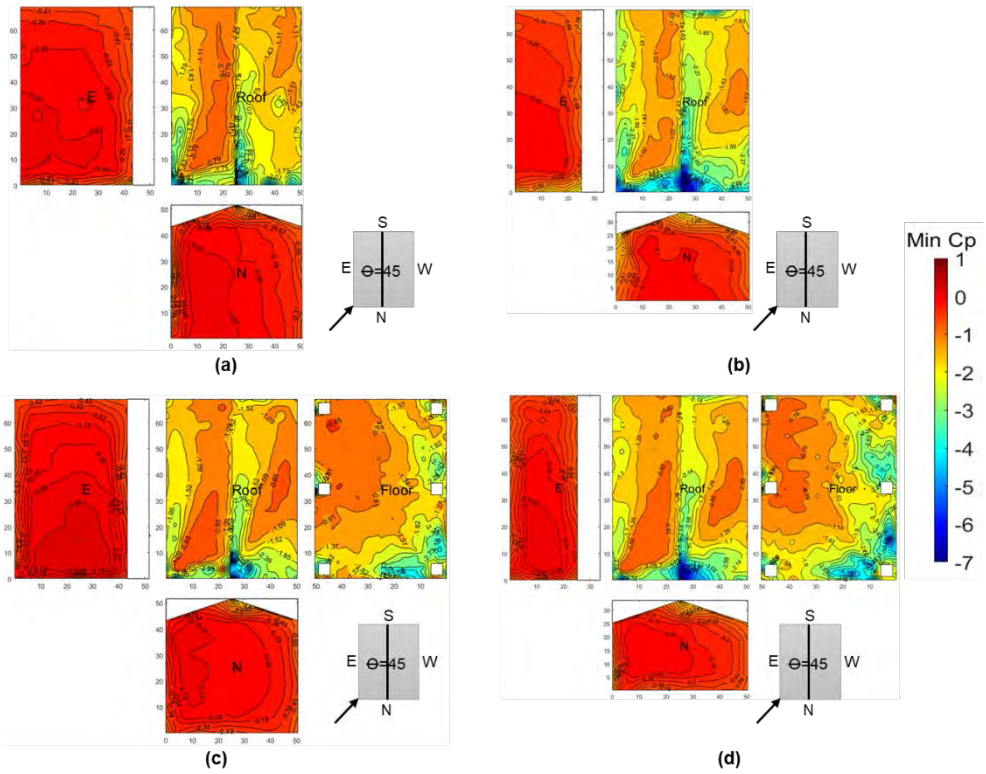

Figure B-9. Observed $C_{p\,min}$ for 45° wind angle (a) 2s-00.0in (b) 1s-00.0in (c) 2s-16.8in (d) 1s-16.8in

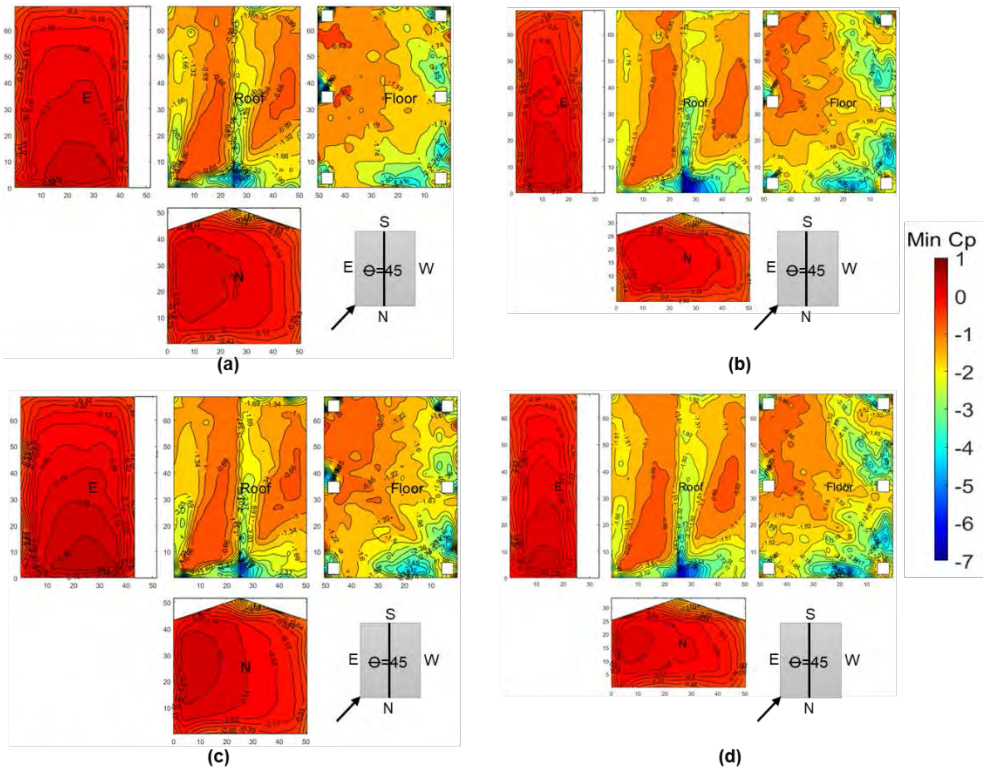

Figure B-10. Observed $C_{p\,min}$ for 45° wind angle (a) 2s-28.8in (b) 1s-28.8in (c) 2s-40.8in (d) 1s-40.8in

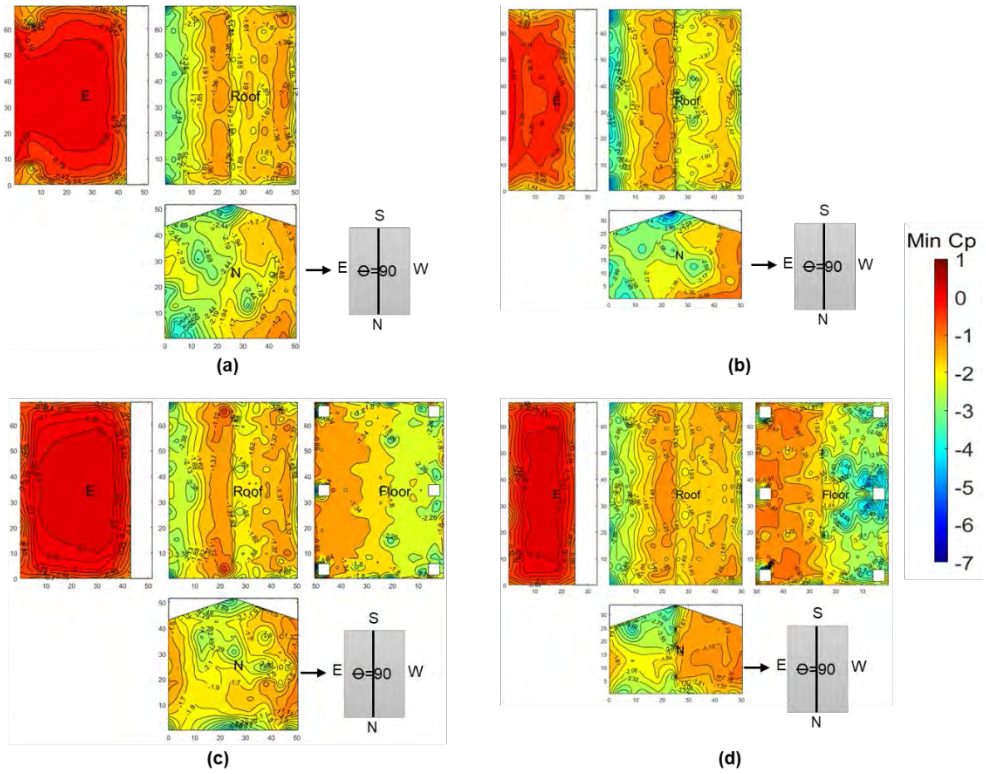

Figure B-11. Observed $C_{p\,min}$ for 90° wind angle (a) 2s-00.0in (b) 1s-00.0in (c) 2s-16.8in (d) 1s-16.8i

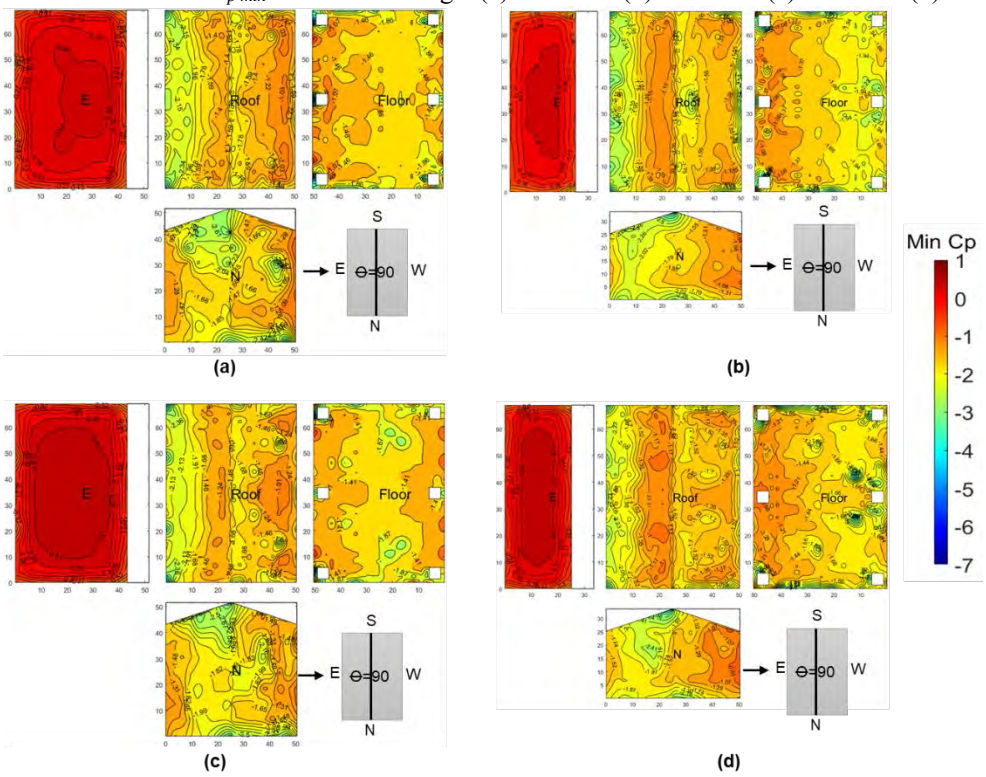

Figure B-12. Observed $C_{p\,min}$ for 90° wind angle (a) 2s-28.8in (b) 1s-28.8in (c) 2s-40.8in (d) 1s-40.8in

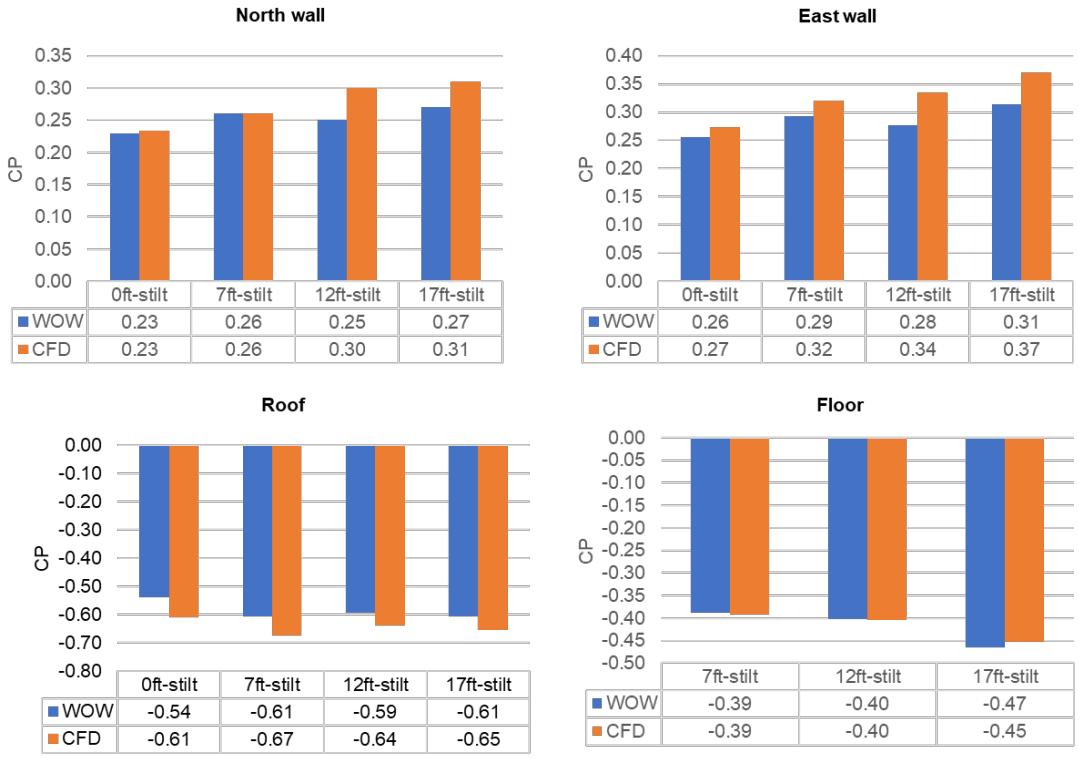

Figure B-13 Mean pressure coefficient of each surface of two-story 7 ft elevated case CFD vs WOW 45º wind direction

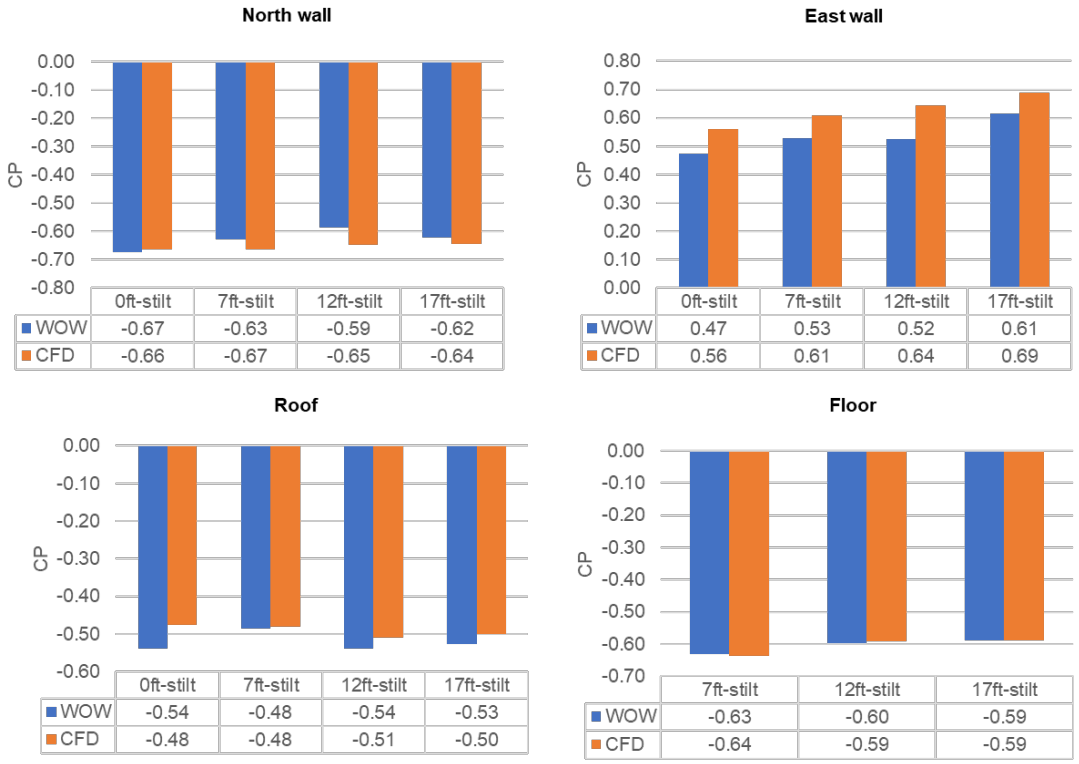

Figure B-14 Mean pressure coefficient of each surface of two-story 7 ft elevated case CFD vs WOW 90º wind direction

SECTION 4
WIND-INDUCED LOADS ON IRREGULAR SHAPED BUILDINGS WITH FLAT ROOF

A Report Submitted to:
The State of Florida Division of Emergency Management

Prepared by:
Principal Investigator:
Ioannis Zisis, PhD (izisis@fiu.edu)
Manuel A. Matus (mmatu016@fiu.edu)

Department of Civil and Environmental Engineering
Florida International University
In Partnership with
The International Hurricane Research Center (IHRC)
Florida International University

April 15, 2021

Executive Summary

Extreme wind events impact the United States on an annual basis. These events have been responsible for numerous fatalities and yearly loses of $34 billion dollars in the residential sector. Considerable research has been performed to mitigate the impact of such events, however, a significant portion of the investigations has been directed towards mid- and high-rise structures, while the effect of residential building shape on the overall pressure distributions has been somewhat overlooked. The current wind load provisions provide information on the design of residential structures; however, these provisions have been developed by results obtained from regular shaped studies in the late 70's and improved by several other field and wind tunnel studies since then. With the advancement of technology and building techniques, the shapes of the residential structures have become much more complex than rectangles and squares. This report presents findings on the wind-induced effect on residential buildings with irregular plans and flat roofs.

The first task of this investigation was to identify common irregular shapes that structures may take. This was done by taking multiple satellite images of residential areas and identifying the shapes that were more common. The next task was to construct and test the building models at the Wall of Wind Experimental Facility at FIU, to assess the effect of building shape on the overall pressure distribution. Four irregular shaped modes, (shapes T, L and C) were constructed and tested. In parallel with the above tasks, the team designed and constructed a small-scale Atmospheric Boundary Layer (ABL) Wind Tunnel (WT) that is to be used in the next set of tests (DEM 2020-2021 cycle). The findings include mean and peak pressure coefficient contour plots along with area averaging envelope curves that provide information for the preliminary comparison with the current wind standards. Overall, the findings indicate that there is an increase of the pressures/suctions experienced by structures with irregular plan shapes. This is especially true in internal corners where high suction zones appear to develop due to complex flow separation events.

Table of Content

Table of Figures

1. Introduction

Extreme wind events, such as hurricanes and tornadoes, are responsible for $34 billion dollars yearly worth in damages in the residential sector. These losses are expected to increase to $39 billion dollars by 2075 (UDO Commerce 2010, CBO 2019). The significant losses due to natural hazards show the necessity to do more studies on the response and/or performance of residential structures under extreme wind events. With the current advancements in technology and construction techniques, the shapes of structures in today's-built environment have become far more complex than the typical square or rectangular floor plans. In fact, there have been several studies to assess the performance of irregular shaped structures in both wind tunnel testing and numerical model studies (Shuai et al., 2019; Uematsu et al., 1999; Stathopoulos et al., 1993; Mashalkar et al., 2015; Gomez et al., 2005; Young et al., 2016; Souvik et al., 2014; Yi et al., 2016; Yi et al., 2017; Yi et al., 2020; Dong-Xue et al., 2017). Nevertheless, the great majority of these studies were focused on structures that range from mid- to high-rise heights and overlooked low-rise residential structures.

The current wind provisions (ASCE 7-16) provide design guidelines for structures of regular shapes that could be used, under engineering judgement, to design irregular-shaped buildings. However, these guidelines are based on wind tunnel testing performed in the late 70's and that was based on regular shaped models (Akins et al., 1977; Davenport et al., 1977 and Stathopoulos 1979). Today's construction methods demand for a more precise investigation of the effects of building shape on the pressure distribution to better understand the aerodynamics of such structures. This would allow to better understand and design low-rise residential structures with enhanced survivability and resiliency to reduce the losses produced by extreme wind events.

The research presented in this report adds to the work done under DEM's last funding period (2018-2019) and aims to better understand the effect of building shape in the overall pressure distribution. For this, attempts have been made to make use of artificial intelligence to identify the most common irregular shapes that low-rise residential structures can take by feeding an algorithm with thousands of satellite images containing identified and labeled building shapes (T, L, S, C, R, etc.) (Figure 1 to Figure 3). Based on the identified shapes, four scaled models were constructed to be tested at the Wall of Wind Experimental Facility (WOW-EF). A previous

investigation (DEM 2018-2019) focused on irregular shaped models with gable roofs and this report shows results of irregular shaped models with flat roofs.

Figure 1. South Florida Satellite Image from Residential Area

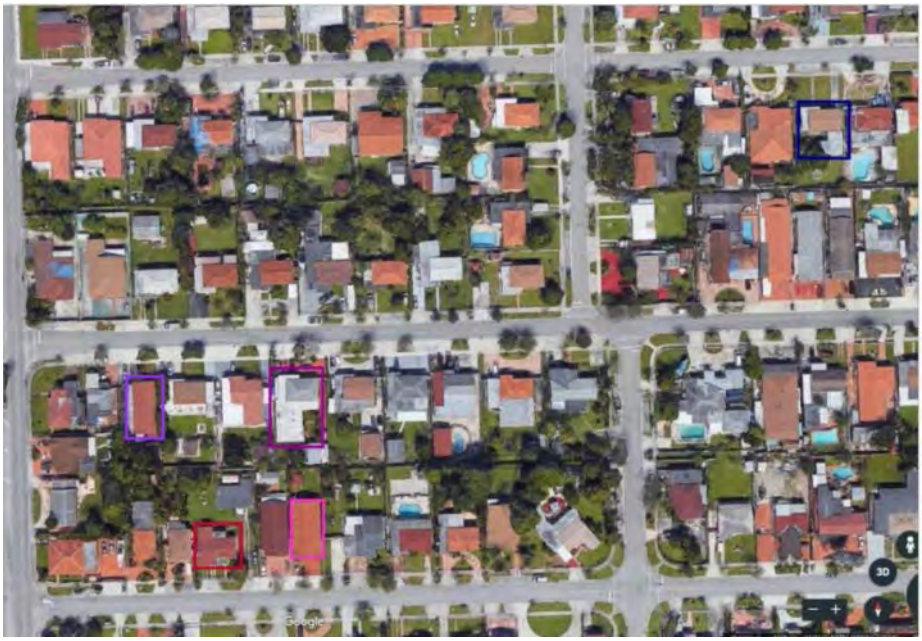

Figure 2. Satellite Image Shapes Identification

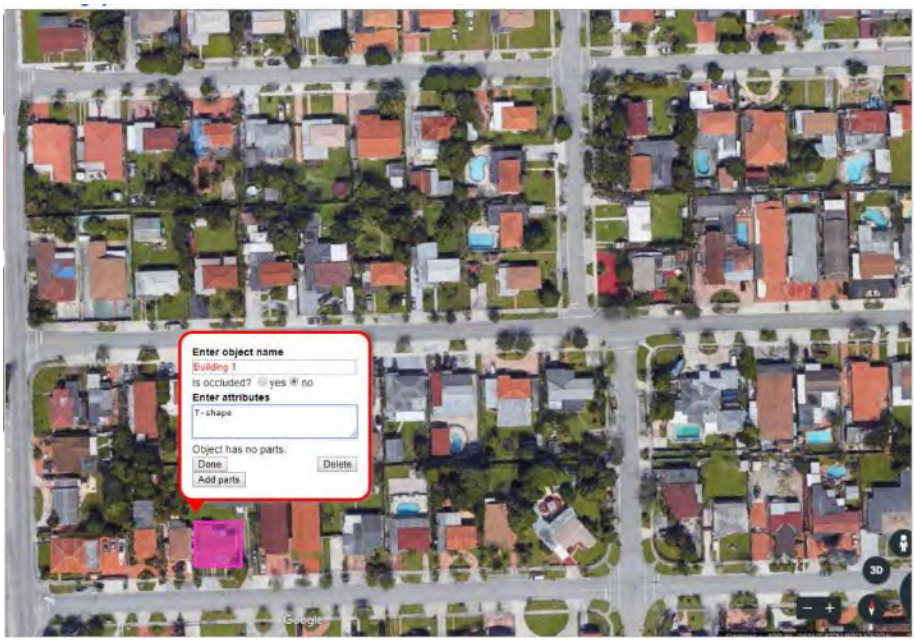

Figure 3. Satellite Image Shapes Labeling

2. Facility and Experimental Procedure

2.1. Large-scale Testing at the Wall of Wind Experimental Facility

The tests were carried out at the NSF NHERI Wall of Wind Experimental Facility (WOW-EF). This facility, located at Florida International University (FIU), is a full/large-scale facility capable of generating wind speeds of up to 157 mph (rated as category-5 on the Saffir-Simpson scale) thanks to the twelve 700-horsepower fans (Chowdhury et al., 2017, 2018). The flow management section can condition the flow by means of spires and automated roughness elements that allow for generating different exposures, or atmospheric boundary layer conditions, such as open and suburban terrains. A turntable, downwind of the flow management system, allows for models to be rotated during the test, see Figure 4. For this project, the spires and automated roughness elements were set to 60 degrees (Figure 5). Due to the scaling of the models, which was 1:50, the roughness was extended from the exit of the flow management box to the entirety of the turn table (Figure 6) to achieve the desired open terrain exposure.

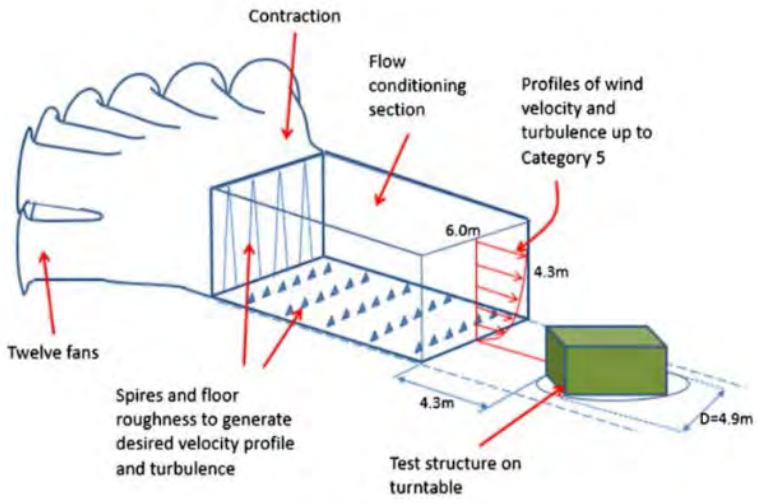

Figure 4. ABL Flow Conditioning Chamber (Chowdhury et al., 2017).

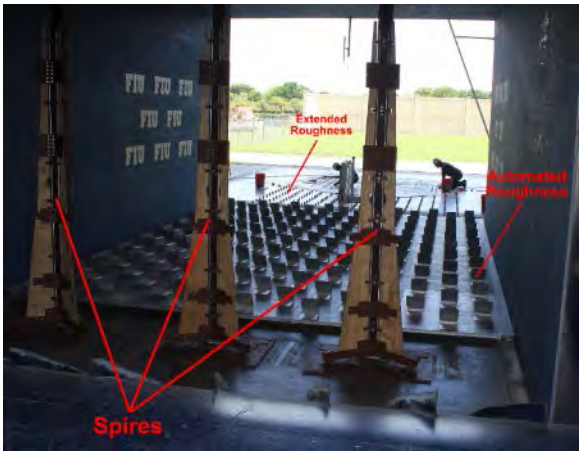

Figure 5. Roughness System.

Figure 6. Extended Roughness Elements.

2.2. Models Description

From aerial satellite imagery, it was observed that irregular shaped low-rise residential structures had T, L, C, S and H shapes, among others. In a previous study carried at the WOW-EF, seven models of T, L, U and Rectangular shapes were constructed. The seven, previously tested models, had gable roofs. For this project, the experiments were aimed to investigate the pressure distribution on irregular shaped models with flat roofs instead. For this, four of the seven models were constructed with flat roofs (See Figure 7 and Table 1). All models were made of 3/8" thick plexiglass and the sections and pressure-tap holes were laser-cut. The models were instrumented with pressure taps connected by means of two-foot-long urethane flexible tubing from the model walls and roof sections plus one-foot-long urethane flexible tubing from the connector side joined by a stainless steel tubulation linking tube (Figure 8).

The four models were tested to obtain pressure measurements at (520 Hz) by means of a Digital Service Module (DSM 4000) data acquisition system in combination with ZOC33/64Px pressure scanners and Thermal Control Units (TCU) and a transfer function was applied to the raw data to compensate for the distortion caused by the length of the tubing (Irwin et al., 1979).

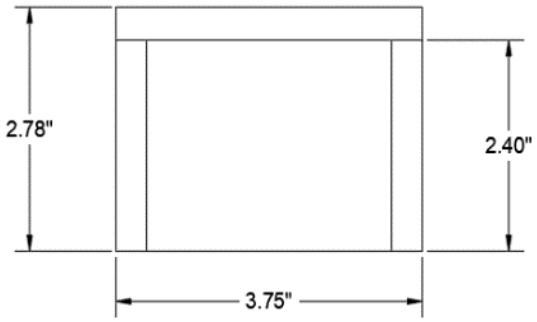

Figure 7. Models Elevation (model-scale dimensions).

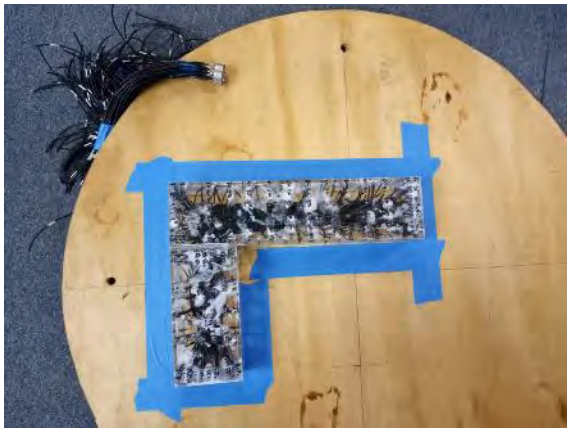

Figure 8. Pneumatic Connector Attached to Model L.

Table 1. Flat Roof Models (model-scale dimensions).

Model	Top View with Dimensions
T1	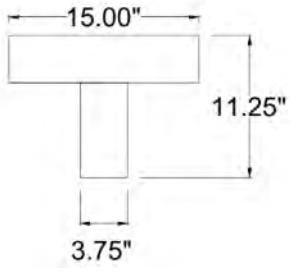
L2	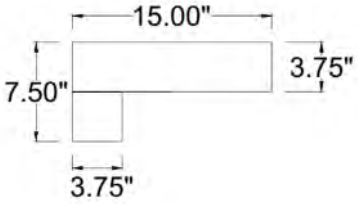
C1	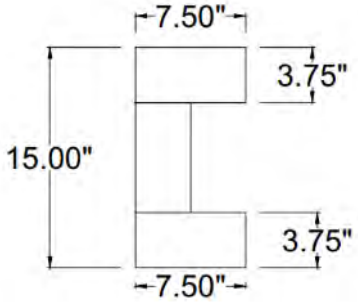

C2	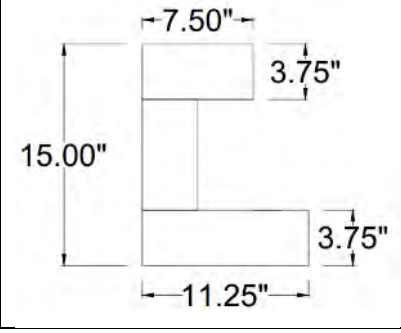

2.3. Flow Simulation

For this experiment, the Wall of Wind flow field was calibrated to generate an open terrain atmospheric boundary layer exposure. Previous wind speed measurements used Cobra Probes installed at heights of 1.75, 2.75 (Zref), 3, 4.5 and 6 inches to measure wind speed and turbulence intensity profiles. The results were compared against Engineering Science Data Unit (ESDU) profiles and provided a good match for heights at the roof level (Z/Zref = 1), see Figure 9 and Figure 10. A power spectrum density profile was obtained to check that the exposure configuration was able to simulate the entire wind turbulence domain in the low-frequency and high-frequency range (Figure 11).

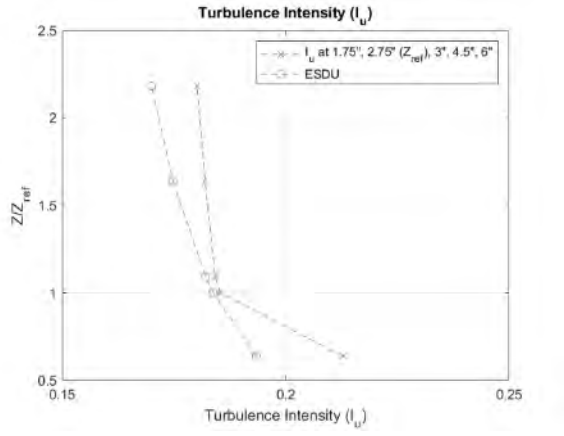

Figure 9. Turbulence Intensity Profile.

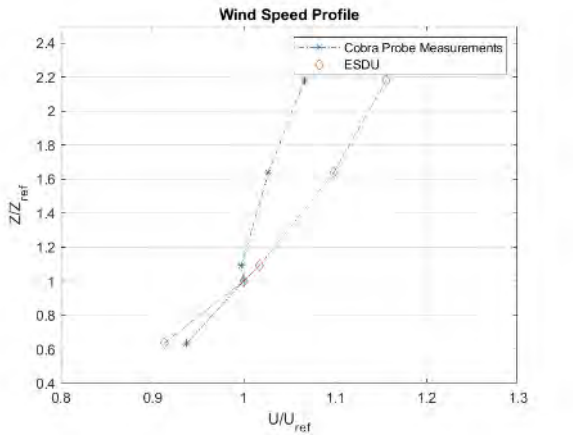

Figure 10. Wind Speed Profile.

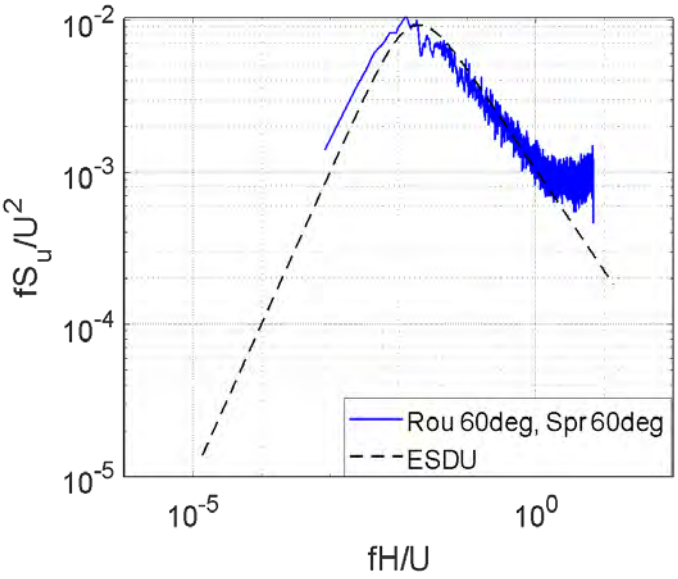

Figure 11. Power Spectrum Density.

2.4. Test Protocol

The models were tested at wind speed of 30 mph and at wind directions ranging from 0 to 345 degrees at 15 degrees increments (Figure 12). The sampling time and frequency for the data acquisition were 60 seconds per wind angle of attack and 520 Hz (for the recording of pressures), respectively.

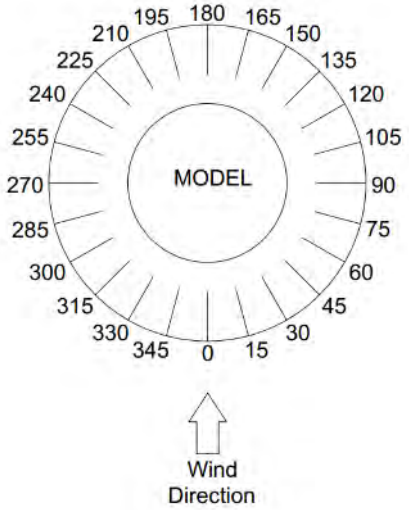

Figure 12. Wind Angles of Attack.

3. Results

The mean and peak pressure coefficients (C_P) are presented in this section. Pressure coefficients (C_P) are dimensionless values obtained from pressure sensors located in the models reading the pressures in multiple locations of the models surfaces (roof, walls, etc.) and describe the relative pressures acting on the models surfaces. The formula used to obtain the fluctuating C_P values was:

$$C_p = \frac{p - p_0}{\frac{1}{2}\rho V^2} \quad (1)$$

Where, $p - p_0$ is the pressure (obtained from the Scanivalve) readings and it is the pressure difference between the static pressure and the pressure read by the pressure taps. The dynamic pressure is $\frac{1}{2}\rho V^2$, where ρ is air-density and V is wind-speed. For simplicity, the units were manipulated to end up with a simpler equation that would require to input the pressure difference in $\frac{lb}{ft^2}$ and the wind speed in MPH. The formula for this is then:

$$C_p = \frac{p - p_0}{0.002556\, V^2} \quad (2)$$

The wind speed used as V is the wind speed obtained from wind speed measurements obtained from the cobra probe installed at mean roof height (that is 2.75" height). For the mean pressure coefficient, the mean wind speed was used, for what the formula would then become:

$$C_{p,mean} = \frac{p - p_0}{0.002556 V_{mean}^2} \quad (3)$$

The 3-second peak pressure coefficients ($C_{p,3sec}$) were obtained using the Best Linear Unbiased Estimate (BLUE) extreme value analysis. This method estimates extreme values for negative and positive pressures applied to n epochs. Extremes were estimated for probabilities of non-exceedance P1, which was set to 80%, while n was set to 100 (Cook, 1985), it must be noted that Adam Pintar extended n from 17-24 to 100 in 2016.

3.1. Mean Pressure Coefficients

Mean pressure coefficients are shown in this section by means of contour plots. It must be noted that only wind directions result for 0, 45, 90, 135, 180, 225, 270, 315 degrees are shown. (see Figure 10 for wind direction notation). Overall, it can be observed that the edges of the roofs experienced high suction at the edges facing the wind. The walls, when oriented along the flow of the wind, underwent suction at the edge that is facing the wind due to the separation of the flow. Also, the walls that faced the wind perpendicularly, underwent positive pressures and there was a concentration of positive pressures at the model sections joint.

3.1.1. Model T1

Figure 13 to Figure 20 show mean pressure coefficient contour plots for model T1.

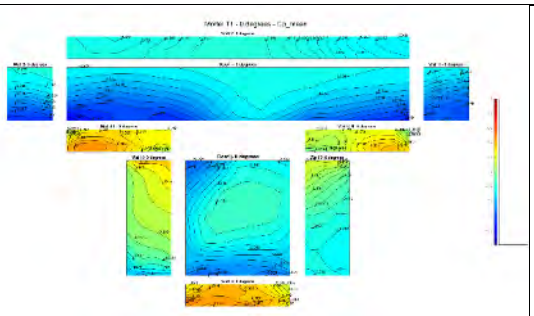

Figure 13. Mean Cp 0 degrees T1.

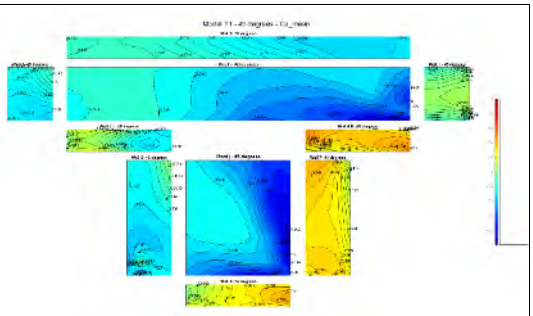

Figure 14. Mean Cp 45 degrees T1.

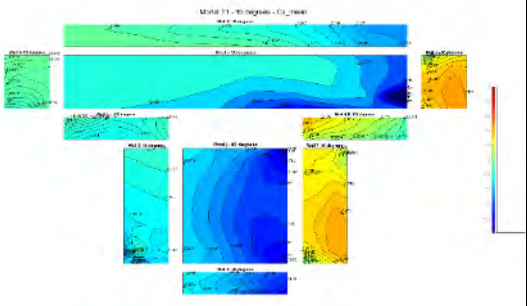

Figure 15. Mean Cp 90 degrees T1.

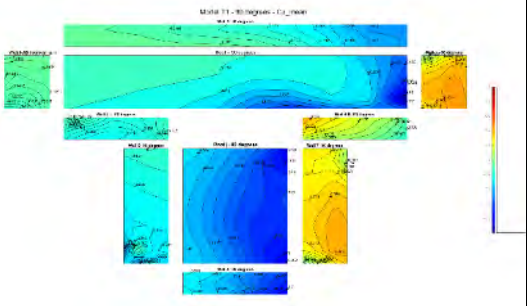

Figure 16. Mean Cp 135 degrees T1.

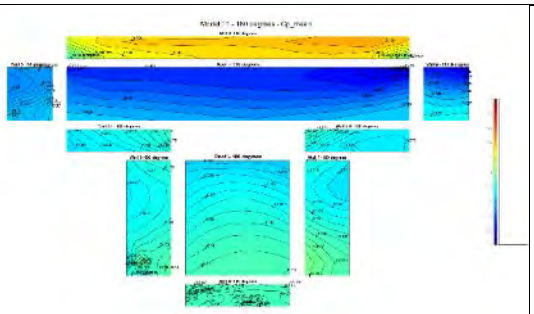

Figure 17. Mean Cp 180 degrees T1.

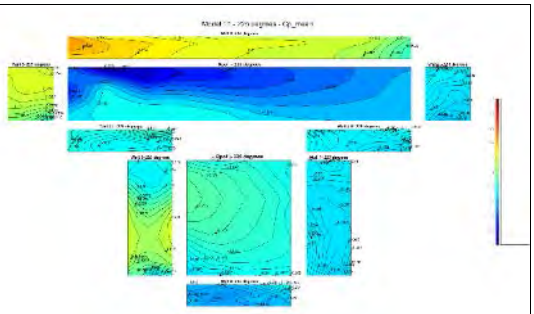

Figure 18. Mean Cp 225 degrees T1.

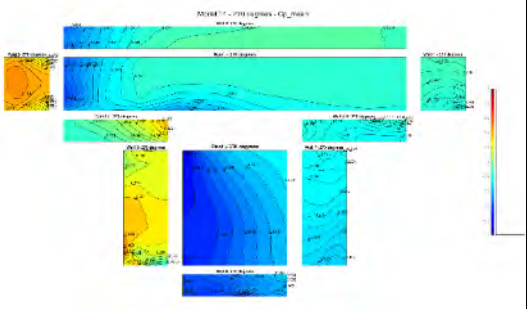

Figure 19. Mean Cp 270 degrees T1.

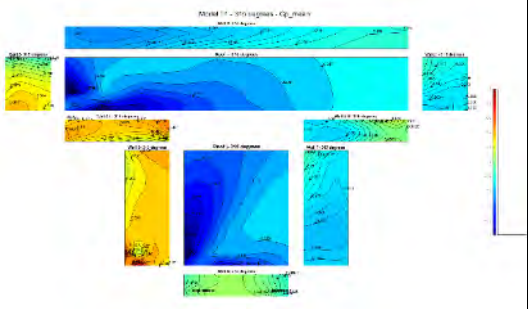

Figure 20. Mean Cp 315 degrees T1.

3.1.2. Model L1

Figure 21 to Figure 28 show mean pressure coefficient contour plots for model L1.

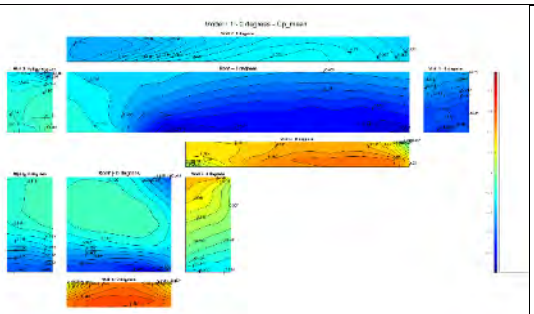

Figure 21. Mean Cp 0 degrees L1.

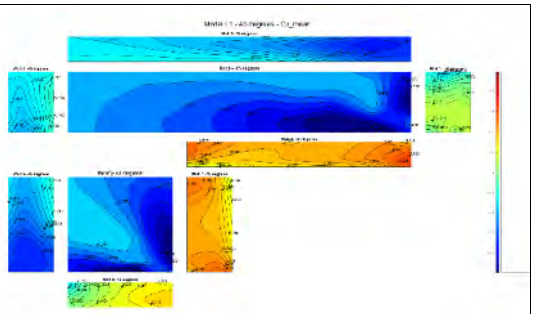

Figure 22. Mean Cp 45 degrees L1.

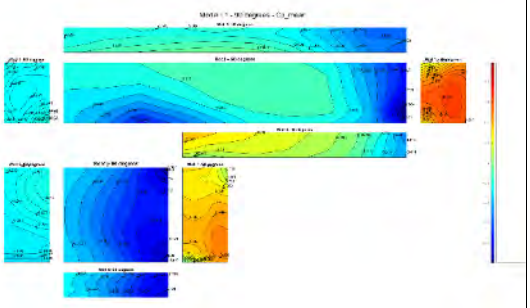

Figure 23. Mean Cp 90 degrees L1.

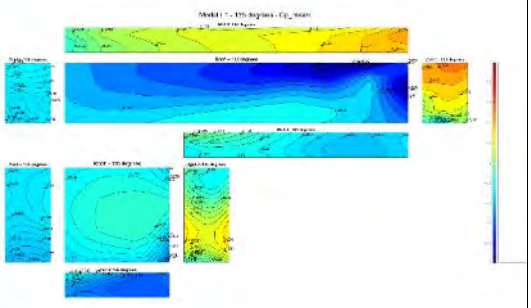

Figure 24. Mean Cp 135 degrees L1.

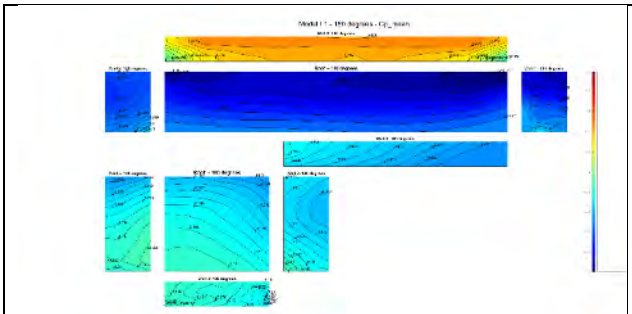

Figure 25. Mean Cp 180 degrees L1.

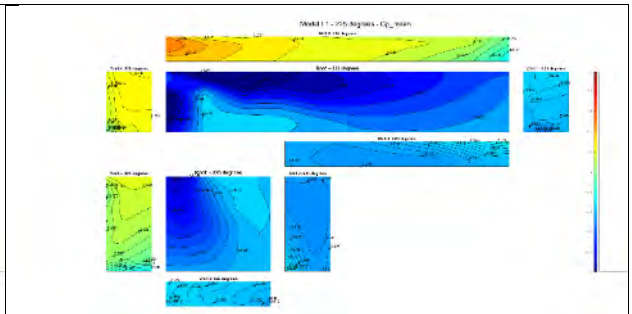

Figure 26. Mean Cp 225 degrees L1.

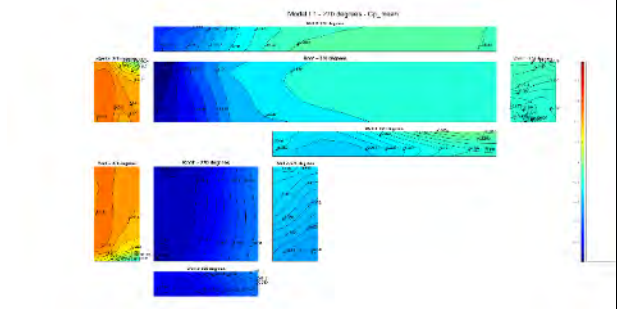

Figure 27. Mean Cp 270 degrees L1.

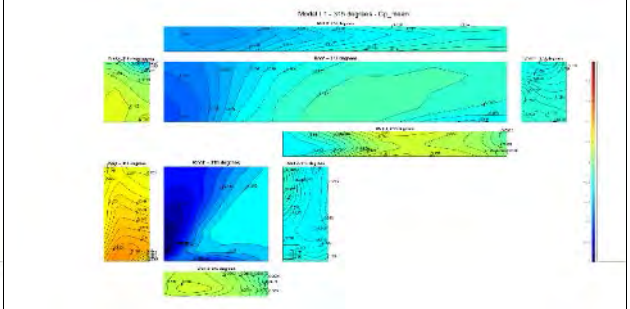

Figure 28. Mean Cp 315 degrees L1.

3.1.3. Model C1

Figure 29 to Figure 36 show mean pressure coefficient contour plots for model C1.

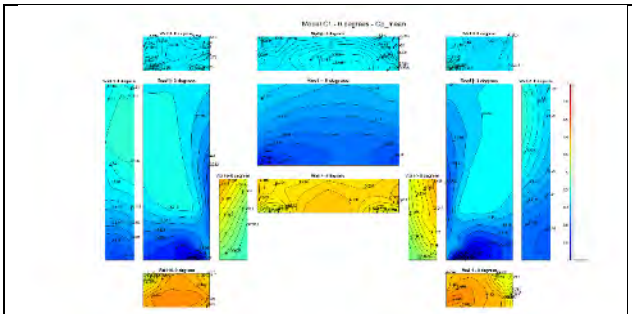

Figure 29. Mean Cp 0 degrees C1.

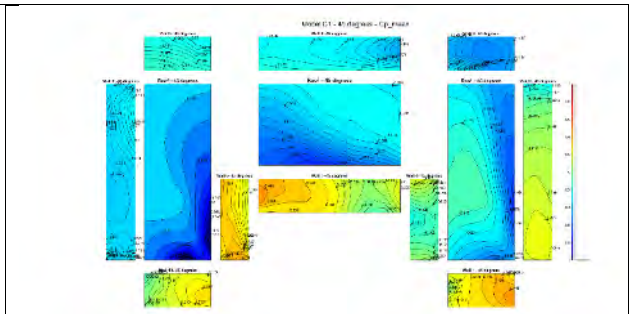

Figure 30. Mean Cp 45 degrees C1.

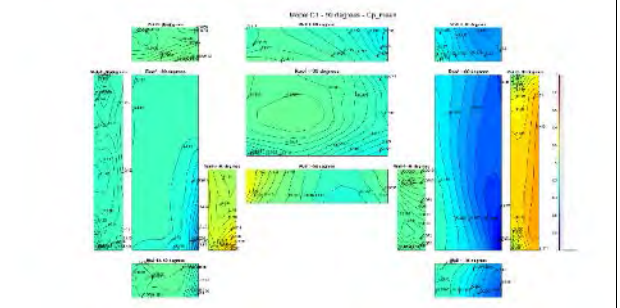

Figure 31. Mean Cp 90 degrees C1.

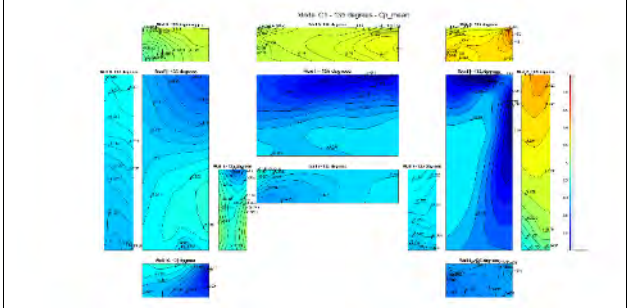

Figure 32. Mean Cp 135 degrees C1.

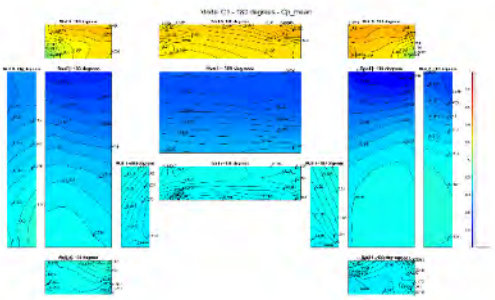

Figure 33. Mean Cp 180 degrees C1.

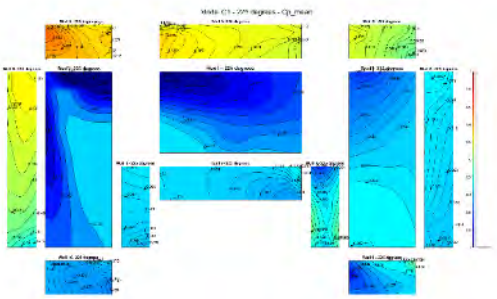

Figure 34. Mean Cp 225 degrees C1.

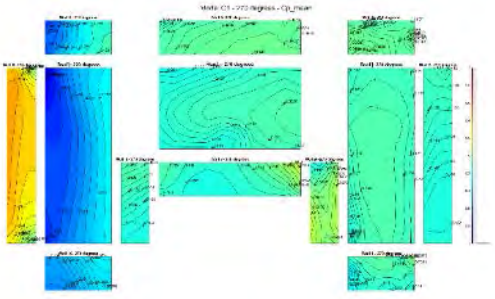

Figure 35. Mean Cp 270 degrees C1.

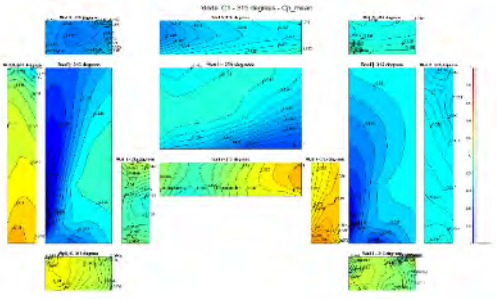

Figure 36. Mean Cp 315 degrees C1.

3.1.4. Model C2

Figure 37 to Figure 44 show mean pressure coefficient contour plots for model C2.

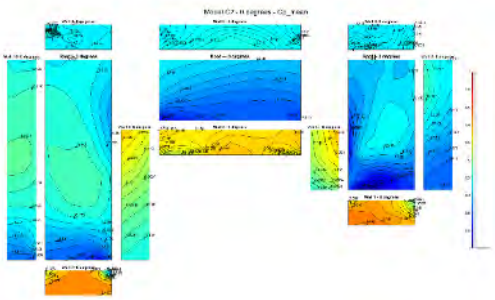

Figure 37. Mean Cp 0 degrees C2.

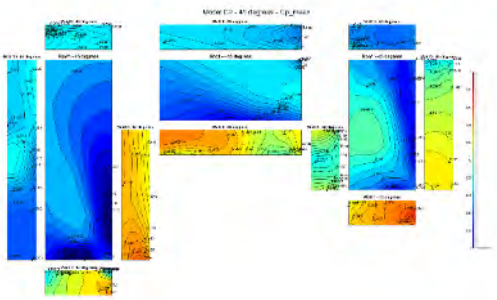

Figure 38. Mean Cp 45 degrees C2.

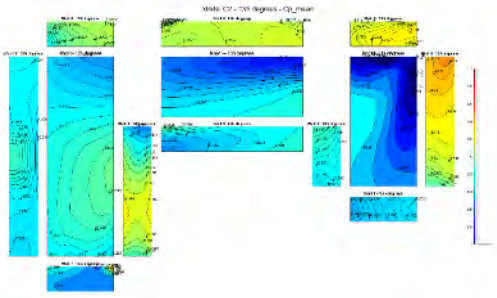

Figure 39. Mean Cp 90 degrees C2.

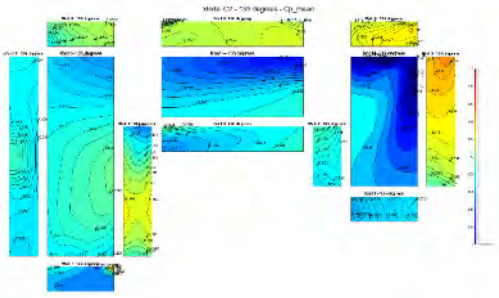

Figure 40. Mean Cp 135 degrees C2.

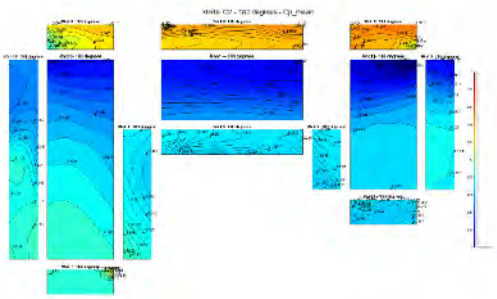

Figure 41. Mean Cp 180 degrees C2.

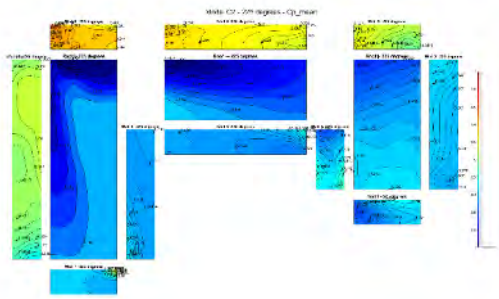

Figure 42. Mean Cp 225 degrees C2.

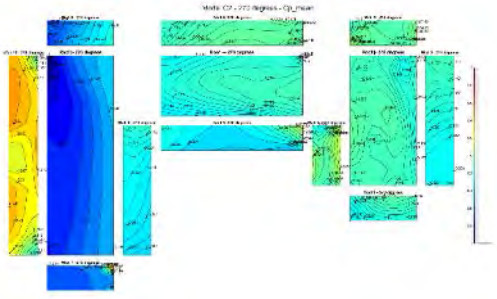

Figure 43. Mean Cp 270 degrees C2.

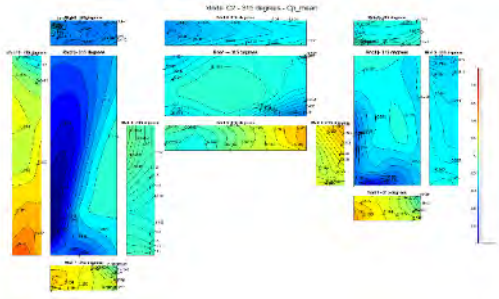

Figure 44. Mean Cp 315 degrees C2.

3.2. Peak Pressure Coefficients

The peak pressure coefficients (C_{Pmin} and C_{Pmax}) are presented in this section. It must be noted that these values were obtained by using the BLUE method analysis, developed by NIST (Ho et al., 2005). The maximum value of all wind direction of each pressure tap was identified along with the respective wind direction. A contour plot showing the highest peak pressure coefficients (of all wind directions) was created and the wind direction at which the peak pressure coefficient occurred is shown by an arrow/quiver (pointing in the corresponding wind direction).

3.2.1. Model T1

Minimum peak pressure coefficients for model T1 are shown in Figure 45. It can be observed that the highest suction areas are found in the edges of the roof as well as edges of the walls where the flow separates. Interestingly, the junction between the vertical and horizontal section of the model is a concentration for suction, reaching a minimum peak pressure coefficient

of -5.3 and the higher peak was found to develop at the edge of the roof reaching a value of -6.7. Maximum pressure coefficients are shown in Figure 46. The maximum peak pressure coefficients concentrate at the higher areas of the walls and range between 2.2 to 3.

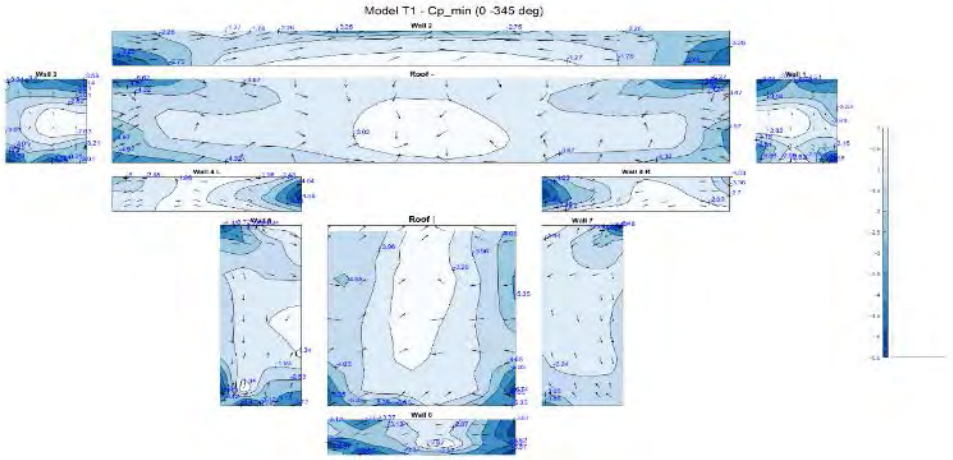

Figure 45. Minimum peak Cp T1.

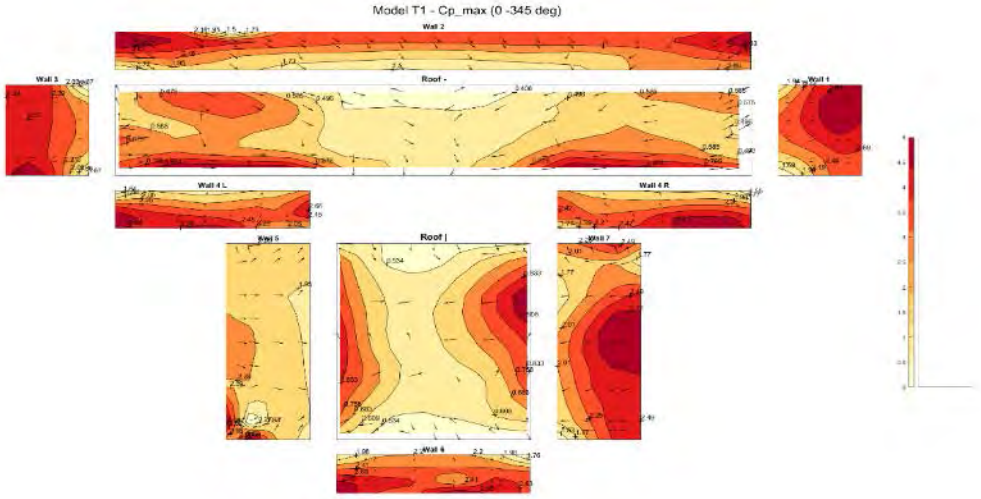

Figure 46. Maximum peak Cp T1.

3.2.2. Model L1

Minimum and maximum peak pressure coefficients for model L1 are shown in Figure 47 and Figure 48. From this figure, and like model T1 results, it was observed that there is a suction

concentration in the junction between the vertical and horizontal sections of the building, reaching a peak value of 4.72. The most susceptible areas of the model were the edges where flow separation occurs. For the maximum peak pressure coefficients, it can be observed that the wall sections, top parts, underwent higher pressure coefficients, reaching values as high as 3.2.

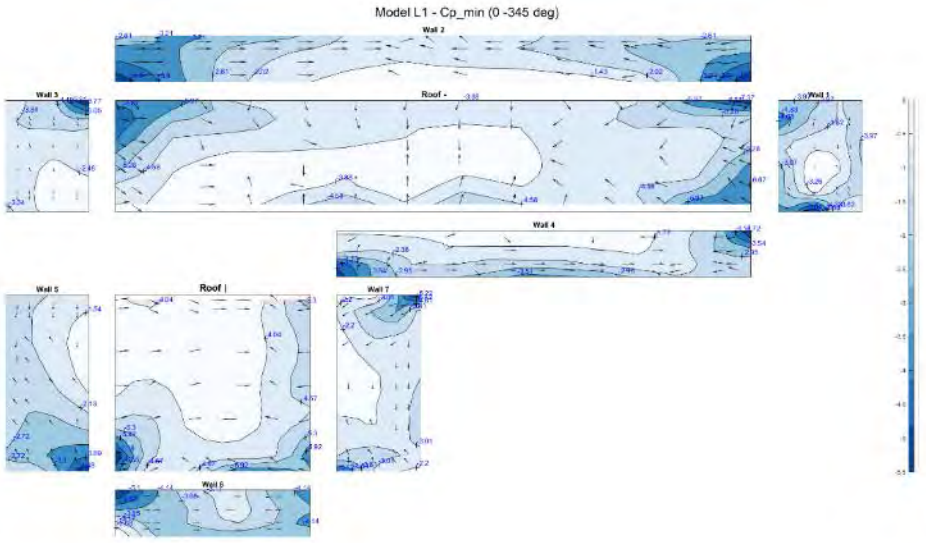

Figure 47. Minimum peak Cp L1.

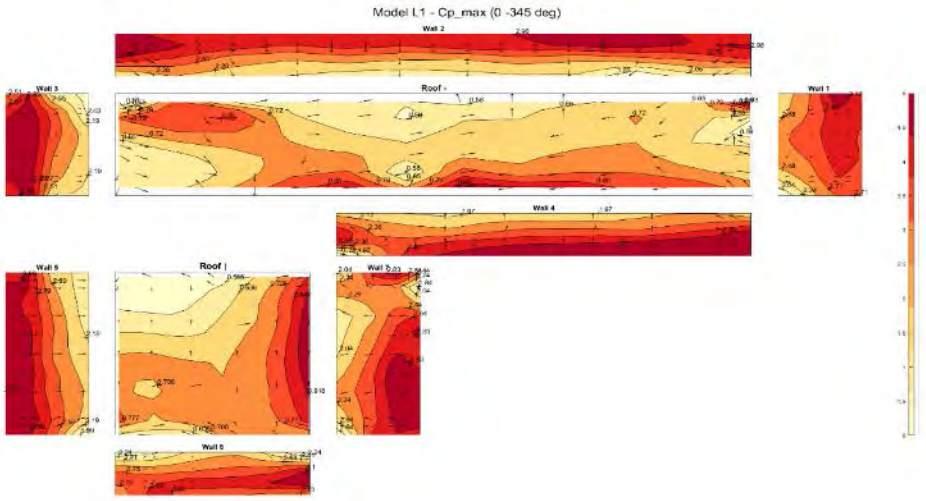

Figure 48. Maximum peak Cp L1.

3.2.3. Model C1

Minimum and maximum peak pressure coefficients for model C1 are shown in Figure 49 and Figure 50. The minimum peak pressure coefficients were observed to develop at the roof and walls edges where flow separation occurs and range from as low as -1 to -7. For the maximum peak pressure coefficients were observed to range from 0.5 to as high as 3.2.

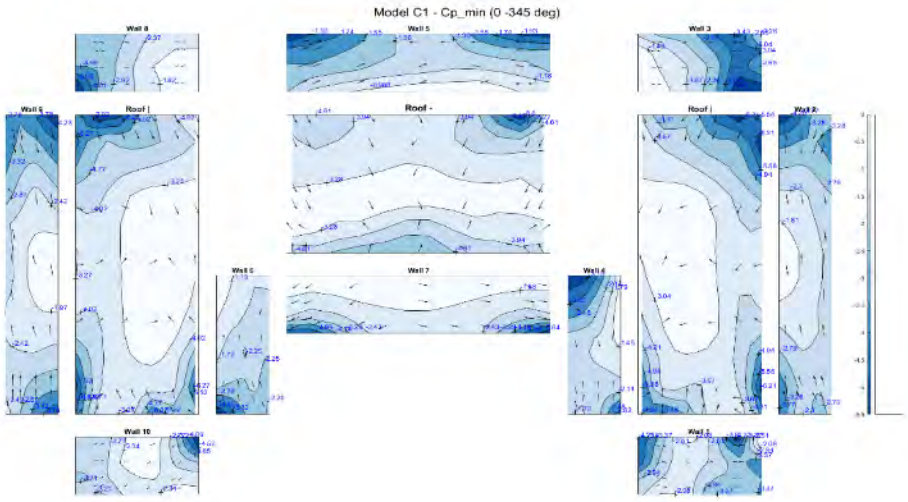

Figure 49. Minimum peak Cp C1.

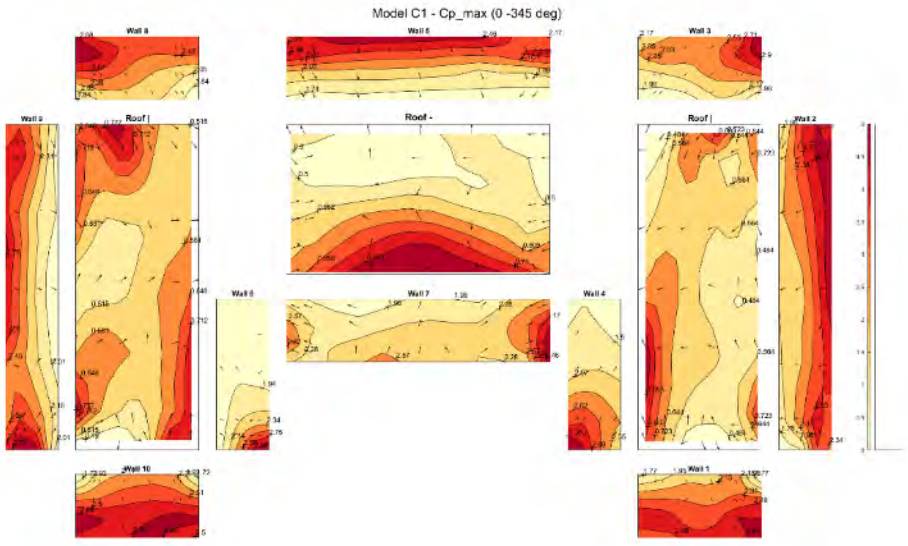

Figure 50. Maximum peak Cp C1.

3.2.4. Model C2

Minimum and maximum peak pressure coefficients for model C2 are presented in Figure 51 and Figure 52. In this case, the minimum peak pressure coefficients, which are found to be more critical at the roof and wall edges, ranged between -1.6 and -9.5. For the positive pressures, 3.1 was observed in one of the wall sections.

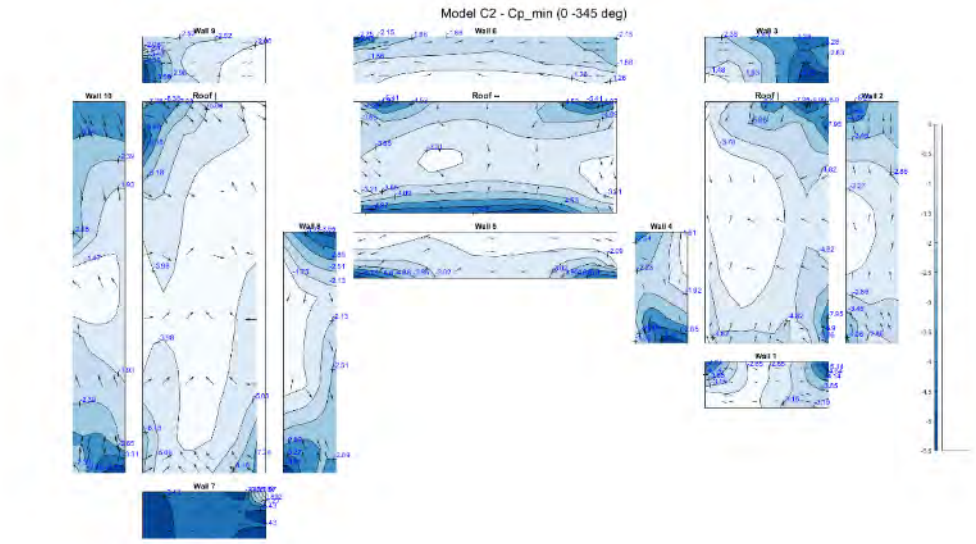

Figure 51. Minimum peak Cp C2.

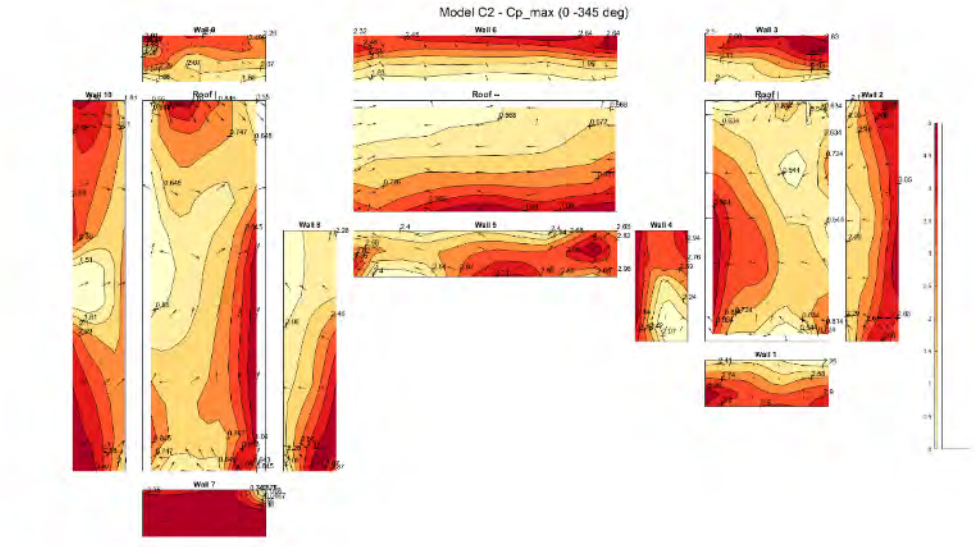

Figure 52. Maximum peak Cp C2.

3.3. Area Averaging

The area-averaged graphs were generated by obtaining the worst peak pressure coefficient by finding different combinations of pressure-tap tributary areas. These combinations varied from a single pressure tap to sets of several pressure taps. The formula used to obtain the area-averaged values was the summation of the product of the pressure-tap pressure coefficient and the tributary area divided by the total summation of the tributary area:

$$Area\ Averaged\ C_p = \frac{\sum_1^i C_{pi} * A_i}{\sum_1^i A_i}$$

The results obtained from the different combinations were used to generate preliminary scatterplots for the wall sections and the roof (Figure 53 and Figure 54). The values for area are reported as full-scale. It should be noted that this is a very useful interpretation approach of the obtained data which is expected to be further refined and enhanced when data from additional building shapes become available.

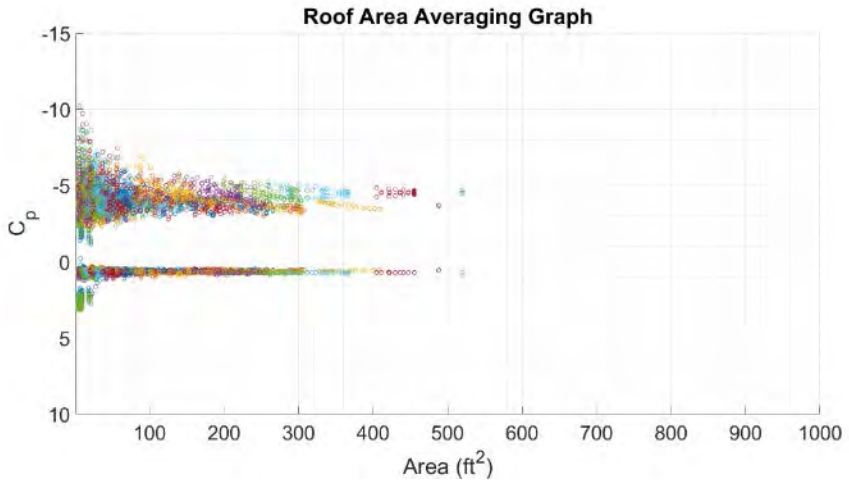

Figure 53. Area-averaged results for roofs.

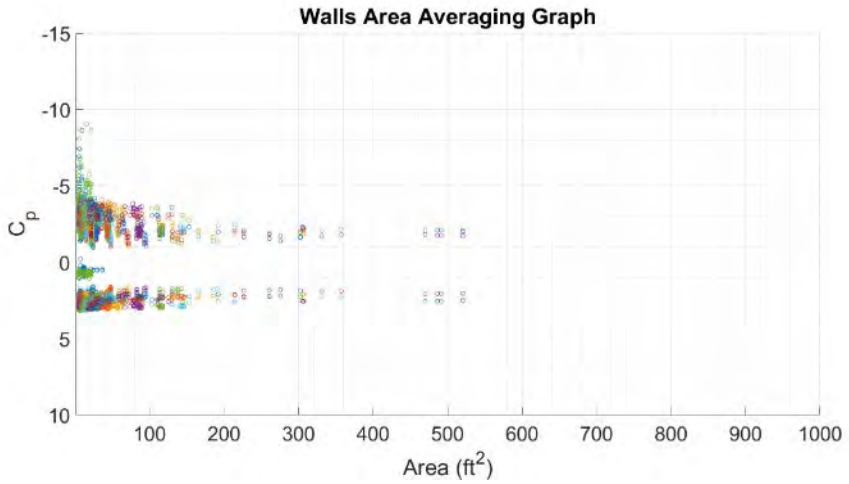

Figure 54. Area-averaged results for walls.

3.4. Codification Example

To attempt to codify the results obtained from Figure 53 and Figure 54, the graphs were modified to have an x-axis with a logarithmic scale to match the properties of the graphs provided by ASCE 7-16 (ASCE 7-16). While the current wind load provisions provide envelope curves for different zones of the walls and roofs sections, for this investigation an overall graph was generated for both, wall, and roof sections (as shown in Figure 55 and Figure 56). The graphs were added envelope lines that extend from 1 to 10, 10 to 500 and 500 to 1000 ft^2 (for positive and negative pressure coefficients) for the wall sections while for the roof envelope curves, the envelope lines extended from 1 to 2, 2 to 100 and 100 to 1000 ft^2 for the positive pressure coefficients and from 1 to 10, 10 to 100 and 100 to 1000 ft^2 for the negative pressures. The red dotted lines correspond to the graphs provided by ASCE 7-16 while the solid black lines are the envelop curves developed based on the results obtained from the Wall of Wind testing. It should be noted that no additional reduction factor has been considered in the experimental data.

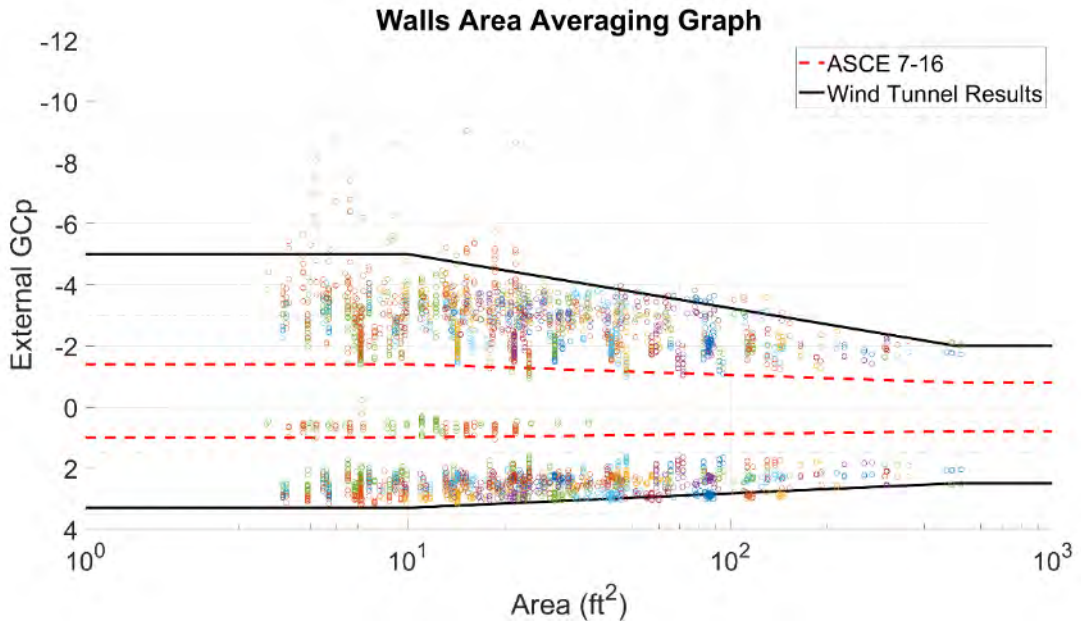

Figure 55. Walls codification graph.

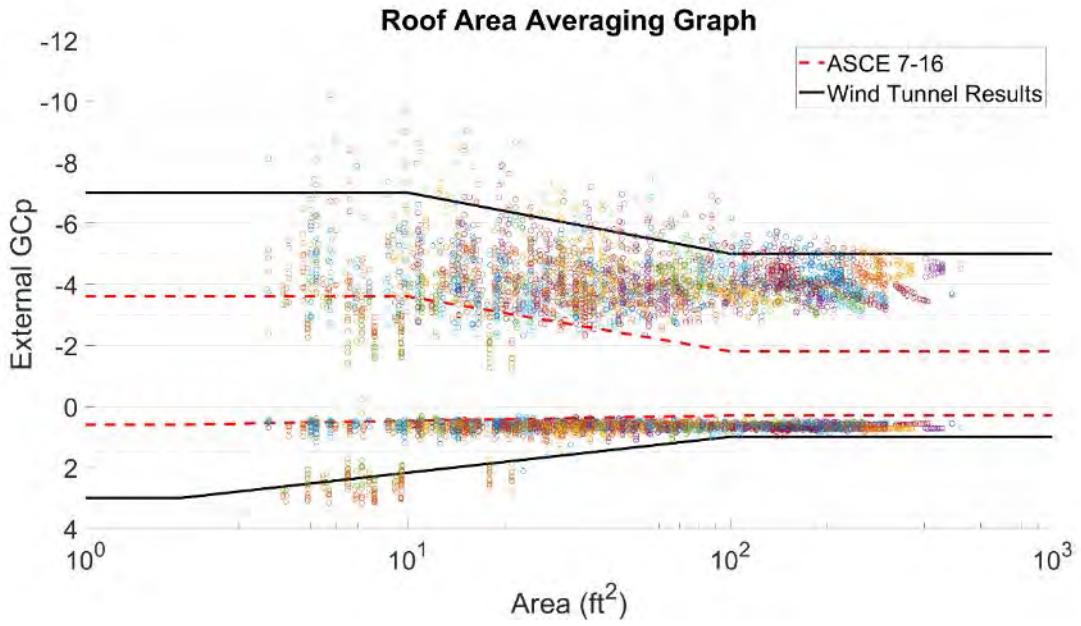

Figure 56. Roofs codification graph.

4. Atmospheric Boundary Layer Wind Tunnel

Wind-tunnel testing has been widely used to investigate fluid phenomena and is one of the most accurate and cost-effective approaches to investigate the effect of wind on civil infrastructure

(Louis et al., 2010, Jewel et al., 1999). As part of this study, it was decided that the use of a smaller Atmospheric Boundary Layer (ABL) Wind Tunnel would greatly benefit and enhance the vision of this research project. The purpose of this wind tunnel is to reduce the time and costs of testing to increase the number of models considered. This chapter will provide information on the design of this ABL wind tunnel and will provide preliminary results obtained from the wind field.

4.1. Design

There are several variables that need to be carefully considered during the design of a boundary layer wind tunnel. In the current research project, the design of the wind tunnel was primarily influenced by the available space, desired testing section and motors to drive the wind through the wind tunnel. Keeping in mind the before mentioned parameters, it was decided to have an open-jet wind tunnel with an aimed wind speed of 44 ft/s and a test section of 6 ft by 8 ft (height x width).

4.1.1. Motors

There were two axial fans available to be used in the construction of the wind tunnel (see Figure 57). These fans dictated the design parameters of the wind tunnel as they needed to be powerful enough to provide a constant volume of inflow to the wind tunnel. Based on the motor factory information and an estimation on the desired test section area for the wind tunnel of 48 ft^2 with an average wind speed of 44 ft/s, the fans would have to be capable of supplying a constant airflow of 126,820 cfm.

Figure 57. Axial Fans.

4.1.2. Wide-angle Diffuser

The diffuser is the section that decelerates and expands the airflow coming from the motors. This sections also serves to reduce the load on the motors, to increase the static pressure and to reduce the overall length of the wind tunnel (Jewel et al., 1999). The design parameters for the design of the wide-angle diffuser were 1) size and shape requirements, 2) diffuser angle and 3) screens as boundary layer control devices.

The size and shape requirements were highly dependent on the available fans. The available fans provided an inlet area of approximately 36 ft^2. Based on this area, the wide-angle diffuser outlet area and fans inlet area ratio required was estimated as 2.65, providing a total outlet area for the wide-angle diffuser of 96 ft^2. For the requirement of the diffuser angle, a maximum diffuser angle of 55 degrees was taken into consideration for the avoidance of flow separation (Mehta, 1979). To reduce the overall length of the wide-angle diffuser, and thus gain more length on the fetch section, a progressive wide angle-diffuser was designed (Figure 58 and Figure 59).

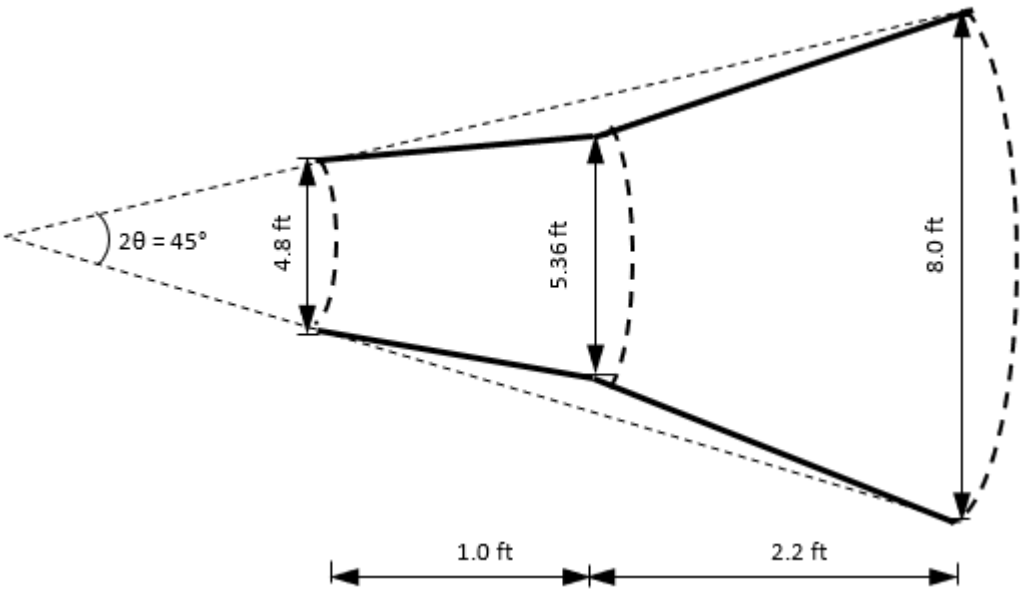

Figure 58. Wide Angle Diffuser Side View.

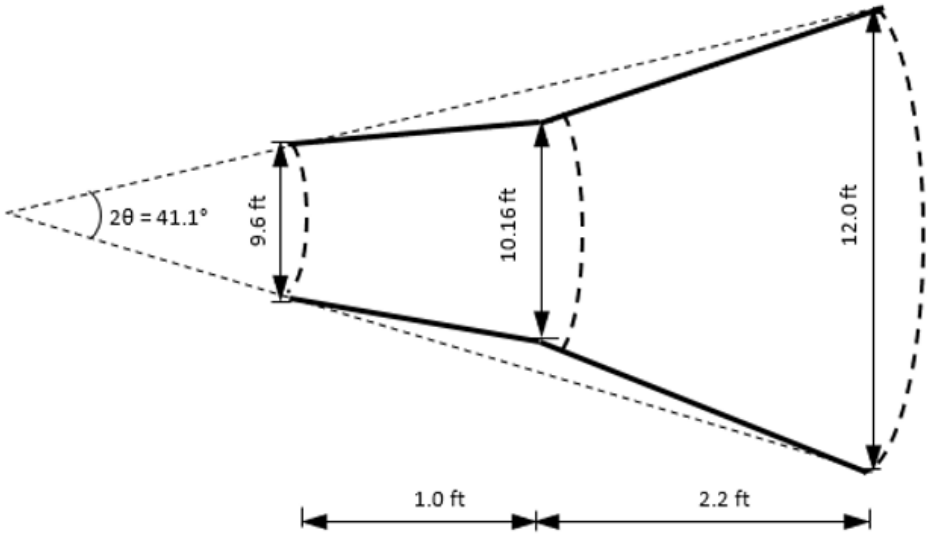

Figure 59. Wide Angle Diffuser Top View.

4.1.3. Settling Chamber

The settling chamber serves for settling the flow and managing it to feed a smooth laminar flow to the contraction section, therefore the design of the settling chamber, wide-angle diffuser

and contraction are interrelated. To settle the flow coming from the wide-angle diffuser, honeycombs and screens are used to straighten the flow and reduce any turbulence produced by the fans and/or flow separation that might have been developed in the wide-angle diffuser (Marshall, 1985). For the honeycomb, the required cell diameter is dependent on the hydraulic diameter of the settling chamber, which was calculated to be 9.6 ft. The required honeycomb cell diameter required was 0.75 inches, ~8 inches length and porosity greater than 80%. The settling chamber was also designed to house 3 screens of different porosities (wire diameters of 0.06, 0.04 and 0.02 in) downwind of the honeycomb with spacing of 10 in (Kulkarni et al.; 2011, Dommelen, 2013), see Figure 60.

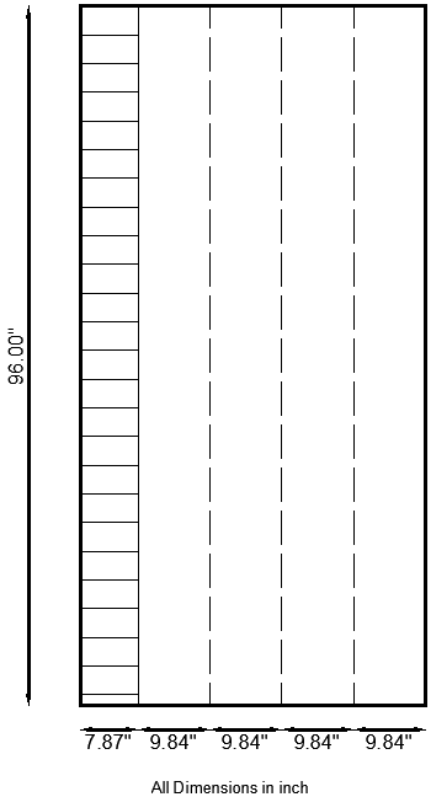

Figure 60. Settling Chamber Elevation View.

4.1.4. Contraction

The main purpose of the contraction section (also known as nozzle) is to accelerate the flow coming from the settling chamber and generate a uniform flow velocity profile adequate to be used in the test section (Mauro et al., 2017). The aim for this wind tunnel was to have a test

section with dimensions of 8 by 6 feet (width and height). The area ratio between the inlet and outlet of the nozzle section was based on the reservoir ratio criteria of 2:1. The fan to reservoir-area ratio was set to be 2.6:1, thus allowing reduction of overall length of this section to gain more overall length for the fetch section. The shape of the contraction was a key design parameter because it must be designed to avoid any flow separation (Mehta et al., 1979; Marshal 1985; James et al., 1988), see Figure 61 and Figure 62.

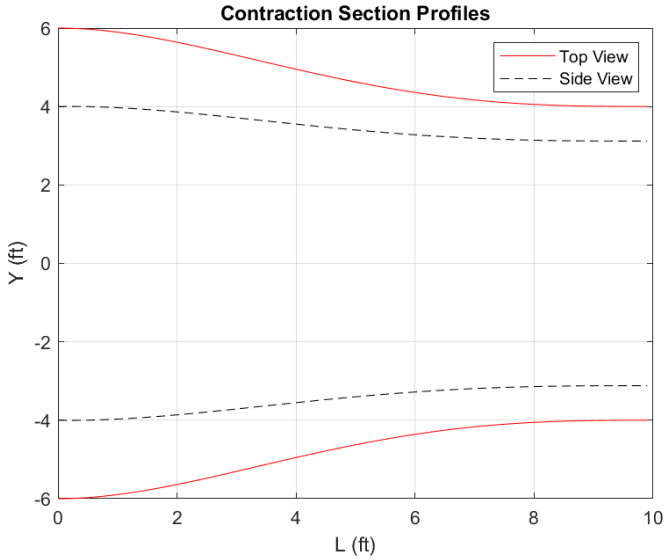

Figure 61. Top View and Side View Nozzle Profiles.

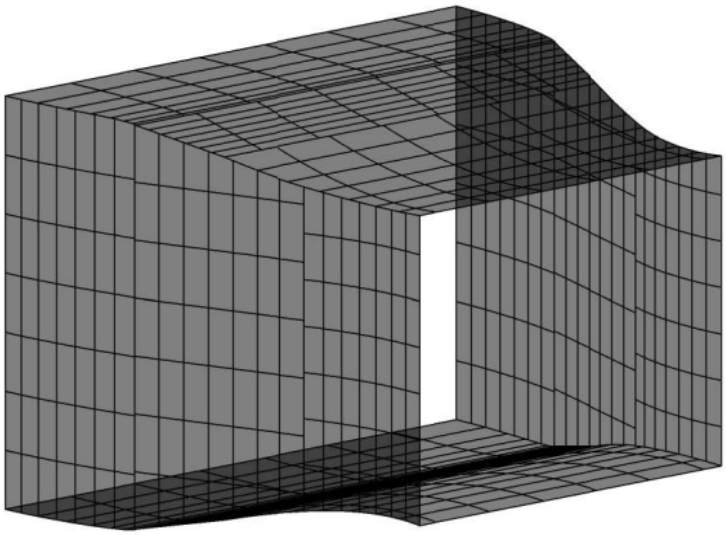

Figure 62. 3D View of Contraction Section.

4.1.5. Fetch

The fetch is the section which will manage the flow coming from the contraction section to simulate the desired atmospheric boundary layer exposure. This will be achieved by the installation of spires, castellated walls, and surface roughness elements. At the end of this section, a turntable with a diameter of 7.5 feet was designed and installed to which the models will be attached for testing at different wind directions. Due to the space limitation, the total distance of this section was of 27 feet and provides a sectional area for testing of 6 by 8 feet (height and width), see Figure 63.

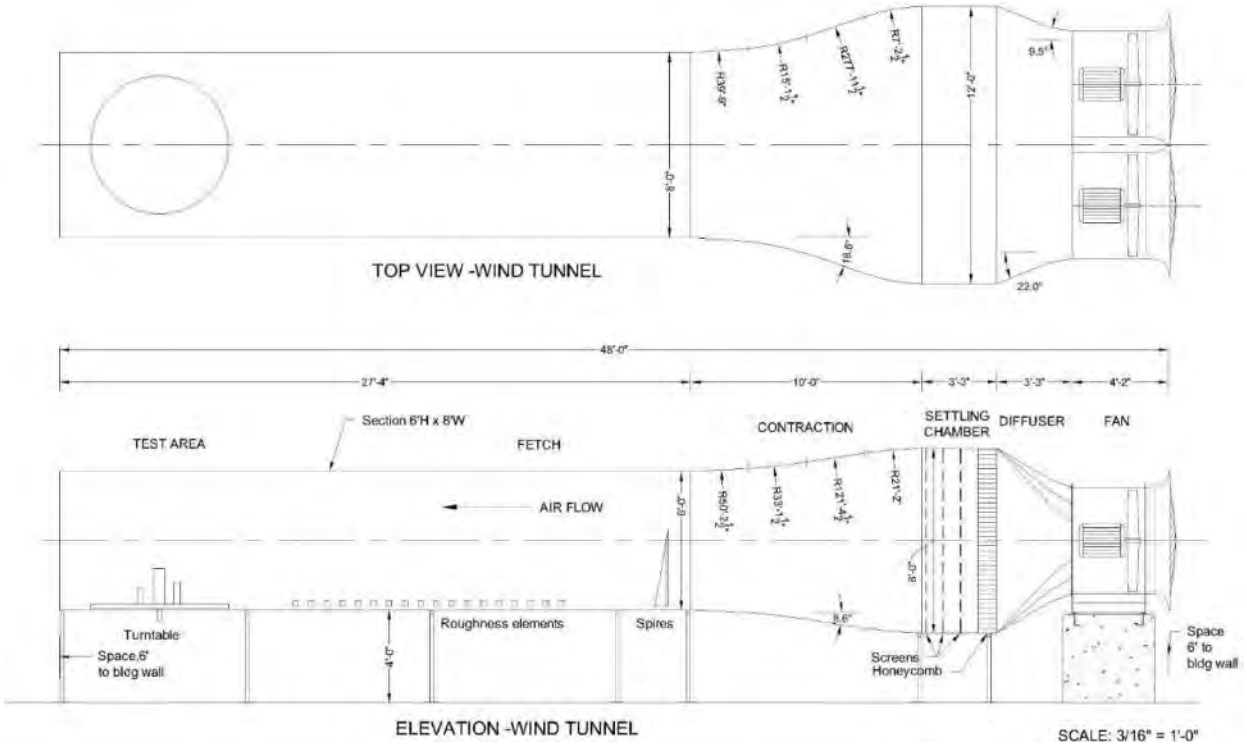

Figure 63. Wind Tunnel Top and Elevation View.

4.1.6. Boundary Layer Generators

The lowest part of the earth atmosphere is called the atmospheric boundary layer (ABL). This part is highly affected by the roughness (human made or naturally made) of the ground level (mountains, trees, hills, buildings in general, and so forth), temperature, pressure, etc. This causes the wind to be naturally turbulent, with its turbulence and wind speed varying in height (Ahmed, 2013).

Since the late 1960's, spires combined with roughness elements have been used to match the planetary boundary-layer profiles (Irwin P, 1980). These "devices" serve for the purposes of gradually modifying the wind speed as well as generating wind turbulence intensity at varying heights. It must be noted that the wind profile increases from lower heights while turbulence intensity profiles decrease with height (Figure 64, Figure 65 and Figure 66). The boundary layer profile may be of different exposures, being open, sub-urban and urban the interest in the civil engineering applications. To manipulate the ABL to the desired exposure, the wind tunnel must be capable of generating a smooth flow. Preliminary measurements of smooth flow are shown in Chapter 4.3.

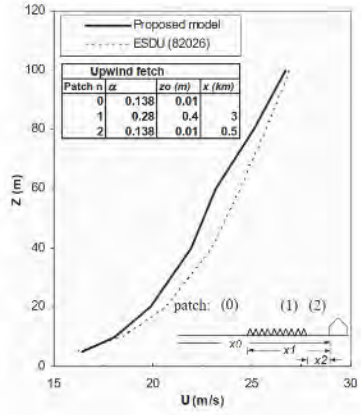

Figure 64. Wind speed profile (Stathopoulos et al., 2007).

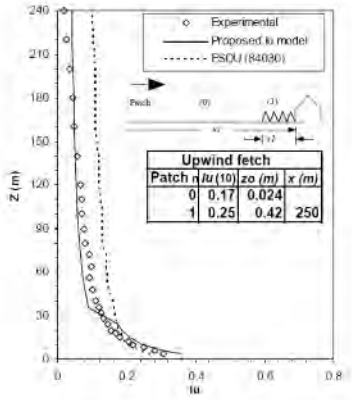

Figure 65. Turbulence intensity (Iu) profile (Stathopoulos et al., 2007).

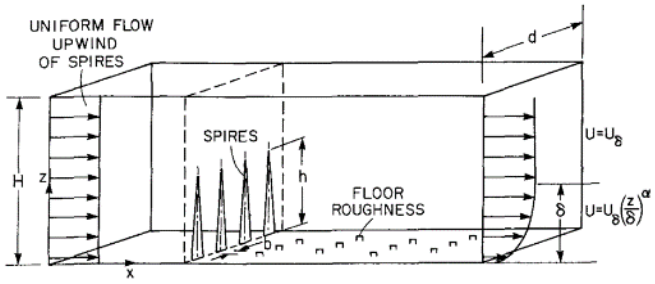

Figure 66. Spires and roughness (Irwin, 1980).

4.2. Construction

For the construction of the wind tunnel, it was decided to create an 80/20 aluminum frame of 3x3 inches. The walls of the sections were sent to a machine shop to be CNC cut out of 3/4 in

plywood. Each section was built separately and then installed adjacent to the corresponding section (wide angle diffuser, settling chamber, contraction (nozzle), and fetch). It must be noted that the longest section (the fetch) was made up of three equal sections, with the last section housing the turntable (Figure 67), this was done for convenience to move the different sections independently from the other for future maintenance, adjustments, repairs, and modification purposes. The built sections are shown from Figure 68 to Figure 74.

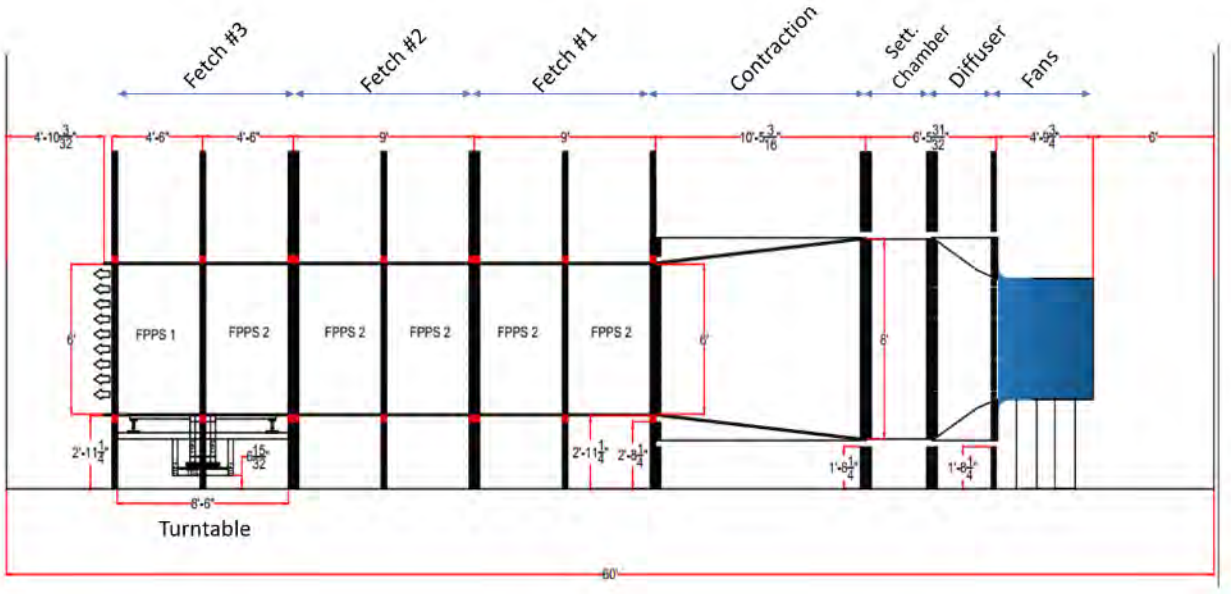

Figure 67. Wind tunnel sections.

Figure 68. Fans.

Figure 69. Wide angle diffuser.

Figure 70. Settling Chamber.

Figure 71. Settling Chamber with Screens.

Figure 72. Contraction.

Figure 73. Fetch (one half of the 3 sections).

Figure 74. Wind Tunnel with all Sections.

4.3. Preliminary Results

The wind tunnel smooth wind field was measured to obtain wind speed (U) and turbulence intensity (I_u) profiles. This was done to get an idea of how turbulent the wind field was when there

are no spires, castellated walls nor roughness elements. To measure the wind field, a rake with 13 pitot tubes fixed at 1, 2, 3, 5, 7, 9, 21, 26, 31, 36, 41, 46 and 71 inches from the floor, was installed at five different locations in front of the turntable (across the fetch). Besides the 13 pitot tubes, four Cobra Probes were installed at 4, 18.5, 38.5 and 64.5 inches from the floor. The advantage of cobra probes vs pitot tubes is the capability to measure across wind speed as well as across wind turbulence intensity at much higher sampling rate (500 Hz vs 2500 Hz). The location of the rake across the test section and the elevation at which the pitot tubes and cobra probes were installed are shown in Figure 75, Figure 76 and Figure 77.

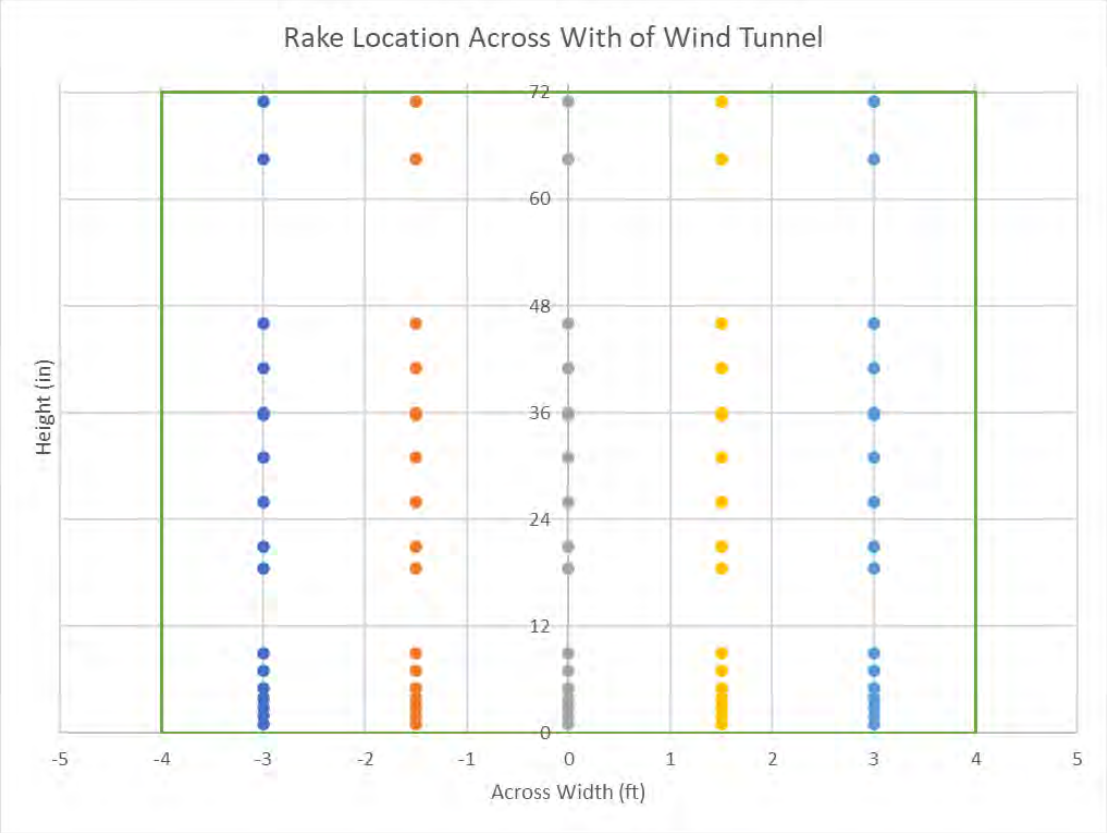

Figure 75. Rake locations with locations of pitot tubes and cobra probes (rear view).

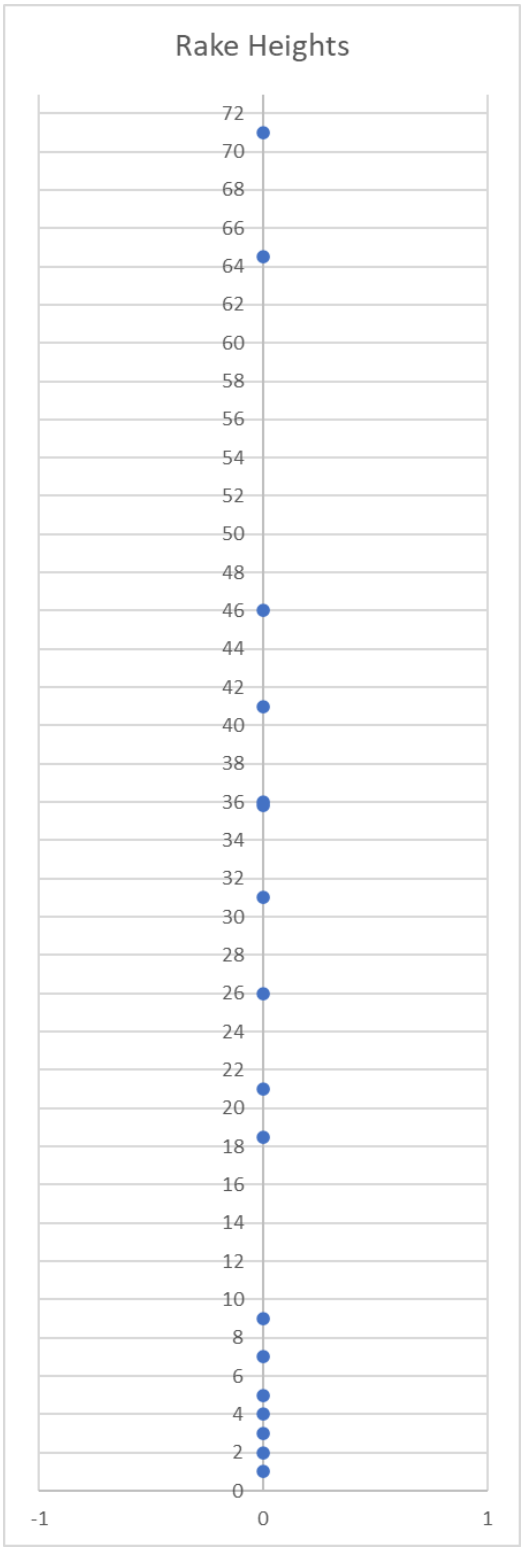

Figure 76. Rake heights (side view).

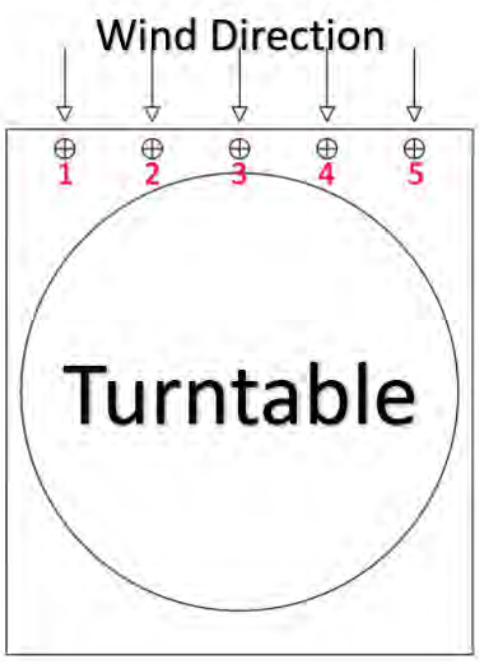

Figure 77. Wind speed measurement locations.

4.3.1. Wind Speed Profiles

The wind speed profiles, with neither roughness elements nor spires installed, was measured at five different locations across the width of the fetch right in front of the turntable. From Figure 78 to Figure 82, it can be observed that the design of the wind tunnel successfully provided a smooth flow coming from the wide-angle diffuser, settling chamber, contraction and their respective screens. These measures provide us with the certainty that there is no separation produced at any point before the fetch section that could induce considerable wind speed fluctuations and high turbulence in the measurements obtained. As it can be observed, and as expected, there is a reduction in the wind speed at heights very close to the floor and ceiling of the fetch section. This is due to the friction of the plywood that induced a reduction of the flow of air. These results provide the basis to start with the calibration of the wind tunnel to generate the ABL exposures desired.

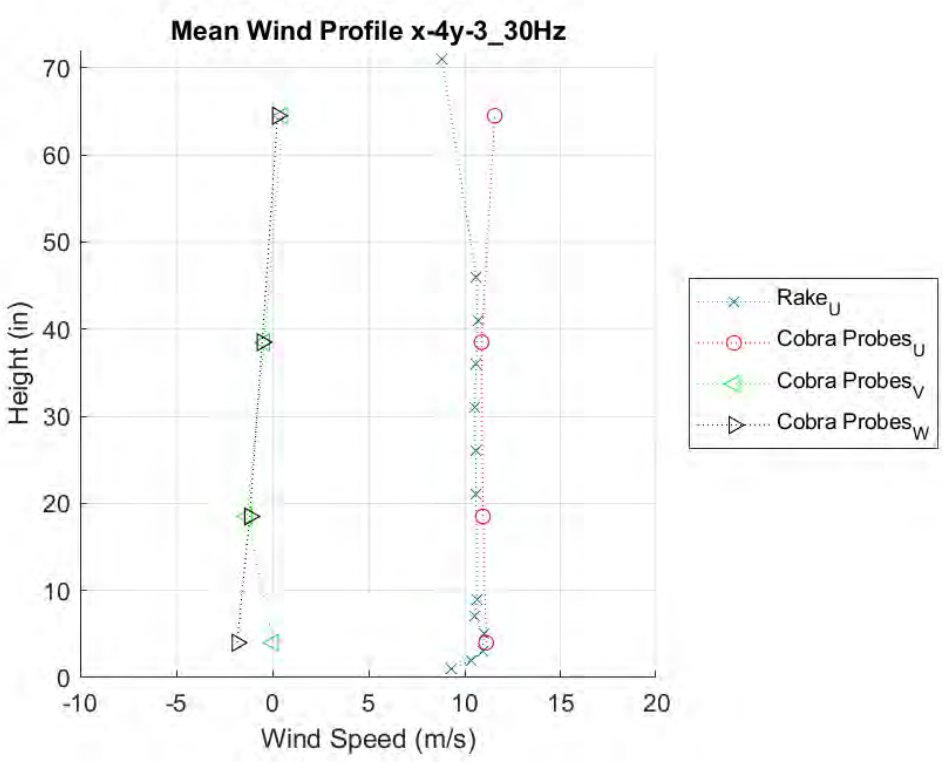

Figure 78. Wind speed profile at location 1

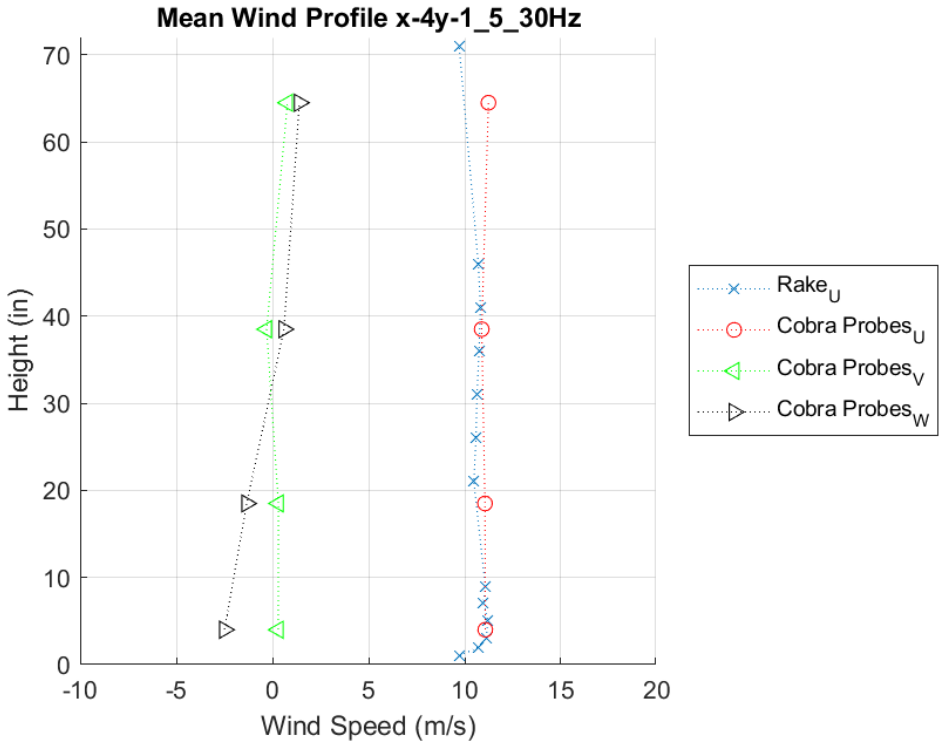

Figure 79. Wind speed profile at location 2.

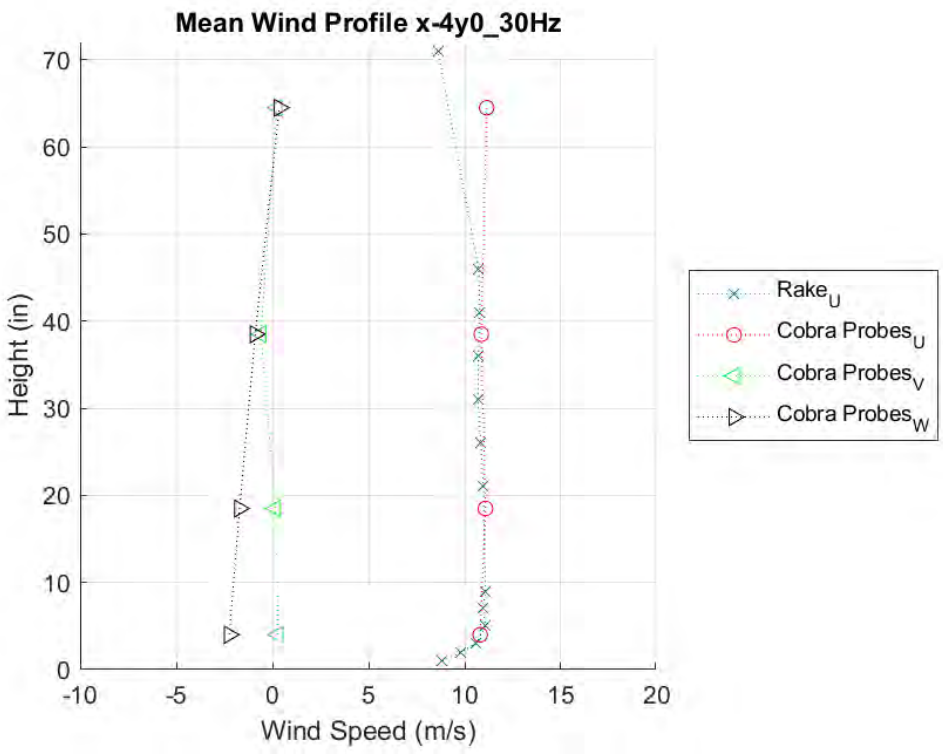

Figure 80. Wind speed profile at location 3.

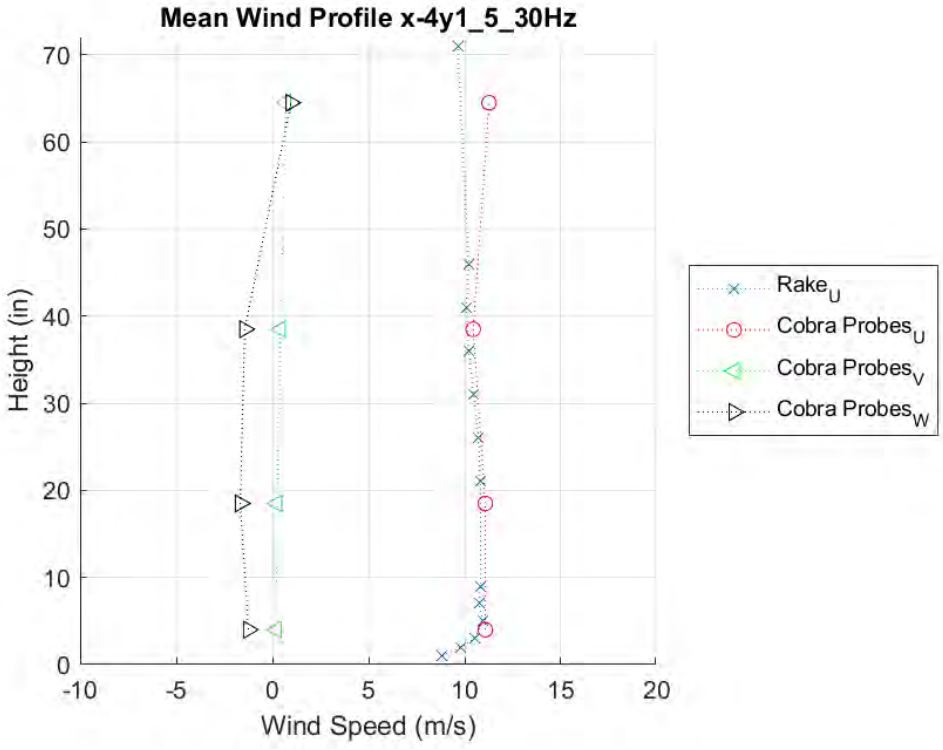

Figure 81. Wind speed profile at location 4.

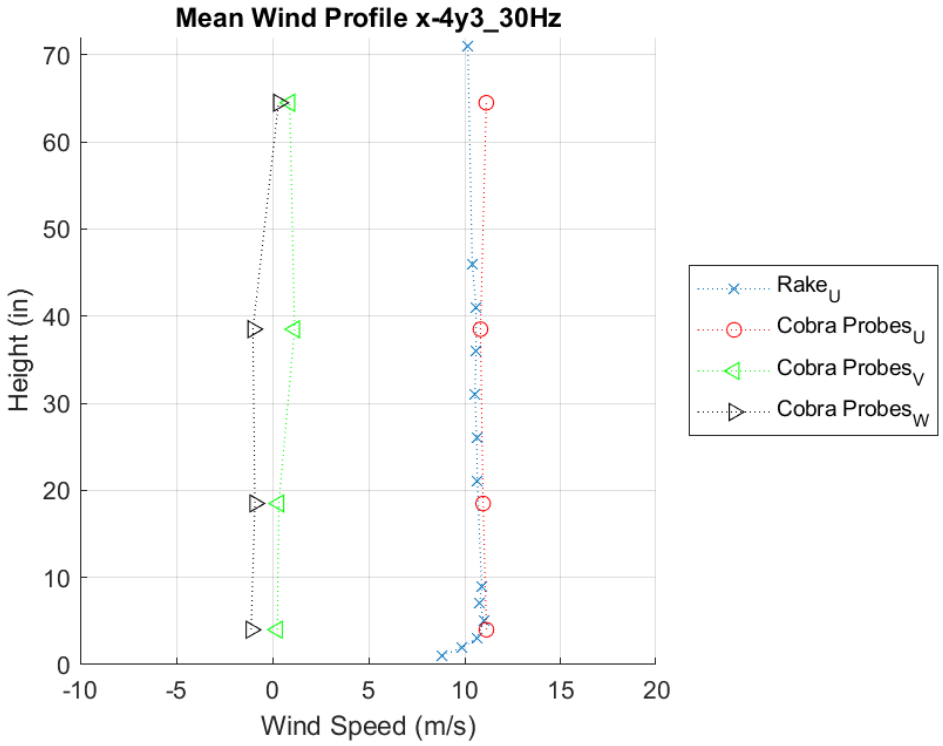

Figure 82. Wind speed profile at location 5.

4.3.2. Turbulence Intensity Profiles

From the pitot tubes as well as cobra probes, the turbulence intensity profiles were obtained (see Figure 83 to Figure 87). As it can be observed from the findings, the turbulence intensity profiles are near equal from floor to ceiling being of approximately 4%. However, and inversely proportional to the wind speed profiles, there is an increased turbulence intensity observed at the pitot tubes closer to the floor and ceiling. As previously mentioned, this is because of the roughness of the plywood that induced a small friction which produces a somewhat higher turbulence in the flow closer to the floor and ceiling.

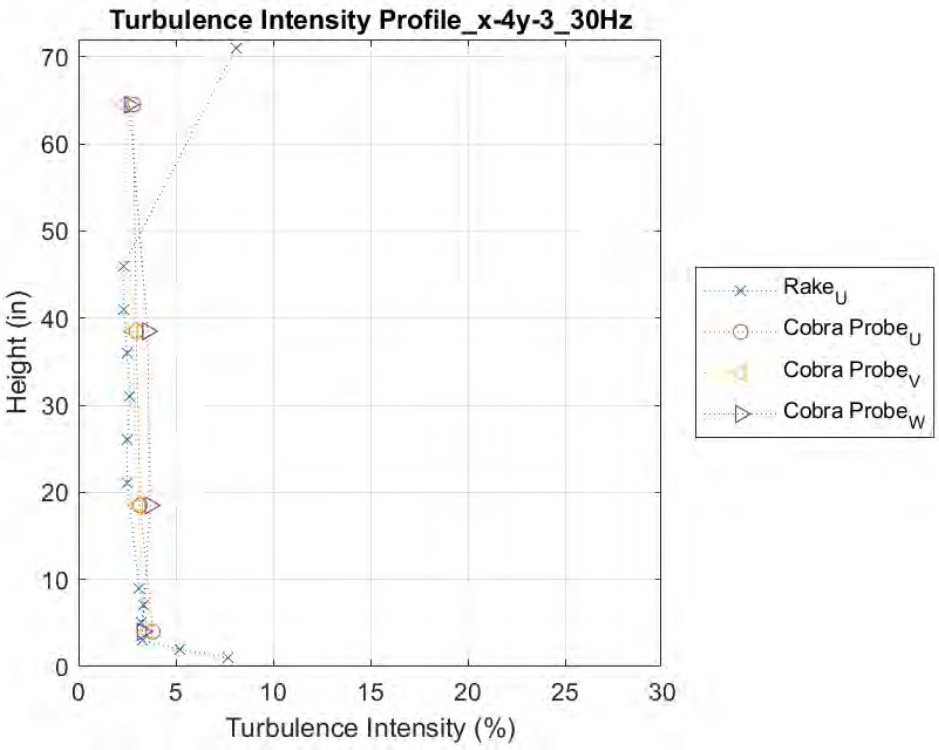

Figure 83. Turbulence intensity profile at location 1.

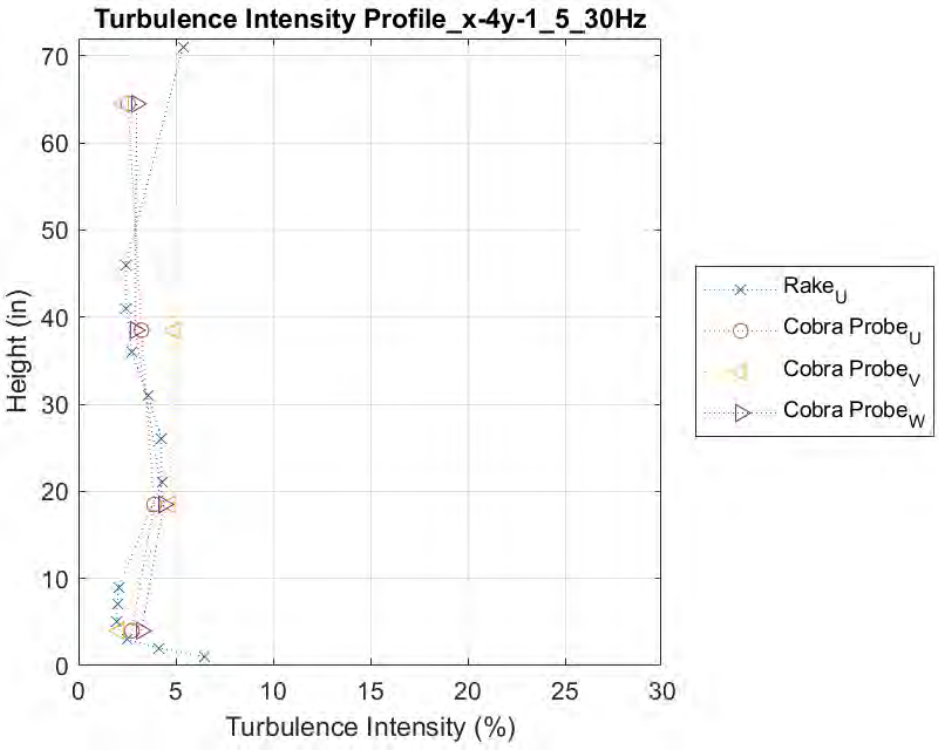

Figure 84. Turbulence intensity profile at location 2.

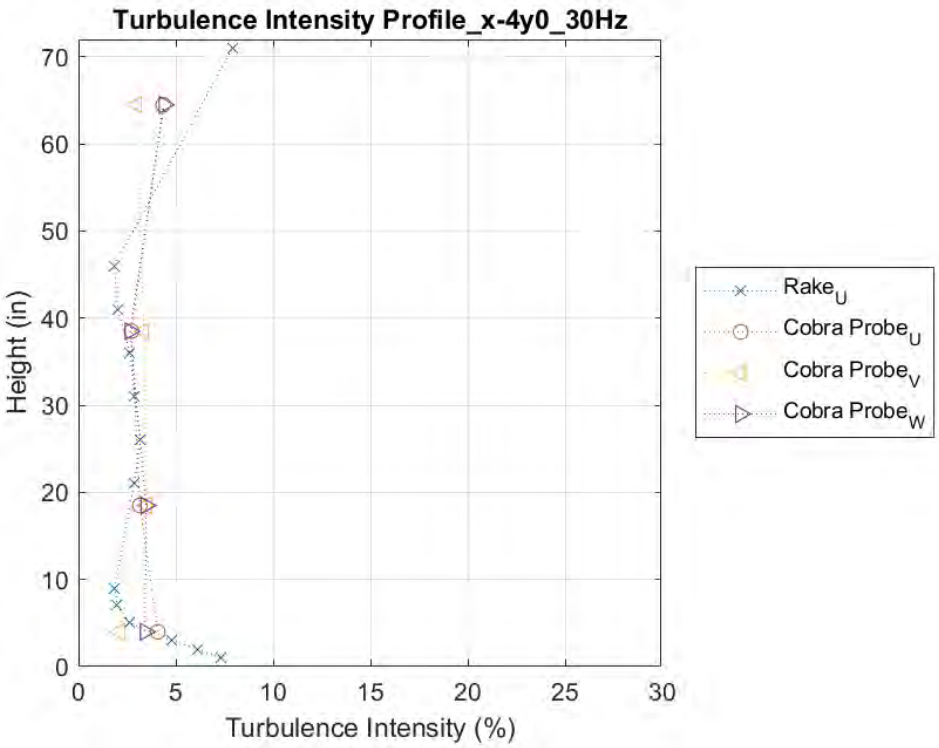

Figure 85. Turbulence intensity profile at location 3.

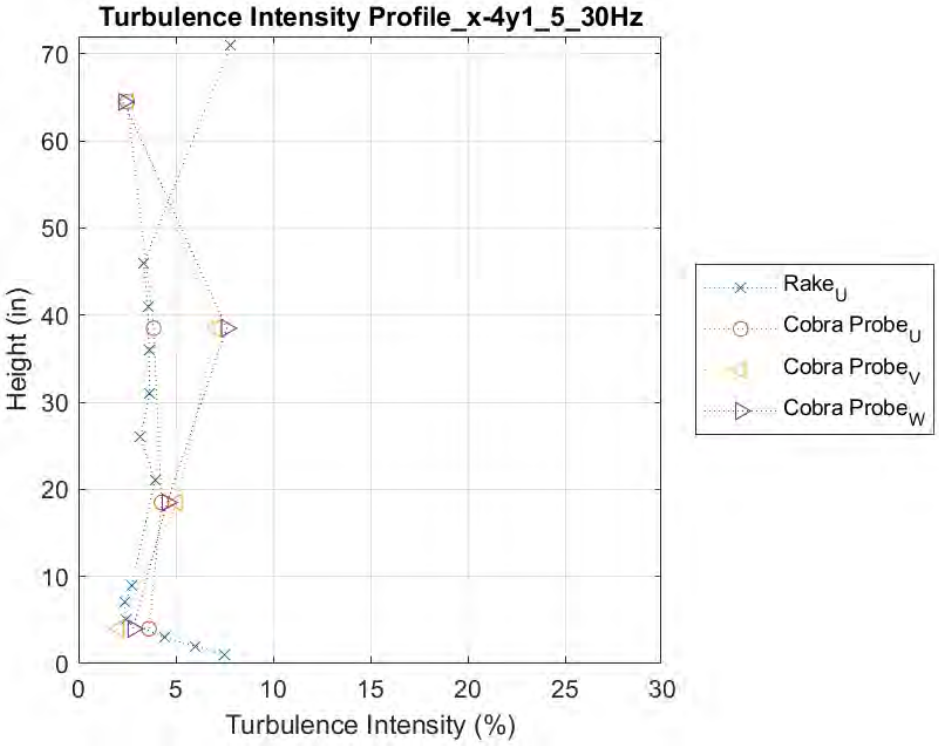

Figure 86. Turbulence intensity profile at location 4.

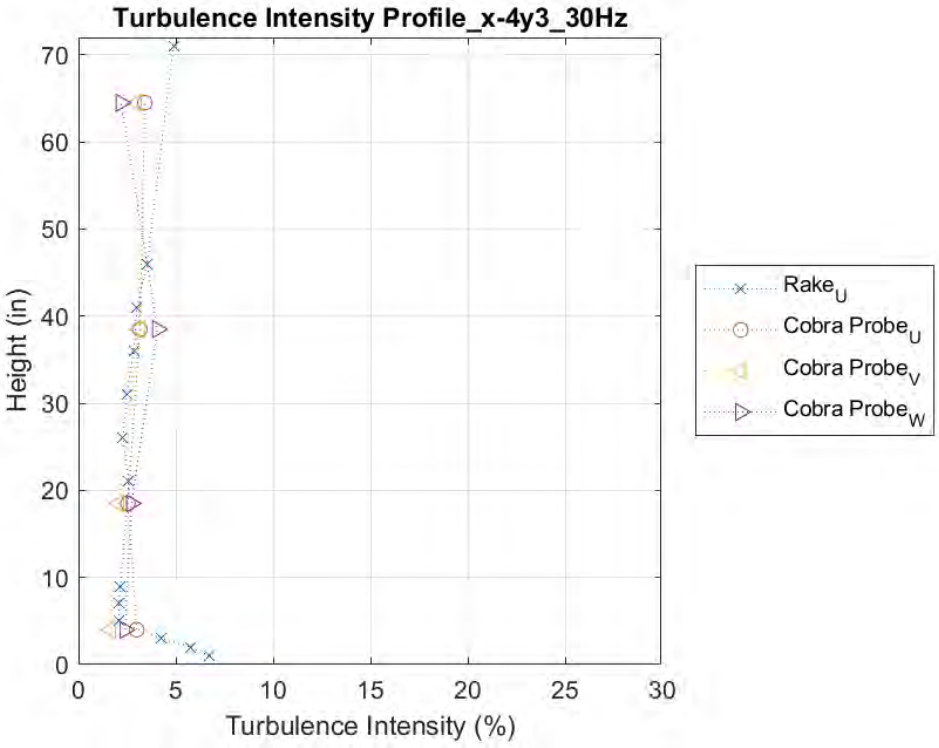

Figure 87. Turbulence intensity profile at location 5.

5. Conclusions

Extreme wind events have been responsible for billions of dollars in losses in the United States. To reduce the losses and improve the survivability of our built environment, several investigations have been carried out to better understand the behavior of structures under wind induced loads and to mitigate the damages produced by extreme wind events. The current wind load provisions provided by ASCE 7-16 are based on wind tunnel testing performed on predominantly regular shaped models, which is not representative of modern-day construction methods. This report presents results obtained from four 1:50 scaled models with irregular shaped plans that were designed, built, and tested at the Wall of Wind Experimental Facility at Florida International University.

Results showed that the pressure distributions on buildings with irregular shapes is considerably more dependent on the direction of the approaching wind. The roofs and walls were observed to develop high suction pressure coefficients at the edges when facing the wind, while the walls (parallel to the wind) experienced somewhat similar pressure coefficients than those experienced by the roof. For the positive pressure coefficients, it was observed that the effect of shape irregularity produced the pressure distribution to be significantly different than those experienced by a regular shaped model. The wall sections facing the wind flow were observed to undergo significant positive pressure coefficients. With the pressure coefficient data obtained from the experiments, area-averaged graphs were developed for both wall and roof sections. These graphs provide good insight when comparing the obtained results to the Components and Cladding (C&C) design curves provided in ASCE 7-16.

It must be noted that there is a considerable need to do more testing to fully understand the effects of building shape irregularities in the overall pressure coefficient distribution and attempt to create a database that can be used to better design residential structures. On that end, an atmospheric boundary layer wind tunnel was designed and constructed in the Laboratory for Wind Engineering Research at FIU. This smaller wind tunnel will allow to test a large number of models with irregular shapes in a cost-effective manner and thus build a more robust database to be used for codification purposes. The database will be available for public use through the NSF funded DesignSafe-CI domain.

References

Ahmed, N.A. 2013. “Wind-tunnel Designs and Their Diverse Engineering Applications.” Janeza Trdine 9, 51000 Rijeka, Croatia. DOI: http://dx.doi.org/10.5772/3403.

Akins, R. E., Peterka, J. A., Cermak, J. E. 1977. “Mean force and moment coefficients for buildings in turbulent boundary layers.” Journal of Wind Engineering and Industrial Aerodynamics. 2 (3): 195–209. https://doi.org/10.1016/0167-6105 (77)90022-8.

American Society of Civil Engineers (ASCE), ASCE Standard, Minimum Design Loads for Buildings and Other Structures, ASCE, 2016.

CBO (Congressional Budget Office). 2016. "Potential Increase in Hurricane Damage in the United States: Implications for the Federal Budget." Congressional Budget Office of the United States.

Chowdhury, A.G., Vutukuru, K., Moravej, M. 2018. “Full- and Large-Scale Experimentation Using the Wall of Wind to Mitigate Wind Loading and Rain Impacts on Buildings and Infrastructure Systems.” Proceedings of the 11th Structural Engineering Convention (SEC18), Jadavpur University, Kolkatta, India.

Chowdhury, A.G., Zisis, I., Irwin, P.A., Bitsuamlak, G., Pinelli, J-P., Hajra, B., Moravej, M. 2017. "Large-Scale Experimentation Using the 12-Fan Wall of Wind to Assess and Mitigate Hurricane Wind and Rain Impacts on Buildings and Infrastructure Systems." Journal of Structural Engineering.

Cook, N.J. 1985. "The designer's guide to wind loading of building structures." British Research Establishment 1985 Table C3, vol. Part 1, pp. 321-323, 2016.

Davenport, A. G., Surry, D., Stathopoulos, T. 1977. “Wind loads on low-rise buildings: Final

report of phases I and II, parts 1 and 2." BLWT Rep. No. SS8-1977. London, ON, Canada: University of Western Ontario.

Dommelen, V.R. 2013. "Design of an atmospheric boundary layer wind tunnel." Ms. Thesis, Technishe Univeriteit Eindhoven, Eindhoven, Netherlands.

Dong-Xue Zhao, Bao-Jie He. 2017. "Effects of architectural shapes on surface wind pressure distribution: Case studies of oval-shaped tall buildings." Journal of Building Engineering. DOI:http://dx.doi.org/10.1016/j.jobe.2017.06.009.

Gomes, M. G., Rodrigues, A. M., Mendes, P. 2005. "Experimental and numerical study of wind pressures on irregular-plan shapes. Journal of Wind Engineering and Industrial Aerodynamics".

Ho, T.C.E., Surry, D., Morrish, D., Kopp, G.A. 2005. "The UWO contribution to the NIST aerodynamic database for wind loads on low buildings." Part 1: Archiving format and basic aerodynamic data. Journal of Wind Engineering and Industrial Aerodynamics. 93 (1): 1–30. https://doi.org/10.1016/j.jweia .2004.07.006.

Irwin P. 1980. "The Design of Spires for Wind Simulation." Journal of Wind Engineering and Industrial Aerodynamics, 7(1981)861-366.

Irwin, P.A., Cooper, K.R., Girard, R. 1979. "Correction of distortion effects caused by tubing systems in measurements of fluctuating pressures." Journal of Wind Engineering and Industrial Aerodynamics.

James H., Mehta R. 1988. "Contraction Design for Small Low-speed Wind Tunnels." National Aeronautics and Space Administration.

Jewel B. Barlow, William H. Rae, Alan Pope. 1999. "Low-speed Wind Tunnel Testing." United

Kingdom, Wiley. ISBN: 9780471557746.

Kurkarni, V., Sahoo, N., Chavan, S.D. 2011. “Simulation of honeycomb-screen combination for turbulence management in a subsonic wind tunnel.” Journal of Wind Engineering and Industrial Aerodynamics.

Louis C., Chris, B., Jose M. 2010. “Fundamentals of Wind-tunnel Testing.” Encyclopedia of Aerospace Engineering. ISBN: 978-0-470-68665-2.

Marshall, R.D. 1985. “Performance Requirements and Preliminary Design of a Boundary Layer Wind Tunnel Facility.” U.S. Department of Commerce, National Bureau of Standards, Center for Building Technology.

Mashalkar, B. S., Patil, G. R., Jadhav, A. S. 2015. “Effect of plan shapes on the response of buildings subjected to wind vibrations”. IOSR Journal of Mechanical and Civil Engineering (IOSR-JMCE).

Mauro, S., Brusca, S., Lanzafame, R., Famoso, F., Galvagno, A., Messina, M. 2017. “Small-scale open-circuit wind tunnel: Design Criteria, Construction and Calibration.” International Journal of Applied Engineering Research 12, no. 23, 13649-13662.

Mehta, RD. 1979. “The Aerodynamic Design of Blower Tunnels with Wide-angle Diffusers.” Progress in Aerospace Sciences 18:59-120.

Shuai Shao, Tuji Tian, Qingshan Yang, Ted Stathopoulos. 2019. “Wind-induced cladding and structural loads on low-rise buildings with 4:12-sloped hip roofs.” Journal of Wind Engineering and Industrial Aerodynamics, Beijing China.

Souvik, C., Sujit, K. D., Ashok, K. A. 2014. “Wind load on irregular plan shaped tall building - a case study.”

Stathopoulos T., Zhou, Y. 1993. “Computation of wind pressures on L-shaped buildings”. Journal of Engineering Mechanics.

Stathopoulos, T. 1979. “Turbulent wind action on low-rise buildings.” Ph.D. thesis, Dept. of Civil and Environmental Engineering, Univ. of Western Ontario.

Stathopoulos, T., Baniotopoulos, C.C. 2007. “Wind Effect on Buildings and Design of Wind-sensitive Structures.” Springer Science & Business Media. ISBN: 978-3-211-73075-1.

Uematsu, Y., Isyumov, N. 1999. “Wind pressures acting on low-rise buildings”. Journal of Wind Engineering.

USDOC (United States Department of Commerce). 2010. “Coastline Population Trends in the United States: 1960 to 2008”. United States Department of Commerce.

Yi, L., Duan, R.B., Li, Q.S., Li, Y.G., Li, C. 2020. “Research on the characteristics of wind pressures on L-shaped tall buildings.” Advances in Structural Engineering. DOI:10.1177/1369433220906934.

Yi, L., Li, Q.S. 2016. “Wind-induced response based optimal design of irregular shaped tall buildings.” Journal of Wind Engineering and Industrial Aerodynamics. 155 (2016) 1978-207. DOI:http://dx.doi.org/10.1016/j.jweia.2016.06.001.

Yi, L., Li. Q.S., Chen, Fubin. 2017. “Wind tunnel study of wind-induced torques on L-shaped tall buildings.” Journal of Wind Engineering and Industrial Aerodynamics. 167 (2017) 41-50. DOI:http://dx.doi.org/10.1016/j.jweia.2017.04.013.

Young, T.L., Soo, L.B., Hee, C.L., Kunio M. 2016. “Pressure distribution on rectangular

buildings with changes in aspect ratio and wind direction." Wind and Structures. Vol. 23, No. 5 (2016) 465-483. DOI:http://dx.doi.org/10.12989/was.2016.23.5.465.

A Resource for the State of Florida

SECTION 5
DEVELOPMENT OF AN INTEGRATED STORM TIDE AND FRESHWATER FLOODING MODEL PHASE 3

A Report Submitted to:
The State of Florida Division of Emergency Management

Prepared By:
Dr. Yuepeng Li
Dr. Keqi Zhang
Dr. Qiang Chen

The International Hurricane Research Center (IHRC)
Florida International University

April 15, 2021

Executive Summary

During Phase 3 (2019-2021) the development of the SSFOF (Storm Surge and Freshwater Overland Flooding) model, based on the open-source TELEMAC modelling suite continued. In the previous 2017-2018 Phase 1 and 2019-2020 Phase 2 reports, IHRC developed the prototype SSFOF model which can simulate the compound effect of tide, storm surge and rain-fall run-off during hurricane impact. The SSFOF model was proven to be stable, robust, and efficient, and is one of the most advanced full-physics Nonlinear Shallow Water Equation (NSWE) based depth-averaged storm surge models. In the previous phases, the applications of the SSFOF model were focused on South Florida and adjacent coasts and open oceans using both historic and synthetic hurricanes. High resolution basins resolving small-features such as rivers, canals, streams, levees, dams, high ways, and major roads in Miami-Dade County, for example, have been developed to achieve better understanding of the county's vulnerability to storm surge and freshwater overland flooding. In this phase, investigations on hurricane impact to the North Florida region, as well as Lake Okeechobee, have been conducted with the SSFOF model. Moreover, the SSFOF model was further developed to include a full 3D model that is capable of modelling saltwater intrusion due to storm surges and tides.

The North Florida mesh was generated to cover the whole northwest coastline of Florida, where the Continuously Updated Digital Elevation Model (CUDEM) - 1/9 Arc-Second Resolution Bathymetric-Topographic Tiles that is being developed by NOAA's national Centers for Environmental Information (NCEI) have been employed for the bathymetry and topography. The finest grid resolution, however, was limited to the order of 100 m due to the relatively large basin. The storm surges caused by Hurricanes Hermine (2016) and Michael (2018) were simulated with result validation using NOAA tide gauges and USGS High Water Marks.

For Lake Okeechobee investigation, an independent new mesh was generated rather than using the previous South Florida mesh. Researchers determine that a high resolution mesh with spacing around the Herbert Hoover Dike (HHD) at 10 meters was applicable, due to the Lake Okeechobee Composite Bathymetry 2014 SFWMD 5-ft database. Four historic hurricanes, including Frances (2004), Wilma (2005), Matthew (2016), and Irma (2017), have been used for

case studies. Simulation results have been verified using the gauge measurements from the DBHYDRO database managed by SFWMD.

The newly added 3D model for saltwater intrusion modeling under hurricane conditions was developed and tested in a qualitative manner (no validation was conducted at this development stage). Saltwater intrusion modeling inside and around the outlet of Miami River under Hurricane Irma (2017) impact was conducted as an example test. A new mesh with grid resolution of approximately 10 meters was generated around the Miami River outlet. The result shows a high impact of saltwater intrusion inside Miami River due to Irma (2017); the salt water can travel upstream as far as 4 km. The stratification of salinity was also observed at locations around the river outlet.

Phase 3 has again demonstrated that the SSFOF model is robust, efficient and comprehensive with great potential for new functionalities. The model can forecast and hindcast hurricane-induced inundation extent, maximum flooding depth, duration of the flooding, water velocity and salinity at given locations. With new innovations, the SSFOF model can become a reliable tool at either regional or local scales.

1. Background

The newly developed SSFOF (Storm Surge and Freshwater Overland Flooding) model, based on the TELEMAC-2D model, represents a cutting-edge storm surge model which can simulate fully coupled storm tides and overland flooding (due to storm rain) on the same computational domain including head losses due to infiltration. Phase 3 of the SSFOF model development during 2020-2021 period focuses on (1) investigating the hurricane impact to the Lake Okeechobee and surrounding Herbert Hoover Dike (HHD), (2) developing a North Florida Basin covering Apalachicola and Panhandle Bay, with specific emphasis on simulating the surge due to Hurricanes Hermine (2016) and Michael (2018), and (3) investigating saltwater intrusion during extreme storm event. The governing equations for the SSFOF model, as well as general configurations such as the calculation of Manning coefficients, parametric wind field, and tide and river discharge boundaries are given in the reports of Phases 1 and 2 and are not repeated in this report.

For the third task in particular, a number of studies were focused on assessing the extent of Saltwater Intrusion (SI) during extreme events such as hurricanes. With the increase of frequency and intensity of extreme storm events, SI poses a significant challenge for coastal engineering and drinking water resource management in vulnerable coastal areas. In fact, Sawyer, et al. (2016) predicted that 9 percent of the U.S. coastline is already vulnerable to saltwater intrusion, a percentage likely to grow as the world continues to warm. Therefore, researchers improved the SSFOF model to include the essential physical features, which allowed the team to track the saline intrusion into fresh water as a consequence of storm surge. Since salt is an active (dense) tracer it is necessary to move from a two-dimensional, depth–averaged, model to a fully three-dimensional model, so that the behaviour of the salt concentration in the water column can be correctly modelled. The TELEMAC modelling suite contains a 3D hydrostatic model (TELEMAC-3D) that is based on the well known σ-grid approach (Hervouet, 2007). The development of the SSFOF model has thus employed TELEMAC-3D to develop a full 3D storm surge model that is capable of modelling saline intrusion due to storm surge and tides.

2. Objectives

The major tasks during the 2020-2021 phase (Phase 3) required slight modifications. First, regarding the investigation on hurricane impact on Lake Okeechobee, an independent new grid was generated rather than using the previous South Florida Mesh. This modification was made by realizing that during hurricane events the control structures on the major rivers connecting to Lake Okeechobee would be closed, and despite the high impact of recent hurricanes, such as Frances (2004), Wilma (2005), Matthew (2016), and Irma (2017), no major overtopping on the HHD was reported. Second, for the simulation on the newly developed North Florida Mesh, the previously suggested case of using Hurricane Ivan (2004) was replaced with Hurricane Hermine (2016). The reason being that the landfall location of Ivan (2004) is very close to the boundary between Florida and Alabama, which are not covered by the North Florida Mesh. Because of this, simulation results for Ivan (2004) are not reliable due to the unphysically short storm fetch and boundary effects. Third, for the SI modeling, researchers focused on the area around Miami River Outlet and considered Irma (2017) case only. The SI simulation result is also preliminary with more stress on qualitative analysis. The Phase 3 research objectives were as follows:

Part 1 – Investigating Lake Okeechobee

1. Collect the available bathymetry data inside of Lake Okeechobee and the height of surrounding HHD.
2. Generate high resolution mesh (30m-50m) of the Lake.
3. Analyze the impact of the historical hurricanes to Lake Okeechobee using Hurricanes Frances (2004), Wilma (2005), Matthew (2016), and Irma (2017).

Part 2 – Development of a North Florida Mesh

4. Collect and analyze available high resolution (5 meters or higher) Lidar Digital Elevation Model (DEM) data covering the North Florida.
5. Build a new mesh covering the North Florida coastal area including Panhandle and Apalachicola bay. The urban areas of the Pensacola, Panama City, and Mexico Beach will be refined (Order 100m mesh spacing).

6. Simulate the recent historical hurricanes Michael (2018) and Hermine (2016) at North Florida Basin with SSFOF.

Part 3 - Towards full 3D modelling and Salt Water Intrusion

7. Regenerate a finer mesh (~10 m resolution) around the Miami River outlet
8. Use Irma (2017) as an example to qualitatively test the full 3D storm surge model that is capable of modelling saline intrusion due to storm surge and tides.

3. Investigating Lake Okeechobee

Fig. 1 shows the study area of Lake Okeechobee. The surface area of the lake is 1732 km^2, with 20% littoral habit near the western shore and 80% open water. The lake serves the region providing flood control for the surrounding watershed, water supply for regional agriculture, and ground water recharge for the urban areas to the south and east (Li et al., 2016). The Herbert Hoover Dike (HHD) as seen in Fig.1 is 225 km long with a height varying between 9.8 and 14m above National Geodetic Vertical Datum (NGVD 1929). Water levels are regulated through numerous water control structures in the levee. The selected hurricanes Frances (2004), Wilma (2005), Matthew (2016) and Irma (2017) (see tracks in Fig.1) have caused storm surges of different severity within the lake and impacted the HHD significantly. Water elevation measurements were obtained for model verification from the DBHYDRO database that is managed by the South Florida Water Management District (SFWMD) (see selected stations in Fig. 1).

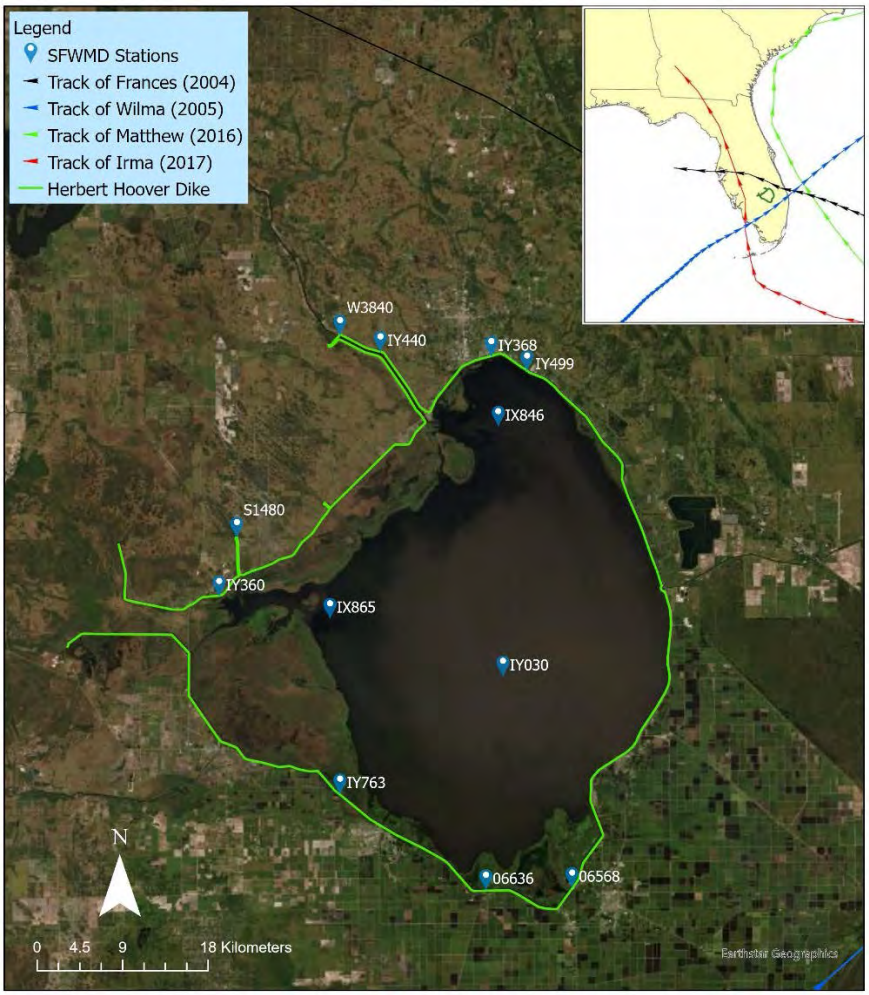

Fig. 1 The Lake Okeechobee study area, measurement stations and hurricane tracks.

The model domain is restricted within the lake area surrounded by the HHD (no overtopping was observed for the selected four hurricanes and it is assumed that all of the water control structures were closed during the passing of hurricanes). Fig.2(a) shows the generated unstructured grid for the computational domain; approximately, a total of 248,000 nodes and 475,000 elements were used, with the resolution ranging from 10 meters along the dike to 1 km at the central area of the lake. The Lake Okeechobee Composite Bathymetry 2014 SFWMD 5-ft (https://geo-sfwmd.opendata.arcgis.com/datasets/acfb4e0d9645452fbe40bbf846d5b255, accessed 2/24/2021) was employed for building the bottom elevation map (see Fig. 2(b)). The Manning friction coefficient was set to be 0.02 in deep areas, and for the wet areas and dry land along the dike, the Manning coefficient was calculated based on the National Land Cover Dataset (NCLD) 2006 (Fig. 2(c)). The initial water level for the whole computational domain was set according to the

averaged water level measured at the water level stations before the storms made a landfall. The duration of the simulation and other parameters for each of the hurricane cases are given in Table 1 using coordinated universal time (UTC).

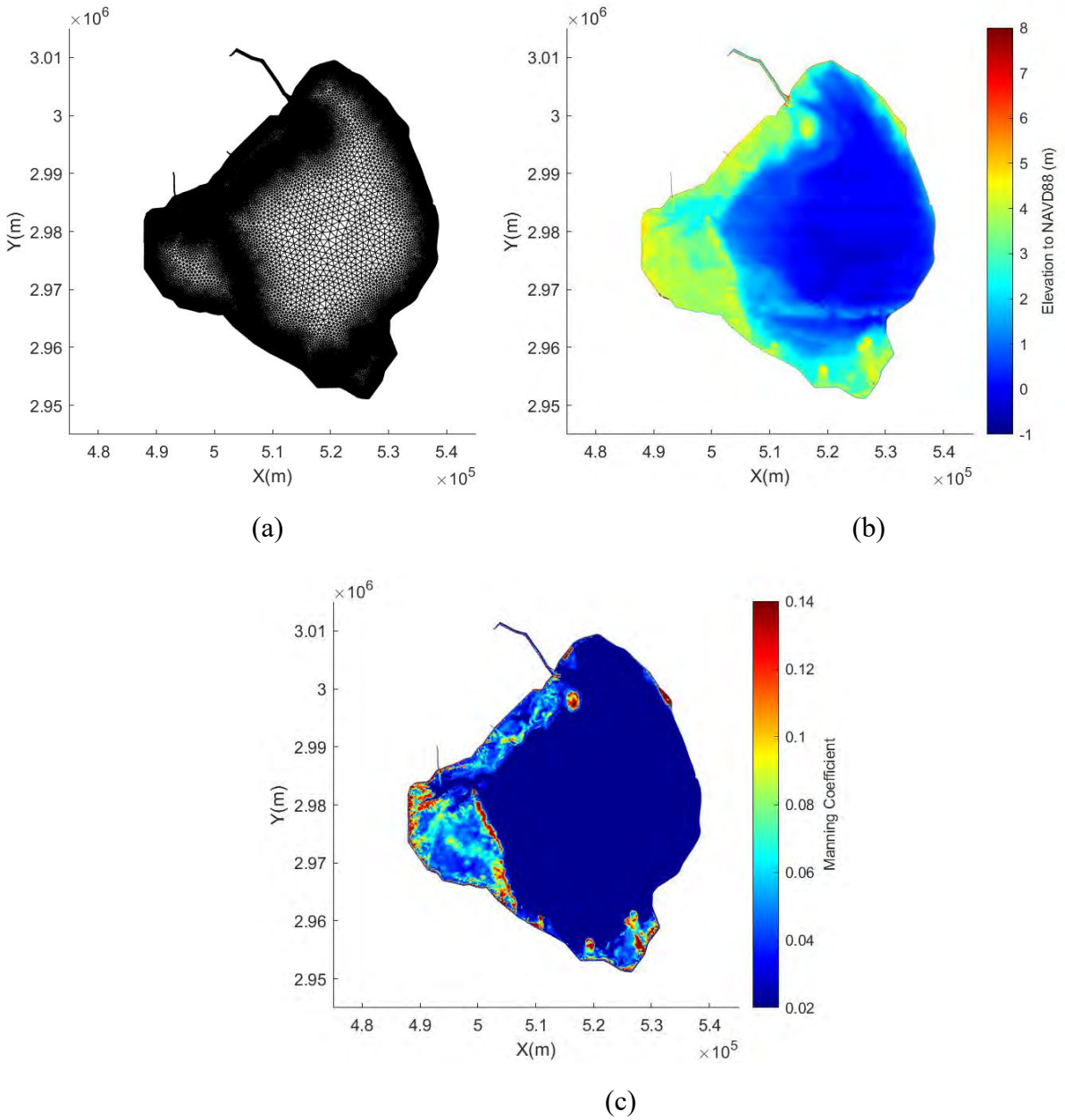

Fig. 2 The computational mesh (in UTM17 coordinate system) (a), the bottom elevation (b) and the Manning coefficient map (c).

Table 1 Computational parameters and CPU time for Frances, Wilma, Matthew and Irma.

	Frances (2004)	Wilma (2005)	Matthew (2016)	Irma (2017)
Simulation start time (UTC)	9:00, 09/02/2004	0:00, 10/22/2005	0:00, 10/06/2016	6:00, 09/08/2017
Simulation Duration (h)	102	90	96	90
Time step (s)	30	30	30	15
CPU cores	14	14	14	14
Computational time (minutes)	36	30	32	49

The simulated maximum surge height across the lake due to the four hurricanes are plotted in Fig.3. It is obvious that Matthew (2016) caused the smallest surge as its track is relatively far away from Lake Okeechobee. Depending on the track direction, Frances (2004), Wilma (2005) and Irma (2017) caused surges propagating to the east, the southwest and the northwest sections of the lake, respectively. Frances and Wilma induced a similar magnitude of maximum surge height around 2 meters, while Irma led to maximum surge of over 3 meters in the west portion of the lake. It is worth noting that no overtopping of storm surge over the HHD are found in the simulation results. Time series of water elevation comparisons between SFWMD measurements and the simulation results are given in Figs. 4 to 7, corresponding to the four hurricanes, respectively. The predictions by the SSFOF model match well with the observations for all scenarios, although slight under-estimation and over-prediction can be seen for Wilma and Irma cases, respectively.

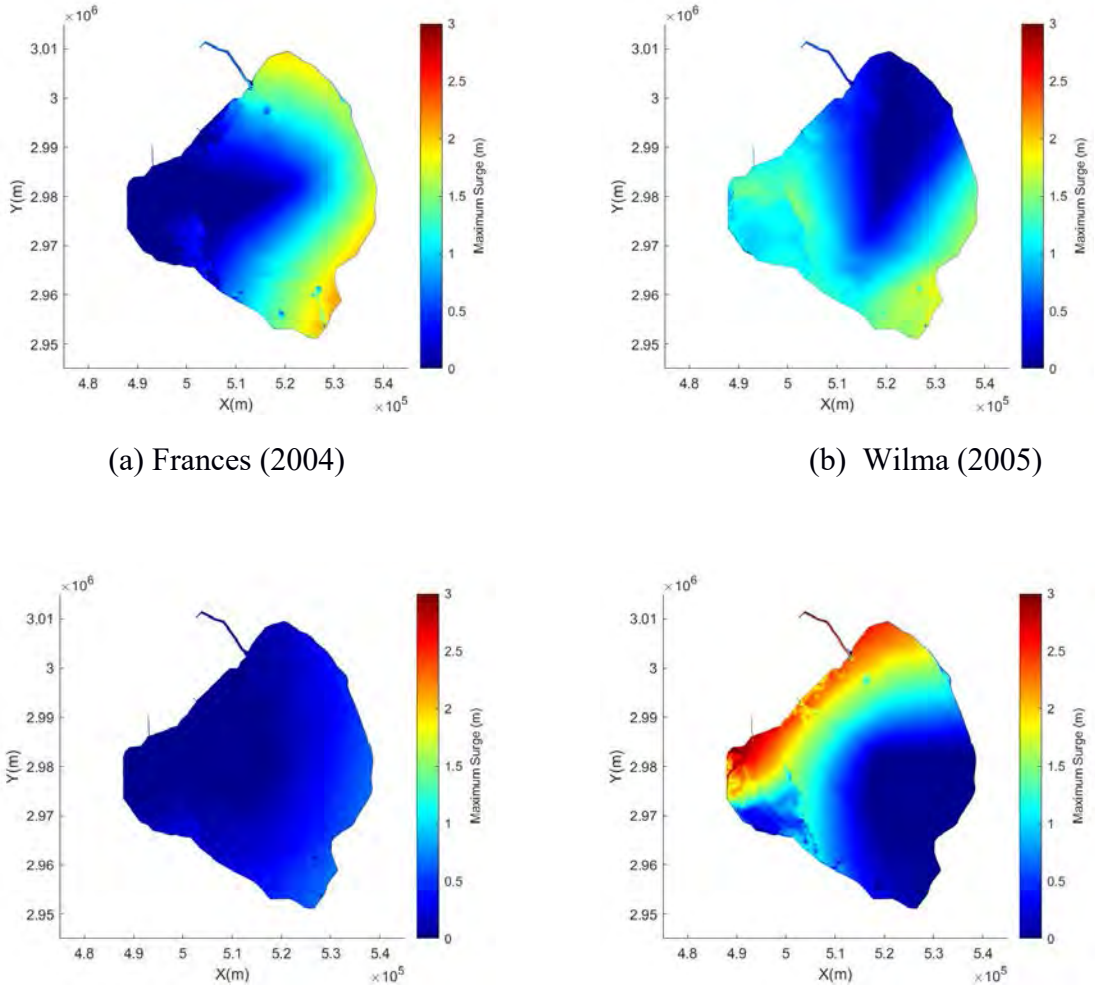

(a) Frances (2004)

(b) Wilma (2005)

(c) Matthew (2016)

(d) Irma (2017)

Fig. 3 Computed maximum storm surge height within Lake Okeechobee for the four hurricanes.

Depending on the relative location of the measurement stations to the hurricane tracks, different pattern of water level change can be observed during hurricane impact (Figs. 4 to 7). Take Frances (Fig. 4) as an example, Stations 06568 and 06636 are located in the south of the lake, while Stations IY368 and IY499 are placed in the north. As all four stations are at the left side of the track direction of Frances, they are expected to experience first southerly and then northerly winds as Frances passes through. Therefore, measurements at Stations 06568 and 06636 exhibit water level increase first followed by a sharp decrease, while those at IY368 and IY499 see the opposite trend. The SSFOF model is capable of capturing this phenomenon.

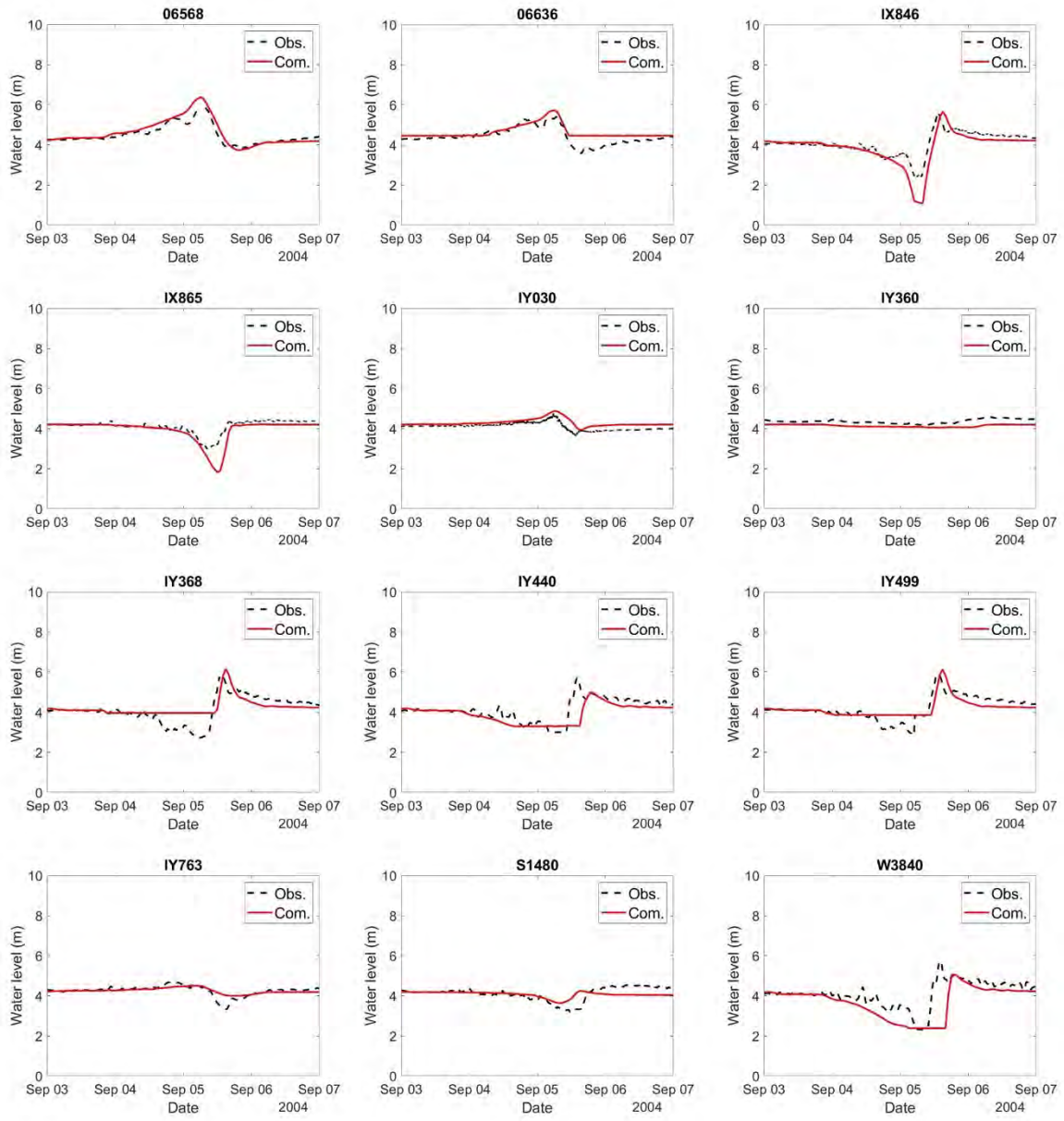

Fig. 4 Comparisons for the time history of water elevations at the measurement stations during Hurricane Frances (2004). Data are referenced to NGVD29.

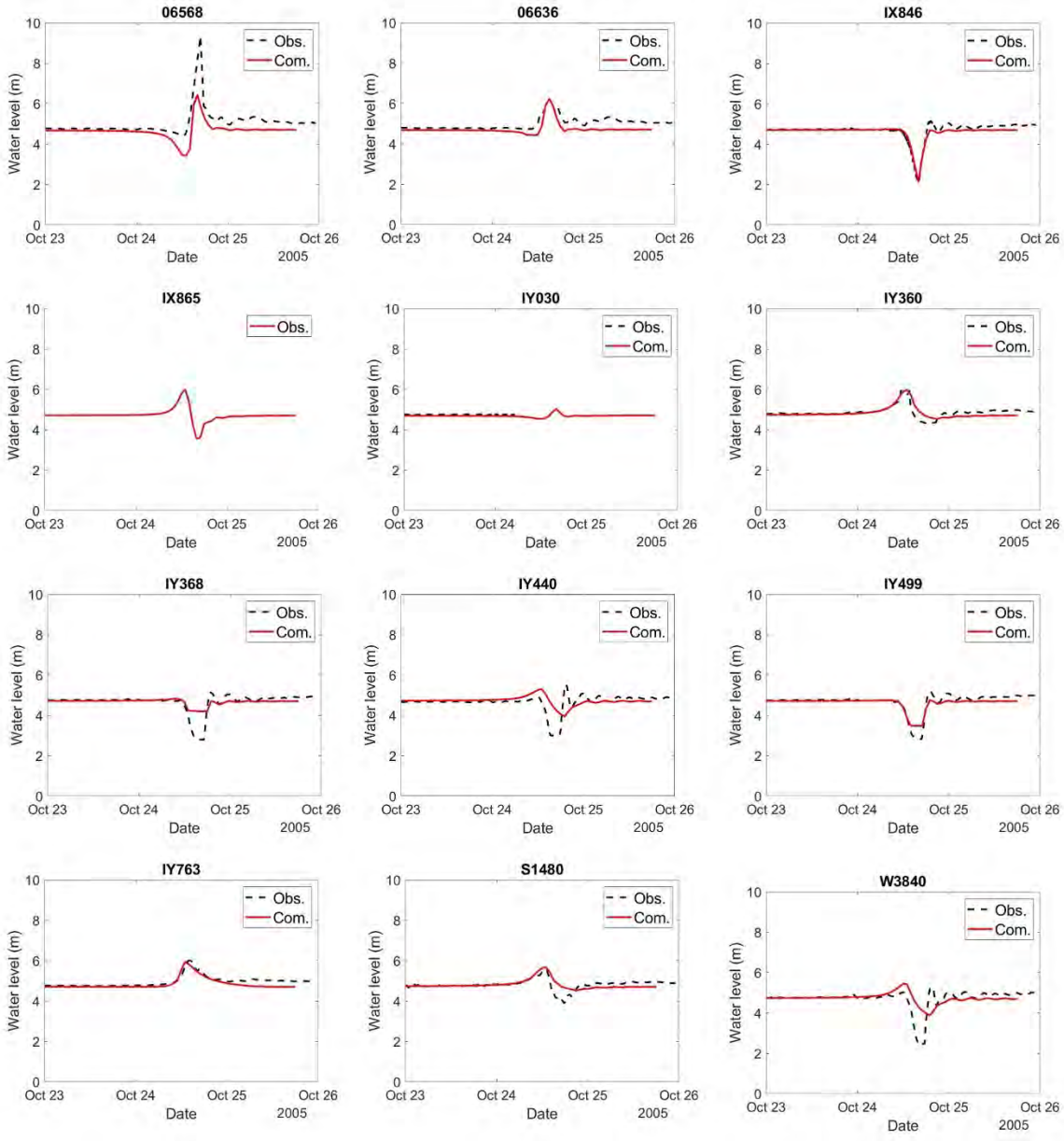

Fig. 5 Comparisons for the time history of water elevations at the measurement stations during Hurricane Wilma (2005). Data are referenced to NGVD29.

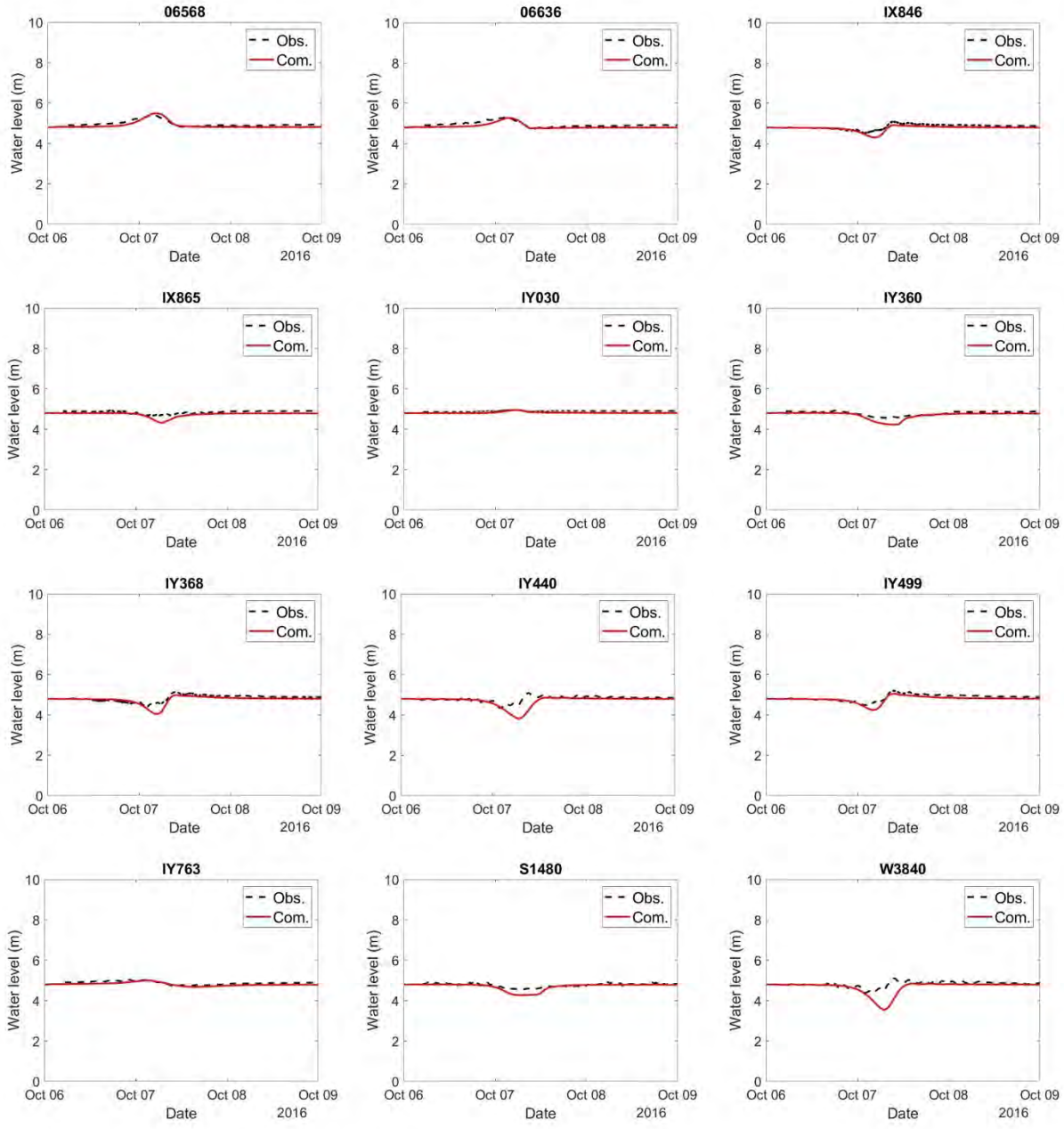

Fig. 6 Comparisons for the time history of water elevations at the measurement stations during Hurricane Matthew (2016). Data are referenced to NGVD29.

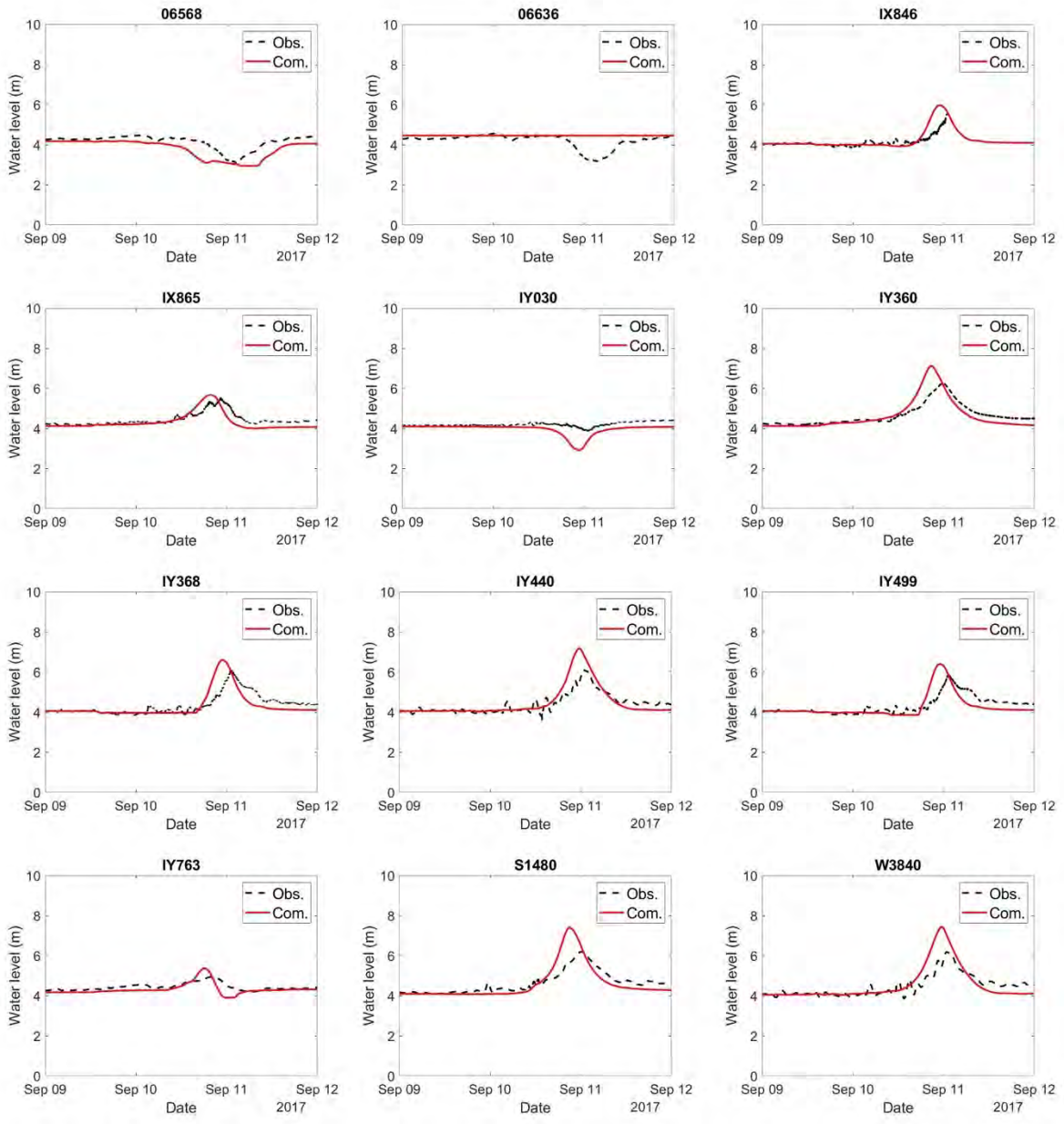

Fig. 7 Comparisons for the time history of water elevations at the measurement stations during Hurricane Irma (2017). Data are referenced to NGVD29.

4. Development of a North Florida Mesh

Fig. 8 shows the model computational domain for the North Florida region, covering almost all of the west coasts of Florida. In this phase of study, two hurricanes, Hermine (2016) and Michael (2018), were employed to test the current model setup and the North Florida mesh. The best

tracks of the two hurricanes are shown in Fig.8, with the NOAA tide gauge location and USGS High Water Marks (HWMs) stations also depicted, where the measured data will be used for model validation. Hurricane Michael (2018) was very powerful and destructive; it was the first Category 5 hurricane to impact Florida since Hurricane Andrew in 1992. Michael (2018) reached peak winds of approximately 160 mph just before making landfall near Mexico Beach on October 10. Hurricane Hermine (2016) struck the Big Bend and made landfall on September 2 just east of St. Marks, Florida, with a maximum sustained winds around 80 mph and a central pressure of approximately 980 mb. Hermine (2016) was the first hurricane to make landfall along the Apalachee Bay coast since 1966.

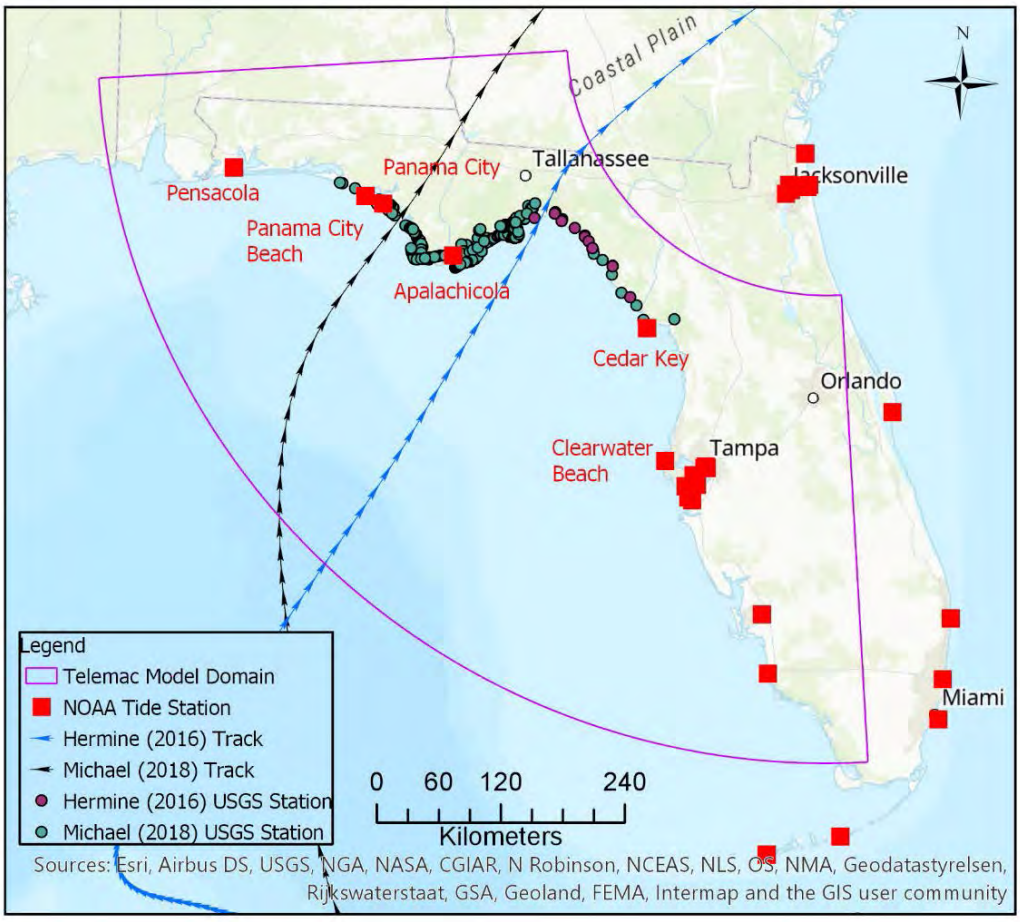

Fig. 8 The North Florida computational domain, the hurricane tracks and the USGS HWM and NOAA tide gauge locations.

Fig. 9 presents the newly generated North Florida mesh. The grid consists of approximately 1 million nodes and 2 million triangular elements, with a grid resolution varying from nearly 10 km in the open ocean area to 100 m along the coastline and other major rivers, roads, and lakes.

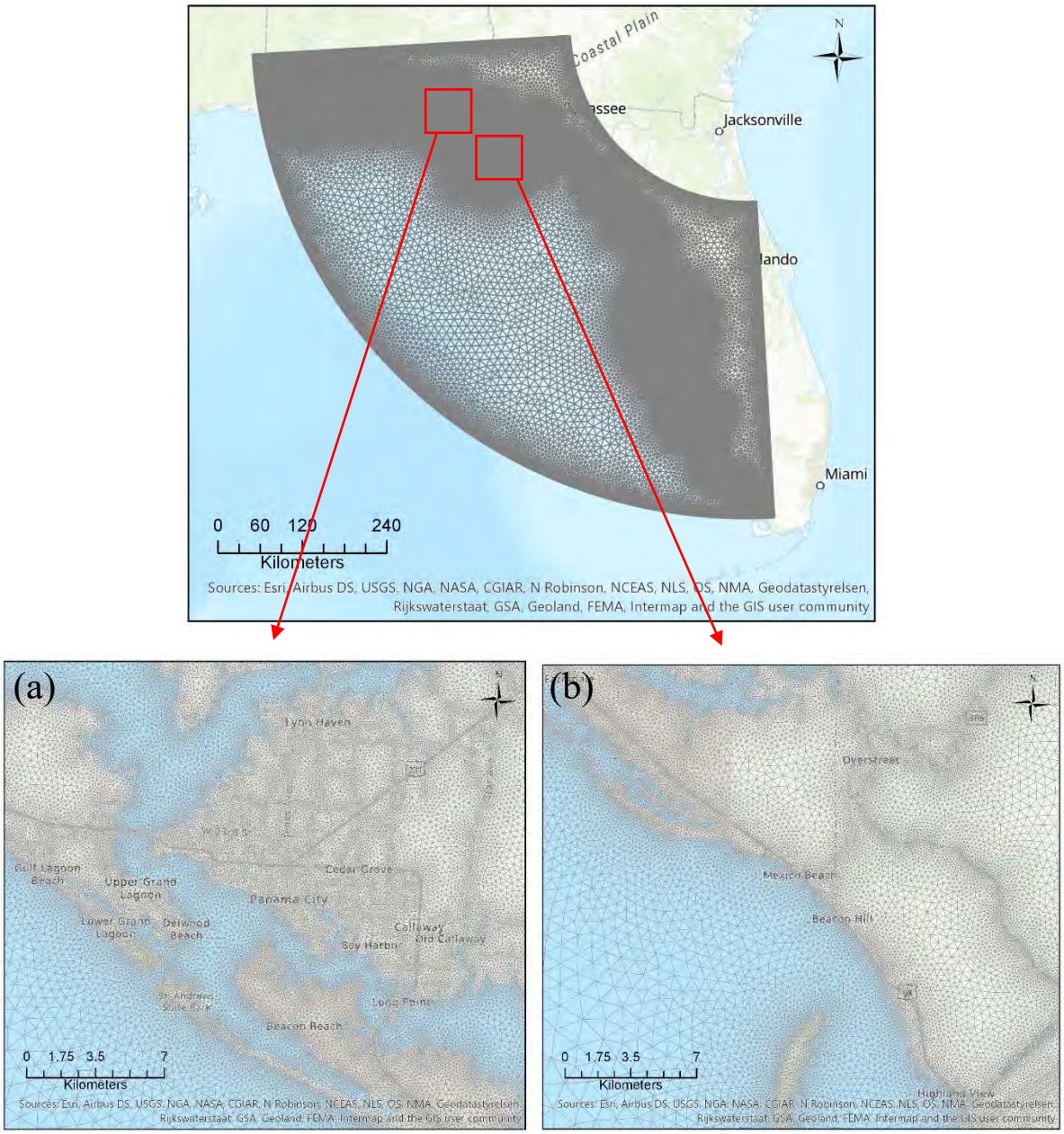

Fig. 9 The North Florida computational mesh (upper panel) and zoomed in views at (a) Panama City and (b) Mexico Beach.

Fig. 10 shows the bottom elevation interpolated on the mesh (referred to NAVD88), which makes use of the Continuously Updated Digital Elevation Model (CUDEM) - 1/9 Arc-Second

Resolution Bathymetric-Topographic Tiles that is being developed by NOAA's national Centers for Environmental Information (NCEI), and NOAA 2-minute Global Relief Model (ETOPO2) (https://www.ngdc.noaa.gov/mgg/coastal/crm.html). The Florida Geographic Data Library (FGDL) 5-m DEM data were employed for the elevation above water (https://www.fgdl.org/metadataexplorer/explorer.jsp) and where the 1/9 Arc-Second Resolution Bathymetric-Topographic Tiles data is not available.

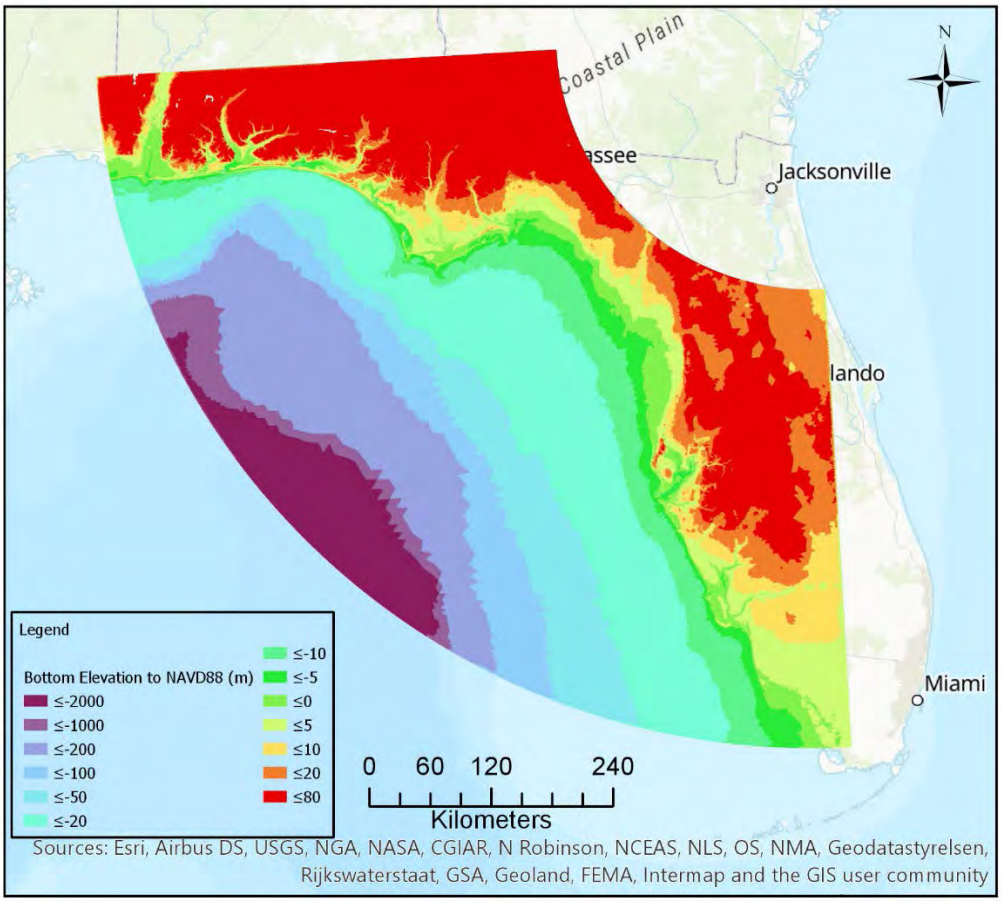

Fig. 10 Interpolated bathymetry and topography on the computational mesh.

The Manning friction coefficient (see Fig. 11) was set to be 0.02 in water areas, and for the wet areas and dry land the Manning coefficient was calculated based on the National Land Cover Dataset (NCLD) 2006, using the method described in Zhang et al. (2012). The initial water level for the whole computational domain was empirically set to 0.4 m according to the NOAA tide gauge measurements before the hurricanes made landfall. The duration of the simulations and

other parameters for each of the hurricane cases are given in Table 2 using coordinated universal time (UTC).

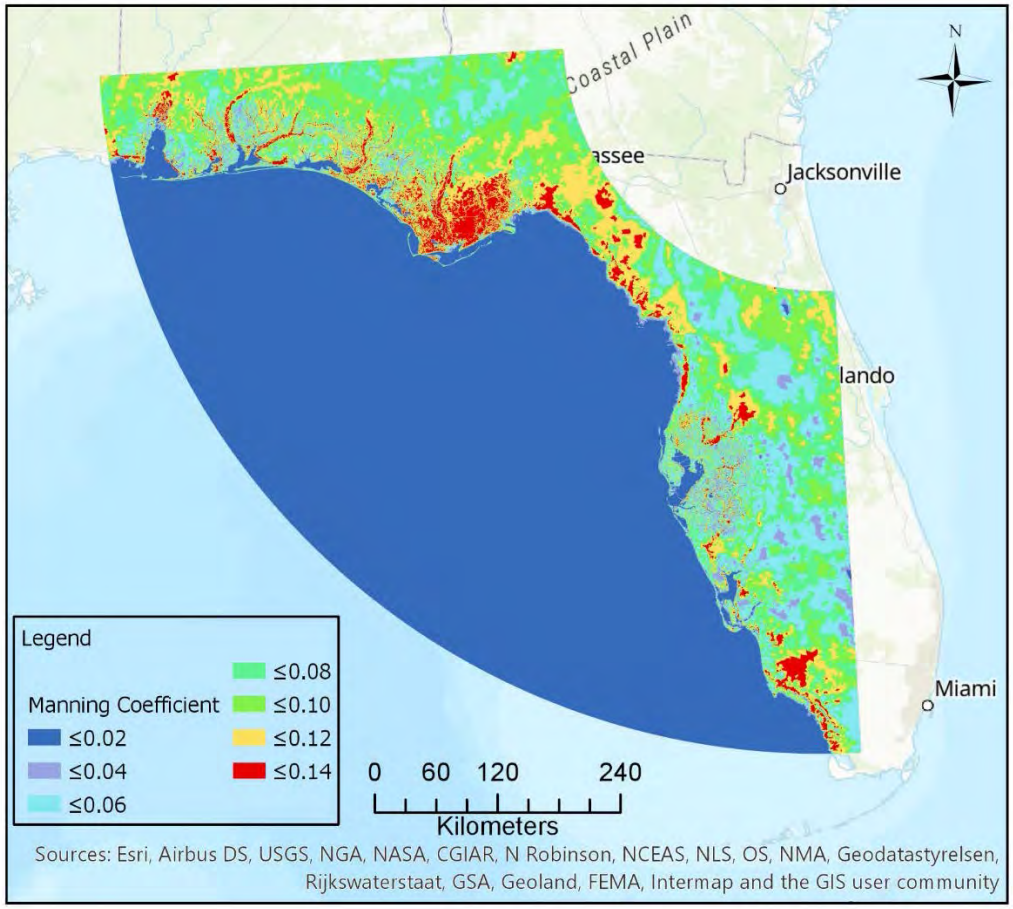

Fig. 11 The calculated Manning coefficients on the computational mesh.

Fig. 12 and Fig. 13 present the computed maximum storm surge height (defined as the maximum value of the increased water level as storms pass through) for Hermine and Michael, respectively. It is obvious that Michael caused much larger storm surge compared to Hermine, in terms of both the overall inundation area and maximum surge height along shorelines. Hermine caused a maximum surge height of approximately 3.5 m in the vicinity of Keaton Beach, the Big Bend, Florida, while Michael resulted in a maximum surge height of around 5 m further north at the Flint Rock Wildlife Management Area, Florida. Furthermore, the peak storm surge heights due to Michael are nearly 3 to 3.5 m from Mexico Beach to Indian Pass, whose locations are at the east side of the track direction and are very close to the landfall point.

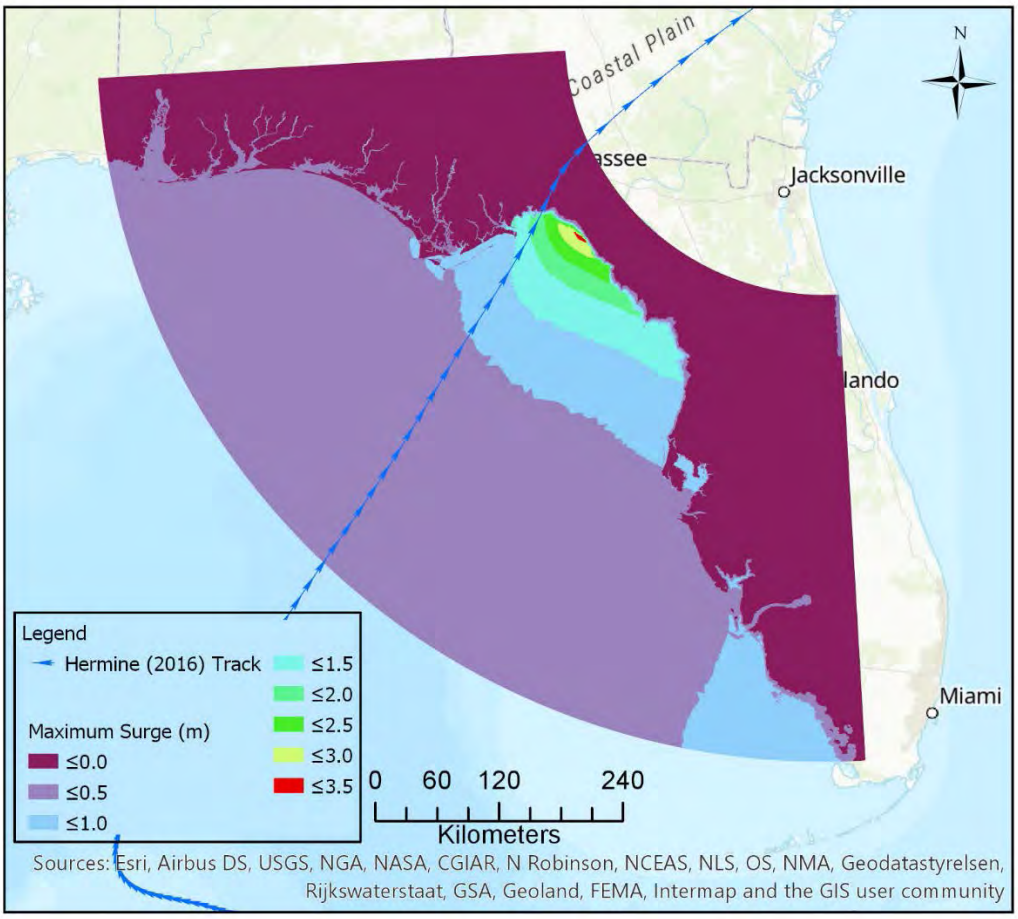

Fig. 12 The computed maximum storm surge height for Hurricane Hermine (2016).

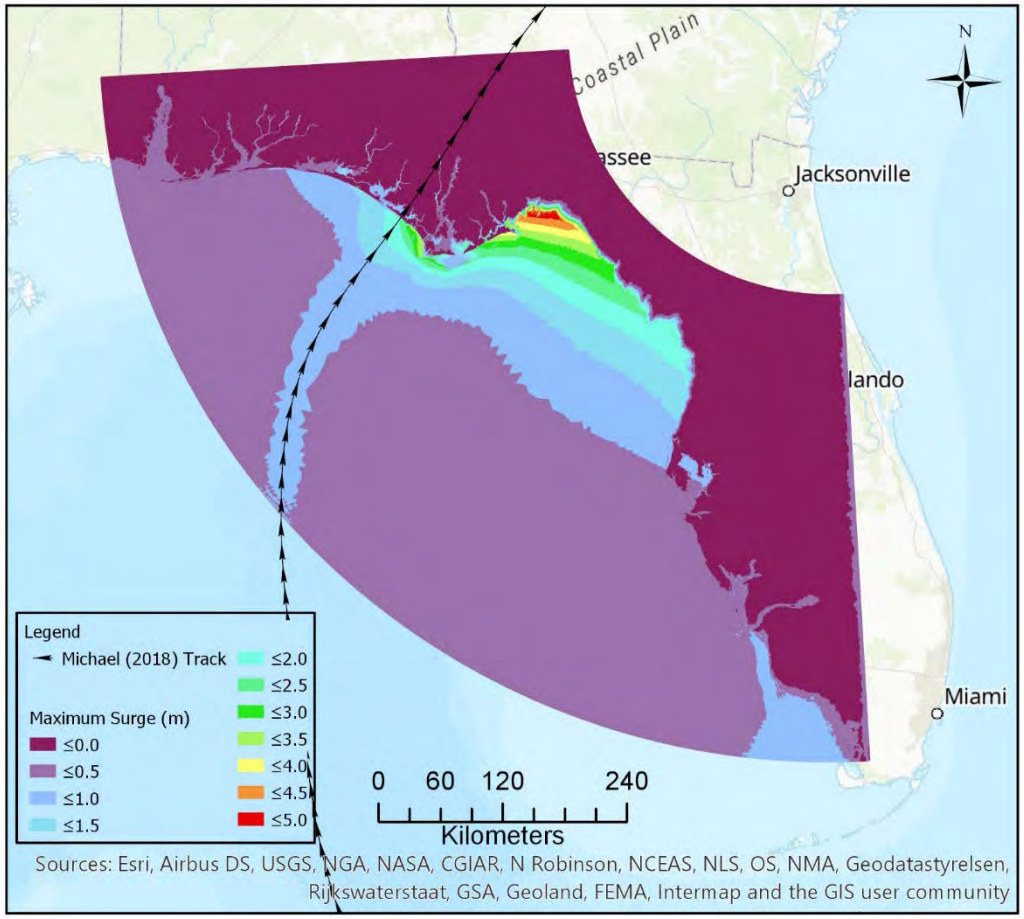

Fig. 13 The computed maximum storm surge height for Hurricane Michael (2018).

Fig. 14 and Fig. 15 plot the comparisons for the water levels at the NOAA tide gauges (see Fig. 8 for the locations) between the computed and observed data. In general, more tide gauges have seen storm impacts during Michael than those in Hermine. The numerical model is able to capture the main trend of the water elevations at these tide gauges for both hurricane scenarios, but produces large discrepancies at some stations for Michael, e.g. Apalachicola. This could be caused by a number of reasons, such as the use of parametric wind fields, accuracy in the bathymetry data, and relatively coarse mesh resolution. These discrepancies can be further researched and improved in the future work.

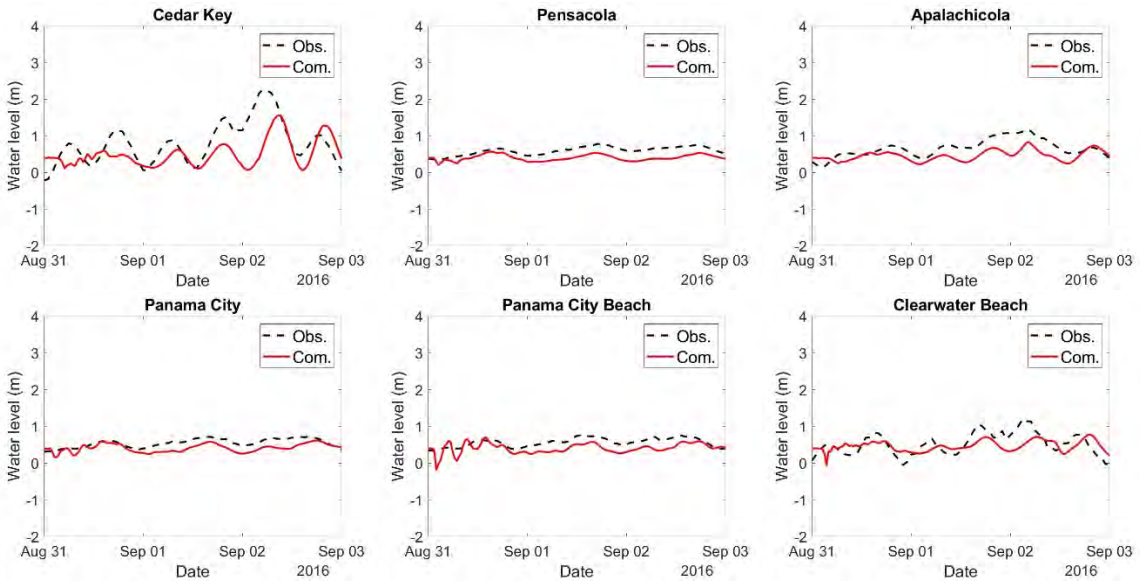

Fig. 14 Comparison between the computed and measured storm tide elevations at the NOAA tide gauges for Hurricane Hermine (2016). Data are referenced to NAVD88 vertical datum.

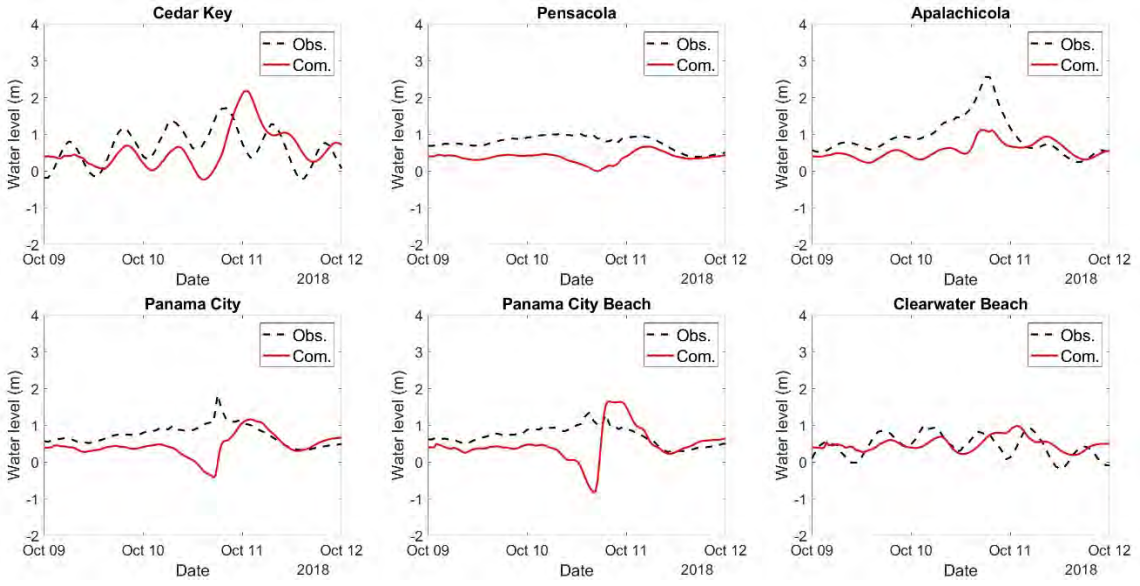

Fig. 15 Comparison between the computed and measured storm tide elevations at the NOAA tide gauges for Hurricane Michael (2018). Data are referenced to NAVD88 vertical datum.

Fig. 16 presents the comparisons for the HWMs at the USGS survey locations (see locations in Fig. 8) between the simulated and measured data. The predicted results for Hermine exhibit smaller root mean square errors (RMSE) and bias compared to those for Michael. In fact, the

HWM result indicates that the storm surge due to Michael was overestimated by the numerical modelling.

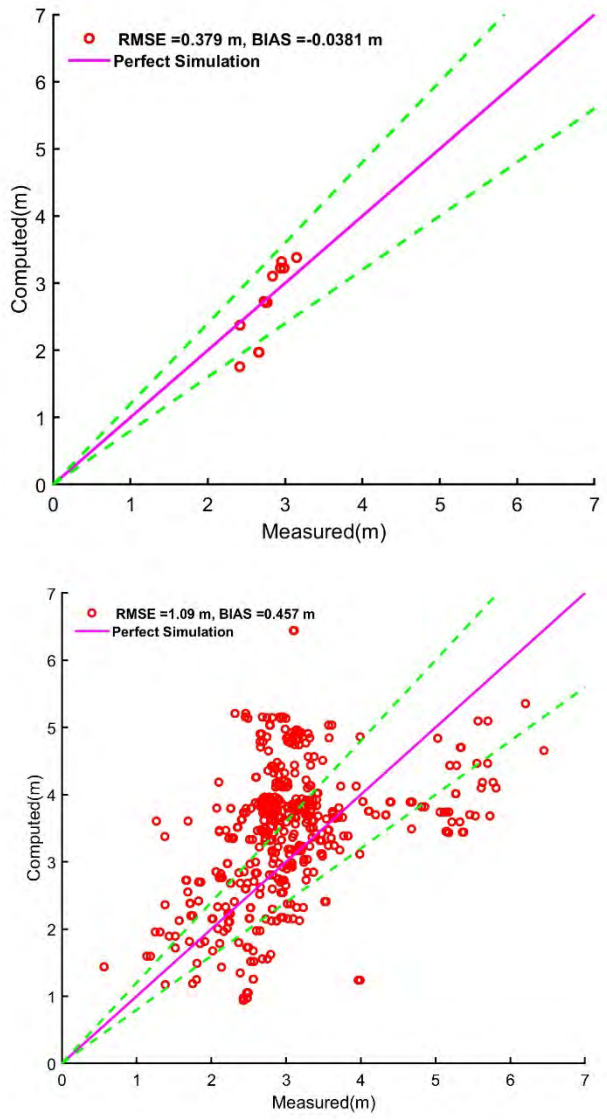

Fig. 16 Comparison between the computed and measured HWMs at the USGS stations for Hurricanes Hermine (upper panel) and Michael (lower panel). Data are referenced to NAVD88 vertical datum. The green dashed lines represent the perfect simulation line multiplied by (100±20)%, respectively.

Table 2 Computational parameters and CPU time for Hermine (2016) and Michael (2018).

	Hermine (2016)	Michael (2018)
Simulation start time (UTC)	0:00, 08/31/2016	0:00, 10/09/2018
Simulation Duration (h)	96	82
Time step (s)	30	30
CPU cores	14	14
Computational time (hours)	2	1.8

5. Towards full 3D modeling and Salt Water Intrusion

Fig.17 presents the TELEMAC3D salinity study area covering Biscayne Bay and particularly Miami River, the focused river to be assessed for Saltwater Intrusion (SI) during storm events. While there are many storms that have struck Miami River directly or indirectly, at this stage of model development, only the case of Hurricane Irma (2017) was used as an initial attempt on SI modeling. Fig.17 also gives the track of Irma, as well as the location of 6 stations for simulation data collection, which are 2.6km (Station 1), 1km (Station 2), 0.4km (Station 3), 0km (Station 4) upstream, and 0.34km (Station 5) and 0.8km (Station 6) downstream (into the bay) from the outlet of Miami River. The Miami River drains out of the Everglades and runs through the city of Miami. Although there are dams on the river to prevent salt water from travelling inland, the SI into fresh water as a consequence of extreme storm events is case dependent and requires detailed investigations.

Fig. 17 The computational domain for saltwater intrusion study, the Irma (2017) track and the simulation result collection stations.

Fig.18 shows the generated 2D grid for the computational domain and a zoom-in view of that around the Miami River outlet. As a 3D modeling, a 6-layer sigma grid setup was used, which leads to approximately 1.3 million nodes and 6.3 million elements. The grid resolution changes from 10 m around the Miami River outlet to approximately 3.5km at the open waters. Fig.18 also presents the interpolated bathymetry and topography. The topographic data used in this study is mainly derived from the US Geological Survey (USGS), and the bathymetric data comes from NOAA. Water depths for grid cells at the open ocean were calculated based on the ETOPO1 global relief dataset from NOAA, which has a resolution of 1 arc minute (~1.8 km). Water depths for grid cells in coastal areas were interpolated from the U.S. coastal relief dataset from NOAA with a resolution of 3 arc second (~90 m) (http://www.ngdc.noaa.gov/mgg/gdas/gd_designagrid.html). The USGS 90 m, 30 m, 10 m, and 3 m digital elevation models (DEM) were used to calculate the elevation of grid cells on the land

(http://viewer.nationalmap.gov/viewer/) in terms of the sizes of grid cells. The interpolated elevations are referred to the NAVD88 vertical datum. For this initial attempt, the Manning coefficient was fixed at 0.02 for water areas and 0.06 for land areas according to the initial water depth.

The current simulation regarding storm-induced saline intrusion was limited to a qualitative study during Phase 3. The salinity setup is as follows: at the upstream river discharge boundary the salinity is set to a constant value of 2 ppt, at the outside tidal boundary salinity is fixed at 35.2 ppt, and inside the computational domain the initial salinity is given 0 ppt in the Miami River and land areas, and 35.2 ppt in the rest water areas. Since 35.2 ppt is the given maximum value, the simulation result with regard to the salinity within the whole computational domain can be expected to be no larger than 35.2 ppt at all times. These values were assumed based on the report of Bellmund et al. (2008). The tide boundary condition in this study employs the TPXO9 tidal data base (https://www.tpxo.net/global/tpxo9-atlas), and the river discharge uses the data from DBHYDRO database that is managed by SFWMD. The simulation, starting from 00:00 September 07, 2017 and ending at 00:00 September 13, 2017, lasts for 6 days and the impact due to Irma occurred at around 10:00am September 10, 2017. The simulation took roughly 7 hours to complete with 30 cores at a workstation in IHRC.

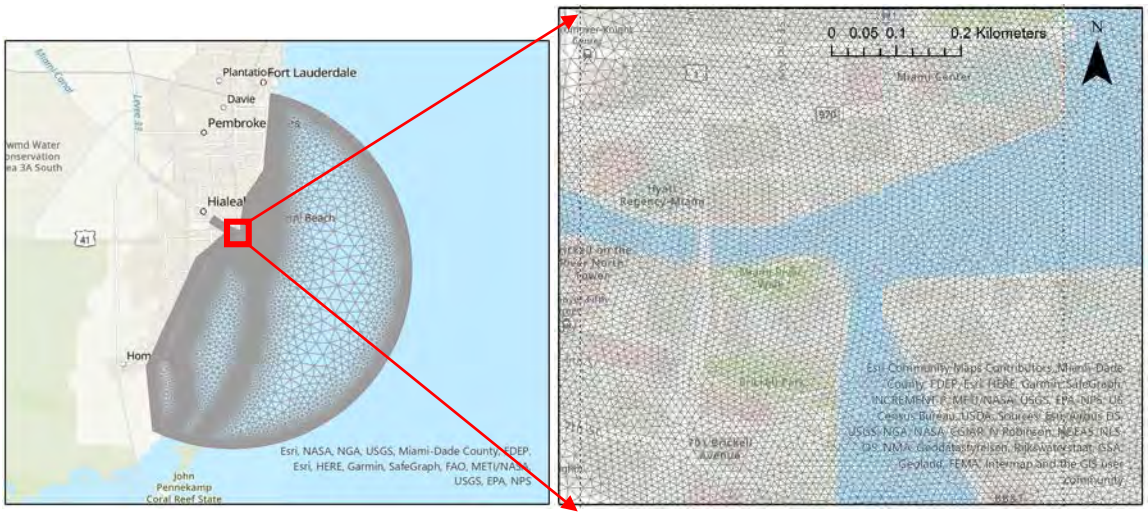

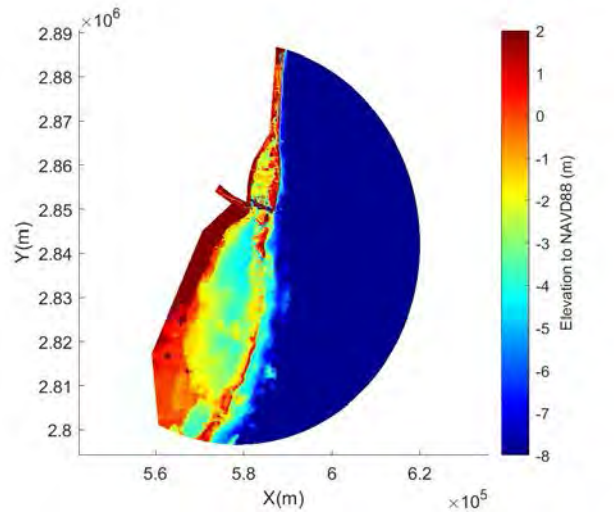

Fig.18 The computational mesh for saltwater intrusion study (upper panels) and the bathymetry and topography interpolated on the computational mesh (lower panel).

Fig.19 shows the snapshots of the simulated salinity distribution at various time instants around the Miami River outlet during the impact of Hurricane Irma (2017). From September 10, 00:00 to September 10, 06:00, the high salinity traveled nearly 1km upstream the river and ebbed afterwards owing to the tidal effect. From September 10, 09:00 onwards, the salinity started to intrude further upstream due to the passing of Irma, which caused storm surge inside the Miami River. The salinity traveled as far as 4km upstream according to the simulation and then receded back into the bay due to the discharged river flows upstream. After Irma has passed through Miami, the salinity inside the Miami River, particularly around the outlet, remained relatively low concentration compared to regular conditions, which is likely to be caused by the continuous large river discharge flows upstream due to rainfalls.

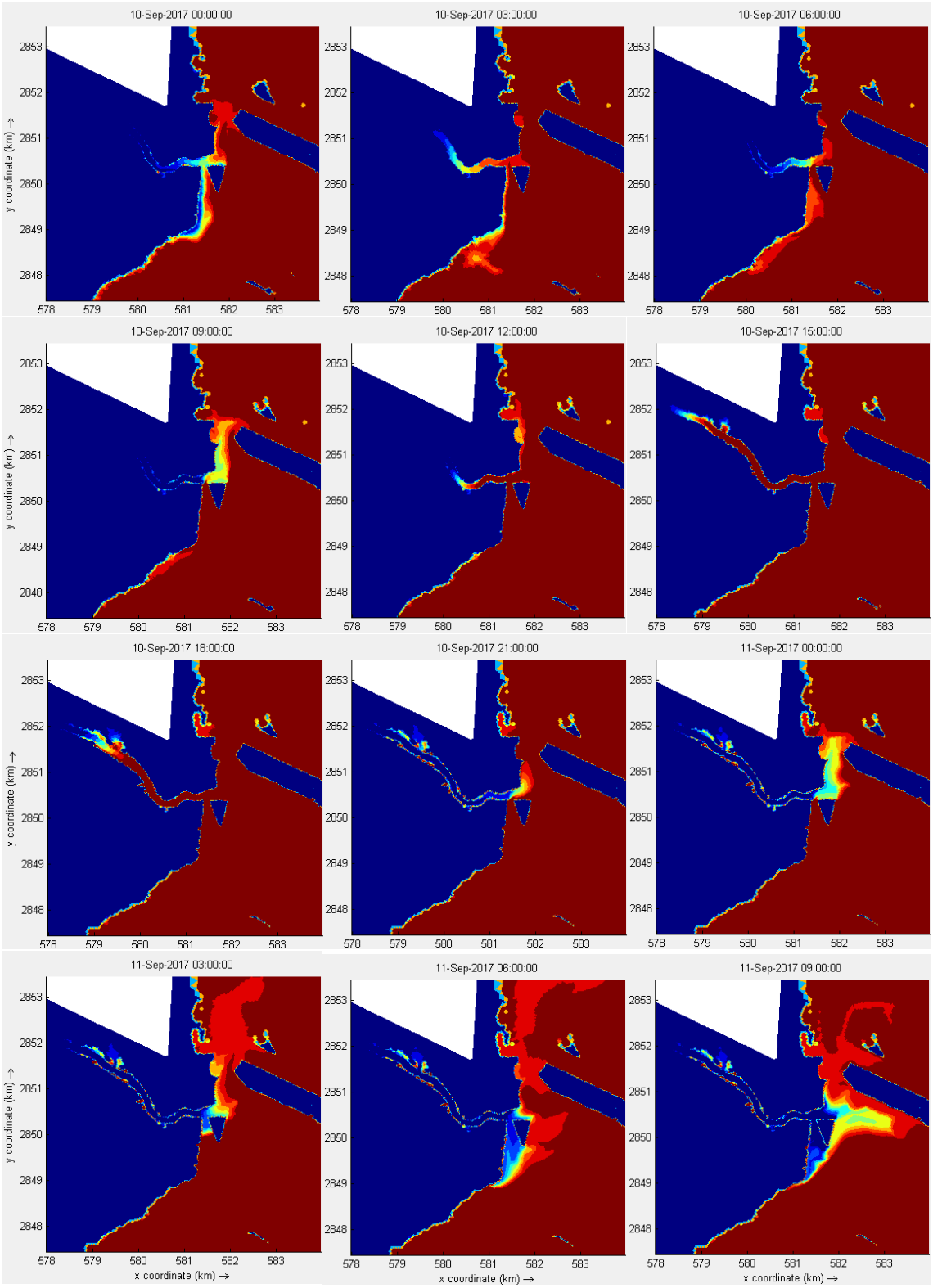

Fig.19 Snapshots of the simulation results for the salinity around the Miami River outlet during and after Hurricane Irma (2017).

Fig.20 shows the time history of salinity concentration at the six data collection stations (see location in Fig.17) during Irma (2017). The salinity at three different sigma layers from the bottom to the top, namely layers 1, 3, and 6, are plotted together for comparison. First of all, it is clear that 85 hours since 00:00 September 07, 2017, the salinity at all six locations reaches a maximum value of 35.2 ppt due to the impact of Irma causing sea water to propagate upriver. The duration of this maxima, however, varies according to the locations; in general, stations at the upstream experience shorter time period of the 35.2 ppt maximum value. It is also seen that at Station 1, 2.6km upstream the outlet, the maximum salinity at regular tidal conditions is the lowest of all stations, and after Irma, the salinity remains at 2 ppt (the same as that given in the upstream river discharge boundary) for a few more days, indicating that the salinity at this station is less affected by the sea water at regular tidal conditions. However, as the stations moving downstream, this maximum salinity at regular tidal conditions increases to 35.2 ppt gradually (see Stations 2, 3 and 4). Specially, Station 4, which is at the Miami River outlet, the salinity appears to be affected by both the tidal effect and the river discharge after Irma has passed; the stratification of salinity is clearly seen that at the top layer the salinity is lower than that at the bottom layer. This salinity stratification is also seen at Station 5, located in the Biscayne Bay near Miami River outlet, during regular tidal conditions and after the passing of Irma. However, this phenomenon almost disappears at Station 6, further far away from the river outlet. This is likely a reflection of the model setup (all six layers were initially given the same 35.2 ppt value), rather than physically correct. Furthermore, it is seen from Stations 5 and 6 that after Irma has passed, the minimum value of salinity is lower than that before the impact of Irma, which is also likely to be an outcome of the large river discharge upstream Miami River.

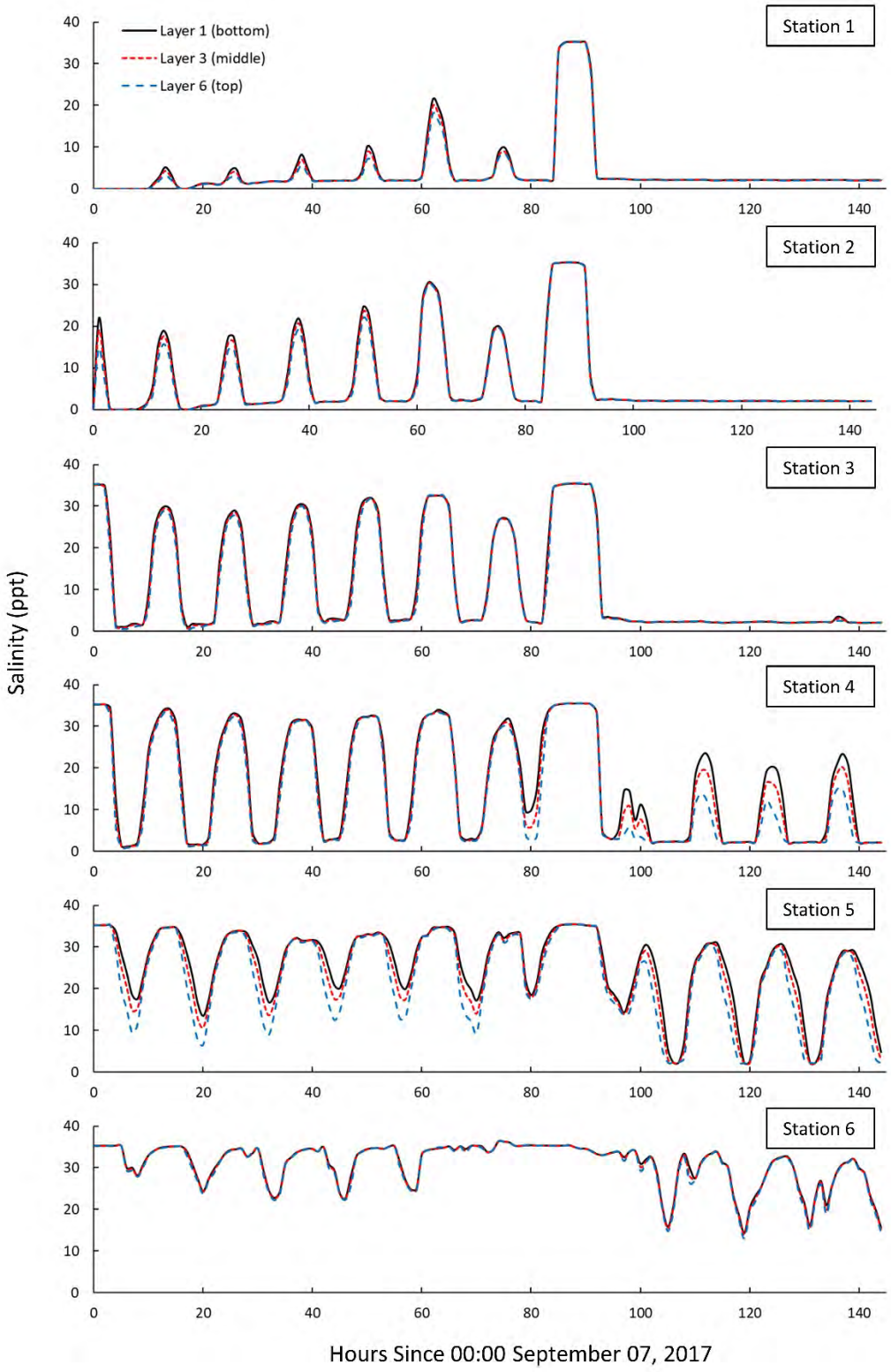

Fig.20 Time series of the salinity extracted at the six stations (see station location in Fig.17), with comparison between values at layers 1 (the bottom layer), 3 (the middle layer) and 6 (the top layer) at each station.

6. Proposed Future Work

This study has demonstrated that the SSFOF model represents the cutting-edge storm surge model. However, as seen from some of the results, there are still areas for improvement in the next phase of study, particularly focusing on the North Florida region.

Re-analysis Wind Data. At present, the SSFOF model generates its own wind field based on parametric wind models. However, it is desirable that the model can read in temporal and spatial varying wind data provided by meteorology models. Wind field is the key drive for storm surge models; this capability will certainly improve the simulation results.

Rainfall Runoff Model. Although the SSFOF model already has a Curve Number (CN) based rainfall runoff model, it was not employed for the simulations in this phase of study. In the next phase, it is planned that simulations will be re-run to include the Next Generation Radar (NEXRAD) data covering North Florida.

Riverine Systems. In the work presented here for the North Florida region, the dynamic interaction between river discharge and storm surge is not included in the modelling. The storm surge propagation upriver currently predicted by the model may be not reliable due to the missing of this physics. Inclusion of this effect could improve the modelling results especially around river outlets.

Reference

Sawyer, A.H., David, C.H. and Famiglietti, J.S., 2016. Continental patterns of submarine groundwater discharge reveal coastal vulnerabilities. *Science*, *353*(6300), pp.705-707.

Hervouet, J.M., 2007. Hydrodynamics of free surface flows: modelling with the finite element method (Vol. 360). New York: Wiley.

Li, Y., Teng, Y.C., Kelly, D.M. and Zhang, K., 2016. A numerical study of the impact of hurricane-induced storm surge on the Herbert Hoover Dike at Lake Okeechobee, Florida. *Ocean Dynamics*, *66*(12), pp.1699-1714.

Zhang, K., Liu, H., Li, Y., Xu, H., Shen, J., Rhome, J. and Smith III, T.J., 2012. The role of mangroves in attenuating storm surges. *Estuarine, Coastal and Shelf Science*, *102*, pp.11-23.

Bellmund, S., Renshaw, A., Jobert, H., Garis, G., 2008. Annual Report-Salinity Sampling in Biscayne Bay (2006-2007). Biscayne National Park.

A Resource for the State of Florida

SECTION 6
INVESTIGATION AND INCORPORATION OF WOW TESTING OUTPUTS IN THE FLORIDA PUBLIC HURRICANE LOSS MODEL

A Report Submitted to:
The State of Florida Division of Emergency Management

Prepared By:
Kurt Gurley, Ph.D.
Professor of Civil and Coastal Engineering
Engineering School for Sustainable Infrastructure and Environment
University of Florida
kgurl@ce.ufl.edu

Jean-Paul Pinelli, P.E., Ph.D.
Professor
Department of Civil Engineering
Florida Institute of Technology
pinelli@fit.edu

The International Hurricane Research Center (IHRC)
Florida International University

April 15, 2021

Executive Summary

The Florida Public Hurricane Loss Model (FPHLM) is a risk hazard model that is updated periodically as new information is discovered regarding the performance of residential construction in hurricane winds. For the current performance period, three tasks were proposed to investigate the possible incorporation of recent FIU Wall of Wind (WOW) experimental outcomes within the FPHLM.

Task 1: Results of roof to wall connection (R2WC) uplift research carried out at the WOW were compared to the current uplift model employed by the FPHLM. The primary finding to date is that the current FPHLM method to load R2WC using component and cladding loading and tributary area is supported by the WOW findings, while the specific load values and distribution with location warrants additional consideration.

Task 2: Non-breach related leakage paths (defects) have long been incorporated in the FPHLM to account for water ingress, but the influence of such paths on internal pressure is not yet well understood nor implemented in the FPHLM. The WOW sequence of tests on internal pressure due to varying controlled aperture sizes provided an initial benchmark to develop an internal pressure model that is sensitive to both approach wind direction and defect size. Preliminary simulations indicate a potentially significant influence on FPHLM loss outputs that requires further model development.

Task 3: Ongoing WOW research concerning pressure loads on non-rectangular building plans offers a potentially significant expansion to the library of rectangular models currently employed in the FPHLM. As of the end of this performance period, results of the WOW research are not far enough advanced to determine whether non-rectangular models should be developed for the FPHLM.

Methods and Findings: Task 1

Feng et al. (2020) documents the primary WOW research that informed the current study. WOW experiments that directly monitored uplift loads at roof to wall connection (R2WC) were compared with calculations of these loads projected using ASCE 7-16 Wind Load Provisions for the test

subject. Both the main wind force resisting system (MWFRS) and component and cladding (C&C) approaches. Although the relative difference between test loads, MWFRS and C&C calculations varied with specific truss and wind direction analyzed, typically the C&C and MWFRS calculations were conservative and un-conservative, respectively, with respect to the measured test loads. Currently the FPHLM employs R2WC loads based on directionalized C&C loads from ASCE 7 (prior to the 2016 guidance). As such the model is not underestimating component loading and therefore damage but is in need of refinement to incorporate ASCE 7-16, which includes significant changes to the C&C roof load coefficients.

The FPHLM is expected to be re-evaluated for certification in Florida based on a planned 2022 fall model submission. A significant portion of the upgrades to FPHLM scheduled for development before fall 2022 is to develop a vulnerability model that utilizes ACSE 7-16 C&C loading to best reflect the latest state-of-knowledge. This will be an 18 month task incorporating overhauls of several FPHLM vulnerability components. The WOW testing of R2WC loads will be among the primary sources of calibration during this development.

Methods and Findings: Task 2

Many of a residential building's exterior components experience an overall net pressure from both internal and external pressure (e.g. roof sheathing, doors, windows), and thus small changes in the internal pressure can influence component loading and thus vulnerability. The current FPHLM internal pressure model assumes simple enclosed status of any building model with no breaches, and then modifies the internal pressure upon breach of door(s) and window(s) from overpressure or debris damage. The primary goal of this investigation is to determine whether this simple internal pressure model is sufficient, or whether the reality of non-breach related building defects and gaps in the building exterior render the enclosed assumption of internal pressure inaccurate and in need of refinement.

An internal report of WOW experimental findings provided by Erwin et al. (2020) included the calculation of 3-second gust internal pressure coefficients of an enclosed building with carefully controlled aperture sizes representing non-breach related building defects such as gaps around fenestration, ridge vents, etc. Figure 1 presents a screen capture from that internal report, and represents the basis for this investigation. The primary finding relevant to the current investigation

is that internal pressure is influenced by small gaps, and this influence can change dramatically with approach wind direction relative to the aperture (defect). Neither affect is currently captured in the FPHLM.

The FPHLM personal residential models (weak, medium and strong strength versions) were modified by replacing the assumed ASCE 7-98 based constant internal pressure value for an enclosed structure with a directionally dependent value based on the data in Figure 1. For the purposes of this preliminary study, the weak model was presumed to have the most gaps, the medium with fewer gaps, and the strong model with the fewest gaps. These were chosen as the data marked as '5', '4' and '2', respectively, in the legend of the right graph in Figure 1.

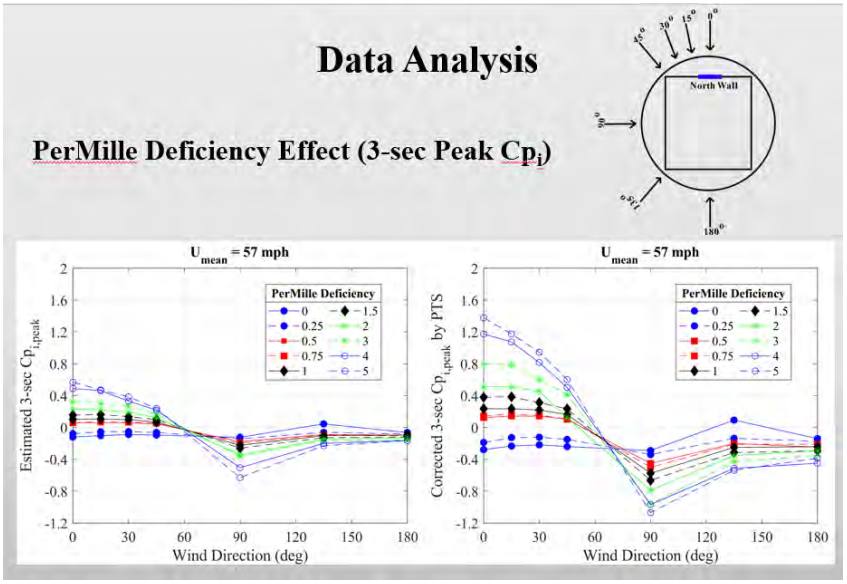

Figure 1: Screen capture from Erwin et al. (2020) FIU WOW report on internal pressure on buildings with controlled aperture sizes.

Figures 2, 3 and 4 present the results for the weak, medium and strong models, respectively. Each figure presents two plots. The left plot presents results prior the internal pressure model modifications, and the right plot presents results after these modifications. Each plot contains the vulnerability of six building components (Legend Key: RC – Roof Cover, Windows from pressure and Windows$_{SM}$ – windows from debris impact, Walls, r2w – roof to wall connections, Decking – roof sheathing, and Doors) as function of 3-second wind gust, averaged over 8 directions using 1000 simulations from each wind speed and direction. The last entry in the legend (IntPresRat) corresponds to the vertical scale on the right side of each plot, and represents the ratio of the

internal pressure at a given speed to the ASCE 7-98 internal pressure coefficient for enclosed buildings. As wind speed increases, windows and doors begin to break, leading to large changes in internal pressure and thus variation in this ratio.

The important outcomes from this study, as observed in each of the Figures 2, 3 and 4, is that the modification in internal pressure model to accommodate non-breach leakage paths does influence the FPHLM modeled vulnerability of most building components, with the exception of window vulnerability to debris impact. In fact, the influence appears to be a universal increase in building vulnerability to some degree. As the incorporation of ASCE 7-16 throughout the model is developed over the next year, this internal pressure modification will be included in this development. When that work is completed, these preliminary findings will be accompanied by monetary loss projections in the form of loss ratios ($ damage over building value).

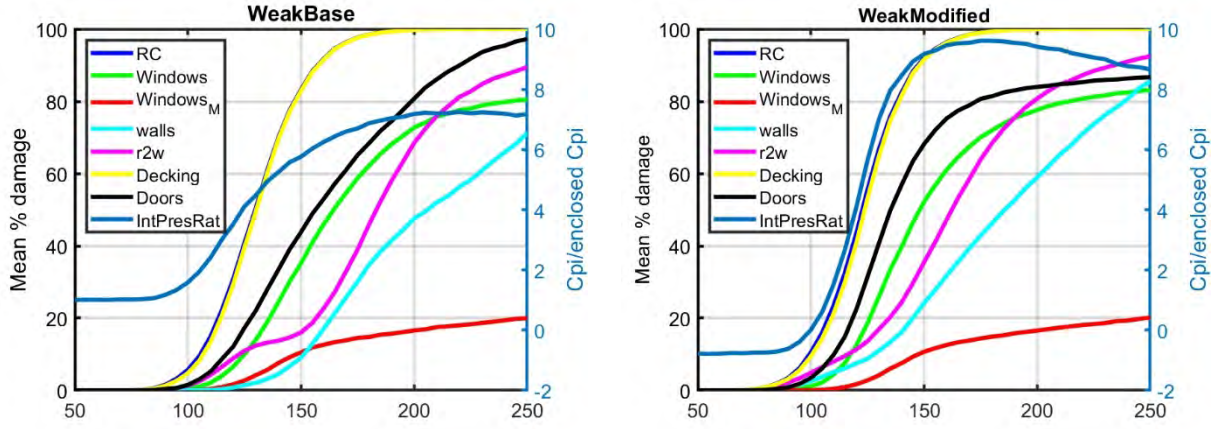

Figure 2: Weak Model - Six component vulnerabilities as a function of wind speed, and actual internal pressure coefficient in ratio with the fixed ASCE 7-98 internal pressure coefficient. Left: prior to modification to internal pressure model (Base). Right: After modification to internal pressure model (Modified).

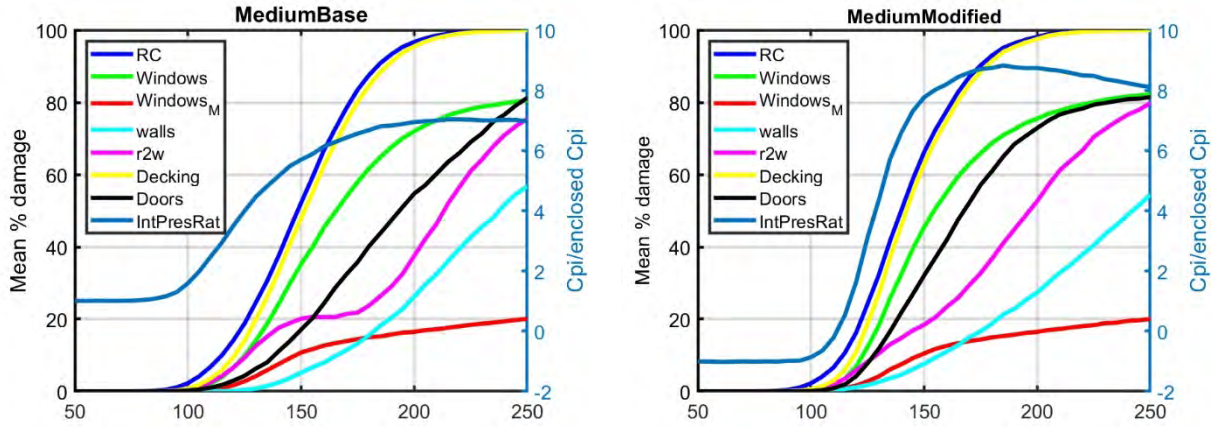

Figure 3: Medium Model - Six component vulnerabilities as a function of wind speed, and actual internal pressure coefficient in ratio with the fixed ASCE 7-98 internal pressure coefficient. Left: prior to modification to internal pressure model (Base). Right: After modification to internal pressure model (Modified).

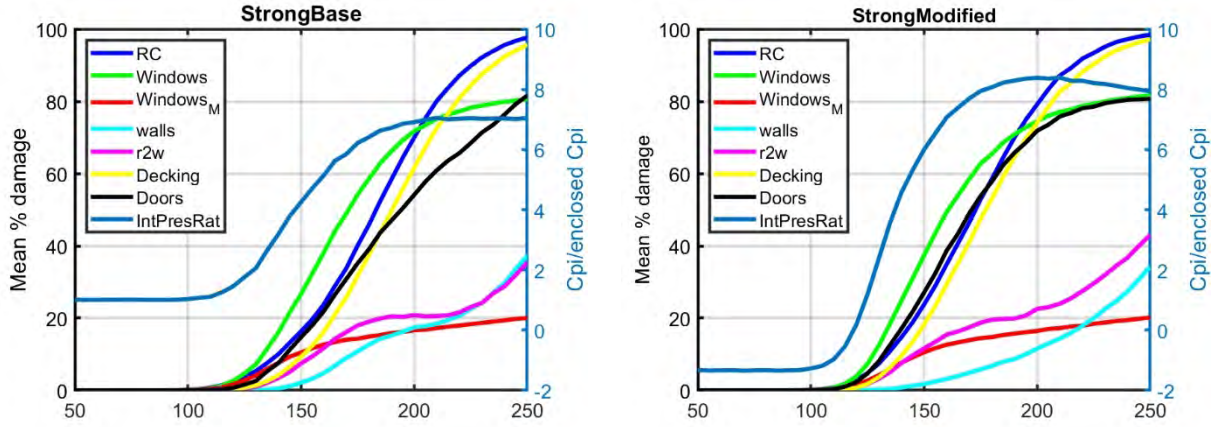

Figure 4: Strong Model - Six component vulnerabilities as a function of wind speed, and actual internal pressure coefficient in ratio with the fixed ASCE 7-98 internal pressure coefficient. Left: prior to modification to internal pressure model (Base). Right: After modification to internal pressure model (Modified).

References:

Feng C, Gan Chowdhury A, Elawady A, Chen D, Azzi Z and Vutukuru KS (2020) Experimental Assessment of Wind Loads on Roof-to-Wall Connections for Residential Buildings. Front. Built Environ. 6:10. doi: 10.3389/fbuil.2020.00010.

Erwin, James and team members. (2020). FIU WOW Wind Internal Report: Experimental and

Analytical Assessments of Effects of Leakage around Doors, Windows, and Other Openings on Internal Pressures in Residential Buildings.

A Resource for the State of Florida

SECTION 7
EDUCATION AND OUTREACH PROGRAMS TO CONVEY THE BENEFITS OF VARIOUS HURRICANE LOSS MITIGATION DEVICES AND TECHNIQUES

A Report Submitted to:
The State of Florida Division of Emergency Management

Prepared By:
Erik Salna

The International Hurricane Research Center (IHRC)
Florida International University

April 15, 2021

Executive Summary:

The FIU International Hurricane Research Center (IHRC) developed and coordinated education and outreach activities to build on the foundation of previous work under this grant and showcased the hurricane-loss mitigation objectives of the HLMP.

For the 2019-20 performance period, the below mentioned educational partnerships, community events, and outreach programs were developed:

Wall of Wind Mitigation Challenge (WOW! Challenge): Cancelled due to COVID-19.

The following was completed before the COVID-19 pandemic closed FIU and Miami-Dade County Public Schools campuses and both went to virtual and remote operations.

- Wall of Wind Research team determined the Challenge would focus on wind mitigation solutions for a flat roof.
- Conducted Wall of Wind Challenge information workshop on February 21st, 2020.
- Registered 9 high school teams for the Challenge which was scheduled for April 24th, 2020 at FIU.
- Rooftops for each team were constructed. It was decided that the 2021 competition would employ the same challenge and the rooftops would be used the following year under the FY 2020-2021 contract.

Hurricane STEM Science, Mitigation and Preparedness Education Learning Modules (6th Grade and High School): March 31st, 2021

A contract modification was executed with the Division when the Wall of Wind Mitigation Challenge was cancelled due to COVID-19. Funds were rededicated to create virtual hurricane learning modules for 6th grade and high school classrooms. The learning modules teach students about hurricane STEM science, mitigation, preparedness, and wind engineering. They also teach about emergency management and the role it plays in the community during a threatening hurricane. The learning modules were developed with the guidance of Miami-Dade County Public Schools (M-DCPS) and available as an educational resource for all teachers.

- IHRC Teacher Resources: http://www.ihrc.fiu.edu/outreach-education/teachers/education-learning-module/
- M-DCPS Department of Science (modules under the outreach tab): M-DCPS District - Science Department (dadeschools.net)

Eye of the Storm (Science, Mitigation & Preparedness) at the Museum of Discovery and Science in Fort Lauderdale: Cancelled due to COVID-19.

Due to COVID-19 the Museum of Discovery and Science (MODS) had to close and the Eye of the Storm Event at the museum was cancelled.

Virtual Eye of the Storm: June 30th, 2020

When the Eye of the Storm Event at the Museum of Discovery and Science (MODS) was cancelled due to COVID-19, a contract modification was executed with the Division and funds were rededicated towards a virtual event. The virtual Eye of the Storm is a 12-episode video series (10-12 minutes each) that educates people about hurricanes and emergency management and connects them with inspiring science.

All the videos are listed on the MODS Virtual Eye of the Storm web-page: https://mods.org/events/eyeofthestorm/

All the videos are also listed on the following MyFloridaCFO web-page: Plan Prepare Protect: Are You Disaster Ready? Eye of the Storm Videos (myfloridacfo.com)

"This video series is a great way to learn about hurricane preparedness and prepare for all possible impacts before a storm makes landfall," said FDEM Deputy Director Kevin Guthrie. "The division is proud to sponsor this informative series so we can help educate all Floridians on how to stay safe before, after and during a hurricane. We look forward to our continued partnership with the International Hurricane Research Center as we continue through the 2020 Atlantic Hurricane Season."

The virtual Eye of the Storm resulted in a hugely successful digital marketing campaign and expanded the reach and impact beyond South Florida to other states on the Gulf of Mexico and the U.S. eastern seaboard at risk of a hurricane landfall.

Digital Marketing Campaign Total Numbers for 12 Videos (The numbers will keep growing because the videos are evergreen.)

- Impressions: 7,054,250+
- Views: 586,320+
- Engagements and Clicks: 23,515+
- Hours Watched: 3,700+

Hurricane Mitigation & Preparedness at FIU: June 30th, 2020

IHRC shared the virtual Eye of the Storm 12-episode video series with the FIU faculty, staff and 55,000 plus students. This was facilitated through the FIU social media channels of LinkedIn, Facebook, and Twitter. IHRC partnered with the FIU Office of Emergency Management and the FIU Division of External Relations and Social Media.

NOAA Hurricane Awareness Tour: Cancelled due to COVID-19.

Get Ready, America! The National Hurricane Survival Initiative: Cancelled due to lack of sponsorships.

Education and Outreach Programs:

Hurricane STEM Science, Mitigation and Preparedness Education Learning Modules (6th Grade and High School): March 31st, 2021

A contract modification was executed with the Division when the Wall of Wind Mitigation Challenge was cancelled due to COVID-19. Funds were rededicated to create virtual hurricane learning modules for 6th grade and high school classrooms. The learning modules teach students about hurricane STEM science, mitigation, preparedness, and wind engineering. They also teach about emergency management and the role it plays in the community during a threatening hurricane. After learning the educational content, there is an activity for students to assume the role of their county emergency management director and record a Zoom video of themselves doing a media conference about a threatening hurricane, which would typically be done at the county EOC with various county officials in attendance. The student media conference (5-10 minutes) would include a brief weather briefing and then information related to county preparations, evacuations, etc.

The learning modules are available as an educational resource for teachers and developed with the guidance of Miami-Dade County Public Schools (M-DCPS). The new modules are located on a new teacher resources web page on the IHRC website and are also located on the M-DCPS Department of Science web page under the outreach tab.

- IHRC Teacher Resources: http://www.ihrc.fiu.edu/outreach-education/teachers/education-learning-module/
- M-DCPS Department of Science (modules under the outreach tab): M-DCPS District - Science Department (dadeschools.net)

To help teachers learn the content, IHRC's Erik Salna provided recorded Zoom presentations describing the educational content in the modules and some guidance for the emergency management activity. After watching the Zoom presentations teachers can then teach the educational content to their students, and guide their preparation for the emergency management activity.

- Hurricane and Emergency Management Module for 6th Grade (PDF)

- Hurricane and Emergency Management Module for 6th Grade Zoom presentation: FIU-IHRC_Hurricane and Emergency Management Module_6th Grade_ZOOM_Presentation
- Hurricane and Emergency Management Module for High School (PDF)
- Hurricane and Emergency Management Module for High School Zoom presentation: FIU-IHRC_Hurricane and Emergency Management Module_High School_ZOOM_Presentation
- Hurricane and Emergency Management Activity for 6th Grade and High School (PDF)

An assessment of the new learning module and student activity was conducted and included student and teacher feedback, and pre and post surveys. All are provided in this Google folder, including an example of a student media conference video: https://drive.google.com/drive/folders/1RU1LFG2PzkiHwcuWVgOYaUXQh10h0Shk?usp=sharing

Virtual Eye of the Storm: June 30th, 2020

When the Eye of the Storm Event at the Museum of Discovery and Science (MODS) was cancelled due to COVID-19, a contract modification was executed with the Division and funds were rededicated towards a virtual event. The virtual Eye of the Storm is a 12-episode video series (10-12 minutes each) that educates people about hurricanes and emergency management and connects them with inspiring science.

All the videos are listed on the MODS Virtual Eye of the Storm web-page: https://mods.org/events/eyeofthestorm/
All the videos are also listed on the following MyFloridaCFO web-page: Plan Prepare Protect: Are You Disaster Ready? Eye of the Storm Videos (myfloridacfo.com)

Topics covered in the videos include hurricane supply kits, power and generator safety, insurance check-ups, pet and boat preparedness, shuttering windows, roofing, debris cleanup, evacuations, storm surge, hurricane forecasting, TV weathercasting and the importance of wind engineering research by the NSF-NHERI Wall of Wind at FIU. The NOAA Hurricane Hunters

even describe what it's like to fly into the eye of a hurricane. The series is unique in that each episode includes a MODS Brainstorm, an interactive science demonstration highlighting the topic being discussed. Demonstrations included creating a liquid nitrogen cloud, the power of air pressure, and the force of an air cannon. Experts also discuss their educational backgrounds and interesting STEM careers, allowing viewers to get a glimpse into their daily lives.

FIU-MODS Media Release: http://www.ihrc.fiu.edu/wp-content/uploads/2021/04/2020-Eye-of-the-Storm-Release-5.28.20-FINAL.pdf
FIU News Story: https://news.fiu.edu/2020/video-series-helps-children,-families-learn-about-hurricanes?utm_source=newsletter&utm_medium=email&utm_campaign=FIU%2520News%2520newsletter
Washington Post News Story: https://www.washingtonpost.com/science/eye-of-the-storm-gives-you-a-better-understanding-about-hurricanes-their-power-and-their-deadliness/2020/07/10/bba1e16c-c147-11ea-b178-bb7b05b94af1_story.html

This collaborative community education outreach project partnered the IHRC with the Florida Division of Emergency Management, Broward County Emergency Management, City of Fort Lauderdale Emergency Management, NOAA's National Hurricane Center, NOAA's Atlantic Oceanographic and Meteorological Laboratory and Hurricane Research Division, NOAA's Miami Office of the National Weather Service. The videos included interviews with National Hurricane Center Director Ken Graham and FDEM Deputy Director Kevin Guthrie.

"This video series is a great way to learn about hurricane preparedness and prepare for all possible impacts before a storm makes landfall," said FDEM Deputy Director Kevin Guthrie. "The division is proud to sponsor this informative series so we can help educate all Floridians on how to stay safe before, after and during a hurricane. We look forward to our continued partnership with the International Hurricane Research Center as we continue through the 2020 Atlantic Hurricane Season."

Other participants who made the video series possible included American Red Cross of Broward County, Broward County Humane Society, International Hurricane Protection Association,

Global Protection Products, Florida Power & Light, Advanced Roofing, Bergeron Emergency Services, Brown & Brown Insurance, State Farm Insurance, Techtronic Industries, Pier Sixty-Six Hotel & Marina, WSVN, NBC 6, Louisiana Children's Museum and the Science Museum of Virginia.

The videos were initially distributed throughout the month of June, 2020 on the MODS YouTube channel, Facebook page, and directly from links on the MODS web-page:

- Hurricane Hunters June 2, 2020
- Forecasting the Storm June 4, 2020
- Weather Tech June 6, 2020
- Wall of Wind June 9, 2020
- Protecting Your Home + Air Cannon June 11, 2020
- Emergency Management & Preparedness June 13, 2020
- Powered Up! Storm Tech & Tools June 18, 2020
- Insurance Check-Up and Boat Safety June 20, 2020
- Pet Prep June 23, 2020
- Tracking & Relief June 25, 2020
- After the Storm June 27, 2020
- Connected & Prepared June 30, 2020

The virtual Eye of the Storm resulted in a hugely successful digital marketing campaign and expanded the reach and impact beyond South Florida to other states on the Gulf of Mexico and the U.S. eastern seaboard at risk of a hurricane landfall. Social media channels included Facebook, Twitter, Instagram, Linkedin and YouTube.

Digital Marketing Campaign Total Numbers for 12 Videos (The numbers will keep growing because the videos are evergreen.)

- Impressions: 7,054,250+
- Views: 586,320+
- Engagements and Clicks: 23,515+

- Hours Watched: 3,700+

Emergency Management & Preparedness Video: https://www.youtube.com/watch?v=fBP1q-i7OS4

- Impressions: 575,570
- Views: 16,735
- Engagements and Clicks: 272
- Hours: 220.7

Staying Connected and Being Prepared for a Hurricane - Interview with FDEM Deputy Director Kevin Guthrie: (https://www.youtube.com/watch?v=UDfgM48PgAY

- Impressions: 600,220
- Views: 21,083
- Engagements and Clicks: 293
- Hours: 276.7

For the complete digital marketing wrap-up report: https://drive.google.com/drive/folders/1gGvlrR22vU0hhc-WFG4DWenaA8kxRaXW?usp=sharing

Hurricane Mitigation & Preparedness at FIU: June 30th, 2020

IHRC shared the virtual Eye of the Storm 12-episode video series with the FIU faculty, staff and 55,000 plus students. This was facilitated through the FIU social media channels of LinkedIn, Facebook, and Twitter. IHRC partnered with the FIU Office of Emergency Management and the FIU Division of External Relations and Social Media.

Digital Summary for LinkedIn: https://www.linkedin.com/posts/florida-international-university_take-your-hurricane-know-how-to-the-next-activity-6683711990952734720-hxy7

- Impressions: 17850
- Likes: 48
- URL Clicks: 53
- Comments: 0

- Shares: 3
- Engagement Rate: 0.58%

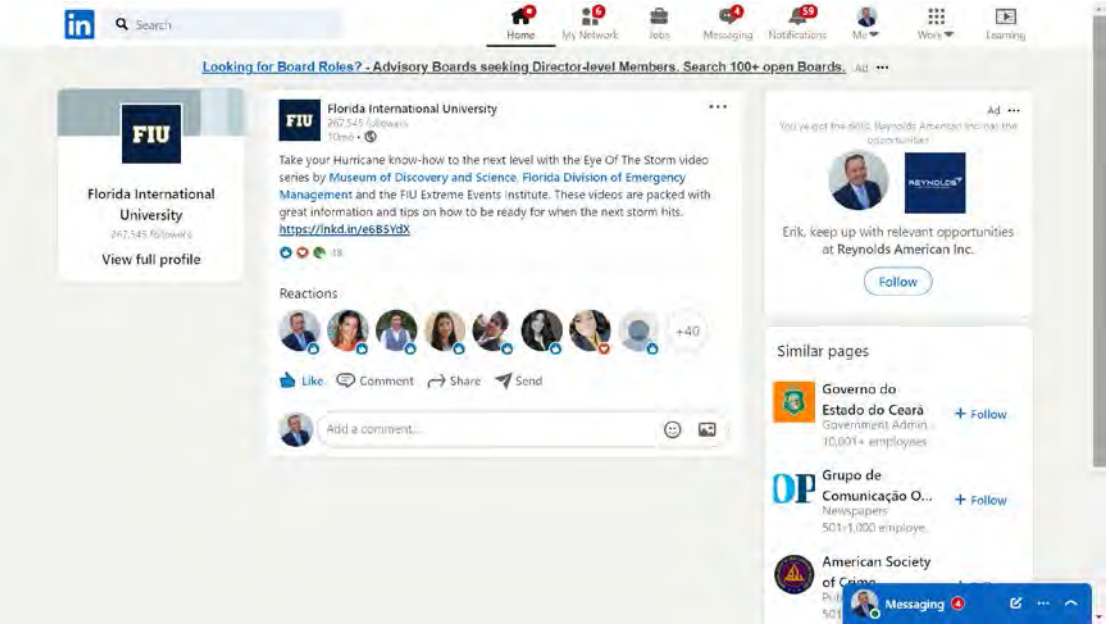

Digital Summary for Facebook:

https://www.facebook.com/floridainternational/posts/10157806869697585

- Impressions: 4878
- Likes: 28
- URL Clicks: 26

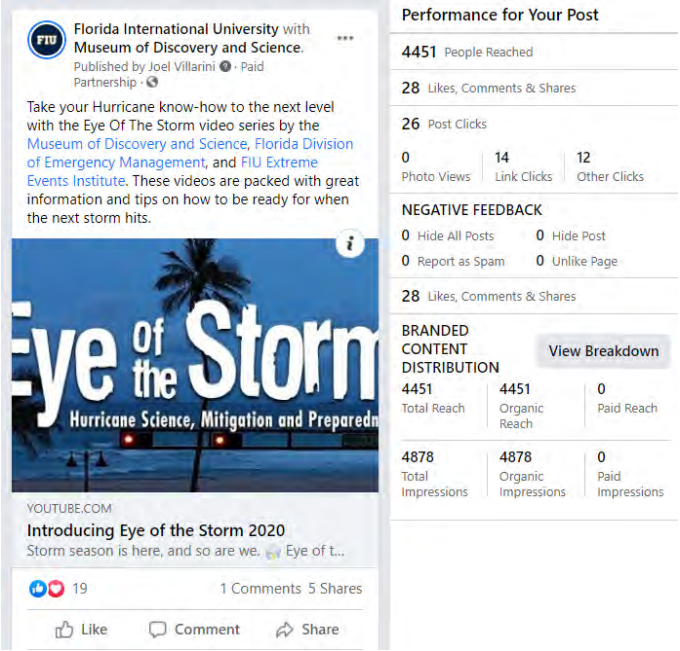

Digital Summary for LinkedIn: https://twitter.com/FIU/status/1277948500206956546

- Impressions: 5453
- Likes: 5
- URL Clicks: 38